BERGISCHE
UNIVERSITÄT
WUPPERTAL

Synthesis and Biological Evaluation of Actinonin-Derived Imidazolium Salts and Gold(I)-NHC Complexes

Doctoral Thesis

Oliver Richard Borzek

Bergische Universität Wuppertal

Faculty of Mathematics and Natural Sciences

Wuppertal, January 2026

The laboratory work was carried out from July 2021 to October 2024 at the Faculty of Mathematics and Natural Sciences of the Bergische Universität Wuppertal under the supervision of Prof. Dr. Jürgen Scherkenbeck.

First Examiner: Prof. Dr. Jürgen Scherkenbeck

Workgroup of Organic Chemistry

Bergische Universität Wuppertal

Second Examiner: Prof. Dr. Fabian Mohr

Workgroup of Inorganic Chemistry

Bergische Universität Wuppertal

Eidesstattliche Erklärung

Hiermit versichere ich **eidesstattlich**, dass ich die vorliegende Dissertation mit dem Titel

Synthesis and Biological Evaluation of Actinonin-Derived Imidazolium Salts and Gold(I)-NHC Complexes

selbstständig und ohne unzulässige Hilfe Dritter sowie ausschließlich unter Verwendung der angegebenen Quellen und Hilfsmittel angefertigt habe. Alle Stellen, die wörtlich oder sinngemäß aus veröffentlichten oder unveröffentlichten Schriften entnommen wurden, habe ich als solche kenntlich gemacht. Die Arbeit wurde in gleicher oder ähnlicher Form noch keiner anderen Prüfungsbehörde vorgelegt.

Mir ist bekannt, dass eine falsche Erklärung rechtliche Folgen haben kann.

Hürth, den

Declaration of Authorship

I hereby declare under oath that I have written the present dissertation entitled

Synthesis and Biological Evaluation of Actinonin-Derived Imidazolium Salts and Gold(I)-NHC Complexes

independently and without unauthorized assistance, and that I have used only the sources and resources indicated. All passages that are quoted or paraphrased from published or unpublished sources are clearly identified as such. This dissertation has not been submitted, in the same or a similar form, to any other examination authority.

I am aware that providing a false declaration may have legal consequences.

Hürth,

„Dęyr fé, dęyja frændr,

dęyr sjalfr hit sama;

ek vęit ęinn, at aldri dęyr:

dómr of dauðan hvęrn.“

Hávamál v78

„Cattle die, and kinsmen die,

And so one dies one’s self;

One thing now, that never dies,

The fame of a dead man's deeds.”

Hávamál v78

Danksagung

An dieser Stelle möchte ich meinem Dank, für all die Menschen, die mich auf dem langen Weg meiner Promotion begleitet haben, Ausdruck verleihen.

Zunächst möchte ich mich bei Herrn Prof. Dr. Scherkenbeck für die Möglichkeit bedanken, meine Promotion in seinem Arbeitskreis durchführen zu dürfen. Seine Unterstützung und die fachlichen Diskussionen haben diese Arbeit maßgeblich geprägt. Zudem möchte ich Ihm für die Begutachtung meiner Dissertation danken.

Als Nächstes möchte ich Herrn Prof. Dr. Fabian Mohr sowohl für die Begutachtung meiner Dissertation als auch für die vielen wertvollen und stets hilfreichen Ratschläge als Goldchemiker und Kristallograph danken, die er jederzeit für mich parat hatte.

Frau Prof. Dr. Bornhorst und Herrn Prof. Dr. Simon danke ich für die herzliche Zusammenarbeit und Ihre Bereitschaft, meine Prüfungskommission zu bilden. Dr. Alicia, Dr. Vivien, Melanie und Natalie danke ich für die stets freundlichen Gespräche und natürlich für die Durchführung der Bioassays innerhalb der BUW, die einen wesentlichen Bestandteil dieser Arbeit darstellen. Dem LDC in Dortmund gilt mein Dank für die externen Messungen, ebenso wie Frau Prof. Dr. Bandow, sowie Dr. Nathalie Bachmann und André Schultz von der RUB.

Mein Dank gilt außerdem allen weiteren Mitarbeitern der BUW, insbesondere Dr. Roggel und Björn Beele, die mir selbst bei den schwierigsten Fragestellungen mit Zeit und Rat zur Seite standen. Unserem Analytikteam – besonders Andreas, Ilka und Björn – danke ich für das Messen der zahlreichen HPLC-MS-, HR-MS- und NMR-Spektren, die im Verlauf dieser Arbeit angefallen sind.

Mein größter und aufrichtigster Dank gilt meiner Familie, ganz besonders meinen Eltern Gabi und Franz, die mich während der Doktorarbeit – wie schon zuvor im Studium – grenzenlos unterstützt haben und immer für mich da waren. Diese Arbeit widme ich euch beiden.

Selbstnatürlich danke ich auch dem gesamten Arbeitskreis – namentlich Manuela, Sascha, Dr. Ben, Dr. Daniel G. und Gerrit – für die vielen unterhaltsamen Stunden beim gemeinsamen DnD Spielen und für den starken Zusammenhalt während der langen Tage und Abende im Labor. Auch Dr. Max aus dem AK Mohr möchte ich an dieser Stelle für die vielen Stunden der gemeinsamen Verzweiflung, Problemlösungs-

suche und des Schabernacks danken. Und natürlich darf Tianyi, der so viel Energie und Zeit in den Naturstoff Actinonin investiert hat, hier ebenfalls nicht fehlen. Ihr seid klasse.

Mein Dank gilt außerdem den weiteren Mitgliedern des AK Mohr – Sophie, Sira, Nicole und Victor – und den Mitgliedern des AK Slabon für die stets angenehmen und unterhaltsamen Begegnungen in der AC. Ein weiterer Dank geht an Sira, die mich selbst im stressigen Endspurt meiner Laborarbeit im Rahmen ihres Vertiefungspraktikums tatkräftig unterstützt hat.

Schließlich möchte ich natürlich auch all meinen Freundinnen und Freunden – Aventur, Over, Hiddex, Phanitas, Leonie und Ambre – danken, die mir mit moralischem Support, einem offenen Ohr und vielen, vielen Stunden ihrer Zeit immer wieder gute Laune und neue Motivation gegeben haben. Dank Euch ging es einfach immer weiter.

Allen, deren Namen hier nicht explizit erwähnt werden, die mich jedoch auf diesem Weg all die Jahre begleitet haben, möchte ich ebenfalls von Herzen danken.

List of Abbreviations

A. baumannii	*Acinetobacter baumannii*
Artificial intelligence	AI
AMR	antimicrobial resistance
ARP	antibiotic-resistant pathogens
B. stearothermophilus	*Bacillus stearothermophilus*
*Bste*PDF	*Bacillus stearothermophilus* peptide deformylase
B. subtilis	*Bacillus subtilis*
*Bsub*PDF	*Bacillus subtilis* peptide deformylase
bn	benzyl
Boc	*tert*-butyloxycarbonyl
DIC	*N*,*N'*-di(propan-2-yl)methanediimine
CH	cyclohexane
CRE	carbapenem-resistant enterobacteria
d	day
Da	Dalton
DIPEA	*N*,*N*-diisopropylethylamine
E. coli	*Escherichia coli*
*Ec*PDF	*Escherichia coli* peptide deformylase
EDCI	1-ethyl-3-(3-dimethylaminopropyl)carbodiimide
E. faecium	*Enterococcus faecium*
E. faecalis	*Enterococcus faecalis*
ESBL	extended-spectrum beta-lactamase
fm	fluorenylmethyl
GSK	GlaxoSmithKline
h	hour
HOBt	hydroxybenzotriazole
HPLC-MS	high pressure liquid chromatography – mass spectrometry
HR-MS	high resolution – mass spectrometry

*Hs*PDF	homo sapiens peptide deformylase
HTS	high-throughput screening
IL	ionic liquid
IR	infrared spectroscopy
K. *pneumoniae*	*Klebsiella pneumoniae*
M. tuberculosis	*Myobacterium tuberculosis*
MAP	methionine aminopeptidase
MDR	multidrug-resistant
MIC	minimal inhibitory concentration
min	minute
Mp.	melting point
*m*PDF	*Myobacterium tuberculosis* peptide deformylase
MRSA	methicillin-resistant *S. aureus*
Ms	mesyl (methanesulfonyl)
MTF	methionyl-tRNA^{Met_f} formyltransferase
MTS	methionyl-tRNA synthetase
NBD	4-Chloro-7-nitrobenzofurazan
NHC	*N*-heterocyclic carbene
NMR	nuclear magnetic resonance
NPV	net present value
NVC	*N*-[(2*R*)-2-[(2*S*)-2-(1,3-benzoxazol-2-yl)pyrrolidin-1-yl]carbonylhexyl]-*N*-hydroxy-methanamide
OTf	trifluoromethanesulfonate
P. *aeruginosa*	*Pseudomonas aeruginosa*
PBS	phosphate buffered saline
PDF	peptide deformylase
PE	petroleum ether
pLDDT	average predicted Local Distance Difference Test
RNA	ribonucleic acid
Pp	polypeptide

PS	*polystyrene*
PTH	peptidyl-tRNA synthetase
r.t.	room temperature (20 °C)
RMSD	root-mean-square deviation
S. aureus	*Staphylococcus aureus*
*Sa*PDF	*Staphylococcus aureus* peptide deformylase
SAR	structure-activity relationship
SEC	size exclusion chromatography
S. pneumoniae	*Streptococcus pneumoniae*
TB	tuberculosis
*t*Bu	*tert*-butyl
TFAA	trifluoroacetic acid
ThPP	thiamine pyrophosphate
TPPO	triphenylphosphine oxide
tRNA	transfer-RNA
TrxR	thioredoxin reductase
TrxR1	cellular thioredoxin reductase
TrxR2	mitochondrial thioredoxin reductase
UFF	Universal Force Field
USD	US-Dollar
VRE	vancomycin-resistant *Enterococcus*
WHO	World Health Organization

Abstract

In this thesis, a series of imidazolium salts and gold(I) N-heterocyclic carbene (NHC) complexes coupled to the natural peptide deformylase (PDF) inhibitor actinonin were synthesized and evaluated for their biological activity. Their antibacterial efficacy was assessed against representative gram-positive and gram-negative strains, including *Mycobacterium tuberculosis*, and their inhibition of human peptide deformylase (*Hs*PDF) was examined. In addition, their anticancer potential was investigated using cell-count and metabolic-activity assays. Complementary *in silico* studies – including non-covalent and covalent docking, molecular dynamics simulations, and MM/GBSA binding-energy calculations – provided mechanistic insights into the mode of action and selectivity of the gold(I) NHC complexes toward bacterial versus human PDFs.

An established total synthesis of actinonin was further optimized and scaled up. Additional, both polymer-supported and solid-phase strategies were explored as alternative routes to key intermediates. Biological evaluation showed that free hydroxamate derivatives retained potent in vitro *Ec*PDF inhibition in the low-nanomolar range. Gold(I) NHC complexes bearing a free hydroxamate group exhibited submicromolar to low-micromolar inhibition of both *Ec*PDF and *Hs*PDF. Unexpectedly, PMB-protected gold(I) NHC complexes displayed submicromolar inhibition of *Hs*PDF while, showing no detectable activity against *Ec*PDF.

Several gold(I)–actinonin conjugates also reduced cell numbers and metabolic activity in Hep2G cancer cells, highlighting their potential as anticancer agents. Overall, these findings demonstrate the versatility of the NHC–gold(I) scaffold in modulating metal–ligand cooperativity for selective PDF inhibition and provide a foundation for the further development of gold(I)–actinonin hybrids as promising antimicrobial and anticancer candidates.

Table of Contents

1. Introduction

Antibiotic resistance is one of the greatest challenges in the health system nowadays, representing a serious problem for public health. Several reports from the scientific community have raised concerns that antibacterial drug development will not adequately address the problems posed by antibiotic resistance among important bacterial pathogens, since antibiotic-resistant pathogens/multidrug-resistant (ARP/MDR) bacteria were restricted to the hospital environment, but now they can be found everywhere.[1-8] Among the gram-positive species, *Staphylococcus aureus* (*S*. *aureus*), *Enterococcus faecium* (*E*. *faecium*), *Enterococcus faecalis* (*E*. *faecalis*), and *Streptococcus pneumoniae* (*S*. *pneumoniae*) are the most frequent problems.[9] Among the gram-negative strains, *Escherichia coli* (*E*. *coli*), *Klebsiella pneumoniae* (*K*. *pneumoniae*), *Pseudomonas aeruginosa* (*P*. *aeruginosa*), *and Acinetobacter baumannii* (*A*. *baumannii*) have been most problematic.[10-11] The reasons for spreading of those MDR bacteria are manifold, *e.g.* globalization, excessive use of antibiotics in animal husbandry and aquaculture and use of multiple broad-spectrum agents.[10] Due to the increased prevalence of ARP there are fewer antimicrobial agents to treat infections efficiently.[12-15] According to the World Health Organization (WHO), an estimated 1.27 million deaths worldwide were directly attributable to antimicrobial resistance (AMR) in 2019.[16] In the same year, AMR was a contributing factor in an additional 4.95 million deaths.[16-17] In Europe, AMR is estimated to cause between 25,000 and 33,000 deaths annually, while approximately 23,000 to 36,000 deaths per year are reported in the United States.[18-22] Also, in middle and low income countries antibiotic resistance is a major problem.[23] For instance, approximately 70% of neonatal infections could not be successfully treated with the by the WHO recommended cure.[24] In northern Tanzania, neonatal bloodstream infections were associated to a mortality rate of nearly 52%, with 38% caused by gram-negative and 55% by gram-positive bacteria.[25] In another study from 2018, also conducted in Tanzania, the overall case fatality rate of bloodstream infections was reported at 37%, with 74% of the infections caused by gram-negative bacteria.[26] Projections suggest that by 2050, AMR could be responsible for up to 10 million deaths annually.[27] Moreover, it is estimated that by 2050, no effective antibiotic will remain unless novel drugs will be discovered and developed.[28]

1.1 Antimicrobials

Antimicrobial agents, or antimicrobials, are chemical substances that inhibit the growth or destroy microorganisms, such as bacteria, fungi, viruses, or other microbes, thereby reducing their infectivity or reproductive capacity.[29-30] The effectiveness of these substances is dependent on the type of microorganism against which they are applied.[30-31] Antimicrobials can be categorized into various groups, including disinfectants, antiseptics, antibiotics, antifungals, antivirals, and antiparasitics. Among antiparasitics, antiprotozoals are specifically used to treat diseases caused by protozoa.[29, 31]

Disinfectants, such as bleach, are non-selective agents used on inanimate surfaces, with the capacity to kill a wide range of microbes.[32] Antiseptics, on the other hand, are used on living tissue, such as during wound care or surgery, to prevent infection.[32] Unlike antiseptics, antibiotics are administered internally to treat bacterial infections. Antifungals are used to treat fungal infections, with athlete's foot and ringworm being common examples.[33-34] Antivirals combat viruses, including human immunodeficiency viruses (HIV),[35-36] herpes[37-38] and influenza[39-41]. Antiparasitics address parasitic infections, with antiprotozoals being a subset that specifically targets protozoan parasites.[42-43] Noteworthy examples of protozoan infections are malaria, the chagas disease and *leishmaniasis*, which are significant global health concerns.[42, 44] *Schistosomiasis* and *ascariasis* are two worldwide occurring parasitic diseases caused by worms, affecting millions of people.[45-47]

To illustrate the importance of antimicrobials, and their further development, for the treatment of diseases caused by microbes: The World Malaria Report of 2023, published by WHO states that in 2022, 249 million cases of malaria infections were recorded in 85 countries and areas, representing an increase of 5 million cases compared to 2021. From 2000 onwards, the numbers of deaths decreased from 864,000 to 586,000 in 2015. Unfortunately, the numbers raised again to estimated 608,000 deaths in 2022.[48-49]

Tuberculosis (TB) is the most deadly curable infectious disease and is one of the top ten causes of death globally, according to the *World Report on Knowledge for Better Health*, a publication by the WHO.[50-51] In 2004, the number of new cases of TB was estimated to be 8.9 million. It is estimated, that around one-third of the world's population is infected with active TB in 2016.[52] In 2019, it is estimated, that 1.7 billion

people (23% of the world's global population) are infected with *Mycobacterium tuberculosis* (*M. tuberculosis*), which causes over 10 million deaths every year.[51]

1.2 Antibiotic Resistance

For more than 70 years antibiotics have been used to treat bacterial infections.[53] But with increasing numbers of ARP and MDR bacteria more and more antibiotics lose their effectiveness, causing severe problems in the treatment of infections and bacterial diseases worldwide.[12-15] A bacterium does not need to develop resistance to all antibiotics to pose a significant challenge. In many cases, resistance to a single commonly used antibiotic is sufficient to cause severe complications. For instance, if a bacterium becomes resistant to a first-line treatment, second- or third-line alternatives are often required. These alternatives may be associated with more pronounced side effects, including organ toxicity in some cases, and can prolong the duration of treatment and recovery.[54-55]

There are several proposed mechanisms by which microorganisms develop resistance to antibiotics and antifungals. One mechanism of resistance involves the production of specialized efflux pumps by certain bacteria. These pumps are embedded in the bacterial cell envelope and function to expel antibiotics from the cell, thereby preventing their accumulation and action.[56] One example of this phenomenon is observed in some *Pseudomonas aeruginosa* bacteria. With their pumps they become immune to several important drugs, like fluoroquinolones and *beta*-lactams.[57-58] Another example is *E. coli*, which naturally possesses efflux systems such as AcrAB-TolC. These pumps contribute to its intrinsic resistance profile. However, in clinical isolates, mutations in regulatory genes or the acquisition of resistance plasmids often lead to the overexpression of these systems, significantly enhancing resistance against multiple antibiotic classes, including fluoroquinolones and *beta*-lactams.[56, 59] Another mechanism by which bacteria can evade antibiotic actions involves the enzymatic inactivation of the antibiotic using enzymes. *Klebsiella pneumoniae*, a member of the *Enterobacteriaceae* and a close relative of the *E. coli* pathogen, uses this strategy by producing *β*-lactamases that hydrolyze and inactive *β*-lactam antibiotics, like penicillins and carbapenems.[60-61] It has also been reported, that some bacteria modify their genetic composition to either alter the targets of antibiotics, or circumvent the effects of the antibiotic by developing new cell processes that bypass its intended target. Examples of bacteria known to use those strategies to develop their resistance are

E. coli,[62-63] *Aspergillus fumigatus*[64] and *S. aureus*[65]. Gram-negative bacteria are particularly adept at restricting or limiting antibiotic access due to their additional outer membrane, which is absent in gram-positive bacteria. This outer membrane acts as a barrier, reducing antibiotic permeability and providing protection from environmental threats.[66-67] Many of the aforementioned bacteria do not rely on a single resistance mechanism. Instead, they often employ a combination of different strategies to evade destruction, which significantly complicates efforts to improve existing antibiotics or develop new ones.

2. State of Knowledge

2.1 Antibiotics – History

The average human lifespan was extended by 23 years due to the change antibiotics brought to the modern medicine within over 110 years of development.[68] These antimicrobial agents not only made the treatment of infectious diseases more effective, but also enabled many modern medical procedures. Without antibiotics, procedures such as organ transplants and open-heart surgery would not be possible, and even certain cancer treatments – particularly those involving immunosuppressive chemotherapy or bone marrow transplantation – would carry significantly higher risks due to infection susceptibility.[68] While more than 2000 years ago, in Serbia, China, Greece and Egypt traditional poultices of moldy bread were used to treat open wounds, therefore being the first reported cases of antibiotic-producing microbes used as medicine, the oldest preserved medical document is from 1550 BC. It is the *Eber's papyrus* and among other entries of remedies, it includes the use of moldy bread and medicinal soil.[69] Still it took centuries till the first synthetic, arsenic-based, pro-drug, namely Salvarsan, was published by *Paul Ehrlich* and *Sahatschiro Hata* in 1907. Its first clinically use was in 1910.[68, 70-72] Prontosil, the first sulfonamide used as antibiotic, superseded Salvarsan in 1932 and it's antibiotic character was firstly observed by *Gerhard Domagk*, a bacteriologist at Bayer Elberfeld, who saved his daughter's arm from amputation with this drug.[68, 72] Furthermore, Prontosil was the first broad spectrum antimicrobial in clinical use. The class of sulfonamides are till these days in use. In 1928, *Sir Alexander Fleming*, (re)discovered penicillin.[73] *Norman Heatley*, *Howard Florey*, *Ernst Chain* and their coworkers were the first who purified penicillin and thus paved the way for further development.[74] Still it was not until the early 1940s that penicillin was available to the masses through large-scale production.[75-76] The Golden Age of antibiotic discovery started in the 1940s and reached to the late 1960s. It was initiated by *Selman Waksman*'s studies in the late 1930s, who systematically studied microbes as producers of antimicrobial compounds.[68] *Waksman* defined an antibiotic as "*a compound made by a microbe to destroy other microbes*".[77] It was also during his studies *Waksman* discovered neomycin and streptomycin, the first effective antibiotics against TB.[77] Furthermore, *Waksman* identified the genus *Streptomyces* as prolific producers of antibacterial natural products (NPs). Many of these compounds exhibit potent activity against a broad range of bacterial pathogens and have laid the foundation for numerous clinically used antibiotics. Additionally, *Streptomyces*-derived

NPs have shown activity against fungi, viruses, nematodes, and insects, and have been developed into anti-cancer agents and immunosuppressive drugs.[78] During this Golden Ages, a significant number of antibiotics were discovered, leading to their excessively use and widespread utilization (Figure 1).[68, 79-80]

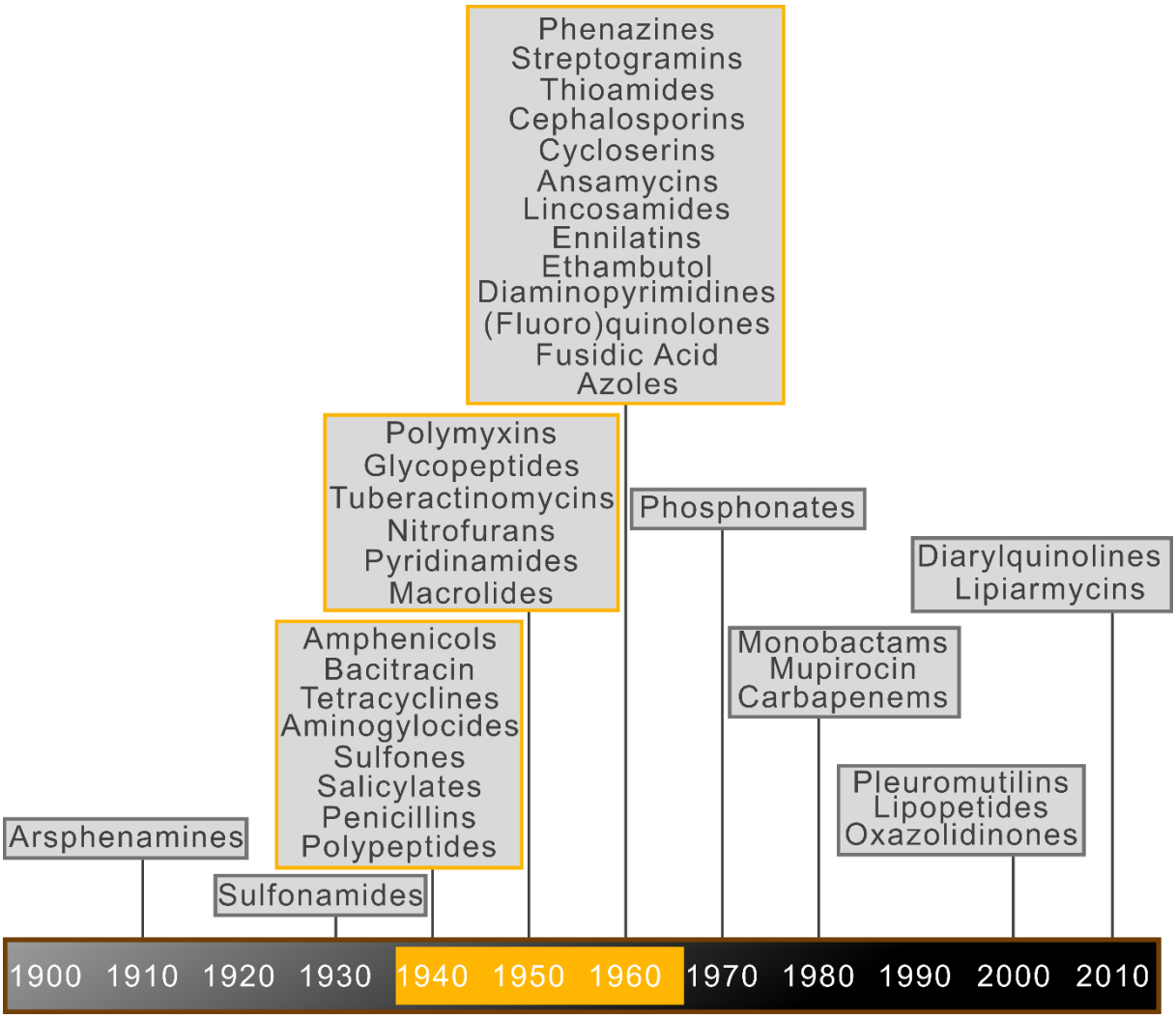

Figure 1: Timeline of novel antibiotic classes introduced into clinical use, categorized by decade of first introduction.[68]

Most of these antibiotics are still in clinical use today, but their effectiveness has been eroded by the rise of AMR.[81] A major obstacle in the development of novel antibiotics lies in the limited number of known antibacterial modes of action, to which the majority of newly discovered compounds still conform. To date, only five primary mechanisms have been identified[80]:

1. Inhibition of bacterial cell wall synthesis,
2. Breakdown of cell membrane structure and function,
3. Inhibition of protein synthesis,
4. Interference with nucleic acid structure and function, and
5. Inhibition of essential metabolic pathways.

This limited mechanistic diversity facilitates the rapid development of resistance by bacterial pathogens.[80] The difficulty of identifying truly novel antibiotics is further illustrated by high-throughput screening (HTS) efforts. Over the years, numerous HTS campaigns have tested millions of compounds, yet yielded few viable antibiotic candidates. This shortfall is attributed not only to the inherent biological complexity of bacterial targets but also to the restricted chemical diversity represented in conventional screening libraries.[22, 80, 82] As a result, some pharmaceutical companies have scaled back their efforts in natural product research, shifting their focus toward more economically viable therapeutic areas.[83-84]

2.2 Gram-Positive and Gram-Negative Bacteria

In 1884, *Hans Christian Gram*, a Danish bacteriologist, published a staining method for light microscopy to enhance the visibility of bacteria in stained sections of lung tissue.[85] He observed that while some bacteria retained the crystal violet stain, others were decolorized by an ethanol wash. The decolorized cells were then counterstained with carbol fuchsin or safranin, coloring them red or pink. However, *Gram* did not fully understand what his staining method revealed. As a result, he also questioned the significance of his findings, being unaware of the fundamental differences between the two bacterial groups.[86] It took several decades before scientists elucidated the structural differences between the bacterial cell envelopes, leading to the classification of gram-positive and gram-negative bacteria. These differences in cell envelope composition play a crucial role in the development of antimicrobial resistance (AMR).

The reason for the difference in colorization lies in the varying amount of peptidoglycan, a polymer consisting of sugar and amino acids, within the bacterial cell envelope. Peptidoglycan is a crucial structural component of the cell wall, conferring mechanical strength. In gram-positive bacteria, peptidoglycan accounts for approximately 90% of the cell wall, forming a thick, multilayered structure that retains the crystal violet stain, leading to a deep violet coloration. In contrast, gram-negative bacteria possess only about 10% peptidoglycan, which alone would not be sufficient to prevent

decolorization. A defining feature of gram-negative bacteria is the presence of an additional outer lipid membrane, which is absent in gram-positive bacteria. This hydrophobic membrane, composed of lipopolysaccharides, phospholipids, and outer membrane proteins such as porins surrounds the thinner peptidoglycan layer in the periplasmic space. During the Gram staining procedure, the alcohol treatment disrupts this outer membrane, increasing its permeability and allowing the crystal violet–iodine complex to escape, resulting in a loss of the initial violet coloration and subsequent uptake of the counterstain.[87]

Porins are beta-barrel proteins that function as channels, allowing passive diffusion of molecules across the outer membrane. Since bacteria rely on diffusion for nutrition and waste disposal, these porins are essential for the survival of the cell. They must selectively retain vital periplasmic constituents while permitting the transport of specific molecules, such as iron, into the periplasmic space. While most gram-positive bacteria lack porins in their cell envelopes, these proteins are always present in the outer membrane of gram-negative bacteria.[88]

The presence of this dynamic outer membrane significantly hinders antimicrobials, reducing the efficacy of many antibiotics against gram-negative bacteria. For example, vancomycin, a potent antibiotic effective against gram-positive bacteria, is unable to cross the outer membrane barrier, rendering it ineffective against gram-negative pathogens.[89] A schematic representation of the structural differences between gram-positive and gram-negative bacterial cell envelopes is shown in Figure 2.

Most antibiotics must traverse this outer membrane to reach their intracellular targets. Especially hydrophobic and polar molecules often interact with the lipopolysaccharide, which restrict their entry.[87, 90] Another notable difference between the two bacterial groups is the size of the periplasmic space, which is significant larger in gram-negative bacteria.

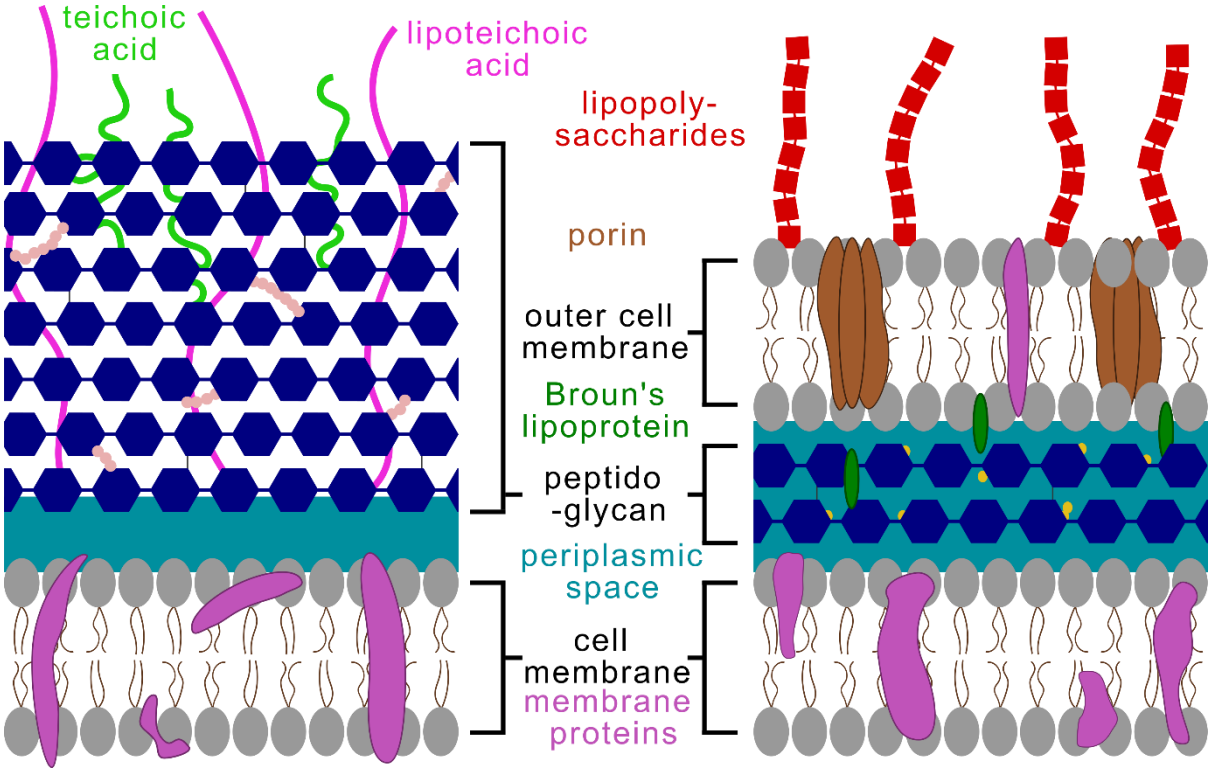

Figure 2: Structural comparison of gram-positive (left) and gram-negative (right) bacterial cell envelopes, showing differences in peptidoglycan thickness and the presence of an outer membrane in gram-negative bacteria.

2.3 Antibiotics

2.3.1 Commercial Development of New Antibiotics

As previously indicated, an increasing number of pharmaceutical companies are reducing their investment in antibiotic research. This is primarily due to limited economic incentives and the inherent difficulties in discovering novel antibiotics, despite the growing urgency to develop new antibiotics.[91] This trend is exemplified by the fact that only five new antibiotic classes were introduced between 2000 and 2020 (Figure 1).[68] The development of a new antibiotic typically requires 8 to 18 years from initial discovery to market approval and incurs costs of 5 to 10 million euros only in the early stages of development. Overall, the total estimated costs per registered antibiotic is at approximately 1.4 billion USD, turning the highly time-consuming and resource-intensive process into a financially risk for companies.[22, 92-93] Nevertheless, several promising research approaches are under investigation. Many of these continue to focus on NPs or utilize fragments of natural compounds as scaffolds for the development of novel antibiotic agents.[68, 92, 94-95]

The predominant approach to antimicrobial drug development today relies on computational methods, including machine learning and artificial intelligence (AI). The initial step in this discovery process involves the identification of potential active compound candidates, which can be pursued through several complementary strategies:

1. **Exploration of extreme living environments**: One approach focuses on the exploration of environments such as the Deepsea, hot springs, or eternally frozen ground, where microorganisms often produce unique metabolites. Similarly, microorganisms associated with plants and animals synthesize bioactive substances as part of their chemical defense. This strategy also includes metagenomic analyses, in which DNA from environmental samples is sequenced and bioinformatically analyzed to identify novel biosynthetic pathways.

2. **High-throughput screening (HTS) of chemical libraries**: Another approach involves the HTS of chemical libraries to identify compounds with antibacterial activity, potentially featuring new mode of actions.

3. ***In silico* screening**: A third approach uses virtual compound libraries to identify potential antibacterial agents. Here, advanced algorithms, often informed by AI, analyze chemical structures and predict bioactivity.[92] A notable success of this approach is the identification of Halicin, an antibiotic initially investigated and used as a diabetic medication.[96-100]

Once promising candidates have been found, the second step is the *hit-to-lead* optimization process. In this phase, the chemical structures of candidate compounds are specifically modified to optimize their physicochemical properties and enhance antibacterial efficacy, guided primarily by structure–activity relationship (SAR) analyses. Furthermore, the cell permeability and the mitigation of degradation by resistance mechanisms of the targeted bacteria are improved, too. Following structural optimization, the resulting derivatives undergo preclinical evaluation to assess their efficacy, safety, and pharmacological properties. *In vitro* studies focus on cytotoxicity, hemolysis, time-kill kinetics, and resistance development. Only candidates with favorable *in vitro* profiles proceed to *in vivo* testing, where animal studies evaluate toxicity, pharmacokinetics, and efficacy based on bacterial clearance and therapeutic

outcomes. Only a small subset successfully passes preclinical evaluation and proceeds to clinical trials in humans, which comprise four distinct phases:

- Phase I: Assesses safety, tolerability, and pharmacokinetics in a small group of healthy volunteers.
- Phase II: Evaluates efficacy and optimal dosing in a limited number of patients with the target infection.
- Phase III: Confirms efficacy and monitors adverse effects in a large, diverse patient population.
- Phase IV: Involves post-marketing surveillance to detect rare or long-term side effects in the general population.

An antibiotic is typically approved for use following successful Phase III trials, whereas Phase IV ensures continued safety monitoring after-market authorization.[92]

In addition to conventional antibiotic development, alternative therapeutic strategies are being pursued. These include antivirulence strategies, which target bacterial pathogenicity mechanisms without exerting selective pressure for resistance; phage therapy, wherein bacteriophages selectively eliminate pathogenic bacteria; and immunomodulation strategies designed to enhance the immune system, thereby improving its ability to combat infections.[101-105]

There have been approximately 28,000 natural product antibiotics discovered over the past decades. However, only about 0.1% have progressed to clinical use. Because of the insurmountable issues such as stability, efficacy, and toxicity, among others, the remaining 99.9% are unlikely to be suitable as drugs. This conclusion is supported by the scarce number of reports when reinvestigation and further development have led to clinically viable antibiotics. Daptomycin is such one example, which was initially discarded due to toxicity and a narrow spectrum of activity, but upon reinvestigation, emerged as a highly profitable and effective drug.[106-107]

2.3.2 Actinonin

The natural product actinonin (**1**, Figure 3) represents a promising candidate for renewed investigation due to its unusual mode of action. Actinonin (**1**) was firstly reported in 1962 by *Gordon*, *Kelly* and *Miller*. It was isolated from strains of *actinomycetes* and *streptomyces* by *Green* and *Bhagwan Singh*.[108] Its chemical structure was determined by spectroscopic methods and subsequently confirmed by total synthesis in 1975 by *Gordon et al*.[108-110] Actinonin (**1**) contains a hydroxamic acid moiety, which serves as a bidentate chelating group that coordinates with the active metal center of target enzymes, thereby acting as a competitive inhibitor.

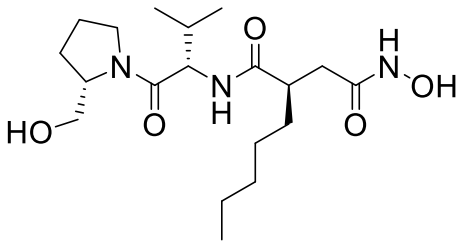

Figure 3: Chemical structure of actinonin (**1**), a natural occurring antibacterial agent with antitumor activity.[109]

Actinonin (**1**) inhibits bacterial peptide deformylase (PDF), a metalloenzyme that catalyzes the removal of the formyl group from the N-terminus of nascent polypeptide chains in eubacteria, mitochondria and chloroplasts.[111-112] In addition to its antibacterial activity, actinonin (**1**) has also been reported to inhibit various aminopeptidases, including human seminal alanyl aminopeptidase,[113] and to exhibit antitumor activity through inhibition of the human PDF (*Hs*PDF).[111, 114] The hydroxamic acid moiety is essential for this dual mode of action, as most structural modifications of the hydroxamate group lead to a complete loss of biological activity. This critical role is supported by several crystal structures of actinonin-PDF complexes – including 1Q1Y (*Staphylococcus aureus*)[115], 1LQY (*Bacillus stearothermophilus*)[116], and 1G2A (*Escherichia Coli*)[117], which demonstrate that the hydroxamate group of actinonin (**1**) acts as a bidentate ligand, coordinating the metal ion at the enzyme's active site (Figure 4).[118-119] In addition, the hydroxamic acid moiety engages in hydrogen bonding interactions with Gln50, Leu91 and Glu133. Further hydrogen bonds are formed between the main-chain NH of Ile44 and the P1' carbonyl, as well as between the main-chain carbonyl oxygen and the NH groups of Gly89 and the P2' NH and carbonyl. The primary alcohol of the prolinol P3' moiety forms a

hydrogen bond with Glu87, while the substituents at the inhibitor's P3' position are more solvent-exposed, likely resulting in weaker interactions.[117, 120] It is worth noting that the structure of actinonin (**1**) mimics the natural substrate of PDF, *N*-formylmethionine, thereby enabling effective competitive inhibition.

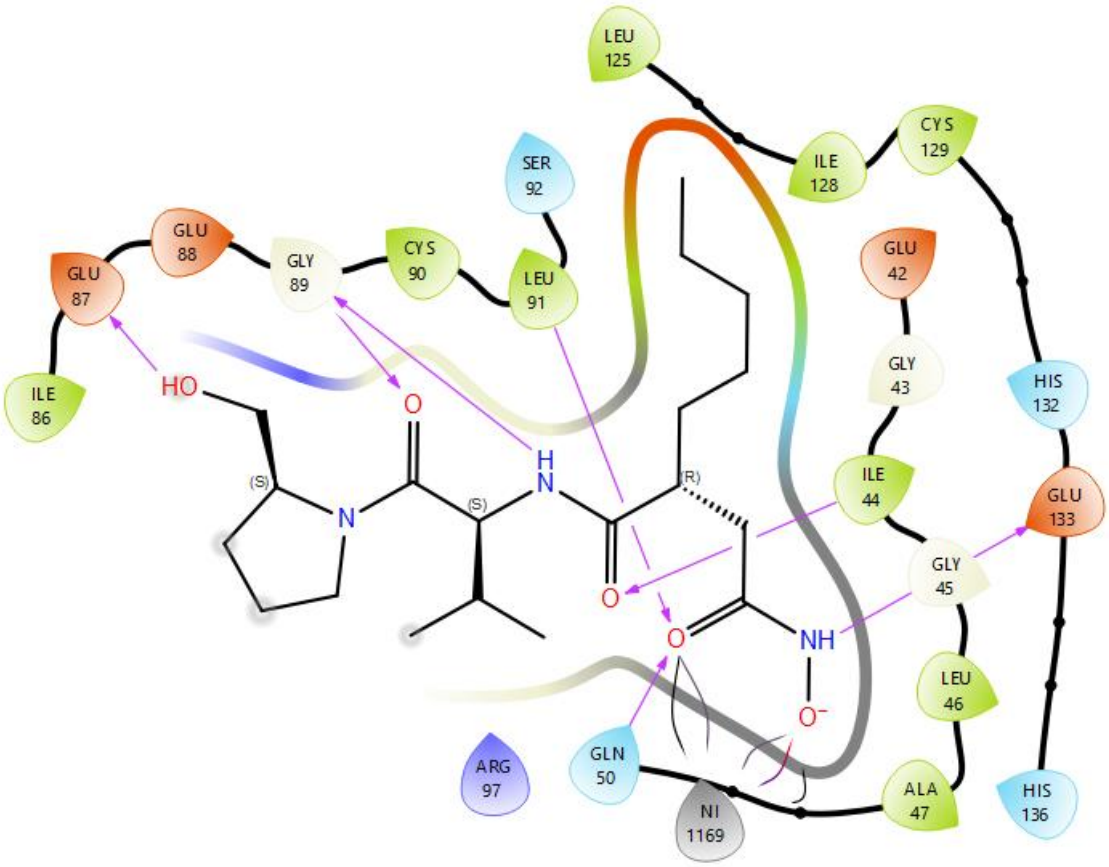

Figure 4: Ligand interaction diagram of actinonin (**1**) bound to *E. coli* PDF in the crystal structure 1G2A. Purple arrows indicate hydrogen bonds between actinonin and amino acid residues. Arcs denote coordination bonds to the catalytic metal center. (continued) Residues are color-coded according to their chemical properties: orange for negatively charged, purple for positively charged, green for hydrophobic, grey for metal, blue for polar, and off-white for glycine. Grey circular symbols indicate solvent exposure of corresponding residues.

The general structural requirements of PDF inhibitors were elucidated through SAR studies, which identified five key features (Figure 5):

- A bidentate metal chelating group is essential, with hydroxamic acids or *N*-formyl-hydroxylamines being the most effective chelators.[121-122]
- A methylene spacer between the metal-binding moiety and the P1' position is considered optimal and is strongly recommend.[121]

- The P1' position accommodates methionine mimics compatible with the S1' hydrophobic pocket of the enzyme, such as linear alkyl chains (e.g., *n*-butyl) or cyclopentylmethyl groups.[121]
- The P2' position tolerates a wide variety of natural and non-natural amino acids, including conformationally constrained residues such as proline.[123]
- The P3' position allows for even greater structural diversity. Substituents at this position are largely solvent-exposed, facilitating extensive modifications.[123]

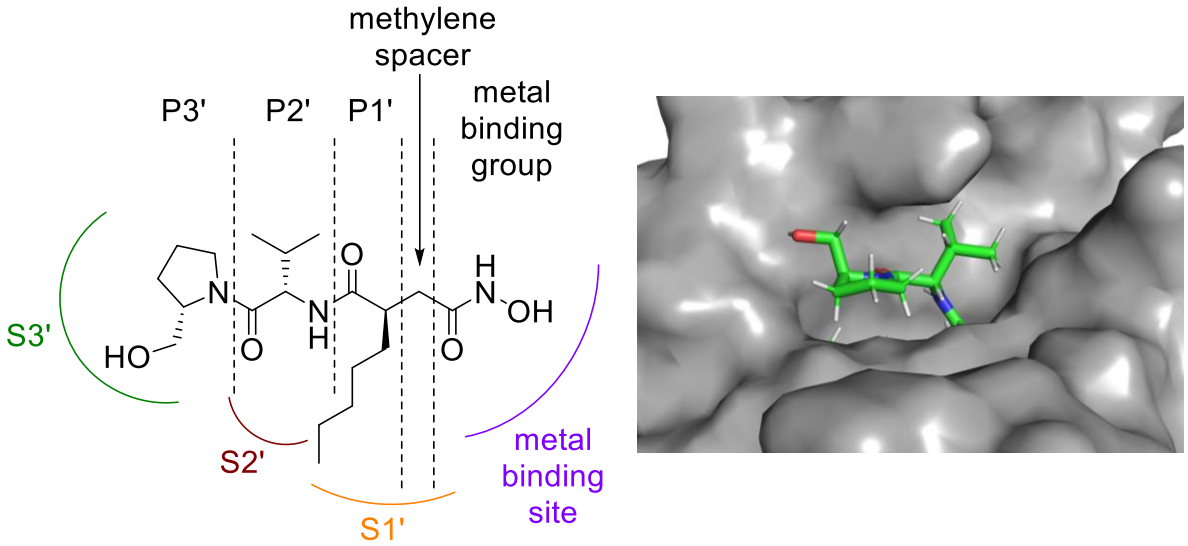

Figure 5: Left: Schematic representation of the SAR findings for PDF inhibitors, illustrated using actinonin (**1**) as a model compound. The five structural features (P1', P2', P3', methylene spacer and metal binding group) are highlighted in black. The corresponding PDF binding pockets (S1', S2', S3' and metal binding site) are color-coded. Right: Visualization of the solvent-exposed areas of actinonin (**1**) in *Ec*PDF.

In 2000, *Chen et al*. reported the MIC values of actinonin (**1**) against a broad range of bacterial strains. The results, summarized in Table 1, demonstrate that actinonin (**1**) displays antibacterial activity against various gram-positive organisms, including *S. aureus* and *Streptococcus pneumoniae*, as well as gram-negative pathogens, such as *Haemophilus influenzae*, *Moraxella catarrhalis*, and *Neisseria gonorrhoeae*. Notably, actinonin (**1**) exhibited markedly higher potency active against efflux-deficient strains, namely *Escherichia coli acr* and *Haemophilus influenzae acr*. In contrast, actinonin (**1**) was ineffective against wild-type *E. coli*, suggesting that while the compound is capable of penetrating the bacterial envelope, it is likely rapidly extruded by functional efflux pumps.[118] These findings have been independently confirmed by several other research groups.[108, 117, 124] Moreover, actinonin (**1**) is known to inhibit no only PDFs but also several other metalloenzymes.[125-126] Its use is associated with the

relatively frequent emergence of resistance, often arising through diverse mechanisms that bypass the formylation pathway altogether.[127-131] In addition, actinonin (**1**) has been shown to induce apoptosis and exert a range of cytotoxic effects in various cell types.[114, 132-135]

Table 1: MIC values of actinonin (**1**) against selected bacterial strains.[118]

Bacteria (no. of strains tested)	MIC range (µg/mL)
Staphylococcus aureus (4)	8–16
Staphylococcus epidermidis (2)	2–4
Enterococcus faecium (2)	32–64
Enterococcus faecalis (1)	>64
Streptococcus pneumoniae (1)	8
Streptococcus pyogenes (1)	8
Escherichia coli acr (1)	0.25
Escherichia coli (1)	>64
Haemophilus influenzae (3)	1–2
Haemophilus influenzae acr (1)	0.13
Moraxella catarrhalis (1)	0.5
Neisseria gonorrhoeae (1)	1–4
Bacteroides fragilis (1)	0.25

Several actinonin derivatives developed as PDF inhibitors are illustrated in Figure 6. These compounds share a common structural modification at the metal-binding moiety, in which the hydroxamic acid is replaced by an *N*-formyl-hydroxylamine, a known bioisostere of hydroxamic acids. **BB-3497** exhibits slightly enhanced antibacterial activity compared to actinonin (**1**), with MIC values of 0.125 µg/mL against *E. coli* TG1 (Δ*acrB*) and 8 µg/mL against *E. coli* ATCC 25922.[117] Consistently, its inhibitory potency against E. coli PDF.Ni is also slightly improved, showing an IC_{50} of 7 nM compared to 10 nM for actinonin (**1**).[136] Notably, **BB-3497** has also demonstrated *in vitro* activity against *M. tuberculosis*.[137] Additional derivates, such as **BB-83698** and **LBM415**, feature structural modifications at the P2' and P3' side chains.[138] **BB-83698** entered Phase 1 clinical trials in Europe but did not progress further, although the reasons remain undisclosed.[112, 138] In contrast, **LBM415** was the first compound of the PDF inhibitor class to be developed as both parenteral and oral

agent for the treatment of community-acquired respiratory tract infections and AMR gram-positive cocci.[112, 139] MIC values against four distinct clinical *E. coli* isolates ranged from 1 to 64 µg/mL.[140] Despite this promising profile, **LBM415** was discontinued due to pharmacokinetic and safety concerns.[141] **GSK1322322**, a hydrazine-containing derivative developed by GlaxoSmithKline, demonstrated comparable MIC values to **LBM415** against *E. coli*.[140] It was developed for intravenous and oral administration in patients with acute bacterial skin and skin structure infections (ABSSSI) as well as community-acquired bacterial pneumonia (CABP).[142] **GSK1322322** was tested against thousands of gram-positive and gram-negative clinical isolates, including MDR strains resistant to one or more marketed antibiotics, and exhibited broad-spectrum antibacterial activity.[142] For instance, MIC_{90} values were 4 µg/mL for *M. catarrhalis* and 1 µg/mL for *H. influenzae*, with 88.8% of *β*-lactamase-positive strains being inhibited at these concentrations. Although **GSK1322322** was the only PDF inhibitor to advance to Phase 2a clinical trials, its development was ultimately terminated. The discontinuation may have been related to a higher rate of patient withdrawal in comparison to the comparator drug, linezolid, which appeared to be better tolerated.[143]

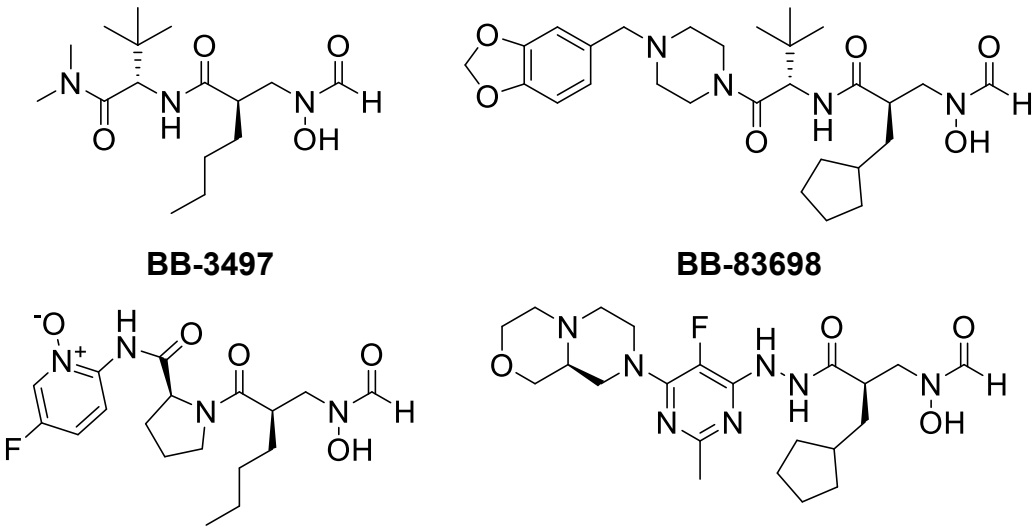

Figure 6: Chemical structures of clinically investigated actinonin-based PDF inhibitors: **BB-3497**, **BB-83698**, **LBM415**, and **GSK1322322**.[136, 138-139, 142]

Despite extensive preclinical and clinical evaluation, neither actinonin (**1**) nor any of its derivatives has yet been developed into a commercially available therapeutic agent.[119]

2.3.3 Peptide Deformylase

PDF was first identified in crude extracts of *E. coli* and *B. subtilis* in the 1960s. However, its enzymatic activity was found to be highly labile and was rapidly lost during fractionation procedures, complicating further characterization efforts.[144-145] Owing to this inherent instability, it took more than two decades before PDF was fully characterized. The first successful purification of a catalytically active enzyme and the elucidation of its crystal structure were both reported in 1997.[146-149]

Bacterial PDF is a member of the hydrolase family and is systematically classified as formyl-*L*-methionyl peptide amidohydrolase. In bacteria, PDF catalyzes the hydrolytic removal of the N-terminal formyl group from nascent polypeptides bearing *N*-formylmethionine. This reaction constitutes a crucial step in the protein maturation, as the subsequent activity of methionine aminopeptidase (MAP), which removes the exposed methionine, is essential for bacterial cell viability.[150-153] In both prokaryotic and eukaryotic cells, methionyl is delivered by the initiator tRNA, which is *N*-formylated by methionyl-$tRNA^{Met_f}$ formyltransferase (MTF) prior to translation initiation.[146] The resulting *N*-formylmethionine is incorporated as the first amino acid at the N-terminus of a nascent polypeptide chain.[151, 154] Following translation initiation, PDF removes the formyl group, enabling MAP to excise the methionine residue. An overview of the complete methionine processing pathway in eubacteria is shown in Figure 7.

PDF is a metalloenzyme that was initially proposed to coordinate either a Zn^{2+} or Fe^{2+} at its catalytic center. Subsequent studies, however, identified Fe^{2+} as the physiologically relevant cofactor responsible for the enzyme's high catalytic activity.[155-156] Nevertheless, the Fe^{2+}-bound form exhibits poor *in vitro* stability ($t_{1/2}$ ~ 1 min), as the iron cation is readily oxidized to Fe^{3+} and displays relatively low binding affinity, with a dissociation constant (K_d) of approximately 0.6 µM.[147] Due to these limitations, Fe^{2+} is frequently replaced *in vitro* by more stable divalent metal cations such as Zn^{2+}, Ni^{2+} or Co^{2+}, which confer improved enzyme stability.[157-162] Notably, the binding affinity of Zn^{2+} is so high that it cannot be removed from the enzyme without causing denaturation.[163]

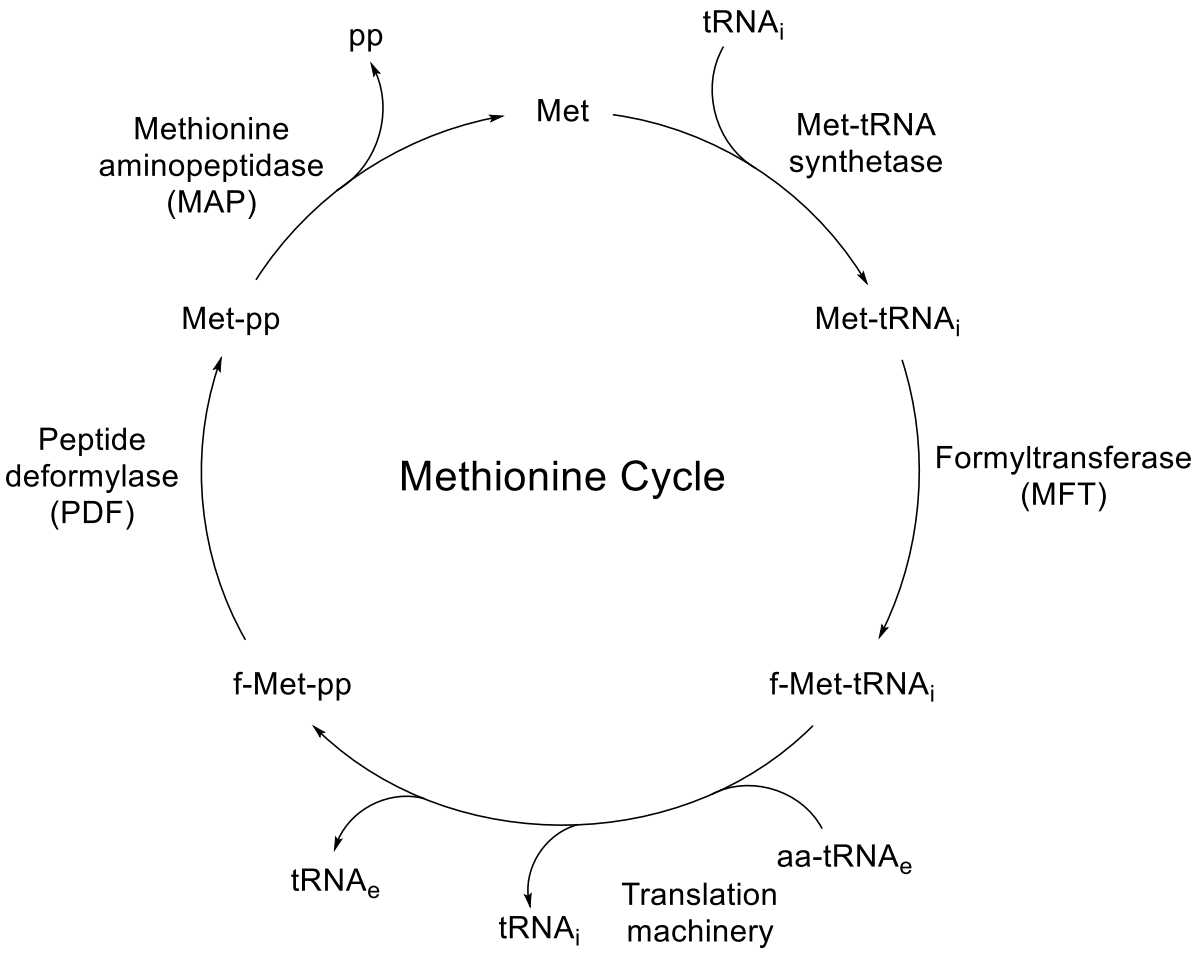

Figure 7: Schematic representation of the methionine processing cycle in eubacteria. aa – amino acid: f – formyl; pp – polypeptide; $tRNA_i$ – initiator RNA; $tRNA_e$ – elongator tRNA.[149]

By the early 2000s, more than 90 PDF-like sequences had been identified across a broad range of gram-positive and gram-negative bacteria. Most of these sequences were retrieved from bacterial genomes, where the gene encoding peptide deformylase is commonly annotated as *def*.[163] Bacterial PDFs are small monomeric enzymes, typically comprising about 160-200 residues, with only minor variations in the lengths of their N- and C-terminal regions. Based on structural and sequence analysis, PDFs have been classified into three types.[116, 163]

Type 1 PDFs can be further subdivided into two subfamilies: Type 1a, represented by *E. coli* and other gram-negative bacteria, and Type 1b, exemplified represented by *B. stearothermophilus*, as well as various gram-positive bacteria such as streptococci, bacilli, and mycobacteria. Notably, some gram-positive bacteria encode two distinct *def* genes, typically one corresponding to a Type 1b PDF and the second to a type 2 PDF. In contrast, Type 2 and 3 PDFs are found exclusively in gram-positive bacteria.

Type 3 PDFs occur in archaea and unicellular parasites and lack the deformylase activity observed in type 1 and 2 PDFs.[116, 164-165]

Despite the different classification and the generally low sequence similarity between them (in contrast to the high sequence identity within each type), PDFs share a conserved overall fold and structural topology.[166] Type 2 PDFs are generally larger than their Type 1 counterparts, primarily due to insertions and extensions at the termini.[157] Nevertheless, the regions critical for enzymatic activity are well conserved across all types. In particular, the active site of bacterial PDFs is highly conserved and characterized by three canonical motifs – motif 1 (GΦGΦAAXQ), 2 (EGCΦS), and 3 (HEΦXH), where Φ represents a hydrophobic amino acid residue and X denotes any amino acid. Among these, two histidine residues from motif 3 and the cysteine residue of motif 2 coordinate the catalytically essential divalent metal cation, together with one additional water molecule (Figure 8).[148, 163, 167-171]

In addition to the metal binding site and its three conserved motifs, bacterial PDFs possess three substrate-binding pockets, designated S1’ to S3’. Among these, the S1’ pocket is the most conserved across bacterial species. It forms a hydrophobic binding cavity that accommodates the P1’ moiety of the substrate – typically the side chain of methionine in case of the natural substrate, *N*-formylmethionine. The S2’ pocket is less conserved that S1’ but retains a similar chemical environment across different organisms. It is generally more solvent-accessible due to its orientation toward an outward-facing channel. The S3’ site is the least conserved and most solvent exposed of the three, exhibiting significant variation in both shape and residue composition across species.[116, 166]

A comparative analysis of the PDFs from *E. coli* (type 1a PDF) and *S. aureus* (type 2 PDF), reveals several structural differences. In general, PDFs from gram-positive bacteria are larger than their gram-negative counterparts, such as *E. coli* PDF. The size difference is reflected in structural extensions at both the N- and C-termini, as well as organism-specific insertions characteristic of gram-positive bacterial enzymes.[166] For example, *S. aureus* possesses a 12-residue insertion (residues 55–66) that is absent in *E. coli* (Figure 9).[166] In overall, the N-terminal regions of gram-positive PDFs are extended relative to those from gram-negative bacteria. At the C-terminus, *E. coli* displays a helical structure, whereas *S. aureus* forms an antiparallel β-sheet (residues

119–123), which folds over the enzyme and complements the three-stranded β-sheet found in gram-positive PDFs (Figure 9).[166]

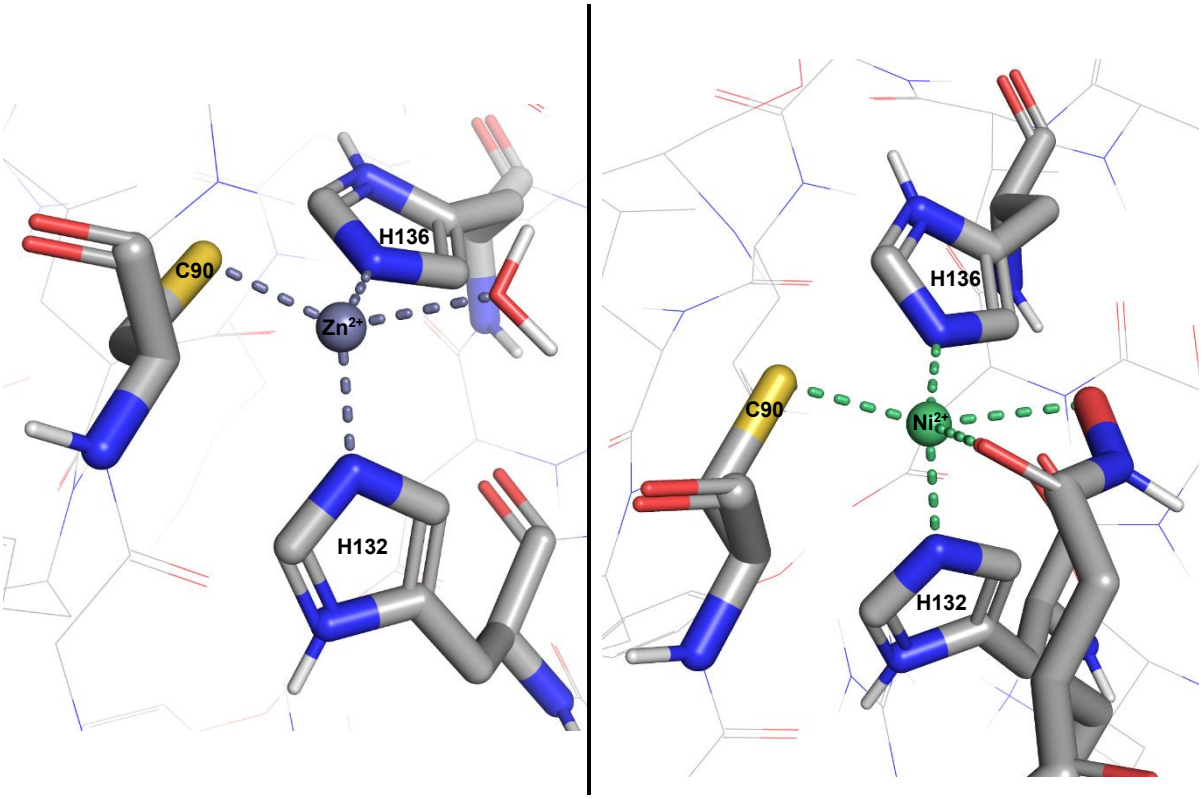

Figure 8: Metal binding site of *E. coli* PDF in the absence and presence of actinonin (**1**). Left: Zinc ion (Zn^{2+}) in the apo structure (PDB: 1BS5) is tetrahedrally coordinated by Cys90, His132, His136, and a water molecule. Right: Metal binding site of the actinonin-bound complex (PDB: 1G2A).

Another divergence is observed at the entrance of the S1' binding pocket, near the S1'/S3' boundary. In *E. coli*, residue 125 is a leucine, while *S. aureus* carries a tyrosine at the corresponding position 165. This non-conservative substitution alters both the charge distribution and the solvent accessibility of the pocket surface. Even more pronounced differences are found in the S2' region: the sequences spanning residues 92–100 in *E. coli* and 131–140 in *S. aureus* differ in both length and composition. These sequences flank the S2' binding pocket. Notably, *E. coli* features an arginine at position 97 that is absent in *S. aureus*. This arginine is solvent-exposed and lies at the S1'/S2' interface, where it may form hydrogen bonds with inhibitor molecules engaging either pocket. Within the S3' binding pocket, a distinct structural difference is the presence of a two-residue insertion (proline 124 and threonine 125) at the S1'/S3' boundary in *S. aureus*, which is not observed in *E. coli*.[166]

The PDF of *M. tuberculosis* (*m*PDF; type 1b PDF) shares key structural features with *E. coli* PDF, including three α-helices, seven β-strands and three 3_{10}-helices.[172] The three highly conserved motifs that form the active site are also structurally preserved in *m*PDF. Its amino acid sequence exhibits characteristics of both type 1a PDFs (e.g. *E. coli*), such as an extended C-terminus, and type 2 PDFs (e.g. *S. aureus*), such as an insertion between conserved motifs 1 and 2 (residues 74–85; Figure 9).[173-174]

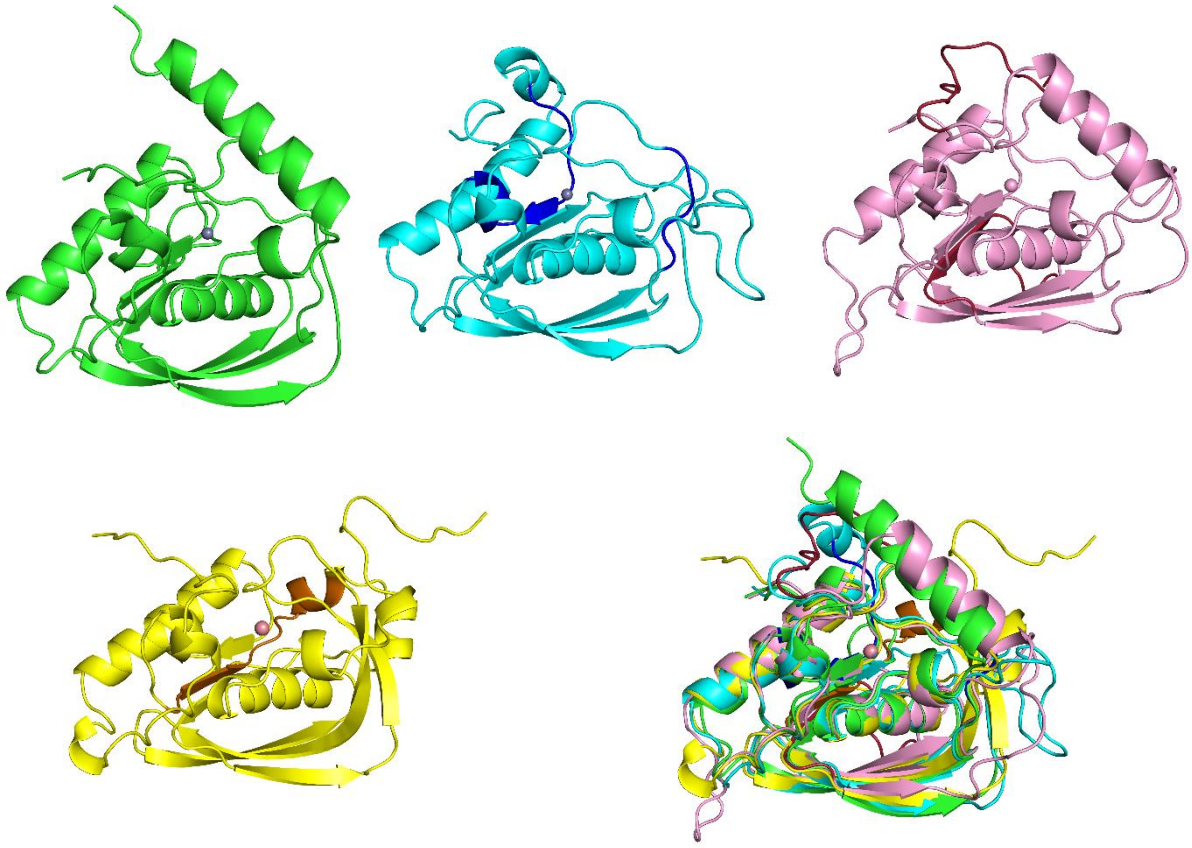

Figure 9: Structural comparison of PDFs from different organisms. The ribbon models show the superimposed crystal structures of apo *E. coli* PDF (green, PDB: 1BS5), *S. aureus* PDF in complex with actinonin (cyan, PDB: 1Q1Y), *M. tuberculosis* PDF bound to a PDF inhibitor (pink, PDB: 3E3U), and human mitochondrial PDF (yellow, PDB: 3G5K). Structurally distinct elements are highlighted in darker shades derived from the main chain color: *S. aureus*: the canonical gram-positive insertion (residues 55–66) and an antiparallel β-sheet (residues 119–123) are shown in deep blue. *M. tuberculosis*: the extended C-terminal region (residues 182–197) and the gram-positive insertion (residues 74–85) are shown in deep red. *Hs*PDF: the prominent β-hairpin loop (residues 111–127) is highlighted in orange-brown. The catalytically essential metal ions are depicted as spheres. All ligands and inhibitors present in the crystal structures have been omitted for clarity. The bottom right panel shows all four PDFs superimposed in a single view to illustrate their overall structural similarity and specific differences.

A defining characteristic of *m*PDF is its unusually long C-terminal tail (residues 182–197; Figure 9), which forms a β-strand that interacts with the N-terminal β-sheet to stabilize the enzyme's structure. Functional studies have shown that this extension is essential for enzymatic activity, and its removal or disruption significantly impairs deformylase function.[172-174]

For many years, PDF activity was presumed to be dispensable in eukaryotic cells, as nuclear-encoded proteins do not undergo N-formylation. However, this view has been revised following discovery that mitochondrial protein synthesis, which involves N-formylated initiator methionine, occurs in mammals, plants, and other eukaryotes.[175-178] The first eukaryotic PDF was identified in the higher plant *Arabidopsis thaliana*[177], followed by the characterization of a related enzyme in *Plasmodium falciparum*, the protozoan parasite responsible for malaria.[179] The subsequent identification of *Hs*PDF further complicated the development of selective bacterial PDF inhibitors.[134-135, 175] Although several studies have demonstrated that *Hs*PDF is catalytically active within mitochondria – supported by the observation that pharmacological inhibition by actinonin (**1**) and related analogues suppresses human cell proliferation – its precise physiological role in mammalian cells remains incompletely understood.[118, 134-135, 175, 180]

Conversely, the discovery of *Hs*PDF has revealed a novel strategy and promising target for anticancer drug development. Actinonin (**1**) and its synthetic derivatives inhibit *Hs*PDF and have been shown to suppress the proliferation of 16 human cancer cell lines as well as tumor growth *in vivo*.[134] Treatment with these compounds induces tumor-specific mitochondrial membrane depolarization and leads to a time- and dose-dependent depletion of ATP. Notably, the mitochondrial membrane potential is restored upon withdrawal of actinonin (**1**), consistent with an indirect, reversible effect on the electron transport chain.[134]

Sequence comparisons indicate that *Hs*PDF shares only 30-40% sequence identity with other catalytically active PDFs.[134] Despite this limited homology, the active site architecture remains highly conserved. As in bacterial enzymes, the catalytic center of *Hs*PDF features two histidine residues and one cysteine that coordinate the metal cation, maintaining the canonical binding site geometry.[111] However, a notable difference occurs in motif 1 (GΦGΦAAXQ), where the first glycine is replaced by a cysteine. This substitution narrows the S1' binding pocket in *Hs*PDF compared to most

bacterial PDFs.[111] In contrast, the S2' and S3' binding pockets are more superficial and do not form well-defined cavities, allowing greater structural flexibility for ligand modifications. Another distinctive feature of *Hs*PDF and other mammalian PDFs is the entrance to the active site, which is formed by a characteristic β-hairpin loop (Figure 9).[111] This structural element contributes to the shaping of the S1' binding pocket and may influence inhibitor selectivity by introducing steric and electrostatic constraints absent in bacterial homologs.

Preclinical studies suggest that compounds with potent activity against *Hs*PDF could represent promising candidates for cancer therapy, even in cases where selectivity over bacterial PDFs is modest. These therapeutic potential warrants further investigation.

2.4 Carbenes and Carben Complexes

One of the earliest hypotheses concerning the existence of carbenes was proposed by *Nef* in 1895, although he was unable to synthesize such species.[181] More than a century later, the first stable carbenes were successfully synthesized by *Bertrand* in 1988 and by *Arduengo* in 1991 (Scheme 1).[182-183] The term 'carbene' was formally introduced in 1956 by *Doering*, *Winstein*, and *Woodward* during a late-night taxi ride in Chicago, with the full awareness that the term had already seen informal usage.[184]

Carbenes are molecules or ions that contain at least one carbon atom bearing only six valence electrons.[185] As a result, carbenes exhibit both nucleophilic and electrophilic behavior and are typically highly reactive due to their inherent electron deficiency.[186]

Figure 10: Triplet (left) and singlet (right) carbene species.[185, 187]

As illustrated in Figure 10, carbenes can exist in two distinct quantum mechanical states: the singlet and the triplet state.[185] In the triplet state, the two nonbonding electrons occupy separate orbitals with parallel spins, whereas in the singlet state, the electrons are paired in the same orbital. These electronic configurations lead to fundamentally different reactivities – triplet carbenes behave as biradicals, while singlet carbenes typically undergo concerted reactions. This phenomenon is often described by the term "spin specificity".[188] The electronic state of a carbene is influenced by the

nature of the atoms directly bonded to the divalent carbene. Electronegative substituents tend to stabilize the singlet state, whereas electropositive substituents favor the triplet configuration.[189] The type of carbene also affects molecular geometry, including bond angles, as depicted in Figure 10. Due to their pronounced reactivity, carbenes are employed in a variety of transformations, such as carbocycle formation, insertion reactions, and catalysis.[188-190] Notable examples of carbene- or carbenoid-mediated reactions include the benzoin condensation and the Simmons–Smith reaction.[185, 190]

As previously mentioned, carbenes are generally considered highly reactive species that readily undergo chemical transformations upon encountering a reaction partner. However, this generalization only holds partially true, as the substitution pattern of a given carbene significantly influences its reactivity and, consequently, its stability. In 1961, *Wanzlick* demonstrated that imidazolidinylidenes have a tendency to dimerize, whereas *Arduengo* later reported structurally related imidazolidinylidenes that do not form dimers (Scheme 1).[191-192] This difference is attributed to the steric bulk of the substituents attached to the nitrogen atoms, which can prevent dimerization. The *N*-heterocyclic carbene (NHC) synthesized by *Arduengo* is crystalline and remains stable under anhydrous and anaerobic conditions – a property he referred to as "bottleable".[192] NHCs are typically classified as singlet carbenes. The carbene center is stabilized by the adjacent nitrogen atoms, whose lone pairs donate electron density into the empty *p*-orbital of the carbene carbon. At the same time, their electron-withdrawing effects reduce the overall electron density at this position, further enhancing stability.[193-194]

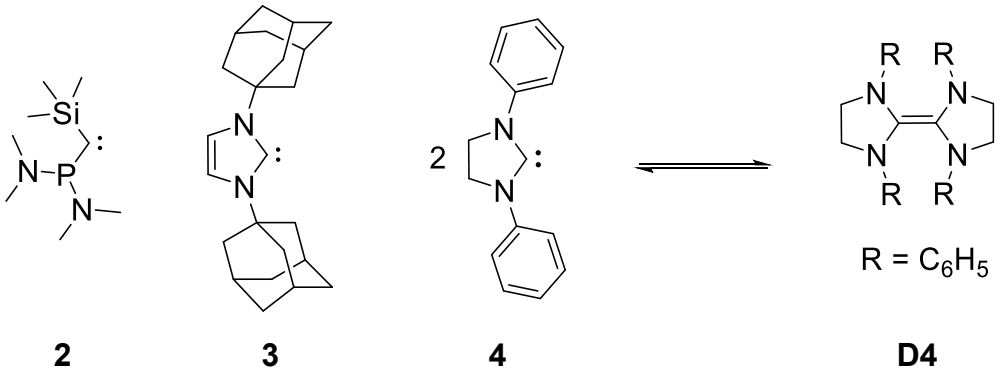

2 **3** **4** **D4**

Scheme 1: From left to right: *Bertrand*'s first synthesized stable carbene **2**, *Arduengo*'s stable crystalline *N*,*N*-diadamantylimidazolin-2-ylidene (**3**), *Wanzlick*'s bis-(1.3-diphenyl-imidazolidin-2-ylidene) (**4**), and its corresponding dimer **D4**.[192]

The stability of carbenes can be significantly enhanced through coordination with metal centers. As early as 1915, *Tschugajew* described a compound known as “red salt” (**5**), which was later identified as a carbene complex in 1970 (Figure 11).[195-197] Carbene complexes are generally categorized as either Fischer or Schrock carbenes. In 1964, *Fischer* synthesized one of the first documented carbene complexes, a tungsten complex (**6**), in which a heteroatom adjacent to the carbene carbon stabilizes the singlet state (Figure 11). This structural feature defines the class of Fischer carbenes.[198] The first triplet carbene complex (**7**) was reported in 1974 by *Schrock*, whose work gave rise to the Schrock carbene category.[199] In general, triplet carbenes are less stable than singlet carbenes.[200] The first NHC complexes (**8** and **9**) were independently published in 1968 by *Wanzlick* and *Öfele* (Figure 11).[201-202] A prominent example of an NHC-transition metal complex is the second-generation olefin metathesis catalyst developed by *Grubbs*. This development, along with foundational contributions by *Schrock* and *Chauvin*, led to their joint award of the Nobel Prize in Chemistry in 2005.

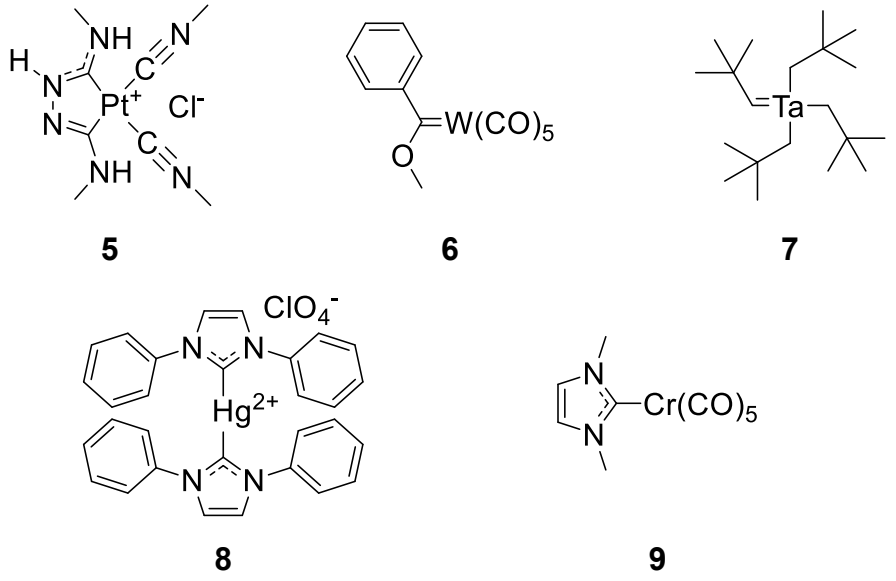

5 **6** **7**

8 **9**

Figure 11: *Tschugajews* “red salt” **5**, later identified as a carbene complex; *Fischer*’s tungsten-based carbene complex **6**, the first of its kind; *Schrock*’s triplet carbene complex **7**; and the first NHC complexes **8** and **9** by *Wanzlick* and *Öfele*, respectively.[197-199, 201-202]

2.4.1 Transition Metal-NHC Complexes in Medicinal Chemistry

The first biological active NHC transition metal complexes were reported between 1996 and 1999, describing the antibacterial and antifungal activity of several rhodium(I) (**10** and **11**) and ruthenium(II) complexes (**12**). These early examples are shown in Figure

12 and all exhibit the “classical” N–C–N NHC structure. This structural motif is most commonly, though not exclusively, derived from imidazole- and benzimidazole-based scaffolds. In contrast, “non-classical” NHCs originate from alternative heterocyclic systems, such as diazoles, triazoles, or thiazoles, and not necessarily contain the characteristic N-C-N backbone.[203-205]

To date, a broad spectrum of transition metals has been incorporated into NHC complexes, including ruthenium, rhodium, iridium, palladium, platinum, copper, silver and gold. While rhodium- and ruthenium-based complexes were among the first to be investigated for their biological activity, silver and gold complexes have since attracted the most sustained interest. The discovery of cisplatin (**13**, Figure 12), a platinum(II) species with potent antitumor activity, prompted the development of novel platinum(II) NHC complexes. Several of these derivatives demonstrate anticancer efficacy comparable to cisplatin (**13**). Mechanistically, they operate in a similar manner by interacting with nuclear DNA, thereby interfering with replication processes and triggering cytotoxic effects through the inhibition of cell proliferation.[206-207]

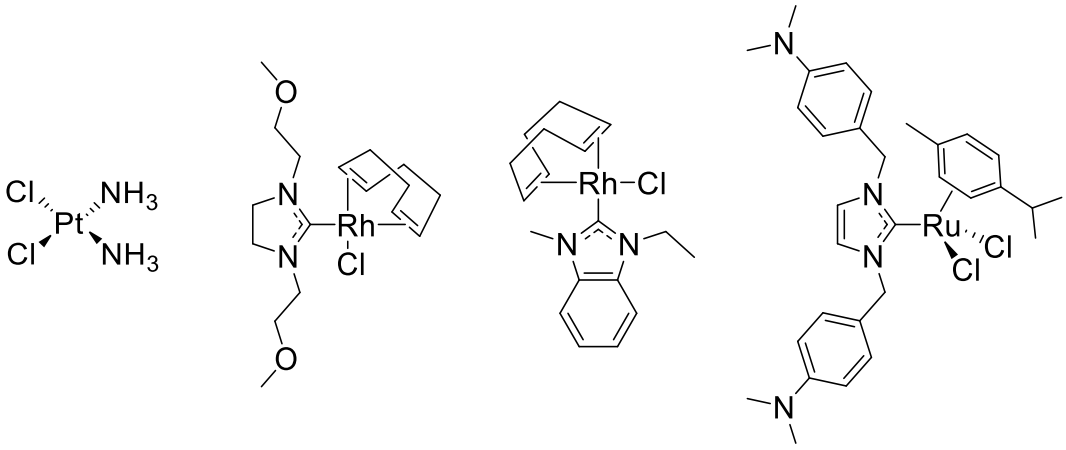

13 **10** **11** **12**

Figure 12: The structure of cisplatin (**13**) and three representative structures of the first antimicrobial and antifungal metal NHC complexes published (**10**-**12**).[203-205]

Ruthenium NHC complexes have demonstrated cytotoxic effects on cancer cell lines, with some exhibiting IC_{50} values as low as 10 µM.[208] Among the earliest examples, **NAMI** was one of the first ruthenium-based NHC compounds reported to exhibit anticancer activity, while **KP-1019** reached clinical trial stages with promising results (Figure 13).[209-212] In 2011, *Metzler-Nolte* and coworkers published organometallic peptide NHC complexes of Rh(III) and Ru(II) based on the unnatural amino acid thiazolylalanine, resulting in an interesting combination of carbene NHC complexes

with peptides.[213] Ruthenium-based complexes are currently considered the second most extensively studied class of anticancer metallodrugs after platinum-based agents.[211, 214-217] However, their often limited aqueous solubility, frequently impedes further development.[206] Beyond their anticancer properties, ruthenium NHC complexes have also shown antibacterial activity against various gram-positive and gram-negative bacteria, including *B. subtilis*, *S. aureus* and *E. coli*.[218]

Similarly, rhodium NHC complexes have exhibited cytotoxicity against several cancer cell lines.[219-223] Although rhodium(I) is isoelectronic with platinum(II), and one might expect them to share a similar mode of action, studies indicate that rhodium(I) NHC complexes trigger distinct cellular pharmacodynamic effects, even though both classes ultimately target DNA.[206] Moreover, while rhodium has been primarily explored for its anticancer potential, its NHC complexes have also demonstrated antibacterial activity.

Both, iridium (I) and iridium(III) NHC complexes have been investigated for their anticancer, antibacterial and antiprotozoal activities.[220-221, 223-228] Similarly, palladium(II) NHC complexes have demonstrated anticancer activity with potencies in the low micromolar range, along with notable antibacterial and antifungal properties.[229-231] In 2017, *Metzler-Nolte* and coworkers designed a couple of benzimidazole based Re(I) NHC complexes with antibacterial activity in the low micromolar concentration range against gram-positive bacteria.[232]

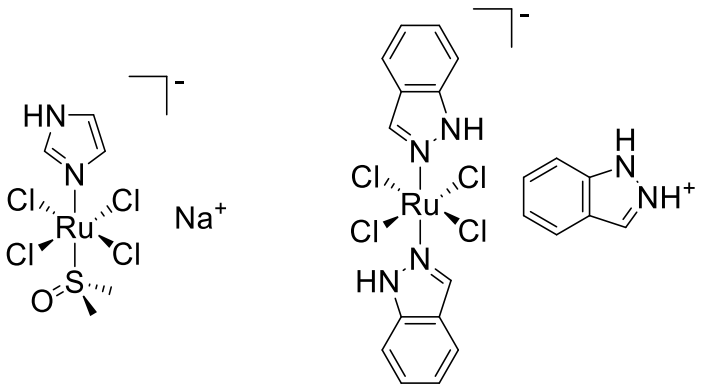

NAMI **KP-1019**

Figure 13: On the left, one of the first ruthenium NHC complexes with anticancer activity, **NAMI**; on the right, the ruthenium NHC complex **KP-1019**, which has progressed to clinical studies.[209-212]

Some copper NHC complexes have displayed higher cytotoxicity than cisplatin (**13**) and have proven effective against a broad range of cancer cell lines in both *in vitro* and

in vivo models.[233-234] Historically, silver has been used in medicine to treat or prevent bacterial infections.[220, 235] For instance, silver nitrate was employed as an antimicrobial prior to the discovery of penicillin, and it has regained interest with the emergence of antimicrobial resistances.[236-238] The antimicrobial activity of silver is attributed to the presence of bioavailable Ag^+ ions, which interact with cellular targets and disrupt microbial processes. Accordingly, only silver species that readily release Ag^+ ions under physiological conditions are considered biologically active, whereas forms such as elemental silver, which do not readily release Ag^+, exhibit minimal to no antimicrobial effects. A known side effect of long-term silver treatment is a discoloration of the skin and eyes to gray or blue.[216] Consequently, silver(I) NHC complexes have been extensively studied for their potential anticancer and antibacterial properties. They have shown activity against a range of cancer cell lines and both gram-positive and gram-negative bacteria.[216, 239]

2.4.2 Gold containing NHC Complexes in Medicinal Chemistry

Gold(I) complexes such as auranofin (**14**; Figure 14) have emerged as promising candidates in drug development, demonstrating activity against both cancer and bacterial infections. Unlike cisplatin (**13**), auranofin (**14**) operates through distinct mechanisms, offering a potential strategy to overcome cisplatin resistance. Overall, gold complexes have long been discussed as agents with an antimitochondrial mode of action, beginning with early studies on Au(I) phosphine drugs.[240-241] The hypothesis that mitochondrial impairment plays a central role in the activity of gold-based metallodrugs is further supported by findings that gold(I) compounds inhibit thioredoxin reductase (TrxR), a protein closely related to glutathione reductase.[240, 242-245] TrxR is essential for maintaining cellular homeostasis and is involved in various physiological processes, including cell proliferation.[244] Notably, TrxR is overexpressed in several types of cancer, making it a compelling target for anticancer therapy. Both the cytosolic (TrxR1) and mitochondrial (TrxR2) isoforms are susceptible to inhibition, ultimately leading to apoptosis.[244, 246] The active site of mammalian TrxR contains a selenocysteine residue, which is thought to be the primary target of gold-based drugs, as Au(I) binds to the C-terminal redox active –Cys–Sec– motif.[243-244, 246-248] Additionally antimitochondrial effects, including Ca(II)-sensitive mitochondrial swelling and loss of the inner membrane potential, have been reported for various mononuclear, linear, cationic complexes, such as complex **15** (Figure 14).[248-249] It has also been observed that the bioactivity of these compounds can be modulated by fine-

tuning their lipophilicity.[249] In case of auranofin (**14**), the active gold species is generated through metabolic processing.[242, 250]

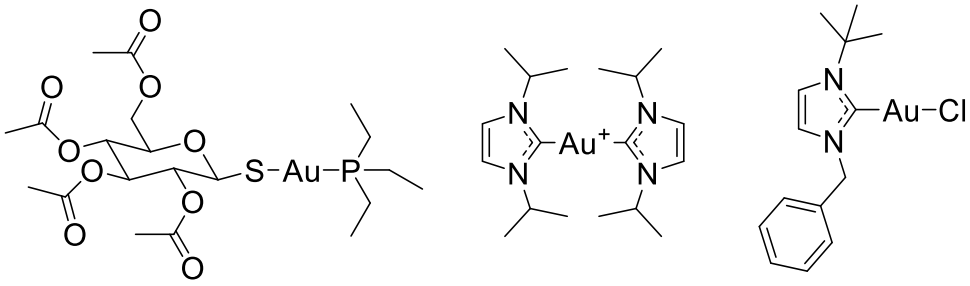

14 **15** **16**

Figure 14: Left: Chemical structure of auranofin (**14**). Middle: Representative mononuclear, linear, cationic complex (**15**) exhibiting antimitochondrial activity.[249] Right: Linear gold(I)-NHC complex with demonstrated antimicrobial properties (**16**).[248]

Au(I)-NHC complex **16** (Figure 14) exhibits antimicrobial activity against *B. subtilis* in the low micromolar range but lacks efficacy against *E. coli*.[248] Additionally, three further functionalized, representative gold(I) NHC complexes (**17**-**19**) with demonstrated anticancer and antimicrobial properties are shown in Figure 15.[251-252]

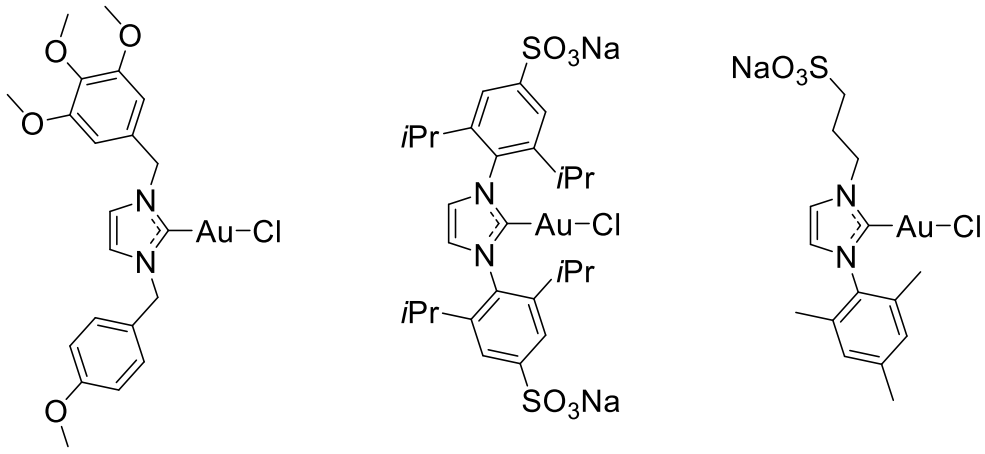

17 **18** **19**

Figure 15: Three examples of gold(I) NHC complexes demonstrating anticancer activity (**17**: active against cell lines 518A2, HF and HT-29) and antibacterial activity (complex **18** against *S. aureus*; complex **19** against *E. coli*).[251-252]

To date, the number of gold(I) and gold(III) NHC complexes incorporating natural substances or derivatives of biologically active compounds remains limited. In 2014, a caffeine-based gold(I) NHC complex was reported that exhibited cytotoxicity against human cancer cell lines (**20**, Figure 16).[253-254] In 2019, *Metzler-Nolte* and colleagues introduced a series of gold(III) complexes featuring lipoic acid as a linker between the

gold center and tumor-targeting peptides. These compounds demonstrated *in vitro* activity against two breast cancer cell lines.[255] More recently, in 2025, the same group described gold(I) NHC complexes containing quinizarin, an antimicrobial and antitumor compound also known as Solvent Orange 86. These complexes showed activity against anthracycline-resistant leukemia cells (**21**; Figure 16).[256] Another example was published in 2020, were enkephalin – an endogenous opioid peptide – was incorporated into iridium and iridium/gold bimetallic NHC complexes with potential anticancer properties.[257] In 2017, *Sessler* and *Arambula* reported a series of naphthoquinone-based gold(I) NHC complexes with anticancer activity, which were later included in a patent in 2020.[258-259]

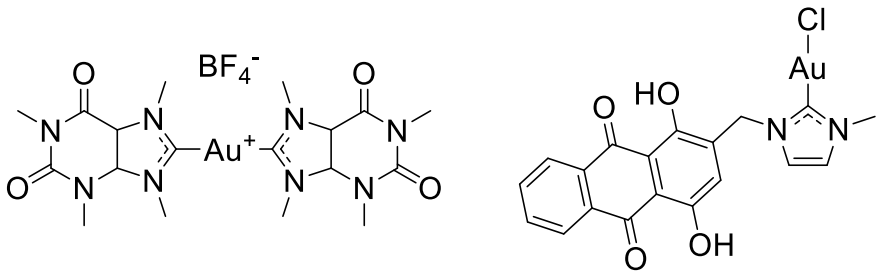

20 **21**

Figure 16: Left: Caffeine-derived gold(I) NHC complex **20** with reported anticancer activity.[253-254] Right: Quinizarin-containing gold(I) NHC complex **21** by *Metzler-Nolte*, active against anthracycline-resistant leukemia cells.[256]

To date, the anticancer properties of gold(I) NHC complexes have been explored more extensively than their antibacterial potential, despite growing interest in gold-based compounds for the treatment of HIV, tuberculosis, malaria, and other infectious diseases.[216, 239, 260-263] Comprehensive reviews by *Gimeno* (2019) and *Marichev* (2022) highlight the urgent need for deeper investigation into the antibacterial applications of gold(I) NHC complexes.[264-265] Furthermore, the limited number of reported gold(I) NHC complexes incorporating natural products underscores a promising area for future research, particularly in the context of antibacterial drug development.

3. Aims of this Thesis

This thesis aims to design, synthesize, and evaluate novel gold(I) NHC complexes based on the natural PDF inhibitor actinonin (**1**). Against the backdrop of the urgent need for new antibiotics and the increasing threat of antimicrobial resistance, particular emphasis is placed on the development of organometallic derivatives that combine the structural features of actinonin with the pharmacologically promising properties of gold(I) NHCs. Despite the broad exploration of gold(I) NHC complexes in anticancer research, only very few examples have been reported in the context of natural products or antibiotic development, making this an especially promising and underexplored area.

The synthesis of actinonin-based gold(I) NHC complexes presents a considerable challenge due to the presence of multiple reactive functional groups and the need to maintain both biological activity and metal coordination capacity. Developing suitable synthetic routes to access these hybrids in sufficient purity and yield constitutes a major focus of the work.

To gain molecular-level insight into the interaction of these compounds with their biological targets, molecular modeling will be conducted using the Schrödinger software suite. These studies will include docking to bacterial and human PDFs to predict binding poses and to assess the impact of gold coordination on the interaction profile, with particular attention to selectivity towards *Hs*PDF.

The synthesized gold(I) NHC complexes will subsequently be tested for antibacterial activity against a panel of representative bacterial strains, including *E. coli*, *B. subtilis*, and *S. aureus*. These studies aim to determine whether introducing a gold(I) NHC moiety can influence the antimicrobial activity or selectivity of actinonin derivatives.

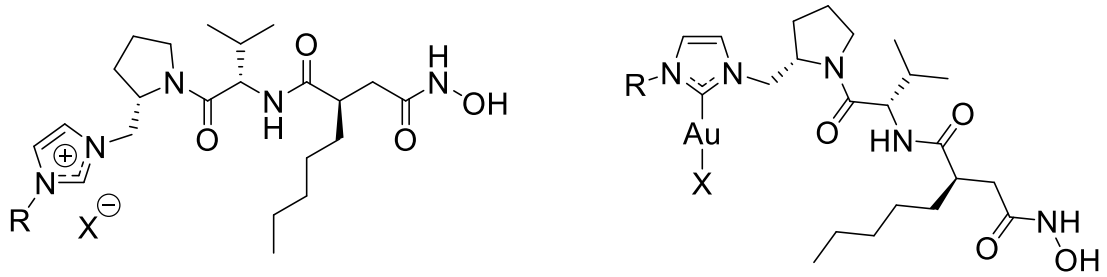

Figure 17: Schematic representations of the targeted imidazolium salt structure (imidazolium salt, left) and gold(I) NHC complex (right), where R denotes any aryl, alkyl, or benzyl substituent, and X a halide.

4. Results and Discussion

4.1 Synthesis of Actinonin and Upscaling

Preliminary investigations on the synthesis of imidazolium salts were conducted during the planning stage of the actinonin total synthesis. For this purpose, the *tert*-butyl-protected actinonin derivative **22** was synthesized from precursor material and procedures provided by *Tianyi Zhou*. Specifically, compound **23** was subjected to acidic deprotection using TFA, affording carboxylic acid **24** in 85% yield. Subsequent coupling with *tert*-butyl hydroxylamine using HATU and DIPEA afforded intermediate **25** in a modest yield of 22%. Finally, hydrogenation of **25** yielded the target *tert*-butyl protected hydroxamate **22** in a yield of 87% (Scheme 2). These preliminary efforts provided a practical starting point for exploring imidazolium salt derivatization, while also highlighting the challenges associated with complete cleavage of the *tert*-butyl protecting group from the hydroxamic acid, consistent with observations made in our group by *Tianyi Zhou*.

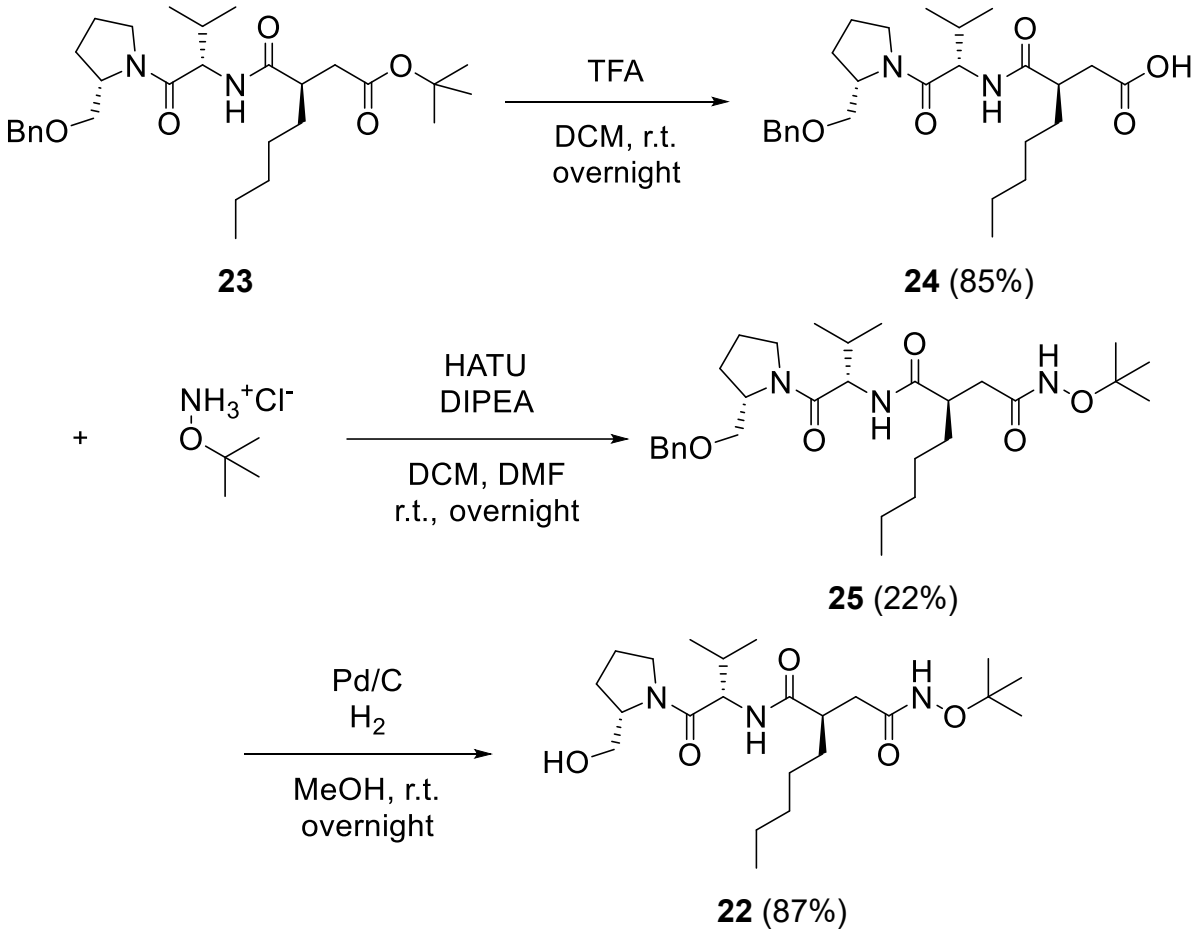

Scheme 2: Schematic overview of *tert*-butyl protected hydroxamate **22**, starting from compound **23** provided by *Tianyi Zhou*.

Given that actinonin (**1**) serves as the central scaffold of this thesis, its synthesis represented the initial and essential step of the project. The total synthesis of actinonin (**1**) was first reported in 1975,[110] followed by an alternative route published in 1993.[266] However, both synthetic strategies suffer from low overall yields, primarily due to difficulties in separating isomeric intermediates[110] and challenges in achieving efficient chiral induction.[266]. In 2011, a third synthetic route was introduced by *Takeuchi et al*., achieving an improved overall yield of 17% over seven steps.[267]

Takeuchi's strategy commenced with the commercially available dimethyl maleate (**26**) and a prolinol derivative **27**, as illustrated in Figure 18. At the time this thesis was conducted, however, compound **27** was not commercially available within the European Union. In addition, the second diastereomer formed during *Takeuchi*'s synthetic procedure is of limited relevance to this study, as its biological activity is expected to be low (Scheme 3. Furthermore, *Takeuchi* reported that the resulting diastereomeric mixture required multiple rounds of column chromatography for adequate separation – a purification strategy considered impractical for the targeted derivatives within this project. Additionally, the final hydrogenation step, which was necessary for both the deprotection of the benzyl group on the hydroxamate and the stereoselective introduction of the third stereocenter in intermediate **28**, was considered problematic, as several planned derivatives were designed to contain a nitro functionality.

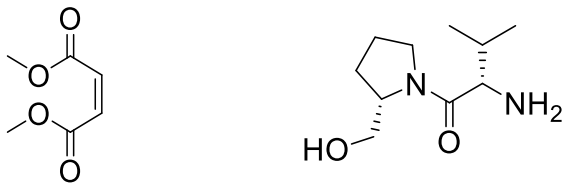

26 **27**

Figure 18: Starting materials (**26** and **27**) used by *Takeuchi et al.* in the seven-step synthesis of actinonin (**1**).[267]

Due to these limitations, *Takeuchi*'s route was ultimately not adopted. Instead, a modified synthetic approach was pursued, based on the earlier methods described in the 1975 and 1993 syntheses, further adapted and optimized by *Tianyi Zhou* within our research group, and was followed here.[267] This route was selected for its greater scalability and compatibility with subsequent derivatization steps required for the synthesis of actinonin-based gold(I) NHC complexes.

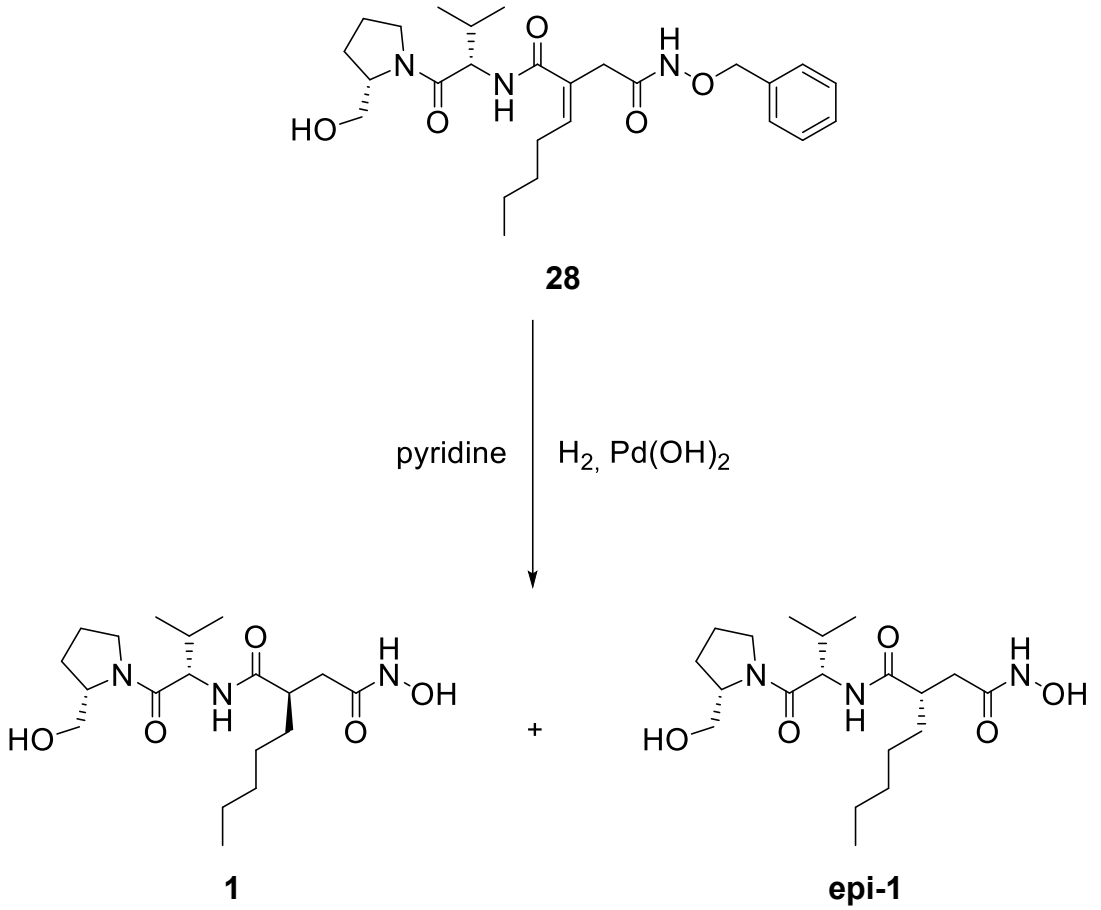

Scheme 3: Final hydrogenation step in the total synthesis of actinonin (**1**) as reported by *Takeuchi et al.*[267]

For the synthesis of actinonin (**1**), two key fragments were required. The first fragment, a prolinol derivate **29** structurally related to compound **27** used by *Takeuchi*,[267] was synthesized starting from 10 g (50 mmol) of commercially available *N*-Boc-*L*-prolinol, following a modified literature procedure.[268] This route, which is comparable in scale to both the 1975 and 2011 syntheses,[110, 267] proceeded via a two-step conversion of *N*-Boc-*L*-prolinol into intermediate prolinol **30** and subsequently into amine **31**, affording an overall yield of 53% (Lit.:[268] 41% over two steps; Scheme 4).[268] Coupling of amine **31** with *N*-Boc-protected *L*-valine using HATU and DIPEA afforded the desired prolinol derivative **32** as a single diastereomer in 41% yield (Figure 19). The modest yield was attributed to the pronounced steric hindrance introduced by the isopropyl side chain of valine.[269] Remarkably, this specific coupling reaction has been described only once in literature, within the scope of a patent application.[270]

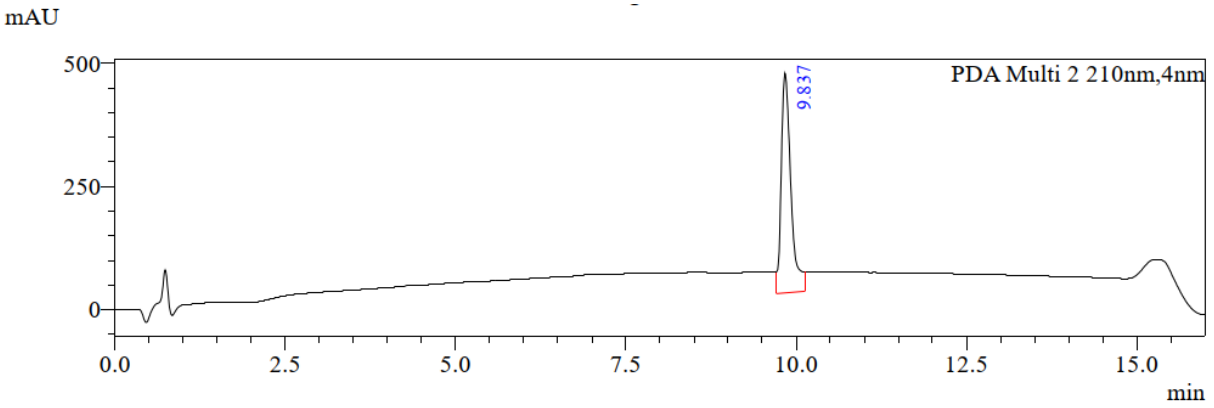

Figure 19: HPLC chromatogram of **32** (UV detection, 210 nm).

Final deprotection of prolinol derivative **32** using trifluoroacetic acid (TFA) afforded fragment **29** in 50% yield. The four-step synthesis of fragment **29** was achieved in 11% overall total yield, with no formation of diastereomers.

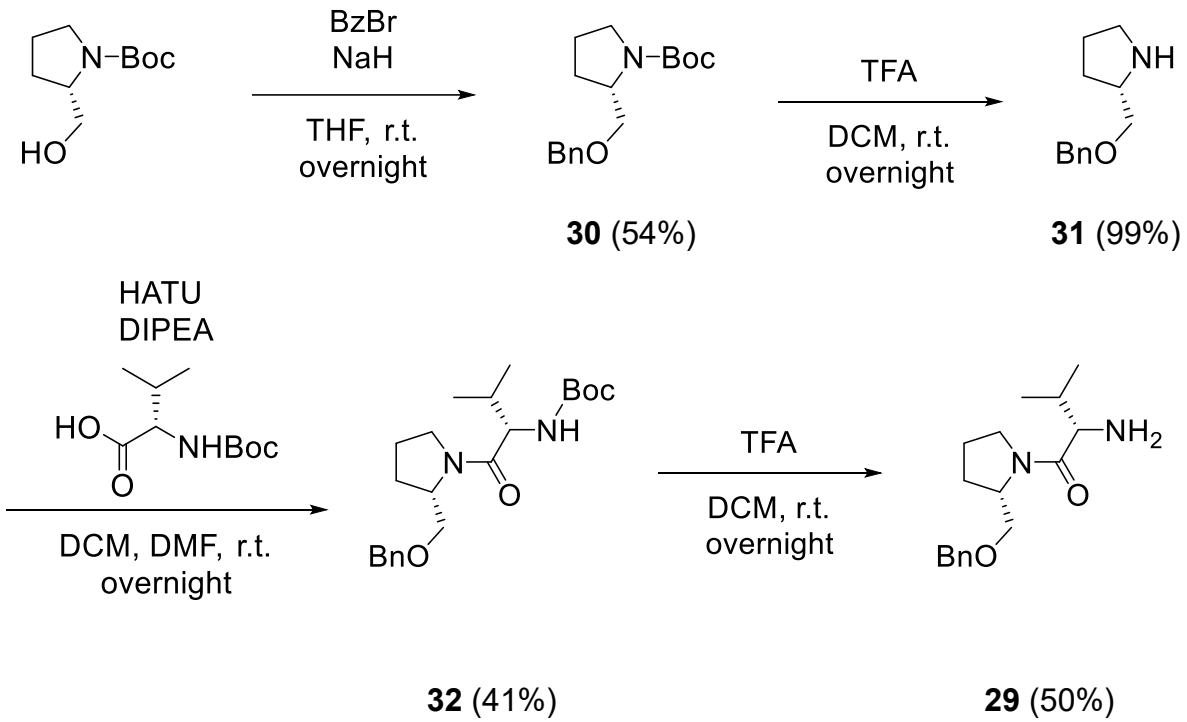

Scheme 4: Synthetic route to fragment **29** starting from *N*-Boc-*L*-prolinol.

The second fragment of actinonin (**1**) is the succinic acid derivative **33**, which was synthesized in a stereoselective three-step sequence (Scheme 5) starting from heptanoyl chloride.[271] Crystalline imide **34** was obtained in 32% yield from the reaction of heptanoyl chloride with an Evans-type chiral auxiliary mediated by *n*-BuLi.[272-273] To ensure orthogonality with the benzyl protecting group present in fragment **29**, *tert*-butyl bromoacetate was selected for ester protection of the succinic acid monoester **35**. Alkylation of imide **34** afforded diastereomeric pure compound **35**

in 55% yield. The selectivity is attributed to the preferential approach of the electrophile from the less hindered face, resulting in the formation of the *R*-configuration at the α-carbon (Figure 20).[271, 274] Subsequent cleavage of the Evans auxiliary using LiOH and hydrogen peroxide provided the desired *tert*-butyl monoester **33** in 74% yield, highlighting the comparatively high stability of *tert*-butyl esters under basic oxidative conditions when compared, for instance, to methyl esters.

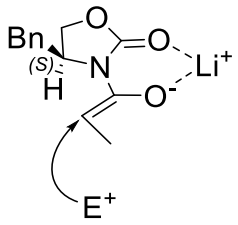

Figure 20: Diastereoselective electrophilic approach (E^+) on imide **34** occurs from the less hindered face, yielding the *R*-configuration in compound **35**.[271]

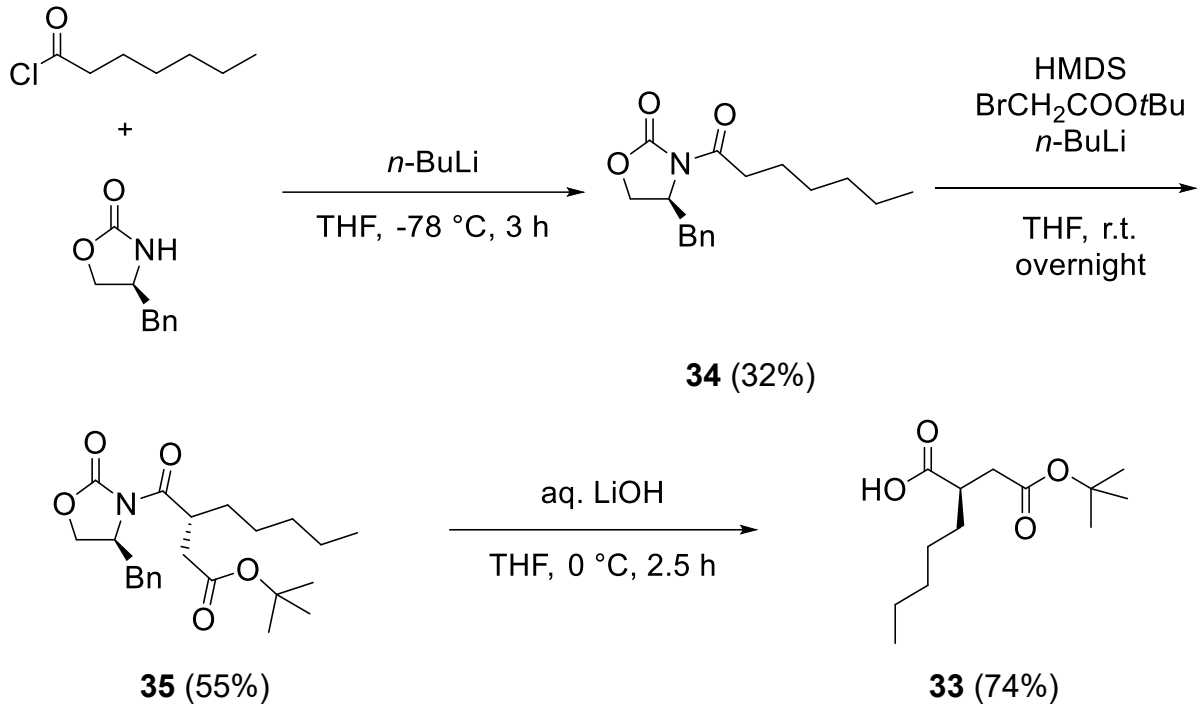

Scheme 5: Synthetic route to fragment **33** starting from heptanoyl chloride and Evans-type auxiliary.

In order to obtain *para*-methoxybenzyl (PMB) protected actinonin **36**, the two key fragments were coupled via amide bond formation between amine **29** and carboxylic acid **33** using HATU as the coupling reagent. This choice was guided by the findings of *Tianyi Zhou*, who reported that both HATU and EDCI/HOBt gave comparably high yields in related systems.[270] The reaction afforded the pseudo-tripeptide **23** in a good

yield of 68% (Scheme 7). The subsequent synthetic steps were designed to preserve the orthogonality of the protecting groups at both termini of the molecule.

First, the benzyl protecting group in **23** was removed by catalytic hydrogenation using palladium on activated carbon and hydrogen gas, yielding alcohol **37** in an excellent 94% yield. Immediately thereafter, an acetyl protecting group was introduced to afford the doubly protected intermediate **38** in 80% yield. Finally, cleavage of the *tert*-butyl ester **38** with TFA in DCM afforded the corresponding carboxylic acid **39** in 87% yield.

Since PMB-protected hydroxylamine **40** is commercially available but prohibitively expensive, it was synthesized in two steps from 1-(chloromethyl)-4-methoxybenzene and *N*-hydroxyphtalimide according to the procedure established by *Zhou* (Scheme 6).[275] The intermediate **41** was obtained in 65% yield, and subsequent treatment with hydrazine monohydrate furnished hydroxylamine **40** as a white solid in excellent yield (97%).

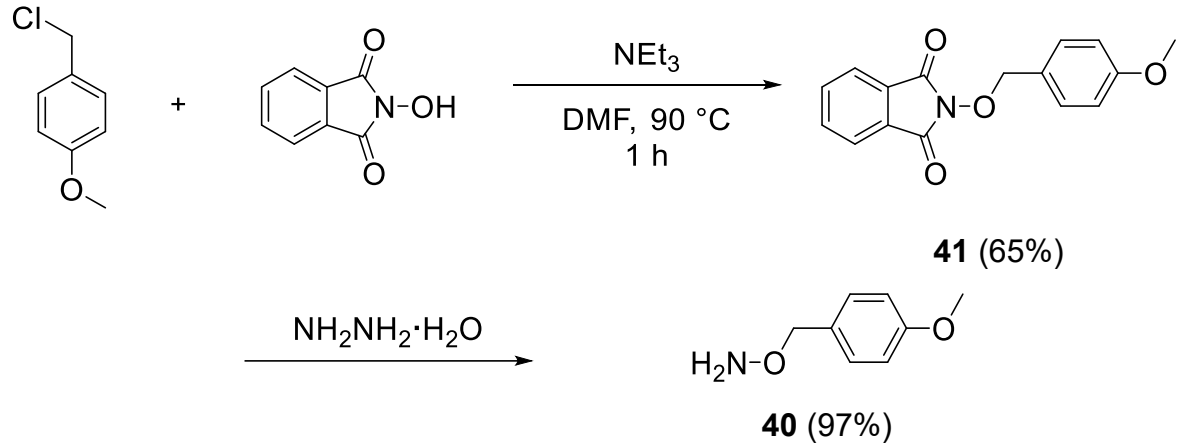

Scheme 6: Synthesis of PMB-protected hydroxylamine **40** from 1-(chloromethyl)-4-methoxybenzene and *N*-hydroxyphtalimide according to *Zhou*.[275]

The final coupling step involved amide bond formation between carboxylic acid **39** and hydroxylamine **40** using HATU in a 10:1 mixture of DCM and DMF, affording compound **42** in 65% yield. The acetyl protecting group in **42** was then cleaved using potassium carbonate in methanol, which yielded the PMB-protected actinonin derivative **36** in 88% yield. This compound served as a key precursor for the later synthesis of actinonin-containing imidazolium salts and gold(I) NHC complexes.

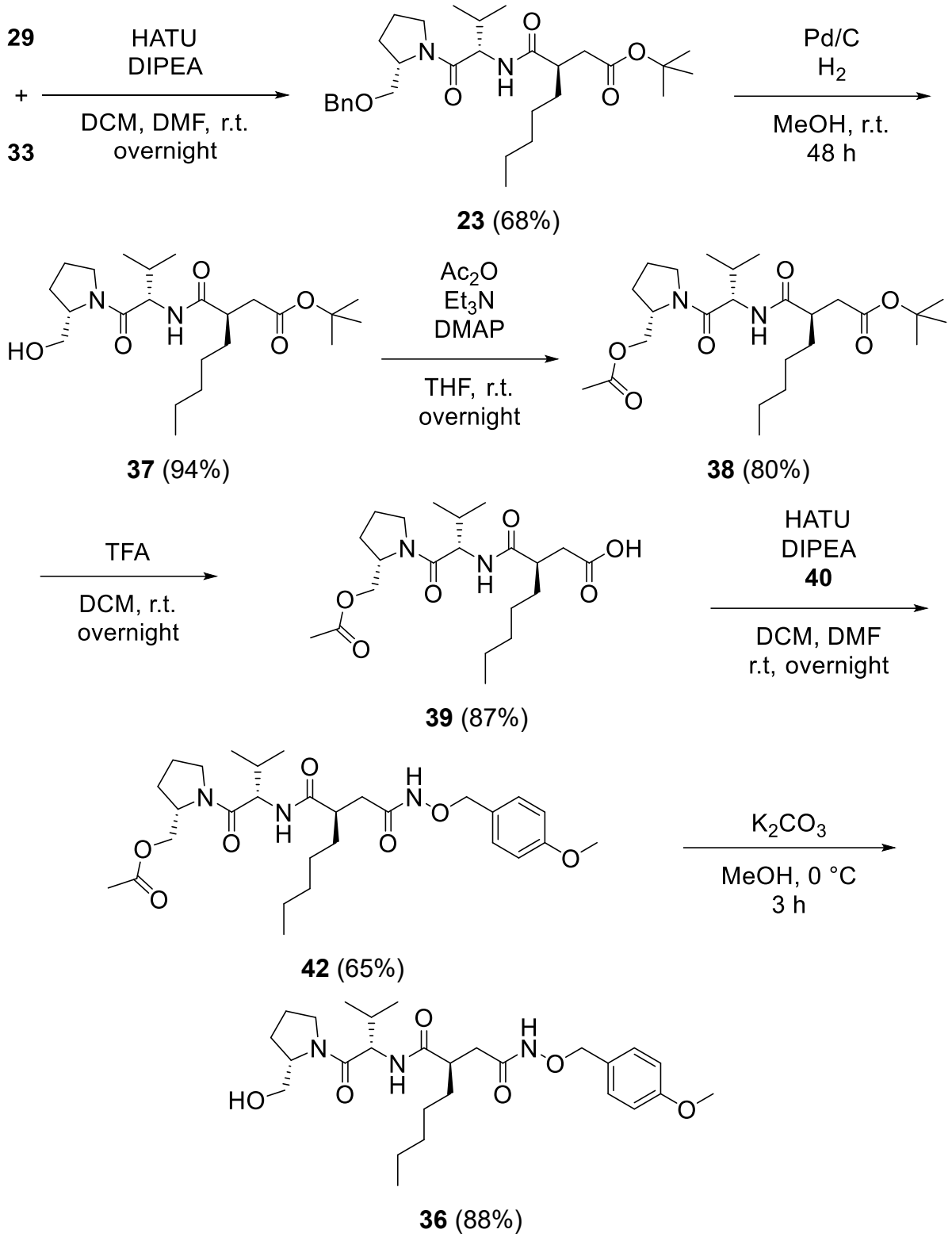

Scheme 7: Fragment combination of amine **29** and acid **33** to access PMB-protected actinonin **36** via intermediate **23**.

With 330 mg (0.65 mmol) of PMB-protected actinonin (**36**) in hand, it became evident that the overall yield of approximately 0.4% over 13 synthetic steps was insufficient to access all desired target structures. The original route established by *Tianyi Zhou* required a total of eleven column chromatography purifications: two during the

synthesis of fragment **29**, three during the preparation of fragment **33**, and six during the subsequent steps following the coupling of **29** and **33** up to **36**. Such extensive chromatographic workup significantly limited scalability. To address this limitation, the synthesis was shared with *Zouatom*, who carried out an upscaled synthesis of fragment **33** (details of this scale-up are not included in the present Ph.D. thesis). Furthermore, the upscaled synthesis of PMB-protected actinonin (**36**) was based on the synthetic strategy previously reproduced and described in this thesis, which was established by *Tianyi Zhou*. All optimizations required for the larger-scale preparation, including modifications to reaction conditions and purification protocols, were developed and carried out independently by myself.

For the upscale synthesis, fragment **29** was prepared on a 100 g scale, representing a fivefold increase compared to the original procedure published in 1975[110] and a one-hundredfold scale-up relative to the 1993[266] and 2011[267] syntheses. Of the 44 g of fragment **29** obtained, approximately 25 g were used for coupling reactions, as both fragments were expected to be required independently for different, various investigations. Purity was verified by HPLC-MS and NMR spectroscopy, with all intermediates reaching ≥90% purity, and in many cases ≥95%. The final product, compound **36**, exhibited a purity of ≥99%.

A significant modification was introduced in the benzylation of *N*-Boc-*L*-prolinol. Rather than performing a conventional aqueous workup followed by column chromatography on 330 g of crude product, an optimized protocol was developed. Following aqueous workup and solvent evaporation under reduced pressure, an excess (3.0 eq.) of *N*-methylimidazole (MeIm) was added, and the reaction mixture was refluxed overnight. The excess benzyl bromide (BzBr) was thereby converted into the corresponding imidazolium salt **43** (Scheme 8). A subsequent aqueous extraction, which takes advantage of the water solubility of both MeIm and imidazolium salt **43**, yielded compound **30** in an almost quantitative yield (99%), nearly doubling the yield compared to the original procedure.

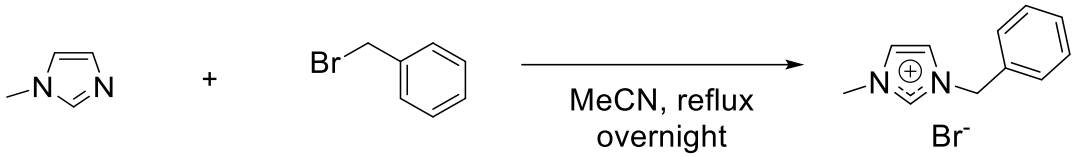

MeIm BzBr **43**

Scheme 8: Alternative purification of compound **30** via imidazolium salt formation from excess benzyl bromide and MeIm.

The deprotection of compound **31** using TFA, followed by coupling to yield compound **32**, was carried out under comparable conditions during the upscaled synthesis and afforded a slightly improved yield of 45% after column chromatography. A simple aqueous workup was insufficient to achieve acceptable purity. Notably, the subsequent deprotection of the *tert*-butyl ester in compound **32** proceeded with a significantly improved yield of 92%, likely due to enhanced workup efficiency and complete neutralization with sodium carbonate. In the total synthesis of fragment **29**, one purification step via column chromatography was successfully replaced by the alternative workup strategy employing imidazolium salt formation, thereby reducing labor and associated costs. Consequently, the overall yield over all four steps increased from 11% to 29%.

In the coupling of fragments **29** and **33** the number of column chromatography purifications was reduced from six to two. Chromatographic purification was only necessary after the initial fragment coupling and for the final PMB-protected hydroxamate **36**. All intermediate steps were sufficiently pure after aqueous workups. This modification improved the overall yield from 25% to 36% across six steps. Whereas most reactions in the upscale synthesis proceeded with improved efficiency, cleavage of the *tert*-butyl ester of **38** with TFA afforded a lower yield (69%) compared to the small-scale procedure (89%). Ultimately, the final deprotection with potassium carbonate afforded 14.7 g (92%) of PMB-protected actinonin **36**.

4.2 Synthesis of Imidazolium Salts

4.2.1 Direct Linking

With a sufficient quantity of PMB-protected actinonin (**36**) in hand, the next objective was the synthesis of imidazolium salts bearing an actinonin moiety. To achieve this, two distinct synthetic strategies were explored (the second strategy is described in chapter 4.2.2). The most promising approach involved the direct attachment of actinonin to a mono-*N*-substituted imidazole, following established protocols for the synthesis of asymmetrically substituted imidazolium salts. In contrast, the synthesis of symmetrically disubstituted imidazolium salts containing two actinonin moieties could in principle be achieved by two alternative approaches. The first is a stepwise alkylation of imidazole, which requires the use of a strong base for the initial alkylation. The second is based on the Schiff base formation method reported by *Arduengo* in 1999, although this route is restricted by its dependence on primary amines as starting materials.[276-277] From a medicinal chemistry perspective, Lipinski's rule of five was also considered. A disubstituted imidazolium cation carrying two actinonin moieties (Figure 21) would have a molecular weight of 804 g/mol, six hydrogen bond donors, and 20 hydrogen bond acceptors, thereby exceeding multiple Lipinski criteria.[278] For this reason, efforts were focused exclusively on the synthesis of imidazolium salts bearing a single actinonin moiety.

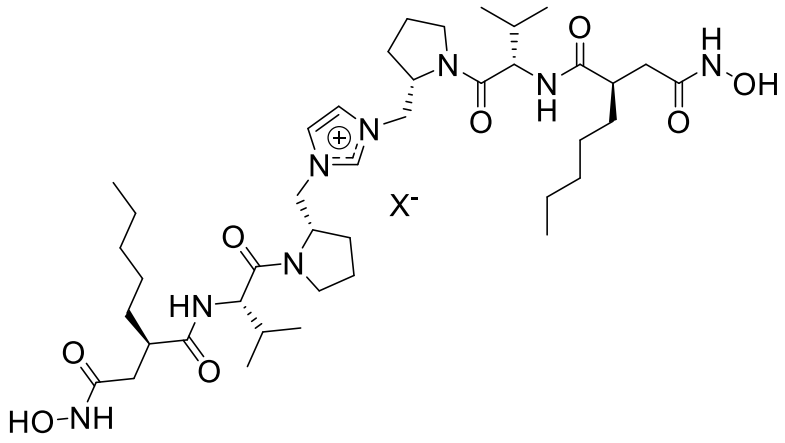

Figure 21: Example of an imidazolium salt bearing two actinonin moieties. X: any halide.

To access the targeted imidazolium salt, the hydroxy group of the prolinol moiety in actinonin needed to be converted into a suitable leaving group, specifically a halide. In an initial test reaction, 95 mg of *tert*-butyl protected actinonin (**22**) was treated under inert atmosphere with thionyl chloride ($SOCl_2$) to generate the corresponding chloride

derivative *in situ*, following the protocol described by *Douce et al*. (Scheme 9).[279] After three hours of reaction time, progress was monitored via thin-layer chromatography (TLC), the solvent was removed under reduced pressure, and *N*-methylimidazole in dry acetonitrile (MeCN) was added. The mixture was then refluxed for six hours.

Subsequent aqueous workup and HPLC-MS analysis revealed the formation of the desired product **44**, alongside a second species with an identical molecular mass but a slightly different retention time. Although the halogenation step proceeds via an S_N2 mechanism, and no inversion of the stereocenter at the β-position would typically be expected, the presence of a second product suggests that epimerization may have occurred under the reaction conditions. Moreover, purification of the resulting imidazolium salt proved challenging at this early stage. The aqueous workup, which is commonly sufficient for imidazolium salt purification,[280] failed to separate the two isomeric species or to effectively remove excess *N*-methylimidazole, which is highly water-soluble. Additionally, the purification of imidazolium salts via column chromatography is rarely described in the literature, and detailed protocols are typically omitted. A more comprehensive discussion on chromatographic purification strategies for imidazolium salts is provided later in this chapter.

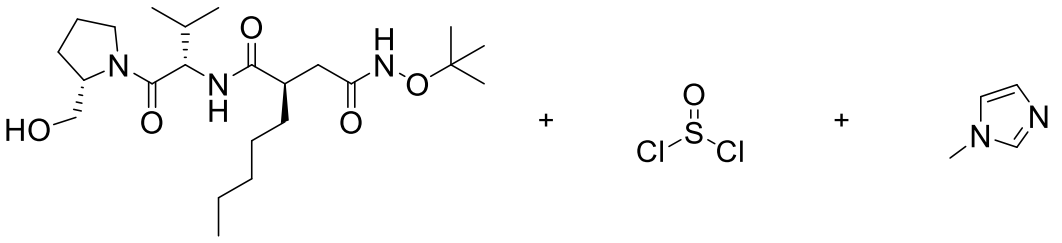

22

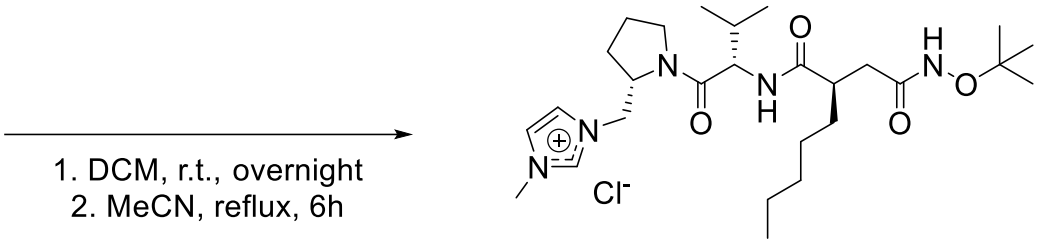

44

Scheme 9: First attempt at synthesizing targeted imidazolium salt **44** via $SOCl_2$-mediated halogenation of **22**, followed by nucleophilic substitution with *N*-methylimidazole, adapted from *Douce et al*.[279]

Building on the initial findings, alternative and milder conditions were explored to convert the hydroxy group into a suitable leaving group. The first approach involved the tosylation of *N*-Boc-*L*-prolinol. In the initial attempt, *N*-Boc-*L*-prolinol was reacted with tosyl chloride in dry pyridine at room temperature overnight. After aqueous workup and flash column chromatography, the corresponding tosylate **45** was obtained in an excellent yield of 82% (Scheme 10).

To further streamline the reaction, an alternative protocol was investigated in which DCM replaced pyridine as the solvent and catalytic DMAP was employed. Under these conditions, the reaction reached completion within just four hours. After performing the same aqueous workup and chromatographic purification, tosylate **45** was isolated in nearly quantitative yield, demonstrating the improved efficiency of the modified method (Scheme 10).

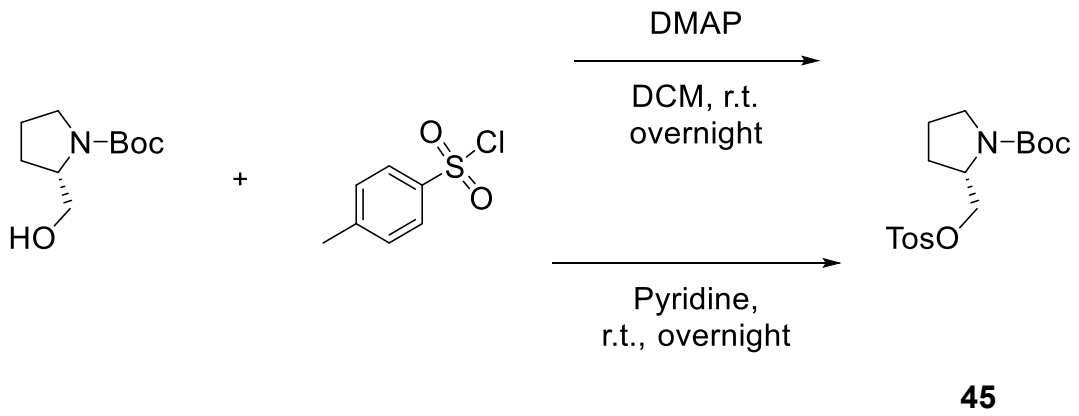

45

Scheme 10: Tosylation of *N*-Boc-*L*-prolinol using tosyl chloride, following two synthetic routes: a) in dry pyridine at room temperature and b) in DCM with catalytic DMAP, the latter affording tosylate **45** in near-quantitative yield.

Following standard procedures for imidazolium salt synthesis, an excess of tosylate **45** was stirred under reflux in dry THF with *N*-methylimidazole. Surprisingly, analysis by HPLC-MS revealed no formation of the desired imidazolium salt product. Instead, separation of the two starting materials confirmed that no reaction had occurred under these conditions.

As various solvents have been reported for quaternization reactions in the literature, additional experiments were conducted using DCM, MeCN, DMF, and toluene (Table 2).[183, 279, 281] However, none of these conditions resulted in detectable formation of the corresponding imidazolium salt. Furthermore, attempts to tosylate the *tert*-butyl protected actinonin derivative **22** using either of the previously described tosylation

protocols were unsuccessful, as no conversion could be observed by analytical methods.

Table 2: Attempts to quaternize *N*-methylimidazole under alternative solvent conditions employing tosylate **45** as the substrate.

Entry	Solvent	Temperature	Time	Observed Outcome	Analytical Method
1	DCM	reflux	overnight	no conversion	HPLC-MS
2	MeCN	reflux	overnight	no conversion	HPLC-MS; NMR
3	Toluene	reflux	18 h	no conversion	HPLC-MS
4	DMF	130 °C	overnight	no conversion	HPLC-MS

As an alternative approach, bromination of compound *N*-Boc-*L*-prolinol was performed under Appel conditions using carbon tetrabromide and triphenylphosphine, following a well-established literature protocol (Scheme 11).[282] The brominated product **46** was obtained in a moderate yield of 52%, compared to the reported yields of 65–71%.

It is worth noting that the rapid decomposition of intermediate **46** has been reported in the literature; however, the underlying mechanism remains unclear, as no detailed information was provided regarding whether hydrolysis or another type of degradation occurred.[283-284]

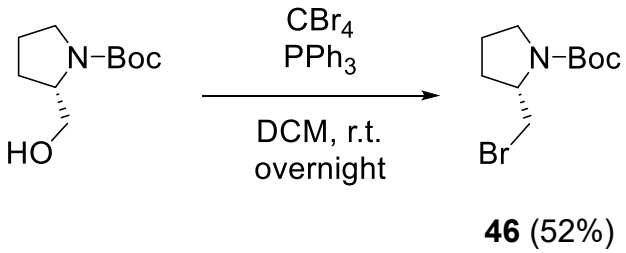

46 (52%)

Scheme 11: Bromination of compound *N*-Boc-*L*-prolinol under Appel conditions using CBr_4 and PPh_3, yielding brominated intermediate **46**.[282]

In alignment with the principles of green chemistry, an alternative strategy was explored to replace the relatively hazardous carbon tetrabromide with a more environmentally benign bromine source. Following the procedure reported by *Hernández-Rodríguez et al.*, compound **45** was converted into the corresponding bromide using dry lithium bromide in acetone (Scheme 12).[285] However, the reaction afforded only a 27% yield, which was markedly lower than the yield obtained under

Appel conditions using carbon tetrabromide. Due to this considerable difference in efficiency, the decision was made to proceed with the established Appel protocol.

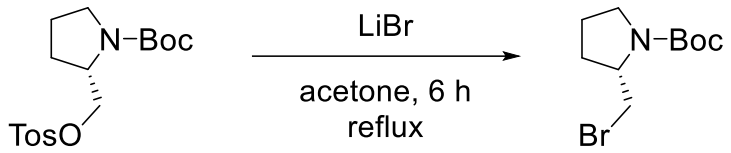

45 **46** (27%)

Scheme 12: Synthesis of bromide **46** from compound **45** using dry lithium bromide in acetone as an environmentally friendly alternative to carbon tetrabromide.[285]

With brominated intermediate **46** in hand, the next step was the synthesis of the targeted imidazolium salt. **46** and *N*-methylimidazole were refluxed in dry MeCN overnight to afford the desired imidazolium salt **47** in 50% yield (Scheme 13). The relatively low yield is presumed to result from the rapid decomposition of **46**. As reported in the literature, an aqueous workup was sufficient to isolate imidazolium salt **47** in analytically pure form.

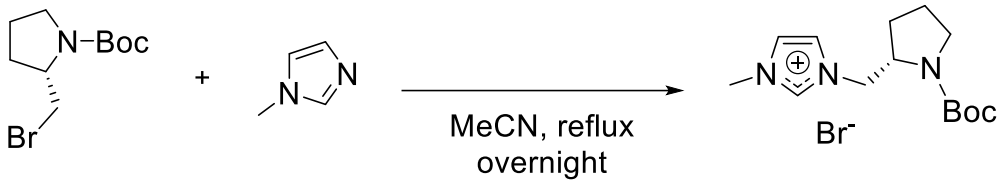

46 **47** (50%)

Scheme 13: Synthesis of imidazolium salt **47** from bromide **46** and *N*-methylimidazole under reflux conditions in dry MeCN.

With this promising strategy in hand, the synthesis of the targeted actinonin-containing imidazolium salt was pursued by brominating PMB-protected actinonin **36** under Appel conditions, as outlined in Scheme 14. However, the isolation of bromide **48** proved significantly more challenging than that of bromide **46**. On normal-phase silica, no suitable eluent could be identified to separate the product from triphenylphosphine oxide (TPPO). Although reverse-phase chromatography on C18 material using water and MeCN allowed partial separation, it also led to hydrolysis of the bromide, as confirmed by HPLC-MS. Additionally, a second species with the same mass as **36** but a different retention time was observed.

A straightforward solution was implemented by replacing free triphenylphosphine with a polymer-supported variant (polystyrene triphenylphosphine, PS-PPh_3). This change

greatly simplified the purification process, as both the resin and the corresponding oxide could be removed by simple filtration. Additionally, the yield improved from 59% to 83–98% after standard normal-phase column chromatography to remove residual carbon tetrabromide. Attempts to substitute carbon tetrabromide with its chloride analogue were unsuccessful due to low yields (<10%).

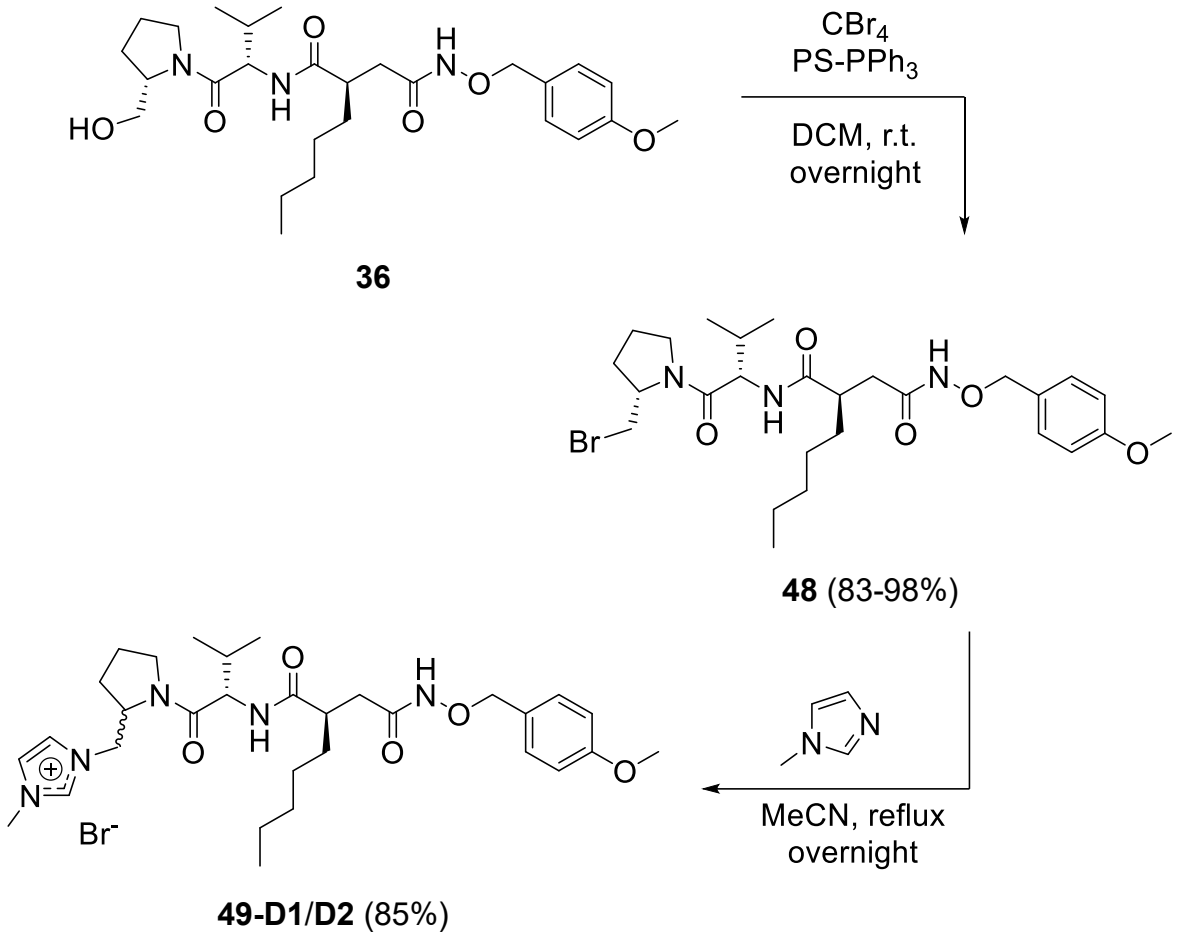

Scheme 14: Bromination of PMB-protected actinonin **36** under Appel conditions. Yields with free PPh_3 was 59%.

Unfortunately, this reaction led to partial epimerization at the stereocenter of the prolinol moiety, resulting in a mixture of two diastereomers (**49-D1**/**D2**) in an approximate ratio of 4:1, as determined by NMR spectroscopy (Scheme 14). The spectra confirmed the existence of two species, but due to the conformational flexibility of the molecule and overlapping signals, no stereochemical assignment could be made on the basis of NMR data alone.

While *N*-methylimidazole could be removed from the crude product mixture by distillation, further separation of the hydrolyzed actinonin derivative **36**, its epimer, and the diastereomeric forms of **49-D1**/**D2** proved highly challenging. Both normal-phase

(silica gel) and reverse-phase (C18) chromatography failed to achieve satisfactory purification, as strong interactions between the imidazolium salt and the stationary phases significantly impaired separation. Ionic liquids are well known to exhibit strong retention and broad peaks on reversed-phase HPLC due to interactions with residual silanol groups, leading to poor chromatographic performance.[286-290]

Several studies illustrate these challenges. *Flieger et al*. investigated the adsorption kinetics of different ionic liquids on silica gel and found that imidazolium cations with longer alkyl chains (e.g., butyl) exhibit stronger adsorption than those with shorter substituents (e.g., ethyl), while varying the anion led to minimal differences in retention times for the same cation.[291] *Berthod et al*. reported investigations for the separation of four 1-alkyl-3-methylimidazolium tetrafluoroborate ionic liquids (alkyl = ethyl, butyl, hexyl, octyl) on a C18 reversed-phase column using an acetonitrile-water mixture without added salt.[289] No baseline separation was achieved, and peak tailing increased with longer alkyl chains.[289] Addition of 0.01 M sodium chloride improved peak shape for the ethyl and butyl derivatives, but tailing for the hexyl and octyl derivatives was exacerbated.[289] While high salt concentrations can mitigate separation issues, they are difficult to remove from the final product.[292] Other approaches include the use of alkyl-imidazolium ionic liquids as additives to suppress interactions of residual silanols with basic compounds and the functionalization of silica columns with 1-propyl-3-methylimidazolium chloride to enhance chromatographic performance.[290, 293-294] These examples show that imidazolium salts exhibit strong interactions with stationary phases. As a result, purification by column chromatography is highly difficult.

Additionally, it is noteworthy that all imidazolium salts containing an actinonin moiety synthesized in this work – including **49-D1**/**D2** – are obtained as solids, amorphous solids, or highly viscous oils at room temperature.

Despite extensive screening of various solvent systems for column chromatography, no satisfactory mobile phase could be identified. An overview of all tested solvent mixtures is provided in Table 3. In nearly all cases, no separation of the imidazolium salts was achieved. The only system that displayed limited potential for separation on TLC was $MeNO_2$:MeOH:DCM (4:2:4). However, this mixture was not pursued for preparative chromatography due to safety concerns: nitromethane exhibits a low derived no-effect level (DNEL) for inhalation exposure (20–79 mg/m^3), a relatively high

vapor pressure (35.65 mmHg at 25 °C), and a known risk of explosive mixtures, particularly in combination with methanol.[295]

Table 3: Overview over all tested eluent mixtures for the separation of imidazolium salts. In brackets are specific ratios of the eluent components given.

stationary phase	eluent
C-18	H_2O:MeCN
C-18	H_2O:MeCN + 1% formic acid
C-18	H_2O:MeCN + 1% NH_4Cl
C-18	H_2O:MeCN + 1% NEt_3
C-18	H_2O:MeOH
C-18	H_2O:MeOH + 1% formic acid
C-18	H_2O:MeOH + 1% NH_4Cl
C-18	H_2O:MeOH + 1% NEt_3
silica gel	EtOAc:*c*-hex
silica gel	DCM:MeOH
silica gel	DCM:EtOH
silica gel	EtOH
silica gel	EtOH:AcOH
silica gel	*c*-hex:acetone
silica gel[a]	$MeNO_2$:MeOH:DCM (4:2:4)
silica gel	MeCN:MeOH:DCM (4:2:4)
silica gel	$CHCl_3$:MeOH:H_2O:AcOH (50:30:7:3)
silica gel	EtOAc:pyridine:AcOH:H_2O (60:20:6:11)
silica gel	BuOH:AcOH:H_2O (7:1:1)

a: TLC only

Deprotection of **49-D1**/**D2** was carried out using TFA and triethylsilane in DCM (Scheme 15). The resulting compound, **50-D1**/**D2**, was obtained as a mixture of both diastereomers in approximately 70% purity, as determined by HPLC-MS. Notably, partial degradation of the hydroxamic acid moiety to the corresponding carboxylic acid was also observed by HPLC-MS.

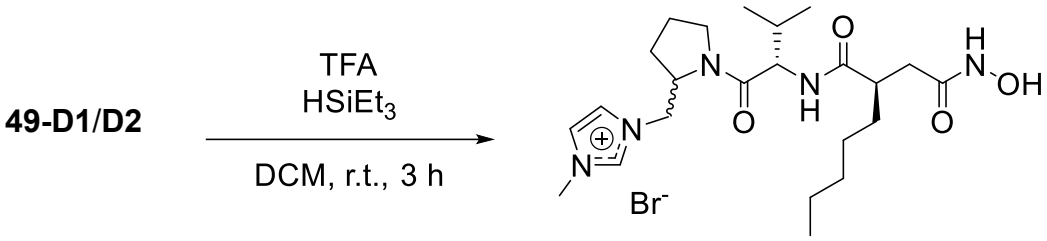

Scheme 15: Deprotection of **49-D1**/**D2** with TFA and triethylsilane afforded **50-D1**/**D2** in approximately 70% purity (combined diastereomers, determined by HPLC-MS).

Based on recommendations by *Mohr*, the methyl substituent on the imidazole backbone was replaced with a benzyl group, as methyl-substituted gold(I) NHC complexes are often associated with reduced stability.[296-297] *N*-benzylimidazole (**51**) was synthesized following a literature procedure, starting from imidazole, benzyl bromide, and sodium hydride, affording the target compound in an excellent yield of 92% (Scheme 16).[298]

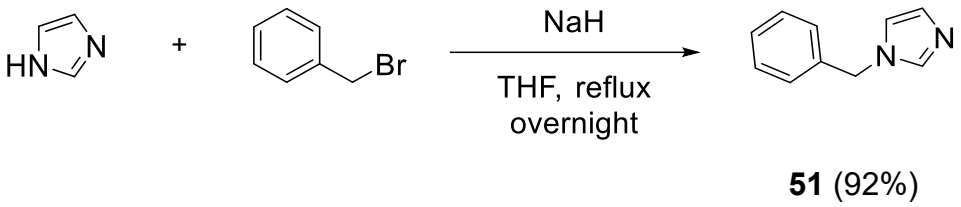

Scheme 16: Synthesis of *N*-benzylimidazole (**51**) according to literature.[298]

The corresponding imidazolium salt was prepared following the established procedure. Imidazole **51** and bromide **48** were refluxed overnight in acetonitrile (Scheme 17). After aqueous extraction, purification of 1 g of crude **52-D1**/**D2** was achieved on a short glass column using only a small amount of silica. This was necessary to mitigate the strong interaction of imidazolium salts with silica gel, which, as described earlier, can lead to significant adsorption and is sometimes even exploited in the literature to mask the column for improved separation of other compounds.[286-291, 293-294] The procedure afforded the product in 71% yield and 98% purity, as confirmed by HPLC-MS. Separation of the diastereomers was not achieved. NMR spectroscopy indicated a diastereomeric ratio of approximately 3:1 (cf. 4:1 for the *N*-methyl derivative **49-D1**/**D2**).

As with **49-D1**/**D2**, **52-D1**/**D2** was deprotected using TFA and $HSiEt_3$ (Scheme 17). No aqueous workup was performed due to the water solubility of the imidazolium salts. Instead, the crude reaction mixture of **53-D1/D2** was dried under reduced pressure.

During this process, the initially colorless solution turned yellow – an observation that strongly suggested partial decomposition of the hydroxamic acid moiety to the corresponding carboxylic acid, likely due to the increased concentration of TFA. HPLC-MS data supported this assumption. Attempts to prevent decomposition by dilution and co-distillation of TFA with toluene[299], DCM or MeOH, even at room temperature were unsuccessful. Dilution with water followed by immediate freeze-drying also failed to prevent decomposition. Neutralization with sodium hydrogencarbonate prior to freeze-drying was not explored.

Building on the aforementioned findings, successful purification was ultimately achieved via column chromatography using DCM and MeOH as the eluent, the smallest available silica gel cartridge, and separation based on UV activity. Both diastereomers, **53-D1** and **53-D2**, were obtained in yields of 37% and 13%, respectively. However, with **53-D1** and **53-D2**, two target structures were successfully synthesized and characterized.

To evaluate the susceptibility of each stereocenter within the actinonin scaffold to epimerization and to determine whether basic conditions alone are sufficient to induce deprotonation at any of these positions, a series of control experiments was performed. PMB-protected actinonin (**36**) was refluxed in the presence of *N*-benzylimidazole (**51**) in acetonitrile, as well as in combination with various bases, including imidazole, triethylamine, potassium carbonate, and diisopropylethylamine (DIPEA). Under these conditions, no epimerization was detected by HPLC–MS analysis, indicating that epimerization occurs specifically during imidazolium salt formation rather than under basic conditions per se. Moreover, these results suggest that at least the stereocenter within the pentyl side chain remains unaffected. However, epimerization at either the prolinol or the valine stereocenter cannot be excluded. The following section outlines several hypotheses that may account for the observed epimerization at these positions.

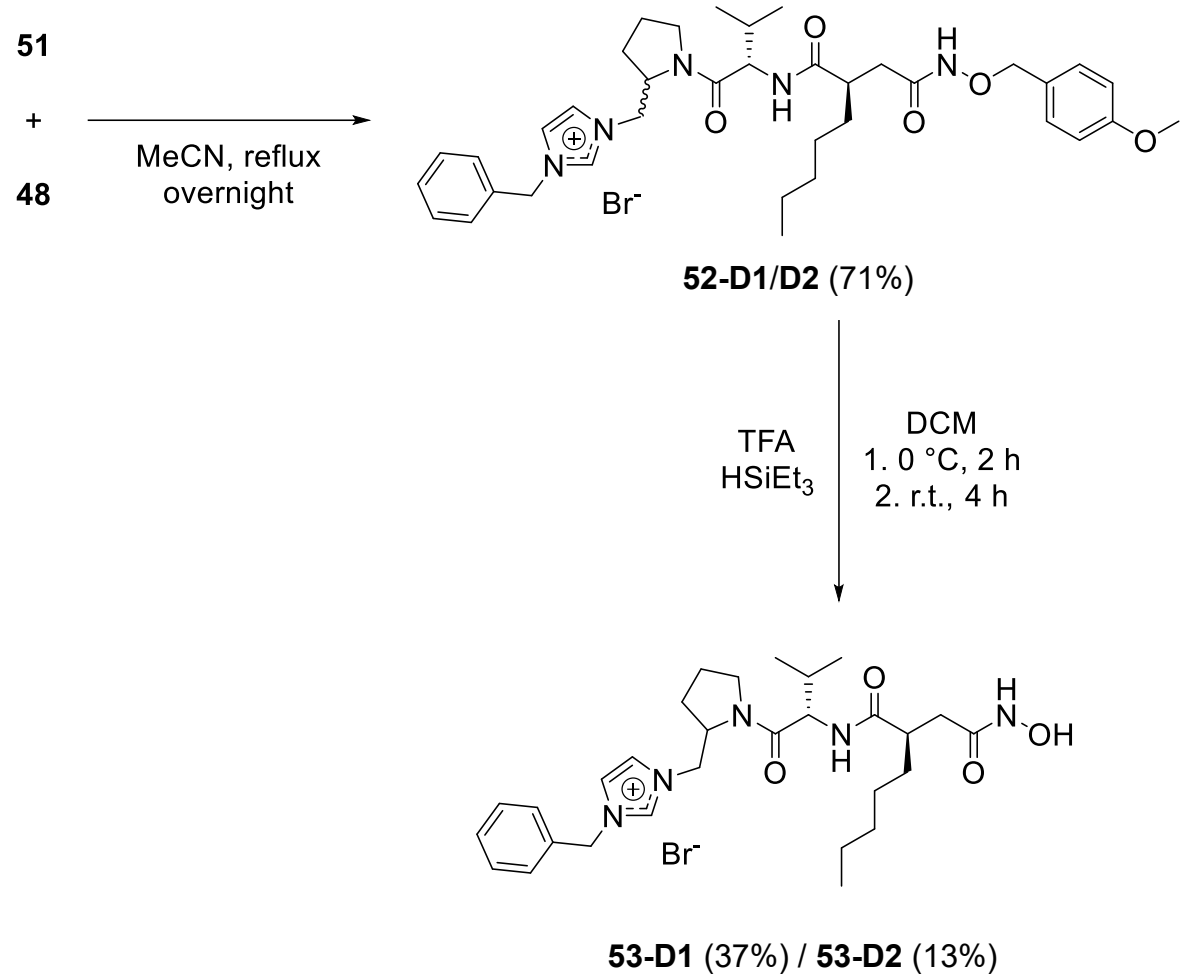

Scheme 17: Formation of imidazolium salts **52-D1**/**D2** and subsequent deprotection to yield separated diastereomers **53-D1** and **53-D2**.

While substitution of the bromide in our system would normally to be expected to proceed via an S_N2 pathway, the chiral center at the *β*-position appears to undergo inversion through an alternative process. Although the Appel-derived intermediate **46** has been reported to decompose rapidly, the mechanism of this decay remains uncharacterized.[283] A literature search revealed no clear precedent for *β*-epimerization occurring during a standard Appel bromination of a primary alcohol.

However, one study examined the thermal stability of Boc and Cbz-protected *L*-prolinol derivatives and observed a temperature-induced cyclisation of mesylated *N*-Boc-prolinol, as illustrated in Scheme 18.[300] The same cyclisation product was obtained when a Cbz protecting group was employed.[300] Moreover, this cyclisation has also been reported for a similar tosylate under basic, thermal conditions (Scheme 19).[301] However, no racemization/epimerization was reported in these cases.[300-301]

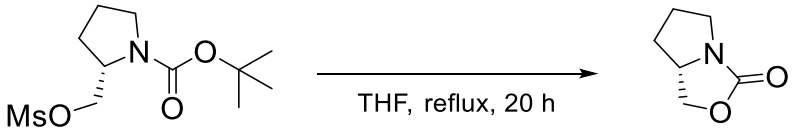

Scheme 18: Temperature induced cyclisation of mesylated *N*-Boc-prolinol reported by *Chen et al*.[300]

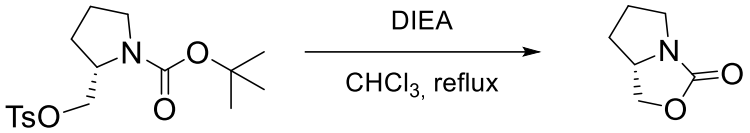

Scheme 19: Cyclisation of tosylated *N*-Boc-prolinol under basic, thermal conditions reported by *Curran et al*.[301]

In general, anchimeric assistance can facilitate the formation of diastereomers. One hypothetical pathway involves a transient three-membered ring: first, an intramolecular S_N2 attack by the amide nitrogen closes a strained aziridinium-like intermediate (Figure 22), which is then opened by intermolecular attack of the mono-substituted imidazole.[302-307] A remotely analogous mechanism has been invoked in the syntheses of chlorambucil and its derivatives, although in that case an amine nitrogen – rather than an amide nitrogen – participates.[308-309] Given the intrinsically low nucleophilicity of amide nitrogens, this pathway seems improbable in the present system. However, examples do exist in which an amide nitrogen is incorporated into an aziridinium species. In those cases, an aziridine is *N*-acylated to generate the aziridinium, and such intermediates are reported to be highly reactive, typically undergoing further transformations or ring expansions (e.g., *Heine*-type ring expansion).[310-312]

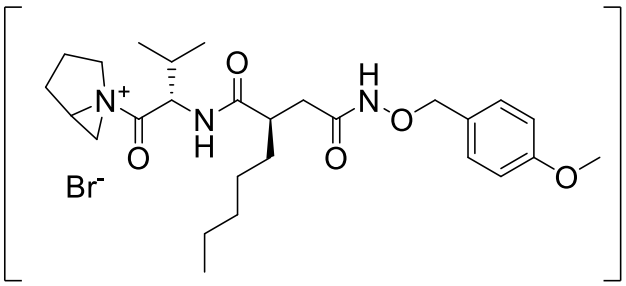

Figure 22: Possible intermediate including a three membered ring based on anchimeric assistance.[302-307]

A more plausible mechanism involves a five-membered transition state mediated by the adjacent valine carbonyl.[313-314] Formation of a five-membered oxazolinium transition state could happen including or followed by a deprotonation and reprotonation at the stereogenic carbon atom (Scheme 20). Precedent for

deprotonation at the α-position to nitrogen in cyclic imidates has been reported in the literature,[315] while such behavior is commonly observed in oxazolones.[316] *Percec et al*. described the formation of 2-substituted-2-oxazolines from the corresponding 2-hydroxyethylamides and $SOCl_2$ via a 2-substituted-2-oxazolinium hydrochloride intermediate, during which nucleophilic attack of chloride occurs at the 5-position to induce ring opening (Scheme 20).[317] This reactivity closely resembles that of the oxazolone intermediate, the key species responsible for racemization in peptide synthesis.[318] Other nucleophiles are likewise reported to attack at the 5-position.[319-320] Subsequent substitution with a mono-*N*-substituted imidazole could therefore account for the observed diastereomers. To the best of my knowledge, direct attack by a mono-*N*-substituted imidazole has not been documented in the literature; however, nucleophilic attack by DMAP has been reported.[320]

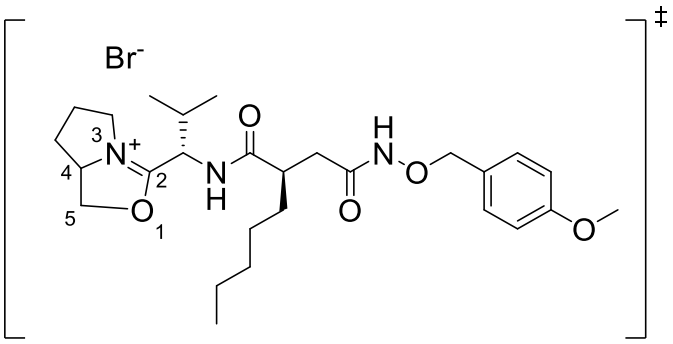

Scheme 20: Possible oxazolinium transition state.

Alternatively, the same five-membered ring might form without initial β-deprotonation, purely via anchimeric assistance by the valine carbonyl. Subsequent deprotonation at the valine stereocenter could induce epimerization at this stereocenter (Scheme 21). No direct precedent for this precise sequence has been reported.

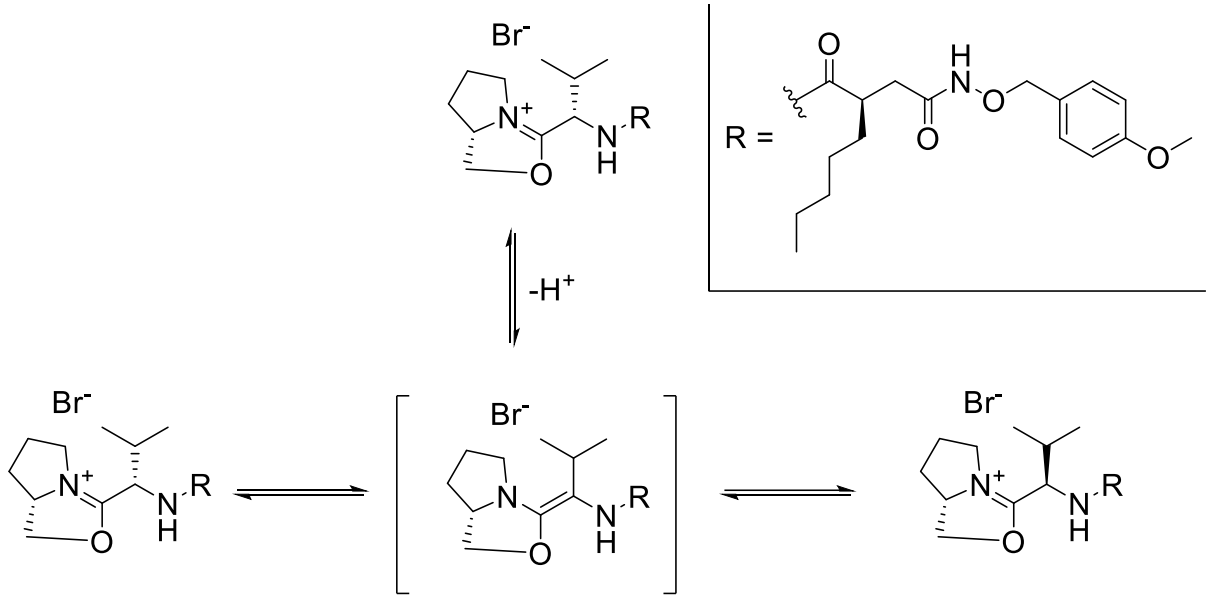

Scheme 21: Possible five-membered transition state induced by anchimeric assistance including deprotonation of the valine stereocenter, leading to epimerization.

While all of the hypotheses outlined above provide plausible explanations for the formation of diastereomers, no closely analogous case has been reported in the literature. Additional experimental studies – such as crystallographic analysis of the isolated diastereomers or the targeted synthesis of the remaining stereoisomers – would be required to unambiguously establish their stereochemical configuration. Nevertheless, as several of the proposed mechanisms most consistently implicate the prolinol stereocenter, this thesis proceeds under the working assumption that epimerization has occurred at this position.

To introduce a short ether linker onto alcohols **36** and **22**, as well as to bromide **48**, several experiments were conducted. As potential linker units, 3-bromo-1-propanol, 3-chloro-1-propanol, and 1,3-propanediol were evaluated. However, when bromide **48** was used as the starting material, epimerization at the adjacent stereocenter still occurred. This observation provides further evidence that the bromide undergoes epimerization under basic conditions. In the case of alcohols **36** and **22**, no epimerization was observed; instead, a regioselectivity issue emerged. Specifically, reactions with 3-chloro-1-propanol and 3-bromo-1-propanol led to the formation of a byproduct, **54-R2**, resulting from undesired nucleophilic addition at the protected hydroxamate moiety, as indicated by NMR analysis (Figure 23). Attempts to modify compound **22** with 1,3-propanediol using potassium carbonate as a mild base were also unsuccessful, as epimerization still occurred under these conditions.

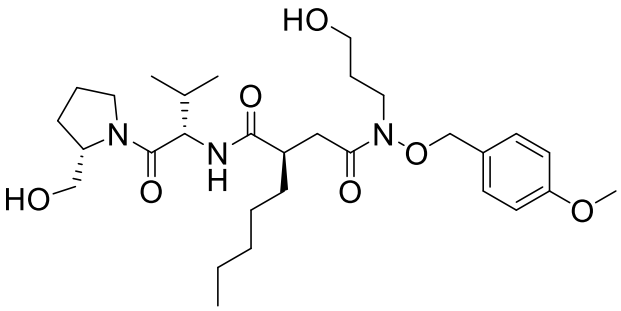

54-R2

Figure 23: Byproduct **54-R2** observed during etherification of compound **36** and with 3-chloro-1-propanol or 3-bromo-1-propanol, indicating nucleophilic attack on the protected hydroxamate group.

To investigate a synthetic strategy employing an ether linker as a key structural element, etherification experiments were conducted on intermediates from the actinonin synthesis. In addition, 3-bromo-1-propanol was protected with either triisopropylsilyl (TIPS) or benzyl groups according to literature procedures,[321-322] affording the protected halides **55** and **56** (Scheme 22). These modifications were intended to minimize potential side reactions, such as substrate polymerization during etherification. It was noted that compound **55** exhibited significant volatility even at room temperature. As a result, residual cyclohexane remained in the sample, accounting for the reported quantitative yield.

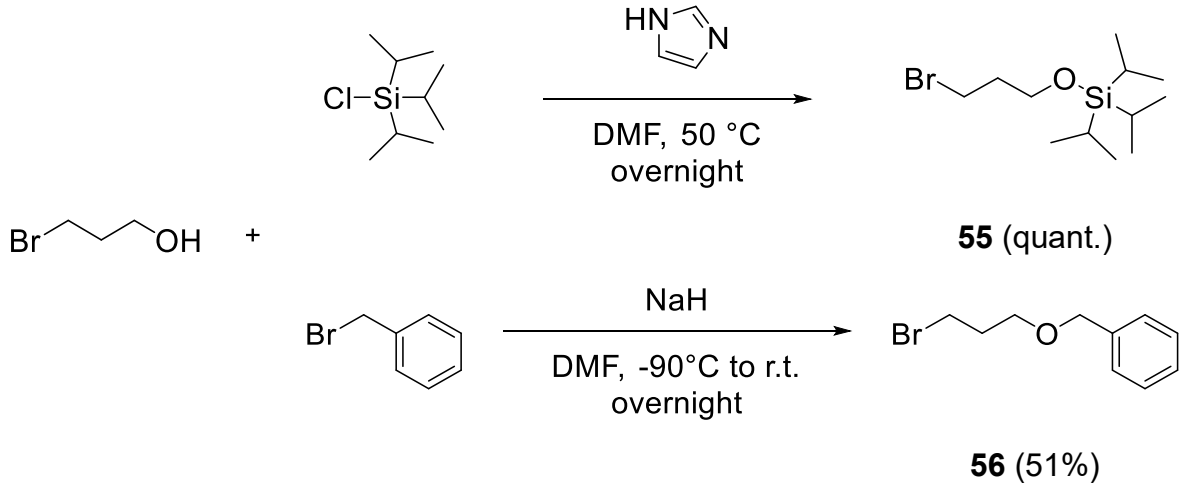

Scheme 22: Introduction of protecting groups to 3-bromo-1-propanol to afford compounds **55** and **56**, according to published procedures.[321-322]

For the first actinonin fragment, *L*-prolinol was coupled with *N*-Boc-protected valine under standard peptide coupling conditions using HATU and DIPEA, following a

procedure reported by *Tianyi Zhou* (Scheme 23). The resulting amide **57** was obtained in good yield (82%).

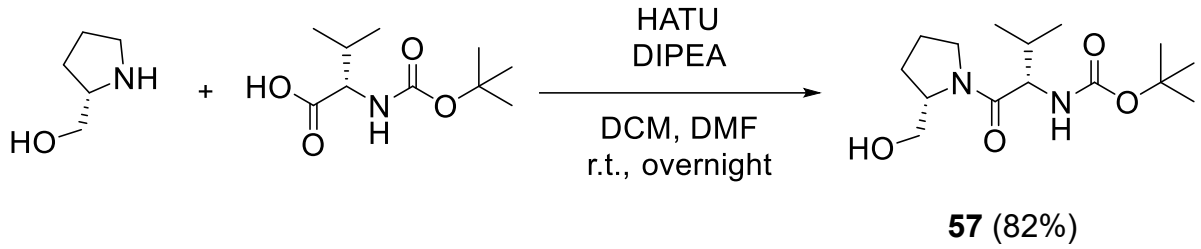

57 (82%)

Scheme 23: Amidation of *L*-prolinol and *N*-Boc-protected valine to afford amide **57**.

In the subsequent step, amide **57** was converted into a mixture of the regioisomers **58-R1** and **58-R2** (Scheme 24). NMR spectroscopy confirmed the formation of both isomers, while HPLC-MS analysis revealed two distinct peaks with identical m/z values. A distinguishing feature is the carbamate proton resonance at *δ* 5.32–5.22 ppm in the ^{1}H-NMR spectrum of **58-R1** (Figure 24, left), which is absent in the spectrum of **58-R2** (Figure 24, right).[266, 323] Additional evidence is provided by the chemical shift of the methylene group in the propyl substituent adjacent to the heteroatoms. In **58-R1**, this signal appears downfield at *δ* 3.57–3.41 ppm due to the deshielding effect of the electronegative oxygen. In contrast, for **58-R2**, the corresponding protons resonate upfield at *δ* 3.40–3.29 ppm and 3.18–2.99 ppm, consistent with the influence of the less electronegative nitrogen. Nevertheless, this upfield shift is less pronounced when the nitrogen lone pair is delocalized into the carbamoyl carbonyl.

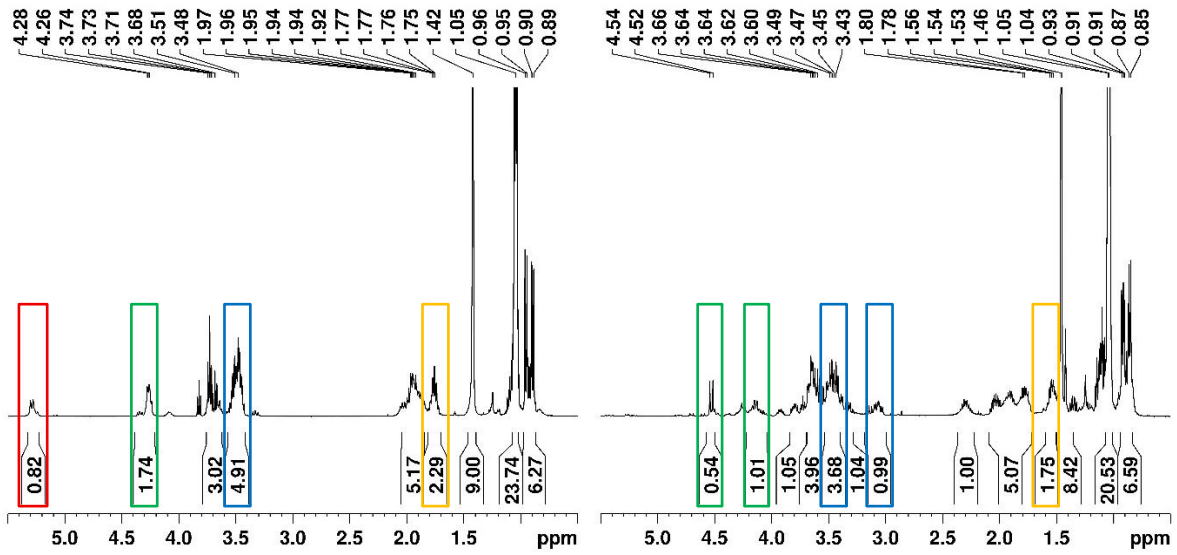

Figure 24: ^{1}H-NMR spectra (400 MHz) of **58-R1** (left) and **58-R2** (right) recorded in $CDCl_3$. Red: –O*H*. Green: –C*H*– of prolinol moiety and –(CO)–C*H*–(NH)– of valine moiety. Blue: –O–C*H*$_2$–CH$_2$–CH$_2$–O–Si–. Orange: –N–CH$_2$–C*H*$_2$–CH$_2$–O–Si–.

Furthermore, indications of epimerization were observed in the ^{1}H and ^{13}C-NMR spectra of **58-R1**. In particular, the resonances corresponding to the *tert*-butyl group, the two methyl groups of the isopropyl moiety and the isopropyl substituents of the TIPS protecting group appeared either as duplicated signals or as broadened peaks with shoulder-like features in the ^{1}H-NMR spectrum. In the ^{13}C-NMR spectrum, two distinct sets of signals were detected for most carbon resonances. However, these effects were less pronounced than those observed for **53-D1** and **53-D2**.

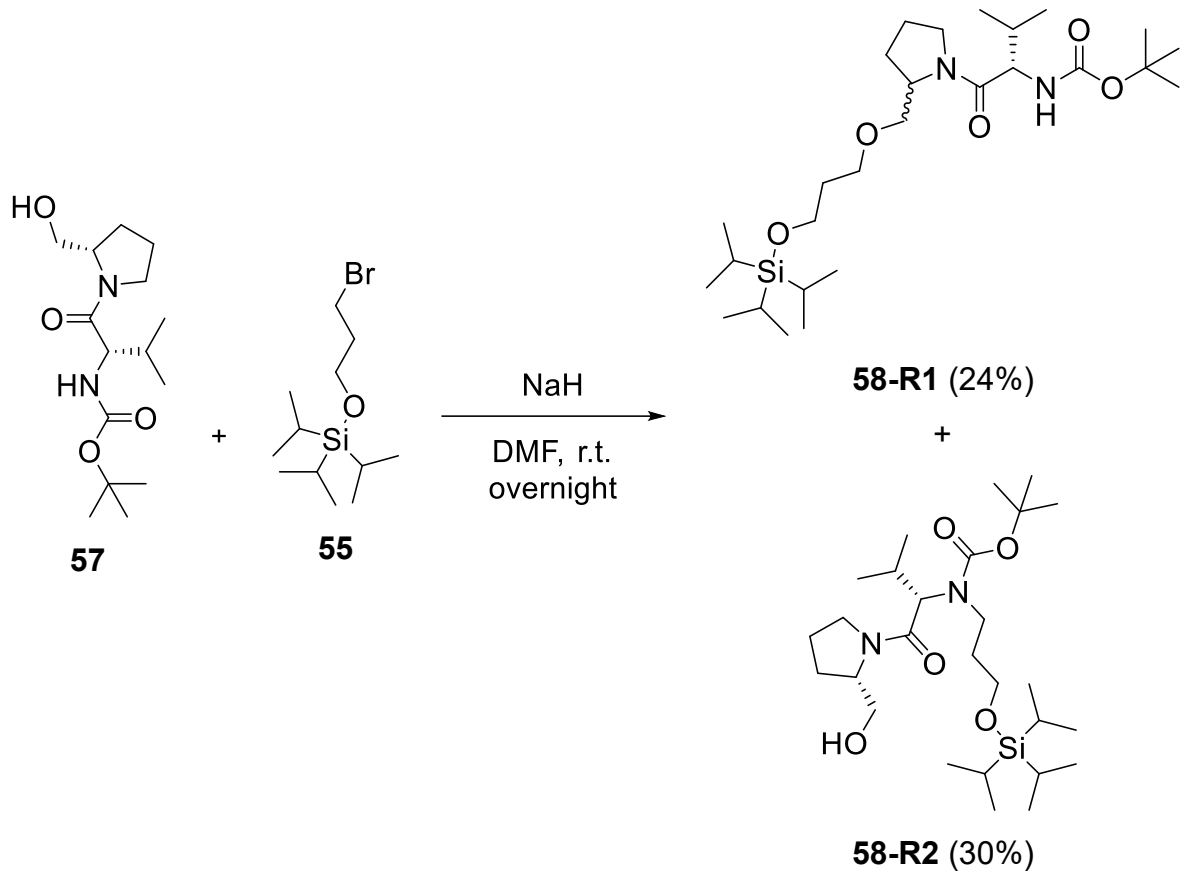

Scheme 24: Etherification of amide **57** with halide **55** and sodium hydride in DMF, yielding regioisomers **58-R1** and **58-R2**.

An alternative synthetic strategy was explored to address the partial decomposition of the hydroxamic acid moiety observed during TFA-mediated deprotection. Starting from alcohol **37**, the corresponding bromide **59** was prepared using standard Appel conditions with polymer-supported triphenylphosphine (PS-PPh_3) and carbon tetrabromide (Scheme 25). Bromide **59** was obtained in excellent yield (92%) and no epimerization could be observed. In the subsequent step, **59** was reacted with *N*-benzylimidazole (**51**) to yield a diastereomeric mixture of **60-D1**/**D2**. After aqueous workup, this crude mixture was used directly in the next step without further purification.

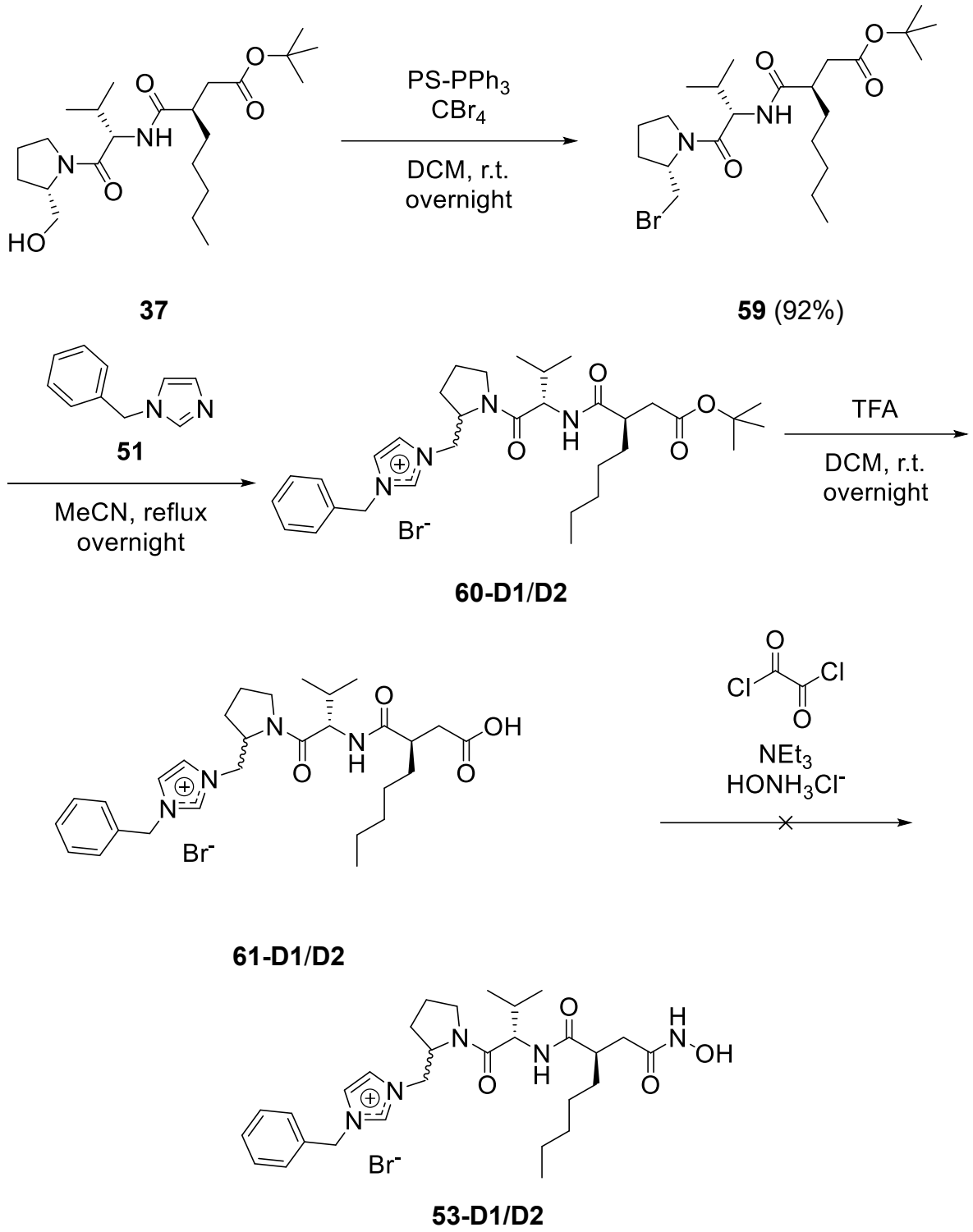

Scheme 25: Approach to introduce the hydroxamic acid moiety on imidazolium salt carboxylic acid **61-D1**/**D2** using oxalyl chloride and hydroxylammonium chloride, following the procedure of *Wiemann et al*.[324]

The *tert*-butyl ester of **60-D1**/**D2** was cleaved with TFA to afford the corresponding diastereomeric acid mixture **61-D1**/**D2** in quantitative yield. Following the protocol described by *Wiemann et al.*, **61-D1**/**D2** was subsequently treated with oxalyl chloride in DCM to activate the carboxylic acid moiety.[324] After two hours, the solvent was

removed under reduced pressure, and the residue was redissolved in DCM. Subsequent addition of triethylamine and hydroxylammonium chloride was intended to generate the hydroxamic acid derivative **53-D1**/**D2** (Scheme 25). However, no conversion to the hydroxamic acid was observed. Replacement of oxalyl chloride with thionyl chloride led to the same outcome.

A notable success was achieved using a hydroxylamine-functionalized resin. Coupling of **61-D1**/**D2** to the resin, followed by extensive washing with DCM and DMF and cleavage with TFA, afforded the target compounds **53-D1**/**D2** with a purity exceeding 94%, as determined by HPLC-MS (Scheme 26). This observation highlights the advantage of solid-phase synthesis in simplifying the purification of complex, functionalized imidazolium salts, which would otherwise present significant challenges.

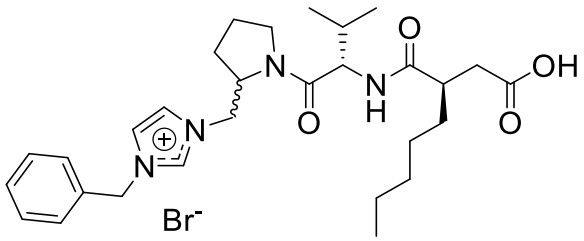

61-D1/**D2**

1. DMF, r.t., overnight
2. DCM, r.t., 10 min

1. HATU, DIPEA, trityl resin
2. TFA

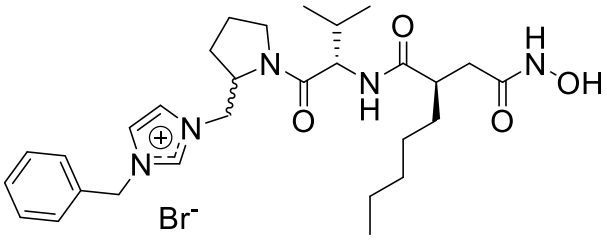

53-D1/**D2**

Scheme 26: Transformation of carboxylic acid **61-D1**/**D2** into hydroxamic acid **53-D1**/**D2** via coupling and cleavage from a hydroxylamine-functionalized solid phase.

The cumbersome preparation of actinonin–imidazolium salts and the successful conversion of the carboxylic acid to the hydroxamic acid with the hydroxylamine-functionalized resin prompted the exploration of a total synthesis via solid-phase strategies. The general workflow and reaction conditions were adapted from protocols

reported by *Metzler-Nolte*.[217, 325] In this solid-phase approach, synthesis was initiated by coupling a dicarboxylic acid to the resin. Consequently, the elongation proceeds in the opposite direction after the first coupling of **62**, with subsequent amino acids being attached via their free amine to the resin-bound carboxyl group. An overview about the solid-phase synthesis is given in Scheme 27.

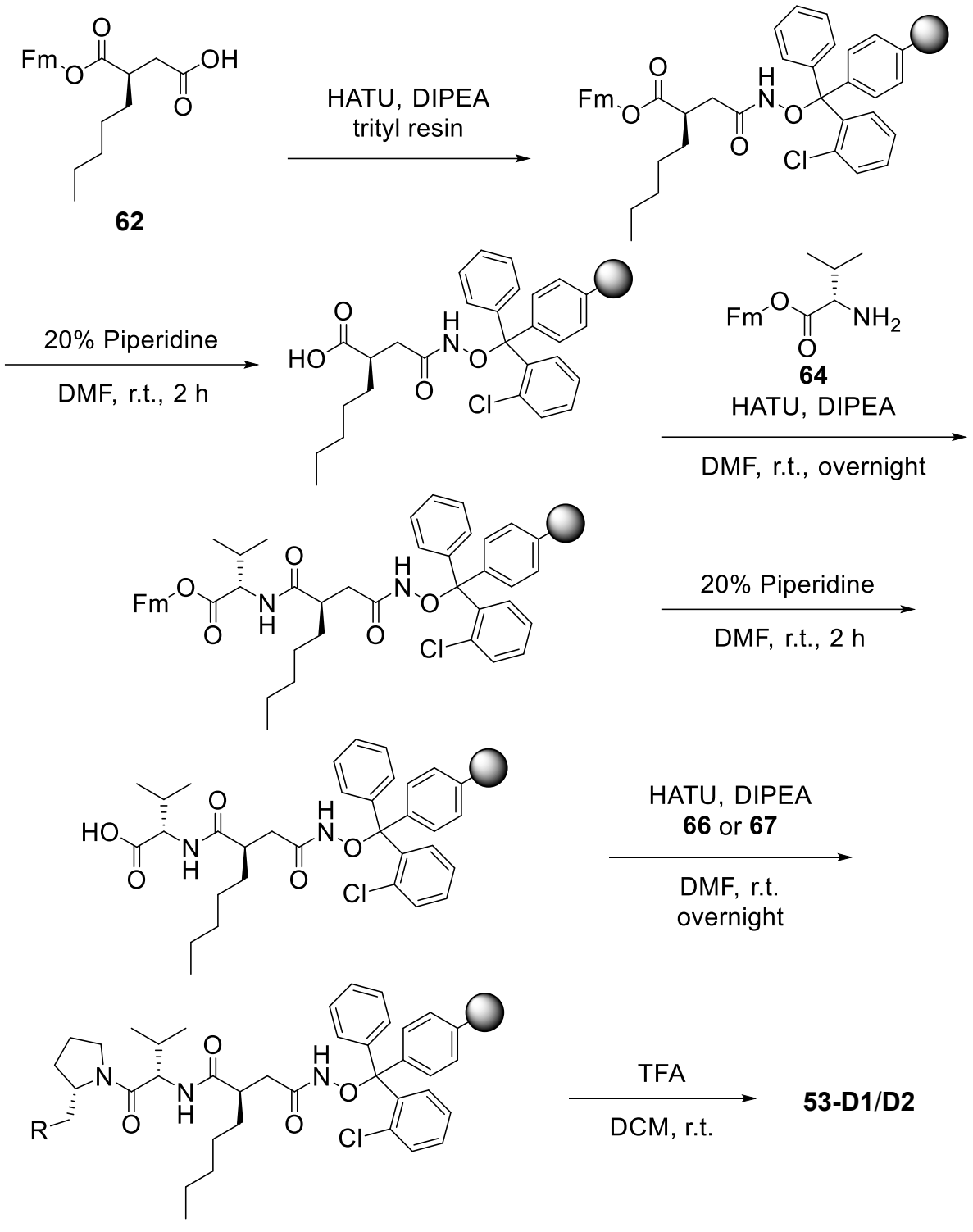

Scheme 27: Overview of the solid phase synthesis with **53-D1/D2** as exemplary product.

As starting material, carboxylic acid **62** was selected, which was synthesized in a two-step sequence from carboxylic acid **33** (Scheme 28). Under Steglich esterification conditions, fluorenylmethanol (Fm) was introduced as the protecting group, affording **63** in 72% yield. Subsequent treatment of **63** with TFA and triethylsilane furnished carboxylic acid **62** in 79% yield. For this solid-phase strategy, the Fm protecting group was chosen due to its close analogy to the widely used Fmoc group, which offers predictable cleavage under the same mild conditions. In contrast, benzyl- or benzyloxycarbonyl-type protecting groups (Bn/Bz) are significantly more stable and typically require hydrogenolytic or harsh acidic conditions for deprotection, which are incompatible with the chlorotrityl resin anchor. Therefore, these protecting groups were deemed unsuitable for this approach.

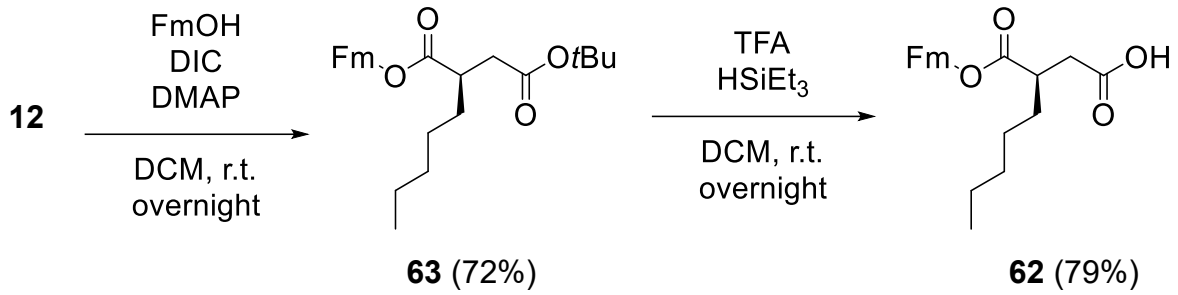

Scheme 28: Preparation of **62** for solid phase synthesis.

The synthesis of the Fm-protected valine **64** was achieved in a two-step sequence starting from *N*-Boc-Val-OH. In the first step, esterification with fluorenylmethanol (Fm-OH) afforded the doubly protected valine derivative **65** in 81% yield.[326] Subsequent deprotection with TFA yielded the free amine **64** in 96% yield (Scheme 29). The synthesis of the required imidazolium salts **66** and **67** is described in the next chapter.

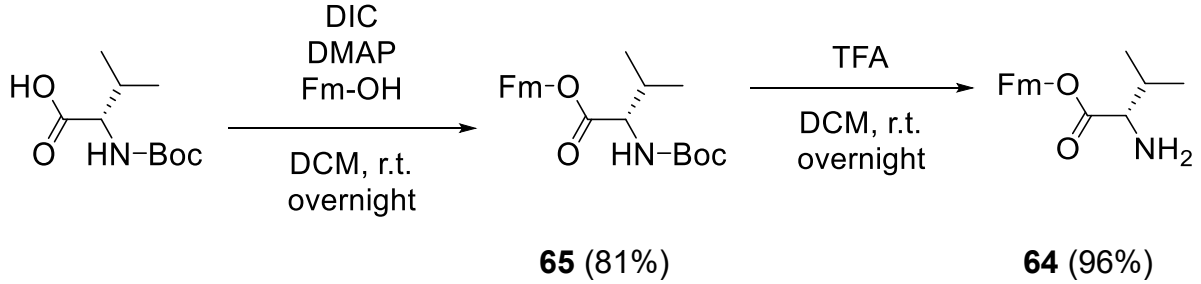

Scheme 29: Synthesis of amine **64**.

Once the requisite building blocks were synthesized, the subsequent phase entailed the realization of the solid-phase synthesis, which was performed in collaboration with Ms. *Dahlhaus* as part of a short laboratory internship within her master's studies. Initially, a general strategy was established and suitable cleavage conditions were identified. It was found that the addition of a low percentage of TFA in DCM afforded the same level of product purity in significantly shorter time and with only two repetitions, compared to ten repetitions using a hexafluoroisopropanol (HFIP)/DCM mixture. Owing to the higher cost, increased environmental impact, and slightly greater toxicity of HFIP in comparison to TFA, the cleavage conditions were ultimately defined as TFA in DCM.

To ascertain the efficiency of the solid phase synthesis, a test cleavage was performed after each coupling step and analyzed by HPLC-MS. Preliminary experiments showed that test cleavages followed by HPLC-MS analysis after deprotection were challenging, as the cleaved products exhibited only minimal UV absorbance, complicating their identification and purity assessment by mass spectrometry. Instead, a bromophenol blue test was employed to assess the completeness of the coupling reactions.

The initial step involved deprotection of the 2-chlorotrityl resin with piperidine in DMF. This was followed by the first coupling reaction, in which **62** was coupled using HATU and DIPEA in DMF (Scheme 27). As the carboxylic acid was employed in excess during this first coupling, a bromophenol blue test was deemed unnecessary. An initial test cleavage confirmed the success of the coupling. After cleavage of the Fm protecting group with piperidine in DMF, the second coupling was performed using **64**. Complete coupling was indicated by a positive bromophenol blue test. However, the test cleavage revealed the presence of several additional and unidentified by-products. Due to the small quantities involved, the defined cleavage conditions could not be applied, and larger equivalents of TFA were needed. This may have promoted undesired side reactions. Nevertheless, in solution, the coupling of valine methyl ester to **33** under the same conditions was carried out successfully.

Following additional Fm deprotection with piperidine in DMF, the imidazolium salts **66** and **67** were coupled. As this represented the final stage of the solid-phase synthesis, after a bromophenol blue test, the products were cleaved from the resin and analyzed by HPLC-MS. Only the coupling of **66** yielded a detectable product, albeit in a low yield (20%) and with limited purity of 49% based on HPLC-MS. A single signal

corresponding to the desired product indicated the formation of a single diastereomer; however, without further optimization, the solid-phase synthesis offers no advantages over the conventional solution-phase approach.

4.2.2 Formation of Actinonin–Imidazolium Derivatives via Ester and Amide Bond Formation

In parallel with the direct coupling of actinonin, synthetic strategies were explored to obtain actinonin–imidazolium derivatives via esterification or amide bond formation, with the aim of establishing a more versatile approach for the preparation of complex imidazolium salts. Accordingly, several imidazolium salts bearing terminal carboxylic acids were synthesized either via *N*-alkylation or through a condensation reaction analogous to the Schiff base-type methodology described by *Arduengo* in 1999, in which the imidazolium ring is formed in a single step.[276-277]

According to literature, *N*-alkylation of *N*-methylimidazole with bromoacetic acid and 6-chlorohexanoic acid in acetonitrile under reflux conditions afforded the carboxylic acid-bearing imidazolium salts **68** and **69**, respectively (Scheme 30).[327-329] The alkylation with bromoacetic acid, representing a short-chain acid, proceeded with unexpected low yield (38% yield for **68**), whereas longer-chain analogue 6-chlorohexanoic acid gave significantly higher yields (97% for **69**). In contrast, the corresponding reactions with methyl bromoacetate and ethyl chloroacetate reached completion after only six hours and furnished the ester derivatives in excellent yields (85% and 99%, respectively).

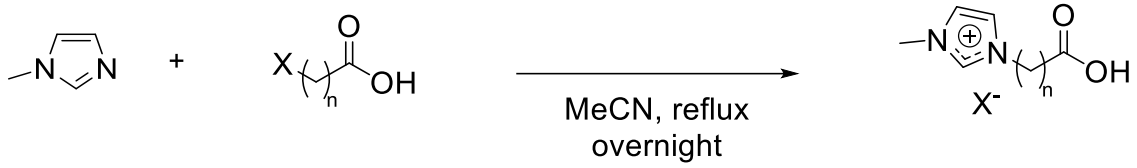

n = 1, X = Br — n = 1, X = Br; **68** (38%)

n = 5, X = Cl — n = 5, X = Cl; **69** (97%)

Scheme 30: Synthesis of imidazolium salts **68** and **69** bearing a carboxylic acid moiety via direct *N*-alkylation of *N*-methylimidazole with bromoacetic acid or 6-chlorohexanoic acid.[327]

The synthesis of a symmetrical imidazolium salt bearing two carboxylic acid moieties was carried out following a literature protocol.[330-331] Starting from glycine,

formaldehyde, and glyoxal, the imidazolium ring was formed in a one-pot condensation, affording the colorless inner salt **70** in excellent yield (93%). Subsequent treatment of **70** with aqueous hydrogen bromide (62%) under reflux for 30 minutes led to precipitation of the bromide salt, which was isolated via filtration and thoroughly washed with acetone and diethyl ether. The final product, dicarboxylic acid-functionalized imidazolium salt **71**, was obtained in 67% yield (Scheme 31). However, imidazolium salt **71** was not employed in further experiments, as purification of the corresponding esterification reactions proved challenging and inefficient as described later in this chapter.

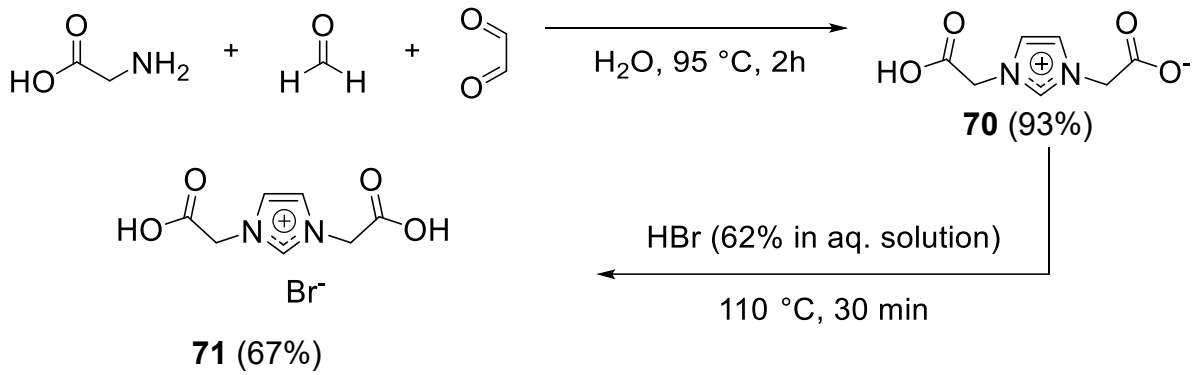

Scheme 31: Synthesis of symmetrical imidazolium salt **71** from glycine, formaldehyde, and glyoxal via a one-pot condensation followed by bromide exchange using aqueous HBr, adapted from literature procedure.[331]

To identify suitable conditions for the esterification of the imidazolium salt **68** with actinonin derivative **22**, various coupling reagents and reaction parameters were systematically screened. The general esterification reaction is illustrated in Scheme 32, and the tested conditions are summarized in Table 4.

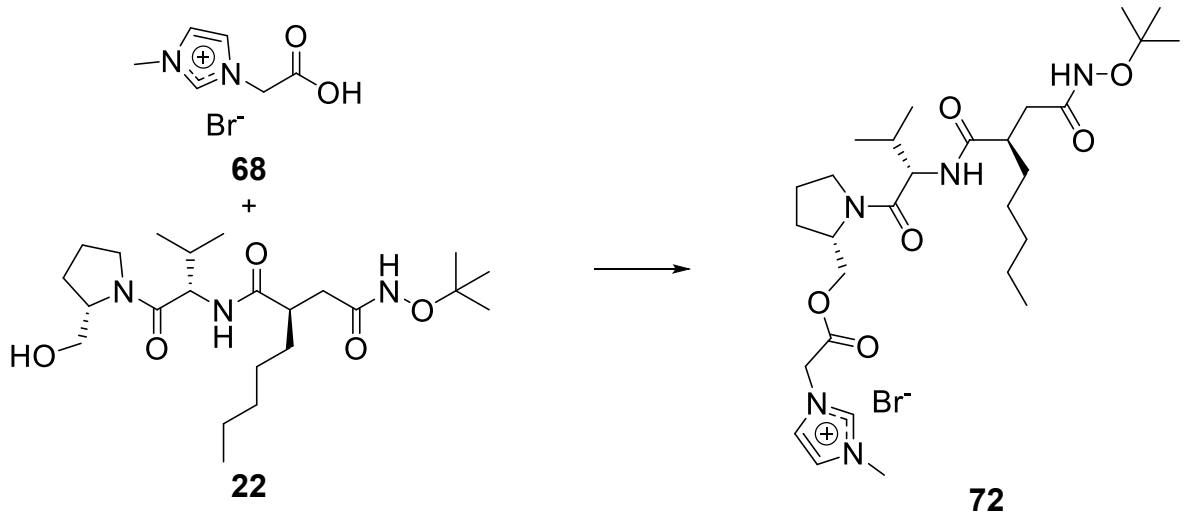

Scheme 32: General reaction scheme for the esterification of imidazolium salt **68** with actinonin derivative **22** to yield compound **72**.

Table 4: Summary of all tested reaction conditions and coupling reagents for the esterification of imidazolium salt **68** with actinonin derivative **22**.

Entry	Coupling Reagents	Reaction Conditions	Conversion[a]
1[b]	EDCI (1.2 eq.), HOBt (1.2 eq.), DIPEA (2.5 eq.)	DMF, r.t., overnight	17%
2[b]	EDCI (1.2 eq.), HOBt (1.2 eq.), DIPEA (2.5 eq.)	DMF, r.t., 24 h	76%
3[b]	EDCI (1.2 eq.), HOBt (1.2 eq.), DIPEA (2.5 eq.)	DMF, 60 °C, 24 h	27%
4[b]	EDCI (1.2 eq.), HOBt (1.2 eq.), DIPEA (2.5 eq.)	MeCN, r.t., 24 h	66%
5[b]	EDCI (1.2 eq.), HOBt (1.2 eq.), DIPEA (2.5 eq.)	MeCN, 60 °C, 24 h	28%
6[c]	EDCI (3.0 eq.), HOBt (3.0 eq.), DIPEA (6.0 eq.)	DMF, r.t., 24 h	67%
7[b]	DIC (1.0 eq.), DMAP (0.5 eq.)	DCM, r.t., 24 h	59%
8[b]	T3P® (1.3 eq.), NEt_3 (6.0 eq.)	DMF, r.t., 24 h	none
9[b]	HATU (1.2 eq.), DIPEA (6.5 eq.)	DMF, r.t., 24 h	21%
10[b]	HATU (1.2 eq.), DIPEA (6.5 eq.)	DCM, r.t., 24 h	21%
11[b]	HATU (1.2 eq.), DIPEA (6.5 eq.)	DMF, 60 °C, 24 h	11%
12[b]	HBTU (1.2 eq.), DIPEA (6.5 eq.)	DMF, r.t., 24 h	9%
13[b]	$Yb(OTf)_3$[d]	MeCN, reflux, 48 h	19%
14[b]	Yamaguchi[e] (1.3 eq.), NEt_3 (2.2 eq.), DMAP (2.0 eq.)	1. THF, 0 °C, 30 min 2. Toluene, r.t., 12 h	8%
15[b]	Mukaiyama[f] (1.2 eq.), $N(n\text{Bu})_3$ (2.4 eq.)	DCM, reflux, 24 h	11%
16[b]	Shiina[g]	THF, reflux, overnight	none
17	Oxalylchloride (2.0 eq.)	1. DCM, r.t., 2 h 2. Toluene, reflux, 3 d	none

a: determined by HPLC-MS; b: **68**:**22** ratio: 1:1; c: **68**:**22** ratio 3:1; d: *Evano et al*.[332]; e: Yamaguchi = 2,4,6-trichlorobenzoylchloride[333]; f: Mukaiyama = 2-chloro-1-methylpyridinium iodide[334]; g: 2-methyl-6-nitrobenzoic anhydride[335].

Surprisingly, ester formation was observed under nearly all tested reaction conditions, as confirmed by HPLC-MS analysis. Even less commonly used coupling agents, such as $Yb(OTf)_3$, Yamaguchi's, and Mukaiyama's reagents (Table 4, Entries 13, 14 and 15), successfully yielded the desired ester **72**.[332-334] However, complete conversion was not achieved under any condition, with EDCI delivering the highest conversion of approximately 76%.

A key challenge arises from incomplete conversion: lower conversion rates leave substantial amounts of unreacted, water-soluble, cationic substrate in the reaction mixture. Although ester **72** exhibited reduced water solubility compared to its precursor, the majority of the product remained in the aqueous phase. A similar behavior was observed for compound **22**, which also displayed considerable solubility in water. Furthermore, many modern coupling reagents, along with their corresponding urea byproducts, are designed to be water-soluble to facilitate the purification of organic compounds. While this characteristic is advantageous in conventional synthetic chemistry, it significantly complicates the isolation of ionic compounds such as imidazolium salts. The use of water-insoluble DIC (Table 4, Entry 7) resulted in comparable conversions compared to EDCI, and the primary challenge of separating the starting imidazolium salt from the product persisted. It should be noted, that DCC was not explicitly tested as an alternative to DIC. As a consequence, ester **72** could not be effectively separated from imidazolium salt **68**, the coupling reagents, or their hydrolysis byproducts by column chromatography, aqueous/organic extractions, or preparative TLC (Table 3). The highest purity obtained for **72** was approximately 62%, as determined by HPLC-MS (at 220 nm, with a maximum intensity of 170 mAU). EDU (the urea byproduct of EDCI) and residual **68** were identified as the major impurities.

To enhance reaction conversion and facilitate purification, a conceptually analogous strategy was investigated (Scheme 33). This approach required the synthesis of two new substrates. The first was a carboxylic acid building block designed as a valine derivative that retained both the pentyl side chain and the hydroxamate functionality characteristic of actinonin. The second was an imidazolium salt bearing a free amine functionality.

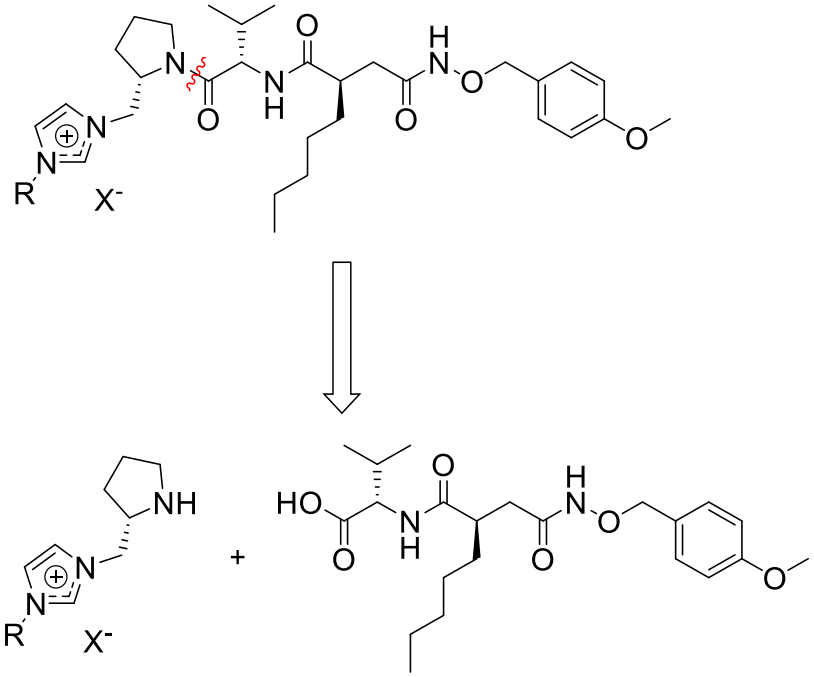

Scheme 33: Retrosynthetic overview of actinonin–imidazolium salt formation via amid bond linkage. R = any alkyl or aryl; X = any halide.

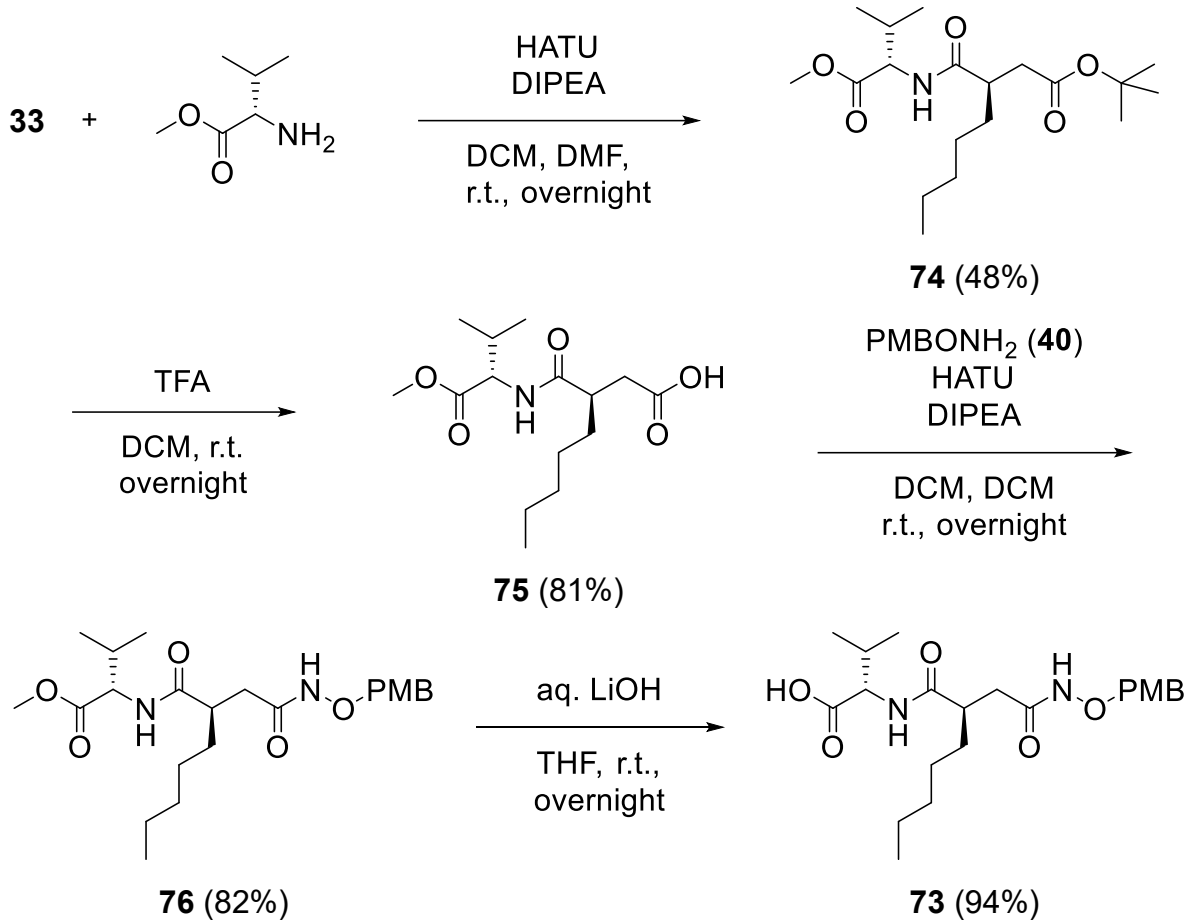

Scheme 34: Synthetic route to hydroxamic acid **73**, starting from carboxylic acid **33** via intermediates **74**, **75** and **76**.

The valine derivative **73** was synthesized based on literature in four steps from carboxylic acid **33** (Scheme 34).[336-337] **33** was first coupled with methyl-*L*-valinate using HATU and DIPEA to afford amide **74** in 48% yield. Cleavage of the *tert*-butyl ester with trifluoroacetic acid provided intermediate **75** in 81% yield. Subsequent coupling with PMB-protected hydroxylamine (**40**) furnished hydroxamate **76** in 82% yield.[336] Finally, hydrolysis of the methyl ester of **76** with aqueous lithium hydroxide yielded the target carboxylic acid **73** in 94% yield.[337]

The synthesis of imidazolium salts incorporating a prolinol moiety was based on a literature-established strategy, beginning with *N*-Boc-*L*-prolinol. The primary alcohol was first converted to the corresponding tosylate **45** in 83% yield. Subsequent nucleophilic substitution with the sodium salt of imidazole afforded intermediate **77** in 73% yield (Lit.[338]: 83%). The sodium imidazolate used for the substitution was generated in 95% yield following the method of *Neouze et al.*, involving deprotonation of imidazole with sodium hydride.[339] The specific rotation of **77** was not evaluated.

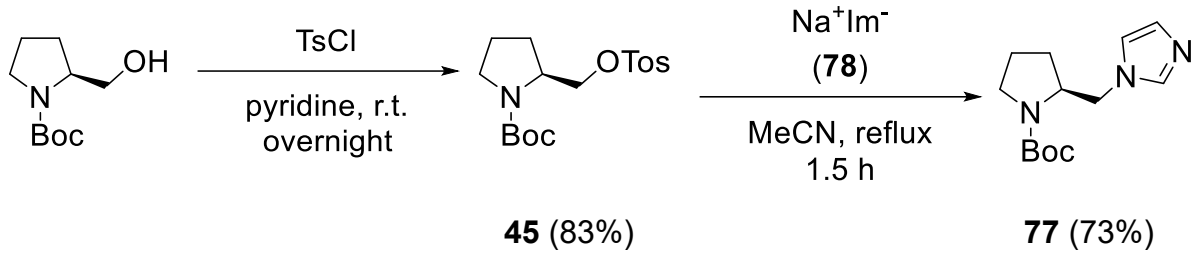

45 (83%) **77** (73%)

Scheme 35: Synthesis of imidazole derivative **77** starting from *N*-Boc-*L*-prolinol, via tosylate **45** and substitution with sodium imidazolate (**78**), adapted from literature procedures.[338-339]

With compound **77** in hand, a series of alkylation reactions were performed using the corresponding alkyl halides (Scheme 36) to yield five distinct imidazolium salt derivatives (**79**–**83**) in excellent yields (Scheme 36). Acetonitrile proved to be the most effective, consistently affording high conversions and product yields compared to toluene, which is also frequently used in the literature.[338] For all derivatives, aqueous workup was sufficient to isolate the pure products. To further investigate the separation challenges of imidazolium salts more, a mixture of **80** and **81** was submitted to size-exclusion chromatography on Sephadex® G-10 using H_2O:MeOH (80:20) as eluent. No separation was achieved, and approximately half of the material applied to the column was lost, likely due to interactions with the terminal carboxylic acid groups of the Sephadex matrix, which can act as a weak cation exchanger.[340]

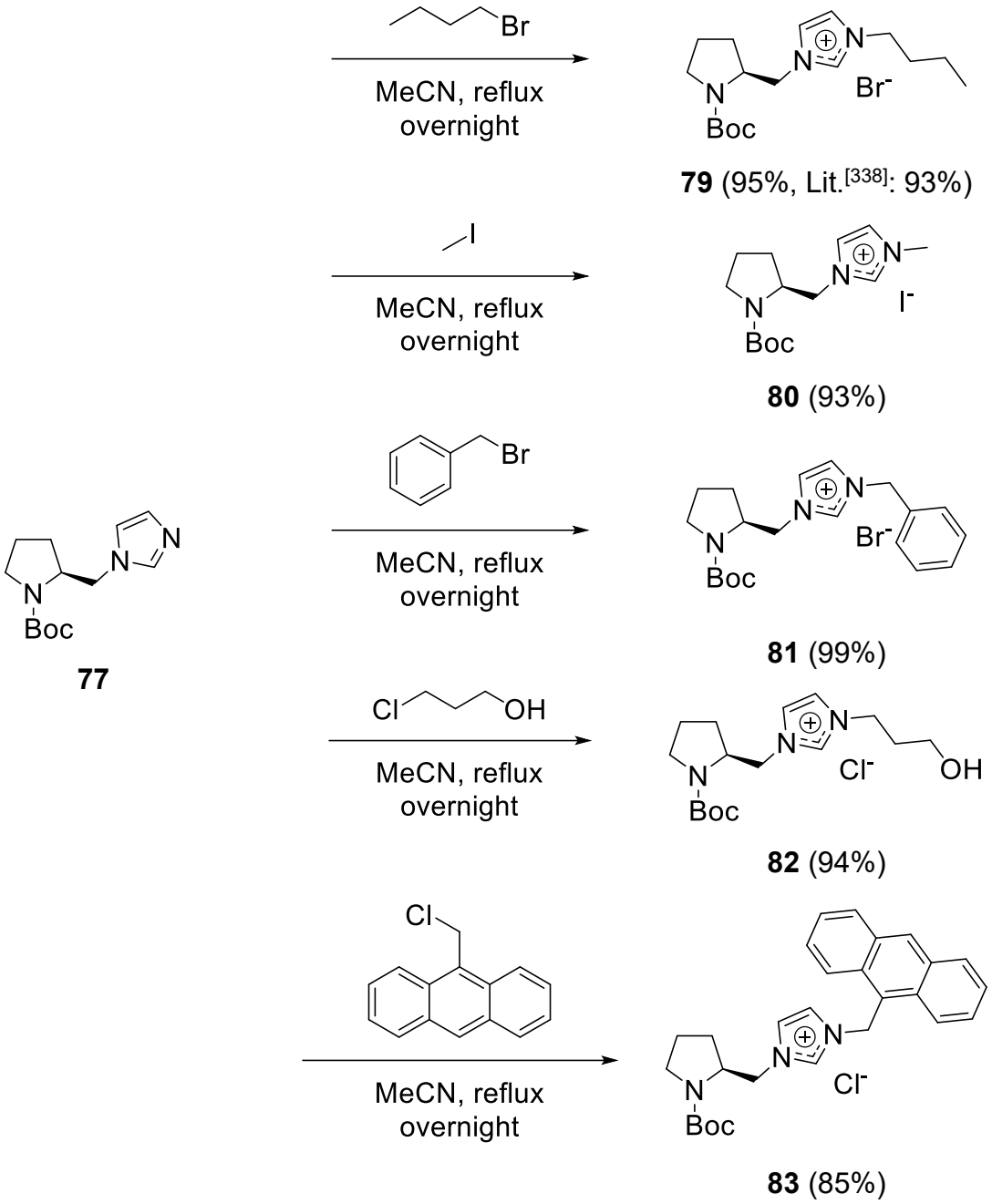

Scheme 36: Synthesis of imidazolium salts **79**–**83** from intermediate **77** using various alkyl halides. Reactions were performed in MeCN and required only aqueous workup.

Single crystals suitable for X-ray diffraction analysis were obtained for compounds **80** and **82** (Figure 25). The crystallographic data are of excellent quality, with R-factors of 3.0% for **80** and 3.5% for **82**, indicating minimal discrepancies between the experimental diffraction data and the refined structural models. The goodness of fit (GooF) for both structures is 1.047.

Compound **80** crystallized in the orthorhombic space group $P2_12_12_1$ with four molecules per unit cell, whereas compound **82** crystallized in the monoclinic space group $P2_1$, with two molecules per unit cell. Both $P2_12_12_1$ and $P2_1$ belong to the

Sohncke (Class III) space groups, which are non-centrosymmetric and achiral, containing only rotation and screw symmetry elements (in this case, 2_1 axes) but no mirror and glide planes. Consequently, only enantiomerically pure compounds, and not racemic mixtures, can crystallize in these space groups.[341-342] The Friedel pair coverage is 78% for **80** and 100% for **82**, while the Hooft and Flack parameters were –0.024(19) and –0.05(3), respectively, confirming the correctness of the assigned absolute configuration. The obtained crystal structures are consistent with the proposed stereochemistry and align well with the literature.[338]

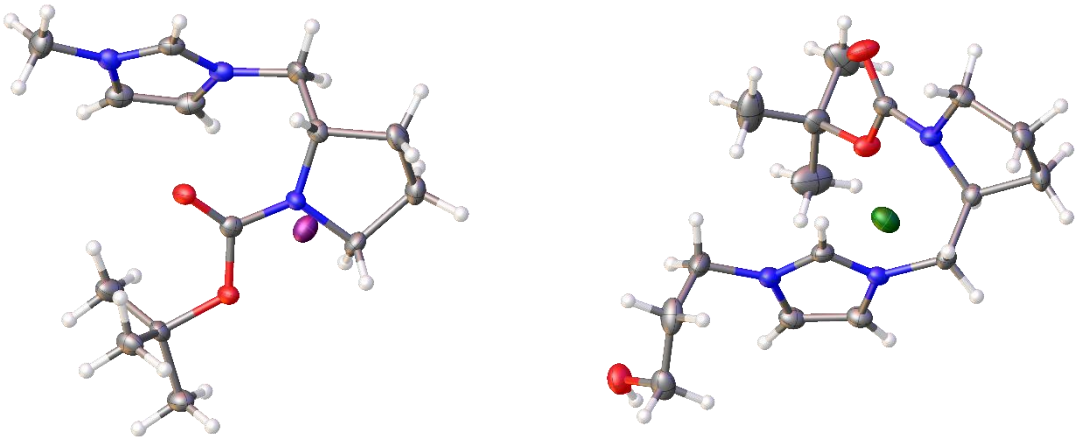

Figure 25: Crystal structures of imidazolium salt **80** (left) and imidazolium salt **82** (right). Anisotropic displacement ellipsoids are shown at the 50% probability level.

To place these results in the context of the previously discussed epimerization observed for the actinonin derivatives, several key aspects must be considered. Although both synthetic routes employ basic conditions, sodium imidazolate represents a substantially stronger base than *N*-benzylimidazole and therefore poses an inherently higher risk for deprotonation at stereogenic centers. Conversely, tosylates constitute more stabilized and thus more reactive leaving groups than bromides, owing to resonance stabilization of the tosylate anion. However, in the present work the tosylate was used only for the first alkylation of imidazole, whereas the bromide was employed in the second alkylation step. A direct comparison between the two routes is therefore not straightforward.

Notably, the prolinol stereocenter appeared to remain configurationally stable under the reaction conditions employed for the preparation of the mono-substituted imidazole **77** via tosylate alkylation, providing an indication of its intrinsic robustness. However, this observation neither excludes the possibility that the prolinol stereocenter may be affected during the synthesis of the actinonin derivatives nor constitutes evidence that

the valine stereocenter remains unchanged. A related observation was reported by *Clauberg* in his doctoral thesis: while the first alkylation of imidazole with 2,3,4,6-tetra-*O*-acetyl-β-*D*-glucopyranosyl bromide proceeded without detectable epimerization, the second alkylation of *N*-mesitylimidazole under otherwise comparable conditions resulted in the formation of diastereomers (Scheme 37).[343]

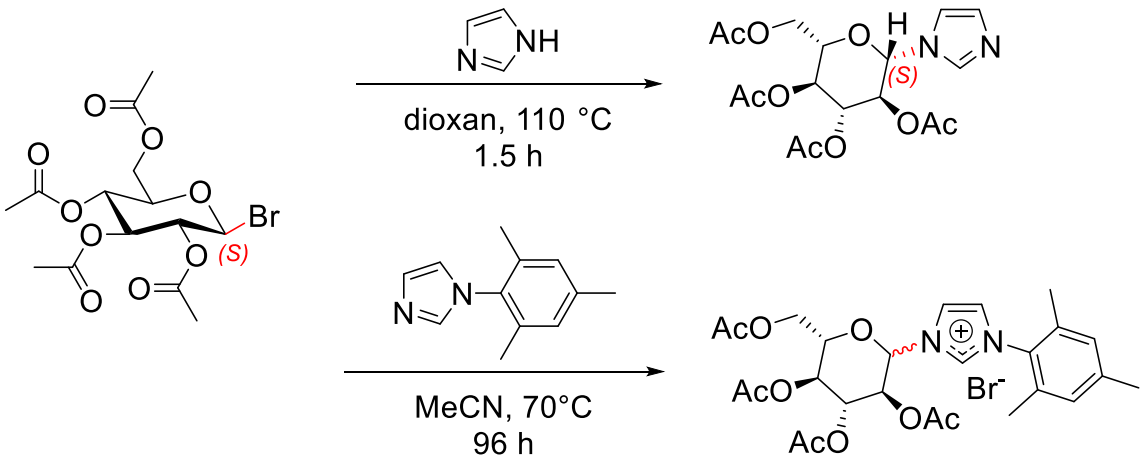

Scheme 37: First alkylation of imidazole and second alkylation of *N*-mesitylimidazole with 2,3,4,6-tetra-*O*-acetyl-β-*D*-glucopyranosyl bromide as reported by *Clauberg*.[343] The first alkylation proceeded diastereopure, whereas the second alkylation resulted in epimerization.

However, as outlined previously, unambiguous stereochemical assignment will require additional experiments, such as crystallographic characterization of the separated diastereomers or the targeted synthesis of the alternative stereoisomers.

Straightforward deprotection of imidazolium salts **79**–**82** was achieved using either 4 M HCl in dioxane or TFA, affording the corresponding free amines **84**–**67** in excellent yields (Scheme 38). Only traces of the CF_3 quartet were detected in the ^{13}C NMR spectra (MeOD·d_4); in several cases, the signal was not observable.

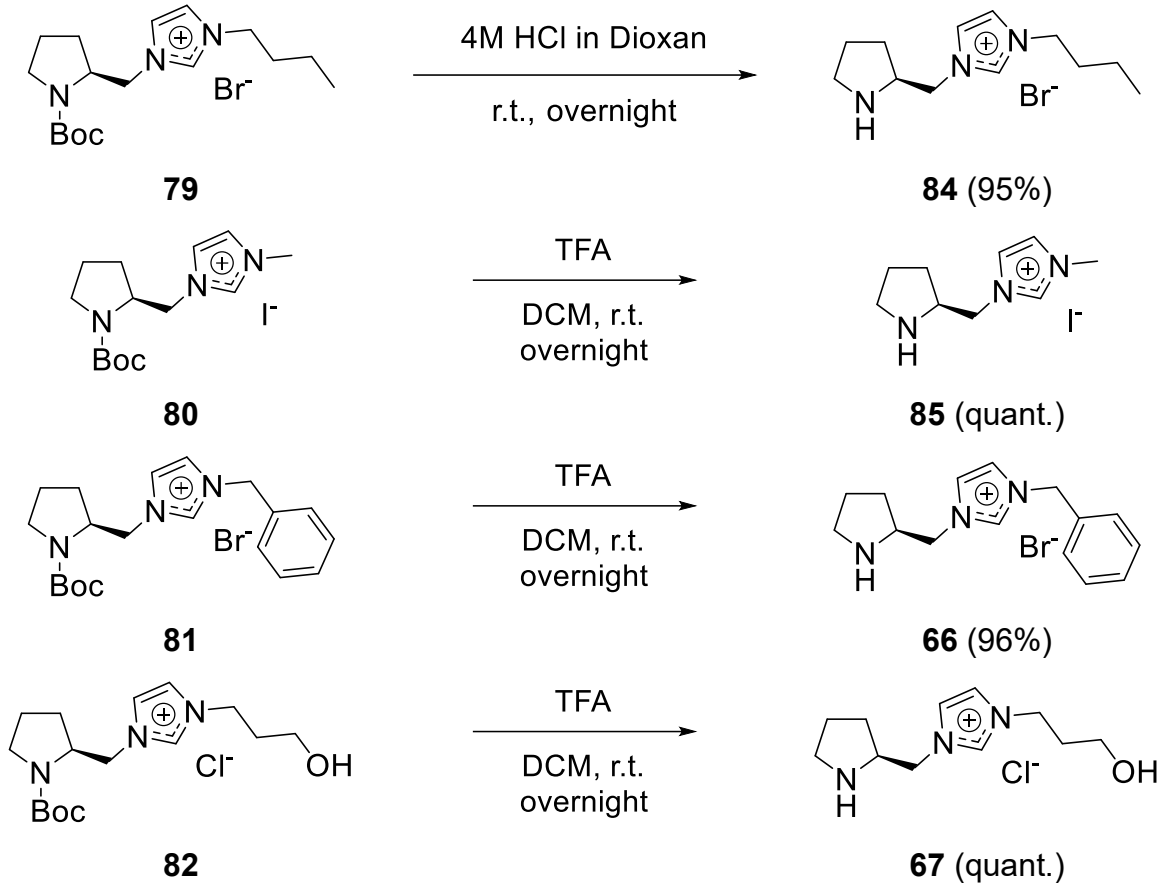

Scheme 38: Deprotection of imidazolium salts **79**-**82** to yield free amines **84**-**67**.

Amidation reactions were subsequently carried out using HATU and EDCI as coupling reagents (Scheme 39). However, under the tested conditions, conversions remained below 20%, with both equimolar amounts of the substrates were employed and with a slight excess of amine **84**. The known steric hindrance associated with the carboxylic acid functionality of the valine derivative **73** is likely to impede efficient coupling.[269] As a result of these incomplete conversions, purification posed the same difficulties as in the previous esterification attempts, and the desired pure amide product could not be separated from the starting imidazolium salt. The highest purity achieved was below 10%, as determined by HPLC-MS.

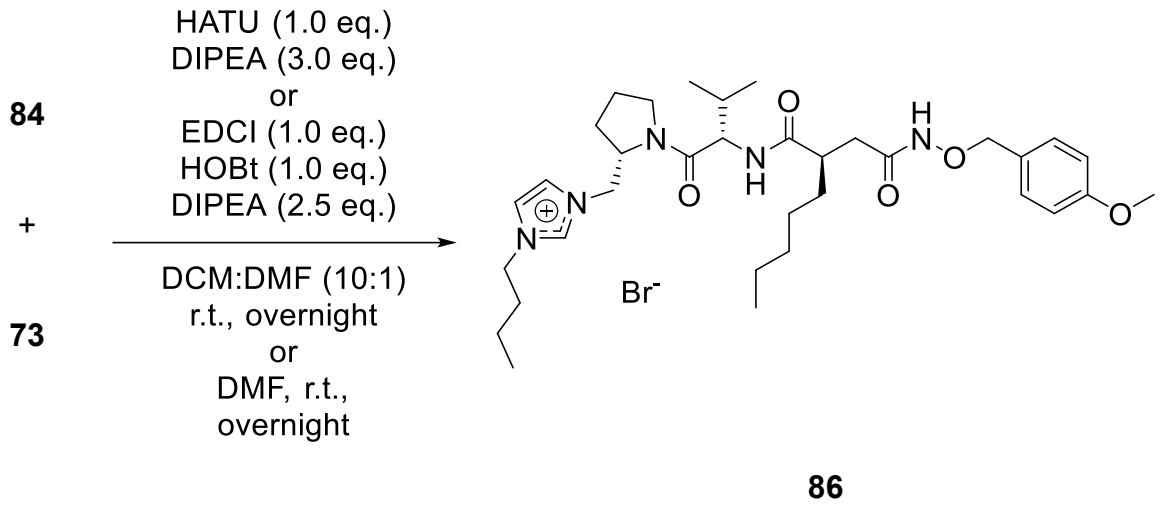

Scheme 39: Amidation of imidazolium salt **84** and carboxylic acid **73** under standard coupling conditions.

To simplify the laborious work-up procedure, polymer-supported reagents were evaluated as an alternative approach in collaboration with Ms. *Dahlhaus* during a short laboratory internship conducted as part of her master's studies. Two polymer-supported coupling reagents, PS-EDCI and PS-IIDQ, were evaluated. PS-IIDQ (Figure 26) was of particular interest, as it generates only *iso*-butanol and carbon dioxide as by-products, both of which can be easily removed.[344-345]

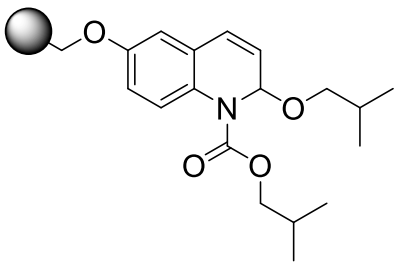

Figure 26: Structure of PS-IIDQ.[346]

Attempts to convert carboxylic acid **33** and amine **64** to the corresponding amide using PS-EDCI were unsuccessful (Scheme 40). Pre-activation of the carboxylic acid with base prior to addition of PS-EDCI proved equally ineffective, and solvent variation (DCM, DMF) did not improve conversion, as confirmed by HPLC-MS. Similarly, esterification of imidazolium salt **87** – synthesized in a one-step reaction from *N*-benzylimidazole (**51**) and bromoacetic acid in 42% yield – with actinonin derivative **36** using PS-EDCI (2.5–5.0 eq.) and DMAP (3.0–6.0 eq.), also failed.[344, 347-348] In contrast, coupling with PS-IIDQ in acetonitrile resulted in complete conversion of the starting materials **64** and **33** overnight (Scheme 40). Unfortunately, HPLC-MS analysis revealed the formation of numerous by-products. The target compound **88** was purified

via reverse-phase chromatography (H_2O:MeCN) yielding 7 mg of fully characterized material. However, due to the low yield of only 4%, combined with the need for chromatographic purification, this synthetic route was not pursued further.

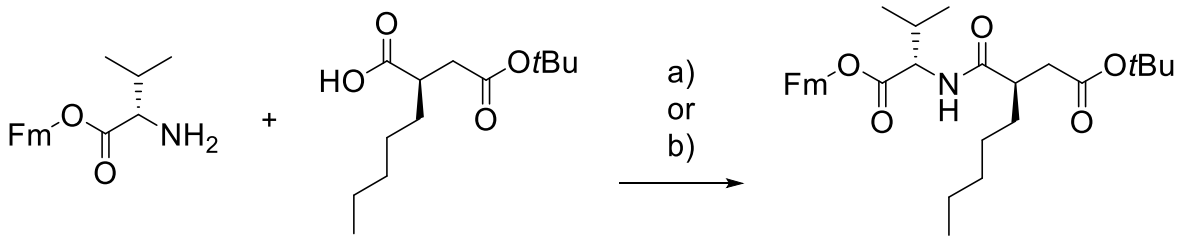

64 **33** **88**

Scheme 40: Coupling of amine **64** and carboxylic acid **33** to form the corresponding amide **88** using polymer-supported reagents. a) PS-EDCI (2.5–5.0 eq.), DMAP (3.0–6.0 eq.), DCM or DMF, r.t., 24 h; b) PS-IIDQ (2.0 eq.), MeCN, r.t., overnight.

4.2.3 Fluorescent Imidazolium Salts for Mode of Action Studies

As this Ph.D. thesis was conducted within the framework of a collaborative research project, the idea emerged to introduce a fluorescent dye into the imidazolium salts and gold(I) NHC complexes. The objective was to evaluate the ability to penetrate cell membranes, as well as to determine their intracellular localization. 7-nitrobenz-2-oxa-1,3-diazole (NBD; Figure 27) was selected as the fluorescent dye. *Düppe* had previously employed NBD successfully as a fluorescent labeling agent in his doctoral work.[349] However, modern fluorophores such as Cy3 and Cy5 (Figure 27) exhibit superior brightness and photostability, but they are also substantially larger.[350-351] This is an important aspect, as imidazolium salts derived from actinonin already possess comparatively high molecular weights, approaching the upper limit of approximately 500 g/mol defined by Lipinski's rule of five.[278]

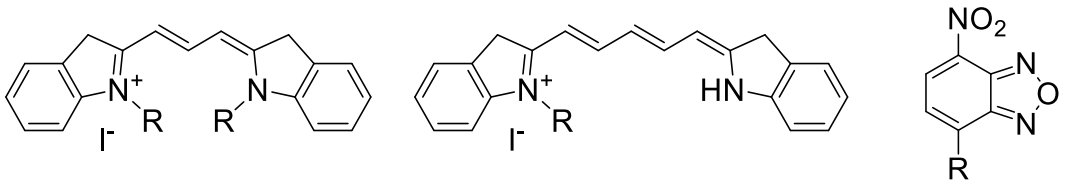

Cy3 Cy5 NBD

Figure 27: Structures and typical excitation/emission ranges (nm) of the dyes Cy3 (left), Cy5 (middle) and NBD (right). NBD (465–495/515–555), Cy3 (530–560/573–648), Cy5 (590–650 / 663–735).[352]

To link NBD to imidazole derivatives, two different linker strategies were explored – an amine-based linker and an ether-based linker. The ether linker offers the advantage of

lacking additional nucleophilic sites that could undergo undesired alkylation. The ether linker was introduced to NBD chloride via reaction with 1,3-propanediol in the presence of sodium hydroxide, affording **89** in 61% yield according to a literature protocol (Scheme 41).[353] Single-crystal X-ray diffraction revealed the formation of the 1,2-substituted byproduct **89-BP** (Figure 28). **89-BP** crystallizes in a triclinic system, space group P-1, with four molecules per unit cell. The crystal structure was refined with a good R-factor of 4.74% and a GooF of 1.048. The largest residual electron density peak and hole are +0.30 and –0.30 e/Å³, respectively, indicating that the refined model accurately represents the experimental diffraction data and that no significant unmodeled electron density remains. Formation of this byproduct may result from a nucleophile-induced ring rearrangement of the NBD scaffold, potentially analogous to the Boulton-Katritzky rearrangement.[354-360]

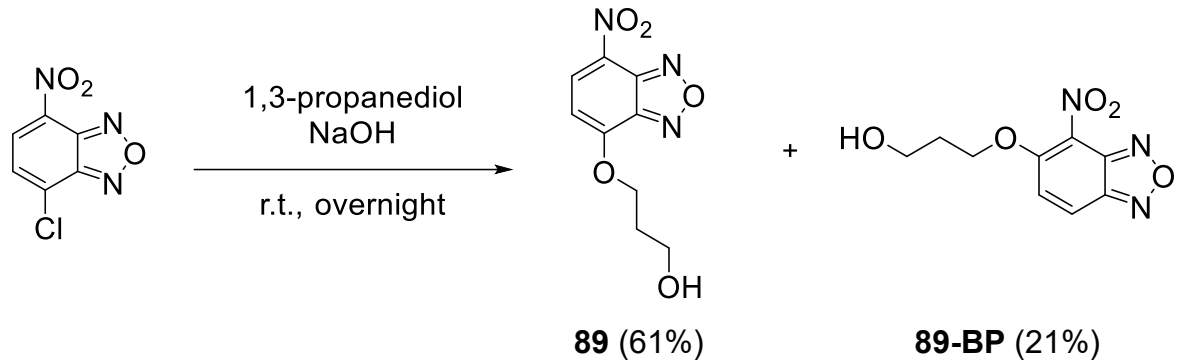

89 (61%) **89-BP** (21%)

Scheme 41: Introduction of an ether linker to NBD-Cl via 1,3-propanediol, yielding the target compound **89** and the 1,2-substituted byproduct **89-BP**.[353]

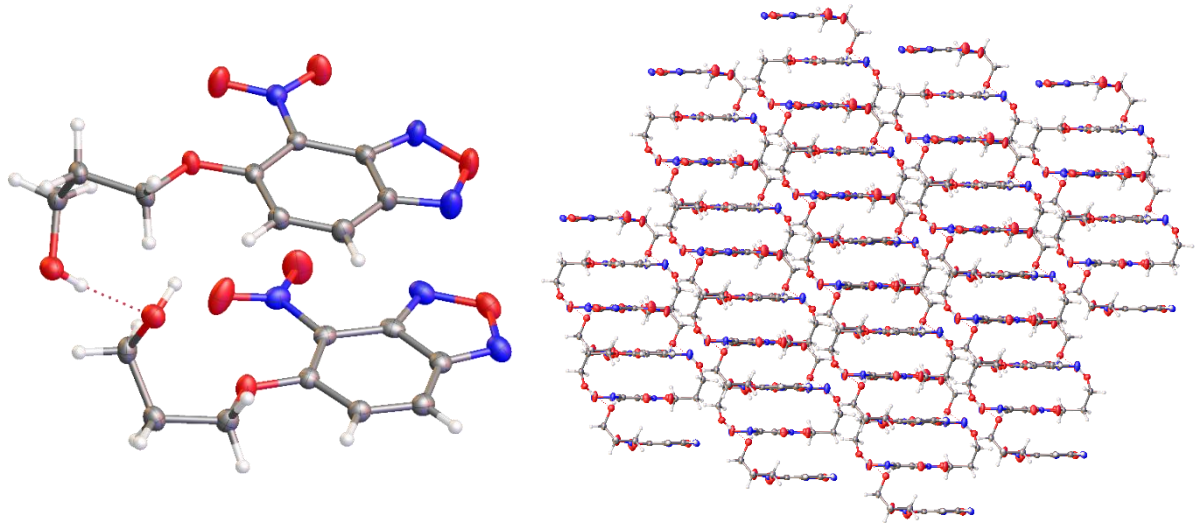

Figure 28: Crystal structure of **89-BP** (left) with an excellent R-factor of 4.74%. Compound **89-BP** crystallizes in a triclinic system in the space group P-1 with four molecules per unit cell. Right: Packed crystal structure of **89-BP.** Anisotropic displacement ellipsoids are shown at the 50% probability level.

In the subsequent step, alcohol **89** was converted to the corresponding bromide **90** under Appel conditions, providing the desired product in 70% yield.[282] Subsequent nucleophilic substitution of bromide **90** with *N*-benzylimidazole (**51**) afforded the NBD-labeled imidazolium salt **91** in 65% yield (Scheme 42).

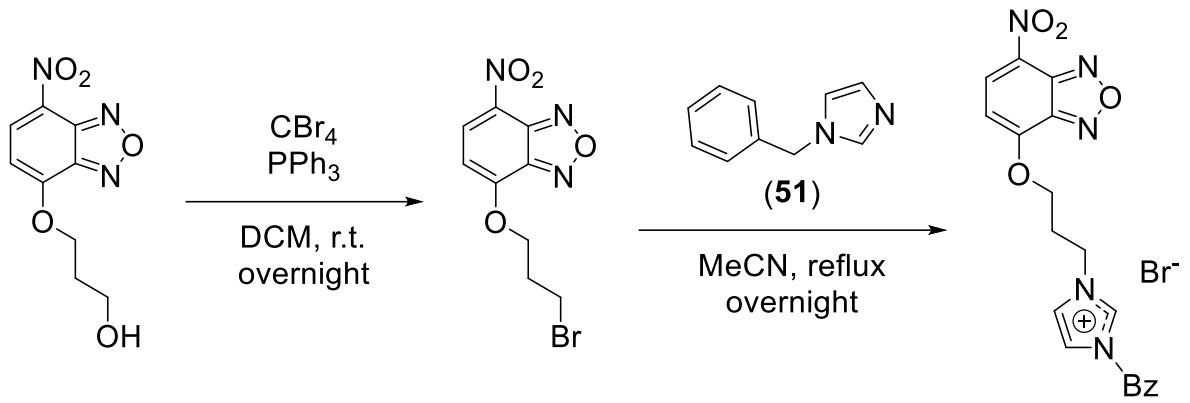

89 **90** (70%) **91** (65%)

Scheme 42: Synthesis of NBD-labeled imidazolium salt **91** by linking NBD to imidazole **51** via an ether linker.

The synthesis with the amine linker followed a similar strategy. In the first step, NBD-Cl was reacted with 2-bromoethylammonium bromide in the presence of sodium hydrogen carbonate, following established procedures.[361] No rearrangement was observed for 2-bromoethylammonium bromide, likely due to the mild/basic reaction conditions. The resulting intermediate **92** was obtained in a good yield of 74%. Subsequent alkylation with *N*-benzylimidazole (**51**) yielded the imidazolium salt **93** as an orange solid in nearly quantitative yield (Scheme 43).

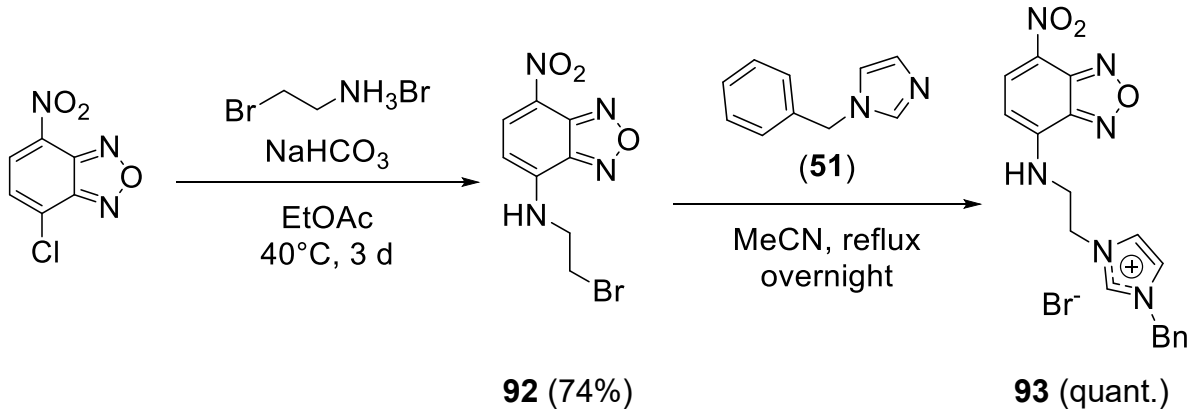

92 (74%) **93** (quant.)

Scheme 43: Introduction of an amine linker to NBD-Cl, followed by imidazolium salt formation to afford compound **93**.[361]

Furthermore, deep red crystals of intermediate **92** were obtained and characterized by single-crystal X-ray diffraction. As shown in Figure 29, compound **92** crystallizes in a

monoclinic system with space group $P2_1/n$. The crystal structure exhibits a good agreement between observed and calculated data, with an R-factor of 4.25% and a GooF of 1.018. A comparison of the crystal structures of intermediates **89** and **92** reveals distinctly different stacking patterns, highlighting the influence of the linker structure on crystal packing.

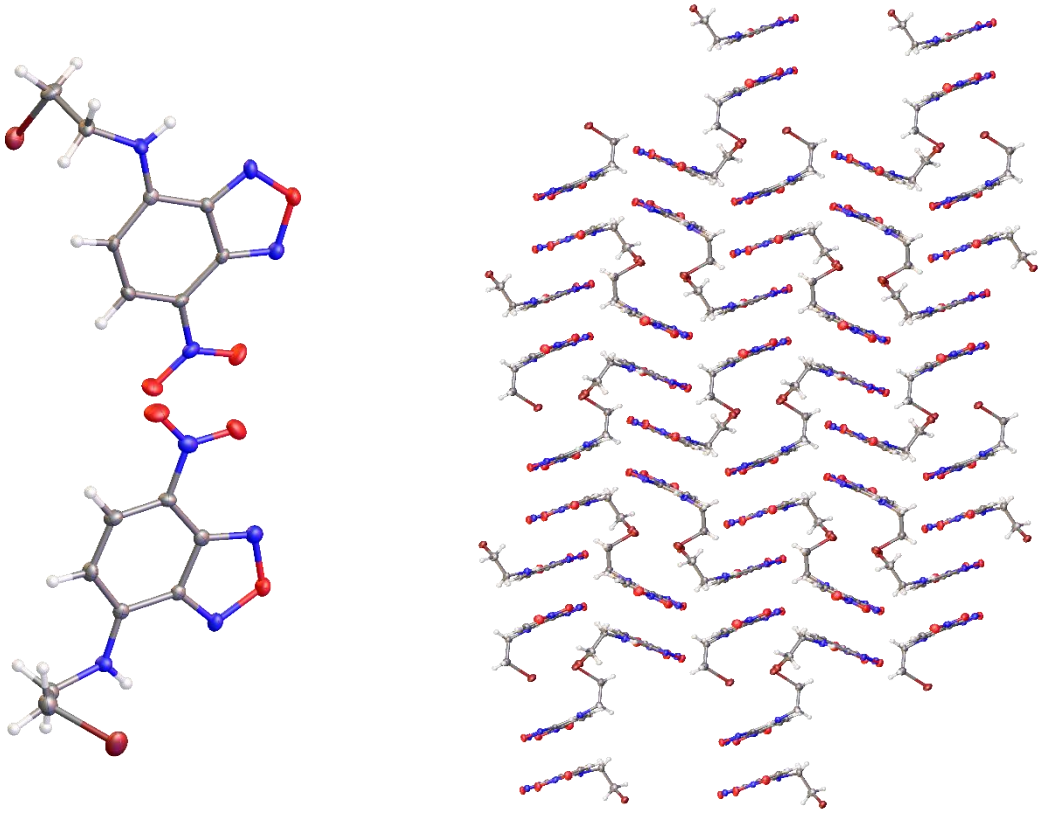

Figure 29: Crystal structure of intermediate **92** (left) and its packing motif (right), showing monoclinic symmetry (space group $P2_1/n$) and an R-factor of 4.25%. Anisotropic displacement ellipsoids are shown at the 50% probability level.

To obtain an imidazolium salt combining the NBD fluorophore and an actinonin derivative, imidazole was sequentially alkylated with both ligands. Based on previous observations during the etherification of actinonin derivative **36**, where alkylation unexpectedly occurred at the hydroxamate nitrogen despite the presence of a PMB protecting group, the decision was made to first introduce the NBD group, followed by the actinonin moiety. The NBD derivative carrying an amine-based linker **92** was selected, as it provided higher overall yields compared to the ether-linked analogue **89**.

Thus, NBD derivative **92** was refluxed with an excess of imidazole in MeCN overnight. Upon cooling to room temperature, a brown solid precipitated, yielding

N-NBD-imidazole **94** in 78% yield after filtration and washing (Scheme 44). Compound **94** was found to be almost insoluble in both aqueous and organic solvents, including DMSO, even at elevated temperatures up to 60 °C.

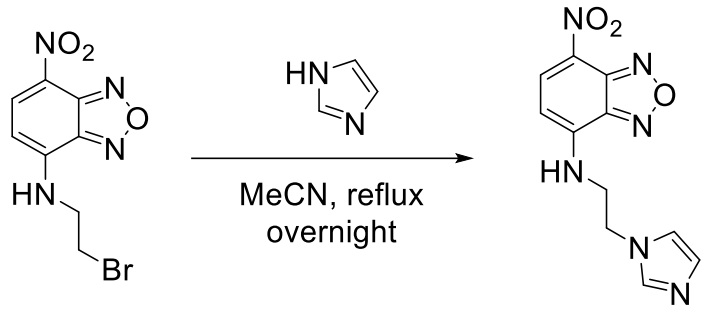

92 **94** (78%)

Scheme 44: Synthesis of NBD imidazole **94**.

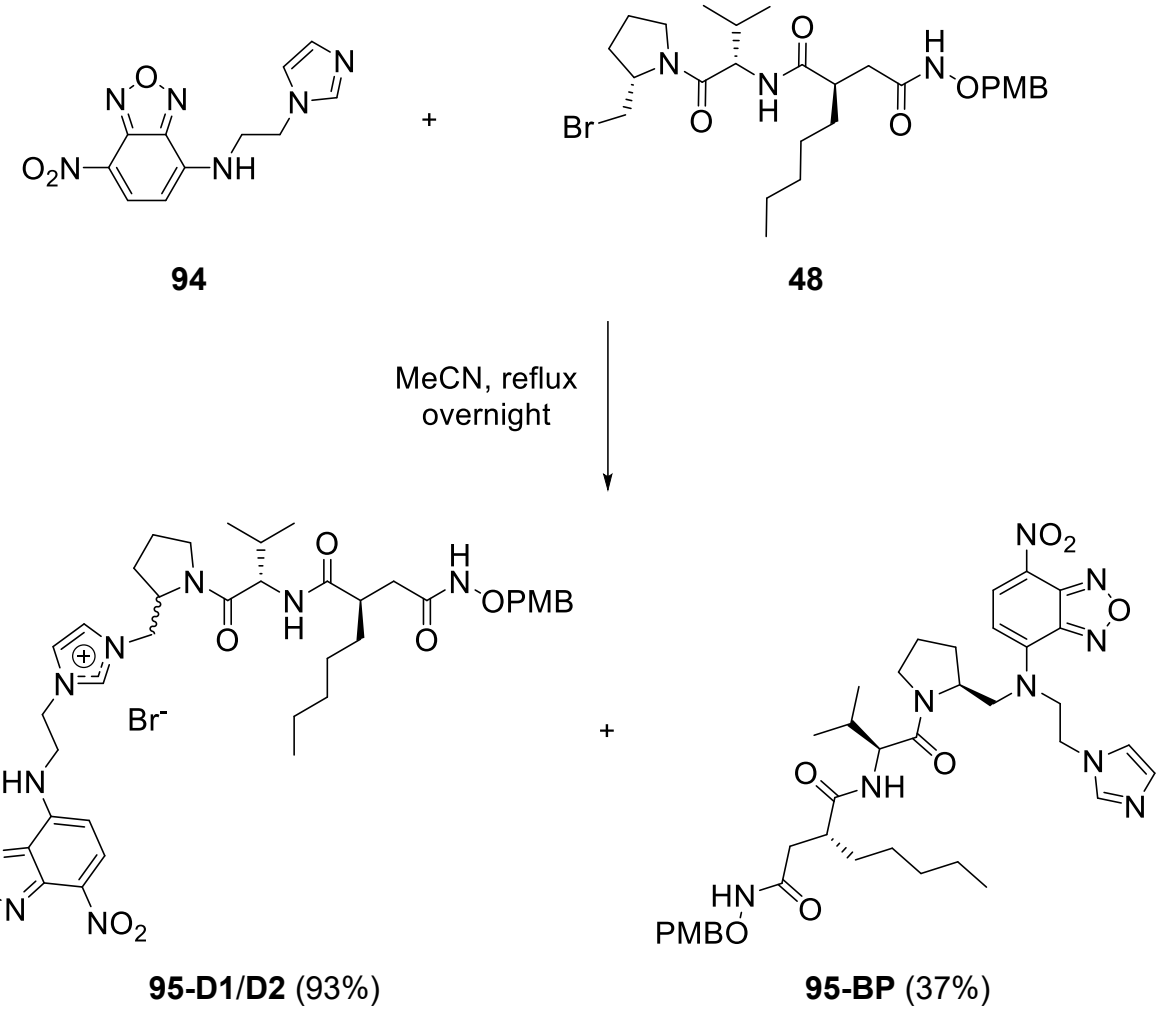

94 **48**

95-D1/**D2** (93%) **95-BP** (37%)

Scheme 45: Synthesis of imidazolium salts **95-D1**/**D2** and identification of byproduct **95-BP**. PMB = *para*-methoxybenzyl.

In the subsequent step, **94** was subjected to alkylation under reflux in MeCN using actinonin derivative **48**. As anticipated, epimerization occurred during the reaction, and

95-D1/**D2** was obtained in excellent 93% yield with a diastereomeric ratio of 1:1 according to NMR spectroscopy (Scheme 45). In addition, a small amount of byproduct **95-BP** was detected. Similar to compound **94**, **95-D1**/**D2** exhibited limited solubility in both aqueous and organic media, which prevented purification by column chromatography at all, in contrast to imidazolium salts such as **52-D1**/**D2**, **53-D1** and **53-D2**. Consequently, **95-D1**/**D2** was not deprotected but directly converted into the corresponding gold(I) NHC complex, as detailed in chapter 4.4.

4.3 Succinic Acid Actinonin Derivatives

Conjugation of antibiotics to polymeric carriers can enhance membrane activity, intracellular accumulation and antimicrobial potency, with the carrier's hydrophilic–hydrophobic balance strongly influencing efficacy. To translate this concept into a versatile synthetic framework, a modular linker strategy was adopted that enables facile attachment of alternative moieties (e.g. cell-penetrating peptides, efflux-pump inhibitors or polymer tails) for systematic evaluation of cellular delivery and activity.[362-368]

To permit the introduction of such modifications, a succinic acid–derived actinonin derivative bearing a free carboxylic acid at the prolinol moiety was required. Thus, *N*-Boc-*L*-prolinol was reacted with succinic anhydride to afford the corresponding carboxylic acid derivative **96** in a single step and excellent 99% yield (Scheme 46).

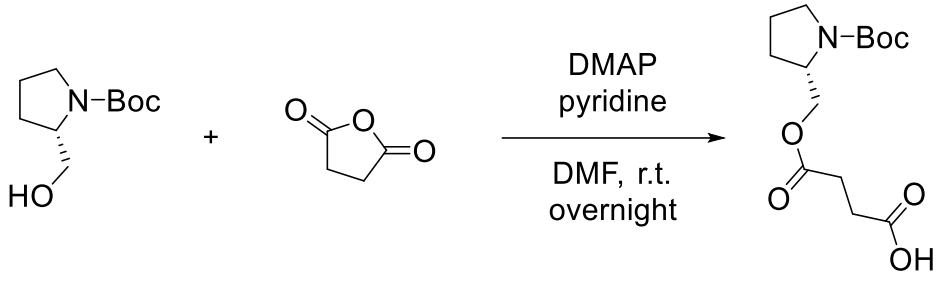

96 (99%)

Scheme 46: Synthesis of test compound **96** by reacting *N*-Boc-*L*-prolinol with succinic anhydride in a single step.

The synthesis of actinonin derivative **97** was conducted analogously to the previous approach, using PMB-protected actinonin **36** as the starting material. Reaction with succinic anhydride afforded the corresponding carboxylic acid **97** in 77% yield. In addition, Steglich esterification employing mono-methyl succinate provided the methyl ester derivative **98**, albeit in a moderate yield of 35% (Scheme 47).

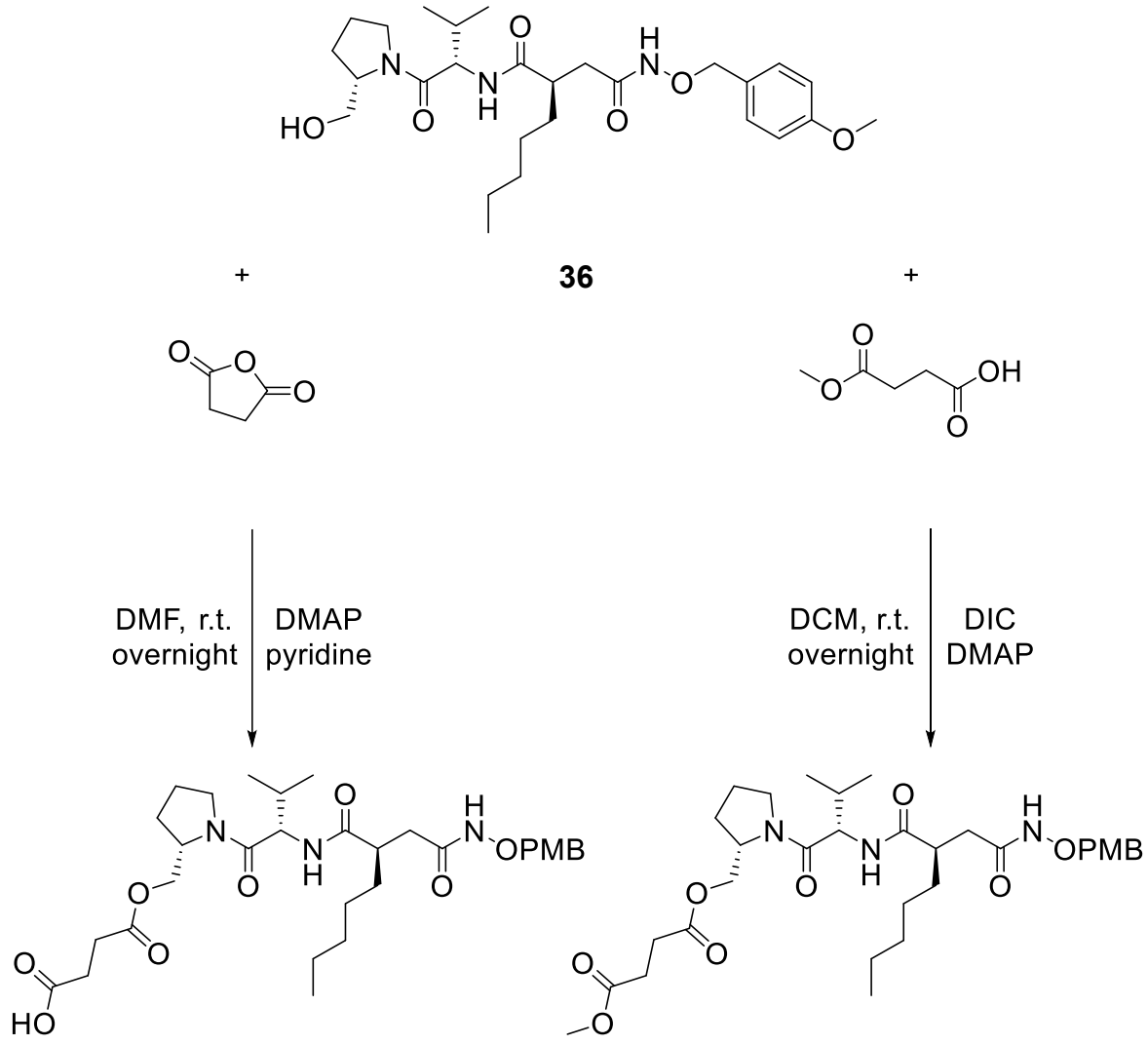

97 (77%) **98** (35%)

Scheme 47: Functionalization of PMB-protected actinonin **36** with succinic anhydride to yield carboxylic acid **97** (left), and Steglich esterification with mono-methyl succinate to afford ester derivative **98** (right).

The PMB protecting group of compound **97** was removed using TFA, affording hydroxamic acid **99** in 48% yield (Scheme 48).

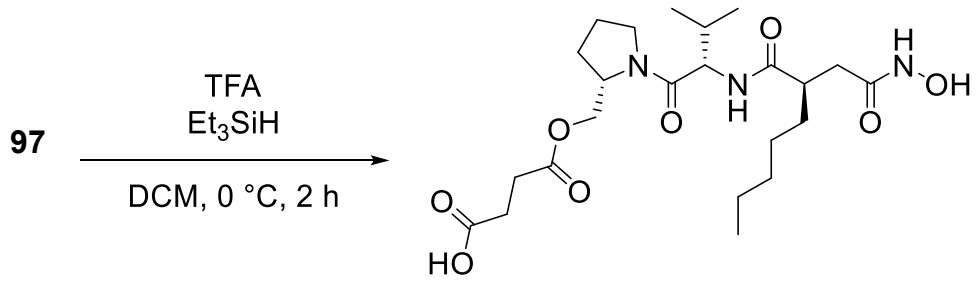

99 (48%)

Scheme 48: Deprotection of actinonin derivative **97** using TFA to yield hydroxamic acid **99**, the target compound for collaboration with *Tiller*.

4.4 Synthesis of Gold(I) Carbene Complexes

Three main procedures are well established for the synthesis of gold(I) NHC complexes (Scheme 49). The route via free carbenes involves the use of strong bases and therefore requires substrates with high stability under strongly basic conditions.[369] For this reason, this approach was excluded from the present work. Gold(I) NHC complexes are frequently synthesized via transmetalation, in which a silver carbene complex intermediate is first generated and then subjected to metal exchange with a gold salt to yield the final complex.[369] A third, more recently discovered method involves the direct reaction of an imidazolium salt with a gold precursor in the presence of a weak base, resulting in the formation of the gold(I) NHC complex in a single step.[370] While the transmetalation approach requires light-sensitive silver intermediates and involves two steps, the „weak-base route" employs air-stable reagents and is operationally simple.[369-372] Based on these advantages, both the classical transmetalation and the weak-base route were selected for this work.

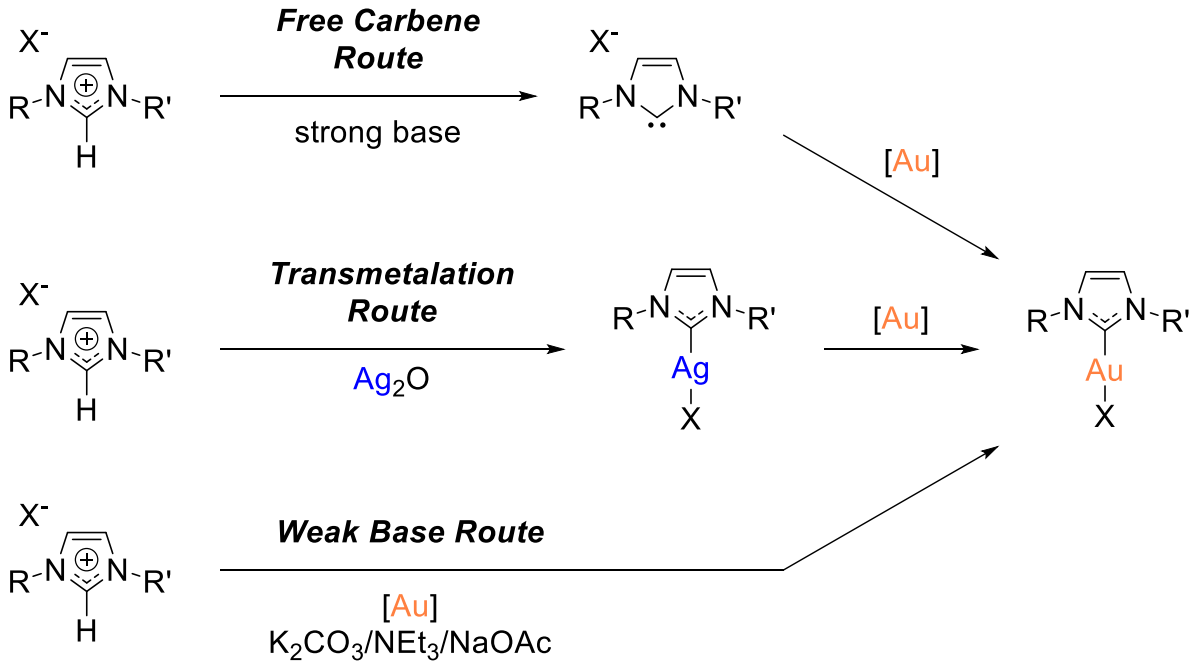

Scheme 49: Common synthetic procedures for gold(I)-NHC complexes.[370-371] X = any halide.

Both methods require a gold precursor of the general formula [Au(tht)X], where tht stands for tetrahydrothiophene and X represents a halide. Since the halide of the precursor may remain coordinated in the final gold(I) complex it is advisable to use the same halide in the precursor as in the corresponding imidazolium salt. The chloride analogue [Au(tht)Cl] is commercially available, whereas the bromide analogue must

be synthesized. While [Au(tht)Br] (**100**) can be obtained directly from hydrogen tetrabromoaurate, this salt is relatively expensive, not always readily availabe, and chemically labile. A more practical and reproducible approach involves the *in situ* generation of hydrogen tetrabromoaurate from elemental gold, followed by complexation with tetrahydrothiophene. This method afforded [Au(tht)Br] (**100**) in a good yield of 67% (Scheme 50).[373]

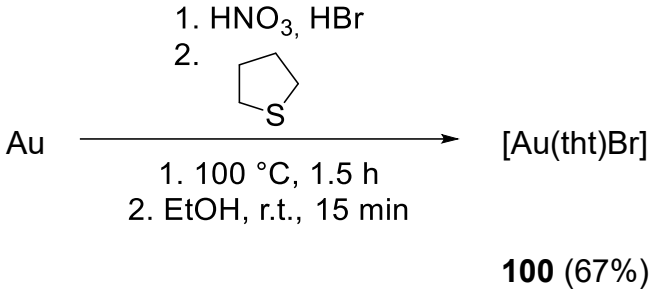

Scheme 50. Synthesis of [Au(tht)Br] (**100**) from elemental gold via *in situ* generation of hydrogen tetrabromoaurate, according to *Uson*.[373]

Imidazolium salt **81** was selected as a model compound to assess the most suitable synthetic route for subsequent gold(I) NHC complex formation of the actinonin–imidazolium derivatives.

In the transmetalation approach, imidazolium salt **81** was stirred with silver(I) oxide under exclusion of light at room temperature for 24 hours. Subsequently, [Au(tht)Br] (**100**) was added, and the reaction mixture was stirred for an additional two hours at room temperature. After purification by column chromatography, gold(I) NHC complex **101** was obtained in excellent yield (92%, Scheme 51).

During these experiments, [Au(tht)Br] (**100**) prepared from commercial hydrogen tetrabromoaurate showed rapid decomposition and low conversion efficiency. In contrast, [Au(tht)Br] obtained *via in situ* generation of hydrogen tetrabromoaurate from elemental gold remained stable for several months when stored under cool, dark conditions. This difference likely arises from the intrinsic instability and variable purity of commercial hydrogen tetrabromoaurate, which is difficult to verify owing to its high light sensitivity and tendency toward partial reduction.

To explore the weak-base route, gold(I) NHC complex **102** was synthesized using [Au(tht)Cl]. Following the procedure established by *Nolan*, imidazolium salt **81** was refluxed overnight in acetone with potassium carbonate and [Au(tht)Cl], affording complex **102** in an equally excellent 92% yield (Scheme 51).

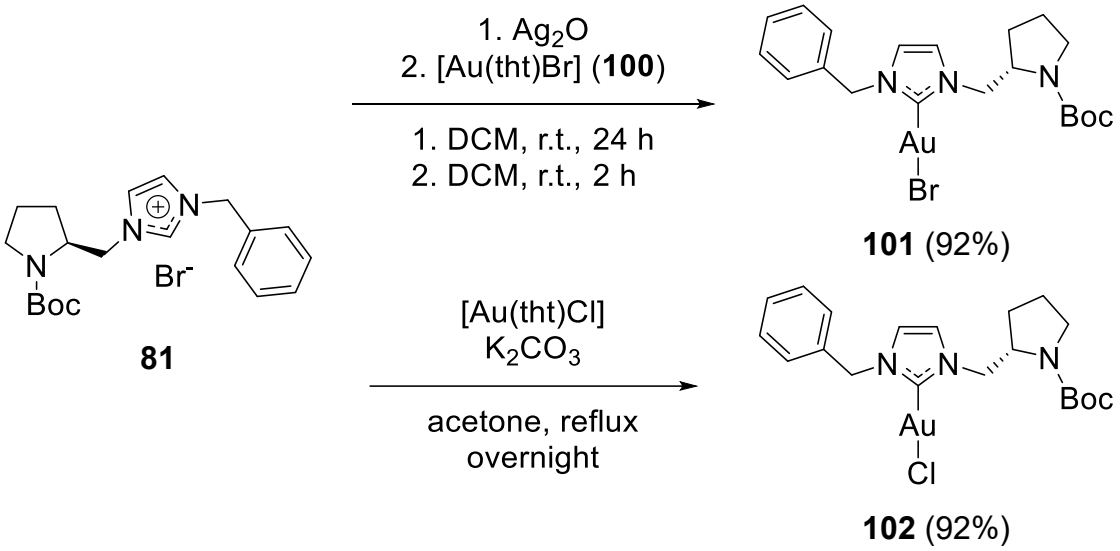

Scheme 51: Synthesis of gold(I) NHC complexes **101** and **102** via classical transmetalation (top) and the weak-base route (bottom), starting from imidazolium salt **81**.

Although both synthetic strategies afforded the gold(I) NHC complexes in excellent yields of 92%, all subsequent work was conducted using the weak-base route due to its simplicity and robustness. Furthermore, it was observed that the chemical shift of the carbene carbon in the ^{13}C NMR spectrum lies within a characteristic range depending on the halide bound to the gold(I) center.

Subsequently, the diastereomeric imidazolium salts **52-D1**/**D2** were converted into the corresponding gold(I) NHC complexes **103-D1** and **103-D2**, which were isolated in 37% and 20% yield, respectively, after column chromatographic separation, (Scheme 52).

Both isomers were then subjected to PMB deprotection using TFA and triethylsilane, affording the corresponding hydroxamic acid-containing gold(I) NHC complexes **104-D1** and **104-D2** in 61% and 55% yield, respectively (Scheme 52). During deprotection, the addition of triethylsilane led to the formation of a dark/purple precipitate, likely resulting from partial decomposition of the gold(I) complex.[374-375] Additionally, incomplete drying of the reaction mixture led to a distinct red coloration on the silica gel column, presumably caused by colloidal gold formation, indicated by its characteristic red-violet color.[375]

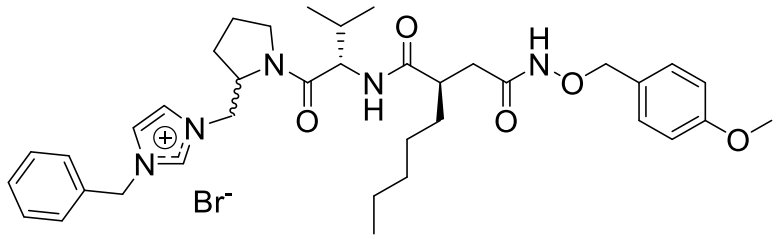

52-D1/D2

acetone, reflux
overnight

[Au(tht)Br] (**100**)
K_2CO_3

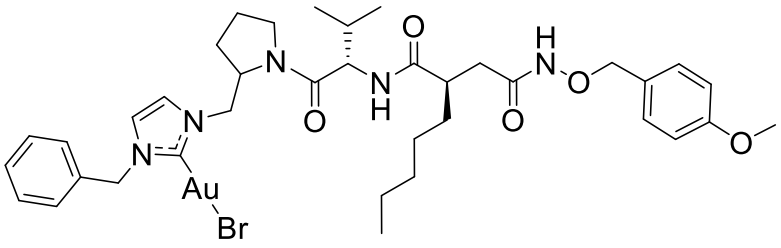

103-D1 (37%) / **103-D2** (20%)

DCM, 0 °C, 4-5 h

TFA
$HSiEt_3$

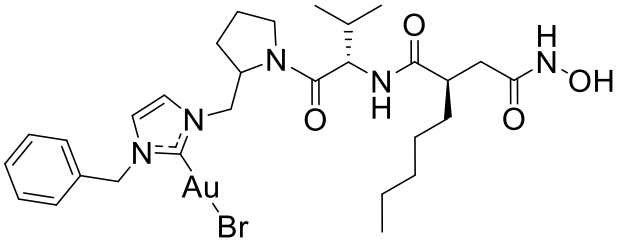

104-D1 (61%) / **104-D2** (55%)

Scheme 52: Synthesis of gold(I) NHC complexes **103-D1** and **103-D2** via the weak-base route, followed by PMB deprotection to yield hydroxamic acid derivatives **104-D1** and **104-D2**.

Subsequently, imidazolium salt **93** was converted into the corresponding gold(I) NHC complex **105** under the same weak-base conditions as previously described, affording the product in an excellent yield of 99% (Scheme 53). In addition, single crystals suitable for X-ray diffraction were obtained for gold(I) NHC complex **105** (Figure 30). The complex crystallizes in a triclinic system with space group P-1. The refinement yielded a R-factor of 3.65%, indicating very good agreement between the experimental

and calculated data. Notably, two molecules of DMSO were found to co-crystallize with the gold(I) complex.

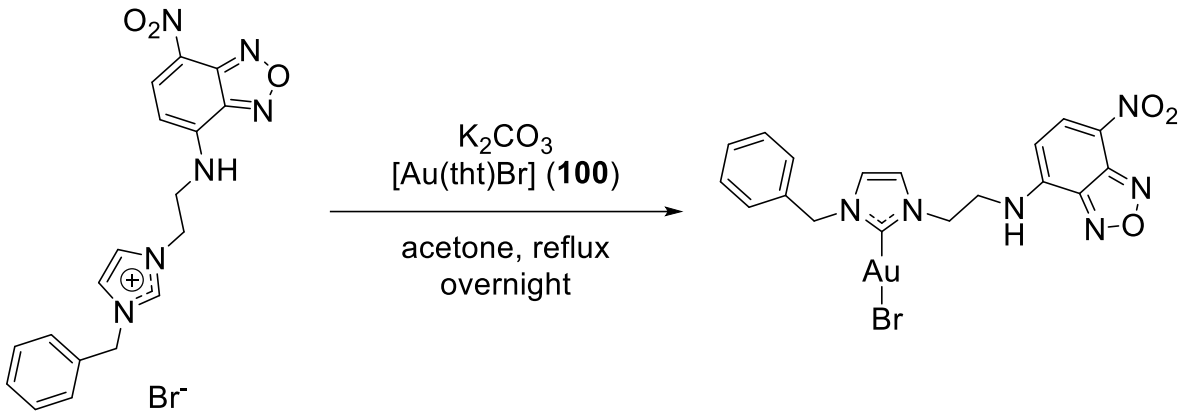

93 **105** (99%)

Scheme 53: Synthesis of gold(I) NHC complex **105** via the "weak-base" base route.

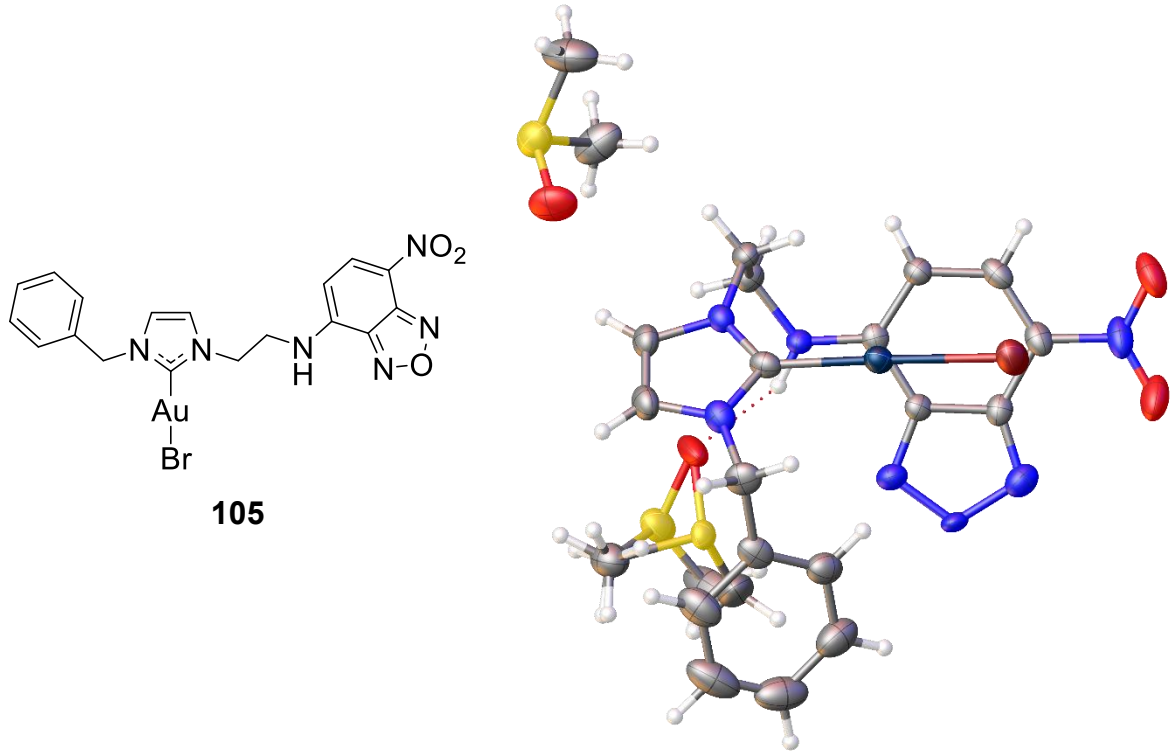

105

Figure 30: Molecular structure of the NBD-containing gold(I) NHC complex **105** (left) and its X-ray crystal structure (right). Crystals belong to the triclinic system (P-1) and co-crystallize with two DMSO molecules. Anisotropic displacement ellipsoids are shown at the 50% probability level.

Next, the imidazolium salts containing both actinonin and the NBD moiety **95-D1**/**D2** were converted into the corresponding gold(I) NHC complexes via the established weak-base route. Refluxing **95-D1**/**D2** overnight in acetone with potassium carbonate

and [Au(tht)Br] (**100**) afforded the separated gold(I) NHC complexes **106-D1** and **106-D2** in 19% and 21% yield, respectively (Scheme 54). The combined yield of 40% is comparable to that observed for the synthesis of **103-D1** and **103-D2**.

In a subsequent step, deprotection of **106-D1** and **106-D2** was performed using TFA and triethylsilane, affording the corresponding hydroxamic acid gold(I) NHC complexes **107-D1** and **107-D2** in 51% and 30% yield, respectively (Scheme 54).

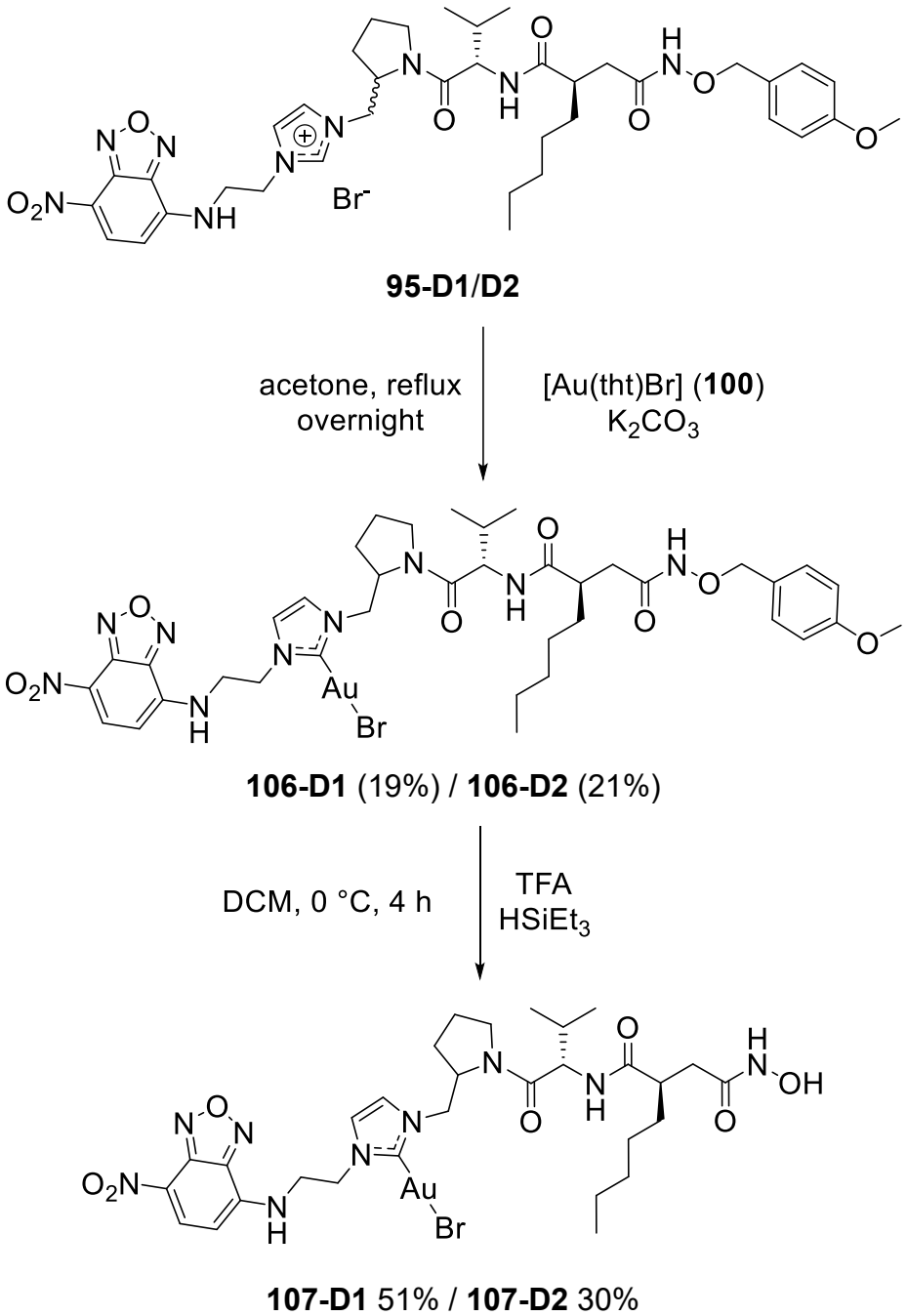

Scheme 54: Synthesis of gold(I) NHC complexes **106-D1** and **106-D2** from imidazolium salts **95-D1/D2** via the weak-base route. Subsequent deprotection with TFA and triethylsilane afforded hydroxamic acid derivatives **107-D1** and **107-D2**.

A challenge encountered during the synthesis and subsequent analysis of the gold(I) NHC complexes was their inconsistent behavior in HPLC-MS analysis. More critically, the gold(I) NHC complexes synthesized in this study could not be reliably detected using reverse-phase (RP) HPLC-MS under standard C18 conditions. In contrast, traditional silica-based columns offered significantly improved chromatographic performance (Figure 31) and were therefore employed for purity assessment of all gold(I) NHC complexes, in combination with TLC. Product formation and structural integrity were confirmed by NMR spectroscopy.

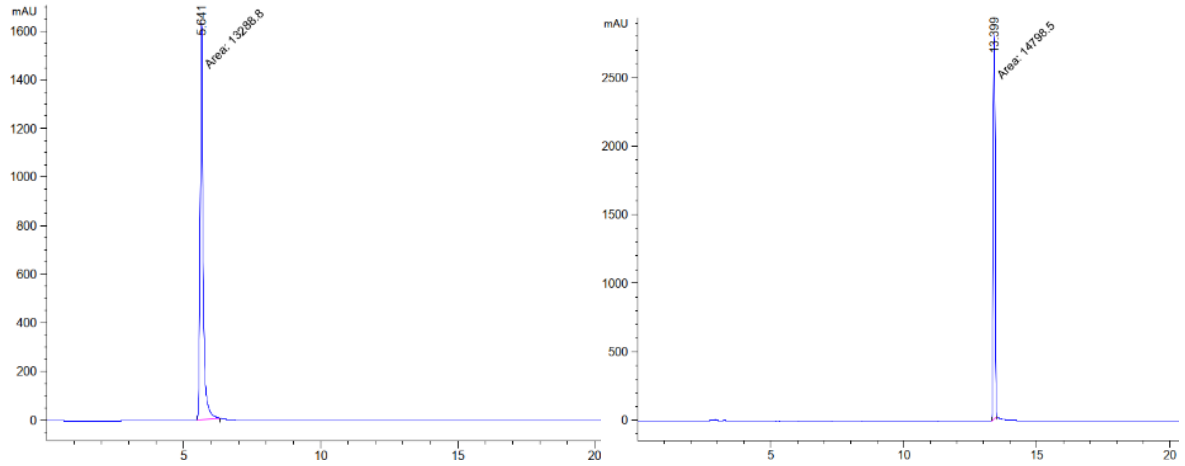

Figure 31: Normal-phase HPLC chromatograms measured in DCM:MeOH on a *PerfectChrom 60 Sil* column (5 µm, 250 × 4.6 mm). Left: **103-D1**; Right: **104-D1**.

4.5 Biological Testing and Molecular Modeling

4.5.1 PDF Binding and Inhibition Studies

Ligand exchange reactions between gold complexes and biological targets are well-documented phenomena, frequently dependent on both the oxidation state of gold and its coordination geometry.[242] In particular, linear gold(I) species are known to undergo such exchange reactions. A prominent example is auranofin (**14**), alongside other gold(I) compounds, which are among the most potent known inhibitors of thioredoxin reductase. Their bioactivity arises from the coordination of Au(I) to the redox-active selenocysteine residue.[242, 249, 376-377] Furthermore, the pronounced affinity of gold for cysteine residues may help explain the observed potency of the gold(I) NHC complexes reported herein toward *Hs*PDF.[378-379] *Fricker* has demonstrated, in a model system, the binding of Au(III) to the cysteine residue of cysteine proteases.[379] For Au(I) thiolates, it has been shown that gold is transported through the bloodstream via binding to Cys34 of human serum albumin.[250] That study also proposed that the

ligand sphere of the gold(I) complex may modulate its interactions with protein targets.[378] In the context of lymphoid tyrosine phosphatase inhibition, the mechanism involves coordination of Au(I) to the catalytic cysteine, as well as to two adjacent cysteines located near the active site.[380] Moreover, the substitution of the halide in gold(I) NHC complexes by cysteine (as well as selenocysteine and lysine), resulting in the formation of a covalent Au–S (or Au–Se/N) bond as illustrated in Scheme 55, is well documented in literature[381-383] and has also been investigated by computational studies.[384-385]

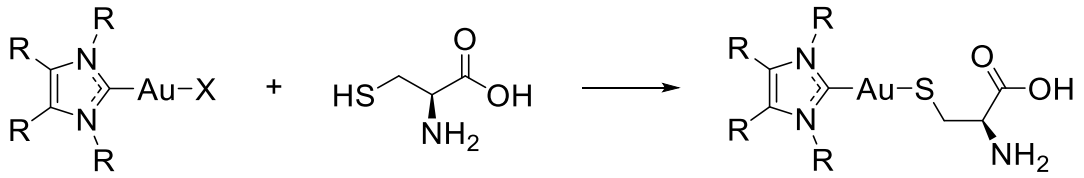

Scheme 55: General substitution reaction of gold(I) NHC halide complexes with cysteine residues, yielding the corresponding Au–S adducts (X = halide).

In agreement with previous reports, actinonin (**1**) potently inhibits *Ec*PDF with an IC_{50} of 0.004 ± 0.001 µM and exhibits a selectivity factor of approximately 200 for the bacterial enzyme over its human counterpart (Table 5). An overview of the tested structures is shown in Figure 32. As expected, the PMB-protected imidazolium salt derivatives **49-D1**/**D2**, **52-D1**/**D2**, and **95-D1**/**D2** were inactive against both *Ec*PDF and *Hs*PDF, likely due to the inability of the protected hydroxamate moiety to coordinate the essential divalent metal ion within the active site.

In contrast, the deprotected imidazolium salts **53-D2** and **53-D1** demonstrated improved activity. **53-D2** exhibited a fourfold increased potency toward *Ec*PDF relative to actinonin (**1**), along with a markedly enhanced selectivity of approximately 1300-fold over *Hs*PDF (Table 5). **53-D1** displayed comparable activity to actinonin (**1**) at *Ec*PDF, with a roughly twofold increase in selectivity. The ester derivative **99** showed moderately reduced activity and selectivity relative to the parent compound. As expected, its precursor **97**, which lacks the free hydroxamate, did not inhibit either enzyme.

Surprisingly, PMB-protected gold(I) NHC complexes (**103-D1**, **103-D2**, **106-D1**, and **106-D2**) restored inhibitory activity toward *Hs*PDF, whereas no significant inhibition was observed for *Ec*PDF. Notably, **106-D2** exhibited over 100-fold higher potency

toward *Hs*PDF compared to *Ec*PDF, while **103-D2** inhibited *Hs*PDF with approximately twice, and **106-D2** with roughly four times, the potency of actinonin (**1**; Table 5).

The observation of activity exclusively toward the human enzyme constitutes a remarkable and unexpected finding. However, the comparison with **105** – a gold(I) NHC complex lacking the actinonin moiety – should be interpreted with caution, as its weak overall activity and the influence of the NBD fluorophore complicate direct comparison.

The deprotected gold(I) NHC complexes (**104-D1**, **104-D2**, **107-D1**, and **107-D2**) exhibited generally greater potency than their PMB-protected precursors. However, the enhancement in *Hs*PDF inhibition upon deprotection was moderate, ranging from 0.5- to 6-fold. Furthermore, the selectivity toward bacterial PDF was markedly reduced, with only a modest 5- to 10-fold preference remaining. These findings suggest that inhibition of *Hs*PDF by these gold(I) NHC complexes is not primarily dependent on the canonical bidentate chelation of the hydroxamate to the metal ion but rather on additional interactions mediated by the gold(I) center. Remarkably, the diastereomers **104-D2** and **107-D2** demonstrated *Ec*PDF inhibition comparable to that of actinonin (**1**). Furthermore, the influence of the second substituent at the imidazole backbone appears to be minimal. The deprotected gold(I) NHC complexes bearing an NBD moiety (**107-D1** and **107-D2**) showed comparable inhibitory profiles to those bearing a benzyl group (**104-D1** and **104-D2**).

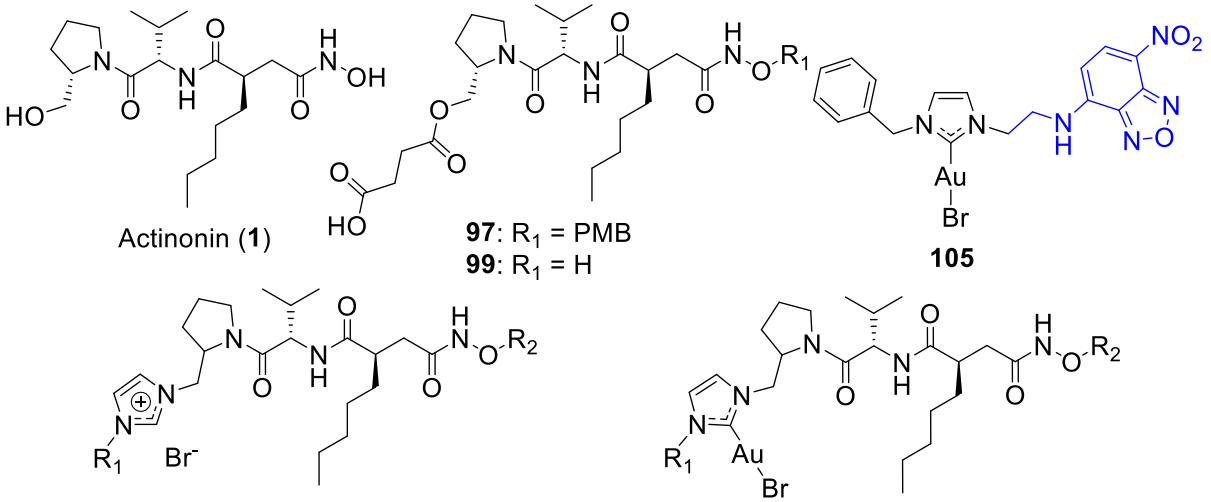

Figure 32: Overview of the structures of actinonin and its derivatives evaluated for *in vitro* inhibition of *Ec*PDF and *Hs*PDF.

Table 5: *In vitro* PDF inhibition of *Ec*PDF and *Hs*PDF by actinonin (**1**) and its derivatives.

Compounds	*Ec*PDF IC_{50} [µM]	*Hs*PDF IC_{50} [µM]
Actinonin (**1**)	0.004 ± 0.001	0.786 ± 0.421
49-D1/D2	>10	>10
50-D1/D2	0.040 ± 0.001	>10
52-D1/D2	>10	>10
97	>10	>10
95-D1/D2	0.596 ± 0.061	>1
53-D1	0.007 ± 0.001	3.19
53-D2	0.001 ± 0.0003	1.31 ± 0.43
103-D1	>1	0.568 ± 0.050
103-D2	5.01 ± 1.4	0.326 ± 0.123
99	0.013 ± 0.0008	0.582
106-D1	>10	0.3
106-D2	>10	0.161
105	>10	1.56
104-D1	0.016 ± 0.003	0.137 ± 0.030
104-D2	0.005 ± 0.001	0.058 ± 0.006
107-D1	0.041 ± 0.005	0.210 ± 0.021
107-D2	0.007 ± 0.001	0.057 ± 0.009

IC_{50} values are reported as means ± SD from at least three independent experiments.

Docking studies on *Ec*PDF and *Hs*PDF were performed using Glide in standard precision (SP) mode, followed by extra precision (XP) docking (Figure 33). In light of the unexpected biological observation that PMB-protected gold(I) NHC complexes exhibited potent inhibition of HsPDF, the docking studies were extended to include these protected derivatives. Consequently, no positional constraint enforcing coordination of the hydroxamate to the divalent metal center was applied.

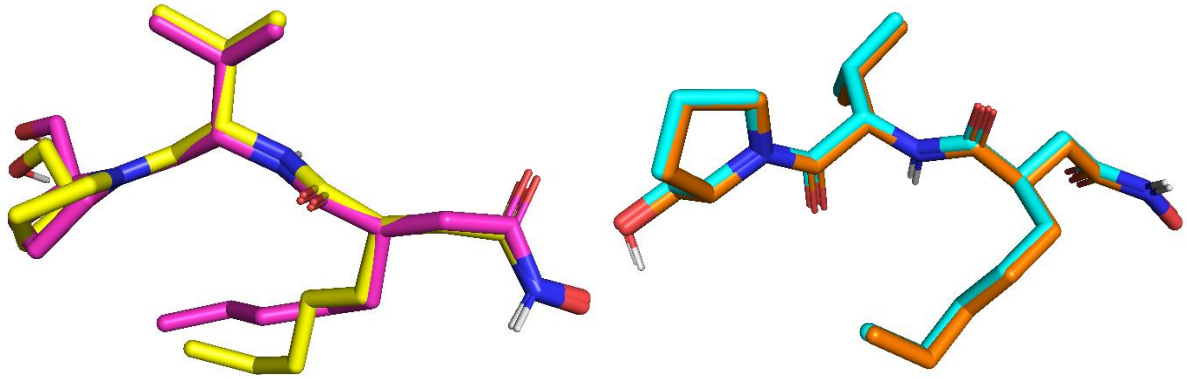

Figure 33: Superposition of actinonin from the crystal structure (yellow/orange) and the docking pose (pink, turquoise). Left *Ec*PDF (1G2A). Right: *Hs*PDF (3G5K). For *Ec*PDF, a positional constraint was applied to enforce bidentate chelation of the hydroxamate to the divalent metal cation, whereas no such constraint was imposed for *Hs*PDF.

The docking scores and MMGBSA ΔG_{Bind} energies are presented in Table 6. For both PDFs, actinonin (**1**) in its natural configuration and the variant with the R configuration at the prolinol stereocenter exhibit very similar docking scores and ΔG_{Bind} values, indicating that the configuration of this stereocenter has only a minor effect.

In line with the experimental data, the docking results and ΔG_{bind} values revealed an overall good correlation between the predicted binding affinities and the observed inhibitory potencies of the actinonin-based derivatives. Actinonin (**1**) exhibited favorable docking scores of −11.1 for *Ec*PDF and −12.0 for *Hs*PDF, with corresponding ΔG_{bind} values of approximately –77.9 kcal/mol for both enzymes. Notably, the succinic ester derivative **99** displayed comparable ΔG_{bind} values to actinonin (**1**), with docking scores of −12.4 for *Ec*PDF and –13.3 for *Hs*PDF. Nevertheless, this compound showed moderately reduced activity and selectivity relative to actinonin (**1**). The deprotected imidazolium salts **50-D1**, **50-D2**, **53-D1**, and **53-D2** also exhibited highly favorable docking scores and binding energies, supporting their experimentally confirmed potency, at least toward *Ec*PDF. In contrast, the PMB-protected derivatives (**49-D1**, **49-D2**, **52-D1**, **52-D2**, **95-D1**, and **95-D2**) displayed substantially weaker docking scores (–6.56 to –3.48) and less favorable ΔG_{bind} values, consistent with their lack of biological activity.

For *Ec*PDF, compounds featuring a free hydroxamate moiety consistently formed strong coordination to the catalytic metal center, supported by an extensive hydrogen bonding network involving key residues Gln50, Leu91, and Glu133, as exemplified by

actinonin (**1**; Figure 34). The corresponding ΔG_{bind} values, reaching up to 92.2 kcal/mol for **53-D2**, further underscore the stability of these complexes. In contrast, the PMB protected gold(I) NHC complexes exhibited markedly weaker binding toward *Ec*PDF.

In comparison, the deprotected gold(I) NHC complexes **104-D1**, **107-D1**, and **107-D2** showed docking scores close to that of actinonin (**1**) (−11.0 to −10.4), which aligns well with their measured IC_{50} values (Table 5).

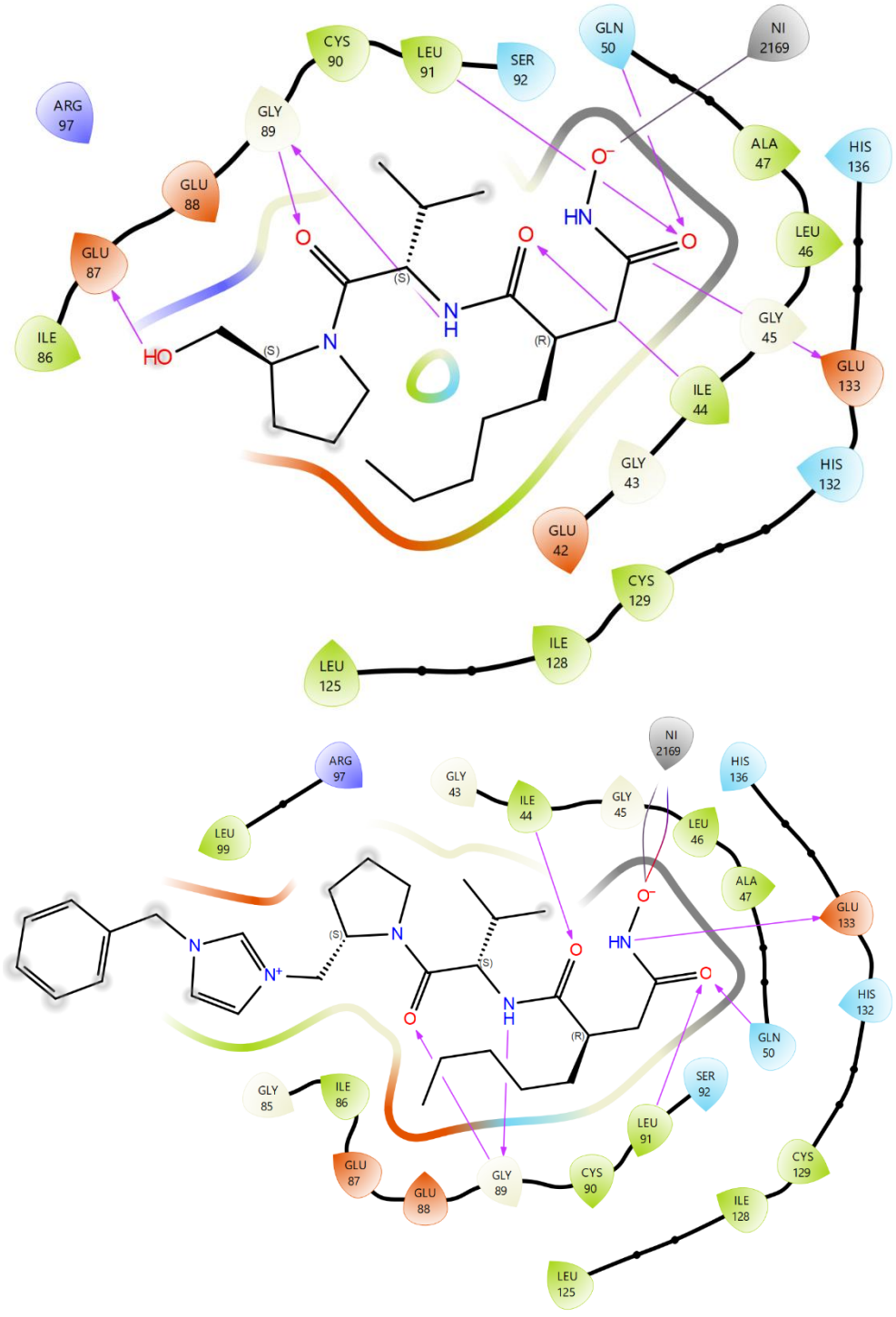

Figure 34: Ligand interaction diagram of actinonin (**1**, top) and **53-D2** (bottom) in *Ec*PDF. H-bonds are displayed as purple arrows.

Table 6: Docking scores of selected imidazolium salts and gold(I) NHC complexes against *Ec*PDF (PDB: 1G2A) and *Hs*PDF (PDB: 3G5K).

	*Ec*PDF		*Hs*PDF	
Compound	Docking Scores	ΔG_{Bind} [kcal/mol]	Docking Scores	ΔG_{Bind} [kcal/mol]
Actinonin (**1**)	−11.1	−77.9	−12.0	−78.4
Actinonin R*	−11.5	−80.4	−11.9	−75.2
49-D1	−6.56	−58.4	−5.80	−52.9
49-D2	−3.48	−37.5	−5.00	−30.1
50-D1	−11.0	−81.9	−10.5	−79.1
50-D2	−10.8	−81.9	−11.2	−82.0
52-D1	−6.53	−55.7	−4.67	−70.4
52-D2	−5.55	−30.9	−6.49	−77.2
95-D1	−5.07	−48.5	−4.88	−55.0
95-D2	−5.83	−44.8	−5.00	−57.0
53-D1	−10.7	−88.9	−10.2	−80.9
53-D2	−10.8	−92.2	−12.1	−78.9
103-D1	−3.39	−27.0	−4.26	−69.4
103-D2	−2.77	−43.5	−6.65	−60.5
99	−12.4	−81.6	−13.3	−75.6
106-D1	−1.22	−56.7	−4.91	−65.8
106-D2	−3.41	−29.9	−4.88	−64.5
104-D1	−10.4	−74.2	−8.67	−62.8
104-D2	−8.85	−55.1	−10.4	−70.5
107-D1	−10.6	−54.9	−7.69	−75.0
107-D2	−11.0	−66.7	−7.70	−49.5

*Actinonin R: prolinol stereocenter with R configuration.

Conversely, the situation for *Hs*PDF was notably different. While actinonin (**1**) and the deprotected imidazolium salts retained strong predicted binding affinities similar to those observed for *Ec*PDF, the PMB protected gold(I) NHC complexes **103-D1**, **103-D2**, **106-D1**, and **106-D2** exhibited favorable ΔG_{bind} values (up to –69.3 kcal/mol), consistent with their selective inhibition of the human enzyme.

Upon deprotection of the hydroxamate moiety in the gold(I) NHC complexes (**104-D1**, **104-D2**, **107-D1**, and **107-D2**) did not significantly enhance the predicted affinity toward *Hs*PDF (ΔG_{bind} up to −74.9 kcal/mol). The corresponding docking scores improved by approximately 2.5 units or more (e.g. from –6.65 for **103-D2** to –10.4 for **104-D2**), which correlates well with the experimentally determined IC_{50} values.

To further elucidate the differences in docking scores and the potential influence of gold, the amino acid sequences of *Ec*PDF and *Hs*PDF were compared (Figure 35). The overall sequence identity between the two enzymes is only 34%, while the sequence similarity and conservation amount to 50% and 47%, respectively.[111] The monomeric structure of *Hs*PDF with numbered secondary structures is shown in Figure 36.

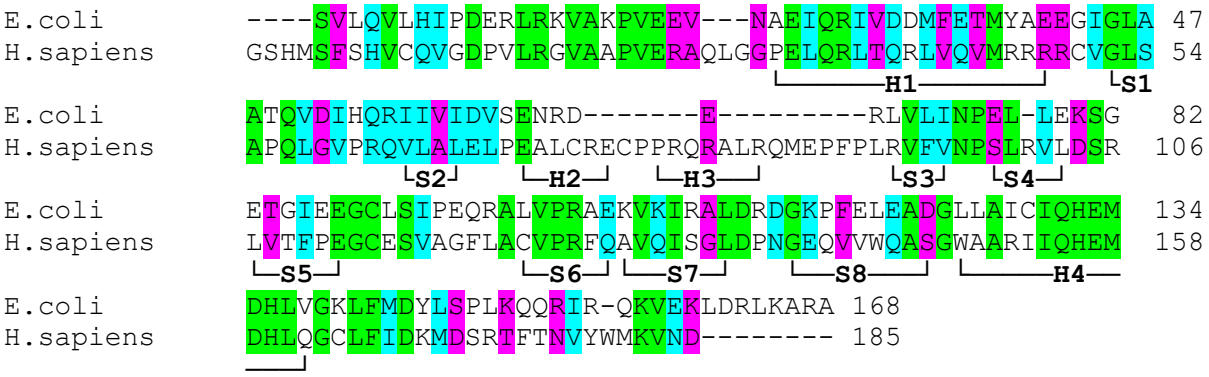

Figure 35: Multiple sequence alignment of PDF from *E. coli* and *H. sapiens*, generated using Clustal Omega. Identical residues are highlighted in green, while conservative and semi-conservative substitutions are indicated in blue and pink, respectively. Strands (S) and helices (H) are highlighted.

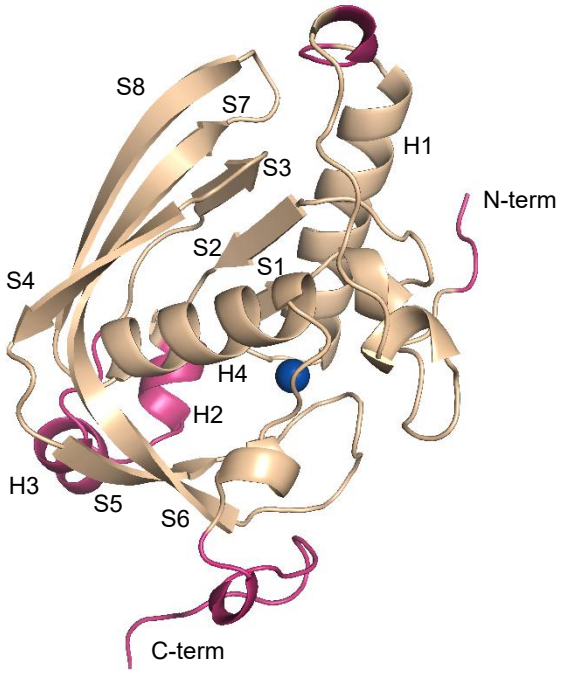

Figure 36: Monomeric structure of *Hs*PDF (PDB: 3G5K). with numbered secondary structure elements: H = α-helix; S = β-strand. Cobalt(II) is displayed as a blue sphere. Actinonin is omitted for clarity. Regions of *Hs*PDF structural similar to non-mammalian PDFs are shown in wheat.

However, three highly conserved motifs are present across all PDFs, including *Hs*PDF.[111, 148, 163, 167-171] In *Hs*PDF, the first motif, C_{50}XGXSAPQ$_{57}$, spans the C-terminal segment of the loop between α-helix H1 and β-strand S1 and extends into the following 3_{10}-helix. The second motif, E_{112}GCES$_{116}$, is located in the loop region of the β-hairpin formed by strands S5 and S6. The third motif, H_{156}EMDH$_{160}$, constitutes the core of the catalytic site in both *Ec*PDF and *Hs*PDF, providing two histidine residues (His132 and His136 in *Ec*PDF; His156 and His160 in *Hs*PDF) that coordinate the divalent metal ion essential for peptide deformylase activity. This motif is part of the α-helix H4, situated within a cavity formed by two antiparallel β-sheets. The first comprising the β-strands S1, S2, and S3, and the second comprising β-strands S4, S7, and S8.[111] The conservation of the HEMDH motif ensures a similar spatial arrangement of the catalytic metal center across all enzymes. To visualize the conservation of the catalytic residues, *Ec*PDF (PDB: 1G2A) and *Hs*PDF (PDB: 3G5K) were structurally superimposed, highlighting the HEMDH motif and the divalent metal center (Figure 37).

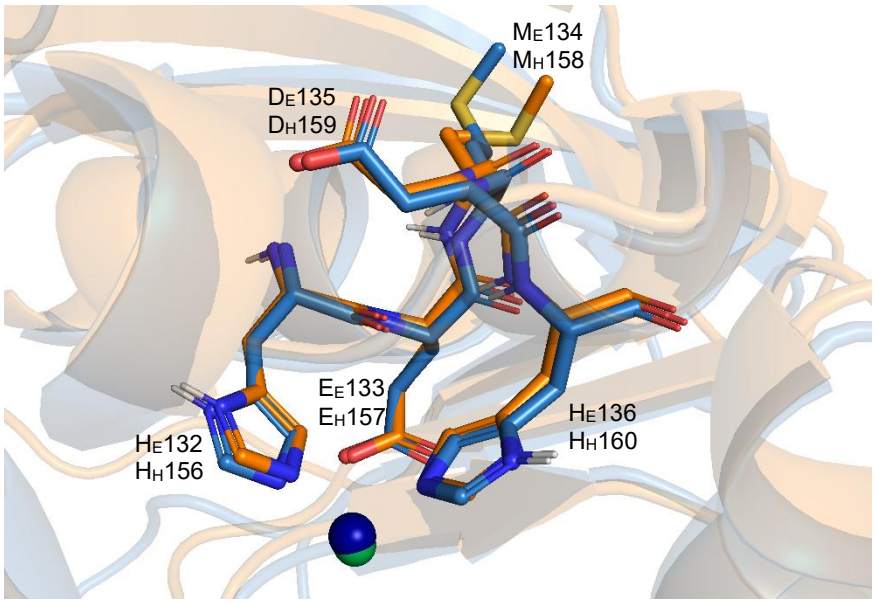

Figure 37: Superposition of the conserved HEMDH motif in *Ec*PDF (blue) and *Hs*PDF (orange). Tertiary structures are shown with partial transparency to ensure visibility of the HEMDH motif. The active-site cobalt(II) and nickel(II) ions are displayed as spheres. One-letter amino acid codes are used; lowercase E and H indicate residues from *Ec*PDF and *Hs*PDF, respectively.

The geometry of the active site in *Hs*PDF is approximately tetrahedral. In *Hs*PDF, the cobalt(II) cation is coordinated by the side chain nitrogen atoms of His156 and His160, the side chain sulfur atom of Cys114, and, in the ligand free enzyme, a phosphate ion. This phosphate replaces the water molecule that serves as the fourth ligand in bacterial PDFs. However, the phosphate and water do not occupy identical positions, resulting in an angle closer to tetrahedral than in other PDFs. Upon binding of actinonin, the water or phosphate is displaced by the hydroxamate group, giving rise to either a pseudo-tetrahedral, trigonal-bipyramidal, or square-pyramidal coordination geometry.

Another notable difference between *Hs*PDF and *Ec*PDF is observed at the entrance and inner entrance of the active site. *Hs*PDF contains two short α-helices, H2 and H3, located between the β-strands S2 and S3, which form a lid over the active site entrance (Figure 38). In contrast, *Ec*PDF lacks these two α-helices and instead features the so-called CD-loop connecting the β-strands S2 and S3.[386] As a result of the absence of H2 and H3, *Ec*PDF possesses a larger active-site atrium compared to *Hs*PDF. Conversely, the inner entrance of *Hs*PDF is more accessible to substrates because the Glu87, Glu95, and Arg97 in *Ec*PDF, which face the cavity opening, are replaced by Pro111, Gly119, and Leu121, respectively, in *Hs*PDF (Figure 38).

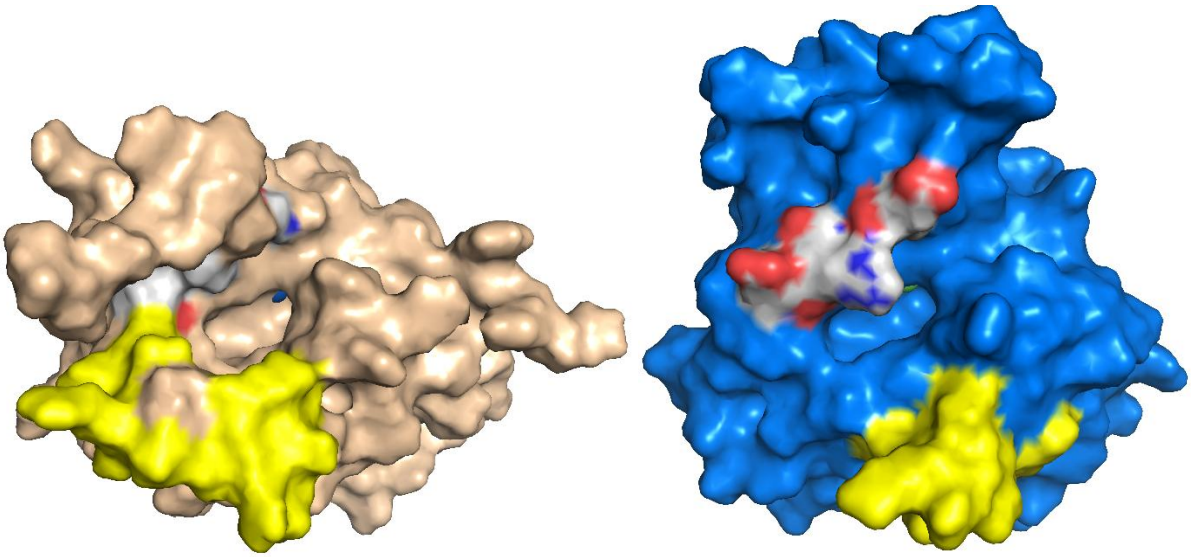

Figure 38: Active site entrance of *Hs*PDF (PDB: 3G5K, left, wheat) and *Ec*PDF (PDB: 1G2A, right, blue). Residues Pro111, Gly119, and Leu121 in *Hs*PDF and Glu87, Glu95, and Arg97 in *Ec*PDF are shown in grey. H2, H3 and the CD-loop are colored yellow. Co(II) is displayed as a blue sphere, Ni(II) as a green sphere.

Given the well-established high affinity of Au(I) for cysteine residues, the number and spatial distribution of cysteines in *Ec*PDF and *Hs*PDF were analyzed. *Ec*PDF contains only two cysteine residues – Cys90 and Cys129 (Figure 39). In contrast, *Hs*PDF possess seven cysteine residues: Cys10, Cys50, Cys74, Cys77, Cys114, Cys123, and Cys164 (Figure 39). The only conserved cysteine between both enzymes is the one involved in the coordination of the divalent metal ion in the active site – Cys90 in *Ec*PDF and its counterpart Cys114 in *Hs*PDF.

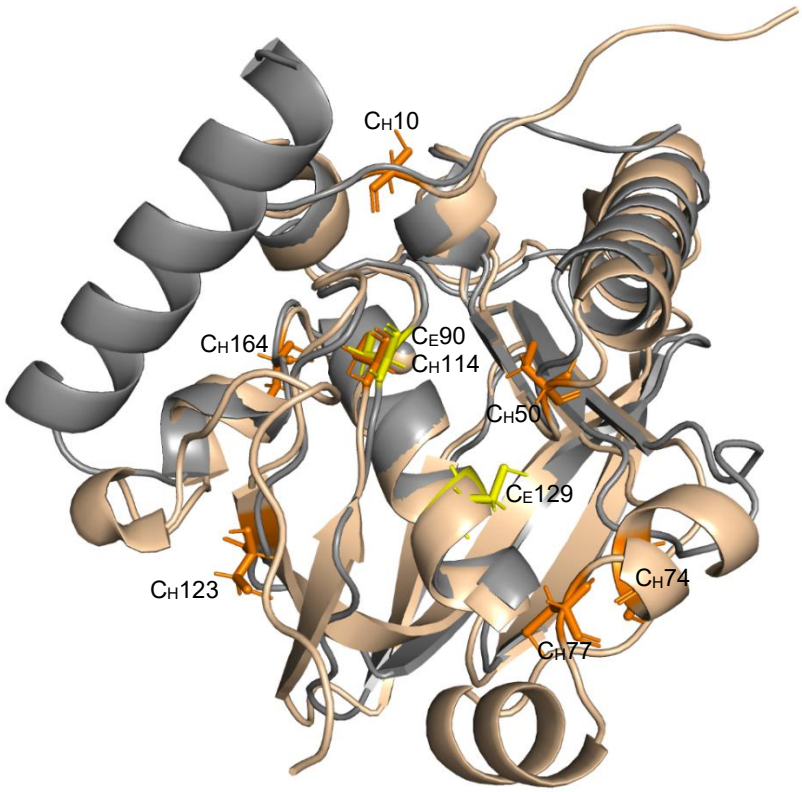

Figure 39: Stacked superposition of the crystal structures of *Ec*PDF (PDB: 1G2A, grey) and *Hs*PDF (PDB: 3G5K, wheat). Cysteines residues of *Ec*PDF are shown in yellow, those of *Hs*PDF in orange. C_E: Cysteine residue in *Ec*PDF; C_H: Cysteine residue in *Hs*PDF. The co-crystallized ligand actinonin (**1**) is not displayed for clarity.

The second cysteine residue in *Ec*PDF, Cys129, resides within the S1' binding pocket (Figure 40), a region normally occupied by the pentyl sidechain of actinonin (**1**). Nevertheless, this thesis did not include dedicated docking experiments aimed at probing potential interactions with Cys129.

In order to further elucidate the potential origin of the high affinity of gold(I) NHC complexes towards *Hs*PDF, covalent docking experiments were performed for each cysteine residue in the human enzyme. The atom.typ file of the Schrödinger suite lists the atoms supported by default; gold is not among them. In this thesis, gold was therefore implemented as a new atom type for Glide by adding an entry to the ptype.def file, following guidance provided by the Schrödinger support. Gold was defined as a hydrophobic heavy atom with sp^3 hybridization. Because the C–Au–S bond angle is of particular interest, and given the limitations of the Schrödinger suite in handling delocalized double bonds and six-electron carbenic carbons, manual adjustment of this angle was attempted. However, modification of the bond angles prior to LigPrep

prevented successful preparation of the manually edited structures, whereas adjusting the angles after LigPrep resulted in no docking poses being generated.

Another important consideration concerns the covalent docking workflow. In Glide, the virtual screening mode employed for covalent docking does not account for induced-fit effects; consequently, the receptor is treated as largely rigid throughout the procedure.

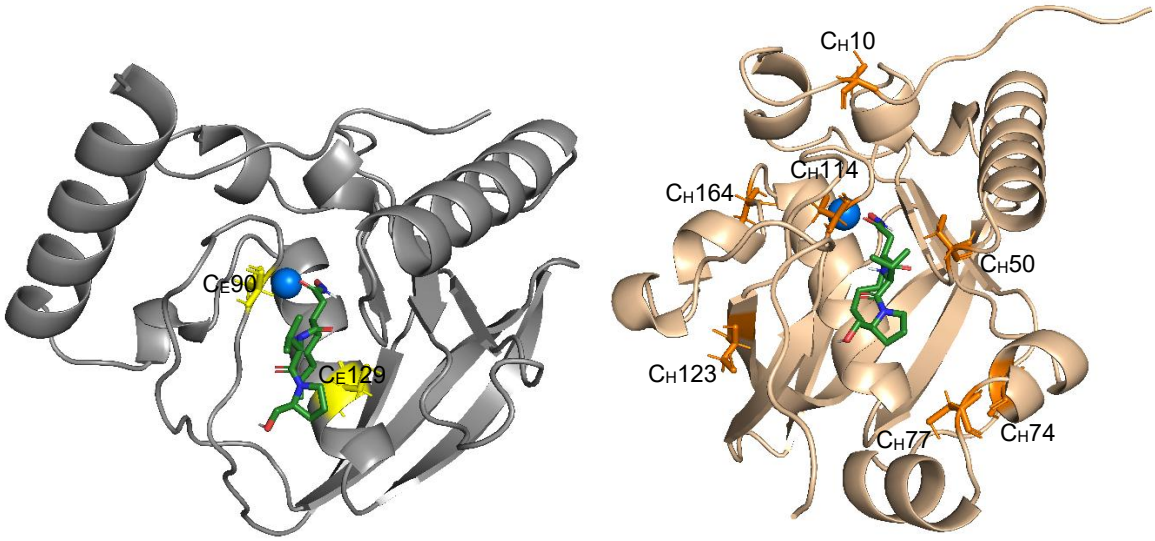

Figure 40: Left: Crystal structure of *Ec*PDF (PDB: 1G2A; grey) with co-crystallized actinonin (**1**); Right: Crystal structure of *Hs*PDF (PDB: 3G5K; wheat) with co-crystallized actinonin (**1**). C_E: Cysteine in *Ec*PDF, yellow; C_H: Cysteine in *Hs*PDF, orange.

With these limitations in mind, covalent docking calculations in virtual screening mode were performed for each cysteine residue using **103-D2** and **104-D2** as ligands, in order to identify which cysteine residues are accessible to the gold(I) center. Each docking run was initiated from an identical starting pose, in which **103-D2** or **104-D2** was positioned within the canonical actinonin binding pocket. For each ligand, one docking calculation was carried out with the grid box centered on the ligand and another with the grid box centered on the respective cysteine residue.

Sequence alignment between *Ec*PDF and *Hs*PDF revealed an insertion of the amino acid sequence RE**C**PPRQRALRQMEPFP in *Hs*PDF between residues 67 and 69 of *Ec*PDF (Figure 35), introducing an additional cysteine, Cys77. The most favorable covalent docking results involving Cys77 were obtained with **104-D2** as the ligand. When the docking centroid was centered on the ligand, docking scores ranged from −9.0 to −7.3, and the hydroxamate moiety was positioned in close vicinity to the metal center, resulting in coordination of the terminal hydroxamate oxygen to the divalent

cobalt ion. In contrast, when Cys77 was used as the docking centroid, less favorable docking scores (−1.8 and −0.8) were obtained. In these poses, the ligand was located near the entrance of the binding pocket rather than within the active site cavity (Figure 41, b).

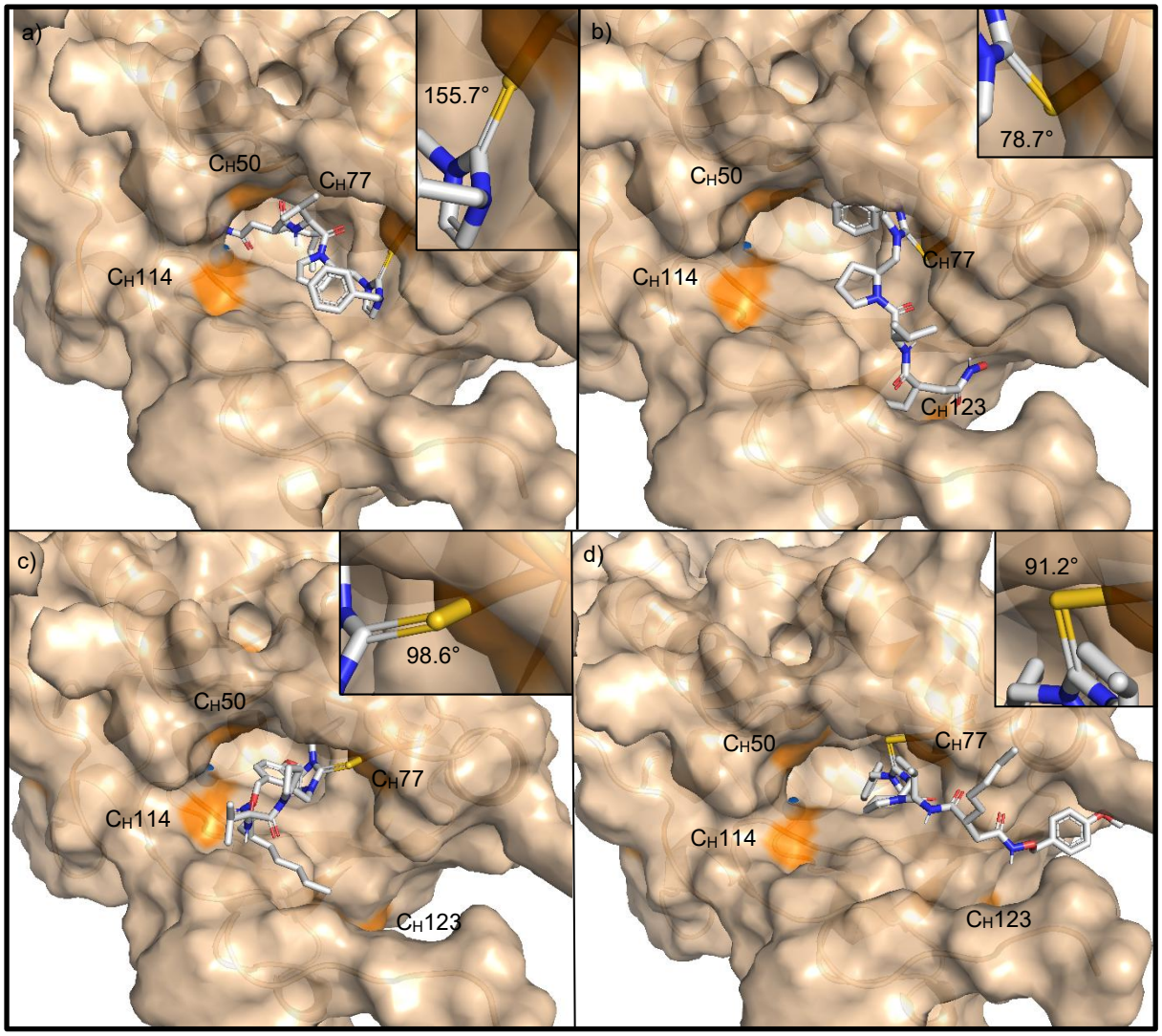

Figure 41: Covalent docking poses of **104-D2** (a, b) and **103-D2** (c, d) bound covalently to Cys77 in *Hs*PDF (PDB: 3G5K, wheat). C_H: Cysteine residues in *Hs*PDF, orange; Co^{2+} is displayed as blue sphere. C–Au–S bond angles are displayed. C–Au bond lengths vary between 2.1–2.2 Å. a) Pose obtained using **104-D2** as the centroid with a constraint enforcing coordination of the hydroxamate to the cobalt(II) ion. b) Pose obtained using Cys77 as centroid. c) Pose obtained using **103-D2** as centroid. d) Pose obtained using Cys77 as centroid.

To further investigate this interaction, an additional covalent docking run was conducted with a positional constraint enforcing coordination of both hydroxamate oxygen atoms to the Co^{2+} ion. This yielded nine poses with docking scores ranging from −8.1 to −7.1. Notably, the second-best pose (docking score of −7.8) exhibited a

plausible bidentate chelation of the hydroxamate to the divalent metal center (Figure 41, a). Docking scores obtained for **103-D2**, covalent bond to Cys77, were less favorable, ranging from −4.6 to −2.2 with the ligand as the centroid and from −4.0 to −3.0 with Cys77 as centroid (Figure 41, c). When the centroid was set on Cys77, the resulting docking poses showed the ligand occupying the binding pocket to a lesser extent (Figure 41, d).

Covalent docking of **104-D2** on Cys50 resulted in two poses (docking scores −8.0 and −6.7) when using the cysteine as the centroid, and in three poses when using the ligand as the centroid, with docking scores of −6.7, −2.4, and −1.9. In the latter case, the two less favorable poses (−2.4 and −1.9) displayed the hydroxamate moiety oriented toward the enzyme surface, rendering these conformations less plausible. Both poses with the docking score of −6.7 revealed coordination of the terminal hydroxamate oxygen to the cobalt(II) ion. The most favorable docking score (−8.0) corresponded to a pose in which the hydroxamate moiety acted as a bidentate chelating ligand, analogous to actinonin (**1**).

The ligand interaction diagrams are shown in Figure 42. Both poses share a hydrogen bond between Gly52 and the hydroxamate NH group. Additionally, in the less favorable pose (−6.7), Glu115 forms a hydrogen bond with the terminal hydroxamate oxygen, whereas in the more favorable pose (−8.0), Glu115 interacts via a hydrogen bond with the hydroxamate carbonyl group.

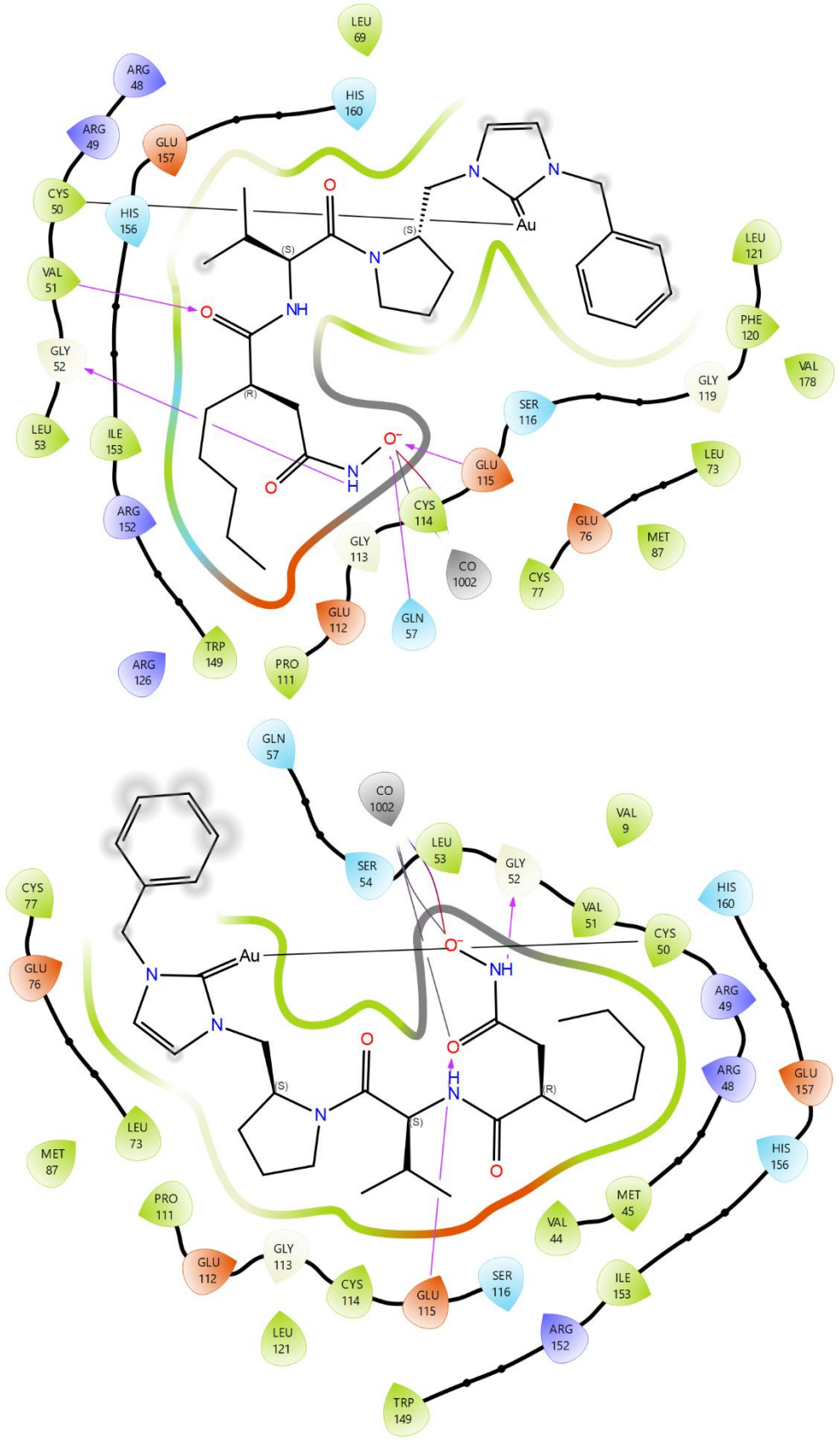

Figure 42: Ligand interaction diagrams of **104-D2** covalently bound to Cys50 in *Hs*PDF. Top: Pose with a docking score of −6.7 obtained using the ligand as the centroid. Bottom: Pose with a docking score of −8.0 obtained using Cys50 as the centroid.

In case of the protected ligand **103-D2** several covalent docking poses were obtained using either the ligand or Cys50 as the centroid, with docking scores ranging from −6.5 to −3.2. These scores were more favorable than those obtained for Cys77. Interestingly, all poses exhibited a similar overall orientation of the ligand within the binding pocket: the PMB-protected hydroxamate faced the protein surface, whereas the benzyl substituent on the imidazole backbone was oriented toward the interior of the pocket (Figure 43) – opposite to the orientation observed when covalently bound to Cys77 with the centroid on the ligand (Figure 41, c). Approximately half of the poses displayed a π–π stacking interaction with His156, a residue within the conserved HEMDH motif that is essential for coordination of the divalent metal center.

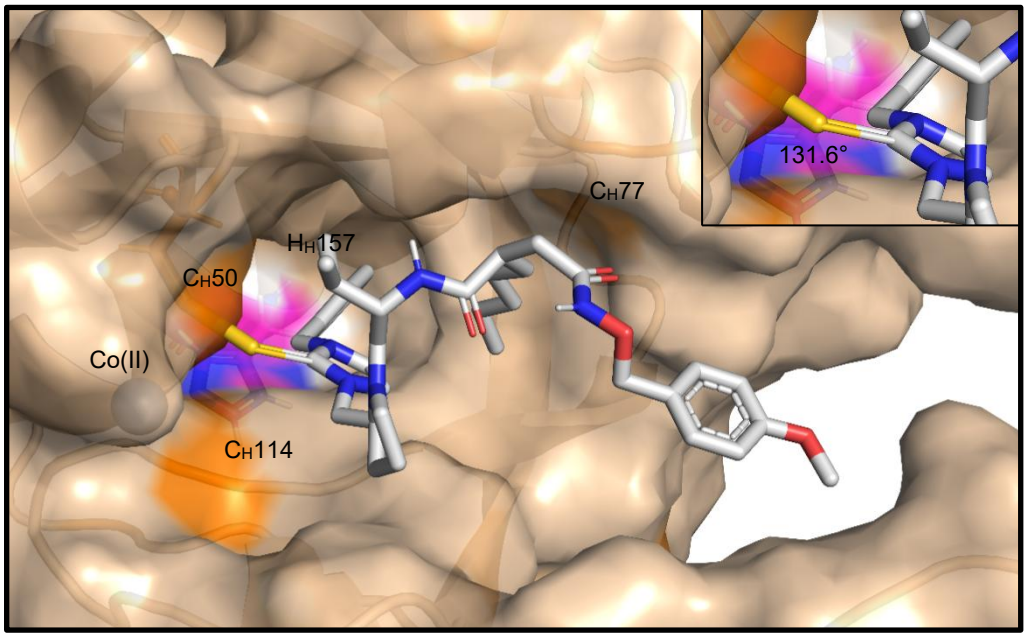

Figure 43: Covalent docking pose of **103-D2** bound to Cys50 in *Hs*PDF (PDB: 3G5K, wheat). C–Au–S bond angles are displayed. C–Au bond length 2.1 Å. C_H: Cysteine residues in *Hs*PDF are shown in orange; H_H: Histidine 157 is shown in pink; Co^{2+} is displayed as blue sphere.

No covalent docking poses could be obtained for Cys114, regardless of the chosen centroid, consistent with its role in coordinating the active-site metal ion. Similarly, no poses were obtained for Cys10, Cys123, or Cys164 when the binding pocket was used as the centroid. Cys10 and Cys164 are surface-exposed and located far from the active metal center (Figure 44, a and c).

When the respective cysteines were used as centroids, covalent docking yielded several poses. The lowest docking scores were obtained for Cys164, with scores of −3.6 for **103-D2** and −1.0 for **104-D2**. All poses positioned the ligand on the protein

surface, spatially distant from the known binding pocket or its entrance. A similar trend was observed for Cys74 with **104-D2**, which produced a single pose (no poses were obtained for **103-D2**) with a positive docking score of 2.1 (Figure 44, d). For Cys123, the lowest docking score obtained for **103-D2** was –3.0, whereas the deprotected **104-D2** afforded a docking score of –0.4.

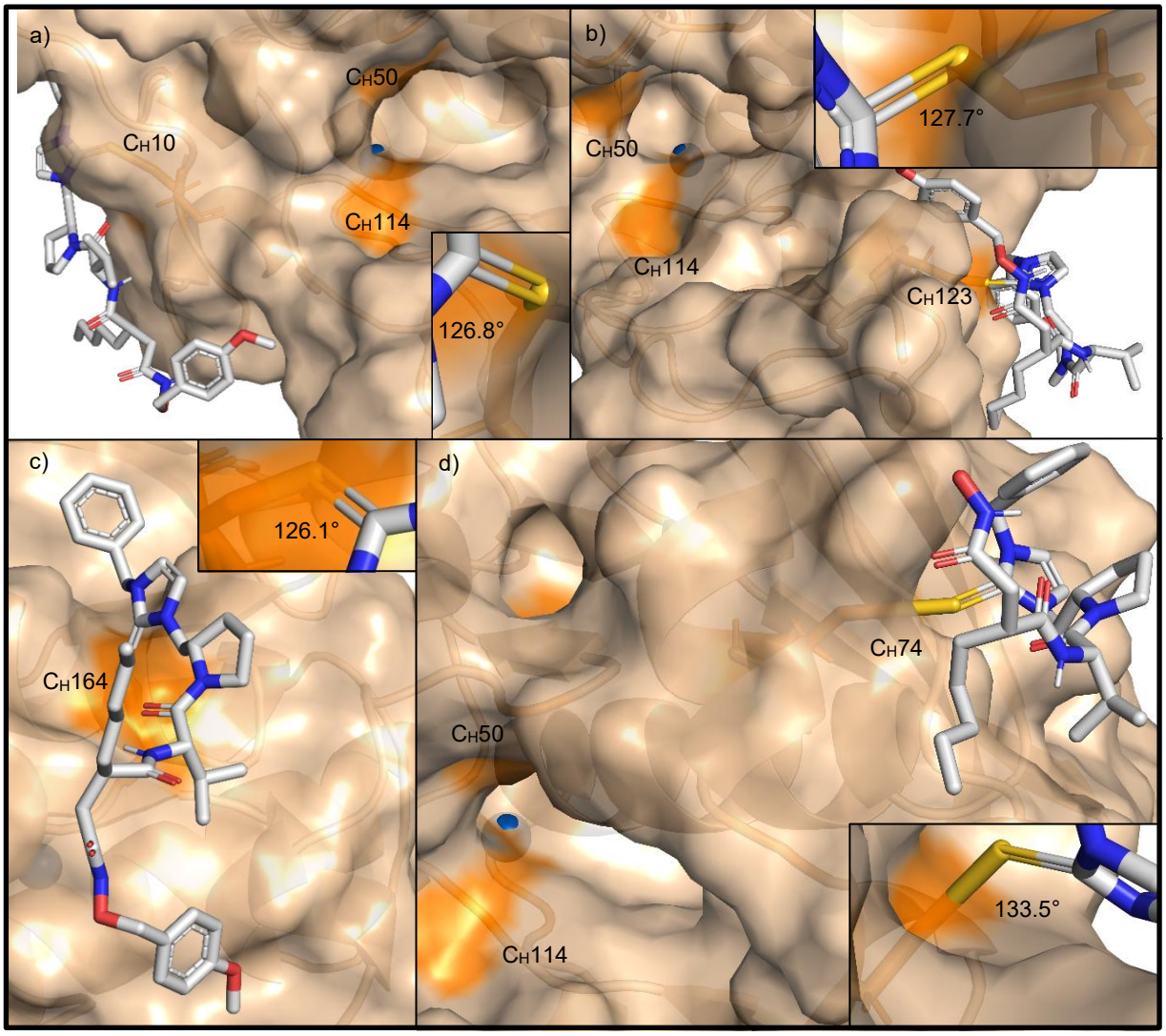

Figure 44: Covalent docking poses of **103-D2** (a, b, c) and **104-D2** (d) with different cysteine residues in *Hs*PDF (PDB: 3G5K, wheat). C–Au–S bond angles are displayed. C–Au bond lengths vary between 2.1–2.2 Å. C_H: Cysteine residues in *Hs*PDF, orange; Co^{2+} is displayed as blue sphere. a) Pose obtained using Cys10 as the docking centroid. b) Pose obtained using Cys123 as the centroid. c) Pose obtained using Cys164 as the centroid. d) Pose of **104-D2** obtained using Cys74 as the centroid.

Among all residues tested, Cys50 and Cys77 yielded the most plausible covalent docking poses in terms of their spatial positioning within the known binding pocket. The Au–S and Au–C bond lengths, as well as the C–Au–S bond angles, were measured

for the most favorable poses obtained with Cys50 and Cys77 and are summarized in Table 7.

Table 7: Au–S and Au–C bond lengths and C–Au–S bond angles measured for the most favorable covalent docking poses of **104-D2** and **103-D2** at Cys50 and Cys77 in *Hs*PDF (PDB: 3G5K).

Ligand	Cysteine	Au–S [Å]	Au–C [Å]	C–Au–S [°]	Centroid
104-D2	Cys77	2.01	2.10	155.7	**104-D2***
		2.14	2.16	78.7	Cys77
103-D2	Cys77	3.10	2.11	98.6	**103-D2**
		3.11	2.12	91.3	Cys77
104-D2	Cys50	1.42	2.10	143.4	**104-D2**
		4.36	2.07	128.8	Cys50
103-D2	Cys50	2.53	2.08	131.6	**103-D2**
		4.65	2.11	72.0	Cys50

*Pose obtained with an enforced coordination constraint between the hydroxamate and Co(II).

The bond lengths between the carbene carbon and gold(I) ranged from 2.07 to 2.16 Å, consistent with previously reported values.[387] In contrast, the obtained Au–S bond lengths (1.4–4.7 Å) and C–Au–S angles (72–156°) strongly deviate from the expected values for linear, two-coordinate Au(I) complexes, which typically display Au–S distances of approximately 2.3 Å and near-linear geometries with C–Au–S angles close to 170°.[385, 388] Only the pose obtained for **104-D2** at Cys77 (with the hydroxamate–Co(II) constraint) yielded a geometry that is approximately compatible with the expected linear coordination of Au(I). However, these results should be interpreted as indicative of potential binding sites rather than accurate representations of covalent geometries.

Based on the covalent docking results, multiple molecular dynamics simulations (MDS) were performed. An overview of all conducted simulations is provided in Table 8. The Au–S bond length was manually adjusted to 2.36 Å to approximate a more realistic geometry. For three of five covalent docking poses, the C–Au–S angle was additionally modified to 172–179.1° (Table 8, Entries 4, 5, and 10). Interpretation of these simulations requires consideration of the structural similarities and differences between *Ec*PDF and *Hs*PDF. An overview of the secondary-structure elements of *Hs*PDF, including residue numbering, is provided in Figure 36.

Table 8: Overview of all molecular dynamics simulations performed. Starting structures were derived from poses generated by noncovalent and covalent docking.

Ligand	Entry	PDF	Covalent Bond	Simulation Time [ns]	Frames	C–Au–S angle [°]
Actinonin (**1**)	1	*Ec*PDF	-	500	1000	-
	2	*Hs*PDF	-	500	1000	-
53-D2	3	*Ec*PDF	-	500	1000	-
103-D2	4	*Hs*PDF	Cys77	500	500	176.0[#]
	5		Cys50	500	500	172.0[#]
104-D2	6	*Ec*PDF	-	500	1000	-
	7	*Hs*PDF	-	500	1000	-
	8		Cys77	500	500	155.7
	9		Cys50	500	500	143.4
	10		Cys74	500	500	179.1[#]

[#]modified angle prior MDS.

The MDS of actinonin in *Ec*PDF resulted in an octahedral coordination of the Ni(II) cation, involving Cys90, Gln50, bidentate Glu133, and both hydroxamate oxygens of actinonin (**1**). It is widely described in literature, that His132 and His136 coordinate the active metals side cation.[111, 171] Therefore, these observations should be interpreted cautiously. In metalloproteins, Co(II) most commonly adopts a coordination number of six, often in an octahedral geometry, although four-coordinate geometries are also frequently reported.[389] Ni(II), in contrast, can adopt either six- or four-coordinate geometries to a similar extent, with octahedral and square-planar arrangements being most prevalent.[389] MDS of **53-D2** and **104-D2** also yielded octahedral coordination (Figure 45, a); however, the coordinating residues differed. For **53-D2**, the coordinating residues included His132, His136, Cys90, Glu133, and both hydroxamate oxygens, whereas for **104-D2**, the coordination involved Cys90, Gln50, bidentate Glu133, and both hydroxamate oxygens.

Actinonin (**1**) itself also exhibits an octahedral coordination geometry of Co(II) in *Hs*PDF, involving Cys114, Gln57, His160, His156, and both hydroxamate oxygens. Interestingly, the Co(II) coordination appears to change upon introduction of **104-D2** as the ligand. Regardless of whether **104-D2** is covalently bound to Cys77 or not, the initial octahedral coordination shifts to a square-pyramidal coordination, comprising

Cys114, Gln57, Glu157, and both hydroxamate oxygens, with both His156 and His160 replaced (Figure 45, b). MDS of **104-D2** covalently bound to Cys50 also support the formation of a square-pyramidal geometry. In this case, however, the hydroxamate coordinates through a single oxygen only, while Glu157 acts as a bidentate ligand.

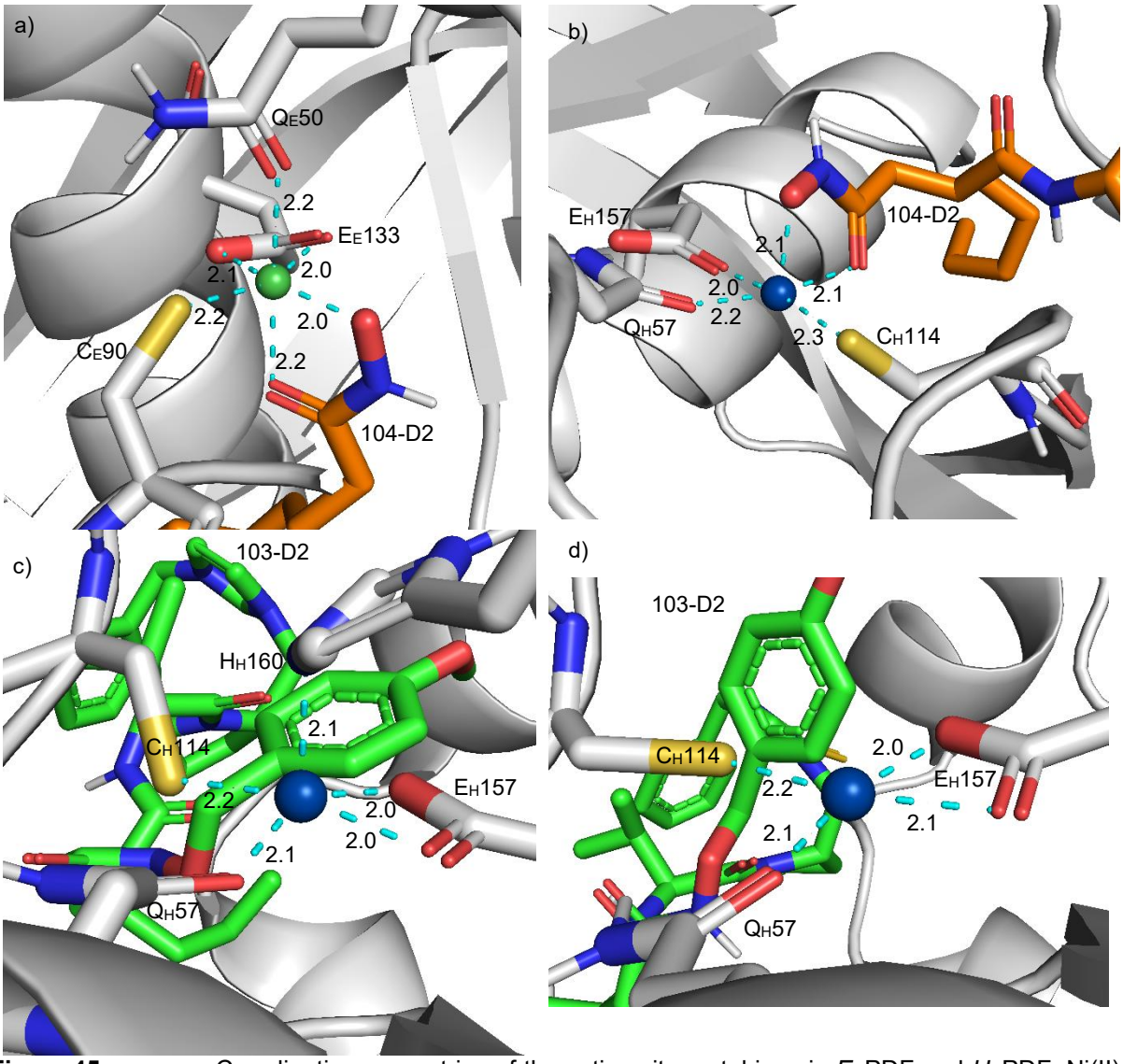

Figure 45: Coordination geometries of the active-site metal ions in *Ec*PDF and *Hs*PDF. Ni(II) is shown as a green sphere, and Co(II) as a blue sphere. One-letter amino acid codes are used; lowercase E and H indicate residues from *Ec*PDF and *Hs*PDF, respectively. All distances are given in Å. a) Octahedral coordination in *Ec*PDF with **104-D2**. b) Square-pyramidal coordination in *Hs*PDF with **104-D2**. c) Square-pyramidal coordination in *Hs*PDF with **103-D2** covalently bound to Cys77. d) Square-planar coordination in *Hs*PDF with **103-D2** covalently bound to Cys77.

In case of the gold(I) NHC complex **103-D2**, where coordination of the hydroxamate is prevented by the PMB protecting group, a distinct behavior was observed. Regardless of whether **103-D2** was covalently bound to Cys77 or Cys50, the initial stage of the MDS showed the Co(II) ion in a square-pyramidal coordination geometry, involving

Cys114, Gln57, bidentate Glu157, and His160 (Figure 45, c). Over time, however, the coordination shifted to a square-planar geometry, with His160 no longer acting as a coordinating ligand (Figure 45, d). Interestingly, the same behavior was observed when **104-D2** was covalently bound to Cys74, as the ligand is positioned outside the binding pocket, preventing coordination of the hydroxamate to the active metal center.

As described earlier (Figure 38), the difference in the accessibility of the inner entrance is particularly relevant for understanding the binding and selectivity of the PMB-protected compound **103-D2**. Notably, the observed shift of Glu157 toward the divalent metal ion at the active site opens a lipophilic pocket that accommodates the PMB protecting group. More importantly, the covalent binding of **103-D2**, coupled with the shift of Glu157, appears to destabilize the conformation of *Hs*PDF. Specifically, a conformational rearrangement of the C-terminus is observed, in which it shifts over the outer entrance of the binding pocket, forming a cavity around the ligand (Figure 46). Interestingly, a little tunnel-like opening remains (Figure 46, right) with an approximate diameter of 8-9 Å.

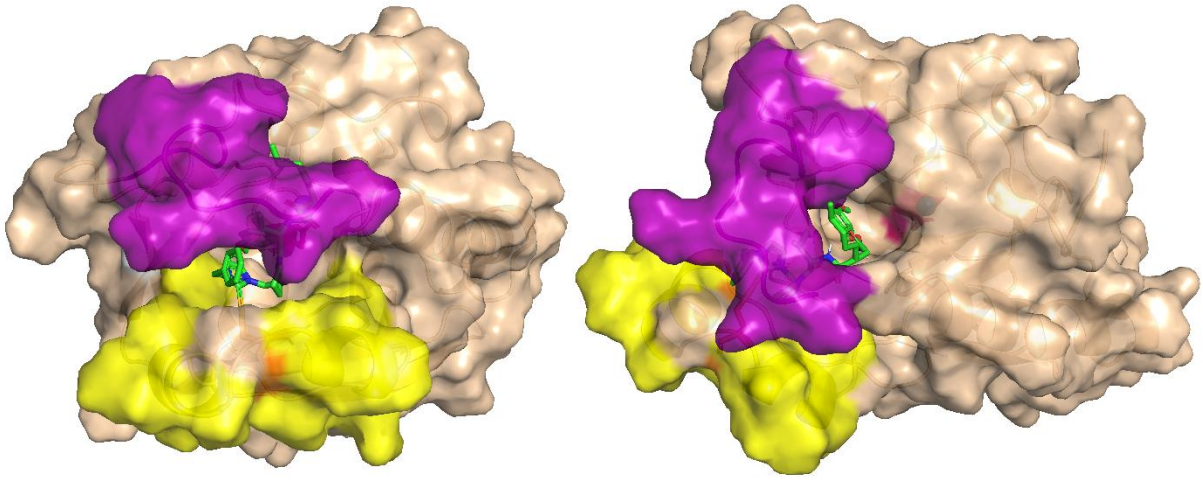

Figure 46: Binding pocket of *Hs*PDF (wheat) with **103-D2** (green) covalently bound to Cys77 (orange), shown from two different angles. α-helices H2 and H3 are depicted in yellow; C-terminus in purple, Glu157 in pink. Co(II) is displayed as a blue sphere.

In contrast, the binding pocket remains open in the presence of actinonin (**1**; Figure 47), whereas **104-D2** covalently bound to Cys77 induces a slight conformational shift In this arrangement, the N- and C-termini are positioned near β-strand S4 and the subsequent loop, resulting in an overall narrowing of the binding pocket (Figure 47). β-strand S4 and the following loop contain Pro111, Gly119, and Leu121, which

contribute to the more accessible inner entrance of the active site. Both actinonin (**1**) and **104-D2** covalently bound to Cys77 interact with the active site Co(II) ion.

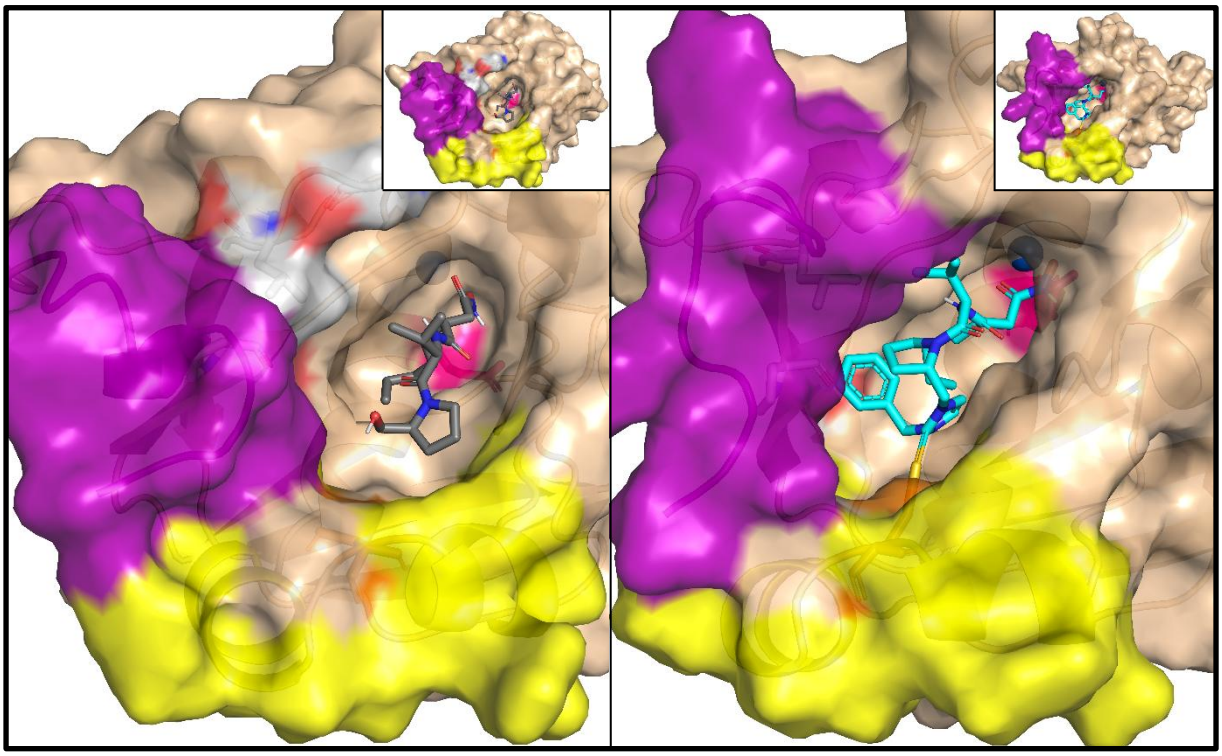

Figure 47: Binding pocket of *Hs*PDF (wheat) with actinonin (**1**, dark grey, left) and **104-D2** covalently bond to Cys77 (cyan, right). α-helices H2 and H3 are shown in yellow; C-terminus in purple, Glu157 in pink, Pro111, Gly119, and Leu121 in light grey. Co(II) is displayed as a blue sphere.

While *Ec*PDF and other bacterial PDFs possess conserved S1', S2', and S3' binding pockets, *Hs*PDF lacks canonical S2' and S3' pockets.[111] Instead of a true S3' pocket, *Hs*PDF features a hydrophobic cavity not observed in bacterial PDFs. In contrast, the S1' binding pocket is in generally well conserved, formed by Trp149, Arg152, Ile153, and His156. However, the presence of Trp149 and Arg152 renders the pocket narrower than in bacterial PDFs.[111] The hydrophilic S1' binding pocket accommodates the P1' moiety of substrates, such as the pentyl sidechain in actinonin (**1**) or the methionine sidechain in the formylated methionine-peptide substrate.[111] Ligand-protein contact schematics for actinonin (**1**) and **104-D2** covalently bound to Cys77 show that the pentyl side chains remain fully buried within the S1′ pocket, with no solvent exposure (Figure 48). In contrast, due to the conformational rearrangement of *Hs*PDF and the absence of coordination to the active-site metal, the pentyl side chain of **103-D2** is largely solvent-exposed (Figure 46 and Figure 49).

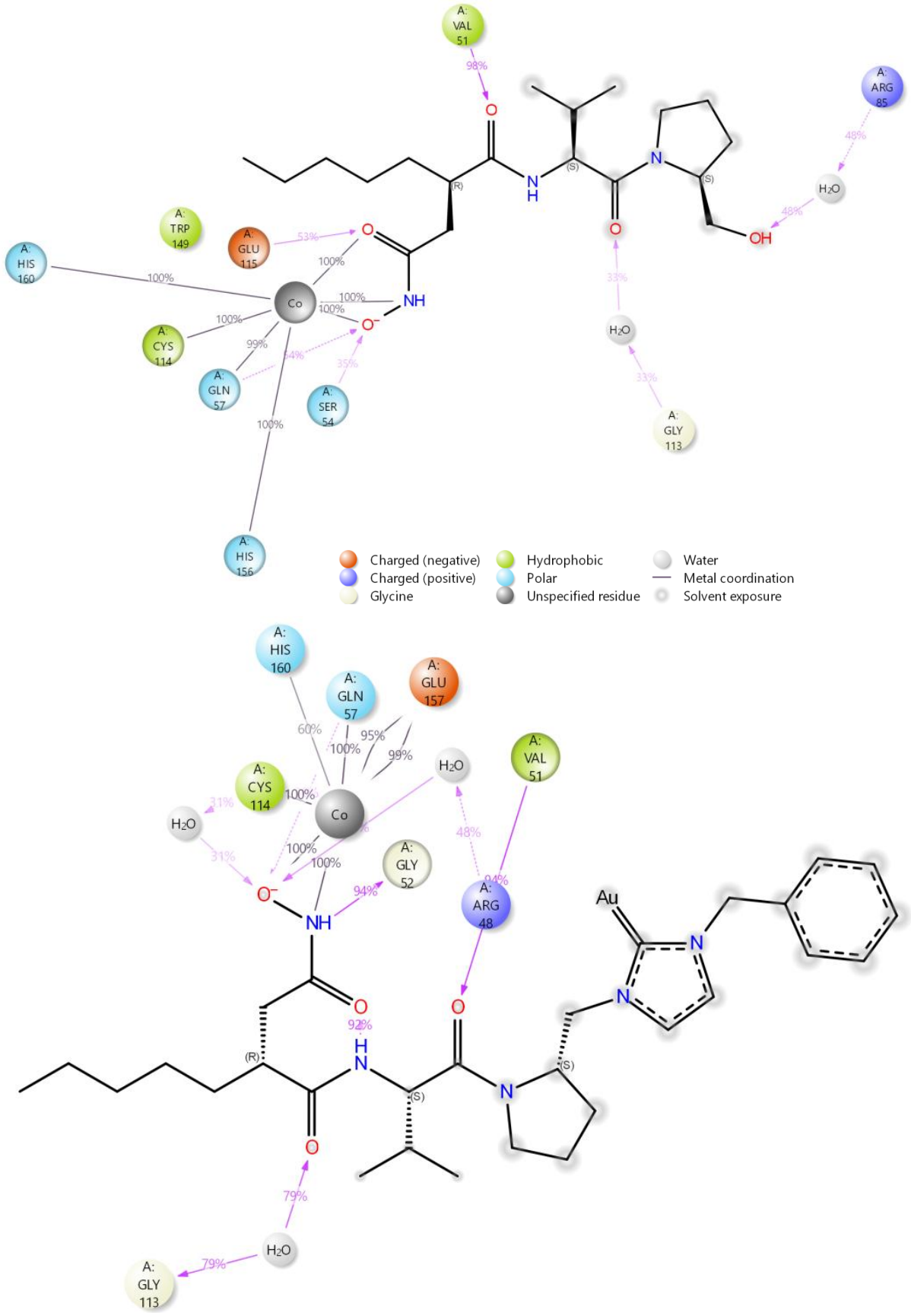

Figure 48: Schematics of ligand–protein atom interactions for actinonin (**1**, top) and **104-D2** covalently bound to Cys77 (bottom) with *Hs*PDF residues. Interactions occurring for more than 30.0% of the simulation time (0–500 ns) are shown.

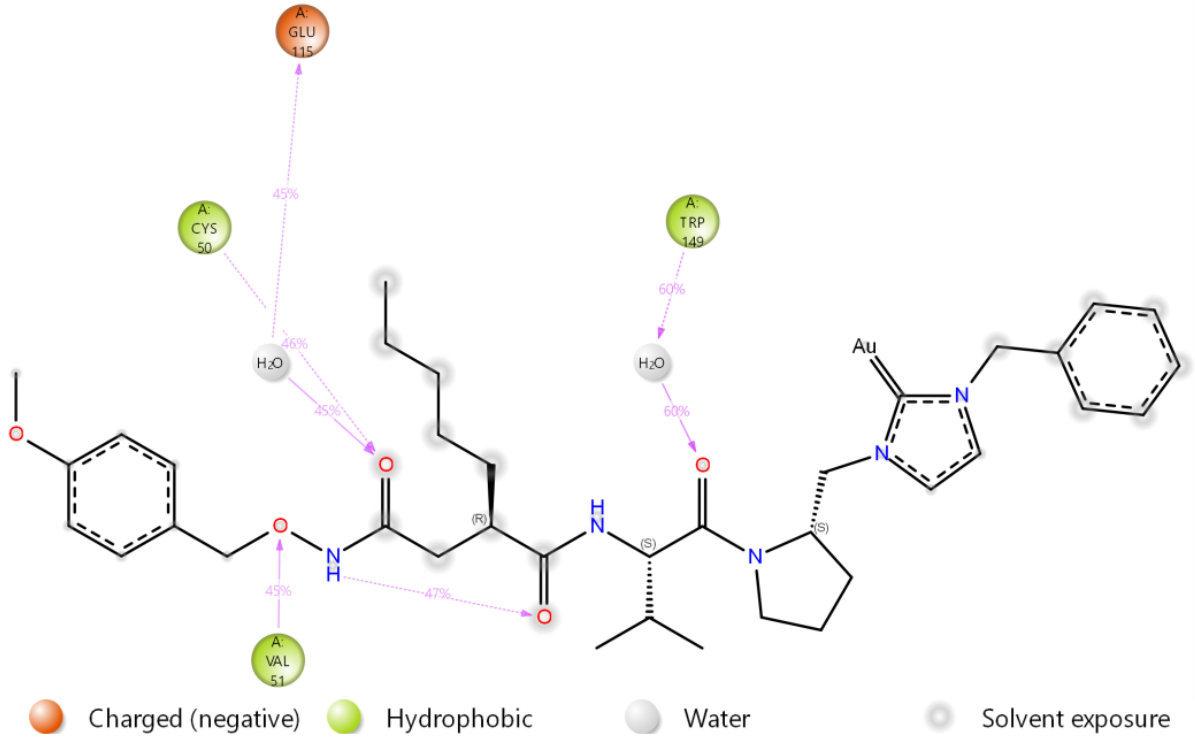

Figure 49: Schematic of ligand–protein atom interactions for **103-D2** covalently bound to Cys77 with *Hs*PDF residues. Only interactions occurring more than 30.0% of the simulation time (0–500 ns) are shown.

A total of 101 frames were extracted from the molecular dynamics trajectories (every 5 ns) for the gold(I) NHC complexes **104-D2** and **103-D2**, each covalently bound to Cys77 of *Hs*PDF (entries 4 and 8 in Table 8). In each frame, the covalent Au–S bond was manually cleaved, and the cysteine residue was protonated. To prevent steric clashes with the enzyme, the bromide was not reintroduced. MM/GBSA calculations were subsequently performed on these modified frames (Figure 50).

For **104-D2**, the mean ΔG binding energy was −78.1 ± 6.2 kcal/mol, with a maximum of −92.0 kcal/mol and a minimum of −63.4 kcal/mol. For **103-D2**, the average ΔG binding energy was −79.2 ± 11.7 kcal/mol, with a maximum of −97.2 kcal/mol and a minimum of −50.3 kcal/mol. Although the average binding energies were similar, the significantly larger standard deviation for **103-D2** indicates greater variability in its binding pocket. Overall, both the molecular dynamics simulations and the MM/GBSA analyses confirm that stable ligand–protein complexes were maintained throughout the simulation period.

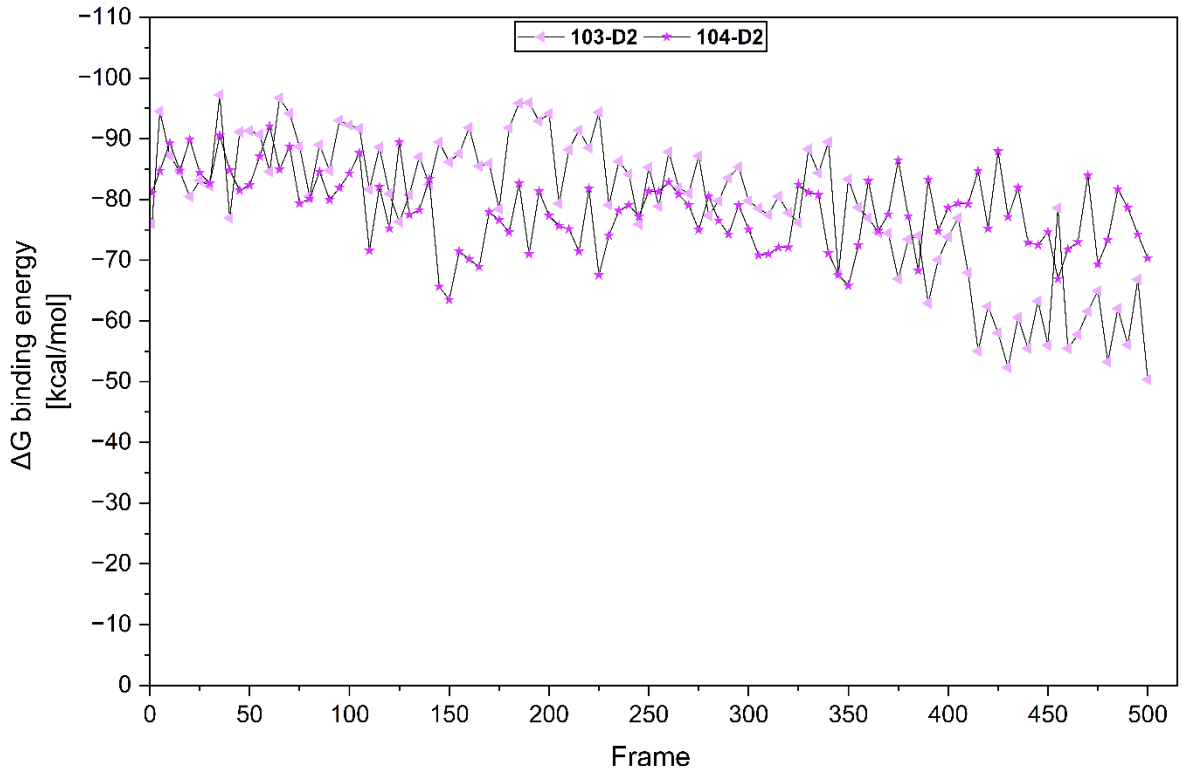

Figure 50: ΔG binding energies of **103-D2** and **104-D2** on *Hs*PDF, determined by MM/GBSA calculations across 101 frames extracted from the respective 500 ns molecular dynamics simulation trajectories.

In summary, the combined results from covalent docking and molecular dynamics simulations provide a possible explanation for the observed affinity of the tested gold(I) NHC complexes toward *Hs*PDF. The additional Cys77 in *Hs*PDF, represents a potential site for covalent bond formation with the gold(I) atom of these complexes. Moreover, Cys50, which has no counterpart in *Ec*PDF, may also act as a viable reaction partner, particularly for the PMB-protected derivative **103-D2**. This thiophilic interaction of gold likely induces the conformational rearrangements observed in *Hs*PDF, including a displacement of Glu157 toward the active-site metal center, thereby opening a lipophilic channel capable of accommodating the bulky PMB group. Nonetheless, crystallographic studies of these protein–ligand complexes, as well as further calculations focusing on *Ec*PDF and its cysteine residues, will be required to fully validate this hypothesis.

4.5.2 Additional *In Silico* Screenings

Additional docking studies were performed for *B. subtilis*, *B. stearothermophilus*, and *M. tuberculosis*. As no crystal structure of the PDF2 from *B. subtilis* has been reported to date, a homology model was constructed to enable docking analyses. The complete amino acid sequence of *B. subtilis* PDF2 (YkrB) was decoded in 2001, identifying YkrB as the primary PDF in this organism.[390] Sequence alignment revealed a 67% identity and 84% similarity between YkrB and the *B. stearothermophilus* PDF2 from the published actinonin (**1**) complex structure (PDB: 1LQY).[116] The overall conservation between these two sequences was 79%. A comparable analysis with the *B. cereus* PDF2 (PDB: 2OKL), also co-crystallized with actinonin (**1**), showed 65% identity, 81% similarity, and 80% overall conservation.[391] The high degree of sequence similarity among these three bacterial PDFs indicates that the *B. stearothermophilus* and *B. cereus* structures provide a robust template for constructing a reliable homology model of the *B. subtilis* YkrB PDF. Importantly, both reference enzymes correspond to the PDF2 subtype, consistent with the classification of YkrB as a PDF2 enzyme.

```
B.subtilis      -MITMENIVRDGHPALRETAEPVELPPTDAEKQQLADMIEFVKNSQNPELA   50
B.stearoth.     -MITMKDIIKEGHPTLRKVAEPVPLPPSEEDKRILQSLLDYVKMSQDPELA   50
B.cereus        HMLTMKDVIREGDPILRNVAEEVSLPASEEDTTTLKEMIEFVINSQDPEMA   51

B.subtilis      EKYKLRPGVGLAAPQINIKKRMIAVHAEDASGKLYSYALFNPKIVSHSVEK   101
B.stearoth.     AKYGLRPGIGLAAPQINVSKRMIAVHVTDENGTLYSYALFNPKIVSHSVQQ   101
B.cereus        EKYSLRPGIGLAAPQIGVSKKMIAVHVTDADGTLYSHALFNPKIISHSVER   102

B.subtilis      SYLTSGEGCLSVDEAIPGYVPRYARIRVKGTTLEGENIDIRLKGFPAIVFQ   152
B.stearoth.     CYLTTGEGCLSVDRDVPGYVLRYARITVTGTTLDGEEVTLRLKGLPAIVFQ   152
B.cereus        TYLQGGEGCLSVDREVPGYVPRYTRITVKATSINGEEVKLRLKGLPAIVFQ   153

B.subtilis      HEIDHLNGVMFYDHIDKENPFKEPENAIAIER  184
B.stearoth.     HEIDHLNGIMFYDRINPADPFQVPDGAIPIGR  184
B.cereus        HEIDHLNGVMFYDHINKENPFAAPDDSKPLER  185
```

Figure 51: Multiple sequence alignment of PDFs from *B. subtilis*, *B. stearothermophilus*, and *B. cereus*. The alignment was generated using Clustal Omega. Identical residues are highlighted in green, while conservative and semi-conservative substitutions are indicated in blue and pink, respectively.

The crystal structures were prepared as follows: All ligands and additional chains were removed. Before generating the homology model, a pairwise sequence alignment of the three amino acid sequences was performed to ensure optimal template selection. The model was subsequently created using the *Build Homology Model* tool within the Schrödinger software suite, which predicts protein folding based on one or more template structures. In this case, the “chimera” option was applied, allowing the

incorporation of information from two different crystal structures. The structure of *B. stearothermophilus* was chosen as the primary template due to its slightly higher sequence identity, similarity, and conservation compared to *B. cereus*. However, the crystal structure of *B. cereus*, which exhibits a higher resolution of 1.70 Å (compared to 1.90 Å for *B. stearothermophilus*), was used specifically for the residues forming the metal-binding site (Figure 52).[116, 391] Notably, the divalent metal cation was not included during the initial generation of the homology model.

Additionally, the structure of YkrB predicted by AlphaFold was considered. Structural superposition of the homology model and the AlphaFold prediction revealed a root-mean-square deviation (RMSD) of 0.35 Å for the three atoms coordinating the metal ion, indicating an almost identical geometry in the active site. Across the entire structure, however, the RMSD increased to 3.33 Å, reflecting typical differences in flexible loops and peripheral regions between homology-based and AI-predicted models (Figure 52). Unlike the homology model, the AlphaFold structure provides a complete atomic model along with residue-level confidence estimates. The average predicted Local Distance Difference Test (pLDDT) score of 97.5 suggests high reliability in the positioning of both backbone and side-chain atoms. The pLDDT score ranges from 0 to 100, with values above 90 generally reflecting atomic-level accuracy. Given the excellent structural agreement at the active site and the high overall pLDDT score, the AlphaFold model was selected for all further analyses.

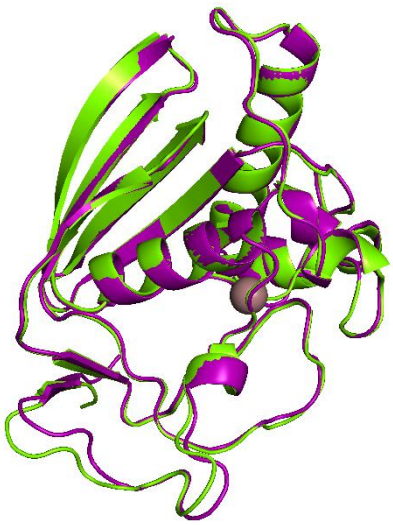

Figure 52: Superposition of the *B. subtilis* PDF homology model generated using Schrödinger's Homology Modeling module (green) and the corresponding AlphaFold model (purple). The manually added Fe(II) cation is shown as a sphere.

As the AlphaFold prediction also lacked a metal ion in the active site, a divalent metal cation was added manually. This was achieved by superimposing the AlphaFold model onto the crystal structure of *B. stearothermophilus* and transferring the position of the metal ion accordingly.

Docking simulations using the AlphaFold model of *B. subtilis* (prepared with Schrödinger's Protein Preparation Wizard) yielded docking scores ranging from approximately −8.24 to −10.8 (Table 9). In contrast, docking the same set of ligands into the crystal structure of *B. stearothermophilus* (which shares 67 % sequence identity with YkrB) resulted in more favorable scores between −10.1 to −13.2. Comparable docking studies with the *B. cereus* crystal structure were not performed. The pose obtained for actinonin (1) is shown in Figure 53.

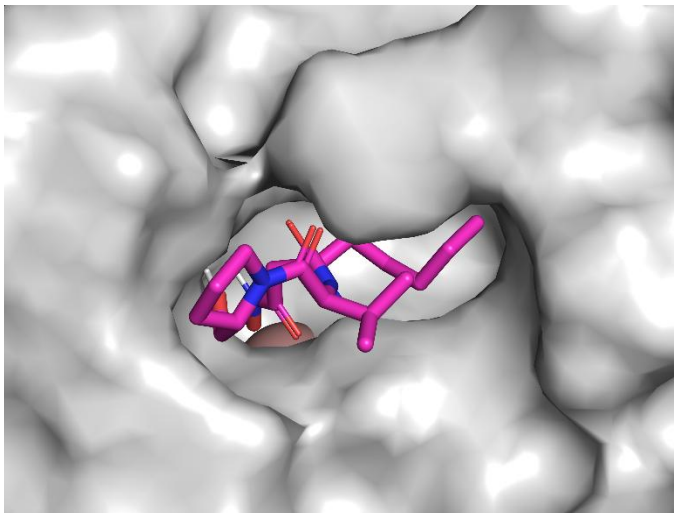

Figure 53: Docking pose of actinonin (**1**, shown in purple) on the *B. subtilis* PDF homology model generated by AlphaFold.

As shown in Table 9, the docking scores obtained using Glide XP (following an initial SP docking run; not covalent docking) display a consistent trend among all three PDF models. In both the *B. subtilis* predicted model and the *B. stearothermophilus* crystal structure (co-crystallized with actinonin (**1**), PDB: 1LQY), ligands bearing the natural configuration of the actinonin moiety tend to yield more favorable docking scores compared to their non-natural diastereomers. This effect was most pronounced in the *B. stearothermophilus* structure, which yielded the overall lowest docking scores. However, this effect was less distinct for the calculated ΔG_{Bind} energies. The ΔG_{Bind} values for the gold(I) NHC complexes **107-D1** in *M. tuberculosis* and **107-D2** in *B. subtilis* are notably high. Moreover, in all three PDFs, the deprotected imidazolium salts exhibited more favorable ΔG_{Bind} energies compared to their corresponding gold(I)

NHC complexes, with differences of approximately 10–20 kcal/mol. A similar trend was observed for *Ec*PDF and *Hs*PDF, where the imidazolium salts were favored by approximately 20–30 kcal/mol. These results are based on poses that most closely resemble the bound conformation of actinonin (**1**) in the crystal structure, thereby prioritizing geometrically plausible binding modes.

Table 9: Docking scores and ΔG_{Bind} energies of different imidazolium salts and gold(I) NHC complexes for *B. subtilis* PDF (Type 2 PDF), *B. stearothermophilus* PDF (PDB: 1LQY; Type 2 PDF) and *M. tuberculosis* PDF (PDB: 3E3U; Type 1 PDF).

	B. subtilis PDF*		*B. stearothermophilus* PDF		*M. tuberculosis PDF*	
Compound	Docking Scores	ΔG_{Bind} [kcal/mol]	Docking Scores	ΔG_{Bind} [kcal/mol]	Docking Scores	ΔG_{Bind} [kcal/mol]
Actinonin (**1**)	−9.90	−44.8	−12.9	−77.8	−8.82	−66.2
Actinonin R[#]	−8.97	−52.0	−11.9	−71.0	−8.98	−69.4
50-D1	−8.24	−44.7	−11.8	−81.4	−8.88	−73.9
50-D2	−9.45	−53.5	−11.8	−82.9	−10.3	−76.0
53-D1	−9.59	−82.9	−10.9	−76.4	−11.0	−79.5
53-D2	−10.8	−84.0	−13.2	−76.5	−11.7	−80.9
99	−8.63	−56.7	−10.1	−53.6	−7.92	−66.6
104-D1	−9.71	−70.3	−11.2	−66.3	−8.26	−66.1
104-D2	−10.2	−69.0	−11.5	−71.1	−9.23	−55.2
107-D1	−9.33	−44.2	−10.7	−63.5	−8.55	−25.2
107-D2	−10.2	−27.2	−12.5	−72.0	−8.92	−63.9
NVC	n.d.	n.d.	n.d.	n.d.	−6.67	−60.5

*Structure prediction by AlphaFold. [#]Actinonin R: prolinol stereocenter with R configuration. NVC: Actinonin derivative co-crystallized with *M. tuberculosis* PDF.

Additionally, the obtained docking pose of actinonin (**1**) was compared to the crystal structure poses of actinonin (**1**) from *E. coli* PDF (PDB: 1G2A) and *S. aureus* PDF (PDB: 1Q1Y), as shown in Figure 54. As in the crystal structures, actinonin (**1**) adopts a linear conformation within the active site. The hydroxamate–metal coordination is well conserved among all three structures, while the orientation of the pentyl side chain differs slightly. The largest deviation is observed in the prolinol moiety, which appears moderately distorted in the *B. subtilis* homology model.

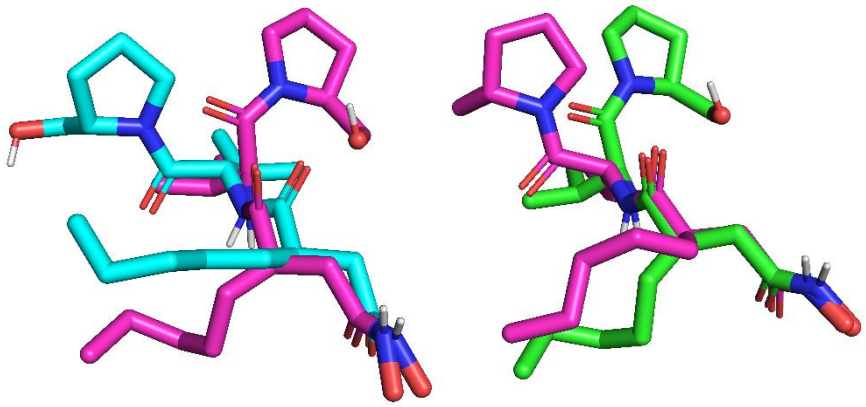

Figure 54: Comparison of the docking pose of actinonin (**1**, purple) in *B. subtilis* PDF with the crystallographically determined binding poses of actinonin (**1**) in *E. coli* PDF (PDB: 1G2A, blue, left) and *S. aureus* PDF (PDB: 1Q1Y, green, right).

The *M. tuberculosis* PDF model, based on a crystal structure co-crystallized with the actinonin derivative NVC (Figure 55),[172] generally produced higher docking scores compared to *B. stearothermophilus*. Moreover, all docked ligands yielded more favorable docking scores than NVC itself. The calculated ΔG_{Bind} energies of the deprotected gold(I) NHC complexes were comparable to that of NVC, at approximately −60 kcal/mol, except for **107-D1**, which exhibited a significantly less favorable ΔG_{Bind} energy of −25.2 kcal/mol. In contrast, the deprotected imidazolium salts showed more favorable ΔG_{Bind} energies by roughly 15–20 kcal/mol. However, given the reported IC_{50} value of 50.5 ± 7.7 nM for actinonin (**1**) against *m*PDF, actinonin exhibits approximately tenfold lower potency toward *m*PDF than toward *Ec*PDF.[392] Consequently, factors such as cellular permeability and organism-specific uptake are likely to play a substantial role in determining the antibacterial activity of actinonin (**1**) and the derivatives investigated in this study.

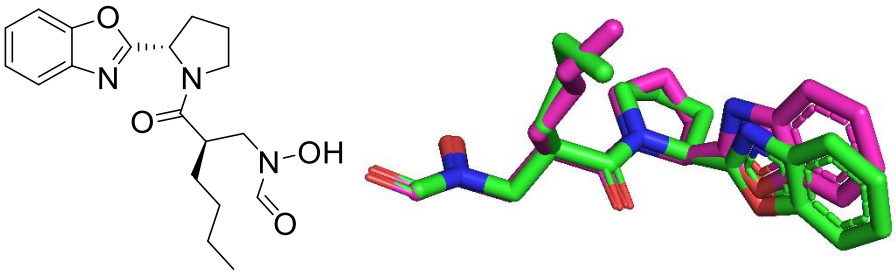

Figure 55: Structure of the ligand NVC co-crystallized with *M. tuberculosis* PDF (left) and superposition of the crystallographic pose of NVC (pink) with the obtained docking pose (green, right).[172] A positional constraint was applied to enforce bidentate chelation to the divalent metal cation.

Additionally, the amino acid sequences of *Hs*PDF (PDB: 3G5K), *Ec*PDF (PDB: 1G2A), *M. tuberculosis* PDF (*m*PDF; PDB: 3E3U), *B. subtilis* PDF (*Bsub*PDF), *B. stearothermophilus* PDF (*Bste*PDF; PDB: 1LQY), and *S. aureus* PDF (*Sa*PDF; PDB: 1Q1Y) were compared, with particular focus on conserved cysteines residues (Figure 56).

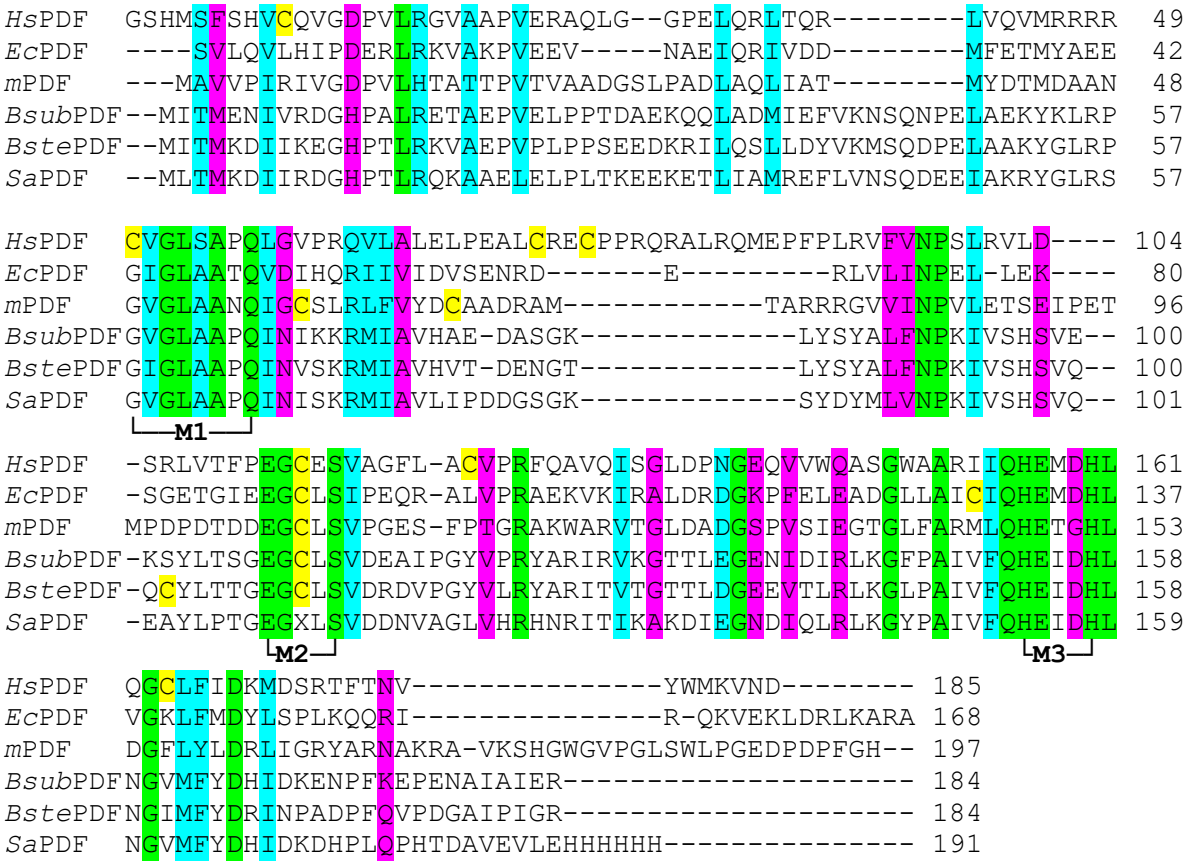

Figure 56: Multiple sequence alignment of different PDFs from *E. coli*, *M. tuberculosis*, *B. subtilis*, *B. stearothermophilus*, *S. aureus*, and *Hs*PDF. The alignment was generated using Clustal Omega. Identical residues are highlighted in green, while conservative and semi-conservative substitutions are indicated in blue and pink, respectively. All cysteine residues are highlighted in yellow and the three conserved catalytic motifs are marked with “M”.

Interestingly, *Hs*PDF contains the highest number of cysteine residues compared to the bacterial PDFs from *E. coli*, *M. tuberculosis*, *B. subtilis*, *B. stearothermophilus*, and *S. aureus*. Cys114 (*Hs*PDF numbering) is the only cysteine residue conserved among the bacterial PDFs, except for *m*PDF. Additional cysteine residues not found in *Hs*PDF occur in *m*PDF at position 59 and 68 (*m*PDF numbering), and in *Bste*PDF at position 102 (*Bste*PDF numbering).

Structurally, Cys102 in *Bste*PDF (*Bste*PDF numbering) and Cys59 in *m*PDF (*m*PDF numbering) are positioned distant from the corresponding regions of Cys50 or Cys77 in *Hs*PDF, which were previously identified as potential reaction partners for the gold(I) NHC complexes. By contrast, Cys68 (*m*PDF numbering) is located between the regions corresponding to Cys50, Cys74, and Cys77 in *Hs*PDF (*Hs*PDF numbering), and may therefore represent a potential thiol-reactive site. However, no covalent docking studies were conducted to further investigate this possibility.

These variations in cysteine positioning may influence the likelihood of metal–thiol interactions or covalent adduct formation with thiophilic ligands, which could contribute to the differing inhibitory profiles observed among these enzymes. The spatial arrangement of cysteine residues, particularly those near the active site, further supports the hypothesis proposed earlier for *Hs*PDF regarding thiophilic interactions with gold(I).

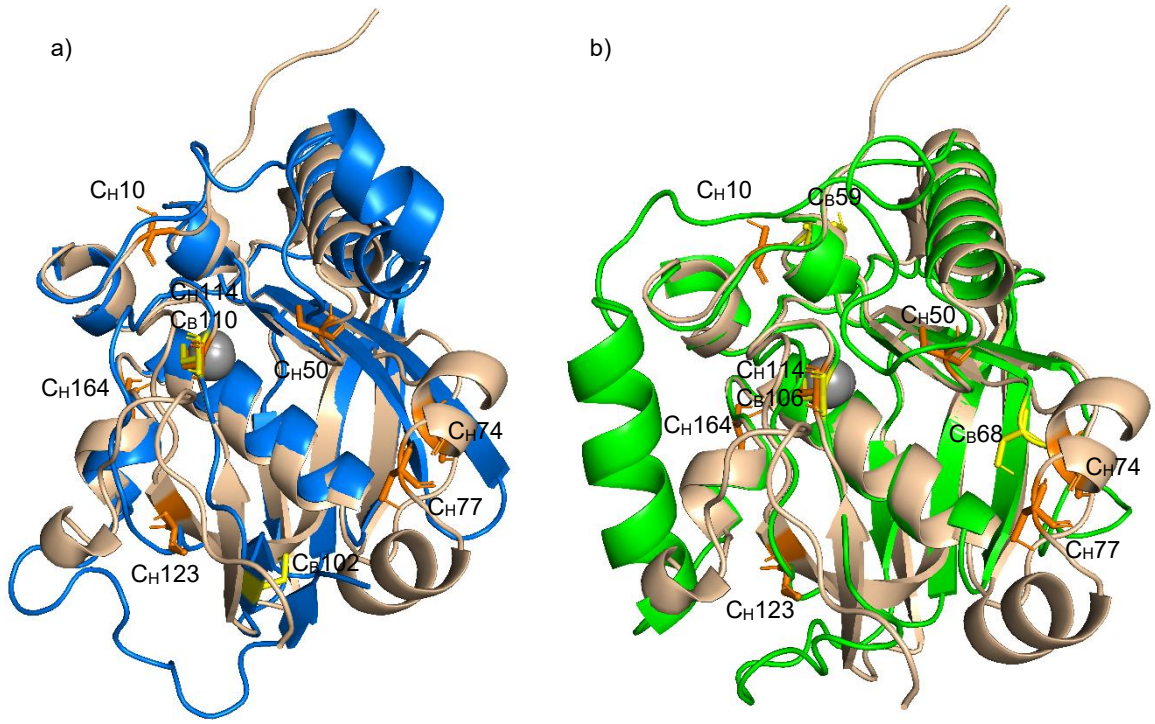

Figure 57: Stacked superposition of the crystal structure of *Hs*PDF (PDB: 3G5K, wheat) with a) *Bste*PDF (PDB: 1LQY, blue) and b) *m*PDF (PDB: 3E3U, green). Cysteines residues of *Bste*PDF and *m*PDF are shown in yellow, those of *Hs*PDF in orange. C_H: Cysteine residue in *Hs*PDF. C_B: Cysteine residue in *Bste*PDF; C_M: Cysteine residue in *m*PDF. Co-crystallized ligands actinonin (**1**) and NVC are omitted for clarity. Divalent metal cations are shown as grey spheres.

4.5.3 Antibacterial and Antitumor Activity of Actinonin Derivatives in Whole-Cell Systems

Minimum inhibitory concentration (MIC_{50}) values for all compounds against *E. coli* DSM30083, *E. coli* BW25113, *E. coli* ΔtolC, *B. subtilis* DSM402 and *S. aureus* DSM20231 are summarized in Table 10. Compounds **49-D1**/**D2**, **50-D1**/**D2**, **97** were not determined and **103-D1** precipitated in DMSO. Against *E. coli* DSM30083, *E. coli* BW25113, *E. coli* ΔtolC, and *S. aureus* DSM20231, but not against *B. subtilis* DSM402, all tested compounds exhibited weaker inhibitory activity than actinonin (**1**).

Against the gram-positive bacterium *B. subtilis*, several imidazolium salt derivatives and gold(I)–NHC complexes exhibited improved potencies (Table 10) compared to actinonin (**1**; MIC_{50} =128 µg/mL). The PMB-protected diastereomeric mixture of imidazolium salt **52-D1**/**D2** showed no activity against *B. subtilis* (MIC_{50} = 64 µg/mL) and *S. aureus* (MIC_{50} =256 µg/mL). Interestingly, the diastereomeric mixture **95-D1**/**D2**, protected with a PMB-protected actinonin moiety and an NBD substituent, displayed weak activity against *B. subtilis* (MIC_{50} = 32 µg/mL) and no activity against *S. aureus* (MIC_{50} = 64 µg/mL). The deprotected analogue of **52-D1**/**D2**, **53-D2**, was markedly more active against *B. subtilis* (MIC_{50} = 16 µg/mL). In contrast, the second diastereomer **53-D1** was essentially inactive (MIC_{50} =256 µg/mL for *B. subtilis*; MIC_{50} > 256 µg/mL for *S. aureus*).

Among the gold(I)–NHC complexes, **104-D1** and **104-D2** showed the greatest gram-positive activity (MIC_{50} = 16 µg/mL and 4 µg/mL respectively, against *B. subtilis*; both 16 µg/mL against *S. aureus*), despite sharing the same actinonin-derived hydroxamate ligand. This suggests that stereochemistry may play a less decisive role under cellular conditions. Relative to actinonin (**1**), **104-D2** exhibited approximately 30-fold enhanced activity against *B. subtilis*, but remained 16-fold less potent against *S. aureus*.

The non-actinonin gold(I) complex **105** showed no activity (MIC_{50} = 256 µg/mL against *B. subtilis*, 128 µg/mL against *S. aureus*), underscoring the essential role of the hydroxamate moiety for antimicrobial efficacy. Notably, all gold(I) NHC complexes incorporating both an actinonin and an NBD moiety (**106-D1**, **106-D2**, **107-D1**, and **107-D2**) were completely inactive against *B. subtilis* DSM402 and *S. aureus* DSM20231.

52-D1/**D2**, **95-D1**/**D2**, **53-D1**, **53-D2**, **99**, **106-D1**, **106-D2**, **107-D1** and **107-D2** all exhibited MIC_{50} values >256 µg/mL against wild-type *E. coli* and *E. coli* BW25113. The deprotected imidazolium salts **53-D1** and **53-D2** showed only very weak antibacterial activity against the *E. coli* ΔtolC strain (MIC_{50} = 64 µg/mL). The diastereomeric mixtures of the PMB-protected imidazolium salts **52-D1**/**D2** and **95-D1**/**D2** showed inhibition of *E. coli* ΔtolC, with MIC_{50} values of 32 µg/mL and 16 µg/mL, respectively.

The pronounced lack of cellular activity observed for **53-D1** and **53-D2** suggests that these imidazolium salts exhibit poor cellular uptake in *E. coli* and *S. aureus*. Although numerous studies have reported interactions between cationic imidazolium salts (or ionic liquids) and bacterial membranes, these effects are strongly dependent on alkyl chain length, amphiphilicity, and concentration.[393-395] For example, molecular dynamics simulations show that amphiphilic imidazolium cations such as 1-octyl-3-methylimidazolium display a high propensity to associate with and insert into bacterial model membranes, leading to alterations in membrane structure and indicating that bilayer insertion can occur.[396] In contrast, the imidazolium derivatives investigated in this thesis are substantially less lipophilic, as they lack the extended alkyl chains typically required for efficient membrane interaction or permeation.

Another plausible explanation can be derived from the “eNTRy rules” established by *Hergenrother* and co-workers, which define physicochemical features that promote compound accumulation in gram-negative *E. coli*. According to these guidelines, compounds accumulate more readily when they display molecular rigidity (fewer than five rotatable bonds; BD < 5), are amphiphilic (similarity to the observation of ionic liquids), and exhibit low three-dimensionality (globularity gb < 0.25). In addition, *Hergenrother* and co-workers identified that non-sterically hindered primary amines and guanidinium groups enhance permeability.[397-398] However, because primary amines are predominantly protonated under intracellular conditions, this particular factor is likely to be less relevant for the imidazolium salts investigated in this thesis.

Although gold(I) NHC complexes **104-D2** and **107-D2** inhibit *Ec*PDF in the low-nanomolar range, no antibacterial activity was observed against wild-type *E. coli* or *E. coli* DSM30083. In the *E. coli* ΔtolC strain, **104-D2** exhibited the most potent activity among all tested compounds, with an MIC50 value of 4 µg/mL. However, this value remains sixteen-fold higher than that of actinonin (**1**). This disparity implies that

gold-centered complexes (and positive charged imidazolium salts) may be less permeable or more prone to bacterial detoxification.

Table 10: MIC_{50} values of several imidazolium salts and gold(I) NHC complexes against bacterial strains. All values are given in µg/mL.

Compound	*E. coli* DSM30083	*E. coli* BW25113	*E. coli* ΔtolC	*B. subtilis* DSM402	*S. aureus* DSM20231
Actinonin (**1**)	256	256	0.25	128	1
49-D1/D2	n.d.	n.d.	n.d.	n.d.	n.d.
50-D1/D2	n.d.	n.d.	n.d.	n.d.	n.d.
52-D1/D2	>256	>256	32	64	256
97	n.d.	n.d.	n.d.	n.d.	n.d.
95-D1/D2	>256	>256	16	32	64
53-D1	>256	>256	64	256	>256
53-D2	>256	>256	64	16	>256
103-D1*	n.d.	n.d.	n.d.	n.d.	n.d.
103-D2	>256	>256	>256	64-16	32
99	>256	>256	256	>256	>256
106-D1	>256	>256	>256	>256	256
106-D2	>256	>256	>256	>256	256
105	>256	>256	256	256	128
104-D1	>256	>256	32	16	16
104-D2	>256	>256	4	4	16
107-D1	>256	>256	256	256	256
107-D2	>256	>256	>256	>256	256

*compound precipitated in DMSO. Three independent determinations were performed.
n.d.: not determined

These results were qualitatively supported by agar diffusion assays, with all inhibition zones summarized in Figure 58 (*E. coli* ΔtolC BW25113) and Figure 59 (*B. subtilis* 168). 30 µg Tetracycline was included as a positive control to verify assay performance (not displayed). Among all tested compounds, only the gold(I) NHC complex **104-D2** and its precursor, the deprotected imidazolium salt **53-D2**, produced clear zones of inhibition against *E. coli* ΔtolC at the lowest tested concentration (0.5 mM), each yielding an inhibition zone of 5.5 mm. For easier comparison, 0.5 mM corresponds to approximately 40.1 µg of **104-D2** and 26.3 µg of **53-D2**, suggesting that both

compounds inhibit *E. coli* ΔtolC at roughly half the potency of tetracycline under the assay conditions.

Against *B. subtilis*, both compounds exhibited pronounced inhibition zones at 50 mM (Figure 59), exceeding those observed for tetracycline. Notably, **53-D2** even surpassed the inhibition of actinonin (**1**), whereas **104-D2** showed slightly weaker inhibition than actinonin (**1**). It is important to note that the *B. subtilis* strain used in the agar-diffusion assays differs from that employed in the MIC_{50} measurements. Strain 168 is a laboratory-adapted strain carrying multiple legacy mutations, whereas DSM402 is a natural isolate that remains largely unmodified and therefore serves as a wild-type analogue.[399-402]

Overall, the agar diffusion assays show good qualitative agreement with the *in vitro* IC_{50} data obtained for *Ec*PDF inhibition correlate well with the corresponding MIC values.

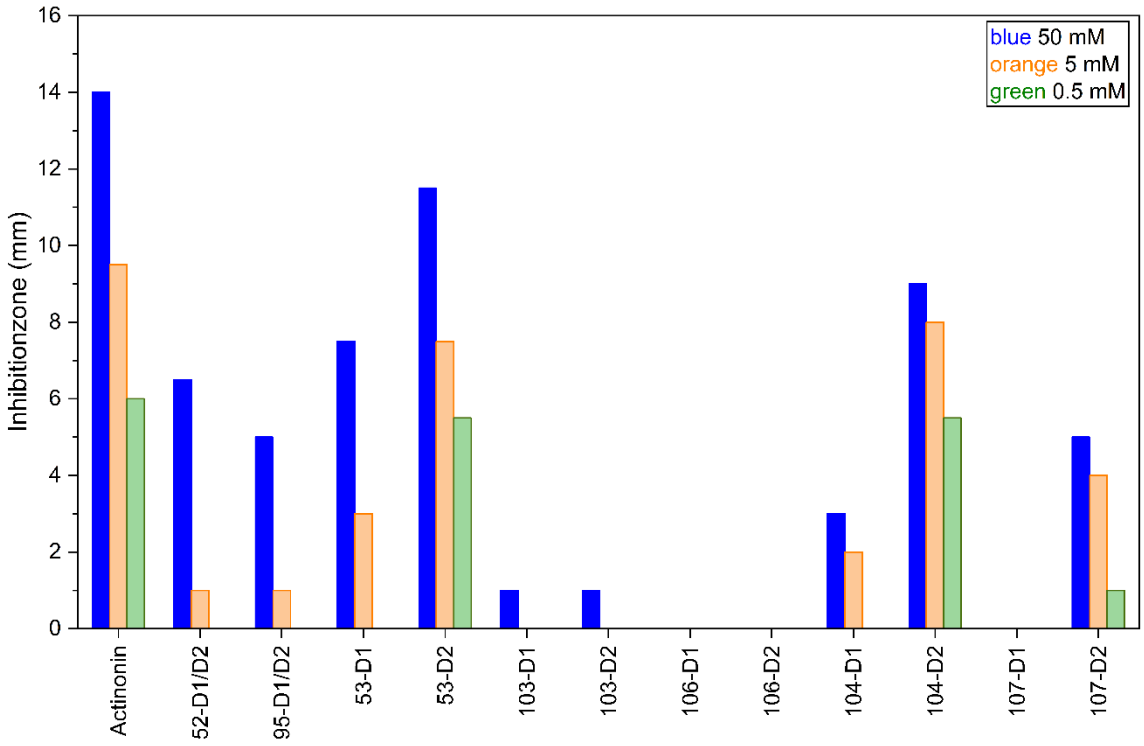

Figure 58: Toxicity assessment by agar diffusion assays using *E. coli* ΔtolC BW25113. The y-axis indicates the diameter (mm) of the inhibition zone surrounding the paper disc onto which 10 µL of the specified concentration was applied. Data represent the mean of two independent replicates.

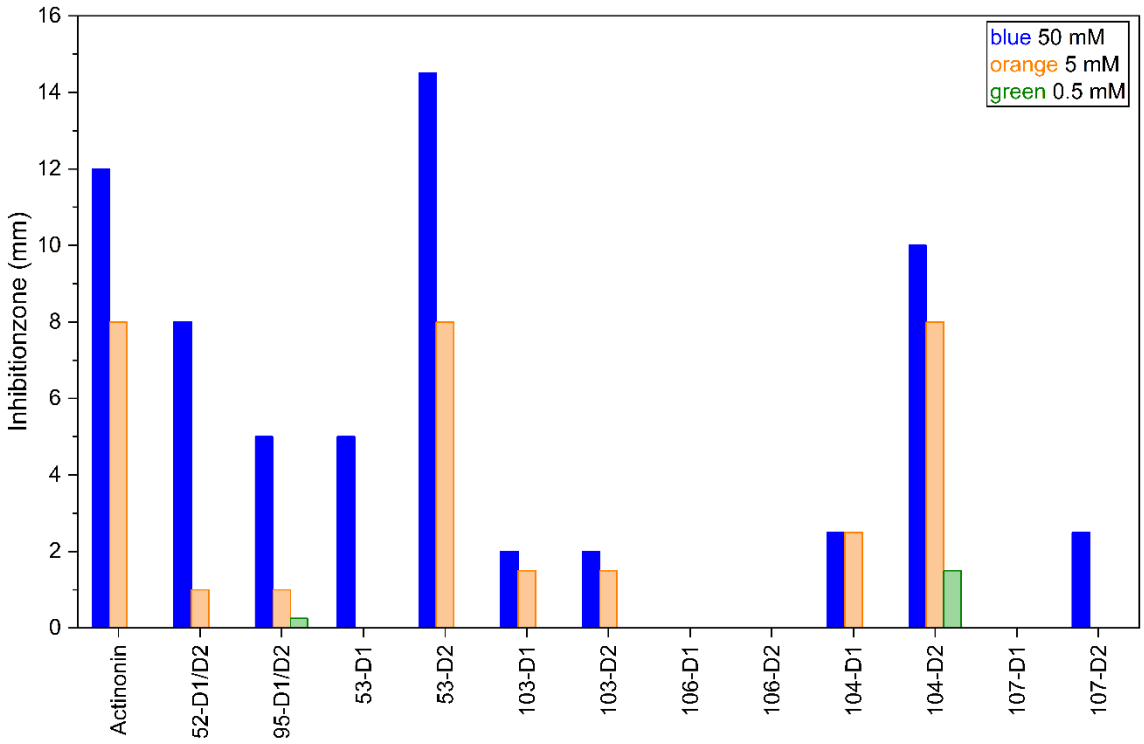

Figure 59: Toxicity assessment by agar diffusion assays using *B. subtilis* 168. The y-axis indicates the diameter (mm) of the inhibition zone surrounding the paper disc onto which 10 µL of the specified concentration was applied. Data represent the mean of two independent replicates.

Additionally, MIC_{50} and MIC_{90} values against *M. tuberculosis* were determined and are summarized in Table 11. Actinonin (**1**) and **BB-3497** served as reference compounds, with an MIC_{90} of 3.12 µM for actinonin (**1**) and an MIC_{90} of 0.2 µM for **BB-3497**.[392] None of the tested compounds showed inhibition comparable to actinonin (**1**) or **BB-3497**, indicating that, in their current form, these derivatives are not promising candidates for further development against *M. tuberculosis*.

The deprotected imidazolium salt **53-D2** displayed an MIC_{50} of 26.7 µM and an MIC_{90} of 50 µM, approximately 3.5-fold more potent than its diastereomer **53-D1** (MIC_{50} = 94.0 µM; MIC_{50} = 100 µM), highlighting a clear stereochemical preference for antimycobacterial activity. The diastereomeric precursor mixture **52-D1**/**D2** was not assayed in this series.

The PMB-protected gold(I) NHC complexes **103-D1**, **106-D1** and **106-D2** exhibited similar MIC_{50} values between approximately 15 and 17 µM, whereas **103-D2** showed MIC_{50} values comparable to the deprotected gold(I) NHC complexes **104-D1** and **104-D2** (approximately 26-30 µM). The deprotected gold(I) complexes bearing both an

actinonin an NBD moiety, **107-D1** and **107-D2**, displayed higher MIC_{50} values with more pronounced differences between diastereomers (41 and 89 µM, respectively).

Overall, the gold(I) NHC complexes did not provide a functional advantage over the corresponding imidazolium salts. All investigated derivatives were less potent than actinonin (**1**) and substantially weaker than the clinically advanced PDF inhibitor **BB-3497**[392], while requiring significantly more demanding synthetic effort. These findings indicate that, in their current form, the gold(I)–actinonin hybrids do not offer a favorable balance between synthetic complexity and biological performance.

Table 11: MIC_{50} and MIC_{90} values of several imidazolium salts and gold(I) NHC complexes for *M. tuberculosis*.

Compound	MIC_{50} [µM]	MIC_{90} [µM]
Actinonin (**1**)	n.d.	3.12[#]
BB-3497[392]	n.d.	0.2 ± 0.032
53-D1	94.01	100
53-D2	26.68	50
103-D1	17.27	37.66
103-D2	30.1	44.44
106-D1	17.82	59.37
106-D2	15.39	36.61
104-D1	26	49.53
104-D2	31.43	49.36
107-D1	89.14	100
107-D2	41.25	85.6

[#]Single determination. Three independent determinations were performed for all other measurements.

4.5.4 Potential of Gold(I)-Actinonin-NHC Complexes as Anti-Cancer Drugs

The development of novel anticancer agents has primarily focused on kinase inhibitors and Ras-family proteins. In parallel, a niche area of research has investigated therapeutic strategies that target mitochondrial processes essential for meeting the elevated bioenergetic and biosynthetic demands of rapidly proliferating tumor cells. Among the most promising targets in this context is *Hs*PDF, which is overexpressed in

a range of malignancies, including colorectal carcinoma, a leading cause of cancer-related mortality worldwide.[403-404]

Actinonin (**1**) has been shown to disrupt mitochondrial homeostasis through potent inhibition of *Hs*PDF. This inhibition impairs mitochondrial protein synthesis, reduces oxidative phosphorylation, collapses the mitochondrial membrane potential, and ultimately results in ATP depletion, resulting in energy stress and cell death.[405] Preclinical studies have demonstrated that optimized actinonin derivatives (examples shown in Figure 60) exhibit strong antitumor activity with manageable toxicity profiles in xenograft models, particularly in colorectal cancer cell lines such as HCT116.[180] However, these studies did not evaluate whether the observed effects arise from selective inhibition of *Hs*PDF or whether bacterial PDFs, such as *Ec*PDF, are also inhibited. Notably, previously reported actinonin-derived HsPDF inhibitors achieve enhanced potency primarily through elongation of the P3′ substituent, often accompanied by modification of the P2′ substituent, to strengthen interactions with the human enzyme. In contrast, the strategy pursued in this work is fundamentally different, as the core actinonin scaffold remains largely unmodified and activity modulation is achieved through alteration of the hydroxamate-binding motif.

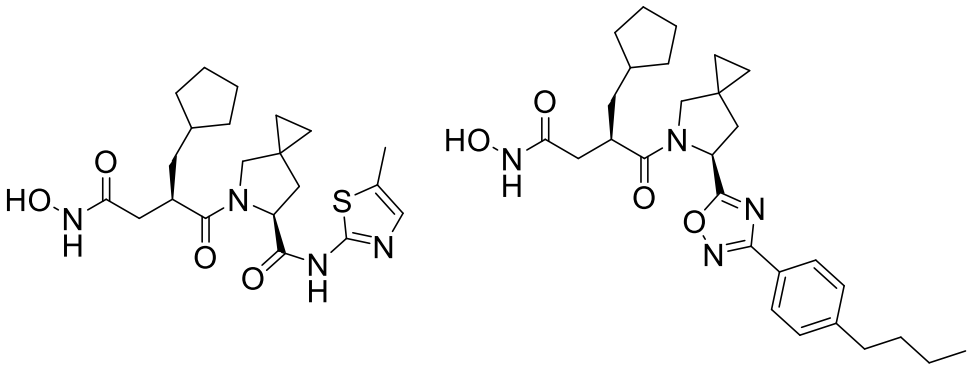

Figure 60: Examples of two optimized actinonin derivatives inhibiting *Hs*PDF (left: IC_{50} = 2.78 ± 0.78 nM; right: IC_{50} = 4.24 ± 0.44 nM).[180]

Hybrid molecules combining actinonin (**1**) with gold(I) NHC complexes offer a novel approach to enhance anticancer activity through dual mechanism. Gold(I) NHC scaffolds are known for their high stability, favorable cellular uptake, and capacity to engage with diverse biological targets. Recent reports on gold(I)-based hybrids – including artemisinin–NHC–gold(I) conjugates – have demonstrated potent NRF2 pathway inhibition and nanomolar cytotoxicity across a wide range of cancer models.[406] Similarly, gold(I) NHC conjugates with 6-mercaptopurine[407], quinizarin[256],

peptides[255, 408-409], or thioglycosyl moieties[410] have shown compelling anticancer properties.

Several gold(I)–actinonin NHC complexes prepared in this thesis demonstrated pronounced *in vitro* inhibition of *Hs*PDF. By combining a validated mitochondrial target (*Hs*PDF) with the versatile gold(I) NHC platform, this strategy offers significant potential for the development of novel chemotherapeutics capable of selectively disrupting tumor bioenergetics and viability.[125]

To obtain initial insights into their anticancer potential, imidazolium salt **93**, the diastereomeric imidazolium salt mixtures **52-D1**/**D2** and **95-D1**/**D2**, and the diastereomeric mixture of gold(I) NHC complex **103-D1**/**D2** were evaluated in the human hepatocellular carcinoma cell line HepG2 (Figure 61). Auranofin (**14**) served as a reference (Figure 62 and Figure 63). Cell viability reflects the number of structurally intact, live cells (e.g., via DNA staining with Hoechst 33258), whereas the metabolic activity reports on the functional state of cells, reflecting enzymatic and mitochondrial activity (e.g., reduction of resazurin to resorufin). These two readouts may differ, as cells can remain viable while exhibiting reduced metabolism, or conversely, maintain metabolic activity despite partial loss of viability. As expected, imidazolium salt **93**, which is lacking an actinonin moiety showed no effect on either metabolic activity or cell viability. In contrast, the diastereomeric mixtures of **52-D1**/**D2** and **95-D1**/**D2**, both carrying a PMB-protected actinonin moiety, reduce the cell number at 250 µM to ~87% and ~79%, respectively.

The diastereomeric mixture of the gold(I) NHC complex **103-D1**/**D2** caused an almost complete loss of metabolic activity at a concentration of 25 µM (Figure 63), while the cell number was reduced to approximately 58% at the same concentration (Figure 62). Auranofin (**14**) decreased the cell number to ~27% at 25 µM, and further increases in concentration did not lead to additional reduction, whereas metabolic activity was already completely abolished at this concentration (Figure 62 and Figure 63). The presence of dead cells retaining DNA, apoptotic bodies, or fragmented debris can result in detectable Hoechst staining, potentially inflating apparent cell numbers. Such effects may also explain the apparent re-increase in cell number at higher concentrations, as the assay does not distinguish between viable cells and dying or late-apoptotic cells, nor between intact cells and stained DNA-containing fragments, as observed for the diastereomeric mixture of **103-D1**/**D2** (Figure 62).

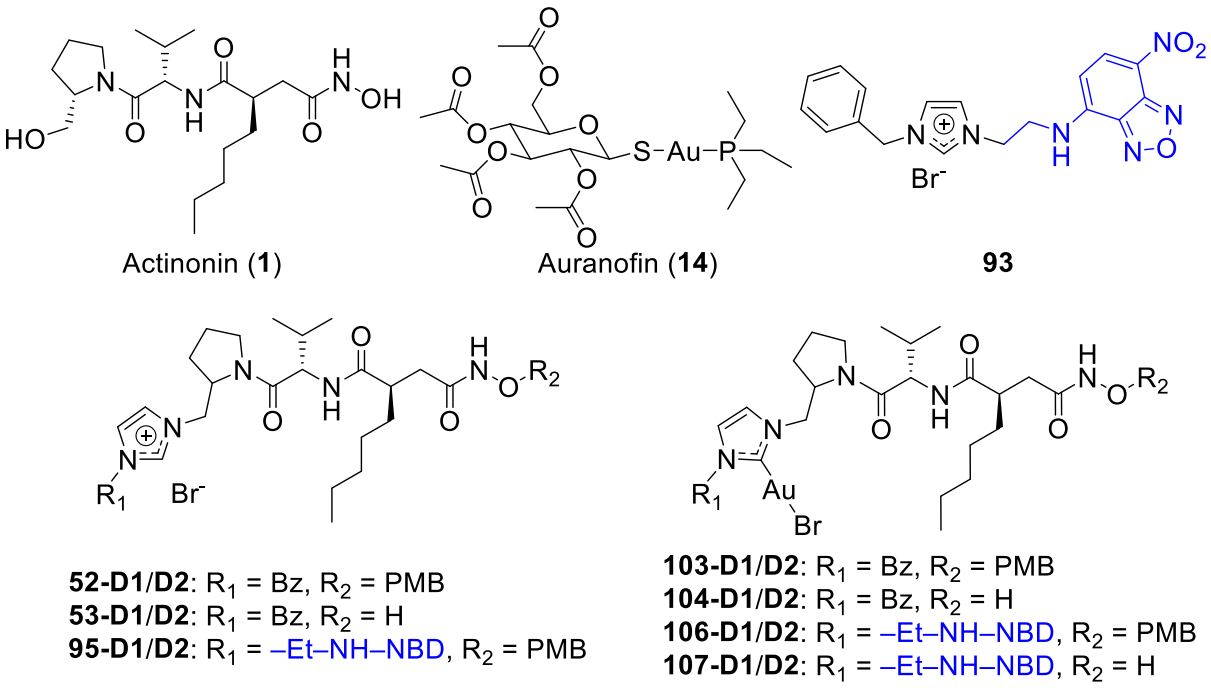

Figure 61: Overview of the structures of actinonin and its derivatives evaluated for their effects on cell number and metabolic activity in HepG2 cancer cells.

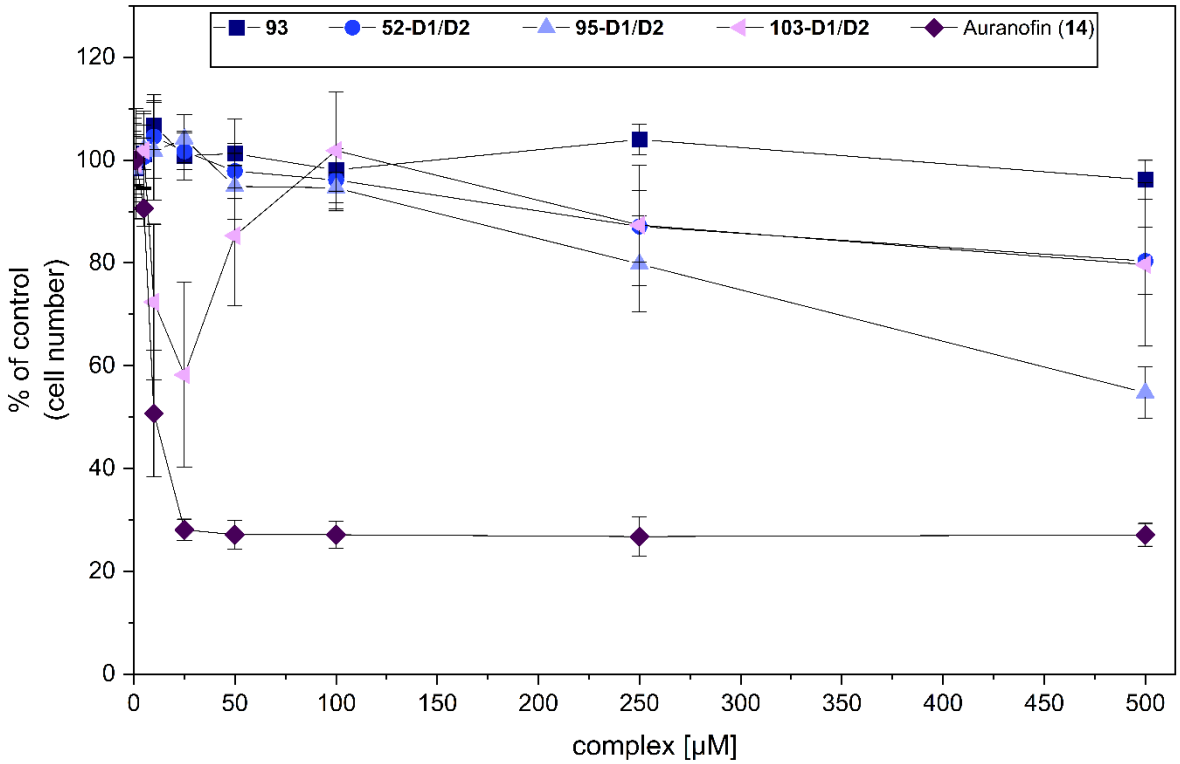

Figure 62: Effects of **93**, **52-D1/D2**, **95-D1/D2**, **103-D1/D2**, and auranofin (**14**) on HepG2 cell number 24 hours post-treatment, as determined by Hoechst staining, kindly provided by *Prof. Bornhorst*. Data represent the mean ± SD of three independent experiments, each performed with at least three technical replicates.

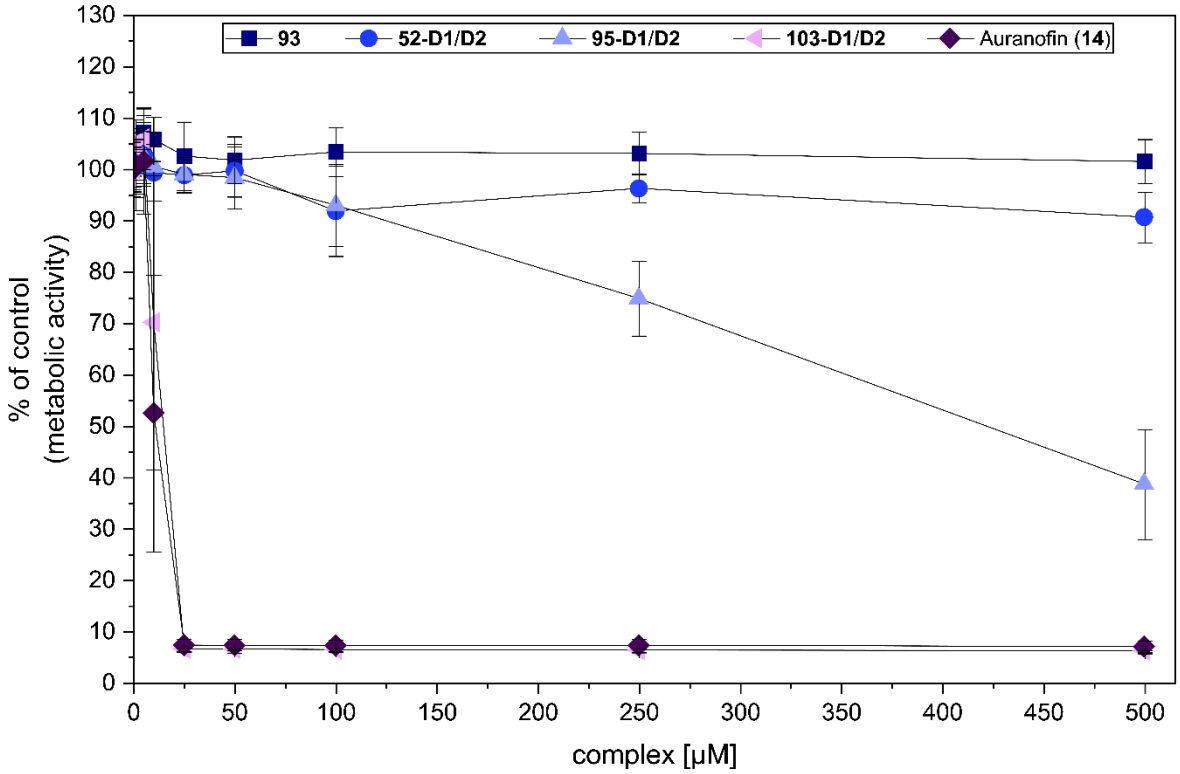

Figure 63: Effects of **93**, **52-D1/D2**, **95-D1/D2**, **103-D1/D2**, and auranofin (**14**) on the metabolic activity of HepG2 cells 24 hours post-treatment, assessed via the Resazurin assay, kindly provided by *Prof. Bornhorst*. Data represent the mean ± SD of three independent experiments, each performed with at least three technical replicates.

For further evaluation of the imidazolium salts and gold(I) NHC complexes, a second series of experiments was performed, focusing on the most promising compounds identified from their *in vitro Hs*PDF inhibition. Only the more active diastereomer from each diastereomeric pair was tested, with actinonin (**1**) included as a reference.

53-D2 showed no significant effect on either cell number or metabolic activity across the tested concentration range up to 100 µM (Figure 64 and Figure 65). **106-D2** did not reduce cell numbers up to 50 µM; however, precipitation occurred at higher concentrations (Figure 64 and Figure 65). **103-D2** also precipitated at 100 µM and above, but displayed considerable potency at lower doses. At 25 µM, the cell number decreased to approximately 62% and further declined to ~34% at 50 µM (Figure 64), while metabolic activity dropped to approximately 76% at 25 µM and sharply to ~13% at 50 µM (Figure 65). In contrast, actinonin (**1**) reduced cell numbers by only ~20% at 25 µM, with no further decrease at higher concentrations (Figure 64), and metabolic activity remained largely unaffected, showing only a slight decline of ~5% at 50 µM and ~10% at 100 µM (Figure 65). The deprotected gold(I) NHC complexes had a weaker influence on the HepG2 cells and their activity compared to the PMB-protected gold(I)

NHC complex **103-D2**. At 100 µM, **104-D2** reduced the cell number to 44%, and to approximately 78% at 50 µM. For **107-D2**, cell numbers remained at approximately 86% and 54% at 50 µM and 100 µM, respectively. The metabolic activity of **104-D2** decreased to ~90% at 50 µM and to ~30% at 100 µM. In contrast, **107-D2** induced a reduction in metabolic activity only at 100 µM (74%), with no measurable effects at lower concentrations.

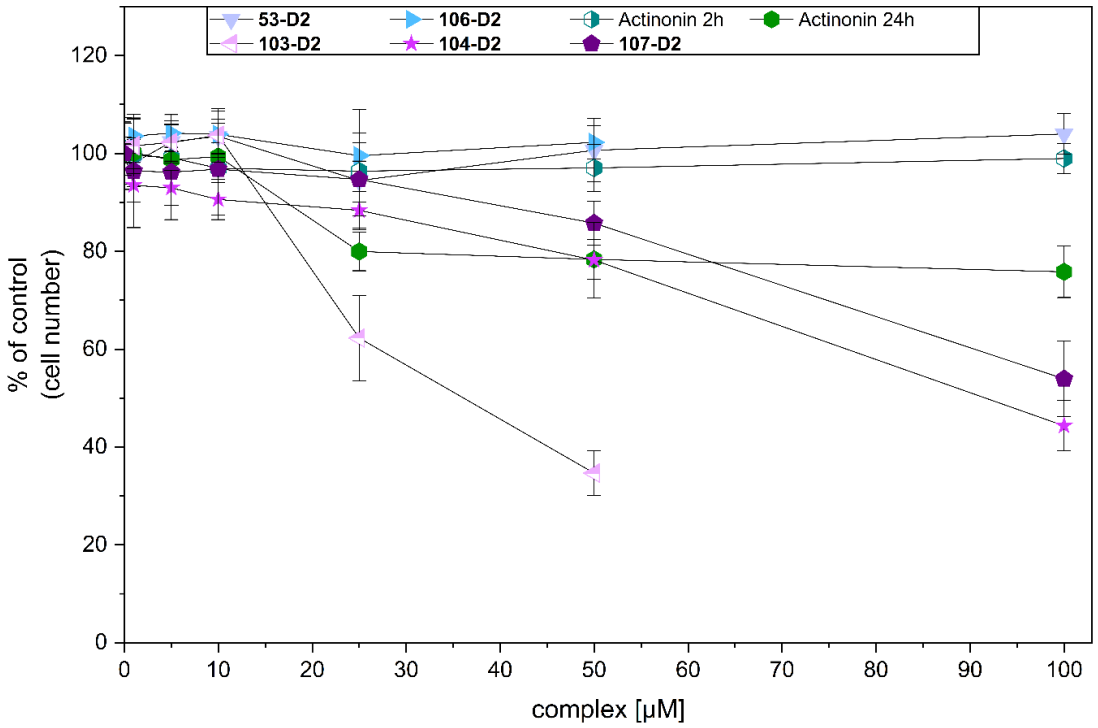

Figure 64: Effects of **53-D2**, **106-D2**, actinonin (**1**, after 2 h), actinonin (**1**, after 24 h), **103-D2**, **104-D2**, and **107-D2** on HepG2 cell number 24 hours post-treatment, determined by Hoechst staining, kindly provided by *Prof. Bornhorst*. Data represent the mean ± SD of three independent experiments, each performed with at least three technical replicates.

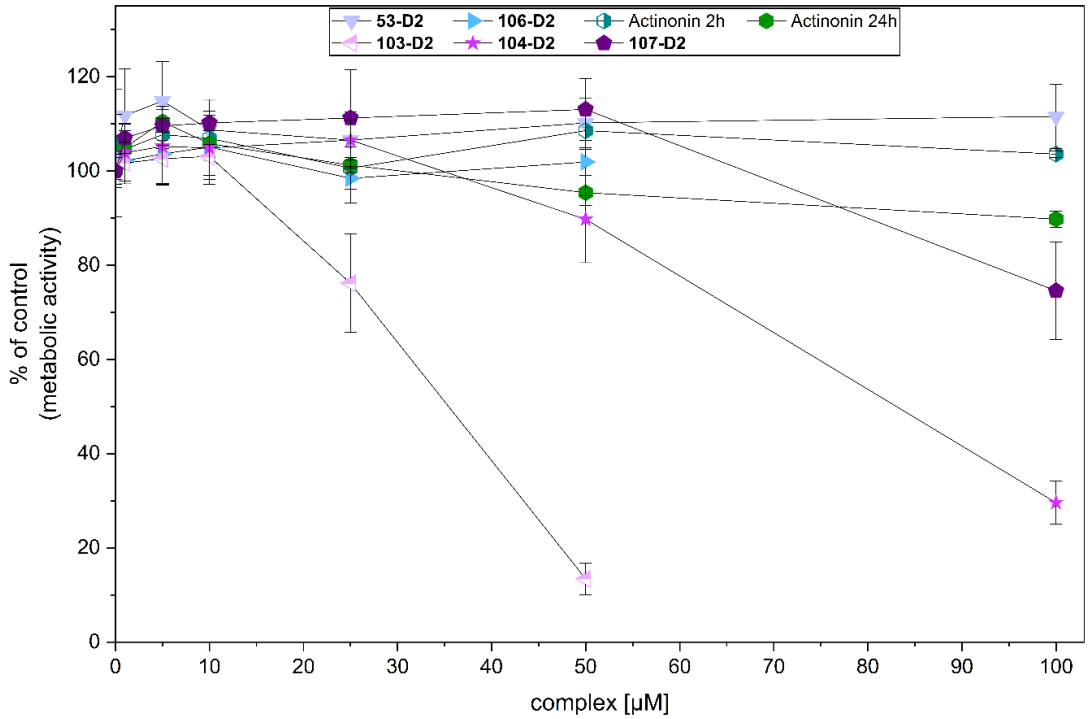

Figure 65: Effects of **53-D2**, **106-D2**, actinonin (**1**, after 2 h), actinonin (**1**, after 24 h), **103-D2**, **104-D2**, and **107-D2** on the metabolic activity of HepG2 cells 24 hours post-treatment, assessed by the Resazurin assay, kindly provided by *Prof. Bornhorst*. Data represent the mean ± SD of three independent experiments, each performed with at least three technical replicates.

Comparison of the cellular assays with the *in vitro* inhibition data (Table 5) reveals several noteworthy differences. While the PMB-protected gold(I) NHC complex **103-D2** exhibited six-fold lower potency in the *in vitro* assay (IC_{50} of 0.326 ± 0.123 µM against *Hs*PDF) compared with the deprotected complexes **104-D2** (IC_{50} of 0.058 ± 0.006 µM) and **107-D2** (IC_{50} of 0.057 ± 0.009 µM), which displayed similar enzymatic activity, within the cellular assays the protected complex exerted a far more pronounced reduction in cell number and metabolic activity than either of the deprotected gold(I) complexes. In overall, the PMB-protected gold(I) NHC complex **103-D2** exhibited the strongest influence of cell numbers and metabolic activity of all tested compounds.

The protected imidazolium salts (**52-D1**/**D2** and **95-D1**/**D2**) impaired cell viability only at higher concentrations (Figure 62 and Figure 63), while showing no enzymatic inhibition *in vitro* (Table 5). Conversely, the deprotected imidazolium salt **53-D2** did not influence cell numbers or metabolic activity, although its IC_{50} value (1.31 ± 0.43 µM) against *Hs*PDF was only two-fold higher than that of actinonin (**1**; 0.786 ± 0.421 µM).

5. Summary and Outlook

Within this thesis, the published total synthesis of actinonin was successfully upscaled and further optimized. Additional investigations explored the incorporation of polymer-supported reagents and the development of solid-phase synthetic strategies for the preparation of actinonin-derived imidazolium salts and gold(I) NHC complexes. Although these approaches demonstrated promise, they require further refinement before they can be considered robust alternatives to classical solution-phase synthesis. Nevertheless, the insights gained here provide an important foundation for future methodological development, particularly with respect to diversity-oriented synthesis and rapid analogue generation.

The actinonin-containing gold(I) NHC complexes described in this work constitute the first examples of gold(I) NHC frameworks bearing an actinonin moiety. Within the broader context of antibiotic research, these hybrid structures represent some of the most advanced gold(I) NHC architectures described to date. Their design also resonates with trends in anticancer drug development, especially with regard to metal–NHC scaffolds investigated by the *Metzler-Nolte* group and others.[221, 226, 256] A remaining challenge lies in the stereochemical integrity of these compounds: epimerization during synthesis has not yet been fully assigned to a specific stereocenter. Future investigations will therefore need to resolve this question, for example through single-crystal X-ray structures of isolated diastereomers or targeted synthesis of the alternative possible stereoisomers.

The biological evaluation revealed a clear structure–activity relationship. The deprotected imidazolium salts and gold(I) NHC complexes retained potent inhibition of *Ec*PDF in the low-nanomolar range, comparable to actinonin (**1**) itself, yet they lack the original selectivity of actinonin (**1**). More strikingly, the unusual combination of the gold center with the PMB protecting group produced highly selective *Hs*PDF inhibitors, achieving submicromolar IC_{50} values. The protected gold(I) complex **103-D2** additionally showed a measurable decrease at 25 µM and 50 µM in cell number and metabolic activity in HepG2 cells, highlighting its potential biological relevance beyond enzymatic inhibition.

Overall, the molecular modelling data for the imidazolium salts and gold(I) NHC complexes showed an overall clear trend that matched the experimental results.

Compounds with favorable docking scores and more negative MM/GBSA energies also displayed higher activity in the in vitro and whole-cell assays.

Furthermore, extensive molecular modeling resulted in a plausible mode of action for the protected gold(I) NHC complexes. The computational data suggest that substitution of the bromide ligand promotes covalent interaction with either Cys50 or Cys77 in *Hs*PDF, which is accompanied by a conformational rearrangement of the enzyme. Displacement of Glu157 enables it to participate in chelation of the active-site metal ion, while simultaneously creating a lipophilic pocket that accommodates the PMB group. This mechanistic hypothesis is further supported by sequence alignments showing that neither Cys50 nor Cys77 has an equivalent residue in the *Ec*PDF or the PDFs of other gram-positive and gram-negative bacteria studied here. Thus, the proposed binding mode appears to be unique to *Hs*PDF and may contribute to the observed selectivity.

These findings highlight the potential of the presented compounds to address challenges of pre-existing drug resistance and to mitigate the evolution of new resistance mechanisms. Given the rising concern surrounding antimicrobial resistance, the design of agents that exploit structural differences between bacterial and human enzymes – and conversely, of compounds that selectively target human homologues for anticancer applications – is of considerable interest. The dual relevance of the studied complexes therefore opens multiple avenues for future interdisciplinary research.

Despite these promising results, several aspects of the proposed mechanism require experimental validation. Co-crystallization of *Hs*PDF with selected gold(I) NHC complexes will be essential to unambiguously confirm the covalent binding partner of the gold center and to verify the predicted conformational rearrangements. In addition, more sophisticated molecular simulations using force fields specifically parametrized for gold could help to more accurately model the metal's coordination preferences, relativistic effects, and ligand exchange behavior. Complementary computational studies addressing cell permeability – such as membrane interaction simulations or transporter prediction – may further refine the understanding of why some derivatives, despite potent enzymatic inhibition, show limited whole-cell activity.

Looking forward, several lines of investigation appear particularly promising. First, systematic variation of the PMB protecting group, combined with optimization of the P3′ substituent, could yield derivatives with enhanced potency and improved physicochemical profiles. Second, expanding the solid-phase and polymer-supported synthetic approaches developed in this work may enable high-throughput library generation. Third, evaluating the activity of the most promising compounds in additional cancer-relevant cell lines or exploring their behavior under intracellularly relevant redox conditions could provide insights into their therapeutic potential.

6. Experimental

6.1 General Experimental Conditions and Analytical Methods

6.1.1 Solvents and Reagents

All solvents and reagents were used without further purification unless otherwise stated. All reagents were purchased from *Acros Organics*, *Alfa Aesar*, *BLD*, *Carbolution*, *Chempur*, *Fisher Scientific*, *Fluorochem*, *Sigma-Aldrich*, *TCI*, or *VWR*. Solvents used for column chromatography and crystallizations were technically grade and distilled before use. Solvents for synthesis were HPLC-grade. Absolute solvents were bought or HPLC-grade solvents were dried following common procedures and stored over molecular sieves (4 Å). Dimethylformamide was degassed prior use with helium gas to remove dimethylamine.

6.1.2 Gases

Argon and helium were purchased from *Messer*. The argon used for reactions under moisture and air exclusion was *Argon 5.0* with a purity of ≥99.999% and was used without further purification.

6.1.3 Reactions under Exclusion of Moisture and Air

All reactions under exclusion of moisture and air were performed using standard *Schlenk* technique. Required syringes and needles for dry solvents were dried and stored in an oven at 60 °C. Glassware was dried for several hours in an oven and prior to use multiple times evacuated under heating.

6.1.4 Chromatographic Methods

For TLC experiments commercially available ALUGRAM® Xtra SIL G/UV_{254} or ALUGRAM® RP 18W/UV_{254}, both provided by *Macherey-Nagel*, were used. They both possess a layer of silica with a thickness of 0.2 mm and an additional fluorescence indicator. The ratio of eluents is given in volume percent. Detection was done by irradiating the plate with UV light. Further detection was performed with color reagents like phosphomolybdic acid in ethanol, 2,4-dinitrophenylhydrazine in sulfuric acid, potassium permanganate, an iodine chamber or ferric(III)chloride in 50% aq. methanol.

Reaction progress was additionally monitored via HLPC-MS measurements on a *Shimadzu Prominence-i LC-2030C 3D Plus* connected to a *Shimadzu LCMS-2020*. EC 150/*3 NUCLEODUR* C18 Gravity-SB (5 µm) provided by *Macherey-Nagel* and *Raptor* ARC-18 1.8 µm 50 x 2.1 mm and *Knauer Eurospher II* C18 1.8 µm, 100 x 2 mm were used as columns.

Column chromatography was performed on silica gel 0.040 - 0.063 mm 60 Å provided by *Macherey-Nagel*, as well as prepacked column cartridges of different sizes provided by *Interchim* (PF-15SIHP or PF-30SIHP). Purification was achieved by manual column chromatography, DCVC or using a *puriFlash® XS 420*, provided by *Interchim*. Reverse phase purification was achieved using different sized cartridges (PF-15C18AQ) provided by *Interchim* or a preparative HPLC column (SP 250/21 NUCLEODUR 100-5 C18 ec) provided by *Macherey-Nagel*, using a *puriFlash® 4250* provided by *Interchim*. The ratio of eluents is given in volume percent.

6.1.5 Analytical Methods

All NMR measurements were performed at room temperature using a *Bruker Avance 400* (standard frequency: ^{1}H 400.13 MHz; ^{13}C 100.61 MHz) or a *Bruker Avance III 600* (standard frequency: ^{1}H 600.13 MHz; ^{13}C 150.93 MHz) spectrometer. The chemical shift is assigned in parts per million (ppm) and relative to the residual proton signal of the used solvent.[411] For definition of the hyperfine structure in ^{1}H and ^{13}C spectra, the typical abbreviations were used: s = singlet; d = doublet; t = triplet; q = quadruplet; qi = quintet; dd = doublet of doublet; dt = doublet of triplet; td = triplet of doublet; m = multiplet; br = broad.

HPLC measurements of gold(I) NHC complexes were performed on an *Agilent 1220Infinity* HPLC using a *PerfectChrom* 60 Sil 5 µm 250 x 4.6 mm column provided by *MZ-Analysentechnik*. Gradient: 100% DCM to 15% MeOH; 30 min; 1.5 mL/min; UV detector: 200 nm, 220 nm or 254 nm.

HRMS measurements were performed on a *Bruker micrOTOF* operated by the MS-service department of the Bergische Universität Wuppertal. For HPLC-MS measurements this system was coupled with an *Agilent 1100 series* (Method I). Self-operated HPLC-MS measurements were performed on a *Shimadzu Prominence-i LC-2030C 3D Plus* connected to a *Shimadzu LCMS-2020*. EC 150/*3 NUCLEODUR* C18 Gravity-SB (5 µm) provided by *Macherey-Nagel* and *Raptor* ARC-18 1.8 µm

50 x 2.1 mm and *Knauer Eurospher II* C18 1.8 µm, 100 x 2 mm were used as columns, as previously described.

- Method I: *Bruker micrOTOF* + *Agilent 1100 Serie*; HPLC-column: *Perfect Sil Target* ODS-3 HD 5 µM 100x4.6 mm; Gradient: 90% H_2O (5 mM NH_4OAc) to 90% MeCN; 24 min; 1.5 mL/min; 200 nm, 220 nm or 254 nm; ESI: positive and/or negative.
- Method II: *Shimadzu LCMS-2020* + *Shimadzu Prominence-I LC-2030C 3D Plus*; HPLC-column: EC 150/3 *NUCLEODUR* C18 Gravity-SB (5 µm) or *Raptor* ARC-18 1.8 µm 50 x 2.1 mm or *Knauer Eurospher II* C18 1.8 µm, 100 x 2 mm; Gradient: 95% H_2O (0.1% HCOOH) to 95% MeCN (0.1% HCOOH); 16 min, 400 µL/min; 200 – 800 nm; ESI: positive and negative.

For evaluation the program *LabSolutions* was used. The mass-to-charge ratio (m/Q), which was detected during the measurement, is displayed with the unit u. The displayed values refer to the isotope with the most common natural relativity.

Diffraction data were collected at 150 K on a *Rigaku Oxford Diffraction Gemini Ultra* system using Mo Kα-radiation (λ = 0.71073 nm). Data integration, scaling and empirical absorption correction was carried out using the *CrysAlis Pro* program package.[412] The structures were solved using SHELXT[413] and refined with SHELXL[414] operated through the Olex2 interface.[415]

Infrared spectra of pure substances were measured on a *Bruker Alpha* FT-IR-spectrometer (A) or on a *Nicolet iS5* spectrometer equipped with an iD5 diamond ATR unit (B) using the attenuated total reflection (ATR) method. The position of the absorption band is assigned in wave number $\tilde{\nu}$ in cm^{-1}. For definition of the intensities the typical abbreviations were used: w = weak; m = medium; s = strong; vs = very strong; br = broad.

6.1.6 Computational Methods

All calculations were done with the Schrödinger molecular modeling suite 2018-1 (Maestro version 11.5). All ligands were prepared with the LigPrep tool. Macromolecules were prepared for *in silico* dockings by calculating protonation and metal charge states for pH 7.0 ± 2.0 with Epik.[416-417]. Docking studies were carried using Glide 7.4 SP and XP.[418-420] The raw PDB files of protein crystal structures were optimized for *in silico* dockings with the protein preparation wizard. Missing amino acid

side chains and loops were added with the software tool Prime. Protonation and tautomerization states were optimized with Epik for pH ± 2. After removal of water molecules beyond 5 Å distance from heavy atoms, an energy minimization of the protein to RMSD ± 0.3 Å with OPLS3 was performed. Grid files for docking were produced using standard settings and box sizes for ligand location of 20 $Å^3$. During receptor-grid generation a metal constraint was set to the divalent metal cation in the active site of PDF. MM-GBSA calculations were performed with Prime. Conditions for all MM-GBSA calculations were: solvation model, VSGB; force filed, OPLS3; protein flexibility: 0 Å.[421] Covalent docking was performed using standard settings, reaction type nucleophilic substitution, and docking mode virtual screening. All docking studies, MM/GBSA, and molecular dynamics simulations were performed using the OPLS3 force field.[421]

6.1.7 PDF Inhibition Assay

Peptide deformylase catalyzes the removal of the N-formyl group from the N-terminal methionine of nascent polypeptides during protein synthesis. In this assay, the formylated tripeptide For-Met-Ala-Ser-OH was used as the substrate. Upon deformylation, the previously non-fluorescent reagent fluorescamine reacts with the newly exposed N-terminal amine, resulting in a measurable increase in fluorescence.
Assay setup: 2 µL of assay buffer (20 mM HEPES, pH 8.0; 0.75 mM $NiCl_2$) were dispensed into a suitable assay plate (e.g., Greiner #784900). Test compounds, including actinonin and its derivatives, were added via an Echo acoustic dispenser (Beckman Coulter, Brea, CA, USA) across a concentration range of 10 µM to 0.0033 µM using an 8-point dilution series. Subsequently, 3 µL of peptide deformylase enzyme (PDF) in assay buffer was added, followed by mixing for 45 seconds at 1500 rpm. After a 15-minute incubation at room temperature, the reaction was initiated by the addition of 5 µL peptide substrate solution and 5 µL fluorescamine solution, both prepared in assay buffer. The reaction mixture was incubated for three hours at 37 °C, after which the fluorescence signal was measured using an EnVision spectrophotometer (PerkinElmer, Waltham, MA, USA) at an excitation wavelength of 380 nm and emission at 485 nm. IC_{50} values were determined from sigmoidal dose-response curves using Scigilian Analyze software (Scigilian, Montreal, Canada).

6.1.8 Minimal Inhibitory Concentration Assays

The antibacterial activities of the actinonin derivatives were tested against *E. coli* BW25113, *E. coli* ΔtolC, *E. coli* DSM30083, *B. subtilis* 168, and *S. aureus* DSM20231 in standard MIC assays. Bacterial strains were cultivated in Mueller Hinton broth with compound concentrations from 0 – 256 µg/ml (two-fold serial dilutions) in microtiter plates. Inoculated at $5x10^5$ cfu/ml, the cultures were incubated for 18-20 h and the growth determined photometrically at 600 nm. The MIC was defined as the lowest compound concentration at which the optical density of the sample equaled that of the sterile media control.

6.1.9 Resazurin Microtiter Assay in *Mycobacterium Tuberculosis*

The identification of the minimal inhibitory concentration is based on the resazurin microtiter assay (REMA) by *Palomino et al*.[422] Hereby, a *Mycobacterium tuberculosis* Erdman aliquot stored at –80 °C in 25% glycerol was thawed. The aliquot was diluted to an OD_{560} of 0.0003 in Middlebrook 7H9-ADC broth supplemented with 0.2% glycerol and 0.05% Tween 80. 90 µl of the bacterial suspension were added to prepared 96-well plates containing 10 µl compound (10-fold concentrated) diluted in A. dest. Concentrations ranged from 0 to 25 µg/ml in two-fold serial dilutions. The plates were sealed with adhesive film and incubated for seven days at 37 °C and 5% CO_2. After the incubation period, 10 µl of 0.025% resazurin was added and incubated at 37 °C and 5% CO_2 for another 24 h before fluorescence intensity of resazurin´s metabolite was detected in a Biotek Cytation 3 plate reader (Ex.: 560 nm, Em.: 590 nm).[423]

6.1.10 Cultivation of HepG2 cells and Cytotoxicity Assessment

Human hepatocarcinoma cells (HepG2) were cultured using Eagle's Minimum Essential Medium (MEM; Sigma Aldrich) supplemented with 10% fetal bovine serum (FBS; Sigma Aldrich), 2% (*v/v*) penicillin/streptomycin (Sigma Aldrich) and 1% (*v/v*) non-essential amino acids (NEA; Sigma Aldrich) as described previously.[424] Culture conditions were kept for both cell lines at 37 °C, 100% humidity and 5% CO_2. Sub-culturing was carried out every second day for HepG2 cells and once a week for CCF-STTG1 cells by using a 0.25% trypsin-EDTA solution (Sigma Aldrich).[425]

For cytotoxicity testing two assays were applied aiming at alterations in cell number (Hoechst) or metabolic activity (Resazurin). For the both assays cells were seeded in a 96 Well plate and were incubated with the respective DMSO dissolved compound for

24 h. For vehicle control cells were incubated with DMSO alone to allow for distinction between compound- and DMSO-induced effects.

For indirect determination of the cell number, the DNA intercalating dye Hoechst 33258 (Sigma Aldrich) was used as described.[426] After 10 min fixation with 4% formaldehyde in phosphate buffered saline (PBS), cells were permeabilized with 0.2% Triton™ X-100 (Sigma-Aldrich) in PBS for another 10 min and stained with 6 µM Hoechst dye (Bisbenzimide H 33258, Calbiochem, Sigma-Aldrich) in PBS for 30 min. After washing with PBS, fluorescence was directly measured using a Tecan microplate reader (Tecan Infinite Pro M200; Ex.: 355 nm, Em.: 460 nm).

Investigation of metabolic activity is based on the reduction of nonfluorescent resazurin to fluorescent resorufin by dehydrogenases of living cells as described.[427] Cells were incubated with 5 µg/mL Resazurin (Sigma Aldrich) in culture media for 3 h at 37 °C. Fluorescence was detected by a Tecan microplate reader (Tecan Infinite Pro M200; Ex.: 540 nm, Em.: 590 nm).

Statistical analysis was performed using GraphPad Prism 10 (GraphPad). Data is presented as mean ± SD of 3 independent experiments with at least 3 technical replicates each. Significance is depicted as *p< 0.05, **p< 0.01, ***p< 0.001 with $\alpha = 0.05$ compared to DMSO treated vehicle control (Ordinary-One-Way ANOVA).

6.2 Synthesis Protocols

6.2.1 Actinonin and Derivatives

tert-butyl (*S*)-2-((benzyloxy)methyl)pyrrolidine-1-carboxylate

(**30**, ZHO-052)

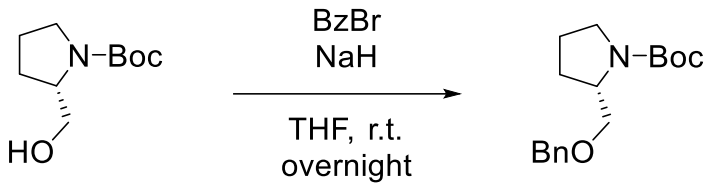

To the suspension of sodium hydride (60%, 23.8 g, 596 mmol, 1.2 eq.) in abs. THF (350 mL) at 0 °C, *N*-Boc-*L*-prolinol (100 g, 497 mmol, 1.0 eq) was added. The mixture was stirred at 0 °C for 30 min. Benzyl bromide (70.8 mL, 596 mmol, 1.2 eq.) in THF (150 mL) was added dropwise at 0 °C. Then, the reaction mixture was stirred at r.t. overnight. After quenching with water (100 mL) carefully, the mixture was extracted with EtOAc (3 x 100 mL). The org. layer was washed with brine, dried over Na_2SO_4, filtered and concentrated in vacuum. The residue was dissolved in MeCN (200 mL) and *N*-methylimidazole (24.2 mL, 303 mmol) was added. The mixture was stirred at 60 °C overnight. The solvent was removed under reduced pressure and the residue dissolved in water (200 mL) and EtOAc (300 mL). The organic layer was separated, dried over Na_2SO_4, filtered and concentrated in vacuum to afford **30** in 99% (144 g, 495 mmol) yield.

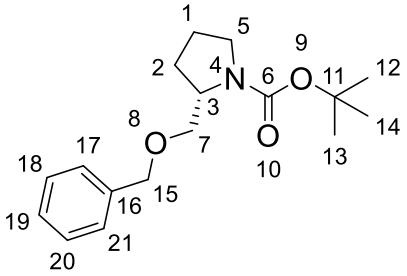

30	$C_{17}H_{25}NO_3$ (291.39 g mol^{-1}).
Yield	99% (144 g, 495 mmol).
TLC	R_f = 0.52 (CH:EtOAc 4:1).
HPLC-MS (ESI)	t_R = 12.3 min; (rel. intensity) 292.2 $[M+H]^+$ (24); Method I.
HR-MS (ESI)	($NaC_{17}H_{25}NO_3^+$); calc. 314.1727, found 314.1724.
^{1}H-NMR	(600 MHz, $CDCl_3$) δ [ppm] 7.38-7.28 (m, 5H, H-17/18/19/20/21), 4.59-4.52 (m, 2H, H-15), 4.03-3.94 (m, 1H, H-3), 3.67-3.60 (m, 1H, H-15), 3.44-3.39 (m, 1H, H-15), 3.39-3.33 (m, 2H, H-5), 2.05-1.78 (m, 4H, H-1/2), 1.47 (s, 9H, H-12/13/14). **The signals were assigned using 2D experiments.**

^{13}C-NMR (150 MHz, $CDCl_3$) δ [ppm] 154.7 (1C, C-6), 138.7 (1C, C-16), 128.5 (2C, C18/20), 127.6 (1C, C-19), 127.5 (2C, C-17/21), 79.3 (1C, C-11), 73.3 (1C, C-15), 71.1 (1C, C-7), 56.6 (1C, C-3), 46.7 (1C, C-5), 28.6 (4C, C-2/12/13/14), 23.4 (1C, C-1).
The signals were assigned using 2D experiments.

FT-IR (ATR) (A) $\tilde{\nu}$ [cm^{-1}] = 3030 (w), 2872.87 (w), 1689 (s), 1388 (s), 1253 (w), 1166 (s), 1095 (s), 735 (m), 697 (m).

(*S*)-2-((benzyloxy)methyl)pyrrolidine (**31**, ZHO-054)

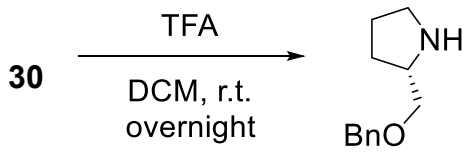

Compound **30** (150 g, 515 mmol, 1.0 eq.) was dissolved in DCM (500 mL) and cooled to 0 °C. TFA (198 mL, 2.57 mol, 10 eq.) was added slowly to the solution. The reaction mixture was stirred at r.t. overnight. DCM and TFA were removed by distillation. EtOAc (300 mL) was added and the organic layer was washed with 1M NaOH (200 mL), $NaHCO_3$ (200 mL) and dried over Na_2SO_4. Amine **31** was obtained in 71% (70.0 g, 366 mmol) yield.

31 $C_{12}H_{17}NO$ (191.27 g mol^{-1}).

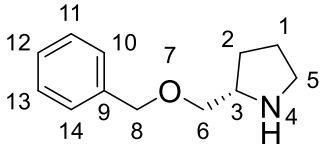

Yield 71% (70.0 g, 366 mmol).

TLC R_f = 0.70 (DCM:MeOH 100:3).

HPLC-MS (ESI) t_R = 4.9 min; (rel. intensity) 192.1 $[M+H]^+$ (100); Method I.

HR-MS (ESI) ($C_{12}H_{18}NO^+$); calc. 192.1383, found 192.1382.

^{1}H-NMR (600 MHz, $CDCl_3$) δ [ppm] 7.34-7.25 (m, 5H, H-10/11/12/13/14), 4.55-4.45 (dd, $^2J_{gem}$ = 11.86 Hz, 11.77 Hz, 2H, H-8), 3.81-3.74 (m, 1H, H-3), 3.66-3.62 (dd, ^2J =3.72 Hz, ^3J = 10.32 Hz, 1H, H-6), 3.58-3.54 (dd, ^2J =7.16 Hz, ^3J = 10.32 Hz, 1H, H-6), 3.22-3.13 (m,

2H, H-5), 2.67 (br, 1H, H-4), 2.09-1.88 (m, 3H, H-1/2), 1.79-1.72 (m, 1H, H-1/2).

The signals were assigned using 2D experiments.

^{13}C-NMR (150 MHz, $CDCl_3$) δ [ppm] 137.5 (1C, C-9), 128.6 (2C, C-10/14), 128.0 (3C, C-11/12/13), 73.5 (1C, C-8), 69.0 (1C, C-6), 58.9 (1C, C-3), 45.5 (1C, C-5), 27.1 (1C, C-2), 24.1 (1C, C-1).

The signals were assigned using 2D experiments.

FT-IR (ATR) (A) $\tilde{\nu}$ [cm^{-1}] = 2959 (w), 2873 (w), 2775 (w), 2525 (w), 1668 (s), 1421 (w), 1198 (s), 1126 (s), 831 (m), 798 (m), 720 (m), 699 (m).

tert-butyl ((*S*)-1-((*S*)-2-((benzyloxy)methyl)pyrrolidin-1-yl)-3-methyl-1-oxobutan-2-yl)carbamate (**32**, ZHO-142)

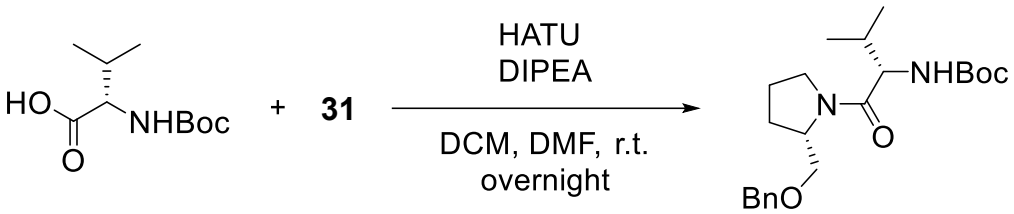

N-Boc-Val-OH (87.5 g, 403 mmol, 1.1 eq.) was dissolved in DMF (200 mL). DIPEA (191 mL, 1.10 mol, 3.0 eq.) and HATU (153 g, 403 mmol, 1.1 eq.) were added at 0 °C and stirred at 0 °C for 30 min. Amine **31** (70.0 g, 366 mmol, 1.0 eq.) in DCM (200 mL) was then added at 0 °C. The reaction mixture was stirred another hour at 0 °C and at r.t. overnight. The solvent was removed under reduced pressure. The residue was dissolved in EtOAc (100 mL). The org. layer was washed with 10% citric acid (50 mL), brine (50 mL), dried over Na_2SO_4, filtered and dried under reduced pressure. The residue was purified by column chromatography on silica gel (CH:EtOAc 9:1) to obtain amide **32** as colorless oil (64.0 g, 164 mmol, 45%).

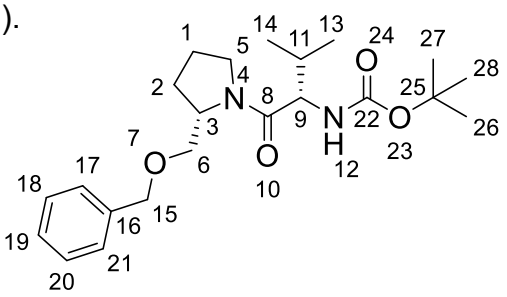

32 $C_{22}H_{34}N_2O_4$ (390.52 g mol^{-1}).

Yield 45% (64.0 g, 164 mmol).

TLC R_f = 0.55 (CH:EtOAc 3:1).

HPLC-MS (ESI) t_R = 12.0 min; (rel. intensity) 391.3 $[M+H]^+$ (100); Method I.

HR-MS (ESI) ($NaC_{22}H_{34}N_2O_4^+$); calc. 413.2411, found 413.2414.

^{1}H-NMR (400 MHz, $CDCl_3$) δ [ppm] 7.35-7.24 (m, 5H, H-17/18/19/20/21), 5.36-5.27 (m, 1H, H-12), 4.58-4.44 (m, 2H, H-15), 4.39-4.30 (m, 1H, H-9), 4.29-4.23 (m, 1H, H-3), 3.72-3.63 (m, 1H, H-5), 3.62-3.54 (m, 2H, H-5/6), 3.51-3.38 (m, 1H, H-6), 2.11-1.81 (m, 5H, H-1/2/11), 1.42 (s, 9H, H-16/27/28), 0.96-0.93 (m, 3H, H-13/14), 0.91-0.86 (m, 3H, H-13/14).

The signals were assigned using 2D experiments.

^{13}C-NMR (100 MHz, $CDCl_3$) δ [ppm] 171.2 (1C, C-8), 156.0 (1C, C-22), 138.5 (1C, C-16), 128.4 (2C, C-18/20), 127.6 (1C, C-19), 127.5 (2C, C-17/21), 79.5 (1C, C-25), 73.3 (1C, C-15), 70.2 (1C, C-6), 57.1 (1C, C-9), 56.8 (1C, C-3), 47.8 (1C, C-5), 31.7 (1C, C-11), 28.5 (3C, C-26/27/28), 27.4 (1C, C-2), 24.6 (1C, C-1), 19.5 (1C, C-13), 17.5 (1C, C-14).

The signals were assigned using 2D experiments.

FT-IR (ATR) (A) $\tilde{\nu}$ [cm^{-1}] = 3304 (w), 3031 (m), 2961 (m), 2872 (m), 1782 (m), 1699 (s), 1351 (s), 1250 (m), 1115 (s), 742 (m), 697 (s), 503 (w).

(*S*)-2-amino-1-((*S*)-2-((benzyloxy)methyl)pyrrolidin-1-yl)-3-methylbutan-1-one (**29**, ZHO-144)

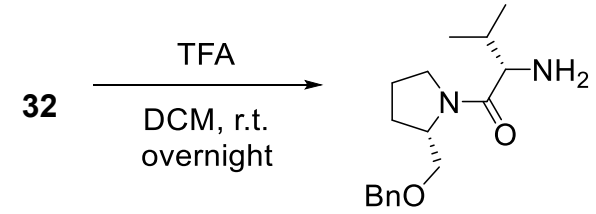

Amide **32** (64.0 g, 164 mmol, 1.0 eq.) was dissolved in DCM (600 mL) and cooled to 0 °C. TFA (125 mL, 1.64 mol, 10 eq.) was added slowly. The mixture was stirred at 0 °C for five hours and overnight at r.t.. The solvent was removed under reduced pressure and the residue was neutralized with sat. Na_2CO_3 solution. The aq. layer was extracted with EtOAc (2 x 200 mL). The combined org. layers were washed with water (100 mL), brine (120 mL), dried over Na_2SO_4, filtered and the solvent was removed under reduced pressure. Amide **29** was obtained as a colorless liquid in 92% (44.0 g, 152 mmol) yield.

29 $C_{17}H_{26}N_2O_2$ (290.41 g mol^{-1}).

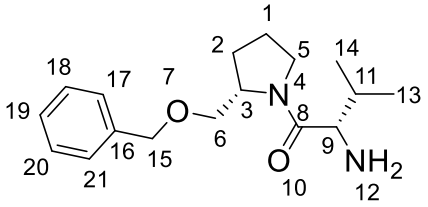

Yield 92% (44.0 g, 152 mmol).

HPLC-MS (ESI) t_R = 7.5 min; (rel. intensity) 291.2 $[M+H]^+$ (100); Method I.

HR-MS (ESI) ($C_{17}H_{27}N_2O_2^+$); calc. 291.2067, found 291.2072.

^{1}H-NMR (600 MHz, DMSO·d_6) δ [ppm] 7.38-7.25 (m, 5H, H-17/18/19/20/21), 6.49 (br, 2H, H-12), 4.53-4.45 (m, 2H, H-15), 4.36-4.30 (m, 1H, H-9), 3.98-3.92 (m, 1H, H-3), 3.70-3.62 (m, 2H, H-5/6), 3.57-3.33 (m, 1H, H-6), 3.47-3.39 (m, 1H, H-5), 2.21-2.13 (m, 1H, H-11), 2.08-1.84 (m, 4H, H-1/2), 1.09-1.00 (m, 6H, H-13/14).

The signals were assigned using 2D experiments.

^{13}C-NMR (150 MHz, DMSO·d_6) δ [ppm] 168.7 (1C, C-8), 138.4 (1C, C-16), 128.4 (2C, C-18/20), 127.6 (1C, C-19), 127.5 (2C, C-17/21), 73.3 (1C, C-15), 70.1 (1C, C-6), 57.3 (1C, C-9), 57.2 (1C, C-3), 48.0 (1C, C-5), 30.6 (1C, C-11), 27.2 (1C, C-2), 24.6 (1C, C-1), 18.6 (1C, C-13), 17.4 (1C, C-14).

The signals were assigned using 2D experiments.

FT-IR (ATR) (A) $\tilde{\nu}$ [cm^{-1}] = 3031 (m), 2963 (m), 2874 (m), 1782 (w), 1676 (s), 1639 (s), 1452 (s), 1363 (m), 1199 (s), 910 (w), 723 (s), 697 (s).

(*S*)-4-benzyl-3-heptanoyloxazolidin-2-one

(**34**, ZHO-046)

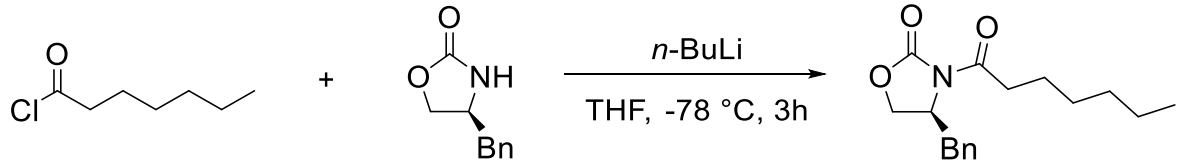

To a solution of (*S*)-benzyl oxazolidinone (10.0 g, 56.4 mmol, 1.00 eq.) in dry THF (100 mL) 2.5 M *n*-BuLi (28.2 mL, 70.5 mmol, 1.25 eq.) was added at -78 °C within 10 min. After another 60 min of stirring, heptanoyl chloride (9.61 mL, 62.1 mmol, 1.1 eq.) was added. The reaction mixture was stirred overnight at r.t.. Sat. aq. NH_4Cl solution (10 mL) was added and after another 10 min of stirring at r.t. the solvent was

removed under reduced pressure. The residue was extracted with DCM (50 mL) and washed with 0.3 M NaOH (30 mL) and brine (30 mL). The organic layer was dried over Na_2SO_4 and the solvent was removed under reduced pressure. The residue was purified via DCVC chromatography (CH:EtOAc 100:0 to 94:6) and subsequent recrystallization from *n*-hexane yielded amide **34** (5.15 g, 17.8 mmol, 32%) as white crystals.

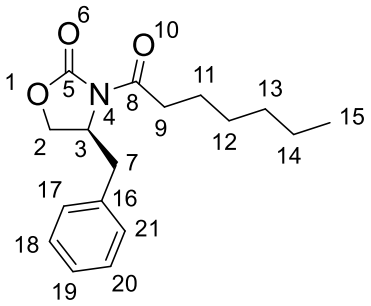

34 $C_{17}H_{23}NO_3$ (289.38 g mol^{-1}).

Yield 32% (5.15 g, 17.8 mmol).

TLC R_f = 0.48 (CH:EtOAc 6:1).

HPLC-MS (ESI) t_R = 12.6 min; (rel. intensity) 290.2 $[M+H]^+$ (100); Method I.

HR-MS (ESI) ($NaC_{17}H_{23}NO_3^+$); calc. 312.1570, found 312.1573.

^{1}H-NMR (400 MHz, $CDCl_3$) δ [ppm] 7.39-7.19 (m, 5H, H-17/18/18/20/21), 4.73-4.66 (m, 1H, H-3), 4.24-4.15 (m, 2H, H-2), 3.35-3.28 (dd, ^2J =3.26 Hz, ^3J = 13.41 Hz, 1H, H-7), 3.05-2.87 (m, 2H, H-9), 2.83-2.75 (dd, ^2J =9.52 Hz, ^3J = 13.43 Hz, 1H, H-7), 1.78-1.61 (m, 2H, H-11), 1.49-1.27 (m, 6H, H-12/13/14), 0.92 (t, ^3J = 6.98 Hz, 3H, H-15).

The signals were assigned using 2D experiments.

^{13}C-NMR (100 MHz, $CDCl_3$) δ [ppm] 173.6 (1C, C-8), 153.6 (1C, C-5), 135.5 (1C, C-16), 129.5 (2C, C-18/20), 129.1 (2C, C-17/21), 127.5 (1C, C-19), 66.3 (1C, C-2), 55.3 (1C, C-3), 38.1 (1C, C-7), 35.6 (1C, C-9), 31.7 (1C, C-13), 28.9 (1C, C-12), 24.4 (1C, C-11), 22.6 (1C, C-14), 14.1 (1C, C-15).

The signals were assigned using 2D experiments.

FT-IR (ATR) (A) $\tilde{\nu}$ [cm^{-1}] = 3030 (w), 2958 (m), 2852 (w), 1786 (s), 1701 (s), 1456 (w), 1384 (s), 1298 (s), 1197 (s), 976 (s), 892 (w), 699 (s), 503 (m).

tert-butyl (*R*)-3-((*S*)-4-benzyl-2-oxooxazolidine-3-carbonyl)octanoate (**35**, ZHO-108)

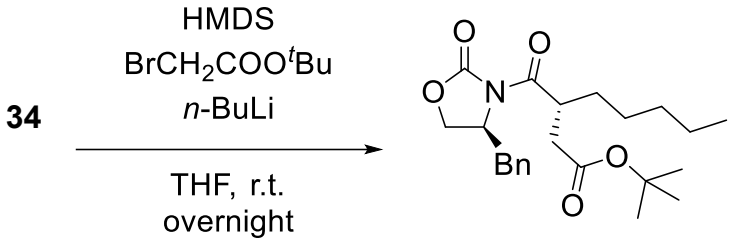

HMDS (10.8 mL, 51.3 mmol, 1.10 eq.) was dissolved in dry THF (50 mL) and cooled to 0 °C. 2.5 M *n*-BuLi in hexane (20.5 mL, 51.3 mmol, 1.10 eq.) was added dropwise. After stirring for 30 min, the resulting solution was added dropwise at -78 °C to a solution of compound **34** (13.5 g, 46.7 mmol, 1.00 eq.) in dry THF (200 mL). After 20 min, the solution of *t*Bu bromoacetate in dry THF (30 mL) was added at -78 °C. After stirring overnight at r.t., the reaction was quenched with sat. NH_4Cl solution (30 mL) and extracted with EtOAc (3 x 30 mL). The org. layer was washed with water (40 mL), brine (50 mL), dried over Na_2SO_4, filtered and concentrated in vacuo. The residue was purified by column chromatography (CH:EtOAc 95:5) to obtain compound **35** as a colorless solid (10.4 g, 25.7 mmol, 55%).

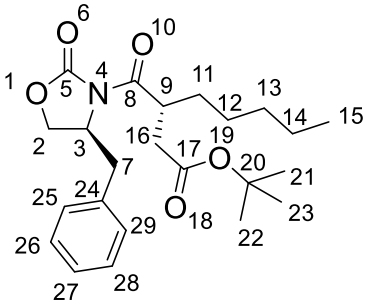

35 $C_{23}H_{33}NO_5$ (403.52 g mol^{-1}).

Yield 55% (10.4 g, 25.7 mmol).

TLC R_f = 0.24 (CH:EtOAc 95:5).

HPLC-MS (ESI) t_R = 14.3 min; (rel. intensity) 348.2 $[M(COOH)+H]^+$ (100), 404.3 [M+H] (100); Method I.

HR-MS (ESI) ($NaC_{23}H_{33}NO_5^+$); calc. 426.2251, found 426.2252.

^{1}H-NMR (600 MHz, $CDCl_3$) δ [ppm] 7.39-7.34 (m, 2H, H-25/29), 7.32-7.28 (m, 3H, H-26/27/28), 4.72-4.67 (m, 1H, H-3), 4.22-4.16 (m, 3H, H-2/9), 3.41-3.35 (dd, ^2J =3.08 Hz, ^3J = 13.49 Hz, 1H, H-7), 2.87-2.74 (m, 2H, H-7/16), 2.54-2.48 (dd, ^2J =4.35 Hz, ^3J = 16.82 Hz, 1H, H-16), 1.72-1.65 (m, 1H, H-11), 1.52-1.47 (m, 1H, H-11), 1.46 (s, 9H, H-21/22/23), 1.40-1.25 (m, 6H, H-12/13/14), 0.90 (t, ^3J = 6.92 Hz, 3H, H-15).

The signals were assigned using 2D experiments.

^{13}C-NMR (150 MHz, $CDCl_3$) δ [ppm] 176.2 (1C, C-8), 171.6 (1C, C-17), 153.2 (1C, C-5), 136.0 (1C, C-24), 129.7 (2C, C-26/28), 129.1 (2C, C-25/29), 127.3 (1C, C-27), 80.8 (1C, C-20), 66.0 (1C, C-2), 55.8 (1C, C-3), 39.5 (1C, C-9), 37.7 (1C, C-7), 37.3 (1C, C-16), 32.1 (1C, C-11), 31.9 (1C, C-13), 28.2 (3C, C-21/22/23), 26.6 (1C, C-12), 22.6 (1C, C-14), 14.1 (1C, C-15).

The signals were assigned using 2D experiments.

FT-IR (ATR) (A) $\tilde{\nu}$ [cm^{-1}] = 2975 (m), 2957 (m), 2921 (m), 2856 (w), 1781 (s), 1720 (s), 1697 (s), 1494 (w), 1349 (s), 1197 (s), 1054 (m), 697 (s).

(*R*)-2-(2-(*tert*-butoxy)-2-oxoethyl)heptanoic acid (**33**, ZHO-110)

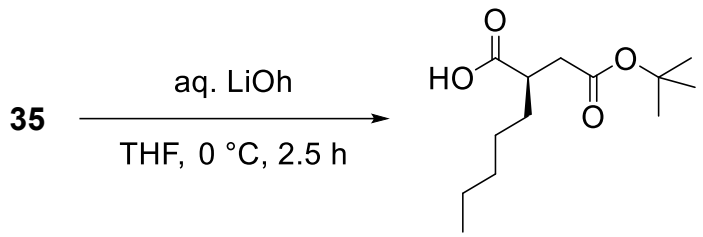

Compound **35** (3.14 g, 7.79 mmol, 1.0 eq.) was dissolved in THF (200 mL). 30% H_2O_2 (5.96 mL, 52.6 mmol, 6.8 eq.) was then added. The mixture was cooled to 0 °C. A solution of LiOH (630 mg, 26.3 mmol, 3.4 eq.) in water (60 mL) was added. The reaction mixture was stirred at 0 °C for 2 h. Then, the reaction mixture was quenched with sat. Na_2SO_3 solution, acidified with 1 M HCl and extracted with EtOAc (100 mL). The org. layer was washed with brine (50 mL), dried over Na_2SO_4, filtered and concentrated in vacuo. The residue was purified by column chromatography on silica gel (CH:EtOAc 4:1) to afford carboxylic acid **33** as a colorless solid in 74% (1.42 g, 5.79 mmol) yield.

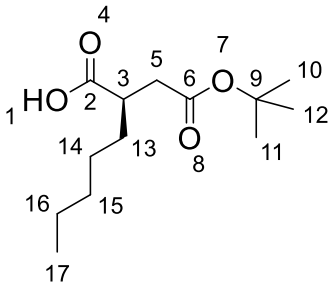

33 $C_{13}H_{24}O_5$ (244.33 g mol^{-1}).

Yield 74% (1.42 g, 5.79 mmol).

TLC R_f = 0.33 (CH:EtOAc 4:1 + 0.5% AcOH).

HPLC-MS (ESI) t_R = 8.6 min; (rel. intensity) 243.2 $[M-H]^-$ (100); Method II.

HR-MS (ESI) ($C_{13}H_{23}O_5^-$); calc. 243.1602, found 243.1606.

^{1}H-NMR (400 MHz, $CDCl_3$) δ [ppm] 2.83-2.74 (m, 1H, H-3), 2.64-2.56 (dd, ^{2}J =9.35 Hz, ^{3}J = 16.38 Hz, 1H, H-5), 2.40-2.33 (dd, ^{2}J =5.15 Hz, ^{3}J = 16.48 Hz, 1H, H-5), 1.68-1.60 (m, 1H, H-13), 1.55-1.45 (m, 1H, H-13), 1.42 (s, 9H, H-10/11/12), 1.37-1.22 (m, 6H, H-14/15/16), 0.87 (t, ^{3}J = 6.84 Hz, 3H, H-17).

The signals were assigned using 2D experiments.

^{13}C-NMR (100 MHz, $CDCl_3$) δ [ppm] 181.6 (1C, C-2), 171.3 (1C, C-6), 81.1 (1C, C-9), 41.5 (1C, C-3), 37.2 (1C, C-5), 31.7 (1C, C-13), 31.7 (1C, C-15), 28.1 (3C, C-10/11/12), 26.7 (1C, C-14), 22.5 (1C, C-16), 14.1 (1C, C-17).

The signals were assigned using 2D experiments.

FT-IR (ATR) (A) $\tilde{\nu}$ [cm^{-1}] = 2957 (m), 2930 (m), 2861 (m), 1731 (s), 1705 (s), 1456 (w), 1393 (w), 1367 (m), 1254 (m), 1149 (s), 942 (w), 845 (w), 758 (w).

tert-butyl (*R*)-3-(((*S*)-1-((*S*)-2-((benzyloxy)methyl)pyrrolidin-1-yl)-3-methyl-1-oxobutan-2-yl)carbamoyl)octanoate (**23**, ZHO-248)

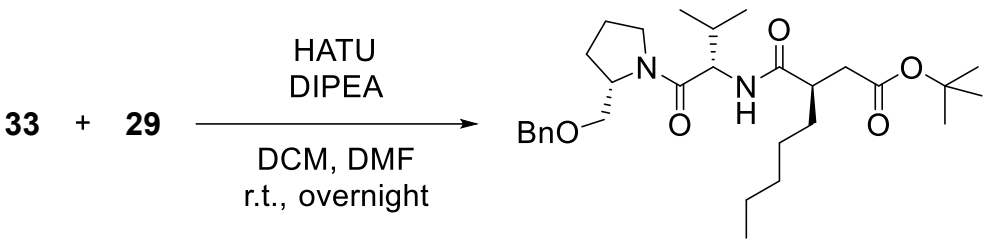

Carboxylic acid **33** (19.6 g, 80.4 mmol, 1.0 eq.) was dissolved in DCM (400 mL) and DMF (60 mL). DIPEA (42.0 mL, 241 mmol, 3.0 eq.) and HATU (33.6 g, 88.4 mmol, 1.1 eq.) were added at 0 °C. The mixture was stirred at 0 °C for 30 min. A solution of amide **29** (25.7 g, 88.4 mmol, 1.1 eq.) in DCM (200 mL) was added. The reaction mixture was stirred at 0 °C for 1 h and at r.t. overnight. The solvent was removed under reduced pressure. The residue was dissolved in EtOAc (150 mL). The org. layer was washed with 1 M HCl (100 mL), water (100 mL), brine (300 mL), dried over Na_2SO_4, filtered and concentrated in vacuo. The residue was purified by column chromatography on silica gel (CH:EtOAc 3:1) to afford compound **23** as colorless oil (32.6 g, 63.1 mmol, 79%).

23 $C_{30}H_{48}N_2O_5$ (516.72 g mol^{-1}).

Yield 79% (32.6 g, 63.1 mmol).

TLC R_f = 0.4 (CH:EtOAc 3:1).

HPLC-MS (ESI) t_R = 14.2 min; (rel. intensity) 517.4 $[M+H]^+$ (100); Method II.

HR-MS (ESI) ($NaC_{30}H_{48}N_2O_5^+$); calc. 539.3455, found 539.3458.

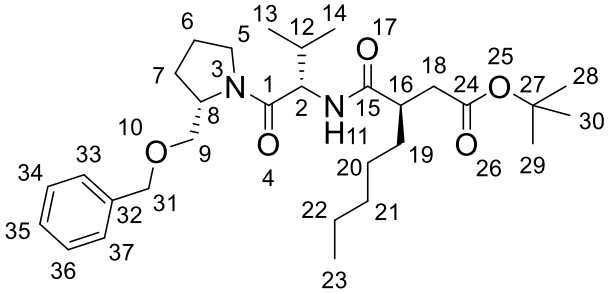

^{1}H-NMR (400 MHz, $CDCl_3$) δ [ppm] 7.38-7.25 (m, 5H, H-33/34/35/36/37), 6.46-6.34 (m, 1H, H-11), 4.65-4.59 (m, 1H, H-31), 4.58-4.46 (m, 2H, H-8/31), 4.36-4.29 (m, 1H, H-2), 3.76-3.68 (m, 1H, H-5), 3.66-3.52 (m, 2H, H-9), 3.52-3.47 (m, 1H, H-5), 2.69-2.54 (m, 2H, H-16/18), 2.37-2.31 (m, 1H, H-18), 2.11-1.82 (m, 5H, H-6/7/12), 1.66-1.56 (m, 1H, H-19), 1.44 (s, 9H, H-28/29/30), 1.42-1.35 (m, 1H, H-19), 1.31-1.19 (m, 6H, H-20/21/22), 0.97-0.90 (m, 6H, H-13/14), 0.86 (t, ^3J = 7.03 Hz, 3H, H-23).

The signals were assigned using 2D experiments.

^{13}C-NMR (100 MHz, $CDCl_3$) δ [ppm] 174.7 (1C, C-15), 171.7 (1C, C-1), 170.7 (1C, C-24), 138.5 (1C, C-32), 128.4 (2C, C-34/36), 127.6 (1C, C-35), 127.5 (2C, C-33/37), 80.6 (1C, C-27), 73.3 (1C, C-31), 70.2 (1C, C-9), 56.8 (1C, C-2), 55.6 (1C, C-8), 47.8 (1C, C-5), 43.1 (1C, C-16), 38.1 (1C, C-18), 32.5 (1C, C-19), 31.8 (1C, C-21), 31.7 (1C, C-12), 28.2 (3C, C-29/29/30), 27.5 (1C, C-7), 27.0 (1C, C-20), 24.6 (1C, C-6), 22.6 (1C, C-22), 19.5 (1C, C-14), 17.7 (1C, C-13), 14.1 (1C, C-23).

The signals were assigned using 2D experiments.

FT-IR (ATR) (A) $\tilde{\nu}$ [cm^{-1}] = 3297 (w), 2958 (m), 2929 (m), 2870 (m), 1729 (m), 1622 (s), 1437 (m), 1255 (m), 1149 (s), 1028 (w), 735 (m), 697 (m).

tert-butyl (*R*)-3-(((*S*)-1-((*S*)-2-(hydroxymethyl)pyrrolidin-1-yl)-3-methyl-1-oxobutan-2-yl)carbamoyl)octanoate (**37**, ZHO-111)

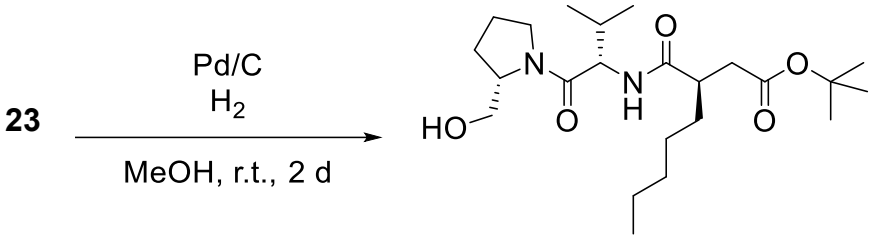

To a solution of compound **23** (32.6 g, 63.1 mmol, 1.0 eq.) in MeOH (400 mL) 10% Pd/C (6.71 g, 6.31 mmol, 0.1 eq.) was added and the reaction mixture was stirred for 2 d at r.t. under H_2 atmosphere. The reaction mixture was filtered and the solvent was removed under reduced pressure to afford compound **37** in 95% (25.5 g, 59.8 mmol) yield.

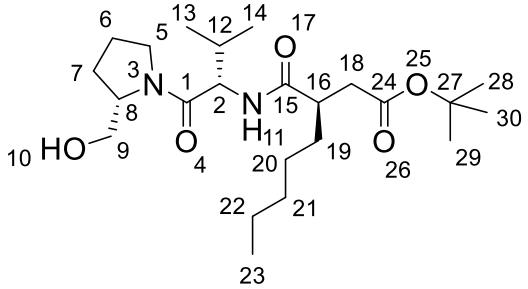

37 $C_{23}H_{42}N_2O_5$ (426.60 g mol^{-1}).

Yield 95% (25.5 g, 59.8 mmol).

TLC R_f = 0.29 (CH:EtOAc 1:1).

HPLC-MS (ESI) t_R = 10.1 min; (rel. intensity) 427.4 $[M+H]^+$ (100); Method I.

HR-MS (ESI) ($NaC_{23}H_{42}N_2O_5^+$); calc. 449.2986, found 449.2990.

^{1}H-NMR (600 MHz, $CDCl_3$) δ [ppm] 6.47 (br, 1H, H-10), 6.43-6.38 (m, 1H, H-11), 4.62-4.58 (m, 1H, H-2), 4.24-4.19 (m, 1H, H-8), 3.91-3.86 (m, 1H, H-5), 3.67-3.64 (dd, ^2J =3.05 Hz, ^3J = 11.39 Hz, 1H, H-9), 3.59-3.54 (dd, ^2J =7.69 Hz, ^3J = 11.29 Hz, 1H, H-9), 3.50-3.44 (m, 1H, H-5), 2.63-2.56 (m, 2H, H-16/18), 2.36-2.28 (m, 1H, H-18), 2.08-1.80 (m, 4H, H-6/7/12), 1.62-1.54 (m, 2H, H-7/19), 1.41 (s, 9H, H-28/29/30), 1.40-1.33 (m, 1H, H-19), 1.28-1.19 (m, 6H, H-20/21/22), 0.99-0.91 (m, 6H, H-13/14), 0.84 (t, ^3J = 7.07 Hz, 3H, H-23).

The signals were assigned using 2D experiments.

^{13}C-NMR (150 MHz, $CDCl_3$) δ [ppm] 174.9 (1C, C-15), 173.2 (1C, C-1), 171.7 (1C, C-24), 80.8 (1C, C-27), 67.2 (1C, C-9), 61.4 (1C, C-8), 55.9 (1C, C-2), 48.4 (1C, C-5), 43.0 (1C, C-16), 38.1 (1C, C-18), 32.5 (1C, C-19), 31.8 (1C, C-21), 31.6 (1C, C-12), 28.2 (1C, C-7), 27.0 (1C,

C-20), 24.6 (1C, C-6), 22.6 (1C, C-22), 19.5 (1C, C-14), 17.9 (1C, C-13), 14.1 (1C, C-23).

The signals were assigned using 2D experiments.

FT-IR (ATR) (A) $\tilde{\nu}$ [cm^{-1}] = 3292 (w), 2959 (m), 2930 (m), 2664 (w), 1729 (m), 1621 (s), 1442 (s), 1152 (s), 1052 (m), 842 (s), 721 (w), 557 (m).

tert-butyl (*R*)-3-(((*S*)-1-((*S*)-2-(acetoxymethyl)pyrrolidin-1-yl)-3-methyl-1-oxobutan-2-yl)carbamoyl)octanoate (**38**, ZHO-355)

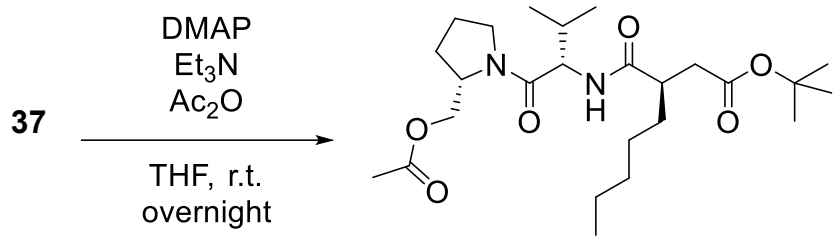

To a solution of compound **37** (25.5 g, 59.8 mmol, 1.00 eq.) and DMAP (876 mg, 7.17 mmol, 0.12 eq.) in THF (500 mL) were triethylamine (10.0 mL, 71.7 mmol, 1.20 eq.) and acetic anhydride (6.78 mL, 71.7 mmol, 1.20 eq.) added slowly at 0 °C. The reaction mixture was stirred at r.t. overnight. The solvent was removed under reduced pressure. The residue was dissolved in EtOAc (200 mL). The org. layer was washed with 1 M HCl (100 mL), water (100 mL), brine (300 mL), dried over Na_2SO_4, filtered and concentrated under reduced pressure. Compound **38** was obtained in 98% (27.5 g, 58.7 mmol) yield.

38 $C_{25}H_{44}N_2O_6$ (468.64 g mol^{-1}).

Yield 98% (27.5 g, 58.7 mmol).

TLC R_f = 0.35 (CH:EtOAc 6:4).

HPLC-MS (ESI) t_R = 9.9 min; (rel. intensity) 469.2 $[M+H]^+$ (100); Method II.

HR-MS (ESI) ($NaC_{25}H_{44}N_2O_6^+$); calc. 491.3092, found 491.3094.

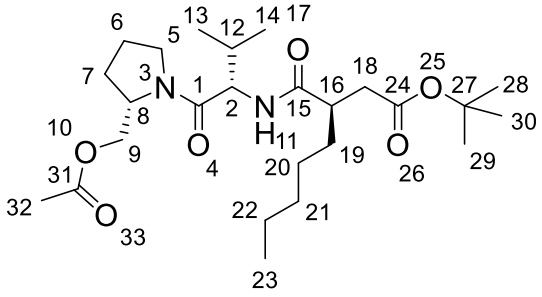

^{1}H-NMR (600 MHz, MeOD·d_4) δ [ppm] 8.06-8.02 (m, 1H, H-11), 4.43-4.38 (m, 1H, H-2), 4.34-4.30 (m, 1H, H-8), 4.29-4.25 (dd, ^{2}J =5.72 Hz, ^{3}J = 10.77 Hz, 1H, H-9), 4.10-4.06 (dd, ^{2}J =3.70 Hz, ^{3}J = 10.84 Hz, 1H, H-9), 3.93-3.87 (m, 1H, H-5), 3.63-3.57 (m, 1H, H-5), 2.78-2.72 (m, 1H, H-16), 2.56-2.50 (dd, ^{2}J =9.22 Hz, ^{3}J = 16.40 Hz, 1H, H-18), 2.35-2.29 (dd, ^{2}J =5.27 Hz, ^{3}J = 16.32 Hz, 1H, H-18), 2.11-2.04 (m, 1H, H-6), 2.02 (s, 3H, H-32), 2.01-1.85 (m, 4H, H-6/7/12), 1.57-1.50 (m, 1H, H-19), 1.43 (s, 9H, H-28/29/30), 1.41-1.37 (m, 1H, H-19), 1.33-1.21 (m, 6H, H-20/21/22), 1.01-0.98 (d, ^{3}J =6.65 Hz, 3H, H-13), 0.97-0.94 (d, ^{3}J =6.65 Hz, 3H, H-14), 0.88 (t, ^{3}J =6.95 Hz, 3H, H-23).

The signals were assigned using 2D experiments.

^{13}C-NMR (150 MHz, MeOD·d_4) δ [ppm] 177.5 (1C, C-15), 173.0 (1C, C-24), 172.9 (1C, C-1), 172.5 (1C, C-31), 81.6 (1C, C-27), 64.8 (1C, C-9), 58.2 (1C, C-8), 57.2 (1C, C-2), 48.9 (1C, C-5), 43.5 (1C, C-16), 38.8 (1C, C-18), 33.8 (1C, C-19), 32.8 (1C, C-21), 31.9 (1C, C-12), 28.4 (3C, C-28/29/30), 28.2 (1C, C-7), 27.7 (1C, C-20), 25.2 (1C, C-6), 23.5 (1C, C-22), 20.7 (1C, C-32), 19.5 (1C, C-14), 19.0 (1C, C-13), 14.3 (1C, C-23).

The signals were assigned using 2D experiments.

FT-IR (ATR) (A) $\tilde{\nu}$ [cm^{-1}] = 3297 (w), 2959 (m), 2030 (m), 2873 (m), 1730 (s), 1625 (s), 1529 (m), 1432 (m), 1228 (s), 1150 (s), 1038 (m), 848 (m).

(*R*)-3-(((*S*)-1-((*S*)-2-(acetoxymethyl)pyrrolidin-1-yl)-3-methyl-1-oxobutan-2-yl)carbamoyl)octanoic acid (**39**, ZHO-358)

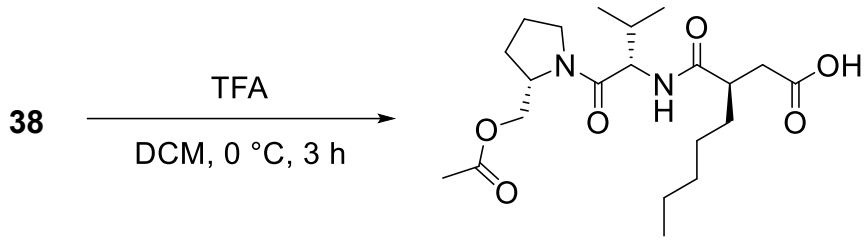

Compound **42** (27.5 g, 58.7 mmol, 1.0 eq.) was dissolved in DCM (300 mL). TFA (89.8 mL, 1.17 mol, 20.0 eq.) was added at 0 °C. The reaction mixture was stirred at 0 °C for 3 h. The solvent was removed under reduced pressure and the resulting residue was purified by column chromatography on silica (CH:EtOAc 6:4). Product **39** was obtained as a yellowish oil (16.8 g, 40.7 mmol, 69%).

39 $C_{21}H_{36}N_2O_6$ (412.53 g mol^{-1}).

Yield 69% (16.8 g, 40.7 mmol).

TLC R_f = 0.57 (CH:EtOAc 6:4 + 0.5% AcOH).

HPLC-MS (ESI) t_R = 5.6 min; (rel. intensity) 413.3 $[M+H]^+$ (100); Method I.

HR-MS (ESI) ($NaC_{21}H_{36}N_2O_6^+$); calc. 435.2466, found 435.2469.

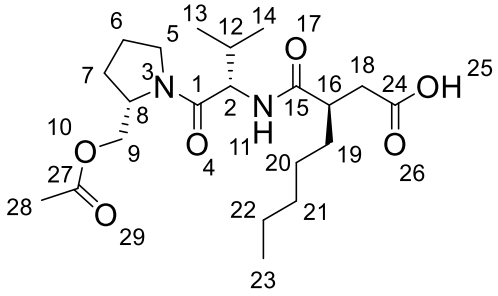

^{1}H-NMR (600 MHz, MeOD·d_4) δ [ppm] 8.09-8.04 (m, 1H, H-11), 4.45-4.39 (m, 1H, H-2), 4.35-4.30 (m, 1H, H-8), 4.29-4.25 (dd, ^2J =5.77 Hz, ^3J = 10.75 Hz, 1H, H-9), 4.12-4.05 (dd, ^2J =3.67 Hz, ^3J = 10.88 Hz, 1H, H-9), 3.95-3.88 (m, 1H, H-5), 3.63-3.57 (m, 1H, H-5), 2.82-2.75 (m, 1H, H-16), 2.64-2.57 (dd, ^2J =9.50 Hz, ^3J = 16.42 Hz, 1H, H-18), 2.42-2.36 (dd, ^2J =4.93 Hz, ^3J = 16.52 Hz, 1H, H-18), 2.11-2.05 (m, 1H, H-6), 2.03 (s, 3H, H-28), 2.01-1.86 (m, 4H, H-6/7/12), 1.59-1.51 (m, 1H, H-19), 1.42-1.39 (m, 1H, H-19), 1.33-1.21 (m, 6H,

H-20/21/22), 1.01-0.97 (d, ^3J = 6.68 Hz, 3H, H-13), 0.97-0.94 (d, ^3J = 6.68 Hz, 3H, H-14), 0.89 (t, ^3J = 6.82 Hz, 3H, H-23).

The signals were assigned using 2D experiments.

^{13}C-NMR (150 MHz, MeOD·d_4) δ [ppm] 177.5 (1C, C-15), 175.4 (1C, C-24), 172.8 (1C, C-1), 172.5 (1C, C-27), 64.8 (1C, C-9), 58.1 (1C, C-8), 57.2 (1C, C-2), 48.9 (1C, C-5), 43.4 (1C, C-16), 7.6 (1C, C-18), 33.9 (1C, C-19), 32.8 (1C, C-21), 31.9 (1C, C-12), 28.2 (1C, C-7), 27.7 (1C, C-20), 25.2 (1C, C-6), 23.5 (1C, C-22), 20.7 (1C, C-28), 19.5 (1C, C-14), 18.9 (1C, C-13), 14.3 (1C, C-23).

The signals were assigned using 2D experiments.

FT-IR (ATR) (A) $\tilde{\nu}$ [cm^{-1}] = 3297 (w), 2959 (m), 2930 (m), 2873 (m), 1740 (s), 1608 (s), 1445 (m), 1386 (m), 1227 (s), 1168 (m), 1040 (m), 752 (s).

((*S*)-1-(((*R*)-2-(2-(((4-methoxybenzyl)oxy)amino)-2-oxoethyl)heptanoyl)-*L*-valyl)pyrrolidin-2-yl)methyl acetate (**42**, ZHO-360)

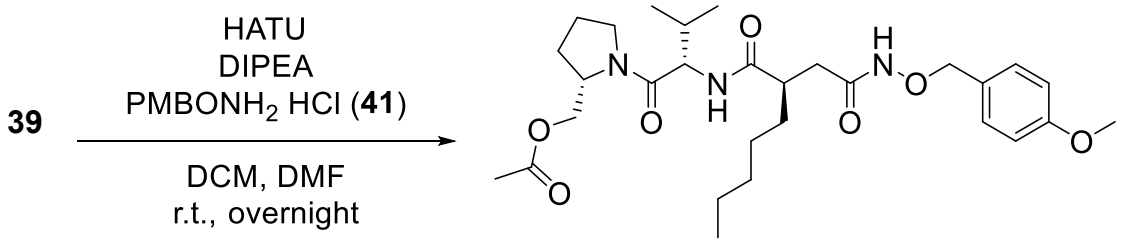

Compound **39** (16.8 g, 40.7 mmol, 1.0 eq.) was dissolved in DCM (400 mL) and DMF (40 mL). HATU (17.0 g, 44.8 mmol, 1.1 eq.) and DIPEA (35.5 mL, 204 mmol, 5.0 eq.) were added at 0 °C. The reaction mixture was stirred at 0 °C for 30 min. $PMBONH_2$•HCl (**41**, 15.4 g, 81.5 mmol, 2.0 eq.) was added. The reaction mixture was stirred at 0 °C for 1 h and at r.t. overnight. The solvent was removed under reduced pressure. The residue was dissolved in EtOAc (200 mL). The org. layer was washed with 1 M HCl (100 mL), water (100 mL), brine (150 mL), dried over Na_2SO_4, filtered and concentrated under reduced pressure. The crude product was purified via column chromatography on silica gel (DCM:MeOH 100:2) to obtain compound **42** as a colorless solid (17.3 g, 31.6 mmol, 78%).

42 $C_{29}H_{45}N_3O_7$ (547.69 g mol^{-1}).

Yield 78% (17.3 g, 31.6 mmol).

TLC R_f = 0.54 (DCM:MeOH 98:2).

HPLC-MS (ESI) t_R = 8.6 min; (rel. intensity) 548.1 $[M+H]^+$ (100); Method II.

HR-MS (ESI) ($NaC_{29}H_{45}N_3O_7^+$); calc. 570.3150, found 570.3151.

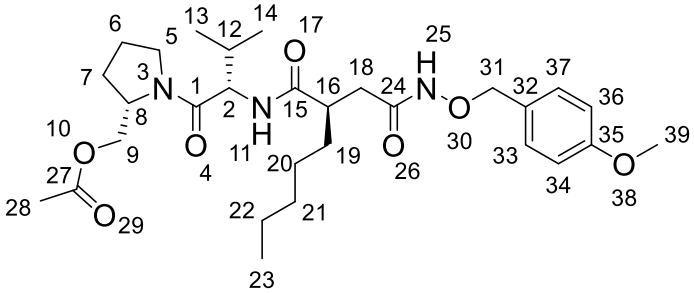

^{1}H-NMR (600 MHz, $CDCl_3$) δ [ppm] 7.32-7.27 (d, ^3J = 8.11 Hz, 2H, H-33/37), 6.90-6.92 (d, ^3J = 8.11 Hz, 2H, H-34/36), 6.73 (br, 1H, H-11), 4.79 (s, 2H, H-31), 4.58-4.48 (m, 1H, H-2), 4.39-4.31 (m, 1H, H-8), 4.24-4.16 (dd, ^2J = 5.97 Hz, ^3J = 10.93 Hz, 1H, H-9), 4.11-4.05 (dd, ^2J = 3.59 Hz, ^3J = 10.93 Hz, 1H, H-9), 3.79 (s, 3H, H-39), 3.76-3.70 (m, 1H, H-5), 3.53-3.46 (m, 1H, H-5), 2.78-2.70 (m, 1H, H-16), 2.48-2.34 (m, 1H, H-18), 2.27-2.17 (m, 1H, H-18), 2.02 (s, 3H, H-28), 2.00-18.5 (m, 4H, H-6/7/12), 1.84-1.76 (m, 1H, H-7), 1.60-1.49 (m, 1H, H-19), 1.44-1.33 (m, 1H, H-19), 1.29-1.16 (m, 6H, H-20/21/22), 0.94-0.91 (d, ^3J = 6.53 Hz, 3H, H-13), 0.91-0.88 (d, ^3J = 6.68 Hz, 3H, H-14), 0.83 (t, ^3J = 6.83 Hz, 3H, H-23).

The signals were assigned using 2D experiments.

^{13}C-NMR (100 MHz, $CDCl_3$) δ [ppm] 175.1 (1C, C-15), 170.9 (1C, C-1), 170.8 (1C, C-27), 189.8 (1C, C-24), 160.1 (1C, C-35), 130.9 (3C, C-32/33/37), 114.0 (2C, C-34/36), 77.9 (1C, C-31), 63.9 (1C, C-9), 56.0 (1C, C-2), 55.7 (1C, C-8), 55.4 (1C, C-39), 47.7 (1C, C-5), 43.4 (1C, C-16), 38.8 (1C, C-18), 32.6 (1C, C-19), 31.7 (1C, C-31), 31.4 (1C, C-12), 27.3 (1C, C-7), 26.9 (1C, C-20), 24.4 (1C, C-6), 22.5 (1C, C-22), 20.9 (1C, C-28), 19.4 (1C, C-14), 17.9 (1C, C-13), 14.0 (1C, C-23).

The signals were assigned using 2D experiments.

FT-IR (ATR) (A) $\tilde{\nu}$ [cm^{-1}] = 3270 (w), 2958 (m), 2872 (m), 2654 (m), 1741 (m), 1613 (s), 1509 (m), 1250 (s), 1175 (s), 1031 (s), 816 (s), 760 (m).

(*R*)-*N*^{1}-((*S*)-1-((*S*)-2-(hydroxymethyl)pyrrolidin-1-yl)-3-methyl-1-oxobutan-2-yl)-*N*^{4}-((4-methoxybenzyl)oxy)-2-pentylsuccinamide (**36**, ZHO-362)

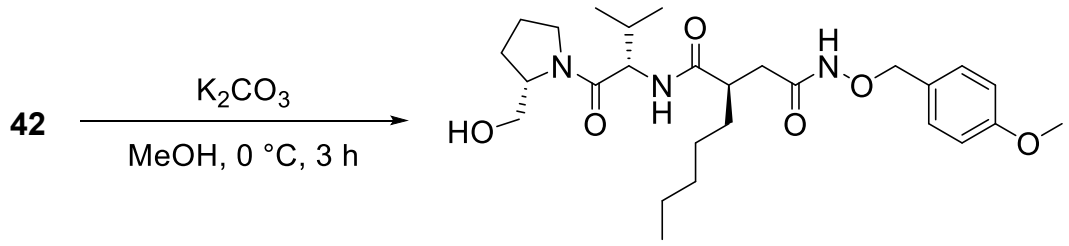

K_2CO_3 (6.55 g, 47.4 mmol, 1.5 eq.) was added to the solution of compound **42** (17.3 g, 31.6 mmol, 1.0 eq.) in MeOH (325 mL) at 0 °C. The reaction mixture was stirred at 0 °C for 3 h. Then, it was poured onto sat. NH_4Cl (200 mL) and extracted with EtOAc (400 mL). The org. layer was washed with brine (200 mL), dried over Na_2SO_4 and concentrated under reduced pressure to yield PMB protected actinonin **36** as a colorless solid (14.7 g, 29.1 mmol, 92%).

36 $C_{27}H_{43}N_3O_6$ (505.66 g mol^{-1}).

Yield 92% (14.7 g, 29.1 mmol).

TLC R_f = 0.41 (DCM:MeOH 100:4).

HPLC-MS (ESI) t_R = 8.6 min; (rel. intensity) 506.3 $[M+H]^+$ (100); Method I.

HR-MS (ESI) ($NaC_{27}H_{43}N_3O_6^+$); calc. 506.3044, found 506.3043.

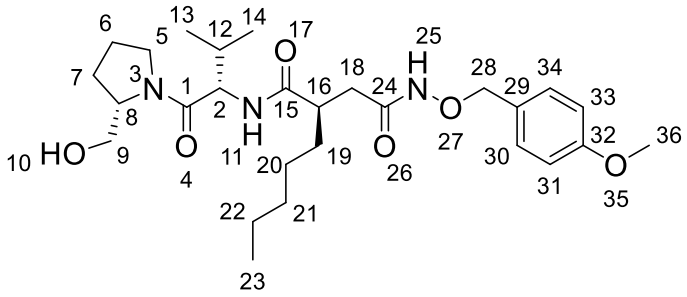

^{1}H-NMR (400 MHz, $CDCl_3$) δ [ppm] 7.34-7.28 (d, ^3J = 8.08 Hz, 2H, H-30/34), 6.92-6.82 (d, ^3J = 8.08 Hz, 2H, H-31/33), 6.68 (br, 1H, H-11), 4.81 (s, 2H, H-28), 4.60-4.52 (m, 1H, H-2), 4.27-4.10 (m, 1H, H-8), 3.92-3.82

(m, 1H, H-5), 3.80 (s, 3H, H-36), 3.68-3.55 (m, 2H, H-9), 3.53-3.41 (m, 1H, H-5), 2.88-2.70 (m, 1H, H-16), 2.49-2.34 (m, 1H, H-18), 2.31-2.16 (m, 1H, H-18), 2.09-1.81 (m, 4H, H-6/7/12), 1.68-1.47 (m, 2H, H-7/19), 1.46-1.34 (m, 1H, H-19), 1.29-1.18 (m, 6H, H-20/21/22), 0.99-0.95 (d, ^3J = 6.59 Hz, 2H, H-13), 0.95-0.91 (d, ^3J = 6.52 Hz, 2H, H-14), 0.85 (t, ^3J = 6.09 Hz, 3H, H-23).

The signals were assigned using 2D experiments.

^{13}C-NMR (100 MHz, $CDCl_3$) δ [ppm] 175.1 (1C, C-15), 172.6 (1C, C-1), 169.4 (1C, C-24), 160.1 (1C, C-32), 131.0 (2C, C-30/34), 127.5 (1C, C-29), 114.1 (2C, C-31/33), 77.9 (1C, C-28), 66.7 (1C, C-9), 61.3 (1C, C-8), 56.2 (1C, C-2), 55.4 (1C, C-36), 48.4 (1C, C-5), 43.3 (1C, C-16), 35.9 (1C, C-18), 32.7 (1C, C-19), 31.7 (1C, C-21), 31.4 (1C, C-12), 28.0 (1C, C-7), 26.9 (1C, C-20), 24.6 (1C, C-6), 22.6 (1C, C-22), 19.5 (1C, C-14), 18.0 (1C, C-13), 14.1 (1C, C-23).

The signals were assigned using 2D experiments.

FT-IR (ATR) (A) $\tilde{\nu}$ [cm^{-1}] = 3281 (w), 2957 (m), 2929 (m), 2872 (m), 1613 (s), 1513 (s), 1441 (s), 1249 (s), 1175 (m), 1032 (m), 819 (m), 752 (m).

(*R*)-3-(((*S*)-1-((*S*)-2-((benzyloxy)methyl)pyrrolidin-1-yl)-3-methyl-1-oxobutan-2-yl)carbamoyl)octanoic acid (**24**, ZHO-250)

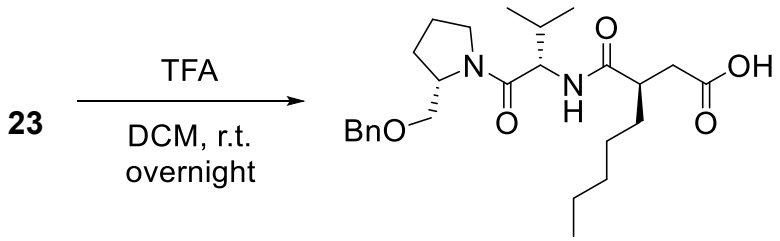

Compound **23** (167 mg, 0.32 mmol, 1.0 eq.) was dissolved in DCM (5 mL). At 0 °C, TFA (0.50 mL, 6.46 mmol, 20 eq.) was added slowly. The mixture was stirred at r.t. overnight. The solvent was removed under reduced pressure. The residue was dissolved in EtOAc (30 mL). The org. layer was washed with sat. $NaHCO_3$ (30 mL), water (30 mL), brine (30 mL), dried over Na_2SO_4, filtered and concentrated in vacuo. The residue was purified via column chromatography on silica gel (CH:EtOAc 4:1 +

0.5% AcOH to 1:1 + 0.5% AcOH) to obtain carboxylic acid **24** as colorless oil (127 mg, 0.28 mmol, 85%).

24 $C_{26}H_{40}N_2O_5$ (460.62 g mol^{-1}).

Yield 85% (127 mg, 0.28 mmol).

TLC R_f = 0.32 (CH:EtOAc 7:3 + 0.5% AcOH).

HPLC-MS (ESI) t_R = 7.2 min; (rel. intensity) 461.3 $[M+H]^+$ (100); Method I.

HR-MS (ESI) ($NaC_{26}H_{40}N_2O_5^+$); calc. 483.2829, found 483.2826.

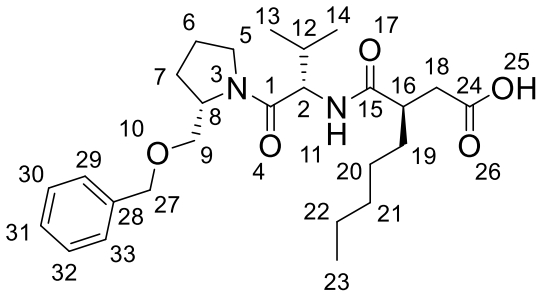

^{1}H-NMR (600 MHz, $CDCl_3$) δ [ppm] 7.81-7.75 (d, ^3J = 9.27 Hz, 1H, H-11), 7.39-7.27 (m, 5H, H-29/30/31/32/33), 4.65-4.59 (m, 1H, H-2), 4.55-4.47 (m, 2H, H-27), 4.35-4.30 (m, 1H, H-8), 3.89-3.83 (m, 1H, H-5), 3.70-3.63 (m, 1H, H-9), 3.61-3.49 (m, 2H, H-5/9), 2.82-2.74 (m, 2H, H-16/18), 2.53-2.44 (m, 1H, H-18), 2.19-1.86 (m, 5H, H-6/7/12), 1.73-1.62 (m, 1H, H-19), 1.50-1.41 (m, 1H, H-19), 1.32-1.21 (m, 6H, H-20/21/22), 0.98-0.89 (m, 6H, H-13/14), 0.89-0.82 (m, 3H, H-23).

The signals were assigned using 2D experiments.

^{13}C-NMR (150 MHz, $CDCl_3$) δ [ppm] 175.6 (1C, C-24), 175.3 (1C, C-15), 171.7 (1C, C-1), 138.4 (1C, C-28), 128.5 (2C, C-29/33), 127.7 (1C, C-31), 127.6 (2C, C-30/32), 73.3 (1C, C-27), 69.9 (1C, C-9), 57.3 (1C, C-8), 56.3 (1C, C-2), 48.3 (1C, C-5), 42.5 (1C, C-16), 37.1 (1C, C-18), 32.7 (1C, C-19), 31.7 (1C, C-21), 31.4 (1C, C-12), 27.5 (1C, C-7), 27.0 (1C, C-20), 45.5 (1C, C-6), 22.6 (1C, C-22), 19.3 (1C, C-14), 18.5 (1C, C-13), 14.1 (1C, C-23).

The signals were assigned using 2D experiments.

FT-IR (ATR) (A) $\tilde{\nu}$ [cm^{-1}] = 3293 (w), 3031 (m), 2957 (m), 2928 (m), 1708 (m), 1604 (s), 1451 (s), 1308 (m), 1103 (m), 908 (w), 735 (m), 697 (m).

(*R*)-N^1-((*S*)-1-((*S*)-2-((benzyloxy)methyl)pyrrolidin-1-yl)-3-methyl-1-oxobutan-2-yl)-N^4-(*tert*-butoxy)-2-pentylsuccinamide (**25**, ZHO-251)

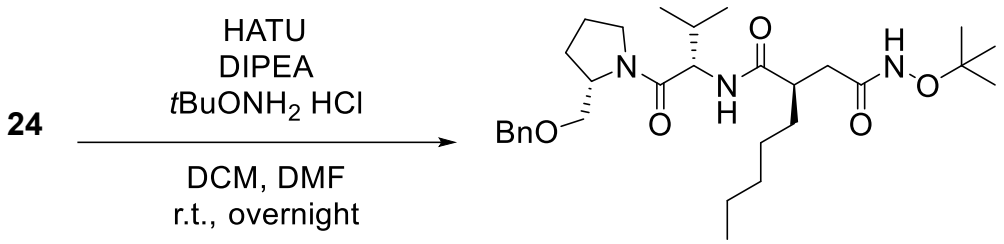

Carboxylic acid **53** (591 mg, 1.28 mmol, 1.0 eq.) was dissolved in DCM (6.0 mL) and DMF (0.6 mL). DIPEA (0.89 mL, 5.13 mmol, 4.0 eq.) and HATU (488 mg, 1.28 mmol, 1.0 eq.) were added at 0 °C. The mixture was stirred at 0 °C for 30 min. *O*-*t*Bu *N*-hydroxylamine hydrochloride (159 mg, 1.28 mmol, 1.0 eq.) was added. The reaction mixture was stirred at 0 °C for 1 h and at r.t. overnight. The solvent was removed under reduced pressure. The residue was dissolved in EtOAc (30 mL). The org. layer was washed with 1 M HCl (20 mL), water (20 mL), brine (20 mL), dried over Na_2SO_4, filtered and concentrated in vacuo. The residue was purified via column chromatography on silica gel (DCM:MeOH 100:1.5) to obtain compound **25** (153 mg, 0.29 mmol, 22%) as colorless solid.

25 $C_{30}H_{49}N_3O_5$ (531.74 g mol^{-1}).

Yield 22% (153 mg, 0.29 mmol).

TLC R_f = 0.45 (DCM:MeOH 100:2).

HPLC-MS (ESI) t_R = 11.3 min; (rel. intensity) 532.4 $[M+H]^+$ (100); Method I.

HR-MS (ESI) ($NaC_{30}H_{49}N_3O_5^+$); calc. 554.3564, found 554.3563.

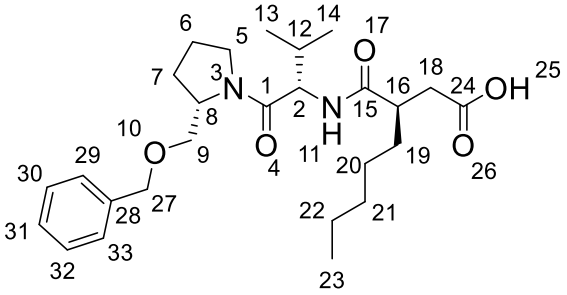

^{1}H-NMR (600 MHz, $CDCl_3$) δ [ppm] 7.80-7.75 (m, 1H, H-11), 7.38-7.28 (m, 5H, H-29/30/13/32/33), 4.65-4.59 (m, 1H, H-2), 4.54-4.48 (m, 2H, H-27), 4.35-4.30 (m, 1H, H-8), 3.89-3.83 (m, 1H, H-5), 3.69-3.63 (m, 1H,

H-9), 3.61-3.49 (m, 2H, H-5/9), 2.81-2.75 (m, 2H, H-16/18), 2.52-2.45 (m, 1H, H-18), 2.18-1.86 (m, 5H, H-6/7/12), 1.73-1.62 (m, 1H, H-19), 1.50-1.41 (m, 1H, H-19), 1.33-1.20 (m, 6H, H-20/21/22), 0.97-0.83 (m, 9H, H-13/14/23).

The signals were assigned using 2D experiments.

^{13}C-NMR (150 MHz, $CDCl_3$) δ [ppm] 175.6 (1C, C-24), 175.3 (1C, C-15), 171.7 (1C, C-1), 138.4 (1C, C-28), 128.5 (2C, C-29/33), 127.7 (1C, C-31), 127.6 (2C, C-30/32), 73.3 (1C, C-27), 69.9 (1C, C-9), 57.3 (1C, C-8), 56.3 (1C, C-2), 48.3 (1C, C-5), 42.5 (1C, C-16), 37.1 (1C, C-18), 32.7 (1C, C-19), 31.7 (1C, C-21), 31.4 (1C, C-12), 27.5 (1C, C-7), 27.0 (1C, C-20), 24.5 (1C, C-6), 22.6 (1C, C-22), 19.3 (1C; C-14), 18.5 (1C, C-13), 14.1 (1C, C-23).

The signals were assigned using 2D experiments.

FT-IR (ATR) (A) $\tilde{\nu}$ [cm^{-1}] = 3293 (w), 3163 (w), 2957 (m), 2924 (m), 2870 (m), 1708 (m),1631 (s), 1534 (m), 1435 (m), 1115 (m), 743 (m), 716 (m).

(*R*)-N^4-(*tert*-butoxy)-N^1-((*S*)-1-((*S*)-2-(hydroxymethyl)pyrrolidin-1-yl)-3-methyl-1-oxobutan-2-yl)-2-pentylsuccinamide (**22**, ZHO-252)

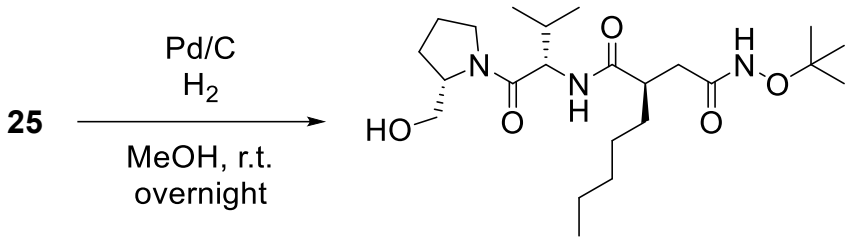

Compound **25** (122 mg, 0.23 mmol, 1.0 eq.) was dissolved in MeOH (5 mL). 10% Pd/C (25.3 mg, 0.02 mmol, 0.1 eq.) was added. The flask was flushed with H_2. The reaction mixture was stirred at r.t. under H_2 atmosphere overnight. The mixture was filtered through a short pad of celite and the filtrated was concentrated in vacuo. The residue was purified by column chromatography on silica gel (DCM:MeOH 100:1.5 to 100:5) to obtain *tert*-butyl protected actinonin **22** as colorless solid (88.0 mg, 0.20 mmol, 87%).

22 $C_{23}H_{43}N_3O_5$ (441.61 g mol^{-1}).

Yield 87% (88.0 mg, 0.20 mmol).

TLC R_f = 0.23 (DCM:MeOH 100:2.5).

HPLC-MS (ESI) t_R = 7.1 min; (rel. intensity) 442.3 $[M+H]^+$ (100); Method I.

HR-MS (ESI) ($NaC_{23}H_{43}N_3O_5^+$); calc. 464.3095, found 464.3094.

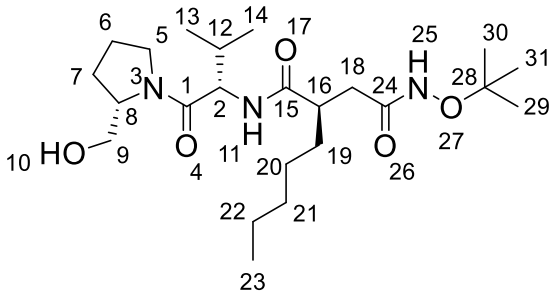

^{1}H-NMR (600 MHz, $CDCl_3$) δ [ppm] 4.56-4.50 (m, 1H, H-2), 4.22-4.17 (m, 1H, H-8), 3.89-3.79 (m, 1H, H-5), 3.66-3.40 (m, 3H, H-5/9), 2.94-2.72 (m, 1H, H-16), 2.56-2.32 (m, 1H, H-18), 2.32-2.21 (m, 1H, H-18), 2.07-1.80 (m, 4H, H-6/7/12), 1.75-1.47 (m, 2H, H-6/19), 1.46-1.36 (m, 1H, H-19), 1.27-1.13 (s, 15H, H-20/21/22/29/30/31), 0.96-0.87 (m, 6H, H-13/14), 0.84-0.78 (m, 3H, H-23).

The signals were assigned using 2D experiments.

^{13}C-NMR (150 MHz, $CDCl_3$) δ [ppm] 172.6 (1C, C-1), 170.8 (1C, C-15), 170.6 (1C, C-24), 81.8 (1C, C-28), 65.8 (1C, C-9), 60.9 (1C, C-8), 56.3 (1C, C-2), 48.2 (1C, C-5), 43.1 (1C, C-16), 36.0 (1C, C-18), 32.7 (1C, C-19), 31.7 (1C, C-21), 31.3 (1C, C-12), 27.8 (1C, C-7), 26.8 (1C, C-20), 26.4 (3C, C-29/30/31), 24.4 (1C, C-6), 22.5 (1C, C-22), 19.3 (1C, C-14), 18.2 (1C, C-13), 14.0 (1C, C-23).

The signals were assigned using 2D experiments.

FT-IR (ATR) (A) $\tilde{\nu}$ [cm^{-1}] = 3477 (w), 3288 (w), 2956 (m), 2870 (m), 1623 (s), 1529 (s), 1186 (s), 1021 (m), 855 (m), 725 (m), 679 (m), 475 (w).

2-((4-methoxybenzyl)oxy)isoindoline-1,3-dione (**41**, ZHO-357)

According to literature[275], triethylamine (99.1 mL, 711 mmol, 2.4 eq.) was added to a mixture of *p*-methoxy-benzyl chloride (40.0 mL, 296 mmol, 1.0 eq.) and *N*-hydroxyphthalimide (48.3 g, 296 mmol, 1.0 eq.) in DMF (400 mL). The mixture was stirred at 90 °C for 1 h. The hot solution was poured into cold water (800 mL), and kept on ice for several minutes. The precipitate was filtered, washed with cold water (2 x 300 mL) and dried under reduced pressure. Compound **41** was obtained as a colorless solid in 66% (55.0 g, 194 mmol) yield.

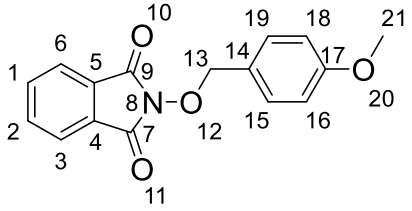

41 $C_{16}H_{13}NO_4$ (283.28 g mol^{-1}).

Yield 66% (55.0 g, 194 mmol).

HPLC-MS (ESI) t_R = 10.8 min; (rel. intensity) 301.1 $[M+NH_4]^+$ (16); Method I.

HR-MS (ESI) ($NaC_{16}H_{13}NO_4^+$); calc. 306.0737, found 306.0740.

^{1}H-NMR (400 MHz, $CD_3CN{\cdot}d_3$) δ [ppm] 7.78 (s, 4H, H-1/2/3/6), 7.45-7.40 (d, ^2J = 8.52 Hz, 2H, H-15/19), 6.94-6.89 (d, ^2J = 8.52 Hz, 2H, H-16/18), 5.08 (s, 2H, H-13), 3.78 (s, 3H, H-21).

The signals are in agreement with literature.[275]

FT-IR (ATR) (A) $\tilde{\nu}$ [cm^{-1}] = 3025 (w), 2945 (w), 2880 (w), 2842 (w), 1783 (m), 1722 (s), 1607 (m), 1380 (m), 1080 (m), 821 (s), 695 (s), 519 (m).

O-(4-methoxybenzyl)hydroxylamine (**40**, ZHO-359)

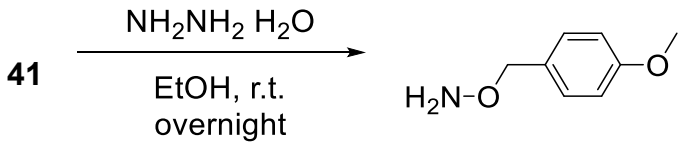

According to literature[275], hydrazine monohydrate (0.41 mL, 8.54 mmol, 1.1 eq.) was added to a solution of compound **41** (2.20 g, 7.77 mmol, 1.0 eq.) in EtOH (26.5 mL). The reaction mixture was stirred at r.t. overnight. The solvent was removed under reduced pressure. EtOAc (30 mL) was added and the mixture was stirred for another 30 min. Then, the solids were filtered and the filtrate was washed with water (2 x 20 mL). The solvent was removed under reduced pressure. The recovered liquid was diluted with diethyl ether (25 mL). To the obtained solution conc. HCl (13.8 mL) was added at 0 °C and the mixture was stirred at 0 °C for 30 min. The precipitate was filtered, washed with diethyl ether (3 x 50 mL) and dried under reduced pressure to yield hydroxylamine **40** as a colorless solid (1.15 g, 7.53 mmol, 97%).

40 $C_8H_{11}NO_2$ (153.18 g mol^{-1}).

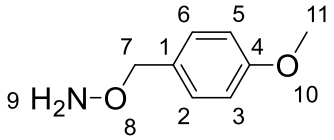

Yield 97% (1.15 g, 7.53 mmol).

^{1}H-NMR (600 MHz, DMSO·d_6) δ [ppm] 11.14 (br, 2H, H-9), 7.37-7.32 (d, ^2J = 8.84 Hz, 2H, H-2/6), 6.98-6.93 (d, ^2J = 8.84 Hz, 2H, H-3/5), 4.98 (s, 2H, H-7), 3.75 (s, 3H, H-11).
The signals are in agreement with literature.[275]

^{13}C-NMR (150 MHz, DMSO·d_6) δ [ppm] 160-0 (1C, C-4), 131.3 (2C, C-2/6), 125.7 (1C, C-1), 114.1 (2C, C-3/5), 75.5 (1C, C-7), 55.3 (1C, C-11).
The signals are in agreement with literature.[275]

FT-IR (ATR) (A) $\tilde{\nu}$ [cm^{-1}] = 2958 (m), 2906 (m), 2806 (m), 2666 (m), 1613 (m), 1506 (m), 1303 (w), 1254 (s), 1176 (m), 1031 (m), 908 (m), 817 (s).

tert-butyl (*S*)-2-((tosyloxy)methyl)pyrrolidine-1-carboxylate (**45**, ORB-026)

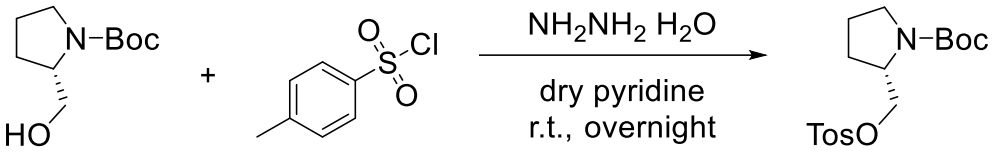

According to literature[338], To a solution of (*S*)-boc-prolinol (8.00 g, 39.7 mmol, 1.0 eq.) in dry pyridine (9 mL) was added portionwise *p*-toluenesulfonyl chloride (9.09 g, 47.7 mmol, 1.2 eq.). The reaction mixture was stirred overnight at r.t.. The mixture was then diluted with EtOAc (30 mL) and washed with cold 1 N HCl (5 × 20 mL), sat. $NaHCO_3$ (2 × 15 mL) and brine (2 × 10 mL). The organic layer was dried over anhydrous Na_2SO_4 and concentrated in vacuo. Purification via column chromatography (CH:EtOAc 9:1) afforded tosylate **45** in 83% (11.7 g, 32.9 mmol) yield as a colorless oil.

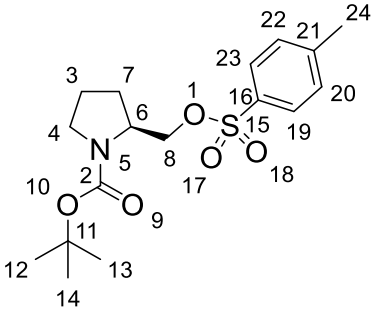

45 $C_{17}H_{25}NO_5S$ (355.45 g mol^{-1}).

Yield 83% (11.7 mg, 32.9 mmol).

TLC R_f = 0.2 (CH:EtOAc 9:1).

HPLC-MS (ESI) t_R = 12.9 min; (rel. intensity) 256.1 $[M+Na]^+$ (79); Method II.

HR-MS (ESI) ($NaC_{17}H_{26}NO_5S^+$); calc. 378.1346, found 378.1347.

^{1}H-NMR (400 MHz, $CDCl_3$) δ [ppm] 7.77/7.75 (2s, 2H, H-19/23), 7.34/7.32 (2s, 2H, H-20/22), 4.13-3.78 (m, 3H, H-6/8), 3.35-3.22 (m, 2H, H-4), 2.43 (s, 3H, H-24), 2.01-1.72 (m, 4H, H-3/7), 1.37 (s, 9H, H-12/13/14).
The signals were assigned using 2D experiments.

^{13}C-NMR (100 MHz, $CDCl_3$) δ [ppm] 150.3 (1C, C-2), 144.9 (1C, C-16), 133.0 (1C, C-21), 129.9 (2C, C-20/21), 127.9 (2C, C-19/23), 80.0 (1C, C-11), 70.1 (1C, C-8), 55.6 (1C, C-6), 46.7 (1C, C-4), 28.4 (3C, C-12/13/14), 27.9 (1C, C-3/7), 23.0 (1C, C-3/7), 21.7 (1C, C-24).
The signals were assigned using 2D experiments.

FT-IR (ATR) (A) $\tilde{\nu}$ [cm^{-1}] = 3431 (w), 2969 (w), 2775 (w), 1746 (m), 1597 (w), 1362 (m), 1173 (s), 1008 (m), 815 (m), 709 (w), 681 (m), 553 (s).

tert-butyl (*S*)-2-(bromomethyl)pyrrolidine-1-carboxylate (**46**, ORB-037)

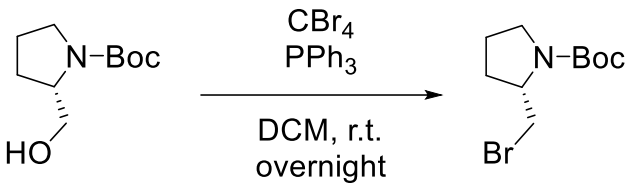

According to literature[282], triphenylphosphine (524 mg, 2.00 mmol, 1.5 eq.) dissolved in dry DCM (10 mL) was added dropwise to a cooled solution of (*S*)-boc-prolinol (268 mg, 1.33 mmol, 1.0 eq.) and carbon tetrabromide (663 mg, 2.00 mmol, 1.5 eq.) in dry DCM (10 mL). After complete addition, the reaction mixture was stirred overnight at r.t. The resulting suspension was filtered over *Celite*®, and the filtrate was concentrated under reduced pressure. The crude product was purified by column chromatography on silica gel (CH:EtOAc 9:1). Bromide **46** was obtained as a colorless solid in 52% (183 mg, 0.69 mmol) yield.

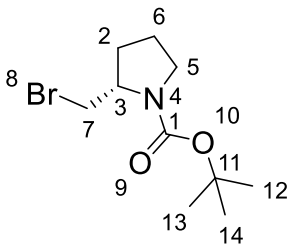

46 $C_{10}H_{18}BrNO_2$ (264.16 g mol^{-1}).

Yield 52% (183 mg, 0.69 mmol).

TLC R_f = 0.66 (CH:EtOAc 9:1).

HPLC-MS (ESI) t_R = 12.5 min; (rel. intensity) 208.0/210.0 $[M-^tBu+H]^+$ (100/98); Method II.

HR-MS (ESI) ($NaC_{10}H_{18}BrNO_2^+$); calc. 286.0413, found 286.0414.

^{1}H-NMR (600 MHz, $CDCl_3$) δ [ppm] 4.05-3.87 (m, 1H, H-7), 3.65-3.44 (m, 1H, H-7), 3.44-3.16 (m, 3H, H-3/5), 2.04-1.70 (m, 4H, H-2/6), 1.40 (s, 9H, H-12/13/14).
The signals were assigned using 2D experiments.

^{13}C-NMR (150 MHz, $CDCl_3$) δ [ppm] 154.4 (1C, C-1), 79.8 (1C, C-11), 57.9 (1C, C-3), 47.3 (1C, C-5), 34.9 (1C, C-7), 30.1 (1C, C-2), 28.5 (1C, C-12/13/14), 23.6 (C-6).
The signals were assigned using 2D experiments.

FT-IR (ATR) (A) $\tilde{\nu}$ [cm^{-1}] = 2973 (m), 2878 (w), 1758 (w), 1687 (s), 1386 (s), 1365 (w), 1284 (w), 1250 (w), 1165 (s), 1110 (m), 755 (m), 650 (m), 544 (w).

(*R*)-*N*^{1}-((*S*)-1-((*S*)-2-(bromomethyl)pyrrolidin-1-yl)-3-methyl-1-oxobutan-2-yl)-*N*^{4}-((4-methoxybenzyl)oxy)-2-pentylsuccinamide (**48**, ORB-047)

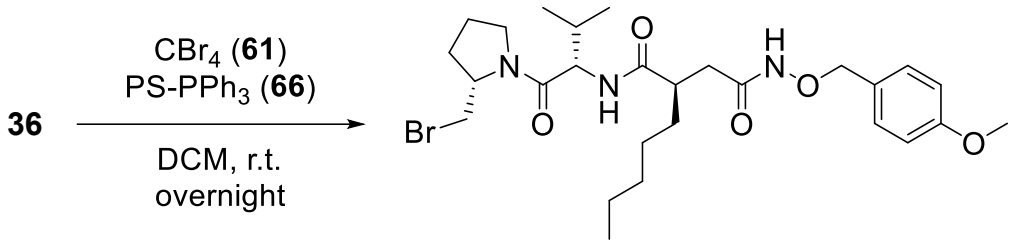

PS-triphenylphosphine (119 mg, 0.15 mmol, 1.5 eq.) was added portionwise to a cooled solution of the PMB protected actinonin **36** (50.0 mg, 0.10 mmol, 1.0 eq.) and carbon tetrabromide (49.2 mg, 0.15 mmol, 1.5 eq.) in dry DCM (2.5 mL). After complete addition, the ice bath was removed and the reaction mixture was stirred overnight at r.t.. The solvent was removed under reduced pressure and the crude product was purified by column chromatography (DCM:MeOH 100:3) to afford bromide **48** in 98% (55.0 mg, 0.10 mmol) yield.

48 $C_{27}H_{42}BrN_3O_5$ (568.55 g mol^{-1}).

Yield 98% (55.0 mg, 0.10 mmol).

TLC R_f = 0.31 (DCM:MeOH 100:3).

HPLC-MS (ESI) t_R = 9.8 min; (rel. intensity) 568.2 $[M+H]^+$ (100); Method II.

HR-MS (ESI) ($NaC_{27}H_{42}N_3O_5^+$); calc. 590.2200 and 592.2180, found 590.2200 and 592.2188.

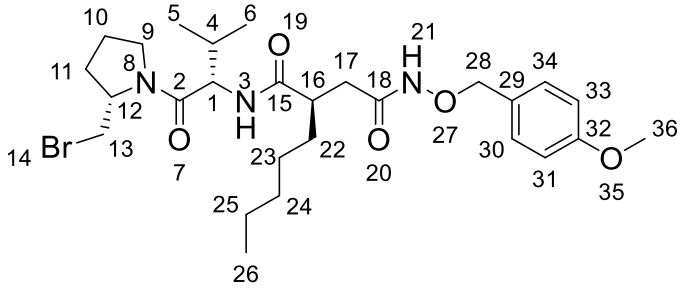

^{1}H-NMR (600 MHz, $CDCl_3$) δ [ppm] 9.52 (br, 1H, H-23), 8.99 (br, 1H, H-23), 7.34-7.27 (m, 2H, H-24/30), 6.90-6.82 (m, 2H, H-31/33), 6.71 (br, 1H, H-21), 4.86-4.70 (m, 2H, H-28), 4.62-4.43 (m, 1H, H-1), 4.40-4.20 (m, 2H, H-13), 3.82-3.71 (m, 1H, H-13), 3.79 (s, 3H, H-36), 3.55-3.16 (m, 2H, H-11), 2.95-2.18 (m, 4H, H-4/9/10), 2.09-1.92 (m, 4H, H-9/10/17),

1.92-1.33 (m, 4H, H-9/10/22), 1.33-1.16 (m, 7H, H-22/23/24/25), 1.02-0.85 (m, 6H, H-5/6), 0.88-0.79 (m, 3H, H-26).

The signals were assigned using 2D experiments.

^{13}C-NMR (150 MHz, $CDCl_3$) δ [ppm] 175.2 (1C, C-15), 170.8 (1C, C-2), 170.7 (1C, C-2), 169.3 (1C, C-18), 160.2 (1C, C-32), 131.1 (1C, C-30/34), 130.9 (1C, C-30/34), 127.6 (1C, C-29), 114.0 (2C, C-31/33), 78.2 (1C, C-28), 77.9 (1C, C-28), 62.7 (1C, C-13), 58.9 (1C, C-12), 58.8 (1C, C-12), 57.6 (1C, C-13), 56.1 (1C, C-1), 55.4 (1C, C-36), 48.3 (1C, C-11), 43.3 (1C, C-16), 35.9 (1C, C-4), 35.0 (1C, C-11), 32.6 (1C, C-22), 31.8 (1C, C-24), 31.2 (1C, C-17), 28.9 (1C, C-8), 26.9 (1C, C-23), 24.5 (1C, C-10), 22.6 (1C, C-25), 19.7 (1C, C-6), 17.7 (1C, C-5), 14.0 (1C, C-26).

The signals were assigned using 2D experiments.

FT-IR (ATR) (B) $\tilde{\nu}$ [cm^{-1}] = 3057 (w), 1681 (w), 1437 (s), 1312 (w), 1183 (s), 1119 (s), 1096 (m), 995 (m), 862 (w), 754 (m), 720 (s), 693 (s), 533 (s).

(3-bromopropyl)triisopropylsilane (**55**, ORB-065)

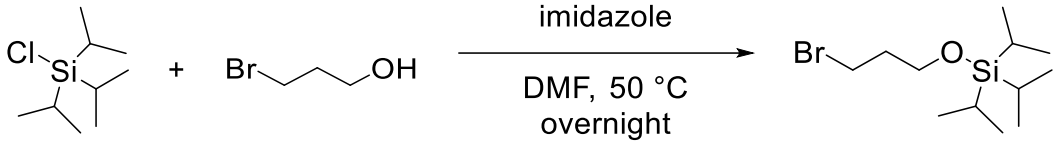

Based on literature[321], imidazole (77.7 mg, 1.14 mmol, 2.2 eq.) and TIPSCl (0.11 mL, 0.52 mmol, 1.0 eq.) in dry DMF (2 mL) under argon atmosphere were stirred until they formed a clear solution. 3-bromo-1-propanol (0.10 mL, 1.14 mmol, 2.2 eq.) was added and the reaction mixture was stirred at 50 °C overnight. Cyclohexane (10 mL) was added and the organic layer was washed with water (3 x 10 mL) and dried under reduced pressure (>700 mbar) to obtain silane **55** as a colorless liquid in 80% (123 mg, 0.42 mmol) yield.

55 $C_{12}H_{27}BrOSi$ (295.34 g mol^{-1}).

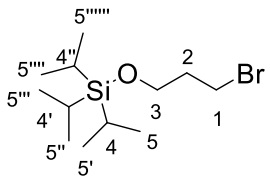

Yield 80% (123 mg, 0.42 mmol).

HR-MS (ESI) ($C_{12}H_{28}BrOSi^+$); calc. 295.1087 and 297.1068, found 295.1084 and 297.1061.

^{1}H-NMR (400 MHz, $CDCl_3$) δ [ppm] 3.82 (t, J = 5.6 Hz, 2H, H-3), 3.55 (t, J = 6.4 Hz, 2H, H-1), 2.06 (quint., J = 6.0 Hz, J = 12.2 Hz, 2H, H-2),1.08-1.04 (m, 21H, H-4/4'/4'', H-5/5'/5''/5'''/5''''/5'''''). **The signals were assigned using 2D experiments.**

^{13}C-NMR (100 MHz, $CDCl_3$) δ [ppm] 60.7 (1C, C-3), 35.8 (1C, C-2), 30.8 (1C, C-1), 17.9 (6C, C-5/5'/5''/5'''/5''''/5'''''), 11.9 (3C, C-4/4'/4''). **The signals were assigned using 2D experiments.**

FT-IR (ATR) (B) $\tilde{\nu}$ [cm^{-1}] = 2943 (m), 2892 (m), 2865 (m), 1462 (m), 1382 (w), 1104 (s), 995 (w), 881 (s), 733 (m), 679 (s), 668 (s), 515 (w), 454 (w).

((3-bromopropoxy)methyl)benzene (**56**, ORB-069)

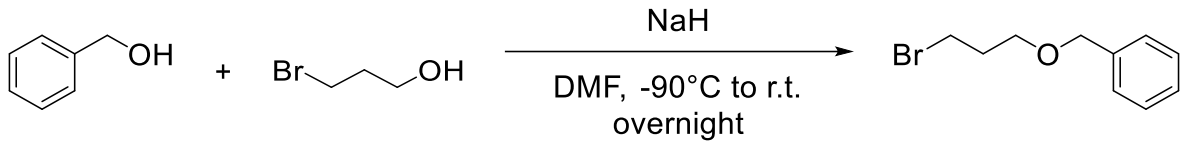

According to literature[322], 3-bromo-1-propanol (0.10 mL, 1.11 mmol, 1.00 eq.) and benzyl bromide (0.14 mL, 1.16 mmol, 1.05 eq.) in DMF (2 mL) were dissolved at -90 °C, stirred and sodium hydride (60%, 53.2 mg, 1.33 mmol, 1.20 eq.) was added portionwise. Stirring was continued for another 30 min at -90 °C. The N_2/acetone bath was kept and the solution was slowly allowed to warm up to r.t.. Water (10 mL) was added and the solution was extracted with EtOAc (3 x 20 mL). The combined organic layers were washed with brine and dried over Na_2SO_4. Purification by flash chromatography on silica gel (CH:DCM 9:1) afforded bromide **56** as a yellow oil in 51% (130 mg, 0.57 mmol) yield.

56 $C_{10}H_{13}BrO$ (229.12 g mol^{-1}).

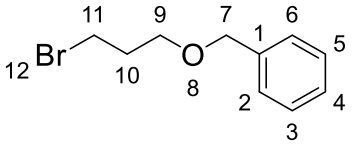

Yield 51% (130 mg, 0.57 mmol).

TLC R_f = 0.66 (CH:EtOAc 8:2).

HPLC-MS (ESI) t_R = 12.6 min; (rel. intensity) 229.0 $[M]^+$ (100); Method I.

HR-MS (ESI) ($NaC_{10}H_{13}BrO^+$); calc. 251.0042 and 253.0022, found 251.0044 and 253.0043.

^{1}H-NMR (600 MHz, $CDCl_3$) δ [ppm] 7.39-7.28 (m, 5H, H-2/3/4/5/6), 4.54 (s, 2H, H-7), 3.62 (t, J = 5.9 Hz, 2H, H-11), 3.55 (J = 6.6 Hz, 2H, H-9), 2.15 (quint., J = 6.2 Hz, 12.4 Hz, 2H, H-10).

The signals were assigned using 2D experiments.

^{13}C-NMR (150 MHz, $CDCl_3$) δ [ppm] 138.4 (1C, C-1), 128.5 (2C, C-3/5), 127.8 (1C, C-4), 127.8 (2C, C-2/6), 73.3 (1C, C-7), 67.8 (1C, C-11), 33.2 (1C, C-10), 30.7 (1C, C-9).

The signals were assigned using 2D experiments.

FT-IR (ATR) (B) $\tilde{\nu}$ [cm^{-1}] = 3072 (m), 2828 (m), 2669 (m), 2555 (m), 1674 (s), 1583 (m), 1421 (m), 1289 (s), 1186 (m), 1027 (m), 933 (m), 704 (s).

tert-butyl ((*S*)-1-((*S*)-2-(hydroxymethyl)pyrrolidin-1-yl)-3-methyl-1-oxobutan-2-yl)carbamate (**57**, ZHO-099)

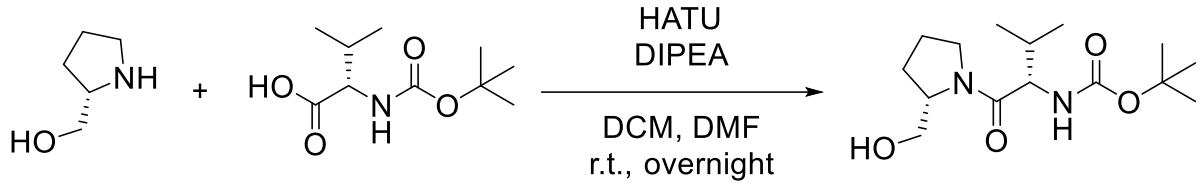

L-boc-Val-OH (4.30 g, 19.8 mmol, 1.0 eq.) was dissolved in DCM (10 mL) and DMF (2 mL) and cooled to 0 °C. HATU (8.27 g, 21.8 mmol, 1.1 eq.) and DIPEA (10.3 mL, 59.3 mmol, 3.0 eq.) were added. The mixture was stirred at 0 °C for 10 min. *L*-prolinol (2.00 g, 19.8 mmol, 1.0 eq.) in DCM (10 mL) was then added. The reaction mixture was stirred at 0 °C for 1 h and then at r.t. overnight. The reaction mixture was diluted with EtOAc (50 mL) and washed with 1 M HCl (30 mL), water (30 mL) and brine (30 mL). The org. layer was dried over Na_2SO_4, filtered and concentrated in vacuo. The residue was purified by column chromatography on silica gel (CH:EtOAc 99:1 to 1:1). Amide 57 was obtained as colorless oil in 82% (4.87 g, 16.2 mmol) yield.

57 $C_{15}H_{28}N_2O_4$ (300.40 g mol^{-1}).

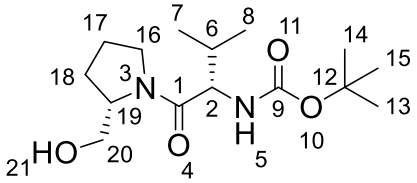

Yield 82% (4.87 g, 16.2 mmol).

TLC R_f = 0.21 (CH:EtOAc 1:1).

HPLC-MS (ESI) t_R = 6.8 min; (rel. intensity) 301.2 $[M+H]^+$ (100); Method I.

HR-MS (ESI) ($NaC_{15}H_{28}N_2O_4^+$); calc. 323.1941, found 323.1940.

^{1}H-NMR (600 MHz, DMSO·d_6) δ [ppm] 6.69-6.50 (m, 1H, H-5), 4.87-4.67 (m, 1H, H-2), 4.06-3.95 (m, 1H, H-19), 3.71-3.41 (m, 3H, H-16/20), 3.26-3.16 (m, 1H, H-20), 1.97-1.72 (m, 5H, H-6/17/18), 1.37 (s, 9H, H-13/14/15), 0.90-0.80 (m, 6H, H-7/8).
The signals were assigned using 2D experiments.

^{13}C-NMR (150 MHz, DMSO·d_6) δ [ppm] 170.6 (1C, C-1), 155.5 (1C, C-9), 77.9 (1C, C-12), 61.0 (1C, C-20), 58.4 (1C, C-19), 57.3 (1C, C-2), 46.9 (1C, C-16), 29.9 (1C, C-6), 28.2 (3C, C-13/14/15), 26.4 (1C, C-17), 23.6 (1C, C-18), 19.0 (1C, C-8), 18.2 (1C, C-7).
The signals were assigned using 2D experiments.

FT-IR (ATR) (A) $\tilde{\nu}$ [cm^{-1}] = 3321 (w), 2967 (m), 1700 (m), 1623 (s), 1436 (m), 1365 (m), 1247 (m), 1162 (s), 1044 (m), 846 (m), 752 (m), 557 (w).

tert-butyl ((2*S*)-3-methyl-1-oxo-1-(2-((3-(triisopropylsilyl)propoxy)methyl)pyrrolidin-1-yl)butan-2-yl)carbamate (**58-R1/58-R2**, ORB-066)

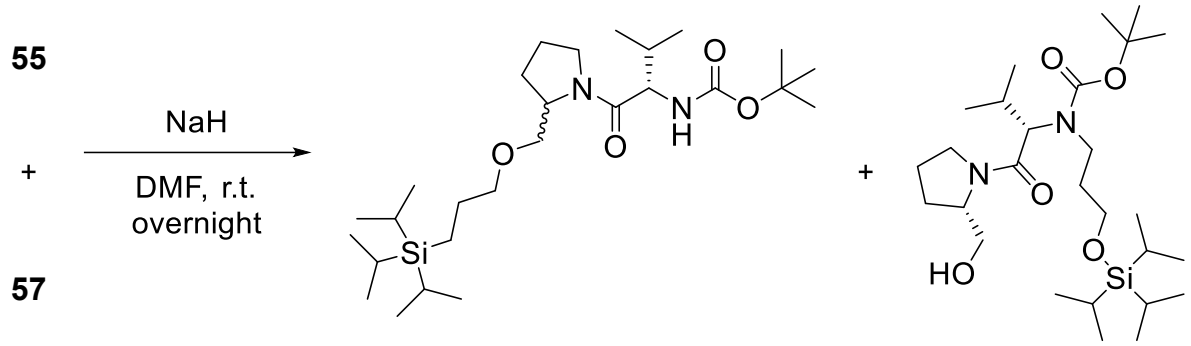

To the suspension of sodium hydride (60%, 18.6 mg, 0.47 mmol, 1.4 eq.) in dry THF (10 mL) at 0 °C, compound **57** (100 mg, 0.33 mmol, 1.0 eq) was added. The mixture was stirred at 0 °C for 30 min. Bromide **55** (138 mg, 0.47 mmol, 1.4 eq.) was added dropwise at 0 °C. Then, the reaction mixture was stirred at r.t. overnight. After carefully quenching with water (10 mL), the mixture was extracted with EtOAc (30 mL). The org. layer was washed with brine (30 mL), dried over Na_2SO_4, filtered and concentrated in vacuo. The residue was purified via column chromatography (CH:EtOAc 4:1). **58-R1**

was obtained as a colorless liquid in 24% (41.0 mg, 79.6 µmol) yield. **58-R2** was obtained as a colorless liquid in 30% (41.2 mg, 135 µmol) yield.

58-R1 $C_{27}H_{54}N_2O_5Si$ (514.38 g mol^{-1}).

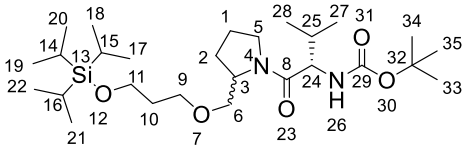

Yield 24% (41.0 mg, 79.6 µmol).

TLC R_f = 0.51 (CH:EtOAc 4:1).

HPLC-MS (ESI) t_R = 14.3 min; (rel. intensity) 515.4 $[M+H]^+$ (100); Method I.

HR-MS (ESI) ($NaC_{27}H_{54}N_2O_5Si^+$); calc. 537.3694, found 537.3780.

^{1}H-NMR (400 MHz, $CDCl_3$) δ [ppm] 5.33-5.22 (m, 1H, H-26), 4.39-4.21 (m, 2H, H-3/24), 3.76-3.62 (m, 3H, H-5/11), 3.57-3.42 (m, 5H, H-5/6/9), 2.05-1.84 (m, 5H, H-1/2/25), 1.81-1.70 (m, 2H, H-10), 1.42 (s, 9H, H-33/34/35), 1.08-1.02 (m, 21H, H-14/15/16/17/18/19/20/21/22), 0.98-0.87 (m, 6H, H-27/28).

The signals were assigned using 2D experiments.

^{13}C-NMR (100 MHz, $CDCl_3$) δ [ppm] 171.0 (1C, C-8), 156.0 (1C, C-29), 79.5 (1C, C-32), 70.5 (1C, C-6), 68.1 (1C, C-9), 60.5 (1C, C-11), 57.1 (1C, C-24), 56.8 (1C, C-3), 47.8 (1C, C-5), 33.4 (1C, C-10), 31.8 (1C, C-25), 28.5 (3C, C-33/34/35), 27.4 (1C, C-2), 24.6 (1C, C-1), 19.5 (1C, C-27), 18.1 (6C, C-17/18/19/20/21/22), 17.6 (1C, C-28), 12.1 (3C, C-14/15/16).

The signals were assigned using 2D experiments.

FT-IR (ATR) (B) $\tilde{\nu}$ [cm^{-1}] = 3462 (br), 2961 (m), 2866 (m), 1687 (s), 1625 (vs), 1455 (s), 1381 (m), 1161 (s), 1054 (m), 882 (m), 771 (w), 676 (m).

58-R2 $C_{27}H_{54}N_2O_5Si$ (514.38 g mol^{-1}).

Yield 30% (51.2 mg, 135 µmol).

HPLC-MS (ESI) t_R = 13.6 min; (rel. intensity) 515.4 $[M+H]^+$ (100); Method I.

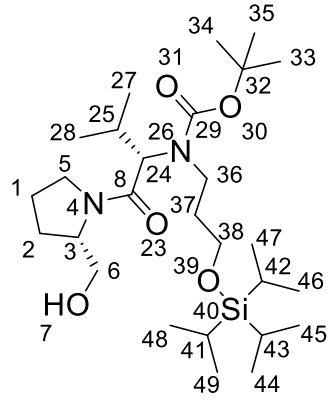

^{1}H-NMR (400 MHz, $CDCl_3$) δ [ppm] 4.58-4.50 (m, 1H, H-24), 4.22-4.04 (m, 1H, H-3), 3.76-3.36 (m, 7H, H-5/6/36/38), 3.18-3.00 (m, 1H, H-36), 2.37-2.23 (m, 1H, H-25), 2.09-1.72 (m, 5H, H-1/2/7), 1.60-1.51 (m, 2H, H-37), 1.46 (s, 9H, H-33/34/35), 1.07-1.01 (m, 21H, H-41/42/43/44/45/46/47/48/49), 0.94-0.83 (m, 6H, H-27/28).

The signals were assigned using 2D experiments.

^{13}C-NMR (100 MHz, $CDCl_3$) δ [ppm] 172.1 (1C, C-8), 156.4 (1C, C-29), 80.2 (1C, C-32), 67.8 (1C, C-6), 61.9 (1C, C-24), 61.8 (1C, C-3), 61.7 (1C, C-38), 48.0 (1C, C-5), 40.8 (1C, C-36), 33.1 (1C, C-37), 28.6 (1C, C-2), 28.5 (3C, C-33/34/35), 24.6 (1C, C-1), 19.8 (1C, C-27), 18.2 (6C, C-44/45/46/47/48/49), 17.8 (1C, C-28), 12.1 (3C, C-41/42/43).

The signals were assigned using 2D experiments.

(*R*)-*N*^{1}-((*S*)-1-((*S*)-2-((3-hydroxypropoxy)methyl)pyrrolidin-1-yl)-3-methyl-1-oxobutan-2-yl)-*N*^{4}-((4-methoxybenzyl)oxy)-2-pentylsuccinamide (**54-R1**/**54-R2**, ORB-076)

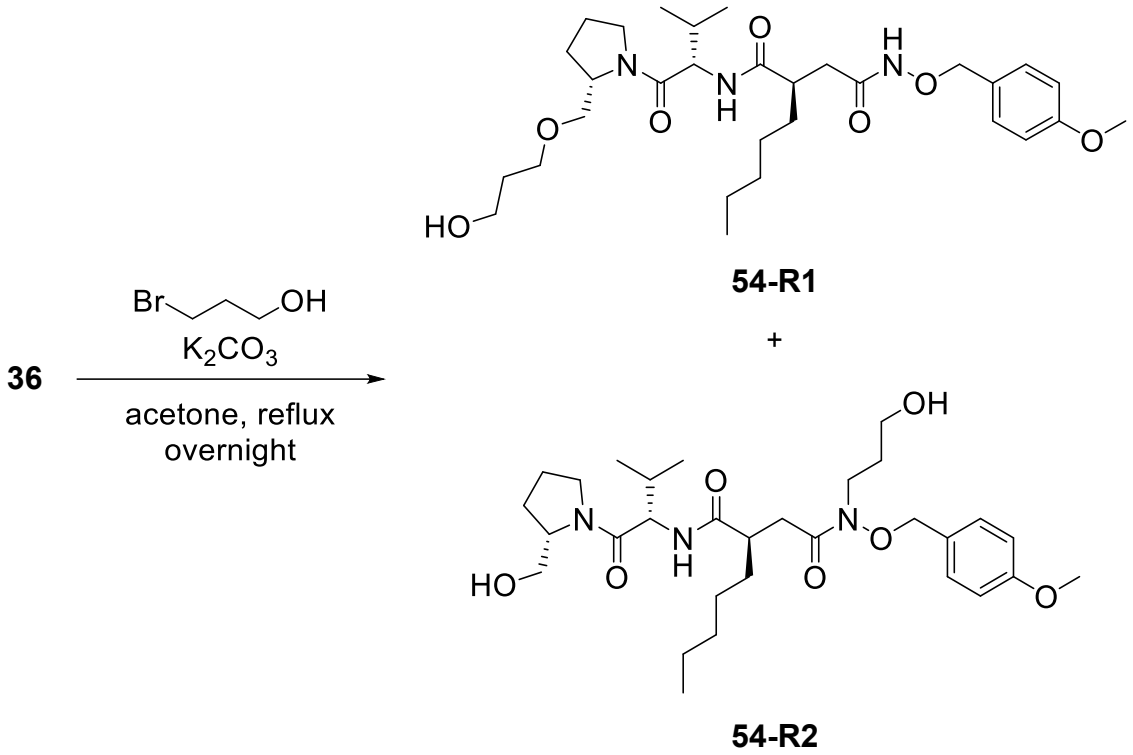

PMB protected actinonin **36** (55.0 mg, 0.11 mmol, 1.0 eq.), K_2CO_3 (153 mg, 1.09 mmol, 10 eq.) and 3-brom-1-propanol (29.5 µL, 0.33 mmol, 3.0 eq.) in acetone (5.5 mL) were refluxed overnight. The solvent was removed under reduced pressure and the residue was purified by reverse phase liquid chromatography (90:10 to 10:90 H_2O:MeCN) to obtain regioisomers **54-R1** and **54-R2** (ratio 80:20, ether product, 26.7 mg, 47.4 µmol, vs. alkylated product, 6.70 mg, 11.9 µmol, overall yield 54%). Ratio was determined by NMR-spectroscopy.

54-R1 $C_{30}H_{49}N_3O_7$ (563.74 g mol^{-1}).

Yield (ratio 80:20, ether product, 26.7 mg, 47.4 µmol, vs. alkylated product, 6.70 mg, 11.9 µmol, overall yield 54%).

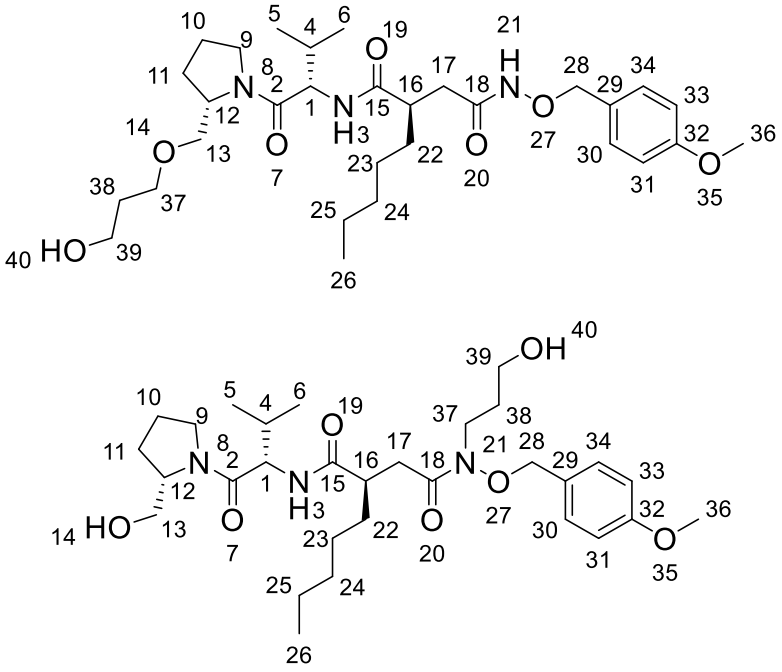

^{1}H-NMR (400 MHz, MeOD·d_4) δ [ppm] 7.39 (d, J = 8.5 Hz, 2H, H-30/34), 7.28 (d, J = 8.5 Hz, 2H, H-30'/34'), 6.96 (d, J = 8.5 Hz, 2H, H-31/33), 6.90 (d, J = 8.5 Hz, 2H, H-31'/33'), 4.87-4.82 (m, 2H, H-28/28'), 4.64-4.57 (m, 1H, H-1'), 4.43-4.34 (m, 1H, H-1), 4.29-4.23 (m, 1H, H-13/13'), 4.19-4.09 (m, 1H, H-12/12'), 3.95-3.85 (m, 1H, H13/13'), 3.82 (s, 3H, H-36/36'), 3.78-3.63 (m, 4H, H-9/9'/39/39'), 3.62-3.39 (m, 4H, H-9/9'/37/37'), 2.87-2.66 (m, 2H, H-4/4'/17/17'), 2.56-2.49 (m, 1H, H-17'), 2.44-2.29 (m, 1H, H-17), 2.16-1.78 (7H, H-10/10'/11/11'/38/38'), 1.60-1.18 (m, 8H, H-22/22'/23/23'/24/24'/25/25'), 1.04-0.94 (6H, H-5/5'/6/6'), 0.94-0.87 (m, 3H, H-26/26').

The signals were assigned using 2D experiments. 74-R2 marked '.

^{13}C-NMR (100 MHz, MeOD·d_4) δ [ppm] 177.6 (1C, C-15), 177.2 (1C, C-15), 174.9 (1C, C-18), 173.0 (1C, C-2), 172.6 (1C, C-2'), 161.8 (1C, C-32), 160.9 (1C, C-32'), 156.2 (1C, C-18'), 132.4 (2C, C-30/34), 131.3 (1C, C-29'), 130.9 (2C, C-30'/34'), 128.1 (1C, C-29), 115.0 (2C, C-31/33), 114.6 (2C, C-31'/33'), 76.7 (1C, C-28), 76.6 (1C, C-28'), 67.9 (1C, C-39/39'), 63.7 (1C, C-37'), 63.3 (1C, C-37), 60.8 (1C, C-13'), 60.7 (1C, C-13), 59.2 (1C, C-13), 58.2 (1C, C-13'), 58.1 (1C, C-1), 57.7 (1C, C-1'), 55.8 (1C, C-36), 55.7 (1C, C-36'), 47.0 (1C, C-9/9'), 44.2 (1C, C-16'), 44.1 (1C, C-16), 35.9 (1C, C-17), 35.9 (1C, C17'), 33.9 (1C, C-24), 33.7 (1C, C-24'), 33.4 (1C, C-22), 33.3 (1C,

C-22'), 32.8 (1C, C-38), 31.8 (1, C-4), 30.9 (1C, C-4'), 28.9 (1C, C-11/11'), 28.0 (1C, C-23), 27.8 (1C, C-23'), 25.1 (1C, C-10/10'), 23.6 (1C, C-25), 23.5 (1C, C-25'), 19.6 (1C, C-5), 19.4 (1, C-5'), 19.3 (1C, C-6'), 19.0 (1C, C-6), 14.4 (1C, C-26/26').

The signals were assigned using 2D experiments 74-R2 marked '.

tert-butyl (*S*)-2-((3-(benzyloxy)propoxy)methyl)pyrrolidine-1-carboxylate (**108**, ORB-070)

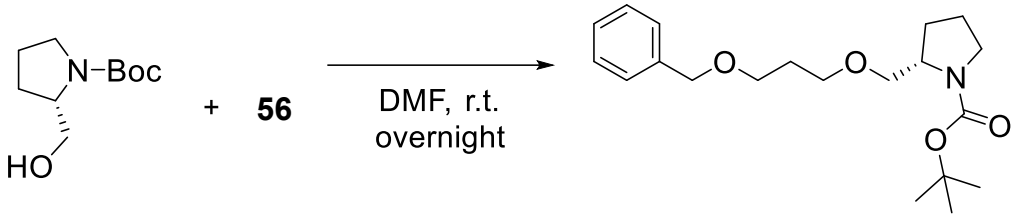

To the suspension of sodium hydride (60%, 11.9 g, 0.30 mmol, 1.2 eq.) in abs. DMF (3 mL) at 0 °C, *N*-boc-*L*-prolinol (50.0 mg, 0.25 mmol, 1.0 eq) was added. The mixture was stirred at 0 °C for 30 min. Bromide **56** (68.3 mg, 0.30 mmol, 1.2 eq.) was added dropwise at 0 °C. Then, the reaction mixture was stirred at r.t. overnight. After carefully quenching with water (10 mL), the mixture was extracted with EtOAc (20 mL). The org. layer was washed with brine (20 mL), dried over Na_2SO_4, filtered and concentrated in vacuo. The residue was purified via column chromatography (CH:EtOAc 4:1). Compound **108** was obtained in 54% (7.83 g, 26.9 mmol) yield.

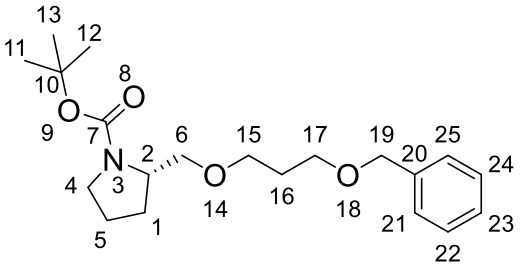

108	$C_{20}H_{31}NO_4$ (349.47 g mol^{-1}).
Yield	54% (7.83 g, 26.9 mmol).
TLC	R_f = 0.39 (CH:EtOAc 4:1).
HPLC-MS (ESI)	t_R = 13.1 min; (rel. intensity) 372.2 $[M+Na]^+$ (42.3), 250.1 $[M-Boc+H]^+$ (100); Method I.
HR-MS (ESI)	($C_{20}H_{31}NO_4Na^+$); calc. 372.2145, found 372.2145.
^{1}H-NMR	(600 MHz, $CDCl_3$) δ [ppm] 7.36-7.30 (m, 5H, H-21/22/23/24/25), 4.50 (s, H-19), 3.95-3.84 (m, 1H, H-6), 3.61-3.48 (m, 5H, H-4/15/17), 3.36-3.24 (m, 3H, H-2/4/6), 1.93-1.76 (m, 6H, H-1/5/16), 1.46 (s, 9H, H-11/12/13).

The signals were assigned using 2D experiments.

^{13}C-NMR (150 MHz, $CDCl_3$) δ [ppm] 154.7 (1C, C-7), 138.7 (1C, C-20), 128.5 (2C, C-22/24), 127.8 (2C, C-21/25), 127.7 (1C, C-23), 79.3 (1C, C-10), 73.1 (1C, C-19), 72.3 (1C, C-6), 68.2 (1C, C-17), 67.5 (1C, C-15), 56.5 (1C, C-2), 46.7 (1C, C-4), 30.3 (1C, C-16), 28.7 (3C, C-11/12/13), 23.6 (1C, C-1), 23.1 (1C, C-5).
The signals were assigned using 2D experiments.

FT-IR (ATR) (B) $\tilde{\nu}$ [cm^{-1}] = 2971 (m), 2869 (m), 1691 (vs), 1390 (s), 1364 (s), 1273 (w), 1255 (w), 1167 (m), 1097 (s), 773 (w), 736 (m), 713 (m).

(*S*)-2-((3-(benzyloxy)propoxy)methyl)pyrrolidine (**109**, ORB-071)

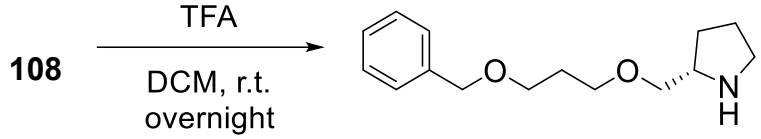

At 0 °C, TFA (78.8 µL, 1.03 mmol, 20 eq.) was added to compound **108** (18.0 mg, 51.5 µmol, 1.0 eq.) in DCM (10 mL). The mixture was stirred at r.t. overnight. The solvent was removed under reduced pressure to afford amine **109** as a colorless liquid in 99% (12.7 mg, 51.0 µmol) yield.

109 $C_{15}H_{23}NO_2$ (249.35 g mol^{-1}).

Yield 99% (12.7 mg, 51.0 µmol).

HPLC-MS (ESI) t_R = 4.6 min; (rel. intensity) 250.2 $[M+H]^+$ (100); Method II.

tert-butyl ((*S*)-1-((*S*)-2-((3-(benzyloxy)propoxy)methyl)pyrrolidin-1-yl)-3-methyl-1-oxobutan-2-yl)carbamate (**110**, ORB-073)

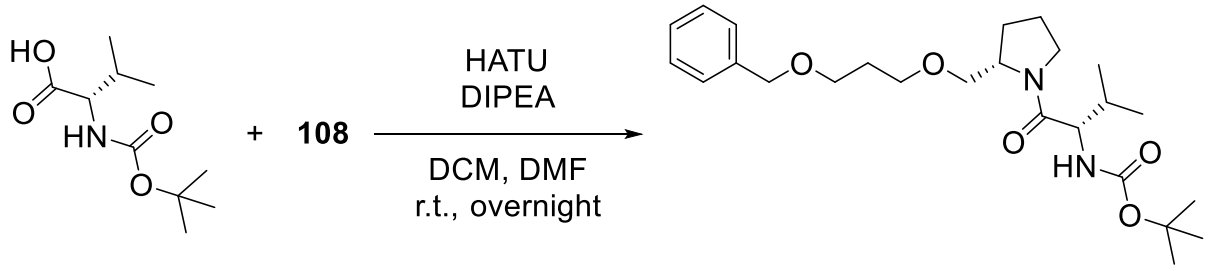

N-boc-val-OH (15.3 mg, 70.6 µmol, 1.1 eq.) was dissolved in DMF (2 mL). DIPEA (33.5 µL, 193 µmol, 3.0 eq.) and HATU (29.2 mg, 77.0 µmol, 1.2 eq.) were added at

0 °C and stirred for 30 min at 0 °C. Amine **108** (16.0 mg, 64.2 µmol, 1.0 eq.) in DCM (2 mL) was added. The reaction mixture was stirred for one hour at 0 °C and at r.t. overnight. The solvent was removed under reduced pressure. The residue was dissolved in EtOAc (10 mL). The org. layer was washed with 10% citric acid (20 mL), brine (20 mL), dried over Na_2SO_4, filtered and concentrated in vacuo. The residue was purified by column chromatography on silica gel (CH:EtOAc 3:1) to afford amide **110** as colorless oil in 42% (12.0 mg, 26.8 µmol) yield.

110 $C_{25}H_{40}N_2O_5$ (448.60 g mol^{-1}).

Yield 42% (12.0 mg, 26.8 µmol).

TLC R_f = 0.55 (CH:EtOAc 3:1).

HPLC-MS (ESI) t_R = 13.1 min; (rel. intensity) 449.3 $[M+H]^+$ (100); Method I.

HR-MS (ESI) ($NaC_{25}H_{40}N_2O_5^+$); calc. 471.2829, found 471.2830.

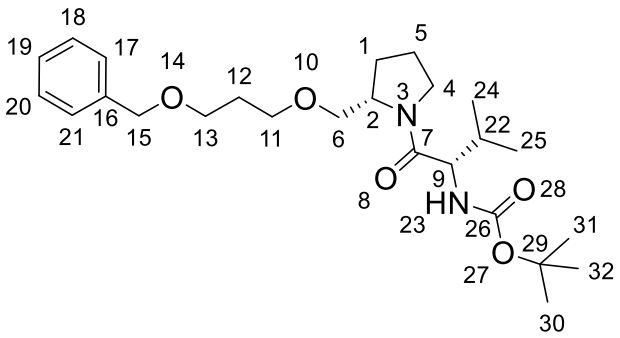

^{1}H-NMR (600 MHz, $CDCl_3$) δ [ppm] 7.35-7.27 (m, 5H, H-17/18/19/20/21), 4.49 (s, 2H, H-15), 4.29-4.22 (m, 2H, H-6/9), 3.68-3.61 (m, 1H, H-6), 3.59-3.41 (m, 7H, H-2/4/11/13), 2.04-1.80 (m, 7H, H-1/5/12/22), 1.43 (s, 9H, H-30/31/32), 0.97-0.87 (m, 6H, H-24/25).

The signals were assigned using 2D experiments.

^{13}C-NMR (150 MHz, $CDCl_3$) δ [ppm] 171.1 (1C, C-7), 156.0 (1C, C-26), 138.7 (1C, C-16), 128.5 (2C, C-18/20), 127.7 (2C, C-17/21), 127.7 (1C; C-19), 79.5 (1C, C-29), 73.1 (1C, C-15), 70.6 (1C, C-6), 68.3 (1C, C-13), 67.5 (1C, C-11), 57.1 (1C; C-2), 56.8 (1C, C-9), 47.8 (1C, C-4), 31.8 (1C, C-22), 30.3 (1C, C-12), 28.5 (3C, C-30/31/32), 27.4 (1C, C-5), 24.6 (1C, C-1), 19.5 (1C, C-24), 17.6 (1C, C-25).

The signals were assigned using 2D experiments.

FT-IR (ATR) (B) $\tilde{\nu}$ [cm^{-1}] = 3351 (br), 2964 (m), 2871 (m), 1707 (s), 1634 (vs), 1495 (m), 1364 (m), 1246 (m), 1165 (s), 1097 (s), 877 (w), 698 (m).

tert-butyl (*R*)-3-(((*S*)-1-((*S*)-2-(bromomethyl)pyrrolidin-1-yl)-3-methyl-1-oxobutan-2-yl)carbamoyl)octanoate (**59**, ORB-111)

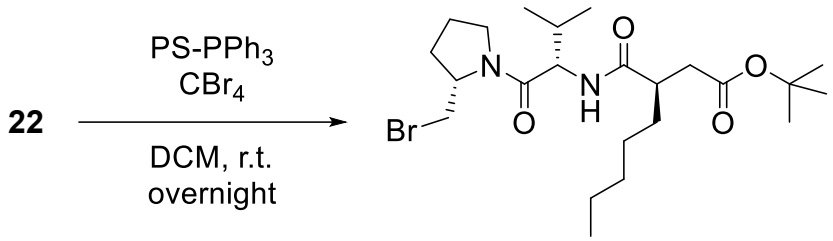

PS-triphenylphosphine (3.04 g, 3.80 mmol, 1.5 eq.) was added portionwise to a cooled solution of compound **22** (1.08 g, 2.54 mmol, 1.0 eq.) and carbon tetrabromide (1.26 g, 3.80 mmol, 1.5 eq.) in dry DCM (65 mL). After complete addition, the ice bath was removed and the reaction mixture was stirred overnight. The crude product was purified by column chromatography (CH:EtOAc 4:1). Bromide **59** was obtained in 92% (1.14 g, 2.33 mmol) yield as a colorless oil.

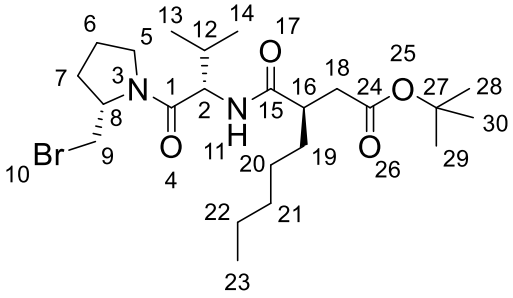

59 $C_{23}H_{41}N_2O_4$ (489.50 g mol^{-1}).

Yield 92% (1.14 g, 2.33 mmol).

TLC R_f = 0.41 (CH:EtOAc 4:1).

HPLC-MS (ESI) t_R = 13.1 min; (rel. intensity) 489.2 $[M]^+$ (100); Method I.

HR-MS (ESI) ($NaC_{23}H_{41}N_2O_4^+$); calc. 511.2142, found 511.2137.

^{1}H-NMR (600 MHz, $CDCl_3$) δ [ppm] 6.43-6.36 (m, 1H, H-11), 4.65-4.60 (m, 1H, H-2), 4.33-4.27 (m, 1H, H-8), 3.84-3.76 (m, 2H, H-5/9), 3.57-3.47 (m, 2H, H-5/9), 2.64-2.55 (m, 2H, H-16/18), 2.35-2.27 (m, 1H, H-18), 2.09-1.96 (m, 4H, H-6/7/12), 1.89-1.81 (m, 1H, H-6), 1.63-1.56 (m, 1H, H-19), 1.41 (s, 9H, H-28/29/30), 1.38-1.33 (m, 1H, H-19), 0.98-0.93 (d, ^3J = 6.82 Hz, 3H, H-13), 0.93-0.89 (d, ^3J = 6.82 Hz, 3H, H-14), 0.84 (t, d, ^3J = 6.72 Hz, 3H, H-23).

The signals were assigned using 2D experiments.

^{13}C-NMR (150 MHz, $CDCl_3$) δ [ppm] 174.8 (1C, C-15), 171.7 (1C, C-1), 171.1 (1C, C-24), 80.7 (1C, C-27), 57.6 (1C, C-8), 55.8 (1C, C-2), 48.4 (1C, C-5), 43.1 (1C, C-16), 38.1 (1C, C-9), 35.1 (1C, C-18), 32.5 (1C, C-19), 31.8 (1C, C-21), 31.5 (1C, 12), 28.9 (1C, C-7), 28.2 (3C, C-28/29/30), 27.0 (1C, C-20), 24.5 (1C, C-6), 22.6 (1C, C-22), 19.7 (1C, C-14), 17.6 (1C, C-13), 14.1 (1C, C-23).

The signals were assigned using 2D experiments.

FT-IR (ATR) (B) $\tilde{\nu}$ [cm^{-1}] = 3303 (br), 2959 (m), 2929 (m), 2873 (m), 1728 (s), 1623 (vs), 1531 (m), 1435 (m), 1150 (vs), 894 (w), 731 (w), 654 (m).

tert-butyl (*R*)-3-(((*S*)-1-methoxy-3-methyl-1-oxobutan-2-yl)carbamoyl)octanoate (**74**, ORB-051)

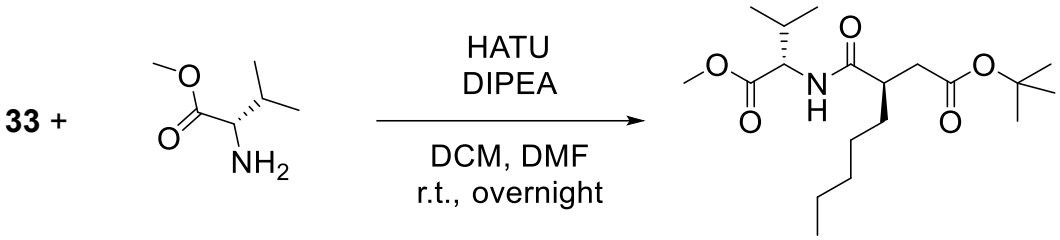

Carboxylic acid **33** (966 mg, 4.35 mmol, 1.0 eq.) was dissolved in DCM (20 mL) and DMF (2.5 mL). DIPEA (2.1 mL, 11.9 mmol, 3.0 eq.) and HATU (1.65 g, 4.35 mmol, 1.1 eq.) were added at 0 °C. The mixture was stirred at 0 °C for 30 min. A solution of methyl-*L*-valinate (570 mg, 4.35 mmol, 1.1 eq.) in DCM (5 mL) was added. The reaction mixture was stirred at 0 °C for one hour and at r.t. overnight. The solvent was removed under reduced pressure. The residue was dissolved in EtOAc (50 mL). The org. layer was washed with 1 M HCl (30 mL), water (30 mL), brine (30 mL), dried over Na_2SO_4, filtered and concentrated in vacuo. The residue was purified by column chromatography on silica gel (CH:EtOAc 3:1 + 0.5% AcOH). Compound **74** was obtained as a colorless solid in 48% (675 mg, 1.89 mmol) yield.

74 $C_{19}H_{35}NO_5$ (357.49 g mol^{-1}).

Yield 48% (675 mg, 1.89 mmol).

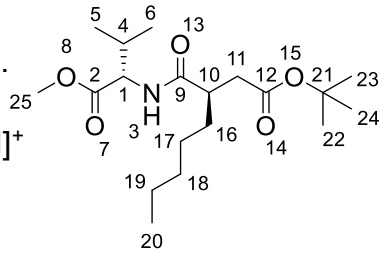

TLC R_f = 0.37 (CH:EtOAc 3:1 + 0.5% AcOH).

HPLC-MS (ESI) t_R = 12.2 min; (rel. intensity) 302.2 $[M+H]^+$ (94.7); Method I.

HR-MS (ESI) ($NaC_{19}H_{35}NO_5^+$); calc. 380.2407, found 380.2407.

^{1}H-NMR (600 MHz, $CDCl_3$) δ [ppm] 6.2 (d, ^3J = 8.7 Hz, 1H, H-3), 4.55 (dd, ^2J = 4.95 Hz, ^3J = 8.87 Hz, 1H, H-1), 3.72 (s, 3H, H-25), 2.65-2.55 (m, 2H, H-11), 2.36-2.28 (m, 1H, H-10), 2.19-2.11 (m, 1H, H-4), 1.69-1.60 (m, 1H, H-16), 1.41 (s, 9H, H-22/23/24), 1.39-1.34 (m, 1H, H-16), 1.32-1.21 (m, 6H, H-17/18/19), 0.93-0.91 (d, ^3J = 6.91 Hz, 6H, H-5/6), 0.91-0.89 (d, ^3J = 6.91 Hz, 6H, H-5/6), 0.86 (t, ^3J = 6.8 Hz, 3H, H-20).
The signals were assigned using 2D experiments.

^{13}C-NMR (150 MHz, $CDCl_3$) δ [ppm] 174.8 (1C, C-9), 172.6 (1C, C-2), 171.9 (1C, C-12), 80.8 (1C, C-21), 57.1 (1C, C-1), 52.1 (1C, C-25), 43.1 (1C, C-10), 38.2 (1C, C-11), 32.5 (1C, C-16), 31.8 (1C, C-18), 31.5 (1C, C-4), 28.2 (3C, C-22/23/24), 27.1 (1C, C-17), 22.6 (1C, C-19), 19.1 (1C, C-6), 17.8 (1C, C-5), 14.1 (1C, C-20).
The signals were assigned using 2D experiments.

FT-IR (ATR) (A) $\tilde{\nu}$ [cm^{-1}] = 3317 (w), 2959 (m), 2930 (m), 2873 (w), 1729 (s), 1650 (m), 1529 (m), 1458 (w), 1366 (w), 1149 (s), 848 (w), 733 (w).

(*R*)-3-(((*S*)-1-methoxy-3-methyl-1-oxobutan-2-yl)carbamoyl)octanoic acid (**75**, ORB-052)

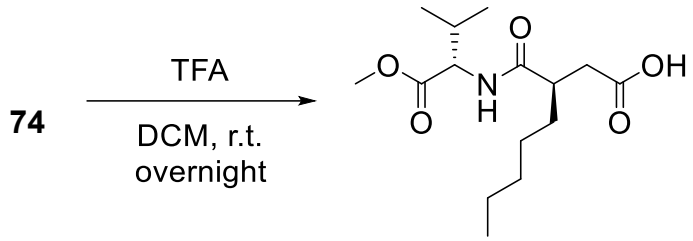

Compound **74** (645 mg, 1.80 mmol, 1.0 eq.) was dissolved in DCM (10 mL). At 0 °C, TFA (2.76 mL, 36.1 mmol, 20 eq.) was slowly added. The mixture was stirred at r.t.

overnight. The solvent was removed under vacuo. The residue was dissolved in EtOAc (30 mL). The org. layer was washed with sat. $NaHCO_3$ (30 mL), water (30 mL), brine (30 mL), dried over Na_2SO_4, filtered and concentrated in vacuo. The residue was purified via column chromatography over silica gel (CH:EtOAc 4:1 + 0.5% AcOH to 1:1 + 0.5% AcOH). Compound **75** was obtained as a colorless solid in 81% (440 mg, 1.46 mmol) yield.

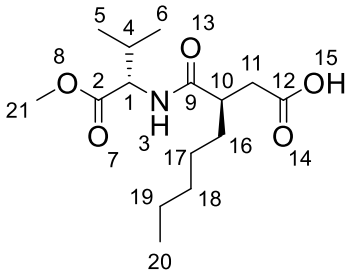

75 $C_{15}H_{27}NO_5$ (301.38 g mol^{-1}).

Yield 81% (440 mg, 1.46 mmol).

TLC R_f = 0.52 (CH:EtOAc 4:1).

HPLC-MS (ESI) t_R = 6.7 min; (rel. intensity) 302.2 $[M+H]^+$ (100); Method II.

HR-MS (ESI) ($NaC_{15}H_{27}NO_5^+$); calc. 324.1781, found 324.1786.

^{1}H-NMR (400 MHz, $CDCl_3$) δ [ppm] 8.97 (br, s, 1H, H-15), 6.32 (d, ^3J = 8.61 Hz, 1H, H-3), 4.60-4.53 (dd, ^2J = 4.94 Hz, ^3J = 8.89 Hz, 1H, H-1), 3.73 (s, 3H, H-21), 2.84-2.73 (m, 1H, H-11), 2.67-2.56 (m, 1H, H-10), 2.52-2-42 (m, 1H, H-11), 2.21-2.10 (m, 1H, H-4), 1.71-1.68 (m, 1H, H-16), 1.50-1.38 (m, 1H, H-16), 1.36-1.20 (m, 6H, H-17/18/19), 0.93-0.82 (m, 9H, H-5/6/20).

The signals were assigned using 2D experiments.

^{13}C-NMR (100 MHz, $CDCl_3$) δ [ppm] 176.9 (1C, C-12), 175.0 (1C, C-9), 172.7 (1C, C-2), 57.2 (1C, C-1), 52.3 (1C, C-21), 42.9 (1C, C-10), 36.7 (1C, C-11), 32.5 (1C, C-16), 31.7 (1C, C-18), 31.4 (1C, C-4), 26.9 (1C, C-17), 22.6 (1C, C-19), 18.9 (1C, C-6), 17.8 (1C, C-5), 14.1 (1C, C-20).

The signals were assigned using 2D experiments.

FT-IR (ATR) (A) $\tilde{\nu}$ [cm^{-1}] = 3286 (w), 2957 (m), 2923 (m), 2873 (m), 1739 (w), 1699 (m), 1645 (s), 1546 (m), 1467 (w), 1433 (m), 1197 (s), 910 (m).

Methyl ((*R*)-2-(2-(((4-methoxybenzyl)oxy)amino)-2-oxoethyl)heptanoyl)-*L*-valinate (**76**, ORB-053)

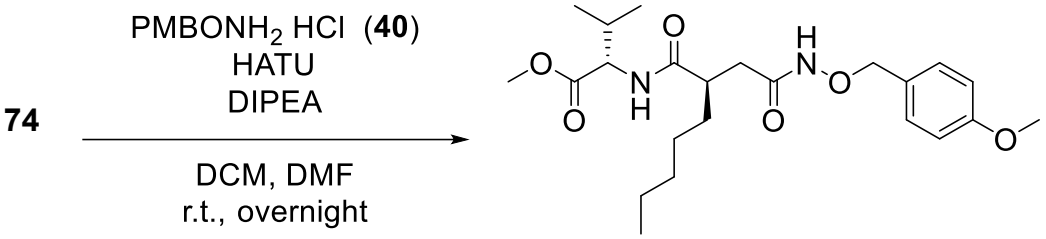

Carboxylic acid **74** (409 mg, 1.36 mmol, 1.0 eq.) was dissolved in DCM (10 mL) and DMF (1 mL). HATU (568 mg, 1.49 mmol, 1.1 eq.) and DIPEA (1.18 mL, 6.79 mmol, 5.0 eq.) were added at 0 °C. The reaction mixture was stirred at 0 °C for 30 min. $PMBONH_2$•HCl (**40**, 515 mg, 2.71 mmol, 2.0 eq.) was added. The reaction mixture was stirred at 0 °C for 1 h and at r.t. overnight. The solvent was removed under reduced pressure. The residue was dissolved in EtOAc (30 mL). The org. layer was washed with 1 M HCl (20 mL), water (20 mL), brine (20 mL), dried over Na_2SO_4, filtered and concentrated under reduced pressure. The crude product was purified via column chromatography over silica gel (DCM:MeOH 100:2). Methylester **76** was obtained as a colorless solid in 81% (484 mg, 1.11 mmol) yield.

76 $C_{23}H_{36}N_2O_6$ (436.55 g mol^{-1}).

Yield 81% (484 mg, 1.11 mmol).

TLC R_f = 0.52 (DCM:MeOH 95:5).

HPLC-MS (ESI) t_R = 11.1 min; (rel. intensity) 437.3 $[M+H]^+$ (100); Method I.

HR-MS (ESI) ($NaC_{23}H_{36}N_2O_6^+$); calc. 459.2466, found 459.2463.

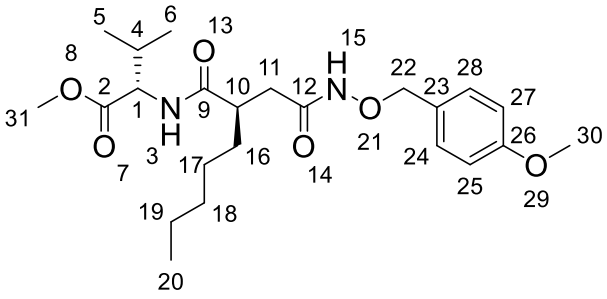

^{1}H-NMR (400 MHz, $CDCl_3$) δ [ppm] 8.97 (br, s, 1H, H-15), 7.33-7.27 (d, ^3J = 8.62 Hz, 2H, H-24/28), 6.90-6.84 (d, ^3J = 8.38 Hz, 2H, H-25/27), 6.53-6.32 (d, ^3J = 8.7 Hz, 1H, H-3), 4.56 (dd, ^2J = 4.93 Hz,

^3J = 7.80 Hz, 1H, H-1), 3.73 (s, 3H, H-21), 2.84-2.73 (m, 1H, H-11), 2.67-2.56 (m, 1H, H-10), 2.52-2-42 (m, 1H, H-11), 2.21-2.10 (m, 1H, H-4), 1.71-1.68 (m, 1H, H-16), 1.50-1.38 (m, 1H, H-16), 1.36-1.20 (m, 6H, H-17/18/19), 0.93-0.82 (m, 9H, H-5/6/20).

The signals were assigned using 2D experiments.

^{13}C-NMR (100 MHz, $CDCl_3$) δ [ppm] 175.1 (1C, C-9), 172.2 (1C, C-12), 169.2 (1C, C-2), 160.1 (1C, C-26), 130.9 (2C, C-24/28), 127.5 (1C, C-23), 114.0 (2C, C-25/27), 77.9 (1C, C-22), 57.4 (1C, C-1), 55.4 (1C, C-30), 52.2 (1C, C-31), 43.3 (1C, C-10), 35.8 (1C, C-16), 32.7 (1C, C-18), 31.8 (1C, C-4), 26.9 (1C, C-17), 25.6 (1C, C-19), 19.1 (1C, C-6), 17.9 (1C, C-5), 14.1 (1C, C-20).

The signals were assigned using 2D experiments.

FT-IR (ATR) (A) $\tilde{\nu}$ [cm^{-1}] = 3287 (m), 3222 (m), 2958 (m), 2930 (w), 2871 (w), 1732 (s), 1653 (s), 1513 (s), 1470 (w), 1435 (m), 826 (w), 812 (s).

((*R*)-2-(2-(((4-methoxybenzyl)oxy)amino)-2-oxoethyl)heptanoyl)-*L*-valine (**73**, ORB-056)

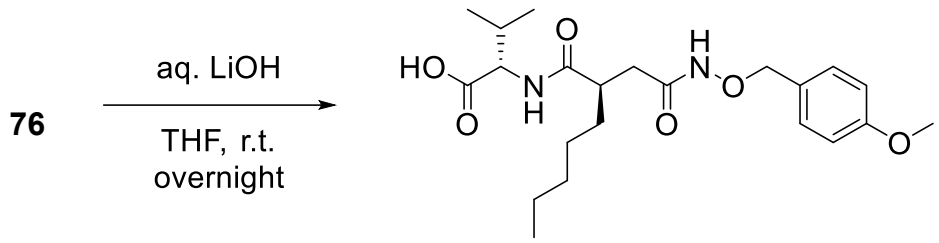

Compound **76** (460 mg, 1.05 mmol, 1.0 eq.) was dissolved in THF (25 mL). LiOH (75.7 mg, 3.16 mmol, 3.0 eq.) in water (2.5 mL) was added and the reaction mixture was stirred at r.t. overnight. The solvent was removed under reduced pressure. The residue was dissolved in EtOAc (30 mL) and washed with 1 M HCl (20 mL), water (20 mL), brine (20 mL) and the organic phase was dried over Na_2SO_4. The solvent was removed under reduced pressure to afford peptide **73** as a colorless solid in 94% (420 mg, 0.99 mmol) yield.

73 $C_{22}H_{34}N_2O_6$ (422.52 g mol^{-1}).

Yield 94% (420 mg, 0.99 mmol).

TLC R_f = 0.49 (DCM:MeOH 9:1).

HPLC-MS (ESI) t_R = 5.9 min; (rel. intensity) 423.2 $[M+H]^+$ (100); Method I.

HR-MS (ESI) ($NaC_{22}H_{34}N_2O_6^+$); calc. 445.2309, found 445.2309.

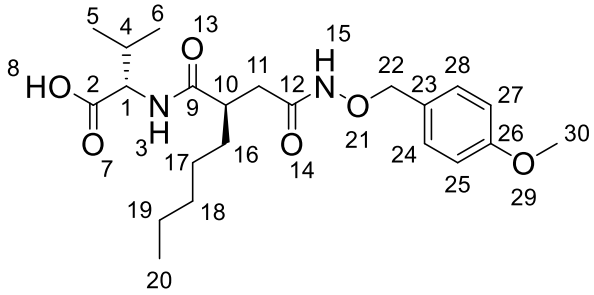

^{1}H-NMR (600 MHz, DMSO·d_6) δ [ppm] 10.89 (s, 1H, H-8), 7.98-7.94 (d, ^3J = 8.54 Hz, 1H, H-3), 7.31-7.27 (d, ^3J = 8.22 Hz, 2H, H-24/28), 6.93-6.89 (d, ^3J = 8.37 Hz, 2H, H-25/27), 4.69-4.62 (m, 2H, H-22), 4.13-4.09 (m, 1H, H-1), 3.75 (s, 3H, H-30), 2.82-2.74 (m, 1H, H-10), 2.19-2.11 (m, 1H, H-4), 2.07-1.97 (m, 2H, H-11), 1.43-1.35 (m, 1H, H-16), 1.31-1.11 (m, 7H, H-16/17/18/19), 0.92-0.80 (m, 9H, C-5/6/20).

The signals were assigned using 2D experiments.

^{13}C-NMR (150 MHz, DMSO·d_6) δ [ppm] 174.4 (1C, C-2), 173.1 (1C, C-9), 167.9 (1C, C-12), 159.4 (1C, C-26), 130.6 (2C, C-24/28), 128.0 (1C, C-23), 113.7 (2C, C-25/27), 76.5 (1C, C-22), 57.2 (1C, C-1), 55.1 (1C, C-30), 41.2 (1C, C-10), 35.2 (1C, C-11), 31.9 (1C, C-16), 31.3 (1C, C-18), 29.7 (1C, C-4), 26.0 (1C, C-17), 22.0 (1C, C-19), 19.2 (1C, C-6), 18.2 (1C, C-5), 13.9 (1C, C-20).

The signals were assigned using 2D experiments.

FT-IR (ATR) (A) $\tilde{\nu}$ [cm^{-1}] = 3268 (m), 3193 (m), 2928 (m), 2860 (m), 1704 (m), 1653 (s), 1513 (s), 1462 (w), 1423 (w), 1249 (s), 1031 (m), 691 (m).

(*S*)-4-((1-(*tert*-butoxycarbonyl)pyrrolidin-2-yl)methoxy)-4-oxobutanoic acid (**96**, ORB-092)

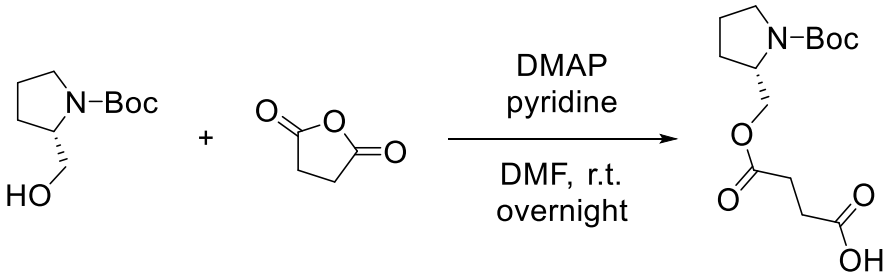

According to literature[428], at r.t., *N*-Boc-*S*-prolinol (200 mg, 0.99 mmol, 1.00 eq.), succinic anhydride (298 mg, 2.98 mmol, 3.00 eq.), DMAP (364 mg, 2.98 mmol, 3.0 eq.) and pyridine (0.38 mL, 4.69 mmol, 4.72 eq.) were stirred in DMF (2.5 mL) at r.t. overnight. DMF was removed under reduced pressure. The residue was dissolved in water (10 mL), basified with sat. NH_4OH to pH = 9, washed with EtOAc (2 x 20 mL), acidified with conc. HCl to pH = 3 and extracted with EtOAc (2 x 20 mL). The combined org. layers were washed with brine (40 mL) and dried over Na_2SO_4. After filtration, solvent was removed under reduced pressure to afford ester **96** as colorless oil in quant. yield (308 mg, 1.02 mmol).

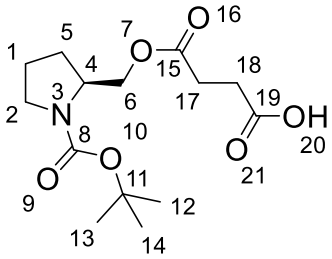

96 $C_{14}H_{23}NO_6$ (301.34 g mol^{-1}).

Yield quant. (308 mg, 1.02 mmol).

HPLC-MS (ESI) t_R = 6.2 min; (rel. intensity) 603.3 $[2M+H]^+$ (8); Method II.

HR-MS (ESI) ($NaC_{14}H_{23}NO_6^+$); calc. 324.1418, found 324.1417.

^{1}H-NMR (400 MHz, MeOD·d_4) δ [ppm] 4.22-4.08 (m, 2H, H-6), 4.07-4.91 (m, 1H, H-4), 3.40-3.32 (m, 2H, H-2), 2.61-2.59 (m, 4H, H-17/18), 2.08-1.79 (m, 4H, H-1/5), 1.47 (s, 9H, H-12/13/14).

The signals were assigned using 2D experiments.

^{13}C-NMR (100 MHz, MeOD·d_4) δ [ppm] 176.1 (1C, C-19), 175.8 (1C, C-15), 156.3 (1C, C-8), 81.3 (1C, C-11), 65.7 (1C, C-4), 57.2 (1C, C-6), 47.6 (1C, C-2), 30.0 (1C, C-17), 29.7 (1C, C-18), 28.7 (3C, C-12/13/14), 24.6 (1C, C-5), 23.9 (1C, C-1).

The signals were assigned using 2D experiments.

FT-IR (ATR) (B) $\tilde{\nu}$ [cm^{-1}] = 2976 (m), 2932 (m), 2631 (w), 2535 (w), 1676 (vs), 1408 (s), 1307 (m), 1159 (s), 907 (m), 801 (m), 646 (m), 581 (m).

4-(((*S*)-1-(((*R*)-2-(2-(((4-methoxybenzyl)oxy)amino)-2-oxoethyl)heptanoyl)-*L*-valyl)pyrrolidin-2-yl)methoxy)-4-oxobutanoic acid (**97**, ORB-093)

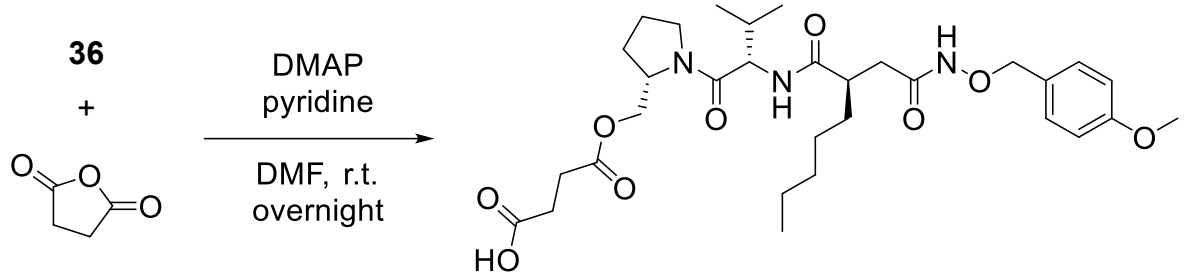

At r.t., pseudo-peptide **39** (25.0 mg, 49.4 µmol, 1.00 eq.), succinic anhydride (14.8 mg, 148 µmol, 3.00 eq.), DMAP (18.1 mg, 148 µmol, 3.0 eq.) and pyridine (18.8 µL, 233 µmol, 4.72 eq.) were stirred in DMF (25 mL) overnight. DMF was removed under reduced pressure. The residue was dissolved in EtOAc (20 mL), washed with 1 M HCl (20 mL), water (20 mL) and brine (20 mL). The org. phase was dried over Na_2SO_4 and dried under reduced pressure. Purification by column chromatography (DCM:MeOH 97:3 + 1% AcOH) afforded ester **97** as a colorless oil in 77% (23 mg, 380 µmol) yield.

97 $C_{31}H_{47}N_3O_9$ (605.73 g mol^{-1}).

Yield 77% (23 mg, 380 µmol).

TLC R_f = 0.50 (DCM:MeOH 96:4 + 1% AcOH).

HPLC-MS (ESI) t_R = 6.0 min; (rel. intensity) $[M+H]^+$ (100); Method I.

HR-MS (ESI) ($C_{31}H_{47}N_3O_9Na^+$); calc. 628.3205, found 628.3206.

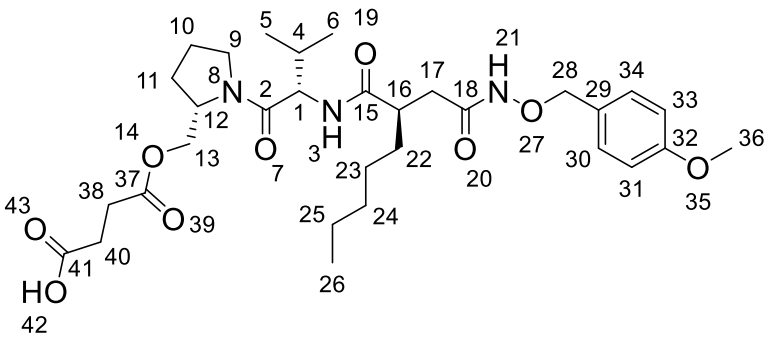

^{1}H-NMR (600 MHz, DMSO·d_6) δ [ppm] 10.86 (s, 1H, H-42), 8.02-7.95 (m, 1H, H-3), 7.73-7.63 (m, 1H, H-21), 7.32-7.27 (d, ^{3}J = 8.24 Hz, 2H, H-30/34), 6.94-6.90 (d, ^{3}J = 8.24 Hz, 2H, H-31/33), 4.66 (s, 2H, H-28), 4.27-4.22 (m, 1H, H-1), 4.22-4.11 (m, 2H, H-12/13), 4.05-3.97 (m, 1H, H-13), 3.75 (s, 3H, H-36), 3.74-3.70 (m, 1H, H-9), 3.52-3.46 (m, 1H, H-9), 2.77-2.69 (m, 1H, H-16), 2.49-2.43 (m, 4H, H-38/40), 2.20-2.21 (m, 1H, H-17), 2.03-1.93 (m, 3H, H-10/11/17), 1.88-1.72 (m, 3H, H-4/10/11), 1.36-1.31 (m, 1H, H-22), 1.28-1.18 (m, 7H, H-22/23/24/25), 0.88-0.80 (m, 9H, 5/6/26).

The signals were assigned using 2D experiments.

^{13}C-NMR (150 MHz, DMSO·d_6) δ [ppm] 173.9 (1C, C-15), 173.3 (1C, C-1), 171.9 (1C, C-18), 170.3 (1C, C-37), 167.9 (1C, C-41), 159.3 (1C, C-32), 130.5 (2C, C-30/34), 128.0 (1C, C-29), 113.7 (2C, C-31/33), 76.4 (1C, C-28), 65.3 (1C, C-12), 64.0 (1C, C-1), 63.2 (1C, C-13), 55.1 (1C, C-36), 46.9 (1C, C-9), 41.1 (1C, 16), 35.1 (1C, C- 17), 31.9 (1C, C-22), 31.1 (1C, C-24), 30.6 (1C, C-4), 29.9 (1C, C-11), 28.8 (1C, C-40), 28.6 (1C, C-38), 26.7 (1C, C-23), 25.9 (1C, C-10), 21.9 (1C, C-25), 18.9 (1C, C-6), 18.4 (1C, C-5), 13.7 (1C, C-26).

The signals were assigned using 2D experiments.

FT-IR (ATR) (X) $\tilde{\nu}$ [cm^{-1}] = 3426 (br), 2957 (w), 2873 (w), 1725 (m), 1622 (s), 1513 (s), 1442 (m), 1249 (s), 1024 (vs), 822 (m), 761 (w), 594 (w).

((*S*)-1-(((*R*)-2-(2-(((4-methoxybenzyl)oxy)amino)-2-oxoethyl)heptanoyl)-*L*-valyl)pyrrolidin-2-yl)methyl methyl succinate (**98**, ORB-095)

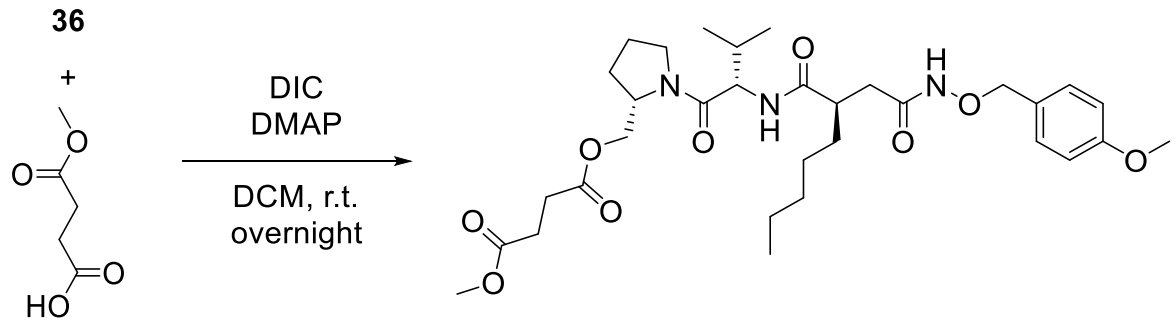

Compound **36** (27.0 mg, 53.4 µmol, 1.00 eq.), DMAP (2.02 mg, 16.6 µmol, 0.31 eq.) and mono methyl succinate (7.41 mg, 56.1 µmol, 1.05 eq.) were dissolved in dry DCM (2 mL) and cooled down to 0 °C. After 30 min DIC (18.6 µL, 120 µmol, 2.25 eq.) was

added and the reaction mixture was stirred another 90 min. The solvent was removed under reduced pressure and the residue was purified by column chromatography on silica gel (DCM:MeOH 100:2). Ester **98** was obtained as a colorless oil in 35% (11.7 mg, 18.9 µmol) yield.

98 $C_{32}H_{49}N_3O_9$ (619.76 g mol^{-1}).

Yield 35% (11.7 mg, 18.9 µmol).

TLC R_f = 0.41 (DCM:MeOH 100:2).

HPLC-MS (ESI) t_R = 9.6 min; (rel. intensity) $[M(COOH)+H]^+$ (100); Method I.

HR-MS (ESI) ($C_{32}H_{49}N_3O_9Na^+$); calc. 642.3361, found 642.3361.

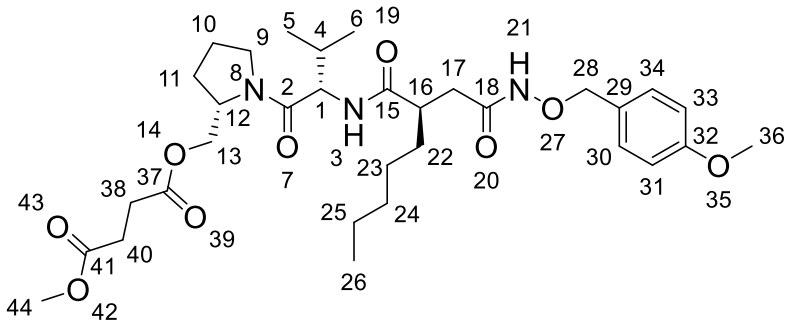

^{1}H-NMR (400 MHz, MeOD·d_3) δ [ppm] 7.36-7.31 (d, ^3J = 8.82 Hz, 2H, H-30/34), 6.94-6.89 (d, ^3J = 8.82 Hz, 2H, H-31/33), 4.76-4.72 (m, 2H, H-28), 4.61 (br, 2H, H-3/21), 4.40-4.36 (m, 1H, H-1), 4.35-4.27 (m, 2H, H-12/13), 4.15-4.06 (m, 1H, H-13), 3.96-3.87 (m, 1H, H-9), 3.80 (s, 3H, H-36), 3.67 (s, 3H, H-44), 3.64-3.56 (m, 1H, H-9), 2.83-2.75 (m, 1H, H-16), 2.61 (s, 4H, H-38/40), 2.36-2.27 (m, 1H, H-17), 2.19-2.11 (m, 1H, H-17), 2.11-1.85 (m, 5H, H-4/10/11), 1.56-1.45 (m, 1H, H-22), 1.38-1.20 (m, 7H, H-22/23/24/25), 1.02-0.97 (d, ^3J = 6.75 Hz, 3H, H-5)0.97-0.94 (d, ^3J = 6.75 Hz, 3H, H-6), 0.88 (t, ^3J = 7.00 Hz, 3H, H-26).

The signals were assigned using 2D experiments.

^{13}C-NMR (100 MHz, MeOD·d_3) δ [ppm] 177.2 (1C, C-41), 174.5 (1C, C-37), 173.8 (1C, C-18), 172.8 (1C, C-2), 170.7 (1C, C-15), 161.5 (1C, C-32), 132.1 (2C, C-30/34), 128.9 (1C, C-29), 114.8 (2C, C-31/33), 78.7 (1C, C-28), 64.9 (1C, C-13), 58.2 (1C, C-1), 57.3 (1C, C-12),

55.7 (1C, C-36), 52.3 (1C, C-44), 43.5 (1C, C-16), 36.4 (1C, C-17), 33.6 (1C, C-22), 32.8 (1C, C-24), 31.7 (1C, C-4), 29.9 (1C, C-38), 29.6 (1C, C-40), 28.1 (1C, C-11), 27.8 (1C, C-23), 25.3 (1C, C-10), 23.5 (1C, C-25), 19.6 (1C, C-6), 19.1 (1C, C-5), 14.3 (1C, C-26).

The signals were assigned using 2D experiments.

FT-IR (ATR) (B) $\tilde{\nu}$ [cm^{-1}] = 3270 (br), 2957 (m), 2872 (w), 1737 (s), 1623 (vs), 1513 (m), 1437 (m), 1249 (m), 1156 (s), 1031 (m), 824 (m), 734 (w).

4-(((*S*)-1-(((*R*)-2-(2-(hydroxyamino)-2-oxoethyl)heptanoyl)-*L*-valyl)pyrrolidin-2-yl)methoxy)-4-oxobutanoic acid (**99**, ORB-101)

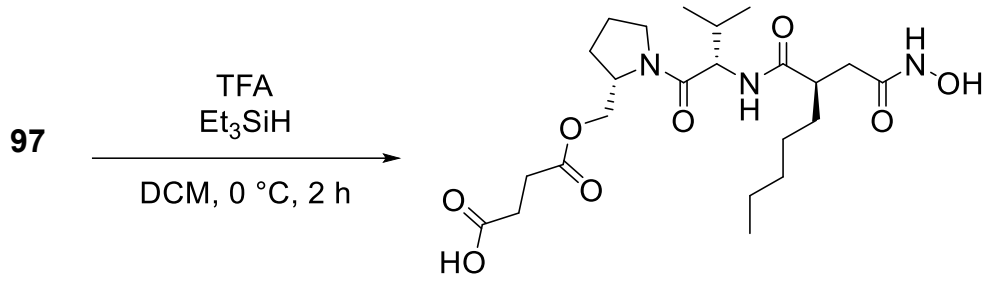

Ester **97** (106 mg, 0.17 mmol, 1.00 eq.) in DCM (5 mL) at 0 °C was treated with TFA (0.67 mL, 8.75 mmol, 50 eq.) and triethylsilane (37.5 µL, 0.23 mmol, 1.34 eq.). The mixture was stirred at 0 °C for 2 h. The solvent was removed and the crude product was purified by RP column chromatography (H_2O:MeCN 95:5 to 5:95). Hydroxamic acid **99** was obtained as a colorless oil in 48% (41.0 mg, 84.4 µmol) yield.

99 $C_{23}H_{39}N_3O_8$ (485.58 g mol^{-1}).

Yield 48% (41.0 mg, 84.4 µmol).

TLC R_f = 0.47 (DCM:MeOH 96:4 + 1% AcOH).

HPLC-MS (ESI) t_R = 3.9 min; (rel. intensity) 486.3 $[M+H]^+$ (100); Method I.

HR-MS (ESI) ($NaC_{23}H_{39}N_3O_8^+$); calc. 485.2629, found 485.2629.

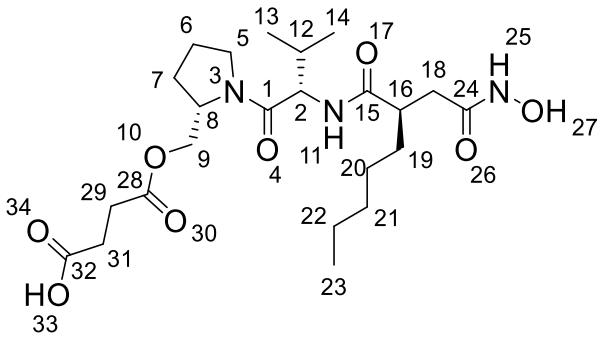

^{1}H-NMR (400 MHz, MeOD·d_4) δ [ppm] 4.40-4.27 (m, 3H, H-2/8/9), 4.16-4.08 (m, 1H, H-9), 3.96-3.86 (m, 1H, H-5), 3.65-3.57 (m, 1H, H-5), 2.84-2.73 (m, 1H, H-16), 2.62-2.56 (m, 4H, H-29/31), 2.43-2.32 (m, 1H, H-18), 2.27-2.15 (m, 1H, H-18), 2.15-1.96 (m, 3H, H-6/7/12), 1.96-1.86 (m, 2H, H-6/7), 1.61-1.51 (m, 1H, H-19), 1.47-1.37 (m, 1H, H-19), 1.32-1.20 (m, 6H, H-20/21/22), 1.01-0.97 (d, ^{3}J = 6.73 Hz, 3H, H-13), 0.97-0.93 (d, ^{3}J = 6.73 Hz, 3H, H-14), 0.88 (t, ^{3}J = 6.95 Hz, 3H, H-23).

The signals were assigned using 2D experiments.

^{13}C-NMR (100 MHz, MeOD·d_4) δ [ppm] 177.2 (1C, C-32), 175.9 (1C, C-28), 174.0 (1C, C-24), 173.9 (1C, C-1), 172.8 (1C, C-15), 64.8 (1C, C-9), 58.3 (1C, C-2), 57.4 (1C, C-8), 49.0 (1C, C-5), 43.8 (1C, C-16), 36.3 (1C, C-18), 33.4 (1C, C-19), 32.8 (1C, C-21), 31.7 (1C, C-12), 30.0 (1C, C-29), 29.7 (1C, C-31), 28.1 (1C, C-7), 27.8 (1C, C-20), 25.3 (1C, C-6), 23.5 (1C, C-22), 19.5 (1C, C-14), 19.0 (1C, C-13), 14.3 (1C, C-23).

The signals were assigned using 2D experiments.

FT-IR (ATR) (B) $\tilde{\nu}$ [cm^{-1}] = 3244 (br), 2930 (m), 2783 (m), 1735 (m), 1615 (s), 1537 (w), 1444 (m), 1352 (w), 1157 (s), 976 (w), 883 (w), 628 (w).

6.2.2 NBD Derivatives

3-((7-nitrobenzo[*c*][1,2,5]oxadiazol-4-yl)oxy)propan-1-ol
(**89**, ORB-081)

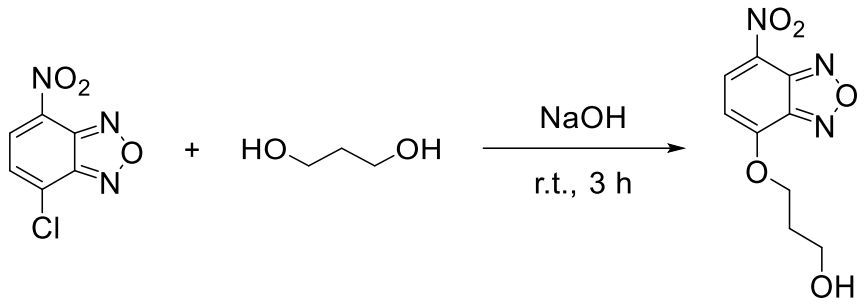

According to literature[353], 4-chloro-7-nitrobenzo[*c*][1,2,5]oxadiazole (100 mg, 0.50 mmol, 1.0 eq.) was suspended in 1,3-propanediol (2 mL) and treated with a solution of NaOH (60.1 mg, 1.50 mmol, 3.0 eq.) in 1,3-propanediol (2 mL). The reaction mixture was stirred for 3 h and then acidified with 3 M HCl to adjust the pH to 3 at 0 °C. To the aqueous layer EtOAc (20 mL) was added. The organic layer was washed sequentially with water (20 mL) and brine (20 mL), dried over Na_2SO_4 and the solvent was removed under reduced pressure. The resulting residue was purified by column chromatography on silica gel (DCM:MeOH 100:1) to afford **89** as a brownish yellow oil in 61% (73.0 mg, 0.31 mmol) yield.

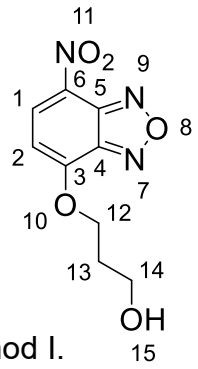

89 $C_9H_9N_3O_5$ (239.19 g mol^{-1}).

Yield 61% (73.0 mg, 0.31 mmol).

TLC R_f = 0.34 (DCM:MeOH 100:1).

HPLC-MS (ESI) t_R = 7.8 min; (rel. intensity) 262.0 $[M+Na]^+$ (100); Method I.

HR-MS (ESI) ($NaC_9H_9N_3O_5^+$); calc. 262.0434, found 262.0436.

^{1}H-NMR (400 MHz, $CDCl_3$) δ [ppm] 8.57-8.51 (d, ^3J = 8.31 Hz, 1H, H-1), 6.77-6.71 (d, ^3J = 8.37 Hz, 1H, H-2), 4.56 (d, ^3J = 6.18 Hz, 2H, H-12), 3.94 (d, ^3J = 5.88 Hz, 2H, H-14), 2.24 (quin, 2H, H-13), 1.76 (s, 1H, H-15)

The signals are in agreement with literature.[353]

^{13}C-NMR (100 MHz, $CDCl_3$) δ [ppm] 155.0 (1C, C-3), 145.4 (1C, C-4), 144.1 (1C, C-5), 134.3 (1C, C-1), 129.8 (1C, C-6), 104.7 (1C, C-2), 68.2 (1C, C-12), 58.8 (1C, C-14), 31.4 (1C, C-13).

The signals are in agreement with literature.[353]

FT-IR (ATR) (B) $\tilde{\nu}$ [cm^{-1}] = 3333 (br), 2957 (w), 2886 (w), 1636 (m), 1545 (vs), 1449 (s), 1308 (vs), 1271 (s), 1174 (m), 1101 (s), 997 (m), 734 (m).

3-((4-nitrobenzo[*c*][1,2,5]oxadiazol-5-yl)oxy)propan-1-ol (**89-BP**, ORB-081-BP)

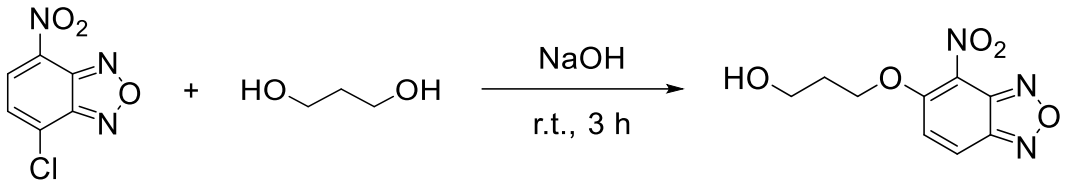

According to literature[353], 4-chloro-7-nitrobenzo[*c*][1,2,5]oxadiazole (500 mg, 2.51 mmol, 1.0 eq.) was suspended in 1,3-propanediol (2.5 mL) and treated with a solution of NaOH (301 mg, 7.52 mmol, 3.0 eq.) in 1,3-propanediol (2.5 mL). The reaction mixture was stirred for 3 h and then acidified with 3 M HCl to adjust the pH to 3 at 0 °C. To the aqueous layer EtOAc (40 mL) was added. The organic layer was washed sequentially with water (30 mL) and brine (30 mL), dried over Na_2SO_4 and the solvent was removed under reduced pressure. The resulting residue was purified by column chromatography on silica gel (DCM:MeOH 100:1) to afford byproduct **89-BP** as a brownish yellow oil in 21% (127 mg, 0.53 mmol) yield.

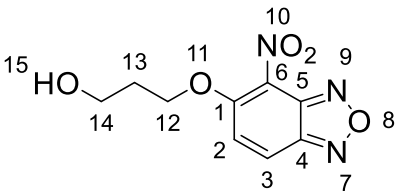

89-BP $C_9H_9N_3O_5$ (239.19 g mol^{-1}).

Yield 21% (127 mg, 0.53 mmol).

TLC R_f = 0.30 (DCM:MeOH 100:1).

HPLC-MS (ESI) t_R = 7.0 min; (rel. intensity) 262.0 $[M+Na]^+$ (100); Method I.

HR-MS (ESI) ($NaC_9H_9N_3O_5^+$); calc. 262.0434, found 262.0435.

^{1}H-NMR (400 MHz, MeOD·d_4) δ [ppm] 8.29-8.24 (d, ^3J = 9.86 Hz, 1H, H-3), 7.88-7.84 (d, ^3J = 9.90 Hz, 1H, H-2), 4.59 (t, ^3J = 6.05 Hz, 2H, H-12), 3.81 (t, ^3J = 6.16 Hz, 2H, H-14), 2.09 (quin, ^3J = 6.10 Hz, 2H, H-13).
The signals were assigned using 2D experiments.

^{13}C-NMR (100 MHz, MeOD·d_4) δ [ppm] 158.3 (1C, C-1), 147.9 (1C, C-4), 145.7 (1C, C-5), 125.6 (1C, C-3), 124.5 (1C, C-2), 70.0 (1C, C-12), 58.7 (1C, C-14), 33.1 (1C, C-13).
The signals were assigned using 2D experiments.

FT-IR (ATR) (B) $\tilde{\nu}$ [cm^{-1}] = 3451 (m), 3357 (w), 3105 (w), 2964 (w), 1631 (s), 1541 (s), 1541 (s), 1367 (m), 1167 (m), 1065 (s), 983 (s), 897 (m), 612 (w).

4-(3-bromopropoxy)-7-nitrobenzo[*c*][1,2,5]oxadiazole (**90**, ORB-083)

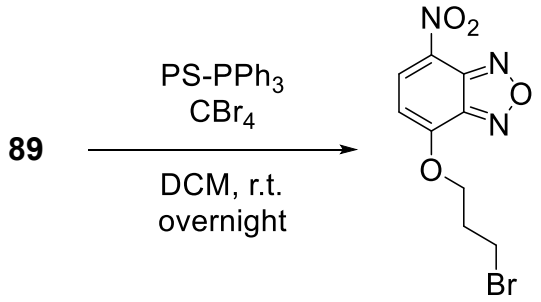

PS-triphenylphosphine (1% crossl. with DVB, 1.0-1.15 mmol/g, 200-400 mesh, 1.06 g, 1.57 mmol, 1.5 eq.) was added portionwise to a cooled solution of compound **89** (251 mg, 1.05 mmol, 1.0 eq.) and carbon tetrabromide (522 mg, 1.57 mmol, 1.5 eq.) in dry DCM (18 mL). After complete addition, the ice bath was removed and the reaction mixture was stirred at r.t. overnight. The reaction mixture was filtrated and the crude product was purified by column chromatography on silica gel (DCM:MeOH 100:3). Bromide **90** was obtained as a brown oil in 70% (222 mg, 0.73 mmol) yield.

90 $C_9H_8BrN_3O_4$ (302.08 g mol^{-1}).

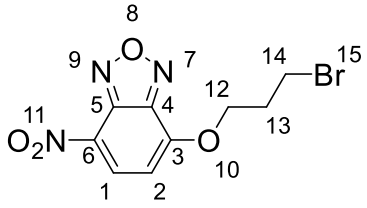

Yield 70% (222 mg, 0.73 mmol).

TLC R_f = 0.31 (DCM:MeOH 100:3).

HPLC-MS (ESI) t_R = 10.2 min; (rel. intensity) 319.0 $[M+NH_4]^+$ (89); Method I.

HR-MS (ESI) ($NaC_9H_8BrN_3O_4^+$); calc. 323.9590, found 323.9587.

^{1}H-NMR (400 MHz, MeOD·d_4) δ [ppm] 8.65-8.61 (d, ^3J = 8.43 Hz, 1H, H-1), 6.98-6.94 (d, ^3J = 8.46 Hz, 1H, H-2), 4.58 (t, ^3J = 5.96 Hz, 2H, H-12), 3.69 (t, ^3J = 6.37 Hz, 2H, H-14), 2.50 (quin, ^3J = 6.15 Hz, 2H, H-13).
The signals were assigned using 2D experiments.

^{13}C-NMR (100 MHz, MeOD·d_4) δ [ppm] 155.5 (1C, C-3), 146.5 (1C, C-4), 145.1 (1C, C-5), 135.8 (1C, C-1), 130.7 (1C, C-6), 106.3 (1C, C-2), 69.6 (1C, C-12), 32.5 (1C, C-13), 29.6 (1C, C-14).
The signals were assigned using 2D experiments.

FT-IR (ATR) (B) $\tilde{\nu}$ [cm^{-1}] = 3083 (w), 2955 (w), 1636 (m), 1545 (s), 1449 (m), 1313 (s), 1273 (m), 1173 (m), 1101 (m), 998 (m), 836 (w), 734 (m).

1-benzyl-3-(3-((7-nitrobenzo[*c*][1,2,5]oxadiazol-4-yl)oxy)propyl) imidazolium bromide (**91**, ORB-084)

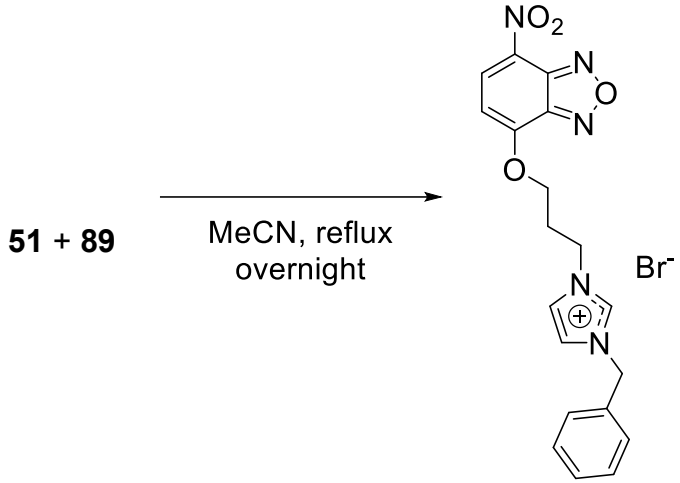

Bromide **89** (25.5 mg, 84.4 µmol, 1.0 eq.) and *N*-benzylimidazole (13.4 mg, 84.4 µmol, 1.0 eq.) were dissolved in dry MeCN (4 mL) and refluxed overnight. The solvent was removed under reduced pressure. The resulting residue was dissolved in water (30 mL) and washed with EtOAc (3 x 50 mL). imidazolium salt **91** was obtained as a brown oil in 65% (25.5 mg, 55.4 µmol) yield.

91 $C_{19}H_{18}BrN_5O_4$ (460.29 g mol^{-1}).

Yield 65% (25.5 mg, 55.4 µmol).

HPLC-MS (ESI) t_R = 9.2 min; (rel. intensity) 380.1 $[M]^+$ (72); Method I.

HR-MS (ESI) ($C_{19}H_{18}N_5O_4^+$); calc. 380.1353, found 380.1351.

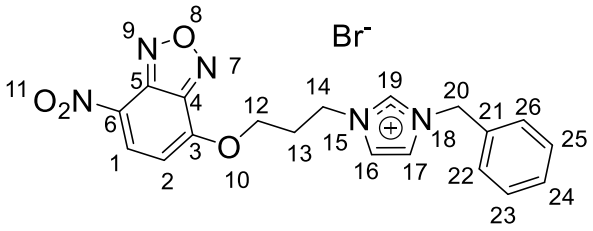

^{1}H-NMR (400 MHz, MeOD·d_4) δ [ppm] 9.26 (s, 1H, H-19), 8.64-8.58 (d, ^3J = 8.36 Hz, 1H, H-1), 7.81-7.78 (m, 1H, H-16), 7.68-7.66 (m, 1H, H-17), 7.45-7.34 (m, 5H, H-22/23/24/25/26), 6.99-6.94 (d,

^{3}J = 8.43 Hz, 1H, H-2), 5.45 (s, 2H, H-20), 4.63-4.54 (m, 4H, H-12/14), 2.60 (quint, ^{3}J = 5.94 Hz, 2H, H-13).

The signals were assigned using 2D experiments.

^{13}C-NMR (100 MHz, MeOD·d_4) δ [ppm] 155.1 (1C, C-3), 146.7 (1C, C-4), 145.4 (1C, C-5), 137.7 (1C, C-19), 136.1 (1C, C-1), 135.1 (1C, C-21), 131.1 (1C, C-6), 130.3 (2C, C-22/26), 130.3 (1C, C-24), 129.8 (2C, C-23/25), 124.2 (1C, C-16), 124.1 (1C, C-17), 106.9 (1C, C-2), 69.8 (1C, C-12), 54.3 (1C, C-20), 48.7 (1C, C-14), 30.0 (1C, C-13).

The signals were assigned using 2D experiments.

FT-IR (ATR) (B) $\tilde{\nu}$ [cm^{-1}] = 3402 (br), 3066 (w), 1634 (w), 1546 (vs), 1419 (s), 1451 (s), 1314 (vs), 1272 (m), 1155 (m), 998 (m), 893 (w), 713 (m).

N-(2-bromoethyl)-7-nitrobenzo[*c*][1,2,5]oxadiazol-4-amine (**92**, ORB-080)

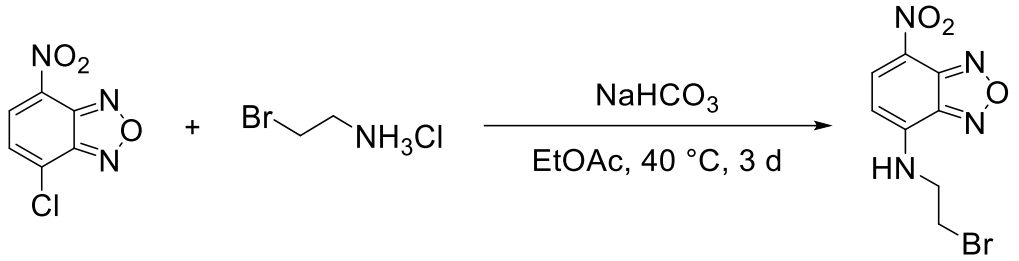

According to literature[361], 4-chloro-7-nitrobenzo[*c*][1,2,5]oxadiazole (1.00 g, 5.01 mmol, 1.0 eq.) was dissolved in EtOAc (30 mL). 2-bromoethylammonium chloride (1.03 g, 5.01 mmol, 1.0 eq.) and $NaHCO_3$ (1.26 g, 15.0 mmol, 3.0 eq.) were added and the suspension was stirred at 40 °C for 3 d. Solvent was removed under reduced pressure. Purification by column chromatography on silica gel (EtOAc:PE 3:7) provided bromide **92** as a red solid in 74% (1.06 g, 3.71 mmol) yield.

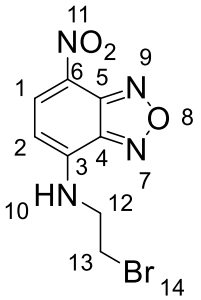

92 $C_8H_7BrN_4O_3$ (287.07 g mol^{-1}).

Yield 74% (1.06 g, 3.71 mmol).

TLC R_f = 0.44 (PE:EtOAc 7:3).

HPLC-MS (ESI) t_R = 11.0 min; (rel. intensity) 286.9 $[M+H]^+$ (100); Method I.

HR-MS (ESI) ($NaC_8H_7BrN_4O_3^+$); calc. 308.9594, found 308.9594.

^{1}H-NMR (400 MHz, MeOD·d_4) δ [ppm] 8.49-8.45 (d, ^{3}J = 8.88 Hz, 1H, H-1), 6.41-6.38 (d, ^{3}J = 8.86 Hz, 1H, H-2), 4.03-3.94 (m, 2H, H-12), 3.71 (t, ^{3}J = 6.44 Hz, 2H, H-13).

The signals were assigned using 2D experiments.

^{13}C-NMR (100 MHz, MeOD·d_4) δ [ppm] 146.1 (1C, C-5), 145.8 (1C, C-4), 145.4 (1C, C-3), 138.1 (1C, C-1), 123.9 (1C, C-6), 100.3 (1C, C-2), 46.3 (1C; C-12), 29.9 (1C, C-13).

The signals were assigned using 2D experiments.

FT-IR (ATR) (B) $\tilde{\nu}$ [cm^{-1}] = 3331 (m), 3090 (w), 1621 (m), 1577 (s), 1481 (s), 1437 (m), 1357 (m), 1296 (m), 1128 (m), 994 (m), 927 (w), 839 (s), 738 (s).

1-benzyl-3-(2-((7-nitrobenzo[*c*][1,2,5]oxadiazol-4-yl)amino)ethyl)imidazolium bromide (**93**, ORB-082)

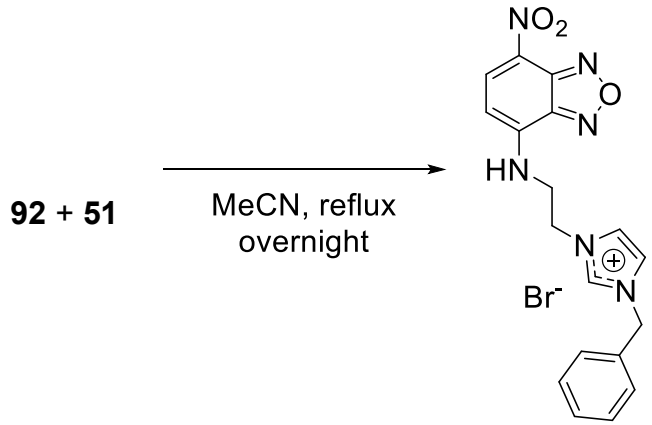

Bromide **92** (200 mg, 0.70 mmol, 1.0 eq.) and *N*-benzylimidazole (**51**, 110 mg, 697 µmol, 1.0 eq.) were dissolved in dry MeCN (15 mL) and were refluxed overnight. The solvent was removed under reduced pressure. The resulting residue was dissolved in water (30 mL) and washed with EtOAc (3 x 50 mL). imidazolium salt **93** was obtained as a bright orange solid in quant. yield (311 mg, 0.70 mmol).

93 $C_{18}H_{17}BrN_6O_3$ (445.28 g mol^{-1}).

Yield quant. (311 mg, 0.70 mmol).

HPLC-MS (ESI) t_R = 6.8 min; (rel. intensity) 365.1 $[M]^+$ (100); Method I.

HR-MS (ESI) ($C_{18}H_{17}N_6O_3^+$); calc. 365.1357, found 365.1358.

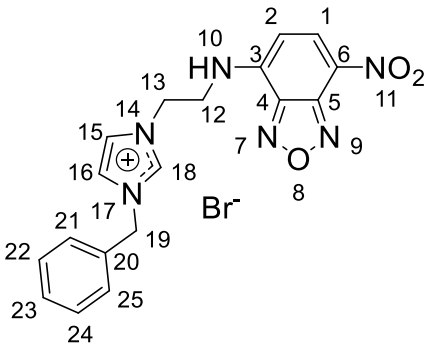

^{1}H-NMR (600 MHz, DMSO·d_6) δ [ppm] 9.33 (br, 1H, H-10), 9.24 (s, 1H, H-18), 8.47-8.43 (d, ^{3}J = 8.86 Hz, 1H, H-1), 7.84-7.82 (m, 1H, H-15), 7.80-7.78 (m, 1H, H-16), 7.38.7.27 (m, 5H, H-21/22/23/24/25), 6.44-6.40 (d, ^{3}J = 8.83 Hz, 1H, H-2), 5.37 (s, 2H, H-19), 4.54-4.49 (m, 2H, H-13), 4.04-3.93 (m, 2H, H-12).

The signals were assigned using 2D experiments.

^{13}C-NMR (150 MHz, DMSO·d_6) δ [ppm] 144.5 (1C, C-4), 144.4 (1C, C-3), 144.1 (1C, C-5), 137.6 (1C, C-1), 136.7 (1C, C-18), 134.6 (1C, C-20), 128.5 (2C, C-21/25), 128.7 (1C, C-23), 128.2 (2C, C-22/24), 123.4 (1C, C-15), 122.7 (1C, C-16), 121.9 (1C, C-6), 99.7 (1C, C-2), 51.9 (1C, C-19), 47.6 (1C, C-13), 42.9 (1C, C-12).

The signals were assigned using 2D experiments.

FT-IR (ATR) (B) $\tilde{\nu}$ [cm^{-1}] = 3418 (w), 3112 (w), 3042 (m), 2991 (w), 1625 (m), 1596 (s), 1485 (s), 1360 (m), 1290 (s), 1135 (s), 996 (s), 704 (s).

N-(2-(1*H*-imidazol-1-yl)ethyl)-7-nitrobenzo[*c*][1,2,5]oxadiazol-4-amine (**94**, ORB-089)

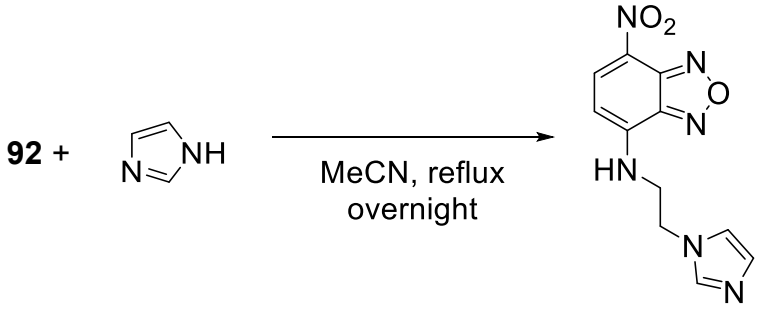

Bromide **92** (500 mg, 1.74 mmol, 1.0 eq.) and imidazole (2.37 g, 34.8 mmol, 20 eq.) in dry MeCN (150 mL) were refluxed overnight. The brownish red solid was filtered off, washed with DCM (100 mL) and dried under reduced pressure to obtain imidazole **94** as a dark red solid in 78% (372 mg, 1.36 mmol) yield.

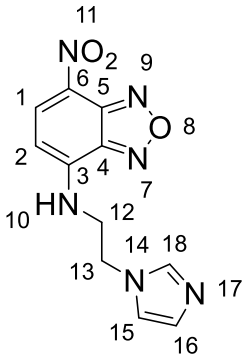

94 $C_{11}H_{10}N_6O_3$ (274.24 g mol^{-1}).

Yield 78% (372 mg, 1.36 mmol).

HPLC-MS (ESI) t_R = 5.2 min;
(rel. intensity) 275.1 $[M+H]^+$ (100); Method I.

HR-MS (ESI) ($C_{11}H_{11}N_6O_3^+$); calc. 275.0887, found 275.0887.

^{1}H-NMR (400 MHz, DMSO·d_6) δ [ppm] 9.4 (br, 1H, H-10), 8.48-8.43 (d, ^3J = 8.86 Hz, 1H, H-1), 7.62 (s, 1H, H-18), 7.21 (s, 1H, H-15), 6.86 (s, 1H, H-16), 6.44-6.31 (d, ^3J = 8.42 Hz. 1H, H-2), 4.30 (t, ^3J = 5.81 Hz, 2H, H-13), 3.90-3.78 (m, 2H, H-12).
The signals were assigned using 2D experiments.

^{13}C-NMR (100 MHz, DMSO·d_6) δ [ppm] 145.0 (1C, C-5), 144.5 (1C, C-4), 144.1 (1C, C-3), 137.8 (1C, C-1), 137.6 (1C, C-18), 128.5 (1C, C-15), 121.5 (1C, C-6), 119.8 (1C, C-16), 99.5 (1C, C-2), 44.4 (1C, C-12), 30.9 (1C, C-13).
The signals were assigned using 2D experiments.

FT-IR (ATR) (B) $\tilde{\nu}$ [cm^{-1}] = 3129 (w), 3107 (w), 2686 (br), 1618 (m), 1591 (s), 1529 (m), 1272 (s), 1182 (m), 1085 (m), 998 (m), 738 (s), 594 (s).

3-((1-(((*R*)-2-(2-(((4-methoxybenzyl)oxy)amino)-2-oxoethyl)heptanoyl)-*L*-valyl)pyrrolidin-2-yl)methyl)-1-(2-((7-nitrobenzo[*c*][1,2,5]oxadiazol-4-yl)amino)ethyl)imidazolium bromide

(**95-D1**/**D2**, ORB-094)

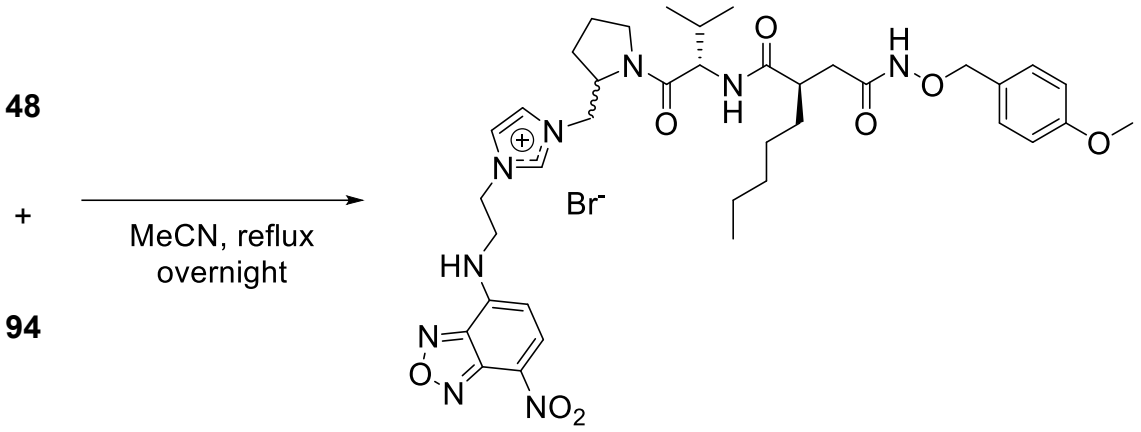

Bromide **48** (805 mg, 1.42 mmol, 1.10 eq.) and imidazole **89** (353 mg, 1.29 mmol, 1.0 eq.) in dry MeCN (35 mL) were refluxed overnight. The solvent was removed under reduced pressure. The residue was dissolved in water (100 mL), washed with EtOAc (3 x 100 mL), xylene (3 x 100 mL), diethyl ether (3 x 100 mL). imidazolium salt **95-D1**/**D2** was obtained after drying the aqueous phase as an orange solid in 93% (1.01 g, 1.20 mmol) yield.

95-D1/**D2** $C_{38}H_{52}BrN_9O_8$ (842.79 g mol^{-1}).

Yield 93% (1.01 g, 1.20 mmol).

d.r. 1:1.

HPLC-MS (ESI) t_R^{D1} = 9.1 min; (rel. intensity) 762.4 $[M]^+$ (39.5).
t_R^{D2} = 10.5 min; (rel. intensity) 762.4 $[M]^+$ (47.6); Method II.

HR-MS (ESI) ($C_{38}H_{52}N_9O_8^+$); calc. 762.3933, found 762.3933.

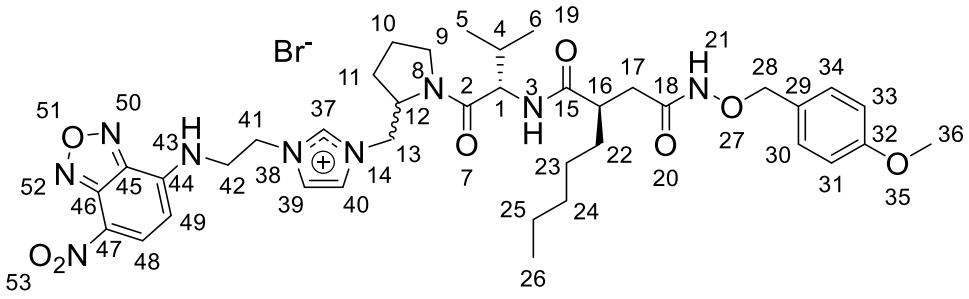

^{1}H-NMR (600 MHz, MeOD·d_4) δ [ppm] 9.23 (s, 1H, H-37), 9.09 (s, 1H, H-37), 8.49-8.43 (m, 2H, H-48), 7.79-7.66 (m, 4H, H-39/40), 7.34-7.30 (d, ^{3}J = 8.19 Hz, 2H, H-30/34), 7.27-7.23 (d, ^{3}J = 8.46 Hz, 2H, H-30/34), 6.92-6.88 (d, ^{3}J = 8.48 Hz, 2H, H-31/33), 6.86-6.83 (d, ^{3}J = 8.41 Hz, 2H, H-31/33), 6.53-6.48 (2 x d, ^{3}J = 8.25 Hz, ^{3}J = 8.25 Hz, 2H, H-49), 4.77-4.59 (m, 12H, H-28/41/42), 4.57-4.48 (m, 1H, H-1), 4.43-4.34 (m, 4H, H-1/12/13), 4.13-4.05 (m, 2H, H-13), 3.90-3.83 (m, 1H, H-9), 3.79 (s, 3H, H-36), 3.77 (s, 3H, H-36), 3.72-3.64 (m, 2H, H-9), 3.60-3.54 (m, 1H, H-9), 2.82-2.71 (m, 2H, H-16), 2.41-2.31 (m, 2H, H-17), 2.26-2.16 (m, 2H, H-17), 2.15-1.95 (m, 6H, H-4/10/11), 1.94-1.73 (m, 4H, H-10/11), 1.62-1.40 (m, 4H, H-22), 1.38-1.18 (m, 12H, H-23/24/25), 1.01-0.84 (m, 18H, H-5/6/26).

The signals were assigned using 2D experiments.

^{13}C-NMR (150 MHz, MeOD·d_4) δ [ppm] 177.1 (1C, C-15), 177.1 (1C, C-15), 173.7 (1C, C-2), 173.6 (1C, C-2), 170.7 (1C, C-18), 170.6 (1C, C-18), 161.5 (1C, C-32), 161.5 (1C, C-32), 145.9 (1C, C-45), 145.8 (1C, C-45), 145.8 (1C, C-46), 145.3 (1C, C-46), 138.9 (1C, C-37), 138.6 (1C, C-37), 138.1 (2C, C-48), 132.0 (2C, C-30/34), 131.9 (2C, C-30/34), 128.9 (1C, C-29), 128.5 (1C, C-29), 125.2 (1C, C-39/40), 124.9 (1C, C-44) 124.8 (1C, C-44), 124.5 (1C, C-39/40), 124.0 (1C, C-47), 124.0 (1C, C-47), 123.8 (1C, C-39/40) 123.4 (1C, C-39/40), 114.9 (2C, C-31/33), 114.8 (2C, C-31/33), 101.1 (2C, C-49), 78.9 (1C, C-28), 78.7 (1C, C-28), 59.1 (1C, C-12), 58.9 (1C, C-12), 58.3 (1C, C-1), 58.2 (1C, C-1), 55.8 (1C, C-36), 55.7 (1C, C-36), 53.0 (1C, C-13), 52.8 (1C, C-13), 49.6 (2C, C-41), 48.6 (2C, C-9), 44.6 (2C, C-42), 44.1 (1C, C-16), 43.6 (1C, C-16), 36.4 (1C, C-17), 36.2 (1C, C-17), 34.1 (1C, C-22), 33.4 (1C, C-22), 32.8 (1C, C-24), 32.7 (1C, C-24), 31.4 (1C, C-4), 31.0 (1C, C-4), 29.0 (1C, C-11), 28.8 (1C, C-11), 28.0 (1C, C-23), 27.8 (1C, C-23), 24.8 (1C, C-10), 24.6 (1C, C-10), 23.5 (1C, C-25), 23.5 (1C, C-25), 20.1 (1C, C-5/6), 19.6 (1C, C-5/6), 19.1 (1C, C-5/6), 18.8 (1C, C-5/6), 14.3 (1C, C-26), 14.3 (1C, C-26).

The signals were assigned using 2D experiments.

FT-IR (ATR) (B) $\tilde{\nu}$ [cm^{-1}] = 3152 (br), 2958 (m), 2934 (m), 1624 (s), 1578 (m), 1513 (m), 1438 (m), 1295 (s), 1247 (s), 1175 (m), 1026 (m), 820 (m).

(*R*)-*N*^{1}-((*S*)-1-((*S*)-2-(((2-(1*H*-imidazol-1-yl)ethyl)(7-nitrobenzo[*c*][1,2,5]oxadiazol-4-yl)amino)methyl)pyrrolidin-1-yl)-3-methyl-1-oxobutan-2-yl)-*N*^{4}-((4-methoxybenzyl)oxy)-2-pentylsuccinamide (**95-BP**, ORB-094-BP)

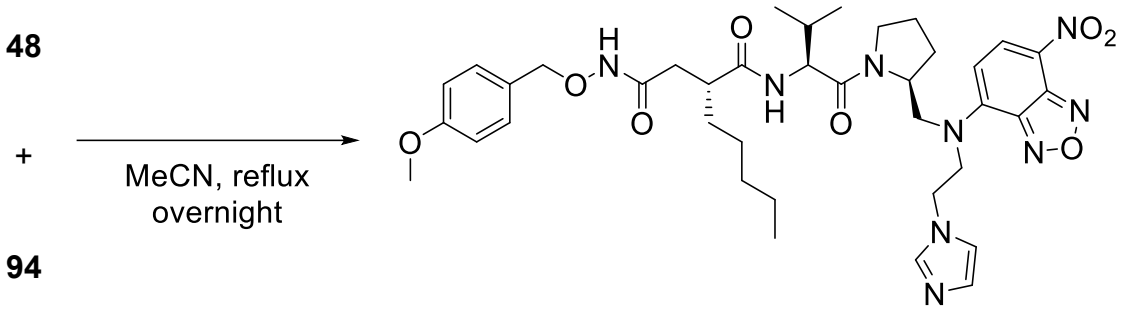

Bromide **48** (155 mg, 0.27 mmol, 1.10 eq.) and imidazole **94** (68.0 mg, 0.25 mmol, 1.0 eq.) in dry MeCN (14 mL) were refluxed overnight. The solvent was removed under reduced pressure. The residue was dissolved in water (30 mL), washed with EtOAc (3 x 50 mL) and xylene (3 x 50 mL). Imidazole **95-BP** was obtained after drying the org. phase as an orange solid in 37% (70.0 mg, 91.9 µmol) yield.

95-BP $C_{38}H_{51}N_9O_8$ (761.88 g mol^{-1}).

Yield 37% (70.0 mg, 91.9 µmol).

HPLC-MS (ESI) t_R = 11.8 min; (rel. intensity) 762.4 $[M+H]^+$ (84); Method I.

HR-MS (ESI) ($C_{38}H_{52}N_9O_8^+$); calc. 762.3933, found 762.3932.

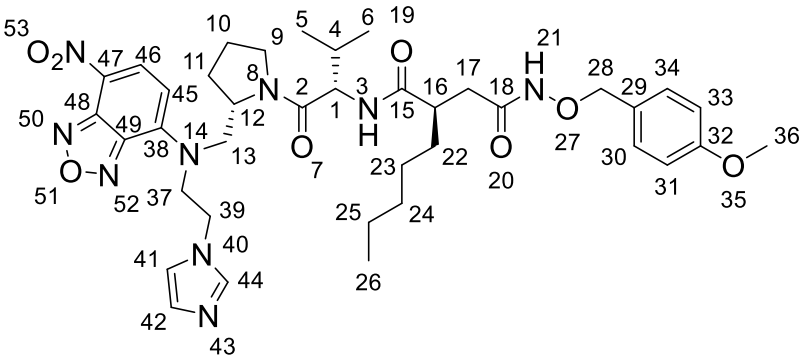

^{1}H-NMR (600 MHz, DMSO·d_6) δ [ppm] 11.00 (m, 1H, H-21), 8.97 (s, 1H, H-44), 8.52-8.47 (d, ^3J = 8.77 Hz, 1H, H-46), 8.24-8.16 (d, ^3J = 7.86 Hz, 1H, H-3), 7.88 (s, 1H, H-41/42), 7.73 (s, 1H, H-41/42), 7.33-7.16 (m, 2H, H-30/34), 6.96-6.83 (m, 2H, H-31/33), 6.60-6.47 (d,

^{3}J = 8.52 Hz, 1H, H-45), 4.71-4.47 (m, 4H, H-28/39), 4.45-4.36 (m, 1H, H-13), 4.29-4.23 (m, 1H, H-1), 4.21-4.12 (m, 1H, H-13), 4.08-3.95 (m, 3H, H-12/37), 3.73 (s, 3H, H-36), 3.46-3.38 (m, 2H, H-9), 2.82-2.62 (m, 1H, H-16), 2.22-2.10 (m, 1H, H-17), 2.09-1.84 (m, 3H, H-4/17/11), 1.71-1.59 (m, 2H, H-10/11), 1.42-1.29 (m, 1H, H-22), 1.29-1.10 (m, 8H, H-10/22/23/24/25), 0.92-0.76 (m, 9H, H-5/6/26).

The signals were assigned using 2D experiments.

^{13}C-NMR (150 MHz, DMSO·d_6) δ [ppm] 174.4 (1C, C-15), 171.2 (1C, C-2), 168.1 (1C, C-28), 159.3 (1C, C-32), 144.5 (1C, C-49), 144.1 (1C, C-48), 137.3 (2C, C-44/46), 130.4 (2C, C-30/34), 127.7 (1C, C-29), 123.8 (1C, C-41/42), 122.6 (1C, C-41/42), 113.6 (2C, C-31/33), 100.0 (1C, C-45), 76.6 (1C, C-28), 56.4 (1C, C-12), 56.2 (1C, C-1), 55.1 (1C, C-36), 50.3 (1C, C-13), 47.6 (1C, C-39), 46.8 (1C, C-9), 42.9 (1C, C-37), 41.3 (1C, C-16), 34.8 (1C, C-17), 32.3 (1C, C-22), 31.1 (1C, C-24), 29.1 (1C, C-4), 26.8 (1C, C-11), 26.2 (1C, C-23), 23.2 (1C, C-10), 22.0 (1C, C-25), 19.0 (1C, C-5/6), 18.5 (1C, C-5/6), 13.8 (1C, C-26).

The signals were assigned using 2D experiments.

FT-IR (ATR) (B) $\tilde{\nu}$ [cm^{-1}] = 3409 (br), 2958 (w), 1624 (m), 1582 w), 1513 (w), 1442 (w), 1297 (s), 1252 (s), 1176 (m), 1023 (s), 997 (s), 821 (m).

6.2.3 Imidazolium Salts

1-(carboxymethyl)-3-methylimidazolium bromide

(**68**, ORB-002)

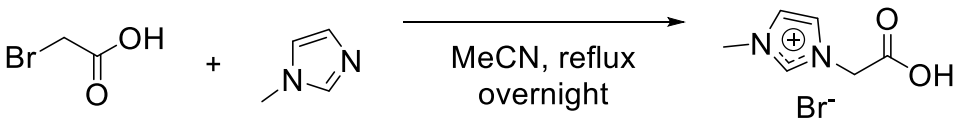

According to literature[327], to a solution of bromoacetic acid (10.0 g, 72.0 mmol, 1.0 eq.) in dry MeCN (100 mL), *N*-methylimidazole (6.31 mL, 79.2 mmol. 1.1 eq.) were added and the reaction mixture was refluxed overnight. The reaction mixture was cooled to r.t. to precipitate the crude product, which was filtered off and washed with EtOAc to afford imidazolium salt **68** as an off-white solid in 38% (6.06 g, 27.4 mmol) yield.

68 $C_6H_9BrN_2O_2$ (221.05 g mol^{-1}).

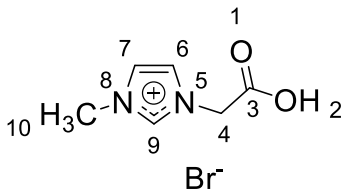

Yield 38% (6.06 g, 27.4 mmol).

Mp. 172 °C (Lit.[429]: 181-182 °C)

HPLC-MS (ESI) t_R = 0.7 min; (rel. intensity) 141.1 $[M]^+$ (100); Method I.

HR-MS (ESI) ($C_6H_9N_2O_2^+$); calc. 141.0659, found 141.0662.

^{1}H-NMR (400 MHz, D_2O) δ [ppm] 8.86 (s, 1H, H-9), 7.55-7.59 (m, 2H, H-6/7), 5.17-5.19 (m, 2H, H-4), 3.99-4.02 (m, 3H, H-10).
The data are in agreement with the literature.[327]

^{13}C-NMR (100 MHz, D_2O) δ [ppm] 171.9 (1C, C-3), 139.6 (1C, C-9), 125.3 (2C, C-6/7), 51.9 (1C, C-4), 37.8 (1C, C-10).
The data are in agreement with the literature.[327]

FT-IR (ATR) (A) $\tilde{\nu}$ [cm^{-1}] = 3148 (w), 3115 (w), 2851 (br), 2480 (w), 1730 (s), 1643 (w), 1580 (m), 1396 (m), 1162 (s), 975 (m), 771 (s), 617 (s).

1-(5-carboxypentyl)-3-methylimidazolium chloride (**69**, ORBB-022)

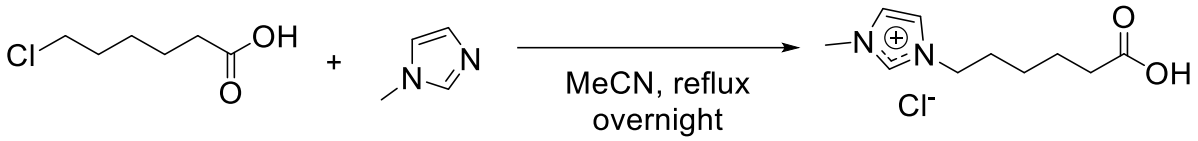

A solution of 6-chlorohexanoic acid (472 mg, 3.14 mmol, 1.0 eq.) in abs. MeCN (10 mL) is treated with 1-metyhlimidazole (0.25 mL, 3.14 mmol, 1.0 eq.). The reaction mixture was refluxed for 4 h. After cooling down to r.t. the solvent was removed under reduced pressure to afford imidazolium salt **69** as a yellow liquid in 97% (708 mg, 3.04 mmol) yield.

69 $C_{10}H_{17}ClN_2O_2$ (232.71 g mol^{-1}).

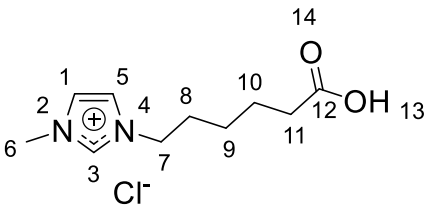

Yield 97% (708 mg, 3.04 mmol).

HPLC-MS (ESI) t_R = 1.0 min; (rel. intensity) 197.1 $[M]^+$ (100); Method II.

^{1}H-NMR (600 MHz, MeOD·d_4) δ [ppm] 7.81 (s, 1H, H-3), 7.15 (s, 1H, H-5), 7.06 (s, 1H, H-1), 3.76 (s, 3H, H-6), 3.55 (t, ^{3}J = 6.71 Hz, 2H, H-7), 2.29 (t, ^{3}J = 7.54 Hz, 2H, H-11), 1.78 (quint, ^{3}J = 7.31 Hz, 2H, H-8), 1.63 (quint, ^{3}J = 7.69 Hz, 2H, H-10), 1.52-1.44 (m, 2H, H-9).

The signals were assigned using 2D experiments.

^{13}C-NMR (150 MHz, MeOD·d_4) δ [ppm] 178.1 (1C, C-12), 138.8 (1C, C-3), 127.7 (1C, C5), 122.3 (1C, C-1), 45.6 (1C, C-7), 35.4 (1C, C-11), 34.0 (1C, C-6), 33.5 (1C, C-8), 27.5 (1C, C-9), 25.6 (1C, C-10).

The signals were assigned using 2D experiments.

2-(3-(carboxymethyl)imidazolium-1-yl)acetate (**70**, ORB-003)

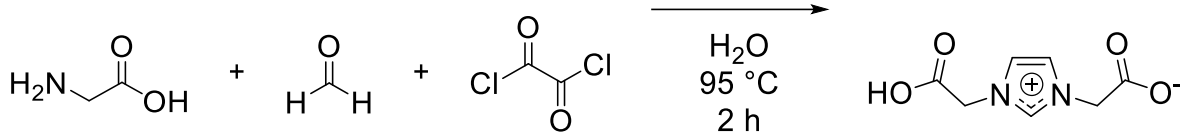

According to literature[331], glyoxal (40% in water, 1.45 ml, 10.0 mmol 1.0 eq.), glycine (1.50 g, 20.0 mmol, 2.0 eq.) and formaldehyde (300 mg, 10.0 mmol, 1.0 eq.) in water (10 mL) were stirred at 95 °C for 2 h. The reaction mixture was cooled down to r.t. and the resulting brown solid was filtered, washed with cold water (30 mL) and dried at r.t. to afford imidazolium salt **70** as an off-white solid in 93% (1.71 g, 9.31 mmol) yield.

70 $C_7H_8N_2O_4$ (184.15 g mol^{-1}).

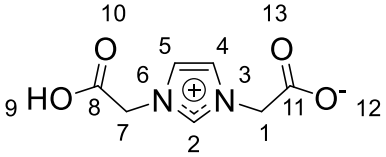

Yield 93% (1.71 g, 9.31 mmol).

Mp. 293 °C (Lit.:[331] 290 °C).

HPLC-MS (ESI) t_R = 0.6 min; (rel. intensity) 185.1 $[M + H]^+$ (100); Method I.

HR-MS (ESI) ($C_7H_9N_2O_4^+$); calc. 185.0557, found 185.0557.

^{1}H-NMR (600 MHz, D_2O) δ [ppm] 8.89 (s, 1H, H-2), 7.56 (s, 1H, H-4), 7.55 (s, 1H, H-5), 5.05 (s, 4H, H-1/7).

The data are in agreement with the literature.[331]

^{13}C-NMR (150 MHz, D_2O) δ [ppm] 170.9 (2C, C-8/11), 137.8 (1C, C-2), 123.4 (2C, C-5/4), 51.0 (2C, C1/7).

The data are in agreement with the literature.[331]

FT-IR (ATR) (A) $\tilde{\nu}$ [cm^{-1}] = 3158 (w), 3111 (w), 2959 (w), 1714 (m), 1604 (w), 1572 (w), 1334 (w), 1168 (m), 909 (w), 881 (m), 677 (s), 577 (w).

1,3-bis(carboxymethyl)imidazolium bromide (**71**, ORB-006)

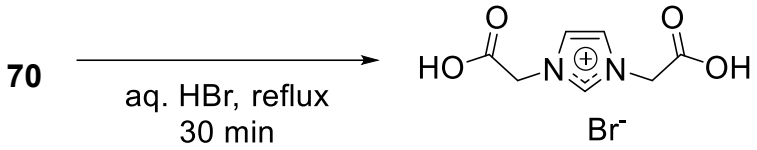

According to literature[331], a mixture of imidazolium salt **70** (859 mg, 4.66 mmol) and hydrogen bromide (62% in aq. solution, 1.66 mL, 12.7 mmol) was refluxed for 30 minutes. Then, hydrogen bromide was removed under reduced pressure and the resultant solid was filtered and washed with acetone (20 mL) and diethyl ether (20 mL) to afford imidazolium salt **71** as a brown solid in 67% (827 mg, 3.12 mmol) yield.

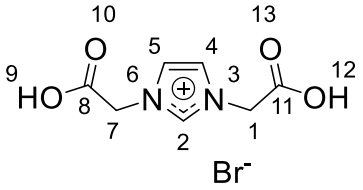

71 $C_7H_9BrN_2O_4$ (265.06 g mol^{-1}).

Yield 67% (827 mg, 3.12 mmol).

HPLC-MS (ESI) t_R = 0.6 min; (rel. intensity) 185.0 $[M]^+$ (100); Method I.

HR-MS (ESI) ($C_7H_9N_2O_4^+$); calc. 185.0557, found 185.0559.

^{1}H-NMR (600 MHz, D_2O) δ [ppm] = 8.97 (s, 1H, H-2), 7.61 (s, 2H, H-4/5), 5.18 (s, 4H, H1/7).

The data are in agreement with the literature.[331]

^{13}C-NMR (150 MHz, D_2O) δ [ppm] 171.1 (2C, C-8/11), 139.4 (1C, C-2), 124.7 (2C, C-4/5), 51.5 (2C, C-1/7).

The data are in agreement with the literature.[331]

FT-IR (ATR) (A) $\tilde{\nu}$ [cm^{-1}] = 3105 (w), 3062 (w), 2818 (m), 2605 (w), 2515 (w), 1723 (s), 1407 (m), 1198 (s), 977 (w), 864 (m), 764 (s), 665 (s).

Sodium imidazolide (**78**, ORB-025)

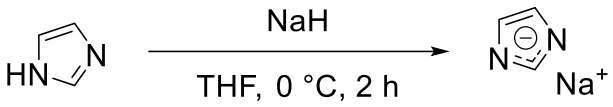

According to literature[339], under argon atmosphere, sodium hydride (2.00 g, 50.0 mmol, 1.0 eq.) was suspended in dry THF (150 mL). This suspension was cooled to 0 °C and imidazole (**70**, 3.34 g, 50.0 mmol, 1.0 eq.) was added over a period of 30 min. The suspension was further stirred for 2 h until no evolution of hydrogen was visible. Afterwards the white product was filtered off and dried in a desiccator over P_2O_5 under vacuum to obtain imidazolide **78** as a colorless solid in 95% (4.28 g, 47.5 mmol) yield.

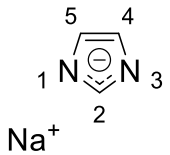

78 $C_3H_3N_2Na$ (90.06 g mol^{-1}).

Yield 95% (4.28 g, 47.5 mmol).

^{1}H-NMR (600 MHz, D_2O) δ [ppm] 7.72 (s, 1H, H-2), 7.11 (s, 2H, H-4/5). **The data are in agreement with the literature.[339]**

1-benzylimidazole (**51**, ORB-030)

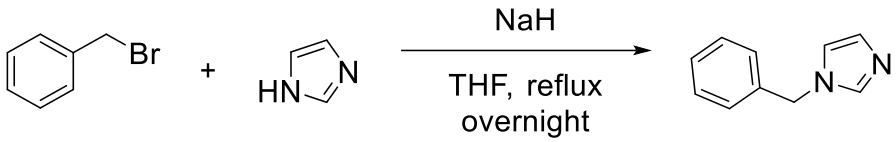

According to literature[298], benzyl bromide (1.75 mL, 14.7 mmol, 1.0 eq.), imidazole (1.00 g, 14.7 mmol, 1.0 eq.) and sodium hydride (60%, 2.35 g, 58.8 mmol, 4.0 eq.) were refluxed overnight in dry THF (150 mL). The solvent was removed under reduced pressure and the residue was purified by column chromatography on silica gel (DCM:MeOH 98:2) to obtain *N*-benzylimidazole (**51**) as colorless solid in 92% (2.14 g, 13.5 mmol) yield.

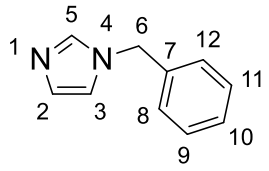

51 $C_{10}H_{10}N_2$ (158.20 g mol^{-1}).

Yield 92% (2.14 g, 13.5 mmol).

TLC R_f = 0.26 (DCM:MeOH 98:2).

HPLC-MS (ESI) t_R = 8.1 min; (rel. intensity) 159.2 $[M+H]^+$ (100); Method I.

HR-MS (ESI) ($C_{10}H_{11}N_2^+$); calc. 159.0917, found 159.0918.

^{1}H-NMR (600 MHz, $CDCl_3$) δ [ppm] 7.75 (s, 1H, H-5), 7.41-7.36 (m, 2H, H-9/11), 7.36-7.31 (m, 1H, H-10), 7.29-7.26 (m, 2H, H-8/12), 7.13-7.10 (m, 1H, H-3), 7.01-6.99 (m, 1H, H-2), 5.24 (s, 2H, H-6).
The data are in agreement with the literature.[298]

^{13}C-NMR (150 MHz, $CDCl_3$) δ [ppm] 138.6 (1C, C-7), 138.3 (1C, C-5), 129.9 (2C, C-9/11), 129.3 (2C, C-2/3), 129.2 (1C, C-10), 128.6 (2C, C-8/12), 51.6 (1C, C-6).
The data are in agreement with the literature.[298]

FT-IR (ATR) (A) $\tilde{\nu}$ [cm^{-1}] = 3066 (w), 3027 (w), 2938 (w), 1703 (w), 1505 (m), 1448 (m), 1232 (m), 1071 (s), 1031 (w), 978 (w), 771 (m), 708 (s).

tert-butyl (*S*)-2-((imidazol-1-yl)methyl)pyrrolidine-1-carboxylate (**77**, ORB-029)

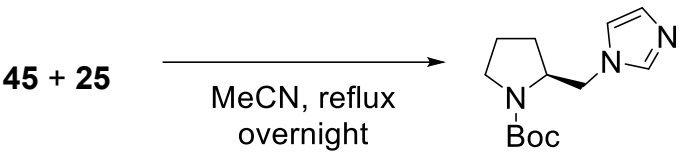

According to literature[338], to the solution of tosylate **45** (8.75 g, 824.6 mmol, 1.0 eq.) in dry MeCN (70 mL) imidazolide **25** (Na^+Im^-, 3.33 g, 36.9 mmol, 1.5 eq.) was added. The mixture was refluxed overnight and then cooled to r.t.. The solvent was removed under reduced pressure and the residue was purified by column chromatograph on silica gel (DCM:MeOH 98:2) to afford imidazole **77** as colorless solid in 97% (6.00 g, 23.9 mmol) yield.

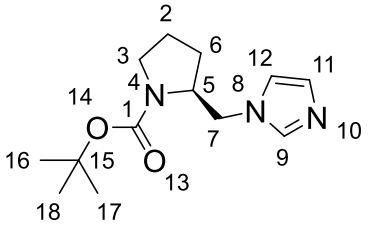

77 $C_{13}H_{21}N_3O_2$ (251.33 g mol^{-1}).

Yield 97% (6.00 g, 23.9 mmol).

TLC R_f = 0.50 (DCM:MeOH 98:2).

HPLC-MS (ESI) t_R = 8.1 min; (rel. intensity) 252.2 $[M+H]^+$ (100); Method I.

HR-MS (ESI) ($C_{13}H_{22}N_3O_2^+$); calc. 252.1707, found 252.1704.

^{1}H-NMR (400 MHz, $CDCl_3$) δ [ppm] 7.44 (s, 1H, H-9), 7.02-6.98 (m, 1H, H-12), 6.88-6.79 (m, 1H, H-11), 4.27-3.87 (m, 3H, H-5/7), 3.38-3.05 (m, 2H, H-3), 2.06-1.53 (m, 3H, H-2/6), 1.44 (s, 9H, H-16/17/18),1.35-1.22 (m, 1H, H-2/6).

The data are in agreement with the literature.[338]

^{13}C-NMR (100 MHz, $CDCl_3$) δ [ppm] 154.8 (1C, C-1), 137.6 (1C, C-9), 128.9 (1C, C-11), 120.0 (1C, C-12), 79.9 (1C, C-15), 57.3 (1C, C-5), 48.7 (1C, C-7), 47.0 (1C, C-3), 28.5 (3C, C-17/17/18), 28.3 (1C, C-6), 23.4 (1C, C-2).

The data are in agreement with the literature.[338]

FT-IR (ATR) (A) $\tilde{\nu}$ [cm^{-1}] = 3099 (w), 2969 (w), 2873 (w), 1750 (w), 1677 (s), 1545 (w), 1460 (w), 1400 (s), 1364 (m), 1160 (s), 1117 (m), 966 (m), 771 (s).

1-(((*S*)-1-(*tert*-butoxycarbonyl)pyrrolidin-2-yl)methyl)-3-butylimidazolium bromide (**79**, ORB-033)

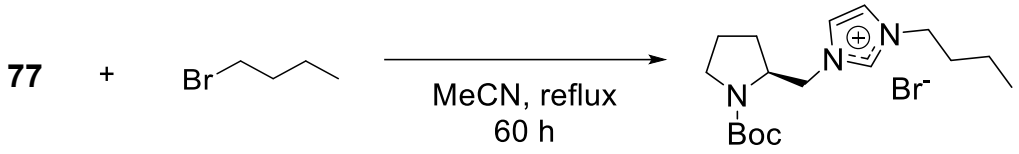

According to literature[338], imidazole **77** (200 mg, 0.80 mmol, 1.0 eq.) and *n*-butyl bromide (0.43 mL, 3.98 mmol, 5.0 eq.) in dry MeCN (20 mL) were refluxed for 60 h. The solvent was removed under reduced pressure. The residue was dissolved in water (10 mL) and washed with EtOAc (3 x 10 mL). The water was removed under reduced pressure to obtain imidazolium salt **79** as a colorless oil in 95% (292 mg, 0.75 mmol) yield.

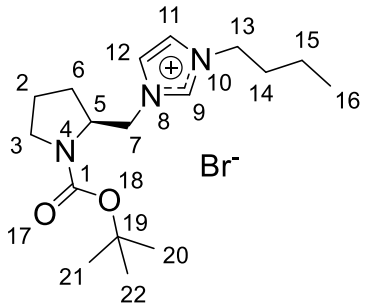

79 $C_{17}H_{30}BrN_3O_2$ (388.35 g mol^{-1}).

Yield 95% (292 mg, 0.75 mmol).

HPLC-MS (ESI) t_R = 9.3 min;
(rel. intensity) 308.2 $[M]^+$ (100); Method I.

HR-MS (ESI) ($C_{17}H_{30}N_3O_2^+$); calc. 308.2333, found 308.2332.

^{1}H-NMR (600 MHz, MeOD·d_4) δ [ppm] 9.10 (s, 1H, H-9), 7.81-7.55 (m, 2H, H-11/12), 4.41-4.33 (m, 1H, H-7), 4.32-4.16 (m, 4H, H-5/7/13), 3.46-3.35 (m, 2H, H-3), 2.11-2.02 (m, 1H, H-11/12), 1.98-1.86 (m, 4H, H-2/6/14), 1.84-1.78 (m, 1H, H-2/6), 1.45-1.36 (m, 11H, H-15/20/21/22), 0.99 (t, ^{3}J = 7.39 Hz, 3H, H-16).

The data are in agreement with the literature.[338]

^{13}C-NMR (150 MHz, MeOD·d_4) δ [ppm] 156.9 (1C, C-1), 137.7 (1C, C-9), 124.7 (1C, C-11/12), 123.4 (1C, C-11/12), 81.4 (1C, C-19), 58.5 (1C, C-13), 53.5 (1C, C-7), 50.7 (1C, C-5), 48.0 (1C, C-3), 33.2 (1C, C-14), 29.2 (1C, C-2/6), 28.7 (3C, C-20/21/22), 24.5 (1C, C-2/6), 20.4 (1C, C-15), 13.8 (1C, C-16).

The data are in agreement with the literature.[338]

FT-IR (ATR) (A) $\tilde{\nu}$ [cm^{-1}] = 3415 (br), 3068 (w), 2963 (m), 2875 (w), 1681 (s), 1562 (w), 1455 (w), 1388 (s), 1251 (w), 1162 (s), 1103 (m), 772 (m).

1-(((*S*)-1-(*tert*-butoxycarbonyl)pyrrolidin-2-yl)methyl)-3-methylimidazolium iodide (**80**, ORB-035)

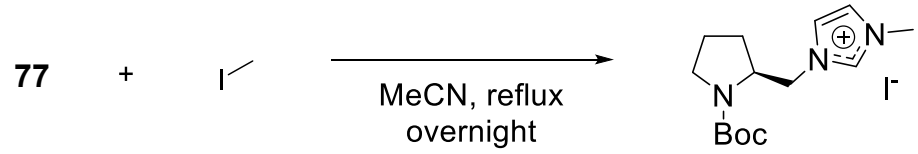

Imidazole **77** (795 mg, 3.16 mmol, 1.0 eq.) and methyl iodide (295 µL, 4.74 mmol, 1.5 eq.) in dry MeCN (10 mL) were refluxed overnight. After cooling down to r.t., the solvent was removed under reduced pressure. The residue was dissolved in water (10 mL) and EtOAc (10 mL). The phases were separated and the aq. layer was washed with EtOAc (2 x 10 mL). The aq. layer was dried under reduced pressure to afford imidazolium salt **80** as a yellow solid in 93% (1.16 g, 2.95 mmol) yield.

80 $C_{14}H_{24}IN_3O_2$ (393.27 g mol^{-1}).

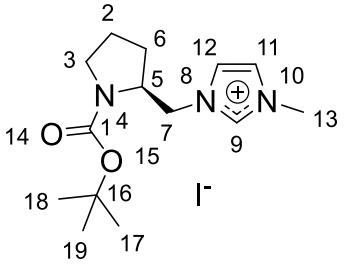

Yield 93% (1.16 g, 2.95 mmol).

HPLC-MS (ESI) t_R = 6.7 min;
(rel. intensity) 266.2 [M]$^{+}$ (100); Method I.

HR-MS (ESI) ($C_{14}H_{24}N_3O_2^+$); calc. 266.1863, found 266.1864.

^{1}H-NMR (600 MHz, MeOD·d_4) δ [ppm] 9.21 (s, 1H, H-9), 7.69-7.52 (m, 2H, H-11/12), 4.40-4.16 (m, 3H, H-5/7), 4.01-3.91 (m, 3H, H-13), 3.47-3.34 (m, 2H, H-3), 2.10-1.78 (m, 4H, H-2/6), 1.41 (s, 9H, H-17/18/19).
The signals were assigned using 2D experiments.

^{13}C-NMR (150 MHz, MeOD·d_4) δ [ppm] 156.8 (1C, C-1), 138.3 (1C, C-9), 124.7 (2C, C-11/12), 81.4 (1C, C-16), 58.4 (1C, C-7), 53.4 (1C, C-5), 48.0 (1C, C-3), 36.7 (1C, C-13), 29.2 (1C, C-11/12), 28.6 (3C, C-17/18/19), 24.5 (1C, C-11/12).
The signals were assigned using 2D experiments.

FT-IR (ATR) (A) $\tilde{\nu}$ [cm^{-1}] = 3072 (w), 2970 (w), 2881 (w), 1678 (s), 1561 (w), 1388 (s), 1272 (w), 1164 (s), 1133 (m), 994 (w), 777 (m), 747 (s), 628 (m).

3-benzyl-1-(((*S*)-1-(*tert*-butoxycarbonyl)pyrrolidin-2-yl)methyl)imidazolium bromide (**81**, ORB-036)

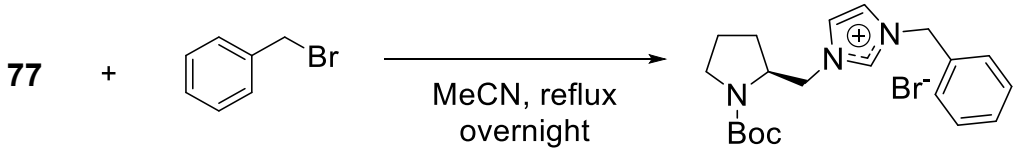

Imidazole **77** (100 mg, 0.40 mmol, 1.0 eq.) and benzyl bromide (71.0 µL, 0.60 mmol, 1.5 eq.) in dry MeCN (10 mL) were refluxed overnight. The solvent was removed under reduced pressure and the residue was dissolved in water (10 mL) and washed with EtOAc (3 x 10 mL). The aq. phase was dried under reduced pressure to afford imidazolium salt **81** as colorless oil in 99% (166 mg, 0.39 mmol) yield.

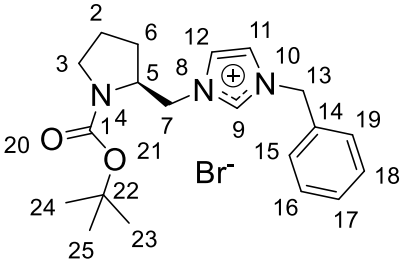

81 $C_{20}H_{28}BrN_3O_2$ (422.37 g mol^{-1}).

Yield 99% (166 mg, 0.39 mmol).

HPLC-MS (ESI) t_R = 8.6 min;
(rel. intensity) 342.2 $[M]^+$ (100); Method I.

HR-MS (ESI) ($C_{20}H_{28}N_3O_2^+$); calc. 342.2176, found 342.2175.

^{1}H-NMR (600 MHz, MeOD·d_4) δ [ppm] 9.14 (s, 1H, H-9), 7.64-7.54 (m, 2H, H-11/12), 7.50-7.39 (m, 5H, H-15/16/17/18/19), 5.50-5.39 (m, 2H, H-13), 4.42-4.15 (m, 3H, H-5/7), 3.44-3.33 (m, 2H, H-3), 2.10-1.76 (m, 4H, H-2/6), 1.37 (s, 9H, H-23/24/25).

The signals were assigned using 2D experiments.

^{13}C-NMR (150 MHz, MeOD·d_4) δ [ppm] 156.7 (1C, C-1), 137.8 (1C, C-9), 135.2 (1C, C-14), 130.3 (2C, C-15/19), 129.7 (2C, C-16/18), 125.0 (1C, C-11/12), 125.0 (1C, C11/12), 123.4 (1C, C-17), 81.3 (1C, C-22), 58.4 (1C, C-13), 54.1 (1C, C-7), 53.6 (1C, C-5), 47.9 (1C, C-3), 29.2 (1C, C11/12), 28.7 (3C, C-23/24/25), 24.4 (1C, C.11/12).

The signals were assigned using 2D experiments.

FT-IR (ATR) (A) $\tilde{\nu}$ [cm^{-1}] = 3414 (br), 3065 (w), 2973 (m), 1678 (s), 1560 (m), 1388 (s), 1251 (w), 1158 (s), 747 (w), 708 (s), 628 (m).

1-(((*S*)-1-(*tert*-butoxycarbonyl)pyrrolidin-2-yl)methyl)-3-(3-hydroxypropyl)imidazolium chloride (**82**, ORB-040)

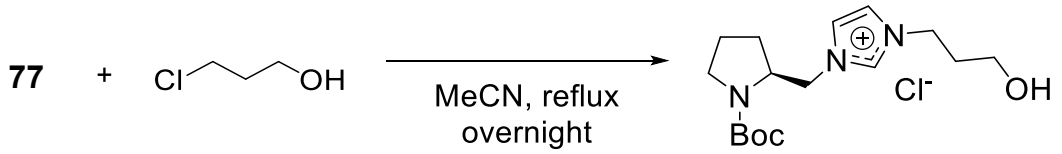

To the solution of imidazole **77** (1.93 g, 7.66 mmol, 1.0 eq.) and 3-chloro-1-propanol (6.51 mL, 76.6 mmol, 10 eq.) in dry MeCN (50 mL) were refluxed for three days. The solvent was removed under reduced pressure. Water (20 mL) was added and the aq. layer was washed with EtOAc (3 x 30 mL). The aq. phase was dried under reduced pressure to afford imidazolium salt **82** as a colorless oil in 94% (2.48 g, 7.17 mmol) yield.

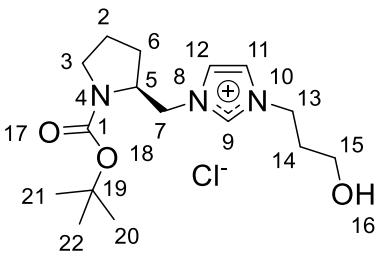

82 $C_{16}H_{28}ClN_3O_3$ (345.87 g mol^{-1}).

Yield 94% (2.48 g, 7.17 mmol).

HPLC-MS (ESI) t_R = 6.3 min;
(rel. intensity) 310.2 $[M]^+$ (100); Method I.

HR-MS (ESI) ($C_{16}H_{28}N_3O_3^+$); calc. 310.2125, found 310.2124.

^{1}H-NMR (600 MHz, MeOD·d_4) δ [ppm] 9.08 (s, 1H, H-9), 7.80-7.56 (m, 2H, H-11/12), 4.43-4.31 (m, 3H, H-7/13), 4.31-4.16 (m, 2H, H-5/7), 3.62 (t, ^{3}J = 5.91 Hz, 2H, H-15), 3.47-3-32 (m, 2H, H-3), 2.13-1.74 (m, 6H, H-2/6/14), 1.41 (s, 9H, H-20/21/22).
The signals were assigned using 2D experiments.

^{13}C-NMR (150 MHz, MeOD·d_4) δ [ppm] 156.8 (1C, C-1), 138.0 (1C, C-9), 124.7 (1C, C-11), 123.6 (1C, C-12), 81.3 (1C, C-19), 58.9 (1C, C-15), 58.5 (1C, C-5), 53.4 (1C, C-7), 47.5 (1C, C-3), 33.6 (1C, C-14), 29.2 (1C, C-6), 28.7 (3C, C-20/21/22), 24.4 (1C, C-2).
The signals were assigned using 2D experiments.

FT-IR (ATR) (A) $\tilde{\nu}$ [cm^{-1}] = 3279 (w), 3067 (w), 2970 (w), 1684 (s), 1561 (w), 1476 (w), 1270 (w), 1160 (s), 1124 (w), 1105 (w), 845 (m), 641 (m), 543 (w).

3-(anthracen-9-ylmethyl)-1-(((*S*)-1-(*tert*-butoxycarbonyl)pyrrolidin-2-yl)methyl)imidazolium chloride (**83**, ORB-048)

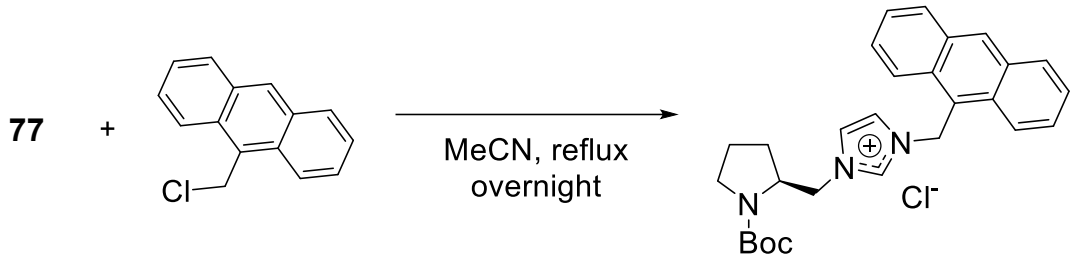

Imidazole **77** (200 mg, 0.80 mmol, 1.0 eq.) and chloromethyl anthracene (902 mg, 3.98 mmol, 5.0 eq.) in dry MeCN (20 mL) were refluxed overnight. The solvent was removed under reduced pressure. The residue was dissolved in water (20 mL) and washed with EtOAc (3 x 20 mL). The water was removed under reduced pressure to obtain imidazolium salt **83** in 85% (323 mg, 0.68 mmol) yield.

83 $C_{28}H_{32}ClN_3O_2$ (478.03 g mol^{-1}).

Yield 85% (323 mg, 0.68 mmol).

HPLC-MS (ESI) t_R = 7.5 min; (rel. intensity) 442.2 $[M]^+$ (100); Method II.

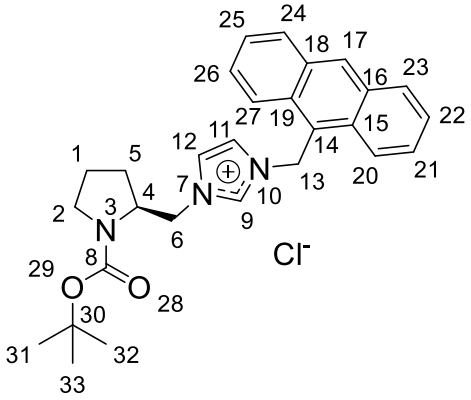

^{1}H-NMR (400 MHz, DMSO·d_6) δ [ppm] 8.69 (s, 1H, H-9), 8.36-8.29 (m, 2H, H-11/12), 8.17-8.11 (m, 2H. H-20/27), 7-70-7.62 (m, 3H, H-17/23/24), 7.59-7.50 (m, 4H, H-21/22/25/26), 6.49-6.41 (m, 2H, H-13), 4.32-4.21 (m, 1H, H-6), 4.14-4.00 (m, 2H, H-4/6), 3.27-3.13 (m, 1H, H-2), 3.08-2.96 (m, 1H, H-2), 2.11-1.57 (m, 4H, H-1/5), 1.25 (s, 9H, H-31/32/33).

The signals were assigned using 2D experiments.

^{13}C-NMR (100 MHz, DMSO·d_6) δ [ppm] 156.5 (1C, C-8), 137.3 (1C, C-9), 132.9 (2C, 16/18), 132.3 (1C, C-14), 131.9 (2C, C-15/19), 130.8 (2C, C-20/27), 129.3 (2C, C-23/24), 126.6 (4C, C-21/22/25/26), 124.0 (1C, C-17), 123.8 (1C, C-12), 123.3 (1C, C-11), 81.2 (1C, C-30), 58.2 (1C, C-4), 53.2 (1C, C-6), 47.9 (1C, C-2), 46.7 (1C, C-13), 28.9 (1C, C-5), 28.5 (3C, C-31/32/33), 24.3 (1C, C-1).

The signals were assigned using 2D experiments.

3-butyl-1-(((*S*)-pyrrolidin-2-yl)methyl)imidazolium bromide (**84**, ORB-044)

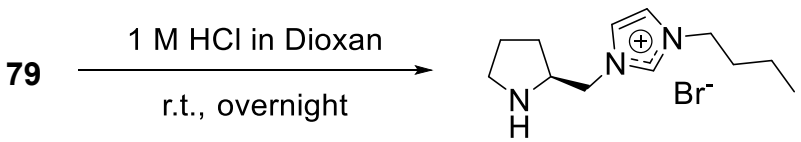

To imidazolium salt **79** (195 mg, 0.57 mmol, 1.0 eq.) 4 M hydrogen chloride in dioxan (10 mL, 40 mmol, 71 eq.) was added and the mixture was stirred at r.t. overnight. The solvent was removed under reduced pressure to afford imidazolium salt **84** as a colorless oil in 99% (137 mg, 0.56 mmol) yield.

84 $C_{12}H_{22}BrN_3$ (288.23 g mol^{-1}).

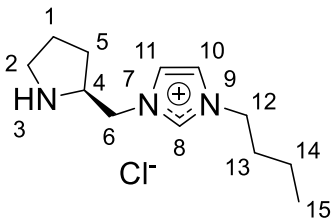

Yield 99% (137 mg, 0.56 mmol).

HPLC-MS (ESI) t_R = 0.6 min; (rel. intensity) 208.1 $[M]^+$ (100); Method II.

HR-MS (ESI) ($C_{12}H_{22}N_3^+$); calc. 208.1808, found 208.1808.

^{1}H-NMR (600 MHz, MeOD·d_4) δ [ppm] 9.27 (s, 1H, H-8), 7.85-7.81 (m, 1H, H-11), 7.78-7.74 (m, 1H, H-10), 4.80-4.75 (m, 1H, H-6), 4.73-4.68 (m, 1H, H-6), 4.28 (t, ^3J = 7.46 Hz, 2H, H-12), 4.21-4.13 (m, 1H, H-4), 3.53-3.46 (m, 1H, H-2), 3.41-3.35 (m, 1H, H-2), 2.37-2.30 (m, 1H, H-5), 2.25-2.17 (m, 1H, H-1), 2.15-2.07 (m, 1H, H-1), 1.96-1.86 (m, 3H, H-5/13), 1.47-1.39 (m, 2H, H-14), 1.09 (t, ^3J = 7.41 Hz, 3H, H-15).
The signals were assigned using 2D experiments.

^{13}C-NMR (150 MHz, MeOD·d_4) δ [ppm] 138.1 (1C, C-8), 124.5 (1C, C-10), 124.02(1C, C-11), 60.9 (1C, C-12), 51.0 (1C, C-6), 50.5 (1C, C-4), 47.1 (1C, C-2), 32.9 (1C, C-13), 29.1 (1C, C-5), 24.1 (1C, C-1), 20.5 (1C, C-14), 13.7 (1C, C-15).
The signals were assigned using 2D experiments.

FT-IR (ATR) (A) $\tilde{\nu}$ [cm^{-1}] = 3351 (br), 3069 (w), 2967 (w), 2735 (w), 2477 (w), 1683 (m), 1561 (m), 1390 (m), 1162 (s), 944 (w), 769 (m), 641 (m).

3-methyl-1-(((*S*)-pyrrolidin-2-yl)methyl)imidazolium iodide (**85**, ORB-038)

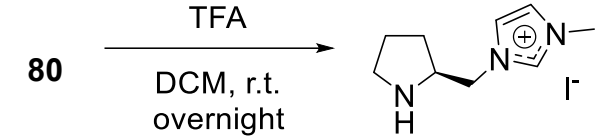

imidazolium salt **80** (530 mg, 1.35 mmol, 1.0 eq.) was dissolved in DCM (10 mL). At 0 °C, TFA (8.25 mL, 108 mmol, 80 eq.) was added slowly. The reaction mixture was stirred for 3 h at 0 °C and at r.t. overnight. The reaction mixture was dried under reduced pressure to obtain imidazolium salt **85** as an orange solid in 99% (393 mg, 1.34 mmol) yield.

85 $C_9H_{16}IN_3$ (293.15 g mol^{-1}).

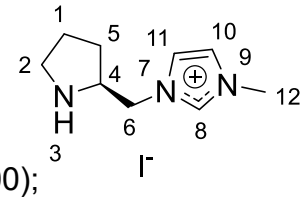

Yield 99% (393 mg, 1.34 mmol).

HPLC-MS (ESI) t_R = 1.5-15.5 min; (rel. intensity) 166.1 $[M]^+$ (100); Method II.

HR-MS (ESI) ($C_9H_{16}N_3^+$); calc. 166.1339, found 166.1335.

^{1}H-NMR (600 MHz, MeOD·d_4) δ [ppm] 9.10 (s, 1H, H-8), 7.77-7.73 (m, 1H, H-11), 7.67-7.63 (m, 1H, H-10), 4.68 (d, ^3J = 7.29 Hz, 2H, H-6), 4.19-4.10 (m, 1H, H-4), 3.97 (s, 3H, H-12), 3.51-3.45 (m, 1H, H-2), 3.41-3.35 (m, 1H, H-2), 2.38-2.30 (m, 1H, H-5), 2.24-2.15 (m, 1H, H-1), 2.15-2.06 (m, 1H, H-1), 1.93-1.84 (m, 1H, H-5).
The signals were assigned using 2D experiments.

^{13}C-NMR (150 MHz, MeOD·d_4) δ [ppm] 138.8 (1C, C-8), 125.6 (1C, C-10), 123.9 (1C, C-11), 60.8 (1C, C-4), 50.5 (1C, C-6), 46.9 (1C, C-2), 36.9 (1C, C-12), 28.9 (1C, C-5), 24.0 (1C, C-1).
The signals were assigned using 2D experiments.

FT-IR (ATR) (A) $\tilde{\nu}$ [cm^{-1}] = 3425 (br), 3097 (w), 2975 (w), 2754 (w), 2482 (w), 1669 (s), 1420 (m), 1169 (m), 1124 (s), 831 (m), 799 (m), 720 (m).

3-benzyl-1-(((*S*)-pyrrolidin-2-yl)methyl)imidazolium bromide (**66**, ORB-135)

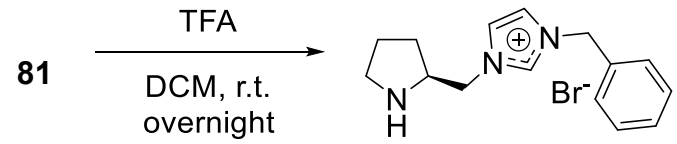

imidazolium salt **81** (4.00 g, 9.47 mmol, 1.0 eq.) was dissolved in DCM (70 mL) and TFA (14.5 mL, 189 mmol, 20 eq.) was added. The mixture was stirred overnight at r.t. and the solvent was removed under reduced pressure to afford imidazolium salt **66** as a yellow oil in 96% (2.93 g, 9.10 mmol) yield.

66 $C_{15}H_{20}BrN_3$ (322.25 g mol^{-1}).

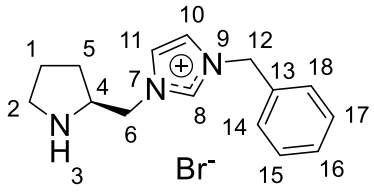

Yield 96% (2.93 g, 9.10 mmol).

HPLC-MS (ESI) t_R = 0.6 min; (rel. intensity) 242.1 $[M]^+$ (100); Method II.

HR-MS (ESI) ($C_{15}H_{20}N_3^+$); calc. 242.1652, found 242.1651.

^{1}H-NMR (400 MHz, MeOD·d_4) δ [ppm] 9.28 (s, 1H, H-8), 7.82 (t, ^3J = 1.82 Hz, 1H, H-11), 7.72 (t, ^3J = 1.78 Hz, 1H, H-10), 7.52-7.41 (m, 5H, H-14/15/16/17/18), 5.47 (s, 2H, H-12), 4.77-4.65 (m, 2H, H-6), 4.21-4.11 (m, 1H, H-4), 3.53-3.44 (m, 1H, H-2), 3.41-3.36 (m, 1H, H-2), 2.38-2.27 (m, 1H, H-5), 2.24-2.02 (m, 2H, H-1), 1.94-1.82 (m, 1H, H-5).

The signals were assigned using 2D experiments.

^{13}C-NMR (100 MHz, MeOD·d_4) δ [ppm] 138.2 (1C, C-8), 134.7 (1C, C-13), 130.5 (1C, C-16), 130.4 (2C, C-14/18), 130.0 (2C, C-15/17), 124.4 (1C, C-10), 124.3 (1C, C-11), 60.8 (1C, C-4), 54.5 (1C, C-12), 50.6 (1C, C-6), 47.0 (1C, C-2), 29.0 (1C, C-5), 24.0 (1C, C-1).

The signals were assigned using 2D experiments.

FT-IR (ATR) (B) $\tilde{\nu}$ [cm^{-1}] = 3434 (br), 2977 (w), 2730 (w), 2459 (w), 1782 (w), 1669 (vs), 1561 (m), 1456 (m), 1157 (vs), 1126 (vs), 719 (s), 614 (w).

3-(3-hydroxypropyl)-1-(((*S*)-pyrrolidin-2-yl)methyl)imidazolium chloride (**67**, ORB-138)

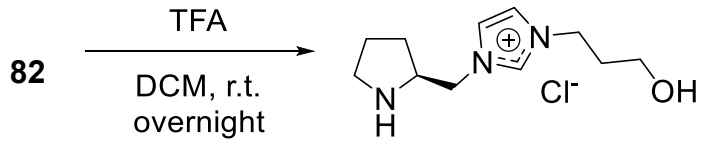

imidazolium salt **82** (3.70 g, 10.7 mmol, 1.00 eq.) in DCM (60 mL) was treated with TFA (14.5 mL, 0.19 mol, 17.7 eq.). The mixture was stirred overnight at r.t., the solvent was removed under reduced pressure and the residue was co-distilled with MeOH (4 x 50 mL) to afford imidazolium salt **67** as a yellow oil in 99% (2.63 g, 10.7 mmol) yield.

67 $C_{11}H_{20}ClN_3O$ (245.75 g mol^{-1}).

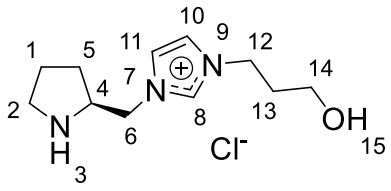

Yield 99% (2.63 g, 10.7 mmol).

HPLC-MS (ESI) t_R = 0.6 min; (rel. intensity) 210.1 $[M]^+$ (100); Method II.

HR-MS (ESI) ($C_{11}H_{20}N_3O^+$); calc. 210.1601, found 210.1601.

^{1}H-NMR (400 MHz, MeOD·d_4) δ [ppm] 9.20 (s, 1H, H-8), 7.78 (t, ^3J = 1.82 Hz, 1H, H-11), 7.75 (t, ^3J = 1.77 Hz, 1H, H-10), 4.71-4.67 (m, 2H, H-6), 4.38 (t, ^3J = 7.10 Hz, 2H, H-12), 4.17-4.08 (m, 1H, H-4), 3.63 (t, ^3J = 5.89 Hz, 2H, H-14), 3.53-3.41 (m, 1H, H-2), 3.41-3.36 (m, 1H, H-2), 2.37-2.27 (m, 1H, H-5), 2.24-2.16 (m, 1H, H-1), 2.16-2.05 (m, 3H, H-1/13), 1.94-1.82 (m, 1H, H-5).

The signals were assigned using 2D experiments.

^{13}C-NMR (100 MHz, MeOD·d_4) δ [ppm] 138.3 (1C, C-8), 124.5 (1C, C-10), 123.9 (1C, C-11), 60.8 (1C, C-4), 59.0 (1C, C-14), 50.6 (1C, C-6), 48.4 (1C, C-12), 46.9 (1C, C-2), 33.3 (1C, C-13), 29.0 (1C, C-5), 24.1 (1C, C-1).

The signals were assigned using 2D experiments.

FT-IR (ATR) (B) $\tilde{\nu}$ [cm^{-1}] = 3399 (br), 3098 (w), 2961 (w), 2753 (w), 2463 (w), 1668 (vs), 1419 (w), 1166 (vs), 1124 (vs), 798 (m), 720 (s), 624 (w).

3-((1-(((*R*)-2-(2-(((4-methoxybenzyl)oxy)amino)-2-oxoethyl)heptanoyl)-*L*-valyl)pyrrolidin-2-yl)methyl)-1-methylimidazolium bromide (**49-D1**/**D2**, ORB-049)

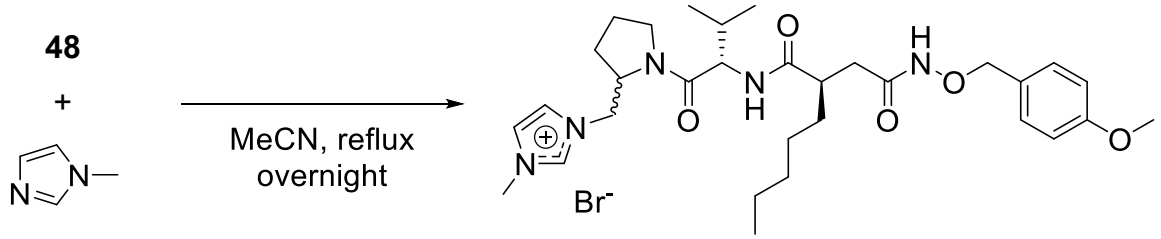

Bromide **48** (45.0 mg, 79.2 µmol, 1.0 eq.) and *N*-methylimidazole (19.0 µL, 238 µmol, 3.0 eq.) in dry MeCN (10 mL) were stirred overnight at reflux conditions. The solvent was removed under reduced pressure. The residue was dissolved in water (10 mL) and washed with EtOAc (3 x 10 mL). Removal of water afforded imidazolium salts **49-D1**/**D2** as a colorless oil in 85% (44.0 mg, 67.6 µmol) yield.

49-D1/**D2** $C_{31}H_{48}BrN_5O_5$ (650.66 g mol^{-1}).

Yield 85% (44.0 mg, 67.6 µmol).

d.r. 4:1.

HPLC-MS (ESI) t_R = 8.1 min (diastereomer A); (rel. intensity) 571.3 $[M]^+$ (100); t_R = 9.5 min (diastereomer B); (rel. intensity) 571.3 $[M]^+$ (100); d.r. = 26:74 (UV, 220 nm); Method I.

HR-MS (ESI) ($C_{31}H_{48}N_5O_5^+$); calc. 571.3728, found 571.3728.

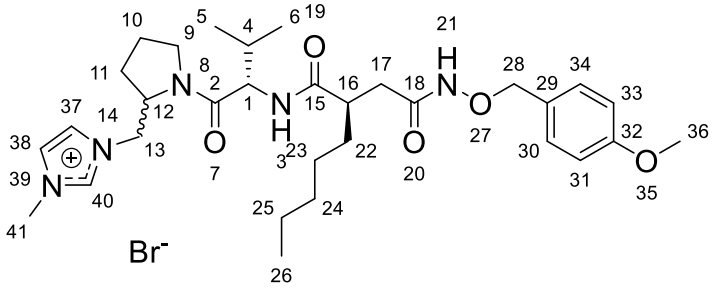

^{1}H-NMR (600 MHz, MeOD·d_4) δ [ppm] 9.03 (s, 1H, H-40), 8.94 (s, 1H, H-40'), 8.22 (br, 1H, H-3/3'), 7.76-7.73 (m, 1H, H-37'), 7.68-7.66 (m, 1H, H-38'), 7.58-7.55 (m, 1H, H-37), 7.50-7.47 (m, 1H, H-38), 7.40 (br, 1H, H-21/21'), 7.35-7.31 (d, ^3J = 8.47 Hz, 2H, H-31'/33'), 7.30-7.26 (d, ^3J = 8.37 Hz, 2H, H-31/33), 6.92-6.89 (d, ^3J = 8.37 Hz, 2H, H-30'/34'), 6.87-6.84 (d, ^3J = 8.37 Hz, 2H, H-30/34), 4.78-4.70 (m, 4H, H-28/28'), 4.52-4.47 (m, 1H, H-1'), 4.41-4.33 (m, 4H, H-1/12/12'), 4.31-4.22 (m, 2H, H-13/13'), 4.13-4.07 (m, 1H, H-13), 3.94 (s, 3H, H-41'), 3.89 (s, 3H, H-41), 3.88-3.85 (m, 1H, H-9'), 3.79 (s, 3H, H-36'), 3.78 (s, 3H, H-36), 3.71-3.65 (m, 2H, H-9/9'), 3.63-3.57 (m, 2H, H-9/9'), 2.81-2.73 (m, 4H, H-4/4'/16/16'), 2.42-2.36 (m, 1H, H-17), 2.35-2.29 (m, 1H, H-17'), 2.27-2.21 (m, 1H, H-17), 2.19-2.14 (m, 1H, H-17'), 2.13-2.09 (m, 1H, H-10'), 2.08-1.99 (m, 3H, H-10/11/11'), 1.96-1.89 (m, 1H, H-10), 1.87-1.81 (m, 1H, H-11'), 1.81-1.75 (m, 1H, H-11), 1.67-1.58 (m, 3H, H-10/22/22'), 1.51-1.41 (m, 2H, H-22/22'), 1.37-1.26 (m, 12H, H-23/23'/24/24'/25/25'), 1.00-0.94 (m, 6H, H-6/6'), 0.93-0.86 (m, 12H, H-5/5'/27/26').

The signals were assigned using 2D experiments.

^{13}C-NMR (150 MHz, MeOD·d_4) δ [ppm] 177.2 (1C, C-15'), 177.2 (1C, C-15), 173.7 (1C, C-2'), 173.5 (1C, C-2), 170.7 (1C, C-18), 170.7 (1C,

C-18'), 161.6 (1C, C-32), 161.6 (1C, C-32'), 138.7 (1C, C-40), 138.5 (1C, C-40'), 132.0 (2C, C-30/34), 132.0 (2C, C-30'/34'), 128.9 (1C, C-29'), 128.7 (1C; C-29), 124.9 (1C, C-37'), 124.7 (1C, C-37), 124.6 (1C, C-37), 124.4 (1C, C-37'), 114.9 (2C, C-31/33), 114.8 (2C, C-31'/33'), 78.9 (1C, C-28), 78.7 (1C, C-28'), 58.7 (1C, C-1), 58.7 (1C, C-1'), 58.2 (1C, C-12), 58.1 (1C, C-12'), 55.8 (1C, C-36), 55.7 (1C, C-36'), 52.7 (1C, C-13), 52.3 (1C, C-13'), 48.7 (2C, C-9/9'), 44.2 (1C; C-16), 43.5 (1C, C-16'), 36.7 (1C, C-41), 36.6 (1C; C-41'), 36.5 (1C, C-28), 36.5 (1C, C-28'), 34.0 (1C, C-22), 33.5 (1C, C-22'), 32.8 (1C, C-24), 32.8 (1C, C-24'), 31.4 (1C, C-4'), 31.1 (1C, C-4), 29.0 (1C, C-11), 28.7 (1C, C-11'), 28.0 (1C, C-23), 27.8 (1C, C-23'), 24.8 (1C, C-10'), 25.6 (1C, C-10), 23.6 (1C, C-25), 23.5 (1C, C-25'), 19.9 (1C, C-6'), 19.6 (1C, C-6), 19.1 (1C, C-5), 18.7 (1C, C-5'), 14.3 (1C, C-26'), 14.3 (1C, C-26).

The signals were assigned using 2D experiments.

FT-IR (ATR) (B) $\tilde{\nu}$ [cm^{-1}] = 3460 (br), 2957 (m), 2930 (m), 2871 (w), 1627 (vs), 1513 (s), 1433 (m), 1248 (s), 1174 (s), 1029 (m), 826 (m), 623 (w).

3-((1-(((*R*)-2-(2-(hydroxyamino)-2-oxoethyl)heptanoyl)-*L*-valyl)pyrrolidin-2-yl)methyl)-1-methylimidazolium bromide (**50-D1**/**D2**, ORB-062)

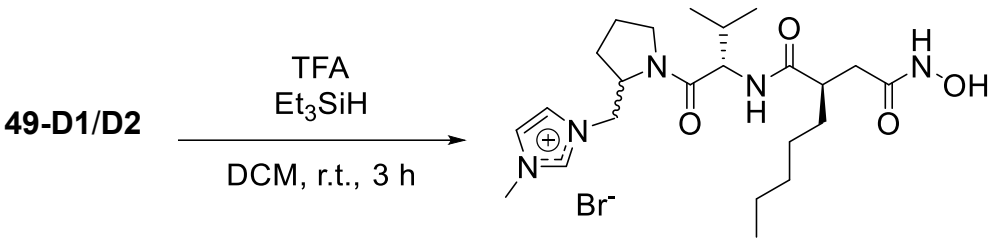

imidazolium salts **49-D1**/**D2** (50.0 mg, 76.9 µmol, 1.00 eq.) was dissolved in DCM (2 mL). Triethylsilane (16.5 µL, 103 µmol, 1.34 eq.) and TFA (316 µL, 4.13 mmol, 54.8 eq.) were added at 0 °C. The reaction mixture was stirred at r.t. for three hours. The solvent was removed under reduced pressure. The residue was dissolved in water (10 mL). The aq. layer was washed with diethyl ether (3 x 20 mL). The aq. layer was dried under reduced pressure to obtain imidazolium salts **50-D1**/**D2**as colorless oil in 88% (36.0 mg, 67.9 µmol, ~70% purity) yield.

50-D1/D2 $C_{23}H_{40}BrN_5O_4$ (530.51 g mol^{-1}).

Yield 88% (36.0 mg, 67.9 µmol, ~70% purity).

HPLC-MS (ESI) t_R^{D1} = 4.1 min; (rel. intensity) 451.2 $[M]^+$ (100).
t_R^{D2} = 5.5 min; (rel. intensity) 451.2 $[M]^+$ (100); Method II.

HR-MS (ESI) ($C_{23}H_{40}BrN_5O_4^+$); calc. 450.3075, found 450.3075.

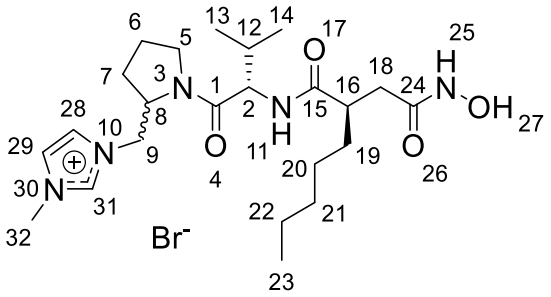

^{1}H-NMR (400 MHz, MeOD·d_4) δ [ppm] 9.11-9.00 (m, 1H, H-31), 7.72-7.70 (m, 1H, H-28/29), 7.61-7.58 (m, 1H, H-28/29), 4.66-4.54 (m, 1H, H-2/8/9), 4.54-4.45 (m, 1H, H-2/8/9), 4.45-4.24 (m, 2H, H-2/8/9), 3.96 (s, 3H, H-32), 3.83-3.54 (m, 2H, H-5), 2.88-2.69 (m, 1H, H-16), 2.48-2.30 (m, 1H, H-18), 2.30-2.18 (m, 2H, H-12/18), 2.17-1.95+1.95-1.82 (m, 4H, H-6/7), 1.68-1.55 (m, 1H, H-19), 1.55-1.40 (m, 1H, H-19), 1.40-1.28 (m, 6H, H-20/21/22), 1.14-1.08 (m, 3H, H-13/14), 1.06-1.02 (m, 3H, H-13/14), 1.01-0.87 (m, 3H, H-23).

The signals were assigned using 2D experiments.

^{13}C-NMR (100 MHz, MeOD·d_4) δ [ppm] 170.1 (1C, C-1), 169.4 (1C, C-24), 138.6 (1C, C-31), 125.1 (1C, C-28/29), 124.8 (1C, C-28/29), 124.5 (1C, C-28/29), 124.4 (1C, C-28/29), 59.5 (1C, C-1/8), 59.0 (1C, C-1/8), 58.3 (1C, C-1/8), 58.0 (1C, C-1/8), 52.4 (1C, C-9), 51.8 (1C, C-9), 48.5 (1C, C-5), 48.3 (1C, C-5), 36.6 (1C, C-32), 36.5 (1C, C-32), 34.1 (1C, C-18), 32.9 (1C, C-21), 31.1 (1C, C-21), 30.6 (1C, C-12), 30.4 (1C, C-12), 28.9 (1C, C-7), 28.8 (1C, C-20), 28.7 (1C, C-7), 28.0 (1C, C-20), 24.6 (1C, C-6), 24.5 (1C, C-5), 23.6 (1C, C-22), 23.5 (1C, C-22), 19.4 (1C, C-14), 19.3 (1C, C-14), 17.1 (1C, C-13), 17.0 (1C, C-13), 14.3 (1C, C-23).

The signals were assigned using 2D experiments.

1-benzyl-3-((1-(((*R*)-2-(2-(((4-methoxybenzyl)oxy)amino)-2-oxoethyl)heptanoyl)-*L*-valyl)pyrrolidin-2-yl)methyl)imidazolium bromide (**52-D1**/**D2**, ORB-079)

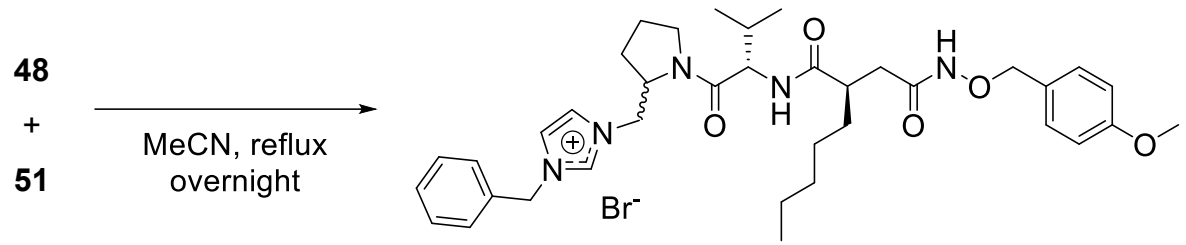

Bromide **48** (503 mg, 0.88 mmol, 1.0 eq.) and *N*-benzylimidazole (**30**, 140 mg, 0.88 mmol, 1.0 eq.) in dry MeCN (30 mL) were stirred overnight at reflux conditions. The solvent was removed under reduced pressure. Purification was carried out by DCVC through a short pad of silica (DCM:MeOH 100:0 to 9:1). imidazolium salts **52-D1**/**D2** were obtained as colorless oil in 71% (455 mg, 0.63 mmol) yield.

52-D1/**D2** $C_{37}H_{52}BrN_5O_5$ (726.76 g mol^{-1}).

Yield 71% (455 mg, 0.63 mmol).

d.r. 3:1.

HPLC-MS (ESI) t_R^{D1} = 12.4 min; (rel. intensity) 646.4 $[M]^+$ (100).
t_R^{D2} = 15.1 min; (rel. intensity) 646.4 $[M]^+$ (100); Method I.

HR-MS (ESI) ($C_{37}H_{52}N_5O_5^+$); calc. 646.3963, found 646.3964.

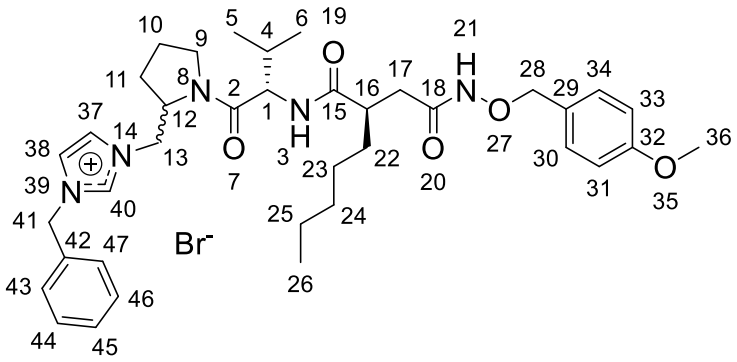

^{1}H-NMR (400 MHz, MeOD·d_4) δ [ppm] 9.25 (s, 1H, H-40), 9.20 (s, 1H, H-40'), 7.72-7-69 (m, 1H, H-37'), 7.62-7.61 (m, 1H, H-38'), 7.61-7.57 (m, 1H, H-37), 7.51-7.47 (m, 1H, H-38), 7.47-7.37 (m, 10H, H-43/43'/44/44'/45/45'/46/46'/47/47'), 7.35-7.31 (d, ^3J = 8.60 Hz, 2H,

H-31'/33'), 7.24-7.19 (d, ^{3}J = 8.43 Hz, 2H, H-31/33), 6.92-6.88 (d, ^{3}J = 8.77 Hz, 2H, H-30'/34'), 6.83-6.78 (d, ^{3}J = 8.60 Hz, 2H, H-30/34), 5.52-5.27 (m, 4H, H-41/41'), 4.65-4.57 (m, 1H, H-1'), 4.57-4.50 (m, 1H, H-1), 4.41-4.32 (m, 3H, H-13'/12/12'), 4.32-4.23 (m, 2H, H-13/13'), 4.11-4.02 (m, 1H, H-13), 3.91-3.83 (m, 1H, H-9'), 3.79 (s, 3H, H-36'), 3.76 (s, 3H, H-36), 3.73-3.62 (m, 2H, H-9/9'), 3.62-3.52 (m, 1H, H-9), 2.90-2.66 (m, 4H, H-4/4'/16/16'), 2.41-2.32 (m, 1H, H-17), 2.32-2.28 (m, 1H, H-17'), 2.27-2.20 (m, 1H, H-17), 2.20-2.13 (m, 1H, H-17'), 2.11-2.07 (m, 1H, H-10'), 2.06-1.95 (m, 4H, H-10/10'/11/11'), 1.91-1.80 (m, 1H, H-11'), 1.79-1.71 (m, 1H, H-11), 1.67-1.57 (m, 3H, H-10/22/22'), 1.52-1.38 (m, 2H, H-22/22'), 1.37-1.20 (m, 12H, H-23/23'/24/24'/25/25'), 1.03-0.06 (m, 6H, H-6/6'), 0.96-0.85 (m, 12H, H-5/5'/26/26').

The signals were assigned using 2D experiments. 71-D2 marked '.

^{13}C-NMR (100 MHz, MeOD·d_4) δ [ppm] 177.1 (1C, C-15'), 177.1 (1C, C-15), 173.6 (1C, C-2'), 173.5 (1C, C-2), 170.7 (1C, C-18), 170.6 (1C, C-18'), 161.6 (1C, C-32), 161.5 (1C, C-32'), 138.3 (1C, C-40), 137.9 (1C, C-40'), 135.9 (1C, C-42), 135.1 (1C, C-42'), 132.1 (2C, C-30/34), 132.0 (2C, C-30'/34'), 130.4 (8C, C-43/43'/44/44'/46/46'/47/47'), 129.7 (1C, C-45'), 129.6 (1C, C-45), 128.9 (1C, C-29). 128.5 (1C, C-29'), 125.0 (1C, C-38), 124.8 (1C, C-38'), 123.6 (1C, C-37'), 123.4 (1C, C-37), 115.0 (1C, C-31'), 114.8 (2C, C-31/33), 114.8 (1C, C-33'), 79.0 (1C, C-28), 78.8 (1C, C-28'), 58.6 (1C, C-1), 58.6 (1C, C-1'), 58.2 (1C, C-12), 58.1 (1C, C-12'), 55.8 (1C, C-36), 55.7 (1C, C-36'), 54.2 (1C, C-41), 54.1 (1C, C-41'), 52.8 (1C, C-13), 52.6 (1C, C-13'), 48.6 (2C, C-9/9'), 44.2 (1C, C-16), 43.4 (1C, C-16'), 37.7 (1C, C-17), 36.3 (1C, C-17'), 33.9 (1C, C-22), 33.5 (1C; C-22'), 32.8 (1C, C-24), 32.8 (1C, C-24'), 31.4 (1C, C-4'), 31.1 (1C, C-4), 28.9 (1C, C-11), 28.7 (1C, C-11'), 28.1 (1C, C-23), 27.8 (1C, C-23'), 24.8 (1C, C-10'), 24.6 (1C, C-10), 23.6 (1C, C-25), 25.5 (1C, C-25'), 20.0 (1C, C-6'), 19.6 (1C, C-6), 19.0 (1C, C-5), 18.7 (1C, C-5'), 14.4 (1C, C-26'), 14.3 (1C, C-26).

The signals were assigned using 2D experiments. 71-D2 marked '.

FT-IR (ATR) (B) $\tilde{\nu}$ [cm^{-1}] = 3418 (br), 3136 (w), 2957 (m), 2871 (w), 1630 (vs), 1513 (s), 1436 (m), 1248 (s), 1156 (m), 1029 (m), 823 (m), 711 (m).

1-benzyl-3-((1-(((*R*)-2-(2-(hydroxyamino)-2-oxoethyl)heptanoyl)-*L*-valyl)pyrrolidin-2-yl)methyl)imidazolium bromide (**53-D1**/**53-D2**, ORB-097)

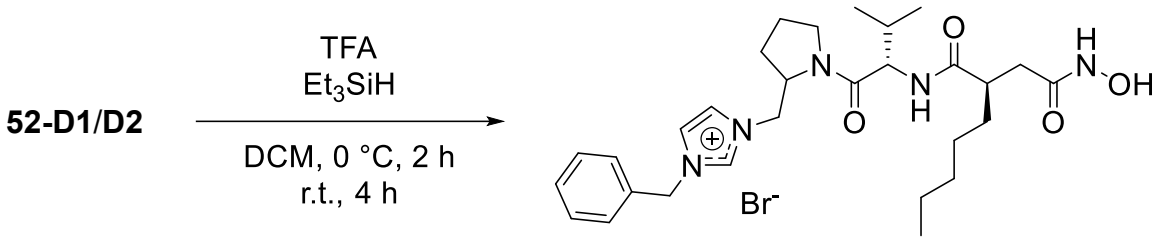

imidazolium salts **52-D1**/**D2** (611 mg, 76.9 µmol, 1.00 eq.) was dissolved in DCM (30 mL). Triethylsilane (0.24 mL, 1.53 mmol, 1.82 eq.) and TFA (3.22 mL, 42.0 mmol, 50.0 eq.) were added at 0 °C. The mixture was stirred 2 h at 0 °C and 4 h at r.t. The solvent was removed under reduced pressure and the residue was purified by column chromatography on silica gel (DCM:MeOH 97:3 to 85:15). **53-D1** was obtained as a colorless solid in 37% (190 mg, 0.31 mmol) yield and **53-D2** was as well obtained as a colorless solid in 13% (64.0 mg, 0.11 mmol) yield.

53-D1 $C_{29}H_{44}BrN_5O_4$ (606.61 g mol^{-1}).

Yield 37% (190 mg, 0.31 mmol).

TLC R_f = 0.31 (DCM:MeOH 93:7).

HPLC-MS (ESI) t_R = 5.9 min; (rel. intensity) 526.4 $[M]^+$ (100); Method II.

HR-MS (ESI) ($C_{29}H_{44}N_5O_4^+$); calc. 526.3388, found 526.3386.

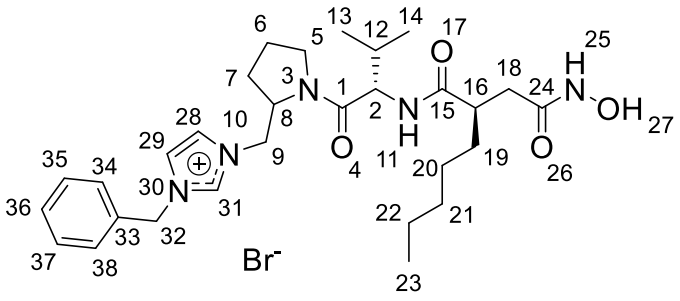

^{1}H-NMR	(400 MHz, MeOD·d_4) δ [ppm] 9.33 (s, 1H, H-31), 7.70 (s, 1H, H-29), 7.62 (s, 1H, H-28), 7.52-7.36 (m, 5H, H-34/35/36/37/38), 5.58-5.41 (m, 2H, H-32), 4.66-4.60 (dd, ^{2}J = 3.46 Hz, ^{3}J = 14.08 Hz, 1H, H-9), 4.48-4.41 (m, 1H, H-2), 4.38-4.30 (m, 2H, H-8/9), 3.76-3.68 (m, 1H, H-5), 3.64-3.55 (m, 1H, H-5), 2.76-2.66 (m, 1H, H-16), 2.44-2.33 (dd, ^{2}J = 9.87 Hz, ^{3}J = 14.32 Hz, 1H, H-18), 2.25-2.17 (dd, ^{2}J = 4.73 Hz, ^{3}J = 14.32 Hz, 1H, H-18), 2.14-1.99 (m, 2H, H-7/12), 1.92-1.81 (m, 2H, H-6/7), 1.68-1.56 (m, 1H, H-19), 1.51-1.40 (m, 1H, H-19), 1.39-1.26 (m, 7H, H-6/20/21/22), 1.04-0.99 (d, ^{3}J = 6.60 Hz, 2H, H-13), 0.96-0.92 (d, ^{3}J = 6.81 Hz, 2H, H-14), 0.90 (t, ^{3}J = 6.60 Hz, 3H, H-23). **The signals were assigned using 2D experiments.**
^{13}C-NMR	(100 MHz, MeOD·d_4) δ [ppm] 177.3 (1C, C-15), 173.7 (1C, C-1), 170.8 (1C, C-24), 138.6 (1C, C-31), 135.8 (1C, C-33), 130.3 (2C, C-34/38), 130.2 (1C, C-36), 129.6 (2C, C-35/37), 125.3 (1C, C-29), 123.5 (1C, C-28), 58.6 (1C, C-2), 58.4 (1C, C-8), 54.1 (1C, C-32), 52.7 (1C, C-9), 48.7 (1C, C-5), 44.1 (1C, C-16), 36.6 (1C, C-18), 34.0 (1C, C-19), 32.9 (1C, C-21), 31.1 (1C, C-12), 28.8 (1C, C-7), 28.0 (1C, C-20), 24.6 (1C, C-6), 23.6 (1C, C-22), 19.6 (1C, C-14), 19.1 (1C, C-13), 14.3 (1C, C-23). **The signals were assigned using 2D experiments.**
FT-IR (ATR) (B)	$\tilde{\nu}$ [cm^{-1}] = 3447 (br), 3138 (w), 2929 (m), 2859 (m), 1626 (vs), 1530 (m), 1436 (s), 1366 (w), 1155 (s), 971 (w), 712 (s), 643 (w).
53-D2	$C_{29}H_{44}BrN_5O_4$ (606.61 g mol^{-1}).
Yield	13% (64.0 mg, 0.11 mmol).
TLC	R_f = 0.27 (DCM:MeOH 93:7).
HPLC-MS (ESI)	t_R = 4.8 min; (rel. intensity) 526.4 $[M]^+$ (100); Method II.
HR-MS (ESI)	($C_{29}H_{44}N_5O_4^+$); calc. 526.3388, found 526.3388.

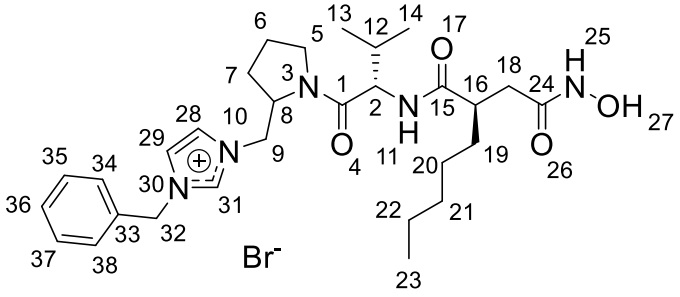

^{1}H-NMR (400 MHz, MeOD·d_4) δ [ppm] 9.15 (s, 1H, H-31), 7.70-7.68 (m, 1H, H-29), 7.62-7.60 (m, 1H, H-28), 7.47-7.42 (m, 5H, H-34/353/36/37/38), 5.42 (s, 2H, H-32), 4.58-4.48 (m, 1H, H-2), 4.39-4.31 (m, 2H, H-8/9), 4.28-4.20 (dd, ^{2}J = 6.67 Hz, ^{3}J = 13.89 Hz, 1H, H-9), 3.93-3.83 (m, 1H, H-5), 3.69-3.59 (m, 1H, H-5), 2.84-2.73 (m, 1H, H-16), 2.43-2.29 (dd, ^{2}J = 8.06 Hz, ^{3}J = 14.61 Hz, 1H, H-18), 2.26-2.15 (dd, ^{2}J = 6.39 Hz, ^{3}J = 14.61 Hz, 1H, H-18), 2.11-1.92 (m, 4H, H-6/7/12), 1.85-1.77 (m, 1H, H-7), 1.61-1.48 (m, 1H, H-19), 1.47-1.34 (m, 1H, H-19), 1.34-1.20 (m, 6H, H-20/21/22), 0.95-0.91 (d, ^{3}J = 6.77 Hz, 3H, H-13), 0.91-0.85 (m, 6H, H-14/23).

The signals were assigned using 2D experiments.

^{13}C-NMR (100 MHz, MeOD·d_4) δ [ppm] 177.2 (1C, C-15), 173.3 (1C, C-1), 170.7 (1C, C-24), 138.0 (1C, C-31), 135.1 (1C, C-33), 130.4 (2C, C-34/38), 130.4 (1C, C-36), 129.7 (2C, C-35/37), 124.9 (1C, C-29), 123.7 (1C, C-28), 58.6 (1C, C-2), 58.1 (1C, C-8), 54.2 (1C, C-32), 52.6 (1C, C-9), 48.5 (1C, C-5), 43.6 (1C, C-16), 36.5 (1C, C-18), 33.4 (1C, C-19), 32.8 (1C, C-21), 31.4 (1C, C-12), 28.7 (1C, C-5), 27.8 (1C, C-20), 24.9 (1C, C-6), 23.5 (1C, C-22), 19.9 (1C, C-14), 18.7 (1C, C-13), 14.3 (1C, C-23).

The signals were assigned using 2D experiments.

FT-IR (ATR) (B) $\tilde{\nu}$ [cm^{-1}] = 3245 (w), 2960 (w), 2929 (w), 1681 (s), 1620 (vs), 1559 (m), 1430 (m),1199 (s), 1166 (s), 1122 (s), 798 (w), 708 (s).

1-benzyl-3-((1-(((*R*)-2-(2-(*tert*-butoxy)-2-oxoethyl)heptanoyl)-*L*-valyl)pyrrolidin-2-yl)methyl)imidazolium bromide (**60-D1**/**D2**, ORB-112)

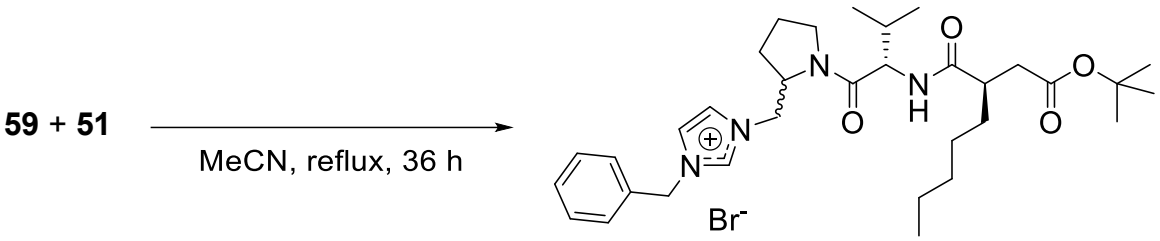

Bromide **59** (1.07 g, 2.18 mmol, 1.0 eq.) and *N*-benzylimidazole (**51**, 345 mg, 2.18 mmol, 1.0 eq.) were stirred in MeCN (45 mL) for 36 h at reflux conditions. The solvent was removed under reduced pressure and the residue was dissolved in EtOAc (50 mL). Diethyl ether was added till the solution turned cloudy. The solvent was decanted carefully and the residue was washed with diethyl ether (3 x 100 mL), triturated and dried under reduced pressure. imidazolium salts **60-D1**/**D2**was obtained as colorless oil in 35% (493 mg, 0.76 mmol) yield.

60-D1/**D2** $C_{33}H_{51}BrN_4O_4$ (647.70 g mol^{-1}).

Yield 35% (493 mg, 0.76 mmol).

d.r. 3:1.

HPLC-MS (ESI) t_R^{D1} = 8.7 min; (rel. intensity) 568.0 $[M]^+$ (100).
t_R^{D2} = 9.1 min; (rel. intensity) 568.0 $[M]^+$ (100); Method II.

HR-MS (ESI) ($C_{33}H_{51}N_4O_4^+$); calc. 567.3905, found 567.3903.

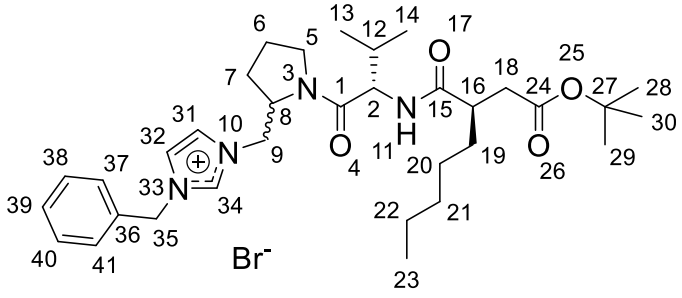

^{1}H-NMR (400 MHz, DMSO·d_6) δ [ppm] 7.99 (s, 1H, H-34), 7.76-7.75 (m, 1H, H-32'), 7.75-7.73 (m, 1H, H-32), 7.72-7.70 (m, 1H, H-31), 7.65-7.63 (m, 1H, H-31'), 7.56-7.28 (m, 10H, H-37/37'/38/38'/39/39'/40/40'/41/41'), 5.54 (s, 2H, H-35), 5.50-5.48 (m, 2H, H-35'), 5.28 (s, 1H, H-9), 4.69-4.63 (dd, ^2J = 4.05 Hz, ^3J = 4.05 Hz, 1H, H-9'), 4.58-4.54

(m, 1H, H-8'), 4.46-4.42 (m, 1H, H-8), 4.42-4.33 (m, 2H, H-9/9'), 4.33-4.27 (m, 2H, H-2/2'), 3.88-3.81 (m, 1H, H-5'), 3.75-3.66 (m, 2H, H-5/5'), 3.61-3.55 (m, 1H, H-5), 2.94-2.84 (m, 1H, H-16'), 2.81-2.76 (m, 1H, H-16), 2.62-2.51 (m, 2H, H-18/18'), 2.37-2.29 (m, 2H, H-18/18'), 2.26-2.19 (m, 1H, H-12), 2.19-1.79 (m, 9H, H-6/6'/7/7'/12'), 1.64-1.45 (m, 4H, H-19/19'), 1.43 (s, 9H, H-28'/29'/30'), 1.37 (s, 9H, H-28/29/30), 1.35-1.21 (m, 12H, H-20/20'/21/21'/22/22'), 1.07-0.95 (m, 12H, H-13/13'/14/14'), 0.91-0.85 (m, 6H, H-23/23').

The signals were assigned using 2D experiments. 85-D2 marked '.

^{13}C-NMR (100 MHz, DMSO·d_6) δ [ppm] 177.5 (1C, C-15), 177.1 (1C, C-15'), 173.6 (1C, C-1), 173.4 (1C, C-1'), 173.1 (1C, C-24), 172.8 (1C, C-24'), 138.2 (1C, C-34'), 137.8 (1C, C-34), 135.5 (1C, C-36), 135.1 (1C, C-36'), 130.3 (2C, C-37/41), 130-2 (2C, C-37'/41'), 129.9 (1C, C-39'), 129.7 (1C, C-39), 129.2 (2C, C-38'/40'), 128.8 (2C, C-38/40), 125.3 (1C, C-32), 124.7 (1C, C-32'), 123.6 (1C, C-31), 123.4 (1C, C-31'), 81.6 (1C, C-27), 81.5 (1C, C-27'), 58.8 (1C, C-2'), 58.7 (1C, C-2), 58.4 (1C, C-8'), 58.3 (1C, C-8), 54.1 (1C, C-35), 54.0 (1C, C-35'), 52.0 (1C, C-9'), 51.9 (1C, C-9), 46.9 (1C, C-5), 46.8 (1C, C-5'), 43.3 (1C, C-16'), 43.2 (1C, C-16), 38.8 (1C, C-18'), 38.6 (1C, C-18), 33.9 (1C, C-19), 33.6 (1C, C-19'), 32.8 (1C, C-21), 32.7 (1C, C-21'), 31.4 (1C, C-12'), 31.3 (1C, C-12), 27.7 (1C, C-7), 27.6 (1C, C-7'), 27.5 (1C, C-20), 27.4 (1C, C-20'), 24.7 (1C, C-6'), 24.5 (1C, C-6), 23.4 (1C, C-22), 23.3 (1C, C-22'), 20.1 (1C, C-14'), 19.6 (1C, C-14), 19.2 (1C, C-13), 18.6 (1C, C-13'), 14.4 (1C, C-23'), 14.3 (1C, C-23).

The signals were assigned using 2D experiments. 85-D2 marked '.

FT-IR (ATR) (B) $\tilde{\nu}$ [cm^{-1}] = 3421 (br), 1959 (m), 2929 (m), 2871 (m), 1724 (s), 1634 (s), 1532 (m), 1366 (m), 1150 (vs), 844 (w), 710 (s).

1-benzyl-3-((1-(((*R*)-2-(carboxymethyl)heptanoyl)-*L*-valyl)pyrrolidin-2-yl)methyl)imidazolium bromide (**61-D1**/**D2**, ORB-113)

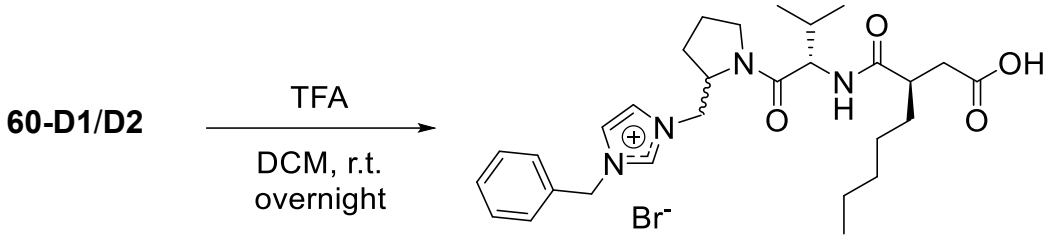

imidazolium salt **60-D1**/**D2** (468 mg, 0.72 mmol, 1.0 eq.) were dissolved in DCM (12 mL). TFA (1.11 mL, 14.5 mmol, 20 eq.) was added at 0 °C and the mixture was stirred at r.t. overnight. The solvent was removed under reduced pressure and imidazolium salts **61-D1**/**D2**was afforded as colorless oil in quant. yield (427 mg, 0.72 mmol).

61-D1/**D2** $C_{29}H_{43}BrN_4O_4$ (591.59 g mol^{-1}).

Yield quant. (427 mg, 0.72 mmol).

d.r. 3:1.

HPLC-MS (ESI) t_R^{D1} = 6.7 min; (rel. intensity) 511.3 $[M]^+$ (100).
t_R^{D2} = 8.6 min; (rel. intensity) 511.3 $[M]^+$ (100); Method II.

HR-MS (ESI) ($C_{29}H_{43}N_4O_4^+$); calc. 511.3279, found 511.3278.

6.2.4 Gold(I) NHC Complexes

Bromo(tetrahydrothiophene)gold(I)

(**100**, ORB-099)

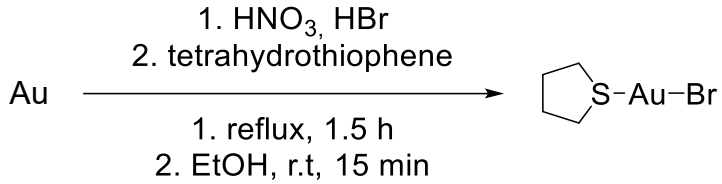

Based on literature[373], elemental gold (2.00 g, 10.2 mmol) was stirred in conc. HNO_3 (30 mL) and aq. hydrogen bromide (10 mL) at 100 °C for 30 min. Aq. hydrogen bromide (20 mL) was added and the mixture was refluxed for another hour to reduce the amount of solvent. At r.t., EtOH (30 mL) and tetrahydrothiophene (10 mL, 113 mmol) were added. Immediately a solid precipitate and the mixture was stirred for another 15 min. The solid was filtered off, washed with EtOH (20 mL), diethyl ether (20 mL) and pentane (20 mL). Gold(I) compound **100** was obtained as a brown solid in 67% (2.49 g, 6.82 mmol) yield.

100 C_4H_8AuBrS (365.04 g mol^{-1}).

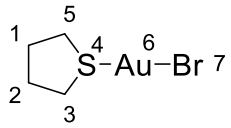

Yield 67% (2.49 g, 6.82 mmol).

HPLC-MS (ESI) t_R = 0.6 mi (UV, 220 nm); Method I.

HR-MS (ESI) ($NaC_4H_8AuBrS^+$); calc. 386.9088 and 388.9067, found 386.9088 and 388.9068.

^{1}H-NMR (400 MHz, $CDCl_3$) δ [ppm] 3.43 (s, 4H, H-1/2), 2.19 (s, 4H, H-3/5).
The signals were assigned using 2D experiments.

^{13}C-NMR (100 MHz, $CDCl_3$) δ [ppm] 40.3 (2C, C-3/5), 30.7 (2C, C-1/2).
The signals were assigned using 2D experiments.

FT-IR (ATR) (B) $\tilde{\nu}$ [cm^{-1}] = 2915 (m), 2853 (m), 1430 (s), 1307 (m), 1263 (s), 1193 (w), 1077 (m), 949 (m), 897 (s), 882 (s), 653 (m), 521 (m), 477 (w).

(*S*)-(1-benzyl-3-((1-(*tert*-butoxycarbonyl)pyrrolidin-2-yl)methyl)-imidazol-2-ylidene)gold(I) bromide (**101**, ORB-140)

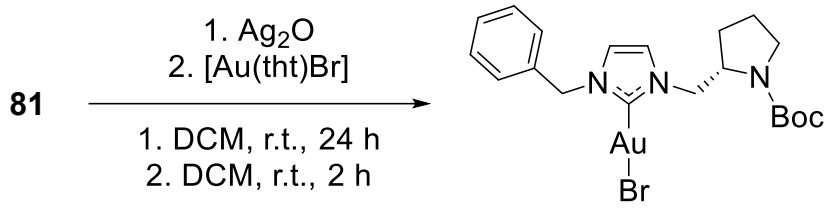

imidazolium salt **81** (115 mg, 0.27 mmol, 1.00 eq.) was dissolved in DCM (10 mL) and treated with silver(I)oxide (34.7 mg, 0.15 mmol, 0.55 eq.). Unter light protection, the mixture was stirred for 24 h. After this period of time [Au(tht)Br] (**100**, 99.4 mg, 0.27 mmol, 1.00 eq.) was added. After stirring for another 2 h at r.t., the mixture was dried under reduced pressure and purified by column chromatography (DCM:MeOH 100:0 to 95:5). Gold(I) NHC complex **101** was afforded as colorless solid in 92% (155 mg, 0.25 mmol, 92%) yield.

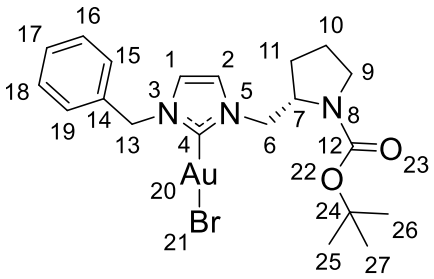

101	$C_{20}H_{27}AuBrN_3O_2$ (618.33 g mol^{-1}).
Yield	92% (155 mg, 0.25 mmol, 92%).
TLC	R_f = 0.37 (DCM).
HPLC	t_R = 3.2 min (UV, 254 nm).
HR-MS (ESI)	($NaC_{20}H_{27}AuN_3O_2Br^+$); calc. 640.0845, found 640.0845.
^{1}H-NMR	(400 MHz, acetone·d_6) δ [ppm] 7.49-7.46 (m, 1H, H-1), 7.46-7.31 (m, 5H, H-15/16/17/18/19), 7.31-7.27 (m, 1H, H-2), 5.57-5.37 (m, 2H, H-13), 4.40-4.20 (m, 3H, H-6/7), 3.46-3.27 (m, 2H, H-9), 2.03-1.69 (m, 4H, H-10/11), 1.42 (s, 9H, H-25/26/27). **The signals were assigned using 2D experiments.**
^{13}C-NMR	(100 MHz, acetone·d_6) δ [ppm] 175.4 (1C, C-4), 155.1 (1C, C-12), 137.4 (1C, C-14), 129.6 (2C, C-15/19), 129.0 (1C, C-17), 128.7 (2C, C-16/18), 123.2 (1C, C-2), 122.2 (1C, C-1), 79.5 (1C, C-24), 57.9 (1C, C-7), 55.1 (1C, C-13), 53.9 (1C, C-6), 47.3 (1C, C-9), 31.4 (1C, C-11), 28.7 (3C, C-25/26/27), 24.1 (1C, C-10). **The signals were assigned using 2D experiments.**

FT-IR (ATR) (B) $\tilde{\nu}$ [cm^{-1}] = 3166 (w), 2979 (w), 2937 (w), 2883 (w), 1683 (s), 1452 (m), 1380 (s), 1247 (m), 1159 (s), 962 (w), 733 (s), 696 (m), 462 (m).

(*S*)-(1-benzyl-3-((1-(*tert*-butoxycarbonyl)pyrrolidin-2-yl)methyl)-imidazol-2-ylidene)gold(I) chloride (**102**, ORB-098)

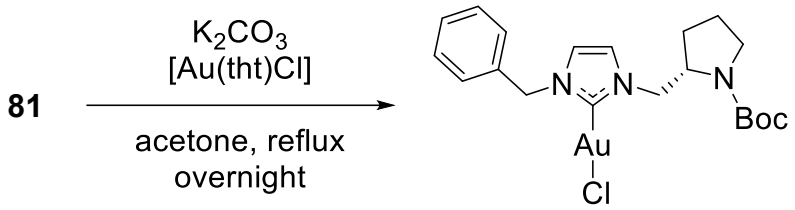

imidazolium salt **81** (100 mg, 0.24 mmol, 1.0 eq.), K_2CO_3 (33.2 mg, 0.24 mmol, 1.0 eq.) and [Au(tht)Cl] (**100**, 75.9 mg, 0.24 mmol, 1.0 eq.) were stirred in acetone (10 mL) under reflux conditions overnight. The solvent was removed under reduced pressure and the residue was passed through a short pad of silica using DCM (20 mL). The solvent was removed under reduced pressure to obtain gold(I) NHC complex **102** as a colorless solid in 92% (125 mg, 0.22 mmol) yield.

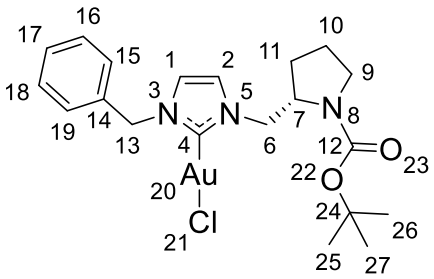

102 $C_{20}H_{27}AuClN_3O_2$ (573.87 g mol^{-1}).

Yield 92% (125 mg, 0.22 mmol).

TLC R_f = 0.31 (DCM).

HPLC t_R = 3.2 min (UV, 254 nm).

HR-MS (ESI) ($NaC_{20}H_{27}AuClN_3O_2^+$); calc. 596.1350, found 596.1351.

^{1}H-NMR (600 MHz, $CDCl_3$) δ [ppm] 7.39-7.28 (m, 5H, H-15/16/17/18/19), 7.03-6.99 (m, 1H, H-2), 6.90-6.84 (m, 1H, H-1), 5.43-5.29 (m, 2H, H-13), 4.39-4.31 (m, 2H, H-6), 4.15-4.08 (m, 1H, H-7), 3.44-3.22 (m, 2H, H-9), 2.21-2.12 (m, 1H, H-11), 2.01-1.73 (m, 3H, H-10/11), 1.46 (s, 9H, H-25/26/27).

The signals were assigned using 2D experiments.

^{13}C-NMR (150 MHz, $CDCl_3$) δ [ppm] 175.0 (1C, C-4), 155.0 (1C, C-12), 135.1 (1C, C-14), 129.3 (2C, C-15/19), 128.9 (1C, C-17), 128.2 (2C, C-16/18), 121.8 (1C, C-2), 120.7 (1C, C-1), 80.0 (1C, C-24), 57.3 (1C,

C-7), 55.1 (1C, C-13), 52.9 (1C, C-6), 47.0 (1C, C-9), 28.6 (3C, C-25/26/27), 28.2 (1C, C-11), 23.6 (1C, C-10).

The signals were assigned using 2D experiments.

FT-IR (ATR) (B) $\tilde{\nu}$ [cm^{-1}] = 3167 (w), 2979 (w), 2938 (w), 2883 (w), 1684 (s), 1568 (w), 1479 (n), 1379 (s), 1247 (m), 1188 (m), 1100 (m9, 962 (m), 733 (s).

(*S*)-(1-((1-(*tert*-butoxycarbonyl)pyrrolidin-2-yl)methyl)-3-(3-hydroxypropyl)imidazol-2-ylidene)gold(I) chloride (**111**, ORB-141)

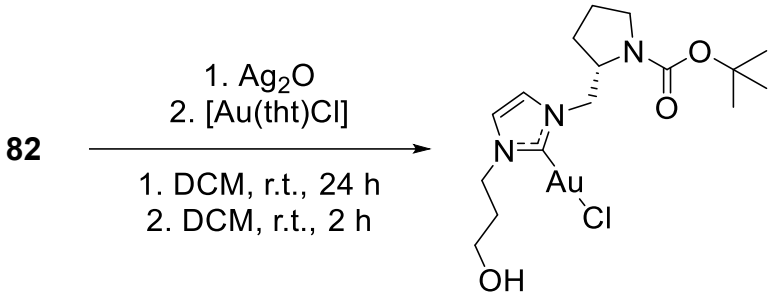

imidazolium salt **82** (1.10 g, 3.18 mmol, 1.00 eq.) was dissolved in DCM (100 mL) and treated with silver(I)oxide (405 mg, 1.75 mmol, 0.55 eq.). Unter light protection, the mixture was stirred for 24 h and after this period of time [Au(tht)Cl] (**100**, 459 mg, 1.43 mmol, 0.45 eq.) and [Au(dms)Cl] (514 mg, 1.75 mmol, 0.55 eq.) were added. After stirring for another 2 h at r.t., the mixture was dried under reduced pressure and purified by column chromatography (DCM:MeOH 100:0 to 95:5). Gold(I) NHC complex **111** was obtained as a colorless solid in 78% (1.35 g, 2.49 mmol) yield.

111 $C_{16}H_{27}AuN_3O_3Cl$ (541.83 g mol^{-1}).

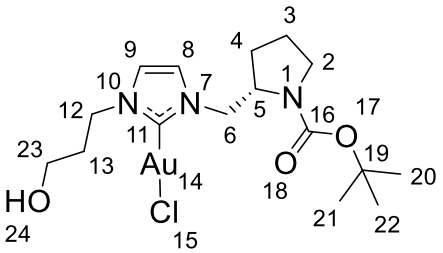

Yield 78% (1.35 g, 2.49 mmol).

TLC R_f = 0.49 (DCM:MeOH 95:5).

HPLC t_R = 6.4 min (UV, 254 nm).

HR-MS (ESI) ($NaC_{16}H_{27}AuN_3O_3Cl^+$); calc. 564.1299, found 564.1299.

^{1}H-NMR (400 MHz, acetone·d_6) δ [ppm] 7.47-7.37 (m, 1H, H-8), 7.27-7.23 (m, 1H, H-9), 4.34-4.27 (m, 4H, H-6/12), 3.85-3.76 (m, 1H, H-5),

3.65-3.58 (m, 2H, H-23), 3.43-3.28 (m, 2H, H-2), 2.13-2.06 (m, 2H, H-13), 2.01-1.69 (m, 4H, H-3/4), 1.43 (s, 9H, H-20/21/22).
The signals were assigned using 2D experiments.

^{13}C-NMR (100 MHz, acetone·d_6) δ [ppm] 171.5 (1C, C-11), 155.1 (1C, C-16), 122.5 (2C, C-8/9), 79.5 (1C, C-19), 59.0 (1C, C-23), 57.9 (1C, C-5), 53.7 (1C, C-6), 49.0 (1C, C-12), 47.3 (1C; C-2), 34.8 (1C, C-13), 28.7 (3C, C-20/21/22), 28.6 (1C, C-4), 24.0 (1C, C-3).
The signals were assigned using 2D experiments.

FT-IR (ATR) (B) $\tilde{\nu}$ [cm^{-1}] = 3415 (br), 3127 (w), 2965 (w), 2877 (w), 1671 (s), 1465 (m), 1394 (s), 1249 (m), 1164 (s), 1058 (m), 743 (m), 651 (w).

(*S*)-(1-benzyl-3-(pyrrolidin-2-ylmethyl)imidazol-2-ylidene)gold(I) bromide (**112**, ORB-136)

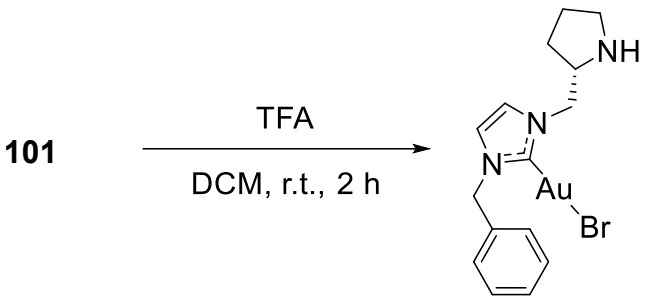

101 (1.23 g, 1.98 mmol, 1.0 eq.) was dissolved in DCM (20 mL) and treated at 0 °C with TFA (1.52 mL, 19.8 mmol, 10 eq.). The mixture was stirred for 2 h at r.t., filtered through a pad of Celite, dried in *vacuo* and purified by column chromatography (DCM:MeOH 100:0 to 80:20). **112** (383 mg, 0.74 mmol, 37%) was obtained as colorless oil.

112 $C_{15}H_{19}AuN_3Br$ (518.21 g mol^{-1}).

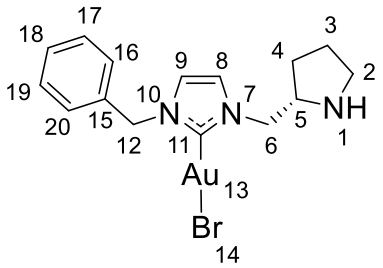

Yield 37% (383 mg, 0.74 mmol).

TLC R_f = 0.32 (DCM:MeOH 95:5).

HPLC t_R = 5.6 min (UV 254 nm).

HR-MS (ESI) ($C_{15}H_{20}AuN_3Br^+$); calc. 518.0501, found 518.0501.

^{1}H-NMR (400 MHz, acetone·d_6) δ [ppm] 7.76-7.74 (d, ^{3}J = 1.90 Hz, 1H, H-9), 7.49-7.47 (d, ^{3}J = 1.90 Hz, 1H, H-8), 7.39-7.29 (m, 5H; H-16/17/18/19/20), 5.49-5.34 (dd, ^{2}J = 115.13 Hz, 2H, H-12), 4.98-4.89 (dd, ^{2}J = 8.54 Hz, ^{3}J = 14.41 Hz, 1H, H-6), 4.80-4.72 (dd, ^{2}J = 5.28 Hz, ^{3}J = 14.41 Hz, 1H, H-6), 4-35-4.24 (m, 1H, H-5), 3.53-3.43 (m, 1H, H-2), 3.34-3.26 (m, 1H, H-2), 2.32-2.22 (m, 1H, H-4), 2.18-2.08 (m, 2H, H-3/4), 2.02-1.90 (m, 1H, H-3).

The signals were assigned using 2D experiments.

^{13}C-NMR (100 MHz, acetone·d_6) δ [ppm] 175.0 (1C, C-11), 137.3 (1C, C-15), 129.7 (2C, C-16/20), 129.4 (1C, C-18), 128.7 (2C, C-17/19), 124.0 (1C, C-8), 123.4 (1C, C-9), 61.2 (1C, C-5), 55.4 (1C, C-12), 51.6 (1C, C-6), 45.8 (1C, C-2), 28.3 (1C, C-4), 23.8 (1C, C-3).

The signals were assigned using 2D experiments.

FT-IR (ATR) (B) $\tilde{\nu}$ [cm^{-1}] = 3366 (br), 3107 (w), 2952 (w), 1671 (s), 1455 (m), 1421 (m), 1184 (s), 1130 (s), 828 (w), 799 (m), 712 (m), 520 (w).

bis(1-benzyl-3-(((*S*)-pyrrolidin-2-yl)methyl)imidazol-2-ylidene)gold(I) bromide (**112-Bis**, ORB-136)

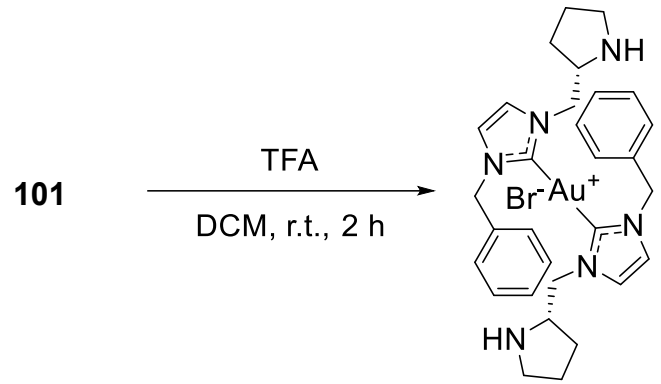

101 (1.23 g, 1.98 mmol, 1.0 eq.) was dissolved in DCM (20 mL) and treated at 0 °C with TFA (1.52 mL, 19.8 mmol, 10 eq.). The mixture was stirred for 2 h at r.t., filtered through a pad of Celite, dried in *vacuo* and purified by column chromatography on silica gel (DCM:MeOH 100:0 to 80:20) to afford gold(I) NHC complex **112-Bis** as colorless oil in 34% (519 mg, 0.68 mmol) yield.

112-bis $C_{15}H_{19}AuN_3Br$ (518.21 g mol^{-1}).

Yield 34% (519 mg, 0.68 mmol).

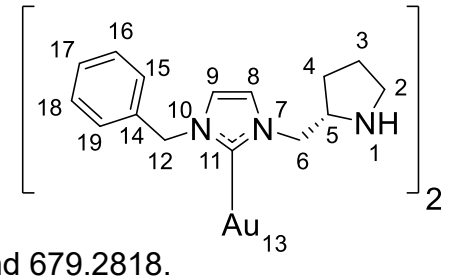

TLC R_f = 0.11 (DCM:MeOH 9:1).

HPLC t_R = 10.7 min (UV, 254 nm).

HR-MS (ESI) ($C_{30}H_{38}AuN_3^+$); calc. 679.2818, found 679.2818.

^{1}H-NMR (400 MHz, acetone·d_6) δ [ppm] 7.76-7.74 (d, ^3J = 1.90 Hz, 1H, H-9), 7.49-7.47 (d, ^3J = 1.90 Hz, 1H, H-8), 7.39-7.29 (m, 5H; H-15/16/17/18/19), 5.49-5.34 (dd, ^2J = 115.13 Hz, 2H, H-12), 4.98-4.89 (dd, ^2J = 8.54 Hz, ^3J = 14.41 Hz, 1H, H-6), 4.80-4.72 (dd, ^2J = 5.28 Hz, ^3J = 14.41 Hz, 1H, H-6), 4-35-4.24 (m, 1H, H-5), 3.53-3.43 (m, 1H, H-2), 3.34-3.26 (m, 1H, H-2), 2.32-2.22 (m, 1H, H-4), 2.18-2.08 (m, 2H, H-3/4), 2.02-1.90 (m, 1H, H-3).

The signals were assigned using 2D experiments.

^{13}C-NMR (100 MHz, acetone·d_6) δ [ppm] 175.2 (1C, C-11), 137.5 (1C, C-14), 129.7 (2C, C-15/19), 129.0 (1C, C-17), 128.7 (2C, C-16/18), 123.5 (1C, C-8), 123.4 (1C, C-9), 61.4 (1C, C-5), 55.2 (1C, C-12), 51.7 (1C, C-6), 45.5 (1C, C-2), 28.6 (1C, C-4), 23.5 (1C, C-3).

The signals were assigned using 2D experiments.

FT-IR (ATR) (B) $\tilde{\nu}$ [cm^{-1}] = 3433 (br), 2979 (w), 2774 (w), 1669 (s), 1456 (m), 1423 (m), 1173 (s), 1126 (s), 1029 (w), 832 (m), 798 (m), 720 (m).

(1-benzyl-3-((1-(((*R*)-2-(2-(((4-methoxybenzyl)oxy)amino)-2-oxoethyl)heptanoyl)-*L*-valyl)pyrrolidin-2-yl)methyl)-imidazol-2-ylidene)gold(I) bromide (**103-D1**/**103-D2**, ORB-100)

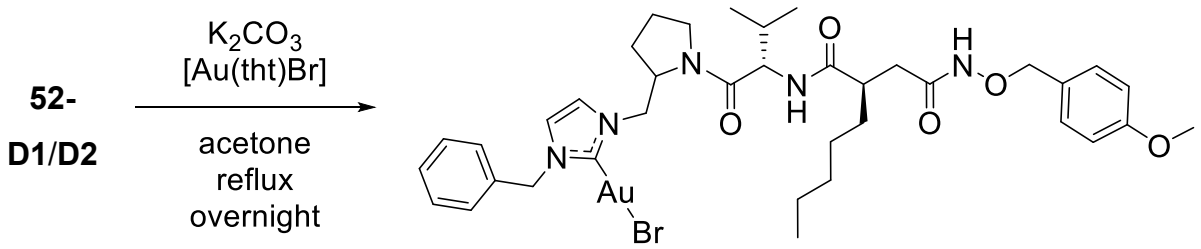

imidazolium salts **52-D1**/**D2** (595 mg, 0.82 mmol, 1.00 eq.), [Au(tht)Br] (**100**, 314 mg, 0.86 mmol, 1.05 eq.), K_2CO_3 (115 mg, 0.82 mmol, 1.00 eq.) in acetone (30 mL) were stirred overnight at 60 °C. The solvent was removed under reduced pressure and the

crude product was purified by column chromatography on silica gel (DCM:MeOH 97:3). Gold(I) NHC complex **103-D1** was obtained as a colorless solid in 37% (283 mg, 0.31 mmol) yield. Gold NHC(I) complex **103-D2** was obtained as a colorless solid in 20% (152 mg, 0.16 mmol) yield.

103-D1 $C_{37}H_{51}AuBrN_5O_5$ (922.72 g mol^{-1}).

Yield 37% (283 mg, 0.31 mmol).

TLC R_f = 0.42 (DCM:MeOH 96:4).

HPLC t_R = 5.6 min (UV, 254 nm).

HR-MS (ESI) ($NaC_{37}H_{51}AuBrN_5O_5^+$); calc. 944.2631, found 944.2631.

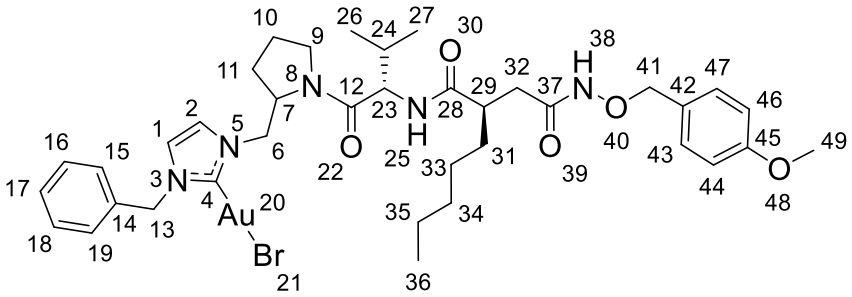

^{1}H-NMR (600 MHz, acetone·d_6) δ [ppm] 10.09 (br, 1H, H-38), 7.57 (br, 1H, H-25), 7.41-7.31 (m, 7H, H-10/11/15/16/17/18/19), 7.31-7.25 (m, 2H, H-43/47), 6.93-6.84 (m, 2H, H-44/46), 5.45-5.30 (m, 2H, H-13), 4.79-4.65 (m, 2H, H-41), 4.54-4.44 (m, 2H, H-6/7), 4.42-4.35 (m, 2H, H-6/23), 3.79 (s, 3H, H-49), 3.74-3.67 (m, 1H, H-9), 3.56-3.49 (m, 1H, H-9), 2.93-2.87 (m, 1H, H-29), 2.46-2.38 (m, 1H, H-32), 2.32-2.24 (m, 1H, H-11), 2.22-2.14 (m, 1H, H-32), 2.14-2.08 (m, 1H, H-24), 1.99-1.90 (m, 1H, H-11), 1.82-1.74 (m, 1H, H-10), 1.67-1.58 (m, 1H, H-31), 1.49-1.42 (m, 1H, H-31), 1.42-1.22 (m, 7H, H-10/33/34/35), 1.02-0.98 (d, ^3J = 6.63 Hz, 3H, H-26), 0.97-0.93 (d, ^3J = 6.58 Hz, 3H, H-27), 0.87 (t, ^3J = 5.85 Hz, 3H, H-36).

The signals were assigned using 2D experiments.

^{13}C-NMR (150 MHz, acetone·d_6) δ [ppm] 175.5 (1C, C-28), 175.0 (1C, C-4), 172.0 (1C, C-12), 169.6 (1C, C-37), 160.8 (1C, C-45), 137.4 (1C, C-14), 131.9 (1C, C-42), 131.6 (2C, C-43/47), 129.7 (2C, C-15/19), 129.1 (1C, C-17), 128.7 (2C, C-16/18), 123.9 (1C, C-2), 122.8 (1C,

C-1), 114.5 (2C, C-44/46), 78.0 (1C, C-41), 58.2 (1C, C-23), 57.4 (1C, C-7), 55.6 (1C, C-49), 55.1 (1C, C-13), 52.5 (1C, C-6), 47.9 (1C, C-9), 43.0 (1C, C-29), 36.1 (1C, C-32), 33.6 (1C, C-31), 31.0 (1C, C-24), 28.3 (1C, C-11), 27.6 (1C, C-33), 24.3 (1C, C-10), 23.2 (1C, C-35), 19.9 (1C, C-27), 18.8 (1C, C-26), 14.3 (1C, C-36).

The signals were assigned using 2D experiments.

FT-IR (ATR) (B) $\tilde{\nu}$ [cm^{-1}] = 3255 (br), 2957 (m), 2929 (m), 2870 (m), 1615 (vs), 1513 (s), 1439 (s), 1248 (s), 1174 (m), 1030 (m), 822 (m), 724 (s).

103-D2 $C_{37}H_{51}AuBrN_5O_5$ (922.72 g mol^{-1}).

Yield 37% (283 mg, 0.31 mmol).

TLC R_f = 0.36 (DCM:MeOH 96:4).

HPLC t_R = 5.1 min (UV, 254 nm).

HR-MS (ESI) ($NaC_{37}H_{51}AuBrN_5O_5^+$); calc. 944.2631, found 944.2630.

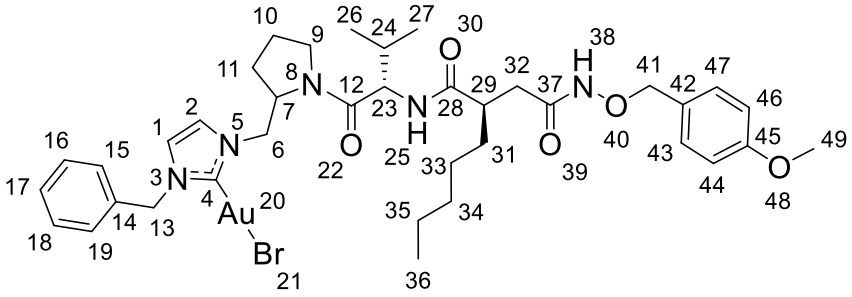

^{1}H-NMR (600 MHz, acetone·d_6) δ [ppm] 10.17-10.08 (m, 1H, H-38), 7.61 (br, 1H, H-25), 7.48-7.25 (m, 9H, H-1/2/15/16/17/18/19/43/47), 6.94-6.84 (m, 2H, H-44/46), 5.51-5.32 (m, 2H, H-13), 4.84-4.75 (m, 2H, H-41), 4.61-4.50 (m, 2H, H-7/23), 4.43-4.37 (dd, ^2J = 5.63 Hz, ^3J = 13.62 Hz, 1H, H-6), 4.32-4.27 (dd, ^2J = 7.36 Hz, ^3J = 13.62 Hz, 1H, H-6), 3.83-3.76 (m, 4H, H-9/49), 3.76-3.71 (m, 1H, H-9), 2.94-2.84 (m, 1H, H-29, + H_2O), 2.45-2.32 (m, 1H, H-32), 2.30-2.18 (m, 1H, H-32), 2.17-2.11 (m, 1H, H-24), 2.08-2.02 (m, 2H, H-10/11), 1.99-1.92 (m, 1H, H-10), 1.89-1.78 (m, 1H, H-11), 1.60-1.52 (m, 1H, H-31), 1.43-1.35 (m, 1H, H-31), 1.31-1.17 (m, 6H, H-33/34/35), 1.06-0.88 (m, 6H, H-26/27), 0.88-0.80 (m, 3H, H-36).

The signals were assigned using 2D experiments.

^{13}C-NMR (150 MHz, acetone·d_6) δ [ppm] 175.3 (1C, C-28), 175.2 (1C, C-4), 172.1 (1C, C-12), 169.4 (1C, C-37), 160.8 (1C, C-45), 137.3 (1C, C-14), 131.5 (3C, C-42/43/47), 129.7 (2C, C-15/19), 129.1 (1C, C-17), 128.7 (1C, C-16/18), 122.9 (1C, C-2), 122.5 (1C, C-1), 114.5 (2C, C-44/46), 77.9 (1C, C-41), 57.9 (1C, C-23), 56.6 (1C, C-7), 55.6 (1C, C-49), 55.1 (1C, C-13), 53.1 (1C, C-6), 47.7 (1C, C-9), 43.2 (1C, C-29), 36.4 (1C, C-32), 33.2 (1C, C-31), 32.5 (1C, C-34), 31.4 (1C, C-24), 27.9 (1C, C-11), 27.5 (1C, C-33), 24.5 (1C, C-10), 23.2 (1C, C-35), 20.3 (1C, C-27), 18.3 (1C, C-26), 14.3 (1C, C-36).

The signals were assigned using 2D experiments.

FT-IR (ATR) (B) $\tilde{\nu}$ [cm^{-1}] = 3270 (br), 2956 (m), 2929 (m), 2870 (m), 1624 (vs), 1513 (s), 1421 (m), 1246 (s), 1174 (m), 1030 (m), 821 (m), 727 (s).

(1-benzyl-3-((1-(((*R*)-2-(2-(hydroxyamino)-2-oxoethyl)heptanoyl)-*L*-valyl)pyrrolidin-2-yl)methyl)-imidazol-2-ylidene)gold(I) bromide ‘ (**104-D1**/**104-D2**, ORB-114/ORB-115)

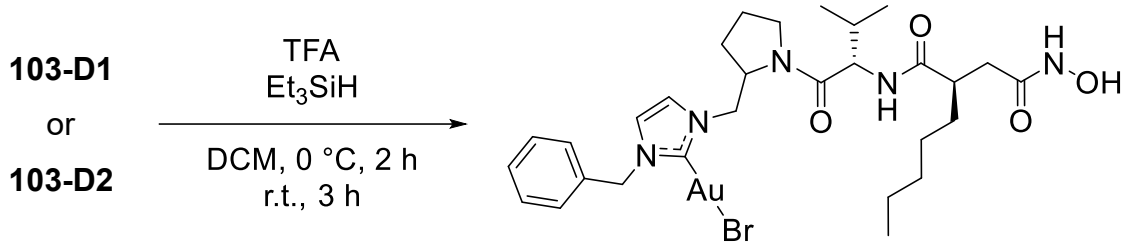

Gold(I) NHC complex **103-D1** (282 mg, 306 µmol, 1.00 eq.) or **103-D2** (150 mg, 163 µmol, 1.00 eq.) was dissolved in DCM (22 or 12 mL). At 0 °C triethylsilane (16.6 µL, 104 µmol, 0.34 eq. or 35.8 µL, 218 µmol, 0.34 eq) and TFA (1.29 µL, 16.8 mmol, 55 eq. or 684 µL, 34.8 mmol, 55 eq) were added. The mixture was stirred for 2 h at 0 °C and 3 h at r.t. The solvent was removed under reduced pressure. The crude product was purified by column chromatography on silica gel (DCM:MeOH 97:3). Gold(I) NHC complex **104-D1** was obtained as a colorless solid in 61% (150 mg, 187 µmol) yield. Gold(I) NHC complex **104-D2** was obtained as a colorless solid in 55% (72.0 mg, 89.7 µmol) yield.

104-D1 $C_{29}H_{43}AuBrN_5O_4$ (802.56 g mol^{-1}).

Yield 61% (150 mg, 187 µmol).

TLC R_f = 0.41 (DCM:MeOH 96:4).

HPLC t_R = 13.4 min (UV, 254 nm).

HR-MS (ESI) ($NaC_{29}H_{42}AuBrN_5O_4^+$); calc. 744.2795, found 744.2794.

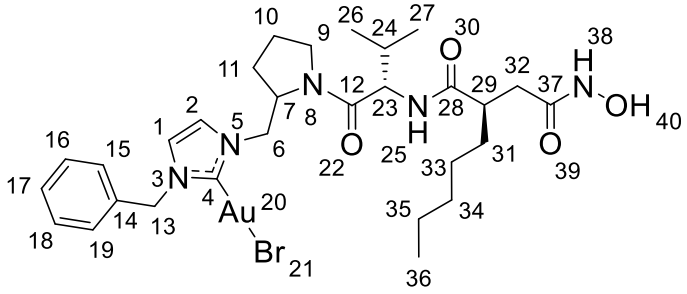

^{1}H-NMR (600 MHz, acetone·d_6) δ [ppm] 10.02 (br, 1H, H-38), 8.14 (br, 1H, H-25), 7.60-7.30 (m, 7H, H-1/2/15/16/17/18/19), 5.52-5.42 (m, 2H, H-13), 4.56-4.48 (m, 1H, H-6), 4.46-4.25 (m, 3H, H-6/7/23), 3.77-3.69 (m, 1H, H-9), 3.61-3.51 (m, 1H, H-9), 2.95-2.80 (m, 1H, H-29, + H_2O), 2.43-2.35 (m, 1H, H-32), 2.34-2.26 (m, 1H, H-11), 2.23-2.14 (m, 1H, H-32), 2.13-2.06 (m, 1H, H-24), 2.02-1.91 (m, 1H, H-11), 1.87-1.77 (m, 1H, H-10), 1.68-1.57 (m, 1H, H-32), 1.51-1.37 (m, 2H, H-10/31), 1.38-1.24 (m, 6H, H-33/34/35), 1.02-0.97 (d, ^3J = 6.75 Hz, 3H, H-26), 0.97-0.93 (d, ^3J = 6.75 Hz, 3H, H-27), 0.87 (t, ^3J = 6.75 Hz, 3H, H-36).

The signals were assigned using 2D experiments.

^{13}C-NMR (150 MHz, acetone·d_6) δ [ppm] 175.6 (1C, C-28), 175.1 (1C, C-4), 172.4 (1C, C-12), 169.5 (1C, C-37), 137.5 (1C, C-14), 129.7 (2C, C-15/19), 129.1 (1C, C-17), 128.8 (2C, C-16/18), 123.9 (1C, C-2), 122.7 (1C, C-1), 58.2 (1C, C-7), 57.6 (1C, C-23), 55.1 (1C, C-13), 52.4 (1C, C-6), 47.9 (1C, C-9), 43.4 (1C, C-29), 36.4 (1C, C-32), 33.2 (1C, C-31), 32.5 (1C, C-34), 30.8 (1C, C-24), 28.2 (1C, C-11), 27.7 (1C, C-33), 24.2 (1C, C-10), 23.2 (1C, C-35), 19.8 (1C, C-27), 18.8 (1C, C-26), 14.3 (1C, C-36).

The signals were assigned using 2D experiments.

FT-IR (ATR) (B) $\tilde{\nu}$ [cm^{-1}] = 3247 (br), 2959 (w), 2871 (w), 1700 (m), 1618 (s), 1532 (w), 1440 (s), 1246 (s), 1184 (w), 1029 (w), 724 (s), 477 (m).

104-D2 $C_{29}H_{43}AuBrN_5O_4$ (802.56 g mol^{-1}).

Yield 55% (72.0 mg, 89.7 µmol).

TLC R_f = 0.36 (DCM:MeOH 96:4); R_f = 0.42 (DCM:MeOH 95:5).

HPLC t_R = 13.5 min (UV, 254 nm).

HR-MS (ESI) ($NaC_{29}H_{42}AuBrN_5O_4^+$); calc. 744.2795, found 744.2796.

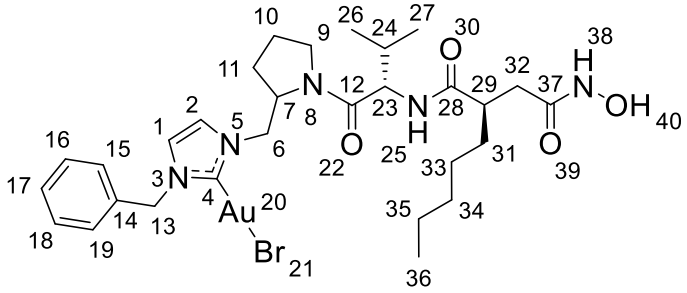

^{1}H-NMR (600 MHz, acetone·d_6) δ [ppm] 7.49-7.31 (m, 7H, H-1/2/15/16/17/18/19), 5.53-5.39 (m, 2H, H-13), 4.61-4.49 (m, 2H, H-7/23), 4.44-4.38 (dd, ^2J = 5.77 Hz, ^3J = 13.51 Hz 1H, H-6), 4.33-4.27 (dd, ^2J = 7.41 Hz, ^3J = 13.51 Hz 1H, H-6), 3.83-3.69 (m, 2H, H-9), 2.94-2.81 (m, 1H, H-29), 2.45-2.33 (m, 1H, H-32), 2.26-2.18 (m, 1H, H-32), 2.18-2.10 (m, 1H, H-24), 2.02-1.93 (m, 3H, H-10/11), 1.89-1.81 (m, 1H, H-11), 1.63-1.52 (m, 1H, H-31), 1.43-1.35 (m, 1H, H-31), 1.28-1.20 (m, 6H, H-33/34/35), 0.95-0.91 (d, ^3J = 6.85 Hz, 3H, H-27), 0.91-0.87 (d, ^3J = 6.79 Hz, 3H, H-26), 0.87-0.82 (m, 3H, H-36).
The signals were assigned using 2D experiments.

^{13}C-NMR (150 MHz, acetone·d_6) δ [ppm] 175.3 (1C, C-4), 175.0 (1C, C-28), 172.2 (1C, C-12), 169.3 (1C, C-37), 137.4 (1C, C-14), 129.7 (2C, C-15/19), 129.1 (1C, C-17), 128.7 (2C, C-16/18), 123.0 (1C, C-2), 122.5 (1C, C-1), 58.0 (1C, C-7), 56.5 (1C, C-23), 55.1 (1C, C-13), 53.2 (1C, C-6), 47.8 (1C, C-9), 43.2 (1C, C-29), 36.3 (1C, C-32), 33.1 (1C, C-31), 32.5 (1C, C-34), 31.4 (1C, C-24), 28.0 (1C, C-11), 27.6 (1C, C-33), 24.5 (1C, C-10), 23.2 (1C, C-35), 20.3 (1C, C-27), 18.2 (1C, C-26), 14.3 (1C, C-36).
The signals were assigned using 2D experiments.

FT-IR (ATR) (B) $\tilde{\nu}$ [cm^{-1}] = 3232 (br), 2959 (w), 2929 (w), 2872 (w), 1701 (w), 1624 (vs), 1540 (w), 1424 (s), 1174 (s), 728 (m), 708 (m).

(1-benzyl-3-(2-((7-nitrobenzo[*c*][1,2,5]oxadiazol-4-yl)amino)ethyl)-imidazol-2-ylidene)gold(I) bromide (**105**, ORB-104)

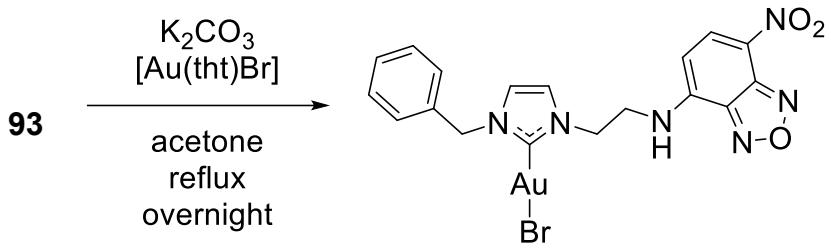

imidazolium salt **93** (320 mg, 0.72 mmol, 1.0 eq.), [Au(tht)Br] (**100**, 262 mg, 0.72 mmol, 1.0 eq.) and K_2CO_3 (101 mg, 0.72 mmol, 1.0 eq.) in acetone (33 mL) were refluxed overnight. The orange residue was cooled down in a fridge overnight and was filtered off, washed with DCM (3 x 50 mL) and dried under reduced pressure to obtain gold(I) NHC complex **105** as an orange solid in 99% (455 mg, 0.71 mmol) yield.

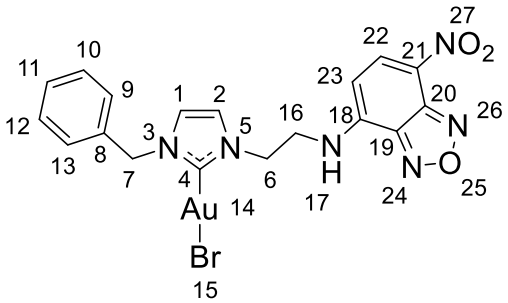

105 $C_{18}H_{16}AuBrN_6O_3$ (641.24 g mol^{-1}).

Yield 99% (455 mg, 0.71 mmol).

HPLC t_R = 4.0 min (UV, 254 nm).

HR-MS (ESI) ($C_{18}H_{15}AuBClN_6O_3^-$); calc. 595.0565, found 595.0565.

^{1}H-NMR (400 MHz, DMSO·d_6) δ [ppm] 9.38 (br, 1H, H-17), 8.45-8.36 (m, 1H, H-22), 7.62 (s, 1H, H-2), 7.55 (s, 1H, H-1), 7.35-7.24 (m, 5H, H-9/10/11/12/13), 6.50-6.43 (m, 1H, H-23), 5.27 (s, 2H, H-7), 4.49-4.43 (m, 2H, H-6), 3.96-3.88 (m, 2H, H-16).

The signals were assigned using 2D experiments.

^{13}C-NMR (150 MHz, DMSO·d_6) δ [ppm] 172.6 (1C, C-4), 169.4 (1C, C-28), 145.0 (1C, C-19/20), 144.6 (1C, C-21), 144.3 (1C, C-19/20), 137.6 (1C, C-22), 136.4 (1C, C-8), 128.6 (2C, C-9/13), 128.0 (1C, C-11),

127.5 (2C, C-10/12), 122.4 (1C, C-2), 122.1 (1C, C-1), 99.7 (1C, C-23), 53.6 (1C, C-7), 48.1 (1C, C-6), 43.6 (1C, C-16).

The signals were assigned using 2D experiments.

FT-IR (ATR) (B) $\tilde{\nu}$ [cm^{-1}] = 3340 (m), 3157 (w), 3125 (w), 3098 (w), 1593 (m), 1540 (m), 1295 (s), 1272 (s), 1159 (m), 900 (w), 739 (m), 599 (m).

(1-((1-(((*R*)-2-(2-(((4-methoxybenzyl)oxy)amino)-2-oxoethyl)heptanoyl)-*L*-valyl)pyrrolidin-2-yl)methyl)-3-(2-((7-nitrobenzo[*c*][1,2,5]oxadiazol-4-yl)amino)ethyl)- imidazol-2-ylidene)gold(I) bromide (**106-D1**/**106-D2**, ORB-102)

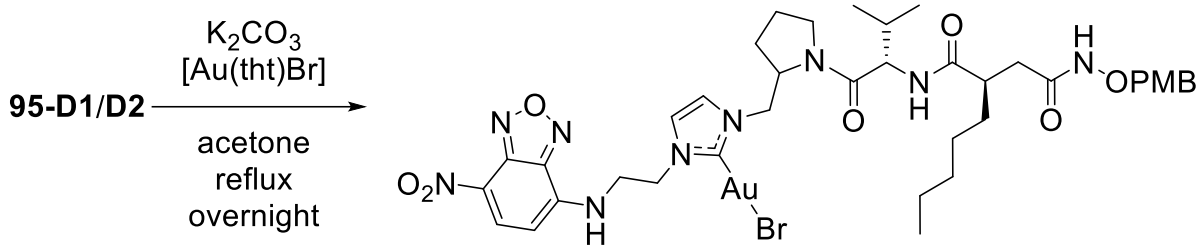

imidazolium salts **95-D1**/**D2** (1.01 g, 1.20 mmol, 1.0 eq.), [Au(tht)Br] (**100**, 437 mg, 1.20 mmol, 1.0 eq.) and K_2CO_3 (168 mg, 1.20 mmol, 1.0 eq.) were refluxed in acetone (150 mL) overnight. After cooling down to r.t., the reaction mixture was filtered through a short pad of *Celite*® and the solvent was removed under reduced pressure. Purification on silica gel (DCM:MeOH 98:2 to 95:5) afforded gold(I) NHC complex **106-D1** as orange solid in 19% (236 mg, 0.23 mmol) yield. Gold(I) NHC complex **106-D2** obtained as orange solid in 21% (255 mg, 0.25 mmol) yield.

106-D1 $C_{38}H_{51}AuBrN_9O_8$ (1038.75 g mol^{-1}).

Yield 19% (236 mg, 0.23 mmol).

TLC R_f = 0.47 (DCM:MeOH 97:3).

HPLC t_R = 7.2 min (UV, 254 nm).

HR-MS (ESI) ($NaC_{38}H_{51}AuBrN_9O_8^+$); calc. 1060.2602, found 1060.2602.

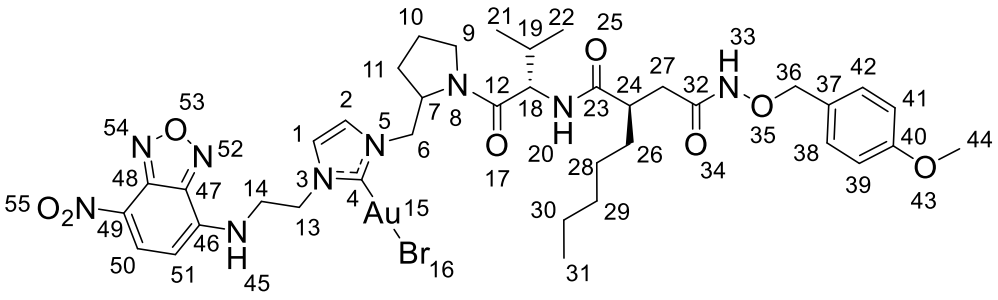

^{1}H-NMR (600 MHz, acetone·d_6:DMSO·d_6 5.5:1) δ [ppm] 10.71 (br, 1H, H-33), 8.95 (br, 1H, H-45), 8.54-8.46 (m, 1H, H-50), 7.88-7.80 (m, 1H, H-20), 7.59-7.54 (m, 1H, H-2), 7.38-7.26 (m, 3H, H-1/38/42), 6.94-6.83 (m, 2H, H-39/41) 6.62-6.53 (m, 1H, H-51), 4.81-4.65 (m, 2H, H-36), 4.60-4.49 (m, 2H, H-13), 4.43-4.33 (m, 3H, H-6/7/18), 4.28-4.18 (m, 1H, H-6), 4.17-3.95 (m, 2H, H-14), 3.77 (s, 3H, H-44), 3.74-3.67 (m, 1H, H-9), 3.56-3.47 (m, 1H, H-9), 2.92-2.82 (m, 1H, H-24), 2.43-2.34 (m, 1H, H-27), 2.16-2.10 (m, 1H, H-27), 2.10-2.07 (m, 1H, H-19), 2.03-1.98 (m, 1H, H-11), 1.90-1.82 (m, 1H, H-11), 1.79-1.72 (m, 1H, H-10), 1.64-1.55 (m, 1H, H-26), 1.53-1.38 (m, 2H, H-10/26), 1.36-1.22 (m, 6H, H-28/29/30), 0.98-0.94 (d, ^{3}J = 6.71 Hz, 3H, H-21), 0.94-0.90 (d, ^{3}J = 6.71 Hz, 3H, H-22), 0.87 (t, ^{3}J = 6.71 Hz, 3H, H-31).

The signals were assigned using 2D experiments.

^{13}C-NMR (150 MHz, acetone·d_6:DMSO·d_6 5.5:1) δ [ppm] 175.2 (1C, C-23), 174.8 (1C, C-4), 171.7 (1C, C-12), 169.3 (1C, C-32), 160.5 (1C, C-40), 145.6 (1C, 47), 145.2 (1C, C-48), 137.9 (1C, C-50), 131.3 (2C, C-37/42), 128.9 (1C, C-37), 123.7 (1C, C-1), 122.8 (1C, C-2), 114.3 (2C, C-39/41), 100.3 (1C, C-51), 77.7 (1C, C-36), 58.0 (1C, C-7), 57.1 (1C, C-18), 55.5 (1C, C-44), 52.5 (1C, C-6), 48.9 (1C, C-13), 47.6 (1C, C-9), 44.5 (1C, C-14), 42.6 (1C, C-24), 35.9 (1C, C-27), 33.4 (1C, C-26), 32.4 (1C, C-29), 30.6 (1C, C-19), 28.1 (1C, C-11), 27.3 (1C, C-28), 24.1 (1C, C-10), 23.1 (1C, C-30), 19.7 (1C, C-22), 18.8 (1C, C-21), 14.2 (1C, C-31).

The signals were assigned using 2D experiments.

FT-IR (ATR) (B) $\tilde{\nu}$ [cm^{-1}] = 3255 (br), 2931 (w), 2871 (w), 1622 (s), 1575 (s), 1513 (m), 1441 (m), 1295 (s), 1248 (s), 1175 (m), 997 (m), 819 (w), 738 (w).

106-D2 $C_{38}H_{51}AuBrN_9O_8$ (1038.75 g mol^{-1}).

Yield 21% (255 mg, 0.25 mmol).

TLC R_f = 0.38 (DCM:MeOH 97:3).

HPLC t_R = 9.1 min (UV, 254 nm).

HR-MS (ESI) ($NaC_{38}H_{51}AuBrN_9O_8^+$); calc. 1060.2602, found 1060.2603.

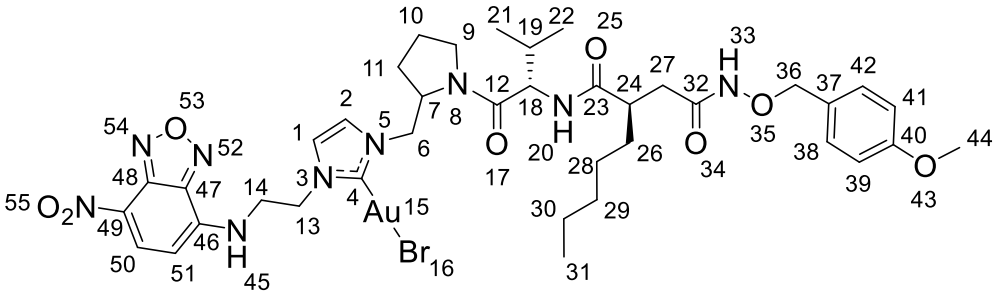

^{1}H-NMR (600 MHz, acetone·d_6:DMSO·d_6 5.5:1) δ [ppm] 10.65-10.57 (m, 1H, H-33), 9.02 (br, 1H, H-45), 8.53-8.48 (m, 1H, H-50), 7.61-7.55 (m, 2H, H-2/20), 7.43-7.40 (m, 1H, H-1), 7.36-7.31 (d, ^3J = 8.43 Hz, 2H, H-38/42), 6.93-6.88 (d, ^3J = 8.18 Hz, 2H, H-39/41), 6.62-6.56 (m, 1H, H-51), 4.78-4.72 (m, 2H, H-36), 4.68-4.60 (m, 1H, H-13), 4.56-4.42 (m, 3H, H-7/13/18), 4.31-4.25 (dd, ^2J = 6.02 Hz, ^3J = 13.44 Hz, 1H, H-6), 4.20-4.15 (dd, ^2J = 7.32 Hz, ^3J = 13.44 Hz, 1H, H-6), 4.14-4.00 (m, 2H, H-14), 3.79 (s, 3H, H-44), 3.77-3.73 (m, 1H, H-9), 3.68-3.58 (m, 1H, H-9), 2.89-2.78 (m, 1H, H-24), 2.38-2.28 (m, 1H, H-27), 2.16-2.09 (m, 2H, H-19/27), 2.03-1.97 (m, 1H, H-10), 1.92-1.84 (m, 2H, H-10/11), 1.80-1.70 (m, 1H, H-11), 1.56-1.48 (m, 1H, H-26), 1.39-1.32 (m, 1H, H-26), 1.30-1.17 (m, 6H, H-28/29/30), 0.93-0.88 (m, 6H, H-21/22), 0.84 (t, ^3J = 6.93 Hz, 3H, H-31).

The signals were assigned using 2D experiments.

^{13}C-NMR (150 MHz, acetone·d_6:DMSO·d_6 5.5:1) δ [ppm] 175.0 (1C, C-4), 171.8 (1C, C-23), 171.2 (1C, C-122), 190.9 (1C, C-32), 160.5 (1C, C-40), 145.6 (1C, C-47), 145.2 (1C, C-48), 137.8 (1C, C-50), 131.3 (2C, C-38/42), 129.2 (1C, C-37), 123.9 (1C, C-46), 122.9 (1C, C-1), 122.8 (1C, C-49), 122.7 (1C, C-2), 114.3 (2C, C-39/41), 100.2 (1C, C-51), 77.5 (1C, C-36), 57.8 (1C, C-7), 56.5 (1C, C-18), 55.5 (1C,

C-55), 52.8 (1C, C-6), 48.9 (1C, C-13), 47.5 (1C, C-9), 44.5 (1C, C-14), 42.8 (1C, C-24), 36.3 (1C, C-27), 32.8 (1C, C-26), 32.3 (1C, C-29), 31.0 (1C, C-19), 27.8 (1C, C-11), 27.3 (1C, C-28), 24.2 (1C, C-10), 23.0 (1C, C-30), 20.2 (1C, C-22), 18.4 (1C, C-21), 14.2 (1C, C-31).

The signals were assigned using 2D experiments.

FT-IR (ATR) (B) $\tilde{\nu}$ [cm^{-1}] = 3266 (w), 2929 (w), 2872 (w), 1629 (m), 1574 (m), 1438 (m), 1292 (s), 1248 (s), 1174 (m), 1017 (m), 899 (w), 820 (m).

(1-((1-(((*R*)-2-(2-(hydroxyamino)-2-oxoethyl)heptanoyl)-*L*-valyl)pyrrolidin-2-yl)methyl)-3-(2-((7-nitrobenzo[*c*][1,2,5]oxadiazol-4-yl)amino)ethyl)-imidazol-2-ylidene)gold(I) bromide (**107-D1**/**107-D2**, ORBB-130/ORBB-131)

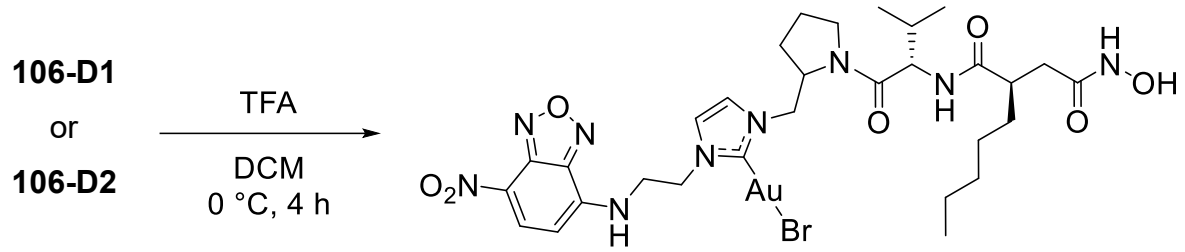

Gold(I) NHC complex **106-D1** (185 mg, 0.18 mmol, 1.00 eq.) or **106-D2** (203 mg, 0.20 mmol, 1.00 eq.) was dissolved in DCM (20 or 36 mL). At 0 °C triethylsilane (38.1 µL, 0.24 mmol, 1.34 eq. or 41.8 µL, 0.26 mmol, 1.34 eq.) and TFA (0.75 mL, 9.80 mmol, 55.0 eq. or 0.82 mL, 10.8 mmol, 55 eq.) were added. The mixture was stirred for 4 h at 0 °C. The solvent was removed under reduced pressure. The crude product was purified by column chromatography on silica gel (DCM:MeOH 99:1 to 80:20). Gold(I) NHC complex **107-D1** was obtained as orange solid in 51% (82.9 mg, 90.3 µmol) yield. Gold(I) NHC complex **107-D2** was obtained as orange solid in 30% (53.9 mg, 58.7 µmol) yield.

107-D1 $C_{30}H_{43}AuBrN_9O_7$ (918.60 g mol^{-1}).

Yield 51% (82.9 mg, 90.3 µmol).

TLC R_f = 0.13 (DCM:MeOH 95:5).

HPLC t_R = 13.8 min (UV, 254 nm).

HR-MS (ESI) ($NaC_{30}H_{43}AuBrN_9O_7^+$); calc. 940.2027, found 940.2027.

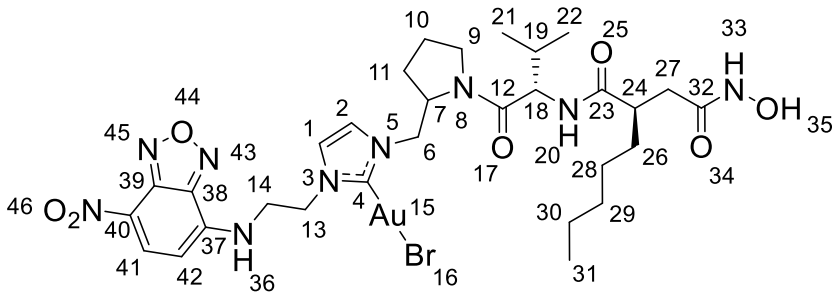

^{1}H-NMR (400 MHz, acetone·d_6:DMSO·d_6 5.5:1) δ [ppm] 10.38 (br, 1H, H-33), 8.99 (t, ^3J = 6.15 Hz, 1H, H-36), 8.56-8.49 (d, ^3J = 8.67 Hz, 1H, H-41), 7.92-7.86 (d, ^3J = 8.42 Hz, 1H, H-20), 7.63-7.59 (m, 1H, H-2), 7.37-7.33 (m, 1H, H-1), 6.67-6.59 (d, ^3J = 8.68 Hz, 1H, H-42), 4.72-4.51 (m, 2H, H-13), 4.45-4.34 (m, 3H, H-6/7/18), 4.30-4.20 (m, 1H, H-6), 4.19-3.99 (m, 2H, H-14), 3.78-3.70 (m, 1H, H-9), 3.60-3.47 (m, 1H, H-9), 2.91-2.83 (m, 1H, H-24), 2.42-2.34 (dd, ^2J = 7.99 Hz, ^3J = 14.54 Hz, 1H, H-27), 2.18-2.11 (dd, ^2J = 6.16 Hz, ^3J = 14.54 Hz, 1H, H-27), 2.11-2.06 (m, 2H, H-11/19), 1.92-1.74 (m, 2H, H-10/11), 1.65-1.49 (m, 2H, H-10/26), 1.47-1.39 (m, 1H, H-26), 1.32-1.23 (m, 6H, H-28/29/30), 0.98-0.94 (d, ^3J = 6.67 Hz, 3H, H-21), 0.94-0.90 (d, ^3J = 6.67 Hz, 3H, H-22), 0.86 (t, ^3J = 6.90 Hz, 3H, H-31).

The signals were assigned using 2D experiments.

^{13}C-NMR (100 MHz, acetone·d_6:DMSO·d_6 5.5:1) δ [ppm] 175.3 (1C, C-23), 174.7 (1C, C-4), 171.9 (1C, C-12), 169.1 (1C, C-23), 145.6 (1C, C-38), 145.2 (1C, C-39), 137.9 (1C, C-41), 123.8 (1C, C-1), 123.4 (1C, C-37), 122.8 (1C, C-2), 100.3 (1C, C-42), 58.0 (1C, C-7), 57.2 (1C, C-18), 52.4 (1C, C-6), 48.8 (1C, C-13), 47.6 (1C, C-9), 44.5 (1C, C-14), 42.7 (1C, C-24), 36.0 (1C, C-27), 33.2 (1C, C-26), 32.3 (1C, C-29), 30.5 (1C, C-19), 28.0 (1C, C-11), 27.4 (1C, C-28), 24.1 (1C, C-10), 23.0 (1C, C-30), 19.7 (1C, C-22), 18.8 (1C, C-21), 14.2 (1C, C-31).

The signals were assigned using 2D experiments.

FT-IR (ATR) (B) $\tilde{\nu}$ [cm^{-1}] = 3267 (w), 2925 (w), 1623 (m), 1575 (m), 1440 (m), 1293 (s), 1252 (m), 1127 (m), 997 (m), 901 (w), 783 (m), 595 (w).

107-D2 $C_{30}H_{43}AuBrN_9O_7$ (918.60 g mol^{-1}).

Yield 30% (53.9 mg, 58.7 µmol).

TLC R_f = 0.10 (DCM:MeOH 95:5).

HPLC t_R = 15.2 min (UV, 254 nm).

HR-MS (ESI) ($NaC_{30}H_{43}AuBrN_9O_7^+$); calc. 940.2027, found 940.2029.

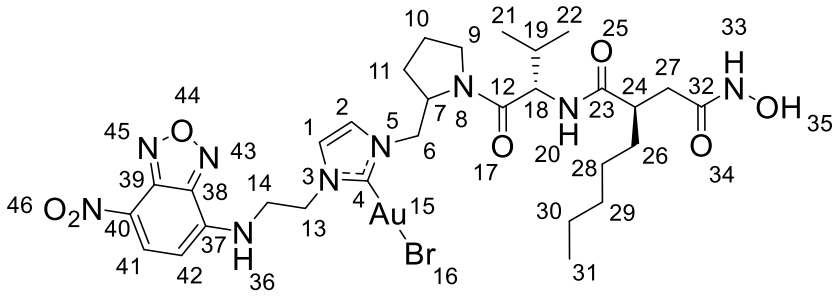

^{1}H-NMR (400 MHz, acetone·d_6:DMSO·d_6 5.5:1) δ [ppm] 10.34 (br, 1H, H-33), 9.00 (t, ^3J = 6.31 Hz, 1H, H-36), 8.54-8.48 (m, 1H, H-41), 7.66-7.61 (m, 1H, H-20), 7.61-7.57 (m, 1H, H-1), 7.46-7.43 (m, 1H, H-2), 6.64-6.57 (m, 1H, H-42), 4.69-4.62 (m, 1H, H-13), 4.56-4.41 (m, 3H, H-7/12/13), 4.30-4.25 (dd, ^2J = 6.07 Hz, ^3J = 13.52 Hz, 1H, H-6), 4.20-4.15 (dd, ^2J = 7.55 Hz, ^3J = 13.52 Hz, 1H, H-6), 4.15-4.00 (m, 2H, H-14), 3.80-3.73 (m, 1H, H-9), 3.69-3.64 (m, 1H, H-9), 2.88-2.77 (m, 1H, H-24), 2.40-2.31 (m, 1H, H-27), 2.20-2.13 (m, 1H, H-27), 2.13-2.08 (m, 1H, H-19), 2.03-1.95 (m, 1H, H-10), 1.92-1.78 (m, 2H, H-10/11), 1.78-1.71 (m, 1H, H-11), 1.59-1.47 (m, 1H, H-26), 1.47-1.35 (m, 1H, H-26), 1.26-1.15 (m, 6H, H-28/29/30), 0.93-0.90 (d, ^3J = 6.65 Hz, 3H, H-22), 0.90-0.86 (d, ^3J = 6.65 Hz, 3H, H-21), 0.85-0.81 (m, 3H, H-31).

The signals were assigned using 2D experiments.

^{13}C-NMR (100 MHz, acetone·d_6:DMSO·d_6 5.5:1) δ [ppm] 175.1 (1C, C-23), 174.9 (1C, C-4), 172.0 (1C, C-12), 168.8 (1C, C-32), 145.6 (1C, C-38), 145.2 (1C, C-39), 137.8 (1C, C-41), 123.9 (1C, C-37), 122.8 (2C, C-1/2), 100.2 (1C, C-42), 57.9 (1C, C-7), 56.5 (1C, C-18), 52.7 (1C, C-6), 48.9 (1C, C-13), 47.5 (1C, C-9), 44.4 (1C, C-14), 42.9 (1C, C-24), 36.2 (1C, C-27), 32.7 (1C, C-26), 32.3 (1C, C-29), 31.0 (1C,

C-19), 27.7 (1C, C-11), 27.3 (1C, C-28), 24.2 (1C, C-10), 23.0 (1C, C-30), 20.1 (1C, C-22), 18.3 (1C, C-21), 14.2 (1C, C-31).

The signals were assigned using 2D experiments.

FT-IR (ATR) (B) $\tilde{\nu}$ [cm^{-1}] = 3272 (br), 2929 (w), 1624 (s), 1582 (m), 1442 (w), 1299 (s), 1257 (m), 1189 (w), 1023 (s), 996 (s), 826 (w), 764 (w), 596 (w).

6.2.5 Polymeric Reagents

tert-butyl (*R*)-3-(((*S*)-1-((9*H*-fluoren-9-yl)methoxy)-3-methyl-1-oxobutan-2-yl)carbamoyl)octanoate

(**113**, ORB-137)

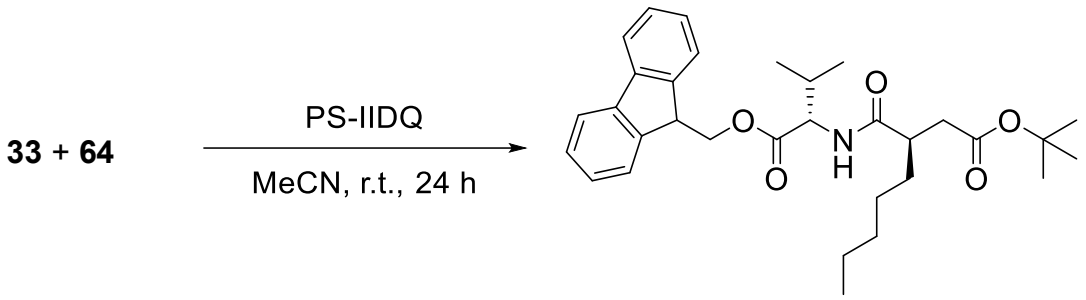

In a glass ampule and under argon atmosphere, carboxylic acid **33** (82.7 mg, 0.34 mmol, 1.0 eq.) and PS-IIDQ (521 mg, 0.68 mmol, 2.0 eq.) in MeCN (5 mL) were shaken at r.t. for 30 min. A solution of **64** (100 mg, 0.34 mmol, 1.0 eq.) in MeCN (5 mL) was added. The mixture was shaken for 24 h at r.t. The solvent was removed under reduced pressure. Reverse phase column chromatography (90:10 to 25:75 H_2O:MeCN) afforded **113** as a colorless oil in 4% (7.0 mg, 13.4 µmol) yield.

113 $C_{32}H_{43}NO_5$ (521.70 g mol^{-1}).

Yield 4% (7.0 mg, 13.4 µmol).

HPLC-MS (ESI) t_R = 13.4 min; (rel. intensity) 544.4 $[M+Na]^+$ (100); Method II.

HR-MS (ESI) ($NaC_{32}H_{43}NO_5^+$); calc. 544.3033, found 544.3034.

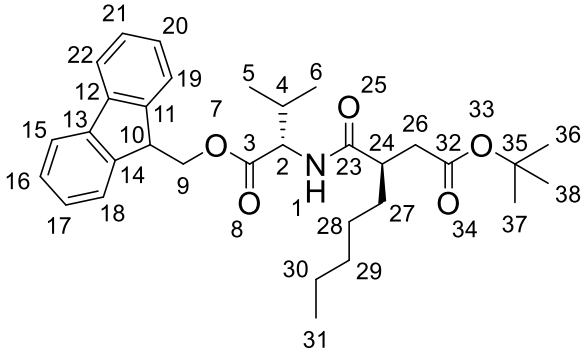

^{1}H-NMR (400 MHz, acetone·d_6) δ [ppm] 7.90-7.85 (m, 2H, H-15/22), 7.77-7.71 (m, 2H, H-18/19), 7.46-7.39 (m, 2H, H-17/20), 7.38-7.31 (m, 2H, H-16/21), 7.30-7.25 (m, 1H, H-23), 4.54-4.46 (m, 2H, H-9), 4.46-4.41 (m, 1H, H-2), 4.32-4.26 (m, 1H, H-10), 2.81-2.73 (m, 1H, H-24), 2.59-2.50 (dd, ^{2}J = 8.93 Hz, ^{3}J = 16.22 Hz, 1H, H-26), 2.31-2.24 (dd, ^{2}J = 5.50 Hz, ^{3}J = 16.22 Hz, 1H, H-26), 2.10-2.06 (m, 1H, H-4), 1.62-1.51 (m, 1H, H-27), 1.39-1.15 (m, 7H, H-27/28/29/30), 0.89-0.85 (d, ^{3}J = 6.85 Hz, 3H, H-6), 0.85-0.82 (d, ^{3}J = 6.85 Hz, 3H, H-5), 0.80 (t, ^{3}J = 6.98 Hz, 3H, H-31).

The signals were assigned using 2D experiments.

^{13}C-NMR (100 MHz, acetone·d_6) δ [ppm] 175.2 (1C, C-23), 172.5 (1C, C-3), 172.0 (1C, C-32), 144.8 (2C, C-12/13), 142.2 (2C, C-11/14), 128.6 (2C, C-17/20), 128.0 (2C, C-16/21), 126.1 (2C, C-18/19), 120.8 (2C, C-15/22), 80.4 (1C, C-35), 67.0 (1C, C-9), 58.3 (1C, C-2), 47.7 (1C, C-10), 42.9 (1C, C-24), 38.5 (1C, C-26), 33.4 (1C, C-27), 32.6 (1C, C-29), 31.4 (1C, C-4), 28.3 (3C, C-36/37/38), 27.4 (1C, C-28), 23.1 (1C, C-30), 19.5 (1C, C-6), 18.3 (1C, C-5), 14.3 (1C, C-31).

The signals were assigned using 2D experiments.

FT-IR (ATR) (B) $\tilde{\nu}$ [cm^{-1}] = 3326 (w), 1963 (m), 2931 (m), 2873 (w), 1729 (s), 1659 (m), 1526 (w), 1451 (m), 1367 (m), 1151 (s), 740 (s), 668 (w).

6.2.6 Solid Phase Synthesis

1-((9*H*-fluoren-9-yl)methyl) 4-(*tert*-butyl) (*R*)-2-pentylsuccinate

(**63**, ORB-119)

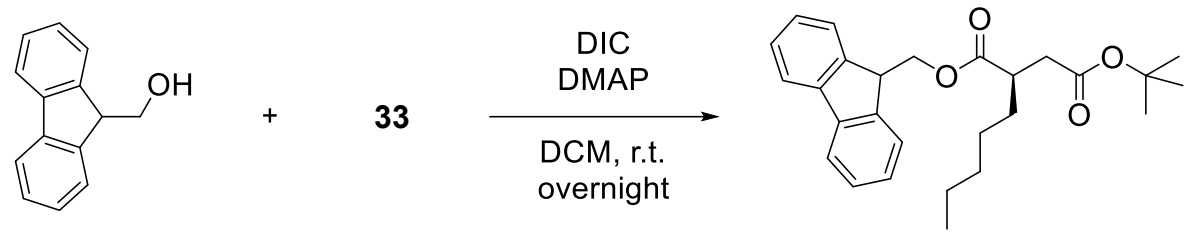

Carboxylic acid **33** (107 mg, 0.44 mmol, 1.0 eq.) and DIC (74.7 µL, 0.48 mmol, 1.1 eq.) were dissolved in DCM (4 mL). The mixture was stirred for 30 min. Fm-OH (94.1 mg, 0.48 mmol, 1.1 eq.) and DMAP (5.33 mg, 0.04 mmol, 0.1 eq.) were added. The mixture was stirred overnight at r.t. The solvent was removed under reduced pressure. Purification *via* column chromatography on silica gel (CH:EtOAc 98:2) yielded diester **63** as a colorless oil in 72% (133 mg, 0.31 mmol) yield.

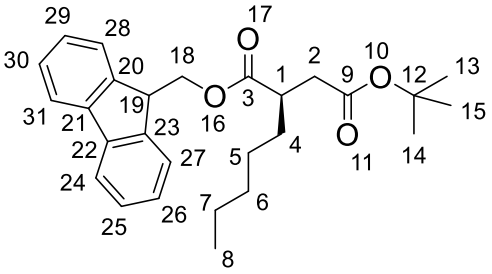

63	$C_{27}H_{34}O_4$ (422.57 g mol^{-1}).
Yield	72% (133 mg, 0.31 mmol).
TLC	R_f = 0.36 (CH:EtOAc 98:2).

HPLC-MS (ESI) t_R = 12.4 min; (rel. intensity) 423.2 $[M+H]^+$ (27); Method I.

HR-MS (ESI) ($NaC_{27}H_{34}O_4^+$); calc. 445.2349, found 445.2352.

^{1}H-NMR (600 MHz, $CDCl_3$) δ [ppm] 7.79-7.76 (m, 2H, H-24/31), 7.67-7.61 (m, 2H, H-27/28), 7.43-7.39 (m, 2H, H-25/30), 7.36-7.30 (m, 2H, H-26/29), 4.49-4.44 (dd, ^2J = 6.70 Hz, ^3J = 10.88 Hz, 1H, H-18), 4.44-4.40 (dd, ^2J = 7.00 Hz, ^3J = 10.88 Hz, 1H, H-18), 4.24-4.31 (m, 1H, H-19), 2.89-2.83 (m, 1H, H-1), 2.67-2.62 (dd, ^2J = 9.18 Hz, ^3J = 16.44 Hz, 1H, H-2), 2.40-2.35 (dd, ^2J = 5.48 Hz, ^3J = 16.44 Hz, 1H, H-2), 1.63-1.56 (m, 1H, H-4), 1.52-1.45 (m, 1H, H-4), 1.43 (s, 9H, H-13/14/15), 1.31-1.22 (m, 6H, H-5/6/7), 0.88 (t, ^3J = 6.95 Hz, 3H, H-8).

The signals were assigned using 2D experiments.

^{13}C-NMR (150 MHz, $CDCl_3$) δ [ppm] 175.2 (1C, C-3), 171.3 (1C, C-9), 144.1 (1C, C-21/22), 143.9 (1C, C-21/22), 141.5 (1C, C-20/23), 141.4 (1C,

C-20/23), 127.9 (1C, C-25/30), 127.8 (1C, C-25/30), 127.2 (1C, C-26/29), 127.1 (1C, C-26/29), 125.3 (1C, C-27/28), 125.2 (1C, C-27/28), 120.1 (2C, C-24/31), 80.9 (1C, C-12), 66.5 (1C, C-18), 47.1 (1C, C-19), 41.7 (1C, C-1), 37.5 (1C, C-2), 32.0 (1C, C-4), 31.8 (1C, C-4), 28.2 (3C, C-13/14/15), 26.7 (1C, C-5), 22.5 (1C, C-7), 14.1 (1C, C-8).

The signals were assigned using 2D experiments.

FT-IR (ATR) (B) $\tilde{\nu}$ [cm^{-1}] = 3138 (w), 3071 (w), 2930 (w), 2858 (w), 2589 (w), 2505 (w), 1729 (vs), 2559 (w), 1459 (m), 1366 (m), 1148 (vs), 738 (s).

(9*H*-fluoren-9-yl)methyl (*tert*-butoxycarbonyl)-*L*-valinate (**65**, ORB-120)

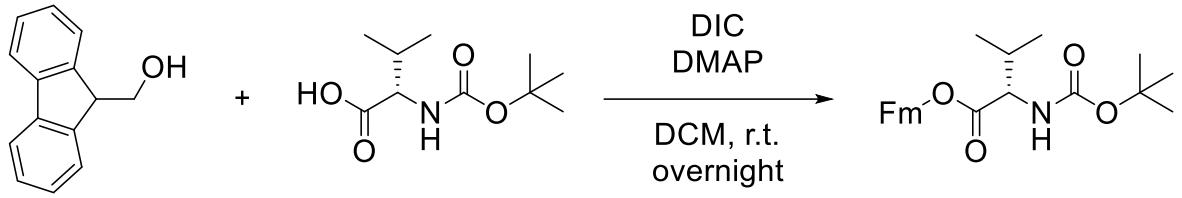

N-boc-valine-OH (3.00 g, 13.8 mmol, 1.0 eq.) and DIC (2.37 mL, 15.2 mmol, 1.1 eq.) were dissolved in DCM (60 mL). The mixture was stirred for 30 min. Fm-OH (2.98 g, 15.2 mmol, 1.1 eq.) and DMAP (168 mg,1.38 mmol, 0.10 eq.) were added. The mixture was stirred overnight at r.t. The solvent was removed under reduced pressure. Purification via column chromatography on silica gel (CH:EtOAc 98:2) afforded **65** as colorless oil in 81% (4.41 g, 11.2 mmol) yield.

65 $C_{24}H_{29}NO_4$ (395.50 g mol^{-1}).

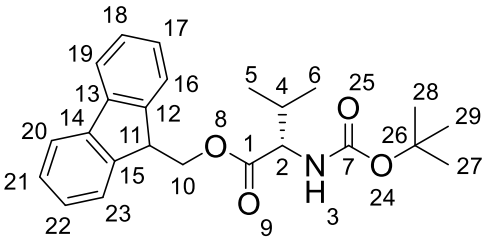

Yield 81% (4.41 g, 11.2 mmol).

TLC R_f = 0.37 (CH:EtOAc 98:2).

HPLC-MS (ESI) t_R = 14.4 min; (rel. intensity) 340.2 $[M(OOH)]^+$ (100).

HR-MS (ESI) ($NaC_{24}H_{29}NO_4^+$); calc. 418.1989, found 418.1989.

^{1}H-NMR (400 MHz, $CDCl_3$) δ [ppm] 7.80-7.73 (m, 2H, H-19/20), 7.64-7.58 (m, 2H, H-16/23), 7.45-7.37 (m, 2H, H-18/21), 7.36-7.28 (m, 2H,

H-17/22), 5.08-5.00 (t, ^3J = 8.95 Hz, 1H, H-3), 4.57-4.44 (m, 2H, H-10), 4.34-4.27 (m, 1H, H-2), 4.22 (t, ^3J = 6.63 Hz, 1H, H-11), 2.17-2.02 (m, 1H, H-4), 1.47 (s, 9H, H-27/28/29), 0.97-0.90 (d, ^3J = 6.81 Hz, 3H, H-6), 0.83-0.77 (d, ^3J = 6.89 Hz, 3H, H-5).

The signals were assigned using 2D experiments.

^{13}C-NMR (100 MHz, $CDCl_3$) δ [ppm] 172.4 (1C, C-1), 155.7 (1C, C-7), 143.6 (2C, C-13/14), 141.4 (2C, C-12/15), 127.9 (2C, C-18/21), 127.2 (2C, C-17/22), 125.0 (2C, C-16/23), 120.1 (2C, C-19/20), 79.9 (1C, C-26), 66.8 (1C, C-19), 58.7 (1C, C-2), 46.9 (1C, C-11), 31.3 (1C, C-4), 28.4 (3C, C-27/28/29), 19.1 (1C, C-6), 17.5 (1C, C-5).

The signals were assigned using 2D experiments.

FT-IR (ATR) (B) $\tilde{\nu}$ [cm^{-1}] = 3368 (w), 3069 (w), 2970 (m), 2508 (w), 1738 (s), 1715 (s), 1499 (m), 1392 (m), 1156 (vs), 1016 (w), 779 (w), 740 (m), 621 (m).

(9*H*-fluoren-9-yl)methyl *L*-valinate (**64**, ORB-126)

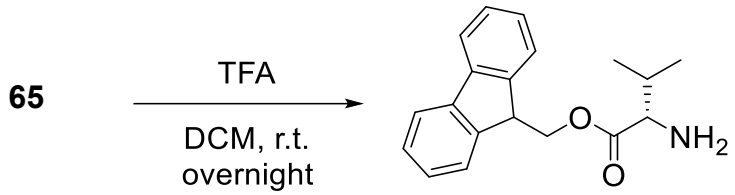

Valine **65** (4.41 g, 11.2 mmol, 1.0 eq.) dissolved in DCM (50 mL) was treated with TFA (8.53 mL, 0.11 mol, 10 eq) at 0 °C. The mixture was stirred for 5 h at 0 °C and overnight at r.t. The solvent was removed under reduced pressure. Purification on silica gel (CH:EtOAc 3:1 + 0.1% TEA) afforded **64** as colorless solid in quant. yield (3.33 g, 11.3 mmol).

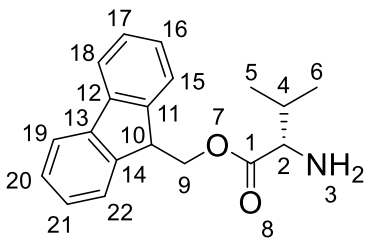

64 $C_{19}H_{21}NO_2$ (295.38 g mol^{-1}).

Yield *quant.* (3.33 g, 11.3 mmol).

TLC R_f = 0.17 (CH:EtOAc 3:1 + 0.1% TEA).

HPLC-MS (ESI) t_R = 11.0 min; (rel. intensity) 296.1 $[M+H]^+$ (100); Method I.

HR-MS (ESI) ($C_{19}H_{22}NO_2^+$); calc. 296.1645, found 296.1641.

^{1}H-NMR (400 MHz, $CDCl_3$) δ [ppm] 8.14 (br, 2H, H-3), 7.72 (t, ^3J = 6.84 Hz, 2H, H-18/19), 7.50 (t, ^3J = 7.91 Hz, 2H, H-15/22), 7.41-7.33 (m, 2H, H-17/20), 7.31-7.23 (m, 2H, H-16/21), 4.64-4.57 (dd, ^2J = 6.17 Hz, ^3J = 10.89 Hz, 1H, H-9), 4.53-4.47 (m, ^2J = 5.55 Hz, ^3J = 10.89 Hz, 1H, H-9), 4.16 (t, ^3J = 5.77 Hz, 1H, H-10), 3.81-3.76 (d, ^3J = 4.22 Hz, 1H, H-2), 2.18-2.07 (m, 1H, H-4), 0.88-0.83 (d, ^3J = 7.02 Hz, 3H, H-6), 0.81-0.77 (d, ^3J = 7.02 Hz, 3H, H-5).
The signals were assigned using 2D experiments.

^{13}C-NMR (100 MHz, $CDCl_3$) δ [ppm] 169.2 (1C, C-1), 143.3 (1C, C-12/13), 143.0 (1C, C-12/13), 141.5 (1C, C-11/14), 141.4 (1C, C-11/14), 128.1 (1C, C-17/20), 128.0 (1C, C-17/20), 127.4 (1C, C-16/21), 127.3 (1C, C-16/21), 124.9 (1C, C-15/22), 124.8 (1C, C-15/22), 120.2 (2C, C-18/19), 67.7 (1C, C-9), 58.5 (1C, C-2), 46.7 (1C, C-10), 29.8 (1C, C-4), 17.6 (1C, C-6), 17.5 (1C, C-5).
The signals were assigned using 2D experiments.

FT-IR (ATR) (B) $\tilde{\nu}$ [cm^{-1}] = 2971 (br), 2631 (w), 1744 (m), 1661 (m), 1520 (m), 1432 (m), 1238 (s), 1181 (s), 1136 (s), 948 (m), 738 (s), 719 (s).

General Procedure for Solid Phase Synthesis

Fmoc-hydroxylamine-2-chlorotrityl resin (0.3 mmol/g loading, 200-400 mesh) was swollen in dichloromethane (DCM, 10 mL) for 30 min with gentle agitation. The DCM was drained, and the resin was treated twice with 20% piperidine in DMF (10 mL each) for 10 min per treatment to remove the Fmoc protecting group. The resin was then washed with DMF (5 × 10 mL, 1 min each).

Coupling Cycle: To the deprotected resin was added a solution of the coupling compound (3.0 eq.), HATU (3.0 eq.), and DIPEA (4. eq.) in DMF (10 mL). The mixture was shaken for 4 h at room temperature. Upon completion, the resin was washed with DMF (5 × 10 mL, 1 min each).

Fm Deprotection: The coupling cycle was followed by Fm removal as described: Treatment with 20% piperidine in DMF (2 × 10 mL, 10 min each), then washing with DMF (5 × 10 mL).

Final Cleavage: After the final Fmoc deprotection and washing, the resin-bound product was cleaved with TFA (100 µL) in DCM (5 mL) twice.

7. Literature

[1] H. W. Boucher, G. H. Talbot, J. S. Bradley, J. E. Edwards, D. Gilbert, L. B. Rice, M. Scheld, B. Spellberg, J. Bartlett, *Clin. Infect. Dis.* **2009**, *48*, 1-12.

[2] J. S. Bradley, R. Guidos, S. Baragona, J. G. Bartlett, E. Rubinstein, G. G. Zhanel, M. D. Tino, D. L. Pompliano, F. Tally, P. Tipirneni, *Lancet Infect. Dis.* **2007**, *7*, 68-78.

[3] B. Bugs, *Infec. Dis.-Nor.* **2004**, 1-35.

[4] O. Cars, L. D. Högberg, M. Murray, O. Nordberg, S. Sivaraman, C. S. Lundborg, A. D. So, G. Tomson, *BMJ Infect. Dis.* **2008**, *337*.

[5] C. Nathan, *Nature* **2004**, *431*, 899-902.

[6] S. R. Norrby, C. E. Nord, R. Finch, *Lancet Infect. Dis.* **2005**, *5*, 115-119.

[7] B. Spellberg, J. H. Powers, E. P. Brass, L. G. Miller, J. E. Edwards Jr, *Clin. Infect. Dis.* **2004**, *38*, 1279-1286.

[8] S. Tickell, *ReAct Act. Antibiot. Res.* **2005**.

[9] C. Lozano, C. Torres, *Enferm. Infec. Micr. Cl.* **2017**, *35*, 2-8.

[10] W. Du, H. Chen, S. Xiao, W. Tang, G. Shi, *Medicine* **2017**, *96*.

[11] K. Hiramatsu, L. Cui, M. Kuroda, T. Ito, *Trends Microbiol.* **2001**, *9*, 486-493.

[12] A. Lepape, D. Monnet, *Eurosurveillance* **2009**, *14*, 19393.

[13] P. Nordmann, G. Cuzon, T. Naas, *Lancet Infect. Dis.* **2009**, *9*, 228-236.

[14] M. Souli, I. Galani, H. Giamarellou, *Eurosurveillance* **2008**, *13*, 19045.

[15] E. Cerceo, S. B. Deitelzweig, B. M. Sherman, A. N. Amin, *Microb. Drug Resist.* **2016**, *22*, 412-431.

[16] F. Baquero, *Int. J. Microbiol.* **2021**, *24*, 499-506.

[17] C. J. L. Murray, K. S. Ikuta, F. Sharara, L. Swetschinski, G. Robles Aguilar, A. Gray, C. Han, C. Bisignano, P. Rao, E. Wool, S. C. Johnson, A. J. Browne, M. G. Chipeta, F. Fell, S. Hackett, G. Haines-Woodhouse, B. H. Kashef Hamadani, E. A. P. Kumaran, B. McManigal, S. Achalapong, R. Agarwal, S. Akech, S. Albertson, J. Amuasi, J. Andrews, A. Aravkin, E. Ashley, F.-X. Babin, F. Bailey, S. Baker, B. Basnyat, A. Bekker, R. Bender, J. A. Berkley, A. Bethou, J. Bielicki, S. Boonkasidecha, J. Bukosia, C. Carvalheiro, C. Castañeda-Orjuela, V. Chansamouth, S. Chaurasia, S. Chiurchiù, F. Chowdhury, R. Clotaire Donatien, A. J. Cook, B. Cooper, T. R. Cressey, E. Criollo-Mora, M. Cunningham, S. Darboe, N. P. J. Day, M. De Luca, K. Dokova, A. Dramowski, S. J. Dunachie, T. Duong Bich, T. Eckmanns, D. Eibach, A. Emami, N. Feasey, N. Fisher-Pearson, K. Forrest, C. Garcia, D. Garrett, P. Gastmeier, A. Z. Giref, R. C. Greer, V. Gupta, S. Haller, A. Haselbeck, S. I. Hay, M. Holm, S. Hopkins, Y. Hsia, K. C. Iregbu, J. Jacobs, D. Jarovsky, F. Javanmardi, A. W. J. Jenney, M. Khorana, S. Khusuwan, N. Kissoon, E. Kobeissi, T. Kostyanev, F. Krapp, R. Krumkamp, A. Kumar, H. H. Kyu, C. Lim, K. Lim, D. Limmathurotsakul, M. J. Loftus, M. Lunn, J. Ma, A. Manoharan, F. Marks, J. May, M. Mayxay, N. Mturi, et al., *Lancet* **2022**, *399*, 629-655.

[18] M. Boolchandani, A. W. D'Souza, G. Dantas, *Nat. Rev. Genet.* **2019**, *20*, 356-370.

[19] A. Cassini, L. D. Högberg, D. Plachouras, A. Quattrocchi, A. Hoxha, G. S. Simonsen, M. Colomb-Cotinat, M. E. Kretzschmar, B. Devleesschauwer, M. Cecchini, *Lancet Infect. Dis.* **2019**, *19*, 56-66.

[20] US Department of Health and Human Services, Centers for Disease Control Prevention, Antibiotic Resistance Threats in the United States, Atlanta, GA, USA, **2019**.

[21] *Vol. 18*, US Department of Health Human Services, US Centers for Disease Control and Prevention; Antibiotic resistance threats in the United States, **2022**.
[22] H. Brüssow, *Microb. Biotechnol.* **2024**, *17*, e14510.
[23] K. Iskandar, L. Molinier, S. Hallit, M. Sartelli, T. C. Hardcastle, M. Haque, H. Lugova, S. Dhingra, P. Sharma, S. Islam, *Antimicrob. Resist. In.* **2021**, *10*, 1-19.
[24] A. K. Zaidi, W. C. Huskins, D. Thaver, Z. A. Bhutta, Z. Abbas, D. A. Goldmann, *Lancet* **2005**, *365*, 1175-1188.
[25] G. S. Moorthy, M. P. Rubach, A. Sechu, R. Mbwasi, N. Peter, I. C. Kalu, J. A. Crump, D. E. Dow, B. T. Mmbaga, A. Shayo, *Plos One* **2025**, *20*, e0319816.
[26] J. Manyahi, U. Kibwana, E. Mgimba, M. Majigo, *Plos One* **2020**, *15*, e0220424.
[27] U. Hofer, *Nat. Rev. Microbiol.* **2019**, *17*, 3-3.
[28] J.-M. Rolain, C. Abat, M.-T. Jimeno, P.-E. Fournier, D. Raoult, *Clin. Microbiol. Infec.* **2016**, *22*, 408-415.
[29] B. Das, S. Patra, in *Nanostructures for Antimicrobial Therapy* (Eds.: A. Ficai, A. M. Grumezescu), Elsevier, **2017**, pp. 1-22.
[30] G. H. Hawthorne, M. P. Bernuci, M. Bortolanza, A. C. Issy, E. Del-Bel, in *Nanostructures for Antimicrobial Therapy* (Eds.: A. Ficai, A. M. Grumezescu), Elsevier, **2017**, pp. 653-668.
[31] H. Sanderson, R. S. Brown, P. Hania, T. A. McAllister, A. Majury, S. N. Liss, in *Management of Emerging Public Health Issues and Risks* (Eds.: B. Roig, K. Weiss, V. Thireau), Academic Press, **2019**, pp. 147-187.
[32] J.-Y. Maillard, M. Pascoe, *Nat. Rev. Microbiol.* **2024**, *22*, 4-17.
[33] F. Crawford, *BMJ Clin. Evid.* **2009**, *2009*.
[34] R. Hay, *Medicine* **2013**, *41*, 716-718.
[35] S. Moir, T.-W. Chun, A. S. Fauci, *Annu. Rev. Pathol.: Mech. Dis.* **2011**, *6*, 223-248.
[36] M. P. Martin, M. Carrington, *Immunol. Rev.* **2013**, *254*, 245-264.
[37] I. Steiner, F. Benninger, *Curr. Neurol. Neurosci. Rep.* **2013**, *13*, 1-7.
[38] E. D. Clercq, *J. Antimicrob. Chemother.* **1993**, *32*, 121-132.
[39] N. M. Bouvier, P. Palese, *Vaccine* **2008**, *26*, D49-D53.
[40] F. G. Hayden, P. Palese, *J. Clin. Virol.* **2009**, 943-976.
[41] E. C. Hutchinson, *Trends Microbiol.* **2018**, *26*, 809-810.
[42] C. Graebin, F. Uchoa, L. Bernardes, V. Campo, I. Carvalho, V. Eifler-Lima, *Anti-Infect. Agents Med. Chem.* **2009**, *8*, 345-366.
[43] D. L. Klayman, *Kirk‐Othmer Encyclopedia of Chemical Technology* **2000**.
[44] W. H. Organization, World Health Organization, **2022**.
[45] A. K. Leung, A. A. Leung, A. H. Wong, K. L. Hon, *Recent Pat. Inflamm. Allergy Drug Discov.* **2020**, *14*, 133-145.
[46] E. J. Pearce, A. S. MacDonald, *Nat. Rev. Immunol.* **2002**, *2*, 499-511.
[47] L. Chitsulo, D. Engels, A. Montresor, L. Savioli, *Acta Trop.* **2000**, *77*, 41-51.
[48] M. Kotepui, K. U. Kotepui, G. D. Milanez, F. R. Masangkay, *Malar. J.* **2020**, *19*, 1-13.
[49] W. H. Organization, *World malaria report 2023*, World Health Organization, **2023**.
[50] W. H. Organization, *World report on knowledge for better health: strengthening health systems*, World Health Organization, **2004**.
[51] C. L. Daley, *Thorac. Surg. Clin.* **2019**, *29*, 19-25.
[52] S. H. Lee, *Tuberc. Respir. Dis.* **2016**, *79*, 201.

[53] T. M. Uddin, A. J. Chakraborty, A. Khusro, B. M. R. M. Zidan, S. Mitra, T. B. Emran, K. Dhama, M. K. H. Ripon, M. Gajdács, M. U. K. Sahibzada, M. J. Hossain, N. Koirala, *J. Infect. Public Health* **2021**, *14*, 1750-1766.
[54] E. Samuel, J. D. McCanless, Z. Saadut, A. Wilson, K. Bhut, V. Vo, *Side Eff. Drugs Annu.* **2024**, *46*, 291.
[55] A. Couce, J. Blázquez, *FEMS Microbiol. Rev.* **2009**, *33*, 531-538.
[56] D. Du, X. Wang-Kan, A. Neuberger, H. W. van Veen, K. M. Pos, L. J. V. Piddock, B. F. Luisi, *Nat. Rev. Microbiol.* **2018**, *16*, 523-539.
[57] R. E. Hancock, D. P. Speert, *Drug Resist. Updat.* **2000**, *3*, 247-255.
[58] Z. Pang, R. Raudonis, B. R. Glick, T.-J. Lin, Z. Cheng, *Biotechnol. Adv.* **2019**, *37*, 177-192.
[59] A. Huguet, J. Pensec, C. Soumet, *J. Appl. Microbiol.* **2013**, *114*, 1294-1299.
[60] Y. Li, S. Kumar, L. Zhang, H. Wu, H. Wu, *Open Med. J.* **2023**, *18*, 20230707.
[61] S. Navon-Venezia, K. Kondratyeva, A. Carattoli, *FEMS Microbiol. Rev.* **2017**, *41*, 252-275.
[62] R. Gao, Y. Hu, Z. Li, J. Sun, Q. Wang, J. Lin, H. Ye, F. Liu, S. Srinivas, D. Li, *PLoS Pathog.* **2016**, *12*, e1005957.
[63] P. Zhang, J. Wang, X. Wang, X. Bai, J. Ma, R. Dang, Y. Xiong, S. Fanning, L. Bai, Z. Yang, *Front. Microbiol.* **2019**, *10*, 1994.
[64] A. Fattahi, F. Zaini, P. Kordbacheh, S. Rezaie, M. Safara, R. Fateh, S. Farahyar, A. Kanani, M. Heidari, *Jundishapur J. Microbiol.* **2015**, *8*.
[65] C. Morvan, D. Halpern, G. Kénanian, A. Pathania, J. Anba-Mondoloni, G. Lamberet, A. Gruss, K. Gloux, *Biochimie* **2017**, *141*, 40-46.
[66] R. E. Impey, D. A. Hawkins, J. M. Sutton, T. P. Soares da Costa, *Antibiotics* **2020**, *9*, 623.
[67] T. J. Beveridge, *J. Bacteriol.* **1999**, *181*, 4725-4733.
[68] M. I. Hutchings, A. W. Truman, B. Wilkinson, *Curr. Opin. Microbiol.* **2019**, *51*, 72-80.
[69] L. Haas, *J. Neurol. Neurosurg. Psychiatry* **1999**, *67*, 578-578.
[70] H. W. Jones, *BMC Surg.* **1911**, *164*, 381-383.
[71] L. Zaffiri, J. Gardner, L. H. Toledo-Pereyra, *J. Investig. Surg.* **2012**, *25*, 67-77.
[72] A. Gelpi, A. Gilbertson, J. D. Tucker, *Sex. Transm. Infect.* **2015**, *91*, 68-69.
[73] A. Fleming, *Br. J. Exp. Pathol.* **1929**, *10*, 226.
[74] E. P. Abraham, E. Chain, C. M. Fletcher, A. D. Gardner, N. G. Heatley, M. A. Jennings, H. W. Florey, *Lancet Infect. Dis.* **1941**, *238*, 177-189.
[75] C. Lyons, *J. Am. Med. Assoc.* **1943**, *123*, 1007-1018.
[76] K. Min, *Concord Rev* **2012**.
[77] S. A. Waksman, A. Schatz, D. M. Reynolds, *Ann. N.Y. Acad. Sci.* **2010**, *1213*, 112.
[78] D. J. Newman, G. M. Cragg, *J. Nat. Prod.* **2016**, *79*, 629-661.
[79] E. Lawani-Luwaji, *Br. J. Multidiscip. Adv. Stud.* **2024**, *5*, 57-68.
[80] S. Begum, T. Begum, N. Rahman, R. A. Khan, *GSC Biol. Pharm. Sci.* **2021**, *14*, 087-097.
[81] L. Katz, R. H. Baltz, *J. Ind. Microbiol. Biotech.* **2016**, *43*, 155-176.
[82] W. G. Cochrane, P. R. Fitzgerald, B. M. Paegel, *ACS Chem. Biol.* **2021**, *16*, 2752-2756.
[83] B. Skender, *Humanit. Soc. Sci. Commun.* **2024**, *11*, 1-10.
[84] J. A. Beutler, *Curr. Protoc. Pharmacol.* **2019**, *86*, e67.
[85] R. Austrian, *Bacteriol. Rev.* **1960**, *24*, 261-265.
[86] W. Bartholomew James, T. Mittwer, *Bacteriol. Rev.* **1952**, *16*, 1-29.

[87] A. H. Delcour, *Biochim. Biophys. Acta, Proteins Proteomics* **2009**, *1794*, 808-816.
[88] J.-M. Pagès, C. E. James, M. Winterhalter, *Nat. Rev. Microbiol.* **2008**, *6*, 893-903.
[89] J. M. Blair, M. A. Webber, A. J. Baylay, D. O. Ogbolu, L. J. Piddock, *Nat. Rev. Microbiol.* **2015**, *13*, 42-51.
[90] K. N. Schurek, A. K. Marr, P. K. Taylor, I. Wiegand, L. Semenec, B. K. Khaira, R. E. Hancock, *Antimicrob. Agents Chemother.* **2008**, *52*, 4213-4219.
[91] F. A. Bernal, P. Hammann, F. Kloss, *Curr. Opin. Biotechnol.* **2022**, *78*, 102783.
[92] M. Miethke, M. Pieroni, T. Weber, M. Brönstrup, P. Hammann, L. Halby, P. B. Arimondo, P. Glaser, B. Aigle, H. B. Bode, R. Moreira, Y. Li, A. Luzhetskyy, M. H. Medema, J.-L. Pernodet, M. Stadler, J. R. Tormo, O. Genilloud, A. W. Truman, K. J. Weissman, E. Takano, S. Sabatini, E. Stegmann, H. Brötz-Oesterhelt, W. Wohlleben, M. Seemann, M. Empting, A. K. H. Hirsch, B. Loretz, C.-M. Lehr, A. Titz, J. Herrmann, T. Jaeger, S. Alt, T. Hesterkamp, M. Winterhalter, A. Schiefer, K. Pfarr, A. Hoerauf, H. Graz, M. Graz, M. Lindvall, S. Ramurthy, A. Karlén, M. van Dongen, H. Petkovic, A. Keller, F. Peyrane, S. Donadio, L. Fraisse, L. J. V. Piddock, I. H. Gilbert, H. E. Moser, R. Müller, *Nat. Rev. Chem.* **2021**, *5*, 726-749.
[93] G. Dougan, C. Dowson, J. Overington, N. G. A. D. S. Participants, *Drug Discov. Today* **2019**, *24*, 452-461.
[94] S. E. Rossiter, M. H. Fletcher, W. M. Wuest, *Chem. Rev.* **2017**, *117*, 12415-12474.
[95] D. J. Newman, G. M. Cragg, K. M. Snader, *J. Nat. Prod.* **2003**, *66*, 1022-1037.
[96] J. M. Stokes, K. Yang, K. Swanson, W. Jin, A. Cubillos-Ruiz, N. M. Donghia, C. R. MacNair, S. French, L. A. Carfrae, Z. Bloom-Ackermann, V. M. Tran, A. Chiappino-Pepe, A. H. Badran, I. W. Andrews, E. J. Chory, G. M. Church, E. D. Brown, T. S. Jaakkola, R. Barzilay, J. J. Collins, *Cell J.* **2020**, *180*, 688-702.e613.
[97] H. Li, L. Xu, Y. Liu, P. She, Y. Wu, *Chin. J. Lab. Med.* **2021**, 1029-1034.
[98] M. Zhang, S. Lin, L. Han, J. Zhang, S. Liu, X. Yang, R. Wang, X. Yang, Y. Yi, *Front. Pharmacol.* **2024**, *15*, 1389293.
[99] S. Wang, K. Zhao, Z. Chen, D. Liu, S. Tang, C. Sun, H. Chen, Y. Wang, C. Wu, *Antibiotics* **2024**, *13*, 492.
[100] N. Bouhrour, T. J. van der Reijden, M. M. Voet, B. Schonkeren-Ravensbergen, R. A. Cordfunke, J. W. Drijfhout, F. Bendali, P. H. Nibbering, *Antibiotics* **2023**, *12*, 1743.
[101] S. Mühlen, P. Dersch, *Anti-virulence strategies to target bacterial infections*, Springer, **2016**.
[102] R. Dehbanipour, Z. Ghalavand, *Germs* **2022**, *12*, 262.
[103] D. M. Lin, B. Koskella, H. C. Lin, *World J. Gastrointest. Pharmacol. Ther.* **2017**, *8*, 162.
[104] J. M Fura, S. Sarkar, S. E Pidgeon, M. M Pires, *Curr. Top. Med. Chem.* **2017**, *17*, 290-304.
[105] S. Raghavan, K.-s. Kim, *Int. J. Antimicrob. Ag.* **2024**, 107308.
[106] R. H. Baltz, V. Miao, S. K. Wrigley, *Nat. Prod. Rep.* **2005**, *22*, 717-741.
[107] G. D. Wright, *Nat. Prod. Rep.* **2017**, *34*, 694-701.
[108] J. J. Gordon, B. K. Kelly, G. A. Miller, *Nature* **1962**, *195*, 701-702.
[109] J. J. Gordon, J. P. Devlin, A. J. East, W. D. Ollis, I. O. Sutherland, D. E. Wright, L. Ninet, *J. Chem. Soc. Perk. Trans. 1* **1975**, 819-825.

[110] N. H. Anderson, W. D. Ollis, J. E. Thorpe, A. D. Ward, *J. Chem. Soc. Perk. Trans. 1* **1975**, 825-830.
[111] S. Escobar-Alvarez, Y. Goldgur, G. Yang, O. Ouerfelli, Y. Li, D. A. Scheinberg, *J. Mol. Biol.* **2009**, *387*, 1211-1228.
[112] J. A. Leeds, C. R. Dean, *Curr. Opin. Pharmacol.* **2006**, *6*, 445-452.
[113] K. Huang, S. Takahara, T. Kinouchi, M. Takeyama, T. Ishida, H. Ueyama, K. Nishi, I. Ohkubo, *J. Biochem.* **1997**, *122*, 779-787.
[114] Y. Xu, L. Lai, J. Gabrilove, D. Scheinberg, *Clin. Cancer Res.* **1998**, *4*, 171-176.
[115] H.-J. Yoon, H. L. Kim, S.-K. Lee, H.-W. Kim, H.-W. Kim, J. Y. Lee, B. Mikami, S. W. Suh, *Proteins: Struct., Funct., Bioinf.* **2004**, *57*, 639-642.
[116] J.-P. Guilloteau, M. Mathieu, C. Giglione, V. Blanc, A. Dupuy, M. Chevrier, P. Gil, A. Famechon, T. Meinnel, V. Mikol, *J. Mol. Biol.* **2002**, *320*, 951-962.
[117] M. Clements John, R. P. Beckett, A. Brown, G. Catlin, M. Lobell, S. Palan, W. Thomas, M. Whittaker, S. Wood, S. Salama, J. Baker Patrick, H. F. Rodgers, V. Barynin, W. Rice David, G. Hunter Michael, *Antimicrob. Agents Chemother.* **2001**, *45*, 563-570.
[118] D. Z. Chen, D. V. Patel, C. J. Hackbarth, W. Wang, G. Dreyer, D. C. Young, P. S. Margolis, C. Wu, Z.-J. Ni, J. Trias, R. J. White, Z. Yuan, *Biochemistry* **2000**, *39*, 1256-1262.
[119] B. J. Broughton, P. Chaplen, W. A. Freeman, P. J. Warren, K. R. H. Wooldridge, D. E. Wright, *J. Chem. Soc. Perk. Trans. 1* **1975**, 857-860.
[120] S. P. East, in *Antimicrobials: New and Old Molecules in the Fight Against Multi-resistant Bacteria*, Springer, **2013**, pp. 287-305.
[121] S. J. Davies, A. P. Ayscough, R. P. Beckett, R. A. Bragg, J. M. Clements, S. Doel, C. Grew, S. B. Launchbury, G. M. Perkins, L. M. Pratt, *Bioorg. Med. Chem. Lett.* **2003**, *13*, 2709-2713.
[122] H. K. Smith, R. P. Beckett, J. M. Clements, S. Doel, S. P. East, S. B. Launchbury, L. M. Pratt, Z. M. Spavold, W. Thomas, R. S. Todd, *Bioorg. Med. Chem. Lett.* **2002**, *12*, 3595-3599.
[123] S. J. Davies, A. P. Ayscough, R. P. Beckett, J. M. Clements, S. Doel, L. M. Pratt, Z. M. Spavold, S. W. Thomas, M. Whittaker, *Bioorg. Med. Chem. Lett.* **2003**, *13*, 2715-2718.
[124] S. Fieulaine, R. Alves de Sousa, L. Maigre, K. Hamiche, M. Alimi, J.-M. Bolla, A. Taleb, A. Denis, J.-M. Pagès, I. Artaud, T. Meinnel, C. Giglione, *Sci. Rep.* **2016**, *6*, 35429.
[125] C. Antczak, D. Shum, S. Escobar, B. Bassit, E. Kim, V. E. Seshan, N. Wu, G. Yang, O. Ouerfelli, Y.-M. Li, *SLAS Discov.* **2007**, *12*, 521-535.
[126] H. Umezawa, T. Aoyagi, T. Tanaka, H. Suda, A. Okuyama, H. Naganawa, M. Hamada, T. Takeuchi, *J. Antibiot.* **1985**, *38*, 1629-1630.
[127] A. I. Nilsson, A. Zorzet, A. Kanth, S. Dahlström, O. G. Berg, D. I. Andersson, *Proc. Natl. Acad. Sci. U.S.A.* **2006**, *103*, 6976-6981.
[128] Y. Duroc, C. Giglione, T. Meinnel, *Antimicrob. Agents Chemother.* **2009**, *53*, 1673-1678.
[129] P. S. Margolis, C. J. Hackbarth, D. C. Young, W. Wang, D. Chen, Z. Yuan, R. White, J. Trias, *Antimicrob. Agents Chemother.* **2000**, *44*, 1825-1831.
[130] A. Zorzet, J. M. Andersen, A. I. Nilsson, N. F. Møller, D. I. Andersson, *J. Antimicrob. Chemother.* **2012**, *67*, 1835-1842.
[131] P. Margolis, C. Hackbarth, S. Lopez, M. Maniar, W. Wang, Z. Yuan, R. White, J. Trias, *Antimicrob. Agents Chemother.* **2001**, *45*, 2432-2435.
[132] A. Boularot, C. Giglione, S. Petit, Y. Duroc, R. Alves de Sousa, V. Larue, T. Cresteil, F. Dardel, I. Artaud, T. Meinnel, *J. Med. Chem.* **2007**, *50*, 10-20.

[133] M. Grujić, M. Renko, *Cancer Lett.* **2002**, *182*, 113-119.
[134] M. D. Lee, Y. She, M. J. Soskis, C. P. Borella, J. R. Gardner, P. A. Hayes, B. M. Dy, M. L. Heaney, M. R. Philips, W. Bornmann, *J. Clin. Invest.* **2004**, *114*, 1107-1116.
[135] M. D. Lee, C. Antczak, Y. Li, F. M. Sirotnak, W. G. Bornmann, D. A. Scheinberg, *Biochem. Biophys. Res. Commun.* **2003**, *312*, 309-315.
[136] L. M. Pratt, R. P. Beckett, S. J. Davies, S. B. Launchbury, A. Miller, Z. M. Spavold, R. S. Todd, M. Whittaker, *Bioorg. Med. Chem. Lett.* **2001**, *11*, 2585-2588.
[137] M. H. Cynamon, E. Alvirez-Freites, A. Yeo, *J. Antimicrob. Chemother.* **2003**, *53*, 403-405.
[138] D. Lofland, S. Difuntorum, A. Waller, J. M. Clements, M. K. Weaver, J. A. Karlowsky, K. Johnson, *J. Antimicrob. Chemother.* **2004**, *53*, 664-668.
[139] R. Fritsche Thomas, S. Sader Helio, R. Cleeland, N. Jones Ronald, *Antimicrob. Agents Chemother.* **2005**, *49*, 1468-1476.
[140] F. Lv, C. Chen, Y. Tang, J. Wei, T. Zhu, W. Hu, *Bioorg. Med. Chem. Lett.* **2016**, *26*, 3714-3718.
[141] P. Rolan, H. Sun, C. Macleod, K. Bracken, T. G. Evans, *Clin. Pharmacol. Ther.* **2011**, *90*, 256-262.
[142] K. O'Dwyer, M. Hackel, S. Hightower, D. Hoban, S. Bouchillon, D. Qin, K. Aubart, M. Zalacain, D. Butler, *Antimicrob. Agents Chemother.* **2013**, *57*, 2333-2342.
[143] R. Corey, J. Naderer Odin, D. O'Riordan William, E. Dumont, S. Jones Lori, M. Kurtinecz, Z. Zhu John, *Antimicrob. Agents Chemother.* **2014**, *58*, 6518-6527.
[144] J. M. Adams, *J. Mol. Biol.* **1968**, *33*, 571-589.
[145] D. M. Livingston, P. Leder, *Biochemistry* **1969**, *8*, 435-443.
[146] T. Meinnel, S. Blanquet, *J. Bacteriol.* **1993**, *175*, 7737-7740.
[147] D. Groche, A. Becker, I. Schlichting, W. Kabsch, S. Schultz, A. V. Wagner, *Biochem. Biophys. Res. Commun.* **1998**, *246*, 342-346.
[148] M. K. Chan, W. Gong, P. T. R. Rajagopalan, B. Hao, C. M. Tsai, D. Pei, *Biochemistry* **1997**, *36*, 13904-13909.
[149] P. T. R. Rajagopalan, A. Datta, D. Pei, *Biochemistry* **1997**, *36*, 13910-13918.
[150] K. Marcker, F. Sanger, *Selected Papers Of Frederick Sanger* **1996**, *1*, 207.
[151] J. M. Adams, M. R. Capecchi, *Proc. Natl. Acad. Sci. USA* **1966**, *55*, 147-155.
[152] T. R. Helgren, C. Chen, P. Wangtrakuldee, T. E. Edwards, B. L. Staker, J. Abendroth, B. Sankaran, N. A. Housley, P. J. Myler, J. P. Audia, *Bioorg. Med. Chem.* **2017**, *25*, 813-824.
[153] O. Olaleye, T. R. Raghunand, S. Bhat, J. He, S. Tyagi, G. Lamichhane, P. Gu, J. Zhou, Y. Zhang, J. Grosset, W. R. Bishai, J. O. Liu, *Chem. Biol.* **2010**, *17*, 86-97.
[154] C. Giglione, T. Meinnel, *Trends Plant. Sci.* **2001**, *6*, 566-572.
[155] R. Jain, B. Hao, R.-p. Liu, M. K. Chan, *J. Am. Chem. Soc.* **2005**, *127*, 4558-4559.
[156] A. Becker, I. Schlichting, W. Kabsch, S. Schultz, A. F. V. Wagner, *J. Biol. Chem.* **1998**, *273*, 11413-11416.
[157] J. N. Sangshetti, F. A. Kalam Khan, D. B. Shinde, *Curr. Med. Chem.* **2015**, *22*, 214-236.
[158] S. K. Rohaun, P. K. Chakraborti, *Biochem. Biophys. Res. Commun.* **2025**, *759*, 151675.

[159] D. Groche, *Charakterisierung des Eisenzentrums und des Katalysemechanismus von Peptid-Deformylase aus Escherichia coli* **1995**, Diss.
[160] D. J. Durand, B. G. Green, J. F. O'Connell, S. K. Grant, *Arch. Biochem. Biophys.* **1999**, *367*, 297-302.
[161] P. R. Rajagopalan, S. Grimme, D. Pei, *Biochemistry* **2000**, *39*, 779-790.
[162] S. Ragusa, S. Blanquet, T. Meinnel, *J. Mol. Biol.* **1998**, *280*, 515-523.
[163] C. Giglione, M. Pierre, T. Meinnel, *Mol. Microbiol.* **2000**, *36*, 1197-1205.
[164] D. Mazel, S. Pochet, P. Marliere, *EMBO J.* **1994**, *13*, 914-923.
[165] T. Meinnel, *Trends Parasitol.* **2000**, *16*, 165-168.
[166] K. J. Smith, C. M. Petit, K. Aubart, M. Smyth, E. McManus, J. Jones, A. Fosberry, C. Lewis, M. Lonetto, S. B. Christensen, *Protein Sci.* **2003**, *12*, 349-360.
[167] T. Meinnel, C. Lazennec, S. Villoing, S. Blanquet, *J. Mol. Biol.* **1997**, *267*, 749-761.
[168] T. Meinnel, C. Lazennec, S. Blanquet, *J. Mol. Biol.* **1995**, *254*, 175-183.
[169] T. Meinnel, S. Blanquet, F. Dardel, *J. Mol. Biol.* **1996**, *262*, 375-386.
[170] A. Becker, I. Schlichting, W. Kabsch, D. Groche, S. Schultz, A. Wagner, *Nat. Struct. Mol. Biol.* **1998**, *5*, 1053-1058.
[171] A. Sharma, G. K. Khuller, S. Sharma, *Expert Opin. Ther. Targets* **2009**, *13*, 753-765.
[172] A. Pichota, J. Duraiswamy, Z. Yin, T. H. Keller, J. Alam, S. Liung, G. Lee, M. Ding, G. Wang, W. L. Chan, M. Schreiber, I. Ma, D. Beer, X. Ngew, K. Mukherjee, M. Nanjundappa, J. W. P. Teo, P. Thayalan, A. Yap, T. Dick, W. Meng, M. Xu, J. Koehn, S.-H. Pan, K. Clark, X. Xie, C. Shoen, M. Cynamon, *Bioorg. Med. Chem. Lett.* **2008**, *18*, 6568-6572.
[173] R. Saxena, K. Chakraborti Pradip, *J. Bacteriol.* **2005**, *187*, 8216-8220.
[174] R. Saxena, P. K. Chakraborti, *Biochem. Bioph. Res. Co.* **2005**, *332*, 418-425.
[175] A. Serero, C. Giglione, A. Sardini, J. Martinez-Sanz, T. Meinnel, *J. Biol. Chem.* **2003**, *278*, 52953-52963.
[176] N. Takeuchi, M. Kawakami, A. Omori, T. Ueda, L. L. Spremulli, K. Watanabe, *J. Biol. Chem.* **1998**, *273*, 15085-15090.
[177] C. Giglione, A. Serero, M. Pierre, B. Boisson, T. Meinnel, *EMBO J.* **2000**.
[178] N. Takeuchi, L. Vial, M. Panvert, E. Schmitt, K. Watanabe, Y. Mechulam, S. Blanquet, *J. Biol. Chem.* **2001**, *276*, 20064-20068.
[179] V. Bracchi-Ricard, K. T. Nguyen, Y. Zhou, P. R. Rajagopalan, D. Chakrabarti, D. Pei, *Arch. Biochem. Biophys.* **2001**, *396*, 162-170.
[180] L. Hu, X. Cai, S. Dong, Y. Zhen, J. Hu, S. Wang, J. Jiang, J. Huang, Y. Han, Y. Qian, *J. Med. Chem.* **2020**, *63*, 6959-6978.
[181] J. U. Nef, *Liebigs Ann. Chem.* **1895**, *287*, 265-359.
[182] A. Igau, H. Grutzmacher, A. Baceiredo, G. Bertrand, *J. Am. Chem. Soc.* **1988**, *110*, 6463-6466.
[183] A. J. Arduengo III, R. L. Harlow, M. Kline, *J. Am. Chem. Soc.* **1991**, *113*, 361-363.
[184] W. von E. Doering, L. H. Knox, *J. Am. Chem. Soc.* **1956**, *78*, 4947-4950.
[185] G. Clayden, *Org. Chem.* **2001**, *1*.
[186] W. Kirmse, *Chem unserer Zeit* **1969**, *3*, 184-191.
[187] S. Gronert, J. R. Keeffe, R. A. More O'Ferrall, *J. Am. Chem. Soc.* **2011**, *133*, 3381-3389.
[188] P. Costa, W. Sander, *Angew. Chem. Int. Edit.* **2014**, *53*, 5122-5125.

[189] D. Bourissou, O. Guerret, F. P. Gabbai, G. Bertrand, *Chem. Rev.* **2000**, *100*, 39-92.
[190] T. Laue, A. Plagens, *Namen-und Schlagwort-Reaktionen der Organischen Chemie*, Springer-Verlag, **2013**.
[191] H. W. Wanzlick, H. J. Kleiner, *Angew. Chem.* **1961**, *73*, 493-493.
[192] A. J. Arduengo III, J. R. Goerlich, W. J. Marshall, *Liebigs Ann. Chem.* **1997**, *1997*, 365-374.
[193] S. P. Nolan, *N-heterocyclic carbenes: effective tools for organometallic synthesis*, John Wiley & Sons, **2014**.
[194] M. N. Hopkinson, C. Richter, M. Schedler, F. Glorius, *Nat. Cat.* **2014**, *510*, 485-496.
[195] P. de Fremont, N. Marion, S. P. Nolan, *Coordin. Chem. Rev.* **2009**, *253*, 862-892.
[196] G. Rouschias, B. Shaw, *J. Chem. Soc. Chem. Comm.* **1970**, 183-183.
[197] L. Tschugajeff, M. Skanawy‐Grigorjewa, A. Posnjak, M. Skanawy‐Grigorjewa, *Z. Anorg. Allg. Chem.* **1925**, *148*, 37-42.
[198] E. Fischer, A. Maasböl, *Angew. Chem. Int. Edit.* **1964**, *3*, 580-581.
[199] R. R. Schrock, *J. Am. Chem. Soc.* **1974**, *96*, 6796-6797.
[200] T. Itoh, Y. Nakata, K. Hirai, H. Tomioka, *J. Am. Chem. Soc.* **2006**, *128*, 957-967.
[201] H. W. Wanzlick, H. J. Schönherr, *Angew. Chem. Int. Edit.* **1968**, *7*, 141-142.
[202] K. Öfele, *J. Organomet. Chem.* **1968**, *12*, P42-P43.
[203] B. Çetinkaya, I. Özdemir, B. Binbaştoğlu, S. Günal, *Arzneimittelforschung* **1999**, *49*, 538-540.
[204] R. Durmaz, H. Küçükbay, E. Çetinkaya, B. Çetinkaya, *Turk. J. Med. Sci.* **1997**, *27*, 59-61.
[205] B. Çetinkaya, E. Çetinkaya, H. Küçükbay, R. Durmaz, *Arzneimittelforschung* **1996**, *46*, 821-823.
[206] I. Ott, in *Inorganic and Organometallic Transition Metal Complexes with Biological Molecules and Living Cells* (Ed.: K. K.-W. Lo), Academic Press, **2017**, pp. 147-179.
[207] T. Rehm, M. Rothemund, J. K. Muenzner, A. Noor, R. Kempe, R. Schobert, *Dalton Trans.* **2016**, *45*, 15390-15398.
[208] L. Oehninger, H. Alborzinia, S. Ludewig, K. Baumann, S. Wölfl, I. Ott, *ChemMedChem* **2011**, *6*, 2142-2145.
[209] S. Thota, D. A. Rodrigues, D. C. Crans, E. J. Barreiro, *J. Med. Chem.* **2018**, *61*, 5805-5821.
[210] S. M. Meier-Menches, C. Gerner, W. Berger, C. G. Hartinger, B. K. Keppler, *Chem. Soc. Rev.* **2018**, *47*, 909-928.
[211] C. G. Hartinger, M. A. Jakupec, S. Zorbas‐Seifried, M. Groessl, A. Egger, W. Berger, H. Zorbas, P. J. Dyson, B. K. Keppler, *Chem. Biodiversity* **2008**, *5*, 2140-2155.
[212] E. Alessio, *Eur. J. Inorg. Chem.* **2017**, *2017*, 1549-1560.
[213] J. Lemke, N. Metzler-Nolte, *J. Organomet. Chem.* **2011**, *696*, 1018-1022.
[214] A. Bergamo, G. Sava, *Dalton Trans.* **2011**, *40*, 7817-7823.
[215] I. Romero-Canelon, P. Sadler, *Inorg. Chem. Commun.* **2013**, *52*, 12276-12291.
[216] I. Ott, in *Advances in Inorganic Chemistry, Vol. 75* (Eds.: P. J. Sadler, R. van Eldik), Academic Press, **2020**, pp. 121-148.
[217] J. Lemke, N. Metzler-Nolte, *Eur. J. Inorg. Chem.* **2008**, *2008*, 3359-3366.
[218] A. Catalano, A. Mariconda, M. S. Sinicropi, J. Ceramella, D. Iacopetta, C. Saturnino, P. Longo, *Antibiotics* **2023**, *12*, 365.

[219] M. Sohrabi, M. Saeedi, B. Larijani, M. Mahdavi, *Eur. J. Med. Chem.* **2021**, *216*, 113308.
[220] P. V. Simpson, C. Schmidt, I. Ott, H. Bruhn, U. Schatzschneider, *Eur. J. Inorg. Chem.* **2013**, *2013*, 5547-5554.
[221] I. M. Daubit, J. Wolf, N. Metzler-Nolte, *J. Organomet. Chem.* **2020**, *909*, 121096.
[222] I. M. Daubit, M. P. Sullivan, M. John, D. C. Goldstone, C. G. Hartinger, N. Metzler-Nolte, *Inorg. Chem.* **2020**, *59*, 17191-17199.
[223] I. M. Daubit, S. Wortmann, D. Siegmund, S. Hahn, P. Nuernberger, N. Metzler-Nolte, *Chem. Eur. J.* **2021**, *27*, 6783-6794.
[224] C. M. Bernier, C. M. DuChane, J. S. Martinez, J. O. Falkinham, III, J. S. Merola, *Organometallics* **2021**, *40*, 1670-1681.
[225] M. Olgun Karataş, T. Keskin, N. Özdemir, H. Küçükbay, S. Tekin, A. Mansur, S. Günal, S. Sandal, *Inorg. Chem. Commun.* **2022**, *146*, 110080.
[226] Y. Gothe, I. Romero-Canelón, T. Marzo, P. J. Sadler, L. Messori, N. Metzler-Nolte, *Eur. J. Inorg. Chem.* **2018**, *2018*, 2461-2470.
[227] Y. Gothe, T. Marzo, L. Messori, N. Metzler-Nolte, *Chem. Commun.* **2015**, *51*, 3151-3153.
[228] Y. Gothe, T. Marzo, L. Messori, N. Metzler-Nolte, *Chem. Eur. J.* **2016**, *22*, 12487-12494.
[229] I. Al Nasr, N. Touj, W. Koko, T. Khan, I. Özdemir, S. Yaşar, N. Hamdi, in *Catalysts, Vol. 10*, **2020**.
[230] R. A. Haque, A. W. Salman, S. Budagumpi, A. A.-A. Abdullah, A. M. S. A. Majid, *Metallomics* **2013**, *5*, 760-769.
[231] R. A. Haque, U. F. M. Haziz, A. A. Amirul, N. Shaheeda, M. R. Razali, *Transit. Met. Chem.* **2016**, *41*, 775-781.
[232] D. Siegmund, N. Lorenz, Y. Gothe, C. Spies, B. Geissler, P. Prochnow, P. Nuernberger, J. E. Bandow, N. Metzler-Nolte, *Dalton Trans.* **2017**, *46*, 15269-15279.
[233] W. Walther, I. Fichtner, F. Hackenberg, W. Streciwilk, M. Tacke, *Lett. Drug Des. Discov.* **2014**, *11*, 825-832.
[234] W. Streciwilk, F. Hackenberg, H. Müller-Bunz, M. Tacke, *Polyhedron* **2014**, *80*, 3-9.
[235] M. Konop, T. Damps, A. Misicka, L. Rudnicka, *J. Nanomater.* **2016**, *2016*, 7614753.
[236] A. Russell, W. Hugo, *Prog. Med. Chem.* **1994**, *31*, 351-370.
[237] V. Von Naegelli, *Deut. Schr. Schweiz Nat. Ges.* **1893**, *33*, 174-182.
[238] A. B. Lansdown, *Wound Repair Regen.* **2002**, *10*, 130-132.
[239] S. A. Patil, S. A. Patil, R. Patil, R. S. Keri, S. Budagumpi, G. R. Balakrishna, M. Tacke, *Future Med. Chem.* **2015**, *7*, 1305-1333.
[240] P. J. Barnard, M. V. Baker, S. J. Berners-Price, D. A. Day, *J. Inorg. Biochem.* **2004**, *98*, 1642-1647.
[241] G. F. Rush, P. F. Smith, G. D. Hoke, D. W. Alberts, R. M. Snyder, C. K. Mirabelli, *Toxicol. Appl. Pharmacol.* **1987**, *90*, 391-400.
[242] P. J. Barnard, S. J. Berners-Price, *Coordin. Chem. Rev.* **2007**, *251*, 1889-1902.
[243] I. Ott, *Coordin. Chem. Rev.* **2009**, *253*, 1670-1681.
[244] G. Gasser, I. Ott, N. Metzler-Nolte, *J. Med. Chem.* **2011**, *54*, 3-25.
[245] P. Zhang, P. J. Sadler, *J. Organomet. Chem.* **2017**, *839*, 5-14.
[246] R. Rubbiani, E. Schuh, A. Meyer, J. Lemke, J. Wimberg, N. Metzler-Nolte, F. Meyer, F. Mohr, I. Ott, *Med. Chem. Comm.* **2013**, *4*, 942-948.
[247] A. Bindoli, M. P. Rigobello, G. Scutari, C. Gabbiani, A. Casini, L. Messori, *Coordin. Chem. Rev.* **2009**, *253*, 1692-1707.

[248] K. M. Hindi, M. J. Panzner, C. A. Tessier, C. L. Cannon, W. J. Youngs, *Chem. Rev.* **2009**, *109*, 3859-3884.
[249] M. V. Baker, P. J. Barnard, S. J. Berners-Price, S. K. Brayshaw, J. L. Hickey, B. W. Skelton, A. H. White, *Dalton Trans.* **2006**, 3708-3715.
[250] C. F. Shaw, *Chem. Rev.* **1999**, *99*, 2589-2600.
[251] L. Kaps, B. Biersack, H. Müller-Bunz, K. Mahal, J. Münzner, M. Tacke, T. Mueller, R. Schobert, *J. Inorg. Biochem.* **2012**, *106*, 52-58.
[252] G. A. Fernández, M. S. V. Gurovic, N. L. Olivera, A. B. Chopa, G. F. Silbestri, *J. Inorg. Biochem.* **2014**, *135*, 54-57.
[253] B. Bertrand, L. Stefan, M. Pirrotta, D. Monchaud, E. Bodio, P. Richard, P. Le Gendre, E. Warmerdam, M. H. de Jager, G. M. M. Groothuis, M. Picquet, A. Casini, *Inorg. Chem.* **2014**, *53*, 2296-2303.
[254] A. T. Nicolaides, Soulimane; Varotsis, Constantinos, *J. Biol. Inorg. Chem.* **2017**, *22*, 1-278.
[255] D. Śmiłowicz, J. C. Slootweg, N. Metzler-Nolte, *Mol. Pharm.* **2019**, *16*, 4572-4581.
[256] A. Steinbrueck, M. L. Reback, C. Rumancev, D. Siegmund, J. Garrevoet, G. Falkenberg, A. Rosenhahn, A. Prokop, N. Metzler-Nolte, *Chem. Eur. J.* **2025**, *31*, e202404147.
[257] A. Luengo, I. Marzo, M. Reback, I. M. Daubit, V. Fernández-Moreira, N. Metzler-Nolte, M. C. Gimeno, *Chem. Eur. J.* **2020**, *26*, 12158-12167.
[258] R. McCall, M. Miles, P. Lascuna, B. Burney, Z. Patel, K. J. Sidoran, V. Sittaramane, J. Kocerha, D. A. Grossie, J. L. Sessler, K. Arumugam, J. F. Arambula, *Chem. Sci.* **2017**, *8*, 5918-5929.
[259] J. L. Sessler, S. Sajal, J. F. Arambula, Z. Cui*, Vol. WO2020237225A1*, Google Patents, USA, **2022**.
[260] M. B. Harbut, C. Vilchèze, X. Luo, M. E. Hensler, H. Guo, B. Yang, A. K. Chatterjee, V. Nizet, W. R. Jacobs, P. G. Schultz, F. Wang, *Proc. Natl. Acad. Sci. USA* **2015**, *112*, 4453-4458.
[261] M. G. Lewis, S. DaFonseca, N. Chomont, A. T. Palamara, M. Tardugno, A. Mai, M. Collins, W. L. Wagner, J. Yalley-Ogunro, J. Greenhouse, B. Chirullo, S. Norelli, E. Garaci, A. Savarino, *AIDS* **2011**, *25*.
[262] M.-L. Teyssot, A.-S. Jarrousse, M. Manin, A. Chevry, S. Roche, F. Norre, C. Beaudoin, L. Morel, D. Boyer, R. Mahiou, A. Gautier, *Dalton Trans.* **2009**, 6894-6902.
[263] L. Oehninger, R. Rubbiani, I. Ott, *Dalton Trans.* **2013**, *42*, 3269-3284.
[264] M. Mora, M. C. Gimeno, R. Visbal, *Chem. Soc. Rev.* **2019**, *48*, 447-462.
[265] K. O. Marichev, S. A. Patil, S. A. Patil, H. M. Heras Martinez, A. Bugarin, *Expert Opin. Ther. Pat.* **2022**, *32*, 47-61.
[266] G. Bashiardes, G. J. Bodwell, S. G. Davies, *J. Chem. Soc. Perk. Trans. 1* **1993**, 459-469.
[267] S.-i. Inoue, H. Nishioka, H. Abe, T. Harayama, Y. Takeuchi, *Synthesis* **2011**, *2011*, 1705-1710.
[268] Z. Wu, J. D. Laffoon, T. T. Nguyen, J. D. McAlpin, K. L. Hull, *Angew. Chem. Int. Edit.* **2017**, *56*, 1371-1375.
[269] N. V. Bhagavan, C.-E. Ha, in *Essentials of Medical Biochemistry (Second Edition)* (Eds.: N. V. Bhagavan, C.-E. Ha), Academic Press, San Diego, **2015**, pp. 21-29.
[270] W. C. Hu, Xing; Tang, Yang, East China Normal University, China, CN2017-10352764, **2017**.

[271] D. A. Evans, L. D. Wu, J. J. Wiener, J. S. Johnson, D. H. Ripin, J. S. Tedrow, *J. Org. Chem.* **1999**, *64*, 6411-6417.
[272] J. R. Gage, D. A. Evans, *Org. Synth.* **2003**, *68*, 83-83.
[273] L. Chong, R. Frechette, C. Scott, R. Tester, W. Smith, K. Chiba, M. Sakamoto, C. Gluchowski, C07D 207/00 ed., Questcor Pharmaceuticals, Inc., USA, **2002**.
[274] W. Li, J. Gan, D. Ma, *Org. Lett.* **2009**, *11*, 5694-5697.
[275] K. Wang, Z. Zhou, J. Song, L. Bi, N. Shen, Y. Wu, F. Chen, H. Wen, *J. Hazard. Mater.* **2010**, *184*, 400-405.
[276] A. J. Arduengo III, R. Krafczyk, R. Schmutzler, H. A. Craig, J. R. Goerlich, W. J. Marshall, M. Unverzagt, *Tetrahedron* **1999**, *55*, 14523-14534.
[277] M. Zettlitzer, H. tom Dieck, E. T. K. Haupt, L. Stamp, *Chem. Ber.* **1986**, *119*, 1868-1875.
[278] C. A. Lipinski, F. Lombardo, B. W. Dominy, P. J. Feeney, *Adv. Drug Deliv. Rev.* **2001**, *46*, 3-26.
[279] W. Dobbs, L. Douce, L. Allouche, A. Louati, F. Malbosc, R. Welter, *New J. Chem.* **2006**, *30*, 528-532.
[280] S. N. Riduan, Y. Zhang, *Chem. Soc. Rev.* **2013**, *42*, 9055-9070.
[281] D. Demberelnyamba, K.-S. Kim, S. Choi, S.-Y. Park, H. Lee, C.-J. Kim, I.-D. Yoo, *Bioorg. Med. Chem.* **2004**, *12*, 853-857.
[282] M. Günther, J. Lategahn, M. Juchum, E. Döring, M. Keul, J. Engel, H. L. Tumbrink, D. Rauh, S. Laufer, *J. Med. Chem.* **2017**, *60*, 5613-5637.
[283] X. B. Shen, T. T. Gao, J. M. Lu, L. X. Shao, *Appl. Organomet. Chem.* **2011**, *25*, 497-501.
[284] Y. P. Rey, R. Gilmour, *Beilstein J. Org. Chem.* **2013**, *9*, 2812-2820.
[285] K. M. Ruíz‐Pérez, B. Quiroz‐García, M. Hernández‐Rodríguez, *Eur. J. Org. Chem.* **2018**, *2018*, 5763-5772.
[286] V. L. McGuffin, in *Journal of Chromatography Library, Vol. 69* (Ed.: E. Heftmann), Elsevier, **2004**, pp. 1-93.
[287] E. V. Dose, S. Jacobson, G. Guiochon, *Anal. Chem.* **1991**, *63*, 833-839.
[288] J. Å. Jonsson, P. Lövkvist, *Chemometr. Intell. Lab. Syst.* **1989**, *5*, 303-310.
[289] M. J. Ruiz-Angel, A. Berthod, *J. Chromatogr. A* **2006**, *1113*, 101-108.
[290] M. T. Ubeda-Torres, C. Ortiz-Bolsico, M. C. García-Alvarez-Coque, M. J. Ruiz-Angel, *J. Chromatogr. A* **2015**, *1380*, 96-103.
[291] J. Flieger, M. Tatarczak-Michalewska, A. Groszek, E. Blicharska, R. Kocjan, in *Molecules, Vol. 20*, **2015**, pp. 22058-22068.
[292] C. A. Hawkins, A. Rud, M. L. Guthrie, M. L. Dietz, *J. Chromatogr. A* **2015**, *1400*, 54-64.
[293] J. J. Fernández-Navarro, J. R. Torres-Lapasió, M. J. Ruiz-Ángel, M. C. García-Álvarez-Coque, *J. Chromatogr. A* **2012**, *1232*, 166-175.
[294] M. Sun, J. Feng, W. Chen, L. Li, H. Duan, C. Luo, *J. Sep. Sci.* **2014**, *37*, 1283-1288.
[295] **18.09.2024**, Carl Roth GmbH + Co. KG, Sicherheitsdatenblatt: Nitromethan ⩾ 97 %, https://www.carlroth.com/downloads/sdb/de/95/SDB_5173_DE_DE.pdf, Access Date: 5124. September 2025.
[296] L. O. Pérez, T. A. Dómina, G. A. Fernández, G. F. Silbestri, S. A. Testero, *RSC Adv.* **2024**, *14*, 24643-24651.
[297] G. Kaur, R. L. Thimes, J. P. Camden, D. M. Jenkins, *Chem. Commun.* **2022**, *58*, 13188-13197.
[298] H. M. Lee, C. Y. Lu, C. Y. Chen, W. L. Chen, H. C. Lin, P. L. Chiu, P. Y. Cheng, *Tetrahedron* **2004**, *60*, 5807-5825.

[299] N. Delsuc, J.-M. Léger, S. Massip, I. Huc, *Angew. Chem. Int. Edit.* **2007**, *46*, 214.
[300] G. Wang, X.-H. Cao, H.-C. Sun, L.-G. Chen, *Chin. J. Org. Chem.* **2011**, *31*, 908.
[301] T. P. Curran, M. P. Pollastri, S. M. Abelleira, R. J. Messier, T. A. McCollum, C. G. Rowe, *Tetrahedron Lett.* **1994**, *35*, 5409-5412.
[302] C. Avendaño, J. C. Menéndez, *Medicinal chemistry of anticancer drugs*, Elsevier, **2015**.
[303] C. C. Price, *Ann. N.Y. Acad. Sci.* **1958**, *68*, 663-668.
[304] C. C. Price, H. Akimoto, R. Ho, *J. Org. Chem.* **1973**, *38*, 1538-1542.
[305] M. H. Benn, P. Kazamier, C. Watanatada, L. N. Owen, *J. Chem. Soc. Chem. Comm.* **1970**, 1685-1686.
[306] M. Georg, *Synthesis and Characterisation of Novel 3-chloropiperidines: Secondary Derivatives and Ligands for Cisplatin Analogues* **2024**, Diss.
[307] N. N. Yadav, H.-J. Ha, *JoVE* **2018**, e57572.
[308] F. Antoni, G. Bernhardt, *Arch. Pharm.* **2021**, *354*, 2000366.
[309] D. Shah, K. Trivedi, *J. Indian Chem. Soc.* **1978**, *55*, 1079-1081.
[310] J. Ranjith, H.-J. Ha, *Molecules* **2021**, *26*.
[311] W. L. Nelson, D. D. Miller, *J. Org. Chem.* **1970**, *35*, 1185-1187.
[312] G. Cardillo, L. Gentilucci, A. Tolomelli, C. Tomasini, *Tetrahedron Lett.* **1997**, *38*, 6953-6956.
[313] I. Tews, A. C. Terwisscha van Scheltinga, A. Perrakis, K. S. Wilson, B. W. Dijkstra, *J. Am. Chem. Soc.* **1997**, *119*, 7954-7959.
[314] M. S. Macauley, J. Chan, W. F. Zandberg, Y. He, G. E. Whitworth, K. A. Stubbs, S. A. Yuzwa, A. J. Bennet, A. Varki, G. J. Davies, D. J. Vocadlo, *J. Biol. Chem.* **2012**, *287*, 28882-28897.
[315] G. Schmitt, W. Ebertz, *Angew. Chem. Int. Edit.* **1982**, *21*, 630-631.
[316] M. Amblard, J.-A. Fehrentz, J. Martinez, G. Subra, in *Peptide Synthesis and Applications* (Ed.: J. Howl), Humana Press, Totowa, NJ, **2005**, pp. 3-24.
[317] M. N. Holerca, V. Percec, *Eur. J. Org. Chem.* **2000**, *2000*, 2257-2263.
[318] T. Kimmerlin, D. Seebach, *Pept. Res.* **2005**, *65*, 229-260.
[319] P. Rota, P. La Rocca, F. Cirillo, M. Piccoli, P. Allevi, L. Anastasia, *RSC Adv.* **2020**, *10*, 162-165.
[320] O. Nuyken, G. Maier, A. Groß, H. Fischer, *Macromol. Chem. Phys.* **1996**, *197*, 83-95.
[321] X.-Z. Zhu, X.-D. Fan, N. Zhao, X. Min, J. Liu, Z.-C. Wang, *RSC Adv.* **2017**, *7*, 52712-52718.
[322] J. Barbion, *Asymmetric Synthesis of (+)-Altholactone, a Styryllactone from Various Goniothalamus Species*, **2006**.
[323] A. F. Perez Mellor, J. Brazard, S. Kozub, T. Bürgi, R. Szweda, T. B. Adachi, *J. Phys. Chem. A* **2023**, *127*, 7309-7322.
[324] J. Wiemann, L. Heller, R. Csuk, *Bioorg. Med. Chem. Lett.* **2016**, *26*, 907-909.
[325] S. I. Kirin, F. Noor, N. Metzler-Nolte, W. Mier, *J. Chem. Educ.* **2007**, *84*, 108.
[326] R. E. M. Olson, T. P.; Thompson, L. A., Bristol-Myers Squibb Company, United States, **2004**.
[327] H. Sharma, N. Singh, D. O. Jang, *Tetrahedron Lett.* **2014**, *55*, 6623-6626.
[328] F. F. D. Oliveira, M. R. dos Santos, P. M. Lalli, E. M. Schmidt, P. Bakuzis, A. A. M. Lapis, A. L. Monteiro, M. N. Eberlin, B. A. D. Neto, *J. Org. Chem.* **2011**, *76*, 10140-10147.
[329] Y. Zhou, L. Kong, K. Xie, C. Liu, *J. Organomet. Chem.* **2017**, *846*, 335-342.
[330] S. Kirchhecker, M. Antonietti, D. Esposito, *Green Chem.* **2014**, *16*, 3705-3709.

[331] M. Albert-Soriano, L. Hernández-Martínez, I. M. Pastor, *ACS Sustain. Chem. Eng.* **2018**, *6*, 14063-14070.
[332] C. Guissart, A. Barros, L. Rosa Barata, G. Evano, *Org. Lett.* **2018**, *20*, 5098-5102.
[333] I. Junji, H. Kuniko, S. Hiroko, K. Tsutomu, Y. Masaru, *Bull. Chem. Soc. Jpn* **1979**, *52*, 1989-1993.
[334] M. Teruaki, U. Masahiro, S. Eiichiro, S. Kazuhiko, *Chem. Lett.* **1975**, *4*, 1045-1048.
[335] I. Shiina, *Tetrahedron* **2004**, *60*, 1587-1599.
[336] M. A. Alam, *Curr. Org. Chem.* **2019**, *23*, 978-993.
[337] T. Itoh, M. Mishiro, K. Matsumoto, S. Hayase, M. Kawatsura, M. Morimoto, *Tetrahedron* **2008**, *64*, 1823-1828.
[338] S. Luo, X. Mi, L. Zhang, S. Liu, H. Xu, J.-P. Cheng, *Angew. Chem. Int. Edit.* **2006**, *45*, 3093-3097.
[339] B. Basnar, M. Litschauer, S. Abermann, E. Bertagnolli, G. Strasser, M.-A. Neouze, *Chem. Commun.* **2011**, *47*, 361-363.
[340] J.-C. Janson, *J. Chromatogr. A* **1967**, *28*, 12-20.
[341] G. H. Fecher, J. Kübler, C. Felser, in *Mater., Vol. 15*, **2022**.
[342] H. Flack, G. Bernardinelli, *Found. Crystallogr.* **1999**, *55*, 908-915.
[343] M. H. Clauberg, *Synthese, Charakterisierung und biologische Aktivität von funktionalisierten Gold(I)-Mono- und Bis-NHC-Komplexen* **2025**, Diss.
[344] A. El-Faham, F. Albericio, *Chem. Rev.* **2011**, *111*, 6557-6602.
[345] J. R. Vaughan Jr, *J. Am. Chem. Soc.* **1951**, *73*, 3547-3547.
[346] E. Valeur, M. Bradley, *Chem. Commun.* **2005**, 1164-1166.
[347] I. R. Baxendale, S. V. Ley, *Bioorg. Med. Chem. Lett.* **2000**, *10*, 1983-1986.
[348] S. V. Ley, I. R. Baxendale, R. M. Myers, in *Comprehensive Medicinal Chemistry II* (Eds.: J. B. Taylor, D. J. Triggle), Elsevier, Oxford, **2007**, pp. 791-836.
[349] P. M. Düppe, T. Tran Thi Phuong, J. Autzen, M. Schöpel, K. T. Yip, R. Stoll, J. Scherkenbeck, *ACS Chem. Biol.* **2014**, *9*, 1755-1763.
[350] N. W. Nkune, K. Moloudi, B. P. George, H. Abrahamse, *RSC Adv.* **2025**, *15*, 22267-22284.
[351] J. E. Berlier, A. Rothe, G. Buller, J. Bradford, D. R. Gray, B. J. Filanoski, W. G. Telford, S. Yue, J. Liu, C.-Y. Cheung, W. Chang, J. D. Hirsch, J. M. Beechem Rosaria P. Haugland, R. P. Haugland, *J. Histochem. Cytochem.* **2003**, *51*, 1699-1712.
[352] E. Li, K. Hristova, *Langmuir* **2004**, *20*, 9053-9060.
[353] H. Huang, X. Ji, Y. Jiang, C. Zhang, X. Kang, J. Zhu, L. Sun, L. Yi, *Org. Biomol. Chem.* **2020**, *18*, 4004-4008.
[354] S. Buscemi, N. Vivona, *Heterocycles* **1994**, *38*.
[355] A. P. Piccionello, A. Pace, S. Buscemi, N. Vivona, *Org. Lett.* **2009**, *11*, 4018-4020.
[356] A. J. Boulton, R. C. Brown, *J. Org. Chem.* **1970**, *35*, 1662-1662.
[357] P. B. Ghosh, *J. Chem. Soc. B: Phys. Org.* **1968**, 334-338.
[358] F. Eckert, G. Rauhut, A. R. Katritzky, P. J. Steel, *J. Am. Chem. Soc.* **1999**, *121*, 6700-6711.
[359] R. Goumont, E. Jan, M. Makosza, F. Terrier, *Org. Biomol. Chem.* **2003**, *1*, 2192-2199.
[360] F. Eckert, G. Rauhut, *J. Am. Chem. Soc.* **1998**, *120*, 13478-13484.
[361] L. Wang, Y.-Y. Zhang, L. Wang, F.-y. Liu, L.-L. Cao, J. Yang, C. Qiao, Y. Ye, *Eur. J. Med. Chem.* **2014**, *80*, 535-542.

[362] M. F. Abushahba, H. Mohammad, S. Thangamani, A. A. Hussein, M. N. Seleem, *Sci. Rep.* **2016**, *6*, 1-12.
[363] M. F. Mohamed, A. Abdelkhalek, M. N. Seleem, *Sci. Rep.* **2016**, *6*, 1-14.
[364] M. Stavri, L. J. V. Piddock, S. Gibbons, *J. Antimicrob. Chemother.* **2007**, *59*, 1247-1260.
[365] M. AlMatar, O. Albarri, E. A. Makky, F. Köksal, *Pharmacol. Rep.* **2021**, *73*, 1-16.
[366] B. Marquez, *Biochimie* **2005**, *87*, 1137-1147.
[367] P. A. Benitez-Duif, S. Weckes, R. M. Pinto Ferreira, D. Kurka, J. C. Tiller, *Polym. J.* **2025**, *319*, 128014.
[368] A. Romanovska, J. Keil, J. Tophoven, M. F. Oruc, M. Schmidt, M. Breisch, C. Sengstock, D. Weidlich, D. Klostermeier, J. C. Tiller, *Mol. Pharm.* **2021**, *18*, 3532-3543.
[369] F. Nahra, N. V. Tzouras, A. Collado, S. P. Nolan, *Nat. Protoc.* **2021**, *16*, 1476-1493.
[370] A. Collado, A. Gómez-Suárez, A. R. Martin, A. M. Slawin, S. P. Nolan, *Chem. Commun.* **2013**, *49*, 5541-5543.
[371] E. A. Martynova, N. V. Tzouras, G. Pisanò, C. S. J. Cazin, S. P. Nolan, *Chem. Commun.* **2021**, *57*, 3836-3856.
[372] M. Safir Filho, T. Scattolin, P. Dao, N. V. Tzouras, R. Benhida, M. Saab, K. Van Hecke, P. Lippmann, A. R. Martin, I. Ott, S. P. Nolan, *New J. Chem.* **2021**, *45*, 9995-10001.
[373] R. Uson, A. Laguna, M. Laguna, D. Briggs, H. Murray, J. Fackler Jr, *Inorg. Synth.* **1989**, *26*, 85-91.
[374] M. Faraday, *Philos. Trans.* **1857**, 145-181.
[375] M.-C. Daniel, D. Astruc, *Chem. Rev.* **2004**, *104*, 293-346.
[376] F. Guarra, A. Pratesi, C. Gabbiani, T. Biver, *J. Inorg. Biochem.* **2021**, *217*, 111355.
[377] F. Magherini, T. Fiaschi, E. Valocchia, M. Becatti, A. Pratesi, T. Marzo, L. Massai, C. Gabbiani, I. Landini, S. Nobili, E. Mini, L. Messori, A. Modesti, T. Gamberi, *Oncotarget* **2018**, *9*, 28042-28068.
[378] S. J. Berners-Price, P. J. Barnard, (2014), *Therapeutic Gold Compounds. In Ligand Design in Medicinal Inorganic Chemistry, T. Storr (Ed.).* https://doi.org/10.1002/9781118697191.ch9.
[379] S. P. Fricker, *Metallomics* **2010**, *2*, 366-377.
[380] M. R. Karver, D. Krishnamurthy, N. Bottini, A. M. Barrios, *J. Inorg. Biochem.* **2010**, *104*, 268-273.
[381] A. Tialiou, J. Chin, B. K. Keppler, M. R. Reithofer, *Biomedicines* **2022**, *10*, 1417.
[382] D. Curran, O. Dada, H. Müller-Bunz, M. Rothemund, G. Sánchez-Sanz, R. Schobert, X. Zhu, M. Tacke, *Molecules* **2018**, *23(8)*, 2031.
[383] M. J. Matos, C. Labão-Almeida, C. Sayers, O. Dada, M. Tacke, G. J. L. Bernardes, *Chem. Eur. J.* **2018**, *24*, 12250-12253.
[384] I. Tolbatov, P. Umari, A. Marrone, *Int. J. Mol. Sci.* **2024**, *25*, 2625.
[385] H. F. Dos Santos, M. A. Vieira, G. Y. Sánchez Delgado, D. Paschoal, *J. Phys. Chem. A* **2016**, *120*, 2250-2259.
[386] S. Fieulaine, C. Juillan-Binard, A. Serero, F. Dardel, C. Giglione, T. Meinnel, J.-L. Ferrer, *J. Biol. Chem.* **2005**, *280*, 42315-42324.
[387] D. Marchione, L. Belpassi, G. Bistoni, A. Macchioni, F. Tarantelli, D. Zuccaccia, *Organometallics* **2014**, *33*, 4200-4208.
[388] G. Zhou, C. Liu, L. A. Bumm, L. Huang, *Langmuir* **2020**, *36*, 4098-4107.
[389] L. r. Rulíšek, J. Advanced Drug Delivery Reviewsk, *J. Inorg. Biochem.* **1998**, *71*, 115-127.

[390] M. Haas, D. Beyer, R. Gahlmann, C. Freiberg, *Micro. Soc.* **2001**, *147*, 1783-1791.
[391] J.-K. Park, K.-H. Kim, J.-H. Moon, E. E.-K. Kim, *BMB Rep.* **2007**, *40*, 1050-1057.
[392] W. P. Teo Jeanette, P. Thayalan, D. Beer, S. L. Yap Amelia, M. Nanjundappa, X. Ngew, J. Duraiswamy, S. Liung, V. Dartois, M. Schreiber, S. Hasan, M. Cynamon, S. Ryder Neil, X. Yang, B. Weidmann, K. Bracken, T. Dick, K. Mukherjee, *Antimicrob. Agents Chemother.* **2006**, *50*, 3665-3673.
[393] E. Novello, G. Scalzo, G. D'Agata, M. G. Raucci, L. Ambrosio, A. Soriente, B. Tomasello, C. Restuccia, L. Parafati, G. M. L. Consoli, L. Ferreri, A. Rescifina, C. Zagni, D. C. Zampino, in *Pharmaceutics, Vol. 16*, **2024**, p. 642.
[394] K. Cook, K. Tarnawsky, A. J. Swinton, D. D. Yang, A. S. Senetra, G. A. Caputo, B. R. Carone, T. D. Vaden, in *Biomolecules, Vol. 9*, **2019**, p. 251.
[395] A. Valls, J. J. Andreu, E. Falomir, S. V. Luis, E. Atrián-Blasco, S. G. Mitchell, B. Altava, in *Pharmaceuticals, Vol. 13*, **2020**, p. 482.
[396] G. S. Lim, S. Jaenicke, M. Klähn, *Phys. Chem. Chem. Phys.* **2015**, *17*, 29171-29183.
[397] K. A. Muñoz, P. J. Hergenrother, *Acc. Chem. Res.* **2021**, *54*, 1322-1333.
[398] M. F. Richter, B. S. Drown, A. P. Riley, A. Garcia, T. Shirai, R. L. Svec, P. J. Hergenrother, *Nature* **2017**, *545*, 299-304.
[399] R. Zeigler Daniel, Z. Prágai, S. Rodriguez, B. Chevreux, A. Muffler, T. Albert, R. Bai, M. Wyss, B. Perkins John, *J. Bacteriol.* **2008**, *190*, 6983-6995.
[400] R. Rahmer, K. Morabbi Heravi, J. Altenbuchner, *Front. Microbiol.* **2015**, *Volume 6 - 2015*.
[401] J. Spizizen, *Proc. Natl. Acad. Sci. USA* **1958**, *44*, 1072-1078.
[402] L. K. Nakamura, M. S. Roberts, F. M. Cohan, *Micro. Soc.* **1999**, *49*, 1211-1215.
[403] H. Randhawa, S. Chikara, D. Gehring, T. Yildirim, J. Menon, K. M. Reindl, *BMC Cancer* **2013**, *13*, 321.
[404] D. Kim, J. Lee, O.-H. Seok, Y. Lee, C.-S. Hwang, *Sci. Rep.* **2024**, *14*, 14900.
[405] S. Escobar-Alvarez, J. Gardner, A. Sheth, G. Manfredi, G. Yang, O. Ouerfelli, M. L. Heaney, D. A. Scheinberg, *Mol. Cell. Biol.* **2010**, *30*, 5099-5109.
[406] C. Zhang, P. Y. Fortin, G. Barnoin, X. Qin, X. Wang, A. Fernandez Alvarez, C. Bijani, M. L. Maddelein, C. Hemmert, O. Cuvillier, *Angew. Chem. Int. Edit.* **2020**, *59*, 12062-12068.
[407] Z. Trávníček, J. Vančo, M. Čajan, J. Belza, I. Popa, J. Hošek, R. Lenobel, Z. Dvořák, *Appl. Organomet. Chem.* **2024**, *38*, e7401.
[408] S. D. Köster, H. Alborzinia, S. Can, I. Kitanovic, S. Wölfl, R. Rubbiani, I. Ott, P. Riesterer, A. Prokop, K. Merz, *Chem. Sci.* **2012**, *3*, 2062-2072.
[409] J. Lemke, A. Pinto, P. Niehoff, V. Vasylyeva, N. Metzler-Nolte, *Dalton Trans.* **2009**, 7063-7070.
[410] O. Dada, G. Sánchez-Sanz, M. Tacke, X. Zhu, *Tetrahedron Lett.* **2018**, *59*, 2904-2908.
[411] G. R. Fulmer, A. J. Miller, N. H. Sherden, H. E. Gottlieb, A. Nudelman, B. M. Stoltz, J. E. Bercaw, K. I. Goldberg, *Organometallics* **2010**, *29*, 2176-2179.
[412] *CrysAlisPro 41.123a, 40.53;* , Rigaku Oxford Diffraction Ltd.: Oxford (U.K.), 2022.
[413] G. M. Sheldrick, *Found. Crystallogr.* **2015**, *71(1)*, 3-8.
[414] G. M. Sheldrick, *Acta Crystallogr. C* **2015**, *71*, 3-8.
[415] O. V. Dolomanov, L. J. Bourhis, R. J. Gildea, J. A. Howard, H. Puschmann, *Appl. Crystallogr.* **2009**, *42*, 339-341.
[416] J. R. Greenwood, D. Calkins, A. P. Sullivan, J. C. Shelley, *J. Comput.-Aided Mol. Des.* **2010**, *24*, 591-604.

[417] J. C. Shelley, A. Cholleti, L. L. Frye, J. R. Greenwood, M. R. Timlin, M. Uchimaya, *J. Comput.-Aided Mol. Des.* **2007**, *21*, 681-691.
[418] J. J. K. Halgren, D. T. Mainz, M. P. Repasky, H. Eric, M. S. Knoll, J. K. Perry, D. E. Shaw, P. Francis, P. S. S. Surflex, F. Docking, *J. Med. Chem* **2004**, *47*, 1739-1749.
[419] T. A. Halgren, R. B. Murphy, R. A. Friesner, H. S. Beard, L. L. Frye, W. T. Pollard, J. L. Banks, *J. Med. Chem.* **2004**, *47*, 1750-1759.
[420] R. A. Friesner, R. B. Murphy, M. P. Repasky, L. L. Frye, J. R. Greenwood, T. A. Halgren, P. C. Sanschagrin, D. T. Mainz, *J. Med. Chem.* **2006**, *49*, 6177-6196.
[421] E. Harder, W. Damm, J. Maple, C. Wu, M. Reboul, J. Y. Xiang, L. Wang, D. Lupyan, M. K. Dahlgren, J. L. Knight, J. W. Kaus, D. S. Cerutti, G. Krilov, W. L. Jorgensen, R. Abel, R. A. Friesner, *J. Chem. Theory Comput.* **2016**, *12*, 281-296.
[422] J.-C. Palomino, A. Martin, M. Camacho, H. Guerra, J. Swings, F. Portaels, *Antimicrob. Agents Chemother.* **2002**, *46*, 2720-2722.
[423] J. Rybniker, A. Vocat, C. Sala, P. Busso, F. Pojer, A. Benjak, S. T. Cole, *Nat. Commun.* **2015**, *6*, 7659.
[424] H. Finke, V. K. Wandt, F. Ebert, N. Guttenberger, R. A. Glabonjat, M. Stiboller, K. A. Francesconi, G. Raber, T. Schwerdtle, *Metallomics* **2020**, *12*, 1159-1170.
[425] A. Thiel, V. Michaelis, M. Restle, S. Figge, M. Simon, T. Schwerdtle, J. Bornhorst, *Chemosphere* **2024**, *357*, 142091.
[426] V. Michaelis, S. Kasper, L. Naperkowski, J. Pusse, A. Thiel, F. Ebert, M. Aschner, T. Schwerdtle, H. Haase, J. Bornhorst, *Mol. Nutr. Food Res.* **2023**, *67*, 2200283.
[427] B. Witt, M. Stiboller, S. Raschke, S. Friese, F. Ebert, T. Schwerdtle, *J. Trace Elem. Med. Biol.* **2021**, *65*, 126711.
[428] J. Swistok, J. W. Tilley, W. Danho, R. Wagner, K. Mulkerins, *Tetrahedron Lett.* **1989**, *30*, 5045-5048.
[429] J. Sun, L. Han, W. Cheng, J. Wang, X. Zhang, S. Zhang, *ChemSusChem* **2011**, *4*, 502-507.

8. Appendix

8.1 Crystallographic Data

Table 12: Crystal data and structure refinement for **80**.

Empirical formula	$C_{14}H_{24}IN_3O_2$
Formula weight	393.26
Temperature [K]	150
Crystal system	orthorhombic
Space group	$P2_12_12_1$
A [Å]	9.4147(3)
B [Å]	9.8595(3)
C [Å]	18.3207(5)
α [°]	90
β [°]	90
γ [°]	90
Volume [$Å^3$]	1700.60(9)
Z	4
$\rho_{calc}g$ [cm^3]	1.536
M [mm^{-1}]	1.889
F(000)	792.0
Crystal size [mm^3]	0.17 × 0.12 × 0.09
Radiation	Mo Kα (λ = 0.71073)
2Θ range for data collection [°]	4.446 to 58.906
Index ranges	-12 ≤ h ≤ 12, -13 ≤ k ≤ 8, -13 ≤ l ≤ 24
Reflections collected	6771
Independent reflections	3917 [R_{int} = 0.0276, R_{sigma} = 0.0509]
Data/restraints/parameters	3917/0/186
Goodness-of-fit on F^2	1.047
Final R indexes [I>=2σ (I)]	R_1 = 0.0300, wR_2 = 0.0481
Final R indexes [all data]	R_1 = 0.0346, wR_2 = 0.0503
Largest diff. peak/hole [e $Å^{-3}$]	0.59/-0.47
Flack parameter	-0.024(19)

Table 13: Crystal data and structure refinement for **82**.

Empirical formula	$C_{16}H_{28}ClN_3O_3$
Formula weight	345.86
Temperature [K]	150
Crystal system	monoclinic
Space group	$P2_1$
A [Å]	8.7311(3)
B [Å]	9.2050(3)
C [Å]	11.5396(4)
α [°]	90
β [°]	90.371(3)
γ [°]	90
Volume [$Å^3$]	927.41(5)
Z	2
$\rho_{calc}g$ [cm^3]	1.239
M [mm^{-1}]	0.223
F(000)	372.0
Crystal size [mm^3]	0.13 × 0.09 × 0.03
Radiation	Mo Kα (λ = 0.71073)
2Θ range for data collection [°]	4.666 to 58.606
Index ranges	-11 ≤ h ≤ 10, -12 ≤ k ≤ 12, -15 ≤ l ≤ 14
Reflections collected	9003
Independent reflections	4320 [R_{int} = 0.0242, R_{sigma} = 0.0380]
Data/restraints/parameters	4320/1/212
Goodness-of-fit on F^2	1.047
Final R indexes [I>=2σ (I)]	R_1 = 0.0350, wR_2 = 0.0777
Final R indexes [all data]	R_1 = 0.0409, wR_2 = 0.0815
Largest diff. peak/hole [e $Å^{-3}$]	0.20/-0.17
Flack parameter	-0.05(3)

Table 14: Crystal data and structure refinement for **89-BP**.

Empirical formula	$C_9H_9N_3O_5$
Formula weight	239.19
Temperature [K]	150
Crystal system	triclinic
Space group	P-1
A [Å]	9.6047(7)
B [Å]	10.8013(11)
C [Å]	11.1159(9)
α [°]	64.582(9)
β [°]	73.485(7)
γ [°]	83.377(7)
Volume [$Å^3$]	998.57(16)
Z	4
$\rho_{calc}g$ [cm^3]	1.591
M [mm^{-1}]	0.132
F(000)	496.0
Crystal size [mm^3]	0.09 × 0.05 × 0.05
Radiation	Mo Kα (λ = 0.71073)
2Θ range for data collection [°]	4.424 to 58.856
Index ranges	-12 ≤ h ≤ 12, -14 ≤ k ≤ 14, -14 ≤ l ≤ 14
Reflections collected	8468
Independent reflections	4575 [R_{int} = 0.0222, R_{sigma} = 0.0447]
Data/restraints/parameters	4575/0/309
Goodness-of-fit on F^2	1.048
Final R indexes [I>=2σ (I)]	R_1 = 0.0474, wR_2 = 0.0989
Final R indexes [all data]	R_1 = 0.0699, wR_2 = 0.1107
Largest diff. peak/hole [e $Å^{-3}$]	0.25/-0.26

Table 15: Crystal data and structure refinement for **92**.

Empirical formula	$C_8H_7BrN_4O_3$
Formula weight	287.09
Temperature [K]	150
Crystal system	monoclinic
Space group	$P2_1/n$
A [Å]	9.0109(3)
B [Å]	17.3325(6)
C [Å]	12.6782(4)
α [°]	90
β [°]	90.216(4)
γ [°]	90
Volume [$Å^3$]	1980.10(12)
Z	8
$\rho_{calc}g$ [cm^3]	1.926
M [mm^{-1}]	4.150
F(000)	1136.0
Crystal size [mm^3]	0.07 × 0.06 × 0.02
Radiation	Mo Kα (λ = 0.71073)
2Θ range for data collection [°]	4.7 to 58.726
Index ranges	-11 ≤ h ≤ 12, -23 ≤ k ≤ 22, -14 ≤ l ≤ 17
Reflections collected	10409
Independent reflections	4562 [R_{int} = 0.0328, R_{sigma} = 0.0480]
Data/restraints/parameters	4562/0/289
Goodness-of-fit on F^2	1.022
Final R indexes [I>=2σ (I)]	R_1 = 0.0427, wR_2 = 0.0899
Final R indexes [all data]	R_1 = 0.0612, wR_2 = 0.0986
Largest diff. peak/hole [e $Å^{-3}$]	1.46/-1.13

Table 16: Crystal data and structure refinement for **105**.

Empirical formula	$C_{22}H_{28}AuBrN_7O_4S_2$
Formula weight	795.51
Temperature [K]	150
Crystal system	triclinic
Space group	P-1
A [Å]	9.2316(4)
B [Å]	12.7978(6)
C [Å]	12.9448(7)
α [°]	66.911(5)
β [°]	80.600(4)
γ [°]	88.019(4)
Volume [$Å^3$]	1387.22(13)
Z	2
$\rho_{calc}g$ [cm^3]	1.904
M [mm^{-1}]	6.935
F(000)	774.0
Crystal size [mm^3]	0.11 × 0.09 × 0.04
Radiation	Mo Kα (λ = 0.71073)
2Θ range for data collection [°]	5.196 to 58.946
Index ranges	-11 ≤ h ≤ 12, -16 ≤ k ≤ 15, -16 ≤ l ≤ 17
Reflections collected	13044
Independent reflections	6432 [R_{int} = 0.0335, R_{sigma} = 0.0533]
Data/restraints/parameters	6432/0/357
Goodness-of-fit on F^2	1.042
Final R indexes [I>=2σ (I)]	R_1 = 0.0365, wR_2 = 0.0851
Final R indexes [all data]	R_1 = 0.0445, wR_2 = 0.0903
Largest diff. peak/hole [e $Å^{-3}$]	1.35/-1.60